

A supramolecular structure in the membrane of *Staphylococcus aureus*

By

Felix Weihs, BSc MSc

(University of Tübingen)

A thesis submitted for the degree of Doctor of Philosophy

September 2016

Department of Molecular Biology and Biotechnology, University of
Sheffield, Firth Court, Western Bank, Sheffield, S10 2TN

Summary

All life demands the temporal and spatial control of essential biological functions. However, the understanding of cellular organization in the prokaryotic kingdom is poorly understood. Bacteria lack many of the known organisers as well as the compartmentalisation of eukaryotic cells and have to count on the cell wall and the membrane as anchoring sites for fundamental processes.

A novel supramolecular localisation pattern was found in the membrane of the apparently spherical bacterium *Staphylococcus aureus*. The phospholipid synthesis enzymes PlsY and CdsA are localised in a punctate pattern, along with a septal localisation in cells that are undergoing cell-division. This localisation pattern is stabilised by the cytoskeletal and cell-division-associated protein MreD.

MreD, which is also localised in punctate pattern, is required for growth at 42 °C. Cells lacking MreD stop growing and exhibit severe morphological defects along with the delocalisation of FtsZ. This phenotype might be explained by a decrease in cardiolipin levels which was revealed by thin layer chromatography and could be relieved by the addition of high amounts of NaCl to the growth medium.

Fluorescence microscopy studies revealed similar localisation patterns as seen for PlsY for membrane proteins involved in phospholipid biosynthesis and other metabolic processes, but not for the secretion protein SecY. A novel protein-interaction system based on Förster Resonance Energy Transfer was established in *S. aureus* and used to demonstrate the interaction of PlsY with CdsA, MreD and PgsA (another phospholipid synthesis enzyme) suggesting the formation of phospholipid synthesis clusters in the membrane that would allow metabolic channelling.

The observed localisation pattern is independent of wall teichoic acids, cardiolipin, lysinylated phosphatidylglycerolphosphate, squalene and peptidoglycan. However, PlsY has been found to localise homogeneously in the membrane when cells are treated with the FtsZ-polymerisation inhibitor PC190723 suggesting a potential role for FtsZ in the punctate patterned distribution of PlsY.

This study illustrates a novel supramolecular structure of membrane proteins in *S. aureus* which could be a common feature across biology.

Publications from this work

García-Lara J., **Weihls F.**, Ma X., Walker L., Chaudhuri R.R., Kasturiarachchi J., Crossley H., Golestanian R., Foster S.J. (2015) Supramolecular structure in the membrane of *Staphylococcus aureus*. *Proc Natl Acad Sci.* 112(51):15725-30.

My contributions: I carried out the complementation of SH1000 $\Delta mreD$ using a chromosomal single-copy native promoter expression approach described in Chapter 3 and the Förster Resonance Energy Transfer based protein-protein system described in Chapter 5. In addition, $\Delta mreC$ null-mutant deletion strains and their whole-genome sequencing analysis (together with Roy Chaudhuri) which are not shown in this thesis were carried out by me. I also wrote parts of the supplementary information and prepared main manuscript figures.

Contributions of other authors: Jorge García-Lara constructed a conditional *plsY* knock-out strain and various GFP fusions along with their characterisation. Xing Ma constructed and characterised the *mreC/mreD/mreCD* deletion strains. Lucas walker contributed towards the establishment of the FRET system. Jagath Kasturiarachchi and Howard Crossley constructed GFP fusion strains. The model to describe how proteins can form the observed localisation patterns was calculated by Ramin Golestanian. The main manuscript was written by Jorge García-Lara and Simon Foster.

Weihls F., Turner R.D., Foster S.J. The localisation pattern of membrane proteins in *Staphylococcus aureus*. *In preparation*.

My contributions: This manuscript encompasses the construction and analysis of GFP/eYFP/mCherry fusions with membrane proteins in *S. aureus* described in Chapter 4 along with their characterisation in dependence of certain membrane constituents and inhibitors. Moreover, the FRET data that was not shown in the previous publication along with the expression of MreD-eYFP in *Escherichia coli* is included and discussed in this manuscript.

Contributions of other authors: Robert Turner contributed towards the quantification of fluorescence signal in a sphere using the coefficient of variation of a polar coordinate image. The manuscript was written by me and Simon Foster.

Acknowledgements

I would like to thank Prof. Simon Foster for giving me the opportunity to carry out my PhD and to allow me to throw money at abstract ideas. I would also like to thank the Harry Worthington Scholarship that financed my tuition fees and living costs. Thanks to Ying (Dr. Jorge García-Lara) and Yang (Dr. Robert Turner) for the very fruitful intellectual inputs, long discussions and CFP.

Many thanks for everyone in F18, F25 and F21 and all my friends in Sheffield and Germany for technical help, advice and most importantly to endure my whining and complaints.

I would also like to thank Prof. Duncan Cameron and Prof. Mike Burrell for helping me with the metabolomics and LC-MS. Thanks to Prof. Peter Taylor and Dr. Helena Rosado for showing me how measure membrane fluorescence anisotropy. Lastly, many thanks to Dr. Ricardo Henriques and Dr. Sian Culley for doing the SRRF analysis.

Special thanks go to Hannah and my family who were always supporting me in bad and in bad times.

Abbreviations

°C	Degree Celsius
~	Approximately
2D	Two dimensional
3D	Three dimensional
a.u.	Arbitrary units
ACP	Acyl carrier protein
ADP	Adenosine diphosphate
Amp	Ampicillin
APS	Ammonium persulphate
ATP	Adenosine triphosphate
ATPase	Adenosine triphosphate hydase
attB	Bacterial attachment site
attP	Phage attachment site
BAR	Bin-Amphiphysin-Rvs
BACTH	Bacterial adenylate cyclase two-hybrid
BHI	Brain heart infusion
BODIPY-FL	Boron-dipyrrromethene
bp	Base pair
c-di-AMP	Cyclic-di-adenosine monophosphate
CDM	Chemically defined medium
CDP	Cytosine diphosphate
CFP	Cyan fluorescent protein
CFU	Colony forming units
CL	Cardiolipin
Cm	Chloramphenicol
CV	Coefficient of variation
D-Ala	D-alanine
D-Glu	D-glutamic acid
D-Ser	D-serine
DAG	Diacylglycerolphosphate
DAPI	4',6-diamidino-2-phenylindole
dH ₂ O	Distilled water
DMSO	Dimethyl sulphoxide
DNA	Deoxyribonucleic acid
DNase	Deoxyribonuclease
dNTP	Deoxyribonucleoside-5'-triphosphate
DPG	Diphosphatidylglycerol (Cardiolipin)
DPH	1,6-diphenyl-1,3,5-hexatriene
DTT	Dithiothreitol
EDTA	Ethylenediamine tetra-acetic acid
EM	Electron microscopy
Ery	Erythromycin
ESI-LC-MS	Electrospray-induced liquid-chromatography mass-spectrometry
eYFP	Enhanced yellow fluorescent protein
FAS II	Fatty acid synthase II
Fig.	Figure
FITC	Fluorescein isothiocyanate
FLIM	Fluorescence lifetime imaging microscopy

FM 1-43	<i>N</i> -(3-Triethylammoniumpropyl)-4-(4-(Dibutylamino) Styryl) Pyridinium Dibromide
FRAP	Fluorescence recovery after photobleaching
FRET	Förster resonance energy transfer
g	Gram
G3P	Glycerol-3-phosphate
GC	Guanine-Cytosine
GDP	Guanosine diphosphate
GFP	Green fluorescent protein
GL	Glycolipid
Glc	Glucose
GlcNAc	<i>N</i> -acetyl glucosamine
GroP	Glycerolphosphate
GSH	Glutathione
GTP	Guanosine triphosphate
GTPase	Guanosine triphosphate hydrolase
GUV	Giant unilamellar vesicles
h	Hour
HADA	Hydroxycoumarin 3-amino- <i>D</i> -alanine
HRP	Horseradish peroxidase
IF	Intermediate filaments
IgG	Immunoglobulin G
IPTG	Isopropyl beta- <i>D</i> -1-thiogalactopyranoside
Kan	Kanamycin
kb	Kilobase pair
kDa	Kilodalton
KOPS	FtsK orienting polar sequences
kV	Kilovolt
l	Litre
L-Ala	L-alanine
L-Lys	L-lysine
LB	Lysogeny broth
Lin	Lincomycin
LPA	Lysophosphatidic acid
LPG	Lysyl-phosphatidylglycerolphosphate
LPS	Lipopolysaccharide
M	Molar
Mbp	Megabase
MCS	Multiple cloning site
mEos2	Monomeric Eos2 fluorescent protein
meYFP	Monomeric enhanced yellow fluorescent protein
mg	Milligram
MIC	Minimum inhibitory concentration
min	Minute
ml	Millilitre
mm	Millimetre
mM	Millimolar
mRNA	Messenger ribonucleic acid
MRSA	Methicillin-resistant <i>Staphylococcus aureus</i>
MurNAc	<i>N</i> -acetyl muramic acid
mW	Milliwatt
NAD	Oxidised nicotinamide adenine dinucleotide

NADH	Reduced nicotinamide adenine dinucleotide
NBS	Noc-binding sequence
ng	Nanogram
nm	Nanometre
nM	Nanomolar
NO	Nucleoid occlusion
nt	Nucleotide
OD ₆₀₀	Optical density measure at 600 nm
OM	Outer membrane
ori	Origin of replication
(p)ppGpp	guanosine (penta)/tetra phosphate
P	Phosphatidylglycerol
PA	Phosphatidic acid
PALM	Photoactivated localisation microscopy
PBP	Penicillin binding protein
PBS	Phosphate buffered saline
PCA	Principal component analysis
PCR	Polymerase chain reaction
PE	Phosphatidylglycerolethanolamine
PG	Phosphatidylglycerolphosphate
PGN	Peptidoglycan
P _i	Inorganic phosphate
PL	Phospholipid
PN	Aminophospholipid
PS	Phosphatidylglycerolserine
P _{spac}	Spac promoter
PTS	Phosphotransferase system
P _{xyl}	Xylose promoter
RBS	Ribosome binding site
rcf	Relative Centrifugal Force
RNA	Ribonucleic acid
rpm	Revolutions per min
s	Second
SALP	SsgA-like proteins
SBS	SlmA-DNA binding sequence
sdH ₂ O	Sterile distilled water
SDS	Sodium dodecyl sulphate
SDS-PAGE	Sodium dodecyl sulphate polyacrylamide gel electrophoresis
SIM	Structured illumination microscopy
Spec	Spectinomycin
SRRF	Super resolution radial fluctuations
STED	Stimulated emission-depletion
STORM	Stochastic optical reconstruction microscopy
TAE	Tris-acetate EDTA
Tab.	Table
Taq	Thermostable DNA polymerase derived from <i>Thermus aquaticus</i>
TBS _i	Tris buffered saline containing a protease inhibitor cocktail
TBST	Tris buffered saline tween
TE	Tris-EDTA (buffer)
TEMED	N,N,N',N'-tetramethyl-ethylenediamine
Tet	Tetracycline
THF	Tetrahydrofuran

TG	Transglycosylase activity
TMDH	Transposon-mediated differential Hybridisation
Tn	Transposon
TP	Transpeptidase activity
Tris	Tris (hydroxymethyl) aminomethane
U	Units (of enzyme activity)
UDP	Uridine diphosphate
UV	Ultra violet
V	Volts
v/v	Volume for volume
w/v	Weight for volume
WTA	Wall teichoic acid
x	Times
X-Gal	5-bromo-4-chloro-3-indolyl- β -D-galactoside
Y2H	Yeast two hybrid
YFP	Yellow fluorescent protein
ZA	Zaragozic acid
μ F	Microfarad
μ g	Microgram
μ l	Microlitre
μ m	Micrometre
μ M	Micromolar
Φ	Phage
Ω	Ohms

Table of Contents

	Page Number
Summary	i
Publications from this work	ii
Acknowledgements	iii
Abbreviations	iv
Table of Contents	viii
List of Figures	xix
List of Tables	xxiii
Chapter 1: Introduction	1-47
1.1 The organisation of life	1
1.2 The bacterial blueprint	2
1.2.1 The different shapes of bacteria	2
1.2.2 Shape determinants or the bacterial cytoskeleton	2
1.2.3.1 Bacterial actin homologues	3
1.2.3.1.1 MreB	3
1.2.3.1.2 ParM	4
1.2.3.1.3 Crenactin	5
1.2.3.2 Bacterial tubulin homologues	5
1.2.3.2.1 FtsZ	5
1.2.3.2.2 TubZ	7
1.2.3.2.3 CetZ	7
1.2.3.3 Bacterial intermediate filament homologues	7
1.2.3.3.1 Crescentin	7
1.2.4 The membrane	8
1.2.4.1 Phospholipid synthesis	8
1.2.4.1.1 FASII initiation module	9
1.2.4.1.2 FASII elongation module	9
1.2.4.1.3 Acyltransferase module	9
1.2.4.1.4 Phospholipid head group synthesis	10
1.2.4.2 Teichoic acids	11
1.2.4.2.1 Lipoteichoic acid synthesis	11

1.2.4.2 Outer membrane.....	16
1.2.4.2.1 LPS synthesis and outer membrane biogenesis	16
1.2.5 Peptidoglycan.....	18
1.2.5.1 Synthesis of UDP-MurNAc and UDP-GlcNAc.....	18
1.2.5.2 Synthesis of lipid II.....	19
1.2.5.3 Transglycosylation and transpeptidation via PBPs.....	19
1.2.5.2 Wall teichoic acid synthesis	20
1.2.6 Nucleoid	20
1.2.6.1 Chromosome replication	24
1.2.7 The bacterial division machinery	24
1.2.7.1 Temporal regulation	24
1.2.7.2 Spatial regulation	26
1.2.7.2.1 The Min system.....	26
1.2.7.2.2 Nucleoid occlusion	28
1.2.7.2.3 Alternative mechanisms	29
1.2.7.2.3.1 MipZ	29
1.2.7.2.3.2 MapZ/LocZ	29
1.2.7.2.3.3 SsgAB.....	30
1.2.7.2.3.4 PomXYZ	30
1.2.7.3 Divisome assembly	32
1.2.8 Cytoplasm	33
1.3 Localisation of membrane proteins.....	37
1.3.1 Membrane curvature as a cue for protein localisation	37
1.3.1.1 DivIVA.....	37
1.3.1.2 SpoVM.....	39
1.3.1.3 Other curvature sensing proteins.....	39
1.3.1.4 BAR-domain containing proteins in eukaryotes	40
1.3.2 Driving forces for membrane curvature.....	40
1.3.2.1 Lipid composition	42
1.3.2.2 Shaped membrane proteins and protein crowding.....	42
1.3.3 Lipid microdomains in bacterial membranes.....	43
1.4 <i>Staphylococcus aureus</i>	44
1.4.1 <i>Staphylococcus aureus</i> as a model to study membrane protein localisation	44
1.5 A supramolecular structure in the membrane of <i>S. aureus</i>	45
1.6 Aims and summary of this study.....	47

Chapter 2: Materials and Methods	48-92
2.1 Media	48
2.1.1 Tryptic Soy Broth (TSB).....	48
2.1.2 Brain Heart Infusion (BHI)	48
2.1.3 Lysogeny broth (LB).....	48
2.1.4 LK medium	48
2.1.5 Lipase activity agar plates.....	48
2.1.6 Chemically defined medium (CDM)	49
2.2 Antibiotics.....	49
2.3 Bacterial strains and plasmids.....	50
2.3.1 <i>Staphylococcus aureus</i> strains	50
2.3.2 <i>Escherichia coli</i> strains	54
2.3.3 Plasmids	54
2.4 Buffers and solutions	58
2.4.1 Phage buffer	58
2.4.2 Phosphate buffered saline (PBS).....	59
2.4.3 TAE (50x)	59
2.4.4 Tris buffered saline (TBS)	59
2.4.5 QIAGEN buffers	59
2.4.5.1 QIAGEN Buffer P1.....	59
2.4.5.2 QIAGEN Buffer P2.....	59
2.4.5.3 QIAGEN Buffer P3.....	59
2.4.5.4 QIAGEN Buffer EB.....	60
2.4.5.5 QIAGEN QBT	60
2.4.5.6 QIAGEN QC.....	60
2.4.5.7 QIAGEN QF	60
2.4.5.8 Buffer N3	60
2.4.5.9 Buffer PB	60
2.4.5.10 Buffer PE.....	60
2.4.5.11 Buffer QG	61
2.4.5.12 Buffers AL, AW1 and AW2	61
2.4.6 Fixative.....	61
2.4.6.1 Preparation of 16 % (w/v) p-formaldehyde	61
2.4.6.1.1 100 mM sodium phosphate buffer	61

2.4.6.1.2 16 % (w/v) p-formaldehyde	61
2.4.7 SDS-PAGE solutions	61
2.4.7.1 SDS-PAGE reservoir buffer (10 x)	61
2.4.7.2 SDS-PAGE loading buffer (5x)	62
2.4.7.3 Coomassie Blue stain	62
2.4.7.4 Coomassie destain	62
2.4.8 Western blotting solutions.....	62
2.4.8.1 Blotting buffer	62
2.4.8.2 TBST (20x)	62
2.4.8.3 Blocking buffer	62
2.4.9 HiTrap purification buffers	63
2.4.9.1 0.1M Sodium phosphate buffer.....	63
2.4.9.2 START Buffer.....	63
2.4.9.3 Elution Buffer.....	63
2.5 Chemicals and enzymes	63
Vancomycin, BODIPY® FL Conjugate	64
2.6 Centrifugation	64
2.7 Determining bacterial cell density	64
2.7.1 Spectrophotometric measurement (OD ₆₀₀)	64
2.7.2 Direct cell counts (CFU ml ⁻¹).....	64
2.8 DNA purification techniques	65
2.8.1 Genomic DNA extraction	65
2.8.2 Small scale plasmid purification	65
2.8.3 Large scale plasmid purification	66
2.8.4 DNA Gel extraction and PCR purification	66
2.8.5 Ethanol precipitation of DNA	67
2.9 <i>In vitro</i> DNA manipulation techniques	67
2.9.1 <i>In vitro</i> DNA manipulation techniques	67
2.9.2 PCR amplification.....	67
2.9.2.1 Phusion polymerase	67
2.9.2.2 Taq polymerase	78
2.9.2.3 Colony PCR screening of <i>E. coli</i>	79
2.9.3 Restriction endonuclease digestion.....	79
2.9.4 Ligation of DNA	79

2.9.5 Gibson Assembly	79
2.9.6 Agarose gel electrophoresis	79
2.9.7 Determination of DNA concentration.....	80
2.9.8 DNA sequencing	80
2.10 Transformation techniques.....	80
2.10.1 Transformation of <i>E. coli</i>	80
2.10.1.1 Preparation of electrocompetent <i>E. coli</i> cells.....	80
2.10.1.2 Electroporation of DNA into <i>E. coli</i> competent cells	81
2.10.1.3 Preparation of chemically competent <i>E. coli</i> cells.....	81
2.10.1.3.1 TFB I buffer	81
2.10.1.3.2 TFB II buffer	81
2.10.1.3.3 Preparation of chemically competent <i>E. coli</i> cells.....	81
2.10.1.4 Heat-shock transformation of DNA into <i>E. coli</i> competent cells	82
2.11.1 Transformation of <i>S. aureus</i>	82
2.11.1.1 Preparation of electrocompetent <i>S. aureus</i> RN4220 cells.....	82
2.11.1.2 Electroporation of DNA into <i>S. aureus</i> RN4220 competent cells	82
2.10 Phage techniques.....	82
2.10.1 Bacteriophage.....	82
2.10.1 Preparation of phage lysate	83
2.10.2 Phage transduction	83
2.11 Protein analysis	83
2.11.1 SDS-PAGE.....	83
2.11.2 Coomassie staining	85
2.11.3 Gel drying	85
2.11.4 Determination of protein concentrations.....	85
2.11.5 Western Blot	85
2.11.5.1 Western Blot transfer	85
2.11.5.2 Antibody treatment	85
2.11.5.2 Western blot development	86
2.12 Production of recombinant protein	86
2.12.1 Expression in <i>E. coli</i> C43 (DE3).....	86
2.12.2 HisTrap HP™ column for protein purification.....	87
2.13 Microscopes	87
2.14 Sample preparation for light-microscopy	88

2.14.1	Fluorescence microscopy	88
2.14.2	Donor photobleaching FRET experiments.....	88
2.14.3	Super resolution microscopy.....	89
2.14.3.1	STORM buffers.....	90
2.14.3.2	Coverslip sample preparation.....	90
2.14.3.3	Sample application	91
2.15	Metabolite analysis.....	91
2.15.1	Harvesting samples	91
2.15.2	Metabolite extraction	91
2.15.3	Electro-spray induced liquid chromatography mass spectrometry	92
Chapter 3: The physiological role of MreD in <i>S. aureus</i>		93-139
3.1	Introduction	93
3.1.1	The roles of MreC and MreD.....	93
3.1.2	Aims of this chapter	94
3.2	Results	95
3.2.1	Effect of temperature on $\Delta mreD$	95
3.2.2	Effect of salts on $\Delta mreD$ growth.....	102
3.2.3	Growth of SH1000 $\Delta mreD$ in a chemically defined medium.....	102
3.2.4	Membrane analysis of SH1000 $\Delta mreD$	103
3.2.4.1	Phospholipid and fatty acid analysis	103
3.2.4.2	Membrane fluidity analysis.....	108
3.2.5	Metabolome analysis of SH1000 and SH1000 $\Delta mreD$	111
3.2.5.1	Sample processing.....	111
3.2.5.2	Principal component analyses between metabolome subgroups	111
3.2.5.3	Identification of altered metabolites.....	114
3.2.5.4	Metabolite identification by tandem mass spectrometry	115
3.2.6	Suppressors of $\Delta mreD$	119
3.2.6.1	Phenotypic characterisation of $\Delta mreD$ suppressors.....	119
3.2.6.2	Whole genomes sequencing of $\Delta mreD$ suppressors	119
3.2.7	Complementation of $\Delta mreD$	124
3.2.7.1	Plasmid-based complementation of $\Delta mreD$	124
3.2.7.2	Single-copy-expression of $mreD$ complementation of $\Delta mreD$	125

3.2.7.2.1 Construction of complementation vector pKASBAR- <i>P_{mreCD}-mreD</i>	125
3.2.7.2.2 Analysis of single-copy <i>mreD</i> expression complementation of SH1000 Δ <i>mreD</i>	127
3.2.7.3 Transduction of Δ <i>mreD</i> into pre-complemented SH1000	127
3.2.7.4 Δ <i>mreD</i> in other strain backgrounds	133
3.3 Discussion	135
3.3.1 Is MreD required for cell viability?	135
3.3.2 Effect of MreD on membrane organisation	136
3.3.4 Suppressors of Δ <i>mreD</i>	138
3.4 Main findings in this chapter	139
3.5 Contributions	139
Chapter 4: Localisation of membrane proteins in	140-253
<i>S. aureus</i>	140
4.1 Introduction	140
4.1.1 Membrane heterogeneity and localisation of phospholipid synthesis enzymes	140
4.1.2 Aims of this chapter	141
4.2 Results	142
4.2.1 Localisation of PlsY	142
4.2.1.1 Growth phase dependent localisation of PlsY	142
4.2.1.2 Cell-cycle dependent localisation of PlsY	143
4.2.1.3 Dose dependent localisation of PlsY	143
4.2.1.4 Verification of the punctate localisation pattern of PlsY	144
4.2.1.4.1 Construction of a PlsY-eYFP and PlsY-meYFP fusion in <i>S. aureus</i>	144
4.2.1.4.2 Localisation of PlsY-eYFP	151
4.2.2 Localisation of other phospholipid synthesis enzymes	151
4.2.2.1 Genes selected for investigation	151
4.2.2.2 Construction of single-copy integrative plasmids for phospholipid synthesis enzyme fusions with eYFP	156
4.2.2.2.1 Construction of a PlsC-eYFP fusion in <i>S. aureus</i>	157
4.2.2.2.2 Construction of a PgsA-eYFP fusion in <i>S. aureus</i>	157
4.2.2.2.3 Construction of an MprF-eYFP fusion in <i>S. aureus</i>	162

4.2.2.2.4 Construction of a Cls2-eYFP fusion in <i>S. aureus</i>	162
4.2.2.3 Localisation studies of phospholipid synthesis enzyme fusions with <i>eyfp</i>	163
4.2.2.3.1 Localisation of PlsC-eYFP	168
4.2.2.3.2 Localisation of PgsA-eYFP	170
4.2.2.3.3 Localisation of MprF-eYFP	172
4.2.2.3.4 Localisation of Cls2-eYFP	174
4.2.2.4 Localisation studies of non-phospholipid synthesis proteins.....	176
4.2.2.5 Cytochrome B subunit (CydB)	176
4.2.2.5.1 Construction of a CydB-eYFP fusion in <i>S. aureus</i>	176
4.2.2.5.2 Localisation of CydB-eYFP	177
4.2.2.6 Flotillin.....	182
4.2.2.6.1 Construction of a FloT-eYFP fusion in <i>S. aureus</i>	182
4.2.2.6.2 Localisation of FloT-eYFP	183
4.2.2.7 Secretion ATPase (SecY).....	189
4.2.2.7.1 Construction of a SecY-GFP fusion in <i>S. aureus</i>	189
4.2.2.7.2 Localisation of SecY-GFP	189
4.2.3 Homogeneity Distribution measurements.....	192
4.2.4 Colocalisation studies of membrane proteins	195
4.2.4.1 Colocalisation studies using overexpression plasmids	197
4.2.4.2 Localisation studies of SNAP-tagged membrane proteins.....	202
4.2.4.2.1 Construction of a PlsY-SNAP fusion in <i>S. aureus</i>	205
4.2.4.2.2 Localisation of PlsY-SNAP (TMR-Star)	205
4.2.4.3.1 Construction of a CydB-SNAP fusion in <i>S. aureus</i>	205
4.2.4.3.2 Localisation of CydB-SNAP (TMR-Star).....	206
4.2.4.4.1 Construction of a PgsA-SNAP fusion in <i>S. aureus</i>	206
4.2.4.4.2 Localisation of PgsA-SNAP (TMR-Star)	206
4.2.4.5 Colocalisation of SecY-GFP and PlsY-SNAP (TMRStar)	207
4.2.4.5.1 Construction of a double tagged SecY-GFP and PlsY-SNAP strain	207
4.2.4.5.1 Colocalisation of SecY-GFP and PlsY-SNAP (TMRStar)	207
4.2.5 Role of membrane components in PlsY-GFP localisation.....	219
4.2.5.1 Inhibition of squalene synthesis.....	219
4.2.5.2 PlsY-GFP localisation in a cardiolipin (<i>cls1/cls2</i>) deletion mutant	220
4.2.5.3 PlsY-GFP localisation in a lys-PG (<i>mprF</i>) deletion mutant	220

4.2.5.4 PlsY-GFP localisation in a wall teichoic acid (<i>tarO</i>) deletion mutant	225
4.2.5.5 Effect of fatty acid synthesis inhibition on PlsY-GFP localisation	230
4.2.5.6 Effect of membrane potential inhibition on PlsY-GFP localisation	237
4.2.5.7 Effect of FtsZ-polymerisation inhibition	238
4.2.5.8 PlsY-GFP localisation in protoplasts	243
4.2.5.9 Effect of SDS treatment on PlsY-GFP localisation	244
4.3 Discussion	247
4.3.1 Localisation of PlsY in <i>S. aureus</i>	247
4.3.2 FtsZ dependent localisation of PlsY	247
4.3.3 The role of lipid domains in the localisation of membrane proteins	248
4.3.4 Dose-dependent localisation of membrane proteins	249
4.3.5 Subcellular localisation of other membrane proteins	251
4.3.6 Conclusion	252
4.4 Main findings in this chapters	253
4.5 Contributions	253
 Chapter 5: Membrane protein interaction studies in	 254-287
<i>S. aureus</i>	254
5.1 Introduction	254
5.1.1 Protein-interaction analysis methods in bacteria	254
5.1.2 Förster Resonance Energy Transfer	257
5.1.3 Measurement techniques	258
5.1.3.1 Sensitized emission	258
5.1.3.2 Fluorescence Lifetime Imaging Microscopy (FLIM)	259
5.1.3.3 Acceptor bleaching	259
5.1.3.4 Donor Photobleaching (pbFRET)	259
5.1.4 Aims of this chapter	259
5.2 Results	261
5.2.1 Genetic and experimental setup	261
5.2.2 Selected controls	261
5.2.3 Genes selected for investigation	263
5.2.4 Construction of FRET plasmids	263
5.2.5 Analysis of functionality	268
5.2.6 FRET measurements	278

5.2.7 FRET measurements in presence the of Daptomycin	281
5.2.8 Single cell subcellular FRET measurements.....	282
5.3 Discussion	285
5.3.1 A novel system to study protein-protein-interactions in <i>S. aureus</i>	285
5.3.2 PlsY is part of a complex protein-interaction network	286
5.3.3 Main findings in this chapter.....	287
3.5 Contributions.....	287
Chapter 6: <i>In vitro</i> studies of MreD	288-313
6.1 Introduction	288
6.1.1 Reconstitution of bacterial proteins <i>in vitro</i>	288
6.1.2 Subcellular localisation and <i>in vitro</i> study examples.....	288
6.1.2.1 DivIVA.....	288
6.1.2.2 SpoVM	288
6.1.2.3 MinCDE	289
6.1.2.4 FtsZ-FtsA	289
6.1.2.5 Other examples of protein reconstitutions	290
6.1.7 Aims of this chapter	290
6.2 Results	291
6.1.1 Heterologous expression of <i>mreD-eyfp</i> in <i>E. coli</i>	291
6.1.1.1 Construction of an IPTG-inducible MreD-eYFP fusion in <i>E. coli</i>	293
6.1.1.2 Localisation of MreD-eYFP and MurJ-GFP in <i>E. coli</i>	293
6.1.2 Localisation of membrane proteins in cytoplasmic vesicles.....	300
6.1.3 Localisation of membrane proteins in liposomes.....	303
6.1.3.1 Liposome formation by lipid emulsion	303
6.1.3.2 Reconstitution of MreD into liposomes	306
6.1.3.2.1 Overexpression and purification of MreD-6-eYFP	306
6.1.3.2.2 FITC-labelling of purified MreD	307
6.1.3.2.3 Reconstitution of FITC-labelled MreD into liposomes	307
6.3 Discussion	311
6.3.1 Punctate patterned distribution of membrane proteins in rod-shaped bacteria	311
6.3.2 Reconstitution of MreD into liposomes	312
6.3.3 Conclusion	313

6.4 Main findings in this chapters	313
3.5 Contributions.....	313
Chapter 7: General Discussion	314-320
7.1 Pattern maintenance	314
7.2 A metabolic perspective.....	317
7.3 A link between phospholipid synthesis and cell-division?	317
7.4 Future work	318
7.4.1 <i>In vivo</i> and <i>Ex vivo</i>	318
7.4.2 <i>In vitro</i>	319
7.5 Conclusion	320
Chapter 8: References	321-354
Chapter 9: Appendix	355-370
9.1 Construction of mCherry and mRFPmars1 fusions with membrane proteins	355
9.1.1 Construction of a PlsY-mCherry fusion in <i>S. aureus</i>	355
9.1.2 Construction of a CdsA-mCherry fusion in <i>S. aureus</i>	355
9.1.3 Construction of a CdsA-mRFPmars1 fusion in <i>S. aureus</i>	356
9.1.4 Construction of a PgsA-mRFPmars1 fusion in <i>S. aureus</i>	356
9.1.5 Construction of a PlsY-GFP (tetracycline resistance) fusion in <i>S. aureus</i> ..	366
9.2 Codon-optimised sequences.....	369
9.2.1 Codon-optimised sequence of <i>mreD</i>	369
9.2.2 Codon-optimised sequence of <i>eyfp</i>	370

List of Figures

	Page Number
Figure 1.1	The different shapes of bacteria 2
Figure 1.2	Initiation and elongation module of fatty acid synthesis 12
Figure 1.3	Acyltransferase module 13
Figure 1.4	Phospholipid headgroup synthesis 14
Figure 1.5	Phospholipid synthesis 15
Figure 1.6	Lipoteichoic acid synthesis in gram positive bacteria 17
Figure 1.7	LPS synthesis and translation in gram-negative bacteria 21
Figure 1.8	Peptidoglycan synthesis in bacteria 22
Figure 1.9	Wall teichoic acid synthesis in gram-positive bacteria 23
Figure 1.10	Chromosome replication 25
Figure 1.11	Temporal regulation of Z-ring formation 27
Figure 1.12	MinCDE oscillation in <i>E. coli</i> 31
Figure 1.13	Cell-division machineries in <i>E. coli</i> , <i>B. subtilis</i> and <i>S. aureus</i> 35
Figure 1.14	Molecule diffusion dynamics in the bacterial cytoplasm 36
Figure 1.15	Examples of membrane curvature sensing protein mechanisms 41
Figure 1.16	Enzymes involved in phospholipid synthesis and MreD are part of a supramolecular structure in the membrane of <i>S. aureus</i> 46
Figure 3.1	Characterization of SH1000 $\Delta mreD$ grown at 42 °C 96
Figure 3.2	Growth phenotype of SH1000 $\Delta mreD$ at various temperatures 97
Figure 3.3	BODIPY-FL-Vancomycin labelling of SH1000 $\Delta mreD$ mutants grown at 42 °C 98
Figure 3.4	FtsZ-eYFP in SH1000 $\Delta mreD$ grown at 42 °C 100
Figure 3.5	Heat-sensitivity phenotype of $\Delta mreD$ in the presence of salts or sucrose 103
Figure 3.6	Growth of SH1000 $\Delta mreD$ in chemically defined medium (CDM) 105
Figure 3.7	Fatty acid and phospholipid composition of SH1000 and SH1000 $\Delta mreD$ 106
Figure 3.8	Membrane fluidity measurements 109
Figure 3.9	Metabolome principal component analyses 111
Figure 3.10	Relative changes of metabolite levels 115
Figure 3.11	Tandem mass spectrometry electron capture induced fragmentation of peak 211.2 da 117
Figure 3.12	SH1000 $\Delta mreD$ suppressor growth on plate 120
Figure 3.13	Restreaking of SH1000 $\Delta mreD$ suppressed derivatives 121
Figure 3.14	SNPs found in SH1000 $\Delta mreD$ suppressed strains 125
Figure 3.15	Plasmid-based complementation of the growth phenotype of SH1000 $\Delta mreD$ and SH1000 $\Delta mreCD$ 125
Figure 3.16	Schematic overview of the native genomic region of <i>mreCD</i> 125
Figure 3.17	Construction of a single-copy chromosomal complementation plasmid for $\Delta mreD$ 127
Figure 3.18	Complementation of SH1000 $\Delta mreD$ by single-copy <i>mreD</i> expression 129
Figure 3.19	Growth on BHI agar of precomplemented SH1000 $\Delta mreD$ 131
Figure 3.20	Growth phenotype of Newman $\Delta mreD$ and NewHG $\Delta mreD$ 133
Figure 3.21	Growth phenotype of the <i>mreD</i> transposon mutant SH1000 NE858 133
Figure 4.1	Growth phase dependent localisation of PlsY-GFP 142

Figure 4.2	SRRF analysis of PlsY-GFP	143
Figure 4.3	Cell-cycle dependent localisation of PlsY-GFP	145
Figure 4.4	Dose-dependent localisation of PlsY-GFP	146
Figure 4.5	Nucleotide and amino acid sequence of <i>eyfp</i> compared to <i>meyfp</i>	147
Figure 4.6	Construction of a chromosomal <i>plsY-(m)eyfp</i> fusion in <i>S. aureus</i> SH1000	148
Figure 4.7	Localisation of PlsY-eYFP in <i>S. aureus</i> SH1000	151
Figure 4.8	Localisation of PlsY-meYFP in <i>S. aureus</i> SH1000	153
Figure 4.9	Construction of a chromosomal <i>plsC-eyfp</i> fusion in <i>S. aureus</i> SH1000	157
Figure 4.10	Construction of a chromosomal <i>pgsA-eyfp</i> fusion in <i>S. aureus</i> SH1000	159
Figure 4.11	Construction of a chromosomal <i>mprF-eyfp</i> fusion in <i>S. aureus</i> SH1000	163
Figure 4.12	Construction of a chromosomal <i>cls2-eyfp</i> fusion in <i>S. aureus</i> RN4220 <i>cls2::Tn</i>	165
Figure 4.13	Localisation of PlsC-eYFP in <i>S. aureus</i> SH1000	167
Figure 4.14	Localisation of PgsA-eYFP in <i>S. aureus</i> SH1000	169
Figure 4.15	Localisation of MprF-eYFP in <i>S. aureus</i> SH1000	171
Figure 4.16	Localisation of Cls2-eYFP in <i>S. aureus</i> RN4220	173
Figure 4.17	Construction of a chromosomal <i>cydB-eyfp</i> fusion in <i>S. aureus</i> SH1000	177
Figure 4.18	Localisation of CydB-eYFP in <i>S. aureus</i> SH1000	179
Figure 4.19	Localisation of FloT-eYFP in <i>S. aureus</i> UAMS-1	181
Figure 4.20	Construction of a chromosomal <i>floT-eyfp</i> fusion in <i>S. aureus</i> SH1000	183
Figure 4.21	Localisation of FloT-eYFP in <i>S. aureus</i> SH1000	185
Figure 4.22	Localisation of FloT-eYFP in <i>S. aureus</i> SH1000	187
Figure 4.23	Localisation of SecY-GFP in <i>S. aureus</i> SH1000	189
Figure 4.24	Coefficient of variation factor calculation	192
Figure 4.25	CV factor calculation of PlsY-GFP and SecY-GFP in <i>S. aureus</i>	193
Figure 4.26	Excitation and emission spectra of selected fluorescent proteins compared to GFP	197
Figure 4.27	Localisation of PlsY-GFP and various membrane proteins fused to mCherry in <i>S. aureus</i> SH1000	198
Figure 4.28	Septal colocalisation of various membrane proteins fused to mCherry with PlsY-GFP	202
Figure 4.29	Overlap coefficient according to Manders using convolved and deconvolved images	202
Figure 4.30	Excitation and emission spectra of TMRStar	203
Figure 4.31	Construction of a chromosomal <i>plsY-SNAP</i> fusion in <i>S. aureus</i> SH1000	207
Figure 4.32	Localisation of PlsY-SNAP in <i>S. aureus</i> SH1000	209
Figure 4.33	Construction of a chromosomal <i>cydB-SNAP</i> fusion in <i>S. aureus</i> SH1000	210
Figure 4.34	Localisation of CydB-SNAP in <i>S. aureus</i> SH1000	212
Figure 4.35	Construction of a chromosomal <i>pgsA-SNAP</i> fusion in <i>S. aureus</i> SH1000	213
Figure 4.36	Localisation of PgsA-SNAP in <i>S. aureus</i> SH1000	215
Figure 4.37	Construction of SH1000 <i>secY-gfp plsY-SNAP</i>	216
Figure 4.38	Colocalisation of SecY-GFP and PlsY-SNAP in <i>S. aureus</i> SH1000	217

Figure 4.39	Inhibitory effect of zaragozic acid on squalene and staphyloxanthin production	220
Figure 4.40	Effect of zaragozic acid on localisation of PlsY-GFP and FloT-eYFP	221
Figure 4.41	Construction of SH1000 $\Delta cls1\Delta cls2$ <i>plsY-gfp</i>	222
Figure 4.42	PlsY-GFP localisation in a $\Delta cls1\Delta cls2$ mutant	223
Figure 4.43	Construction of SH1000 $\Delta mprF::ermB$ <i>plsY-gfp</i>	225
Figure 4.44	PlsY-GFP localisation in a $\Delta mprF$ mutant	226
Figure 4.45	Construction of SH1000 $\Delta tagO::ermB$ <i>plsY-gfp</i>	228
Figure 4.46	PlsY-GFP localisation in a $\Delta tagO$ mutant	230
Figure 4.47	PlsY-GFP localisation in a $\Delta tagO$ mutant and morphology of $\Delta tagO$	232
Figure 4.48	Cerulenin inhibits fatty acid synthesis	233
Figure 4.49	Effect of fatty acid inhibition on PlsY-GFP localisation	234
Figure 4.50	Effect of membrane potential inhibition on PlsY-GFP localisation	239
Figure 4.51	PlsY-GFP localisation in PC190723 treated cells	240
Figure 4.52	Correlation between cell size, PC19072 treatment and coefficient of variation	241
Figure 4.53	Localisation of PlsY-GFP in protoplasts	244
Figure 4.54	Effect of SDS on PlsY-GFP localisation	245
Figure 4.55	Summary of the effect of cardiolipin and lysinylated phosphatidyl-glycerolphosphate on the localisation of PlsY	249
Figure 5.1	Schematic overview of FRET	256
Figure 5.2	Examples for donor photobleaching decay rates	259
Figure 5.3	Excitation and emission spectra of selected fluorophores	261
Figure 5.4	Schematic presentation of the genetic construct used for FRET experiments	261
Figure 5.5	Construction of pWhiteWalker 1-4	268
Figure 5.6	Construction of pWhiteWalker 7, 8, 10-17	270
Figure 5.7	Construction of pWhiteWalker 18	271
Figure 5.8	Localisation of PlsY-GFP and various membrane proteins fused to mCherry in <i>S. aureus</i> RN4220	273
Figure 5.9	Protein-protein-interactions between PlsY-GFP and various membrane proteins fused to mCherry	279
Figure 5.10	Protein-protein-interactions between PlsY-GFP and various membrane proteins fused to mCherry in presence and absence of daptomycin	282
Figure 5.11	Subcellular single-cell FRET analysis of protein-interactions of PlsY-GFP and MreD, CydB and SecY fused to mCherry	283
Figure 6.1	Schematic overview of <i>in vivo</i> and <i>in vitro</i> protein study systems	291
Figure 6.2	Schematic overview of <i>mreD-eyfp</i> fusion expression constructs	291
Figure 6.3	Construction of IPTG-inducible <i>mreD-eyfp</i> fusion constructs in <i>E. coli</i>	293
Figure 6.4	Localisation of MreD-eYFP fusions and MurJ-GFP in <i>E. coli</i>	296
Figure 6.5	Localisation of MreD-eYFP fusions in <i>E. coli</i> at low expression levels	297
Figure 6.6	3D-STORM imaging of MreD-6-eYFP in <i>E. coli</i>	298
Figure 6.7	Localisation of MreD-eYFP in <i>E. coli</i> spheroplasts	300
Figure 6.8	Schematic overview of the preparation of membrane vesicles	300
Figure 6.9	Cytoplasmic membrane vesicles of <i>S. aureus</i>	303

Figure 6.10	Liposome generation using the emulsion method	304
Figure 6.11	Purification of MreD-6-eYFP and MurJ-GFP	308
Figure 6.12	MreD-FITC reconstitution into liposomes	309
Figure 7.1	A mathematical explanation for the punctate patterned distribution of membrane proteins in <i>S. aureus</i>	315
Figure 9.1	Construction of a chromosomal <i>plsY-mCherry</i> fusion in <i>S. aureus</i> SH1000	357
Figure 9.2	Construction of a chromosomal <i>cdsA-mCherry</i> fusion in <i>S. aureus</i> SH1000	359
Figure 9.3	Construction of a chromosomal <i>cdsA-mRFPmarsI</i> fusion in <i>S. aureus</i> SH1000	361
Figure 9.4	Construction of a chromosomal <i>pgsA-mRFPmarsI</i> fusion in <i>S. aureus</i> SH1000	363
Figure 9.5	Construction of a chromosomal <i>plsY-gfp</i> (tetracycline resistance) fusion in <i>S. aureus</i> SH1000	366
Figure 9.6	Nucleotide alignment of <i>S. aureus</i> SH1000 <i>mreD</i> with the optimised <i>mreD</i> sequence	368
Figure 9.7	Nucleotide alignment of <i>eyfp</i> with the optimised sequence	369

List of Tables

	Page Number
Table 2.1	Chemically defined medium composition 49
Table 2.2	Antibiotics 50
Table 2.3	<i>S. aureus</i> strains used in this study 50
Table 2.4	<i>E. coli</i> strains used in this study 54
Table 2.5	Plasmids used in this study 54
Table 2.6	Stock solutions used in this study 63
Table 2.7	Centrifuges used in this study 64
Table 2.8	Primers used in this study 68
Table 2.9	1kb DNA ladder (Thermo Scientific) DNA fragment sizes 80
Table 2.10	Phage transduction 83
Table 2.11	DeltaVision filter sets 88
Table 3.1	Analysed metabolite masses and potential candidates 116
Table 3.2	Single nucleotide polymorphisms of SH1000 $\Delta mreD$ suppressor strains 122
Table 4.1	Bioinformatic analysis of phospholipid synthesis enzymes. 154
Table 4.2	Fluorescence properties of selected fluorescent proteins 195
Table 4.3	Selected proteins used for colocalisation studies with PlsY-GFP 197
Table 5.1	Protein-protein interaction methods 255
Table 5.2	Bioinformatic analysis of selected integral membrane proteins chosen for protein interaction studies with PlsY 263
Table 5.3	Nomenclature of FRET plasmids and their features 265
Table 5.4	Donor photobleaching times 278

Chapter 1: Introduction

1.1 The organisation of life

Life is categorised into three domains: Eubacteria, Archaeobacteria and Eukaryotes. Eukaryotes are composed of highly specialised organelles that fulfil specific tasks within the cell. Importantly, the genetic information of eukaryotes is compacted in the nucleus. Eubacteria and archaeobacteria are much smaller than eukaryotes and possess an apparently more simple structure in which cell functions do not seem to be spatially separated and the nucleoid is located within the cell together with all the cell components. Thus, do bacteria and archaea not require a higher organisation and rely solely on diffusion to maintain cell function and proliferation?

Indeed, diffusion does play a significant role in bacterial cells, however, in a more complex and efficient way than initially anticipated. In 1952, Alan Turing delineated the chemical basis for what we as modern researchers are now able to observe (Turing, 1990). He wanted to understand how two chemicals diffuse in a spatially homogeneous system with differing diffusion coefficients. This work illustrated that diffusion disturbances, such as a chemical diffusing quicker than another, can create local compartments. Although, his work was based on a very simple system of only two components, it illustrated convincingly that chemical and structural compartmentalisation can be achieved based on diffusion mechanics and does not necessarily require organelles. The basis for diffusion disturbances can be due to a variety of factors including reaction-diffusion mechanisms in which one molecule slows down the diffusion of another along through simple geometry. Its outcome is the basis for experimental observations in bacteria in an attempt to understand how an apparently simple organism is capable of completing complex tasks.

The following introduction describes how bacterial cells are structured and how essential biopolymers required for homeostasis and cell-proliferation are generated from a bottom-up view point.

1.2 The bacterial blueprint

1.2.1 The different shapes of bacteria

Bacteria are found in every habitat of the world and are highly adapted to different life styles which led to the development of a wide range of morphologies that determines their inner structure and features. Different cell shapes were initially used for the classification of bacteria into rod, cocci, spiral, comma and corkscrew-shaped bacteria (Fig. 1.1). These shapes are also found in various variations of single-cell, clusters and chains.

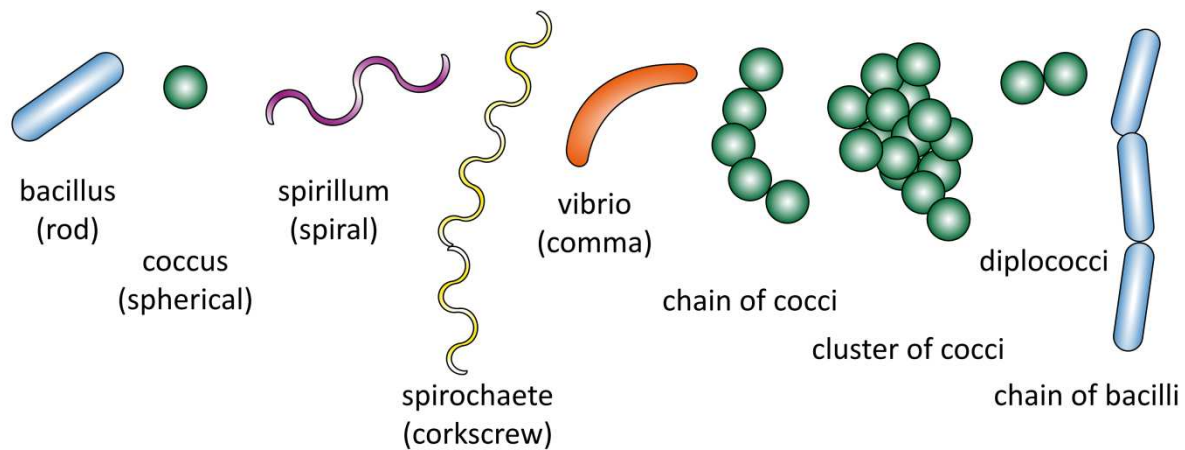


Figure 1.1 The different shapes of bacteria

Image is adapted from: <http://www.microbiologyonline.org.uk/about-microbiology/introducing-microbes/bacteria>.

To outline how a bacterial cell is composed and structured, their shape constitutes a starting point. However, most bacterial aspects are derived from an interplay between different factors and the following blueprint is therefore simplified.

1.2.2 Shape determinants or the bacterial cytoskeleton

As mentioned before, the shape or geometry of bacterial cells facilitates a basic starting point for the localisation of further proteins and subcellular structures. The shapes of eukaryotes are determined by cytoskeletal components that were initially thought to be unique for eukaryotic cells. Tubulin is a dimer that polymerises by GTP hydrolysis into

microtubules and is essential in many pivotal cellular processes such as mitosis and intracellular transport.

Another major cytoskeletal component is the ATPase actin. Actin is a multifunctional protein that assembles into filaments and gives structure to eukaryotic cells by facilitating cell motility, division and bridging to other cells. Its polymerisation is driven by ATP hydrolysis and often involves the interaction with membranes. The third principal cytoskeletal elements, intermediate filaments (IF), are composed of a family of proteins exhibiting a structural rather than a dynamic role within the cell and provide mechanical strength and integrity. Recently, structural homologues of all three eukaryotic elements have been found in bacteria.

1.2.3.1 Bacterial actin homologues

The screen for cytoskeletal components in bacteria based on amino acid sequence homologies to actin, tubulin or IF was unsuccessful and thus it was thought that bacteria lack these components. Advances in structural biology however, changed the focus to examining structural homologues rather than screening for primary structures. In 1992, a comparison of three-dimensional structures of ATPases with actin revealed a set of common conserved residues (Bork *et al.*, 1992). Searching for this pattern in prokaryotic species led to the discovery of bacterial actin-homologues such as MreB and ParM.

1.2.3.1.1 MreB

MreB is widely conserved across non-spherical bacteria. Some species, particularly gram-positive bacteria even possess more than one MreB homolog. The lack of MreB in spherical shaped bacteria gave a hint to the rod-shape determining function of MreB (Daniel & Errington, 2003, Pinho *et al.*, 2013). Like actin, MreB is an ATPase capable of polymerisation (van den Ent *et al.*, 2001, Colavin *et al.*, 2014). MreB forms dynamic and flexible cables in a helical pattern throughout the entire bacterial cell and localises just under the cytoplasmic membrane (Jones *et al.*, 2001). This observation was supported by Cryo-EM and crystal structures showing that MreB forms antiparallel filaments (van den Ent *et al.*, 2014). MreB in cooperation with RodA work together to help synthesise the glycan strands of peptidoglycan (PGN) (Uehara & Park, 2008). In cells depleted of UndP, a lipid-linked cell wall precursor, MreB disassembles into the cytoplasm giving evidence that the membrane association of MreB is dependent on these precursors (Schirner *et al.*, 2015). In *Escherichia coli* and *Caulobacter crescentus*

MreB changes its helical pattern according to the cell cycle, while in *Bacillus subtilis*, MreB stays in its helical pattern even during cell division (Figge *et al.*, 2004, Vats & Rothfield, 2007, Defeu Soufo & Graumann, 2006). Labelling of new peptidoglycan strands using fluorescent vancomycin revealed similar patterns to those observed for MreB, underscoring its involvement in peptidoglycan synthesis (Daniel & Errington, 2003). Pulse-chase labelling of newly synthesised peptidoglycan indicated its heterogeneous insertion that is spatially and temporally correlated with MreB. Furthermore, MreB localises to negatively curved membranes where it also directs peptidoglycan synthesis which results in cell straightening that contributes to the cylindrical shape of *E. coli* (Ursell *et al.*, 2014). However, it has to be highlighted that the helical pattern of MreB is controversially discussed since it turned out that the MreB-YFP fusion used for localisation studies in *E. coli* creates artefacts caused by the yellow fluorescent protein tag (Swulius & Jensen, 2012). Moreover, the question whether MreB directs the peptidoglycan synthesis machinery or is directed by it represents a typical chicken and egg problem. Several authors suggest that MreB forms discontinuous fibres and rotates around the long-axis of the cell in discrete patches driven by the cell wall synthesis enzymes (Reimold *et al.*, 2013, Dominguez-Escobar *et al.*, 2011, van Teeffelen & Gitai, 2011, Garner *et al.*, 2011). Another study raises doubt that rod-shaped cells require a continuous filament of MreB to maintain their shape since coarse-grained simulations revealed that local coordination of cell wall synthesis enzymes alone can be sufficient for their cell integrity during growth (Nguyen *et al.*, 2015). Besides its direct connection to cell wall synthesis, MreB has a global effect on the bacterial membrane. MreB filaments create membrane regions with increased fluidity which might have an affect on membrane protein diffusion (Strahl *et al.*, 2014). The turnover dynamics of MreB are still unclear, but it has been shown that a sub-population of elongation factor Tu interacts with MreB and promotes formation of MreB filaments (Liu *et al.*, 2014, Defeu Soufo *et al.*, 2015). Furthermore, roles for MreB in motility of *Myxococcus xanthus* and competence of *B. subtilis* were described (Treuner-Lange *et al.*, 2015, Mirouze *et al.*, 2015).

1.2.3.1.2 ParM

Equal distribution of plasmids during cell-division is required to ensure their stable inheritance, particularly for low-copy plasmids. ParCMR is the best understood plasmid partitioning system. ParM is an actin-like ATPase that spontaneously forms double-helical polar filaments that either hydrolyse or get stabilised by the DNA binding

protein ParR. ParR binds to plasmid-localised direct repeats sequences named *parC* and forms a nucleoprotein that is attached to the ParM filament. The stabilised ParM bound to ParR then drives the segregation by polymerisation and thereby pushes the plasmid to the cell poles (Gerdes *et al.*, 2010, Bharat *et al.*, 2015, Gayathri *et al.*, 2012, Ebersbach & Gerdes, 2005, Gunning *et al.*, 2015, Schumacher, 2012). Homologues of this system have been found in *B. thuringiensis* (Jiang *et al.*, 2016), *E. coli* (Jiang *et al.*, 2016, Gerdes *et al.*, 2010, Polka *et al.*, 2014, Popp *et al.*, 2010), *B. subtilis* (Polka *et al.*, 2014) and *Staphylococcus aureus* (Popp *et al.*, 2010). In *S. aureus* for instance, ParM secures the maintenance of the clinically relevant pSK41 plasmid that confers resistance to multiple antibiotics (Popp *et al.*, 2010).

1.2.3.1.3 Crenactin

Studies of the generally neglected third domain of life, archaea, added a novel entry to the world of prokaryotic cytoskeletal elements. The actin homologue crenactin was found in the rod-shaped hyperthermophilic archaea *Pyrobaculum calidifontis*. Crenactin forms a helical structure *in vivo* as demonstrated by *in situ* immunostaining and localises between segregated nucleoids suggesting a possible involvement in cytokinesis (Ettema *et al.*, 2011). Although it only shares a low sequence similarity with actin, its three-dimensional structure is highly similar to those observed for actin and MreB (Lindas *et al.*, 2014).

In contrast to MreB and actin that both form helical double stranded filaments, structural studies demonstrated that crenactin forms a single stranded helical filament similar in structure to a single strand of actin (Izore *et al.*, 2014, Braun *et al.*, 2015). Therefore, it has been proposed that crenactin might be an ancestor of the later evolved actin from eukaryotes (Ettema *et al.*, 2011).

1.2.3.2 Bacterial tubulin homologues

Microtubules in eukaryotes facilitate chromosome segregation and intracellular-transport forming tubules by a dynamic assembly-disassembly interplay. GTP hydrolysis of tubulins stabilises the microtubule structure and enable their polymerisation.

1.2.3.2.1 FtsZ

The essential cell-division protein FtsZ was the first protein of the prokaryotic cytoskeleton to be identified. Although it does not share a high level of sequence

similarity with the eukaryotic tubulin, FtsZ turned out to be a tubulin-homologue based on its tertiary structure (Lowe & Amos, 1998) (Nogales *et al.*, 1998, Erickson, 1995). In confirmation of this theory, FtsZ also possesses a self-activating GTPase activity and is capable of polymerisation. Binding of GTP activates the polymerisation of FtsZ that eventually induces its GTPase activity (Lutkenhaus *et al.*, 1980, de Boer *et al.*, 1992, Mukherjee & Lutkenhaus, 1994, Mukherjee *et al.*, 2001, Scheffers & Driessen, 2001, Oliva *et al.*, 2004, Ruiz-Avila *et al.*, 2013, Singh *et al.*, 2007). Thus, GTP hydrolysis is not required for the polymerisation of FtsZ which is supported by a study showing FtsZ polymerisation in the presence of GDP. This mechanism could ensure the disassembly and recycling of FtsZ monomers after cell-division (Erickson *et al.*, 1996, Huecas & Andreu, 2004). FtsZ is considered to be the first protein to move to the division site where it forms a structure called the Z-ring, a molecular scaffold for the recruitment of other cell-division associated proteins that coordinate cell-division in concert with FtsZ (Bi & Lutkenhaus, 1991, Adams & Errington, 2009). Therefore, it is not surprising that *E. coli* and *B. subtilis* cells lacking FtsZ fail to form complete septa, which eventually leads to cell lysis (Lutkenhaus *et al.*, 1980, Dai & Lutkenhaus, 1991, Beall & Lutkenhaus, 1991). The use of immunogold electron microscopy and GFP fusions also revealed that FtsZ localises and assembles in a ring structure at the midcell in a number of bacteria (Bi & Lutkenhaus, 1991). The *in vivo* characterisation of the Z-ring in *E. coli* by photo-activated localisation microscopy demonstrated that the Z-ring is rather composed of a loose bundle of FtsZ protofilaments than forming one single continuous ring. These filaments are randomly overlapping with each other in both longitudinal and radial directions of the cell (Fu *et al.*, 2010)(Holden *et al.*, 2014). Surprisingly, only approximately 30 % of FtsZ in *B. subtilis* and *E. coli* was localised at the septum whereas the rest was distributed in the cytoplasm (Anderson *et al.*, 2004). Recently, the architecture of the Z-ring in *B. subtilis* and *S. aureus* was examined by using 3D-structured illumination microscopy (3D-SIM). It demonstrated that the Z ring is composed of a heterogeneous discontinuous distribution of FtsZ. The authors of that study proposed that FtsZ localises dynamically in a bead-like pattern (Strauss *et al.*, 2012). Amongst bacteria, only members of the obligate intracellular living Chlamydiaceae family and *Ureaplasma urealyticum* lack FtsZ homologues (Vaughan *et al.*, 2004). FtsZ has also been found in eukaryotic organelles having prokaryotic origins such as mitochondria and chloroplasts which possess two homologues of *ftsZ* (Stokes & Osteryoung, 2003, Miyagishima *et al.*, 2004).

1.2.3.2.2 TubZ

Similarly to the actin homologue ParM, TubZ facilitates the partitioning of low-copy plasmids into the two daughter cells during cell-division (Tinsley & Khan, 2006). TubZ is a tubulin homologue that forms filaments upon GTP-hydrolysis and exhibits a treadmilling activity *in vitro* (Larsen *et al.*, 2007, Hoshino & Hayashi, 2012). Its role in plasmid segregation is linked to the DNA adaptor protein TubR that binds *tubC* sequences located on the plasmids. TubZ then binds to TubR and starts to depolymerise on the non-TubR bound end of the filament. In contrast to the ParCMR system which is based on pushing, the dynamic instability of TubZ causes the segregation of plasmids by pulling them to the cell poles. Thus, it has been suggested that a capping mechanism prevents the depolymerisation at the filament pole bound to TubR-plasmid complex (Chen & Erickson, 2008). Furthermore it has been demonstrated that TubZ forms switch between a two-stranded and four-stranded state depending on its ability to bind GTP (Montabana & Agard, 2014).

1.2.3.2.3 CetZ

CetZ is a tubulin homologue found in many archaea that coexists with FtsZ. Deletion studies in *Haloferax volcanii*, which harbours two homologues of CetZ, indicated their role as rod -shape determinants that are required for the transition from a sessile to a motile lifestyle. X-ray crystal structures showed the structural similarity to Tubulin and FtsZ along with the formation of protofilaments. In contrast to FtsZ, CetZ does not seem to be involved in cell-division and cells of *Haloferax volcanii* lacking one of the *cetZ* genes do not exhibit cell-division defects (Duggin *et al.*, 2015).

1.2.3.3 Bacterial intermediate filament homologues

Eukaryotic intermediate filaments (IF) are flexible cables that are extremely resistant to strain forces. These filaments function in the maintenance of cell-shape by bearing tension and organising the internal three-dimensional structure of the cell by anchoring organelles.

1.2.3.3.1 Crescentin

Just as MreB and FtsZ, the intermediate filament homologue crescentin is a major cytoskeletal component and shape determinant that was discovered in *C. crescentus* (Ausmees *et al.*, 2003). Analyses of rod-shaped mutants led to the identification of

crescentin. It is located at the concave face of the cell and is necessary for cell shape (Lew *et al.*, 2011). It shares the common features of intermediate filaments by assembly into filaments that continuously integrate subunits on both ends without energy or cofactor requirements (Ausmees *et al.*, 2003, Charbon *et al.*, 2009). Biochemical and ultrastructural studies revealed that IF can be functionally divided into two subdomains where the first is required for recruiting proteins while the second domain facilitates structural assembly. A linker sequence between both domains prevents the disintegration into non-functional aggregates (Cabeen *et al.*, 2011). Crescentin seems to be a unique cytoskeletal element only found in *C. crescentus*. However, the screen for ‘central segmented coiled-coil rod’ domains that are regarded to be crucial for the structural features of crescentin revealed 21 bacterial genomes harbouring potential IF homologues. Three of these including the ones from *Mycobacterium* and other actinomycetes were tested *in vitro* where all of them spontaneously formed filaments (Bagchi *et al.*, 2008). This suggests that just like tubulin and actin homologues, IF homologues might be a common cytoskeletal component of bacterial cells.

1.2.4 The membrane

All bacteria possess a cytoplasmic membrane that is composed of a phospholipid bilayer. Membranes act as a first barrier to maintain cellular processes in a defined and controllable space. Additionally, membranes serve as chassis for the incorporation of a number of proteins involved in the transport of molecules into the cell, energy conservation and cell signalling.

1.2.4.1 Phospholipid synthesis

Phospholipids are the main component of cell membranes. They are composed of a variable fatty acid chain and a hydrophilic phospholipid headgroup. In general, the biosynthesis of phospholipids can be sub-grouped in four synthetic steps. The initiation module produces building blocks for fatty acid synthesis and feeds the elongation module where fatty acids are gradually extended. Both modules are features of the multiprotein complex fatty acid synthase II (FASII). This process takes place in the cytoplasm. Fatty acids are then incorporated into glycerol-3-phosphate by a membrane associated acyltransferase module synthesising the precursor used for a series of mainly integral membrane bound phospholipid synthesis enzymes that modify the head group

of phospholipids. This procedure is described in detail by Parsons and Rock that also elucidates remaining knowledge gaps (Parsons & Rock, 2013). A summary of fatty acid and phospholipid synthesis is shown in Fig. 1.5.

1.2.4.1.1 FASII initiation module

The first step in phospholipid synthesis is performed by the acetyl-CoA carboxylase by carboxylation of acetyl-CoA which is catalysed by a four protein subunit complex (AccABCD) and its product is subsequently transferred to the acyl carrier protein (ACP) through FabD (see Fig. 1.2) (Cronan & Waldrop, 2002, Choi-Rhee & Cronan, 2003, Li & Cronan, 1992, Zhang & Rock, 2008). Some bacteria such as *B. subtilis* and *S. aureus* preferentially employ acyl-CoA instead of acetyl-CoA (Choi *et al.*, 2000, Qiu *et al.*, 2005, He & Reynolds, 2002, Jackowski *et al.*, 1989). In the last step of the fatty acid initiation module, FabH condenses acyl-CoA with malonyl-ACP to β -Ketoacyl-ACP which, together with malonyl-ACP feed directly into the elongation module (Tsay *et al.*, 1992, Heath & Rock, 1996a, Alhamadsheh *et al.*, 2007).

1.2.4.1.2 FASII elongation module

The second step in fatty acid synthesis elongates the precursors, malonyl-ACP and β -ketoacyl-ACP, derived from the initiation module through four enzymes that differ between bacterial species which act in concert in a cycled process (Fig. 1.2) (Heath & Rock, 1996b). The second keto group of β -Ketoacyl-ACP gets removed and two carbons get added to the acyl chain per cycle. This process is repeated until a long fatty acid chain is generated (Heath & Rock, 1996b, Fisher *et al.*, 2000, Massengo-Tiasse & Cronan, 2008). First, FabF/B decarboxylates malonyl-ACP to β -ketoacyl-ACP that is then reduced by FabG to β -hydroxyacyl-ACP (Prescott & Vagelos, 1970, Parsons & Rock, 2013). The next step is catalysed by FabZ/A hydrolysing β -hydroxyacyl-ACP to form trans-2-enoyl-ACP which leads to the final reaction catalysed by FabI (Heath & Rock, 1995). The resulting acyl-ACP product is either used to begin another round of elongation or it is incorporated into phospholipids by the acyltransferase module (Heath *et al.*, 2000).

1.2.4.1.3 Acyltransferase module

The assembly of fatty acids and glycerophol-3-phosphate (G3P) is mainly facilitated by the PlsB system in γ -proteobacteria bacteria (Bell, 1975) whereas the slightly different PlsX/PlsY system is dominating in gram-positive bacteria. G3P is gained by the

glycolysis through the glycerol-3-phosphate dehydrogenase GspA and two of its acyl chains are connected with the Acyl-ACP derived from the elongation module forming lysophosphatidic acid (LPA) (Fig. 1.3) (Ray & White, 1972, Ray *et al.*, 1972). This reaction is catalysed by PlsB and PlsC. Both enzymes can either use Acyl-ACP or Acyl-CoA for the incorporation of the acyl chain. In gram-positive bacteria, the acyl chain is first phosphorylated by PlsX and subsequently connected to G3P by PlsY to LPA (Paoletti *et al.*, 2007) (Lu *et al.*, 2006). The addition of the second acyl chain is facilitated by PlsC in both the PlsB as well as the PlsX/PlsY systems resulting in the universal bacterial phospholipid precursor phosphatidic acid (PA).

Due to their central role in connecting fatty acid synthesis with phospholipid headgroup generation, enzymes from the acyltransferase module are regarded as key regulators in phospholipid synthesis.

1.2.4.1.4 Phospholipid head group synthesis

The diversity and composition in phospholipids in bacteria determines the topology, properties and localisation of membrane proteins and affects membrane curvature (Zhang *et al.*, 2005b, Xie *et al.*, 2006).

The first step in phospholipid headgroup synthesis is shared among all bacteria. PA gets cytidinylated by CdsA into CDP-diacylglycerol (CDP-DAG) which acts as a precursor for the formation of various phospholipids (Fig. 1.4) (Kanfer & Kennedy, 1964) (Sparrow & Raetz, 1985). PssA and PgsA then convert CDP-DAG to phosphatidylserine (PS) and phosphatidylglycerolphosphate (PG) respectively. Phosphatidylserine is further processed to phosphatidylethanolamine by the Psd enzyme, whereas phosphatidylglycerolphosphate is dephosphorylated to phosphatidylglycerol by PgpA in most bacteria. Some species such as *E. coli* also possess multiple homologues of *pgp* genes (Ames, 1968) (Miyazaki *et al.*, 1985, Li & Dowhan, 1990). Phosphatidylglycerol displays the precursor for cardiolipin (CL) and lysylphosphatidylglycerol (LPG). The former can be catalysed by several enzymes termed ClsA/B/C and the latter is only formed in firmicutes by the enzyme MprF (Miyazaki *et al.*, 1985) (Ernst & Peschel, 2011). MprF also possesses a flippase activity and translocates LPG to the outer leaflet of the phospholipid bilayer which confers resistance to cationic antimicrobial peptides such as daptomycin (Ernst *et al.*, 2009). Currently, it is not known how other phospholipids are flipped and are therefore thought to be independent of a specific membrane protein.

1.2.4.2 Teichoic acids

Teichoic acids are crucial and major constituent cell wall polymers that include two forms. Both phospholipid-anchored lipoteichoic acids (LTA) and the peptidoglycan-bound wall teichoic acids (WTA) are only found in gram-positive bacteria. Firstly, the synthesis of the lipoteichoic acids is discussed. WTA synthesis can be found in Section 1.2.5 since it is anchored at the cell wall which will be described later.

1.2.4.2.1 Lipoteichoic acid synthesis

The synthesis of the LTA lipid anchor diglucosyldiacylglycerol (Glc₂DAG) is catalysed by the cytoplasmic glycosyltransferase YpfP which uses a nucleotide-activated sugar as substrate (see Fig. 1.6) (Fischer, 1990)(Reichmann & Grundling, 2011, Jorasch *et al.*, 2000, Jorasch *et al.*, 1998, Kiriukhin *et al.*, 2001). The putative flippase LtaA translocates Glc₂DAG to the outer leaflet of the membrane where LtaS repeatedly extends Glc₂DAG by glycerolphosphate (GroP) taken from the headgroup of phosphatidylglycerol. Importantly, the sugar chain is highly diverse and species-dependent. *S. aureus* has a GroP-chain based lipoteichoic, whereas for example, *Micrococcus luteus* employs a mannose-phosphate chain attached to Glc₁DAG (Weidenmaier & Peschel, 2008, Powell *et al.*, 1975).

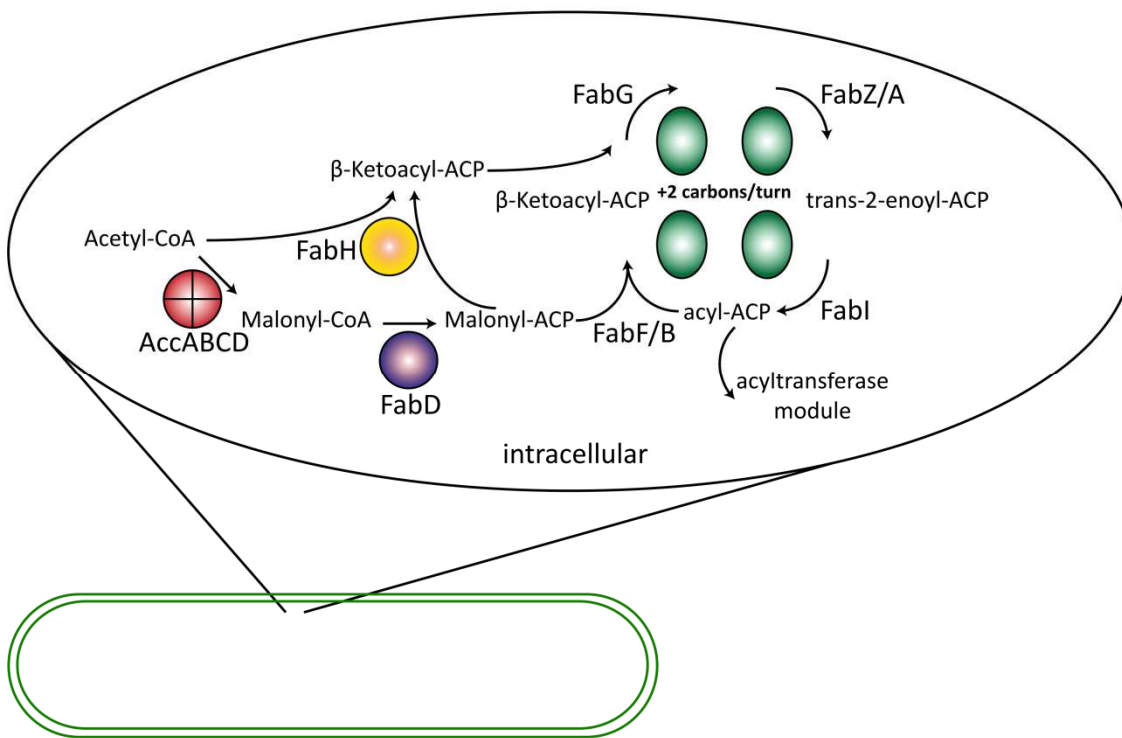


Figure 1.2 Initiation and elongation module of fatty acid synthesis

Schematic overview of fatty acid production in bacteria. Acetyl-CoA is carboxylated and transferred to β -ketoacyl-ACP by FabH or converted to malonyl-ACP by AccABCD and FabD. Both products feed into the elongation module while malonyl-ACP is first converted to β -ketoacyl-ACP by FabF/B. The acyl chain of β -ketoacyl-ACP is extended in a cyclic process involving the enzymes FabG, FabZ/A, FabI and FabF/B and gains two carbon atoms per turn. The final product acyl-ACP feeds into the acyltransferase module. This process takes place in the cytoplasm. Figure is adapted from Parsons and Rock, 2013.

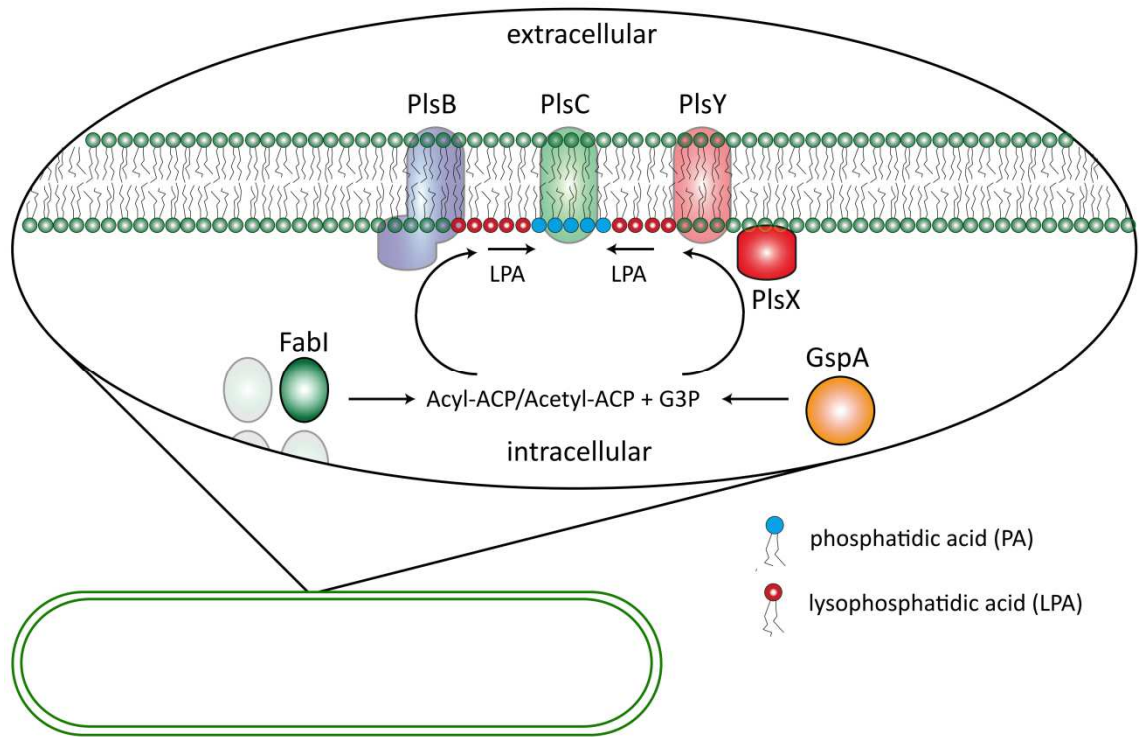


Figure 1.3 Acyltransferase module

Schematic overview of the transfer of acyl groups to glycerol-3-phosphate. Acyl-ACP/Acetyl-ACP fatty acid chains from the fatty acid elongation module are transferred to G3P derived from glycolysis through the glycerol-3-phosphate dehydrogenase GspA. This process is either facilitated by the PlsB/PlsC or PlsX/PlsY/PlsC system. PlsB or PlsY together with PlsX connect the acyl chain to G3P synthesising lysophosphatidic acid which is then used as substrate by PlsC to generate phosphatidic acid. PA is required as a precursor for various phospholipid head group modifications. Figure is adapted from Zhang and Rock, 2008.

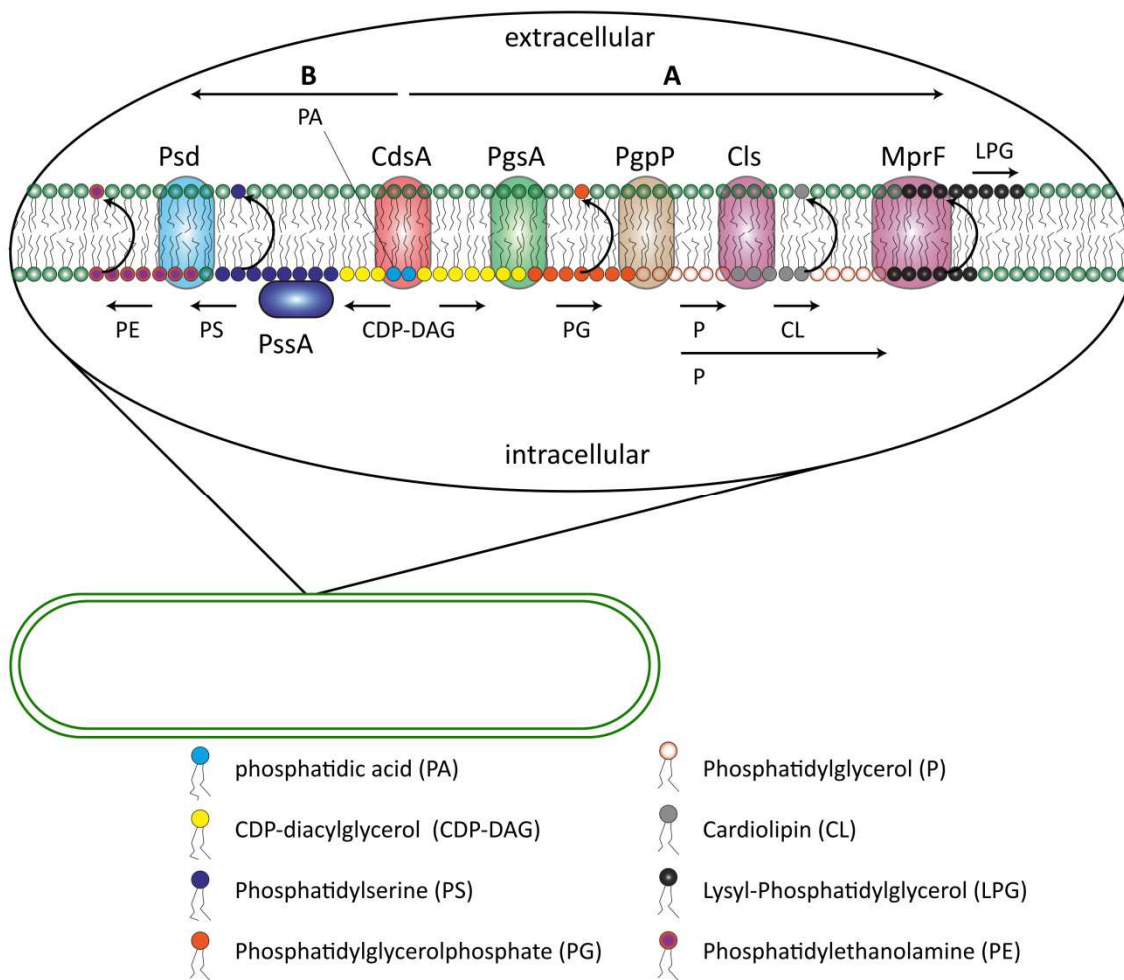


Figure 1.4 Phospholipid headgroup synthesis

Schematic overview of the modification of phospholipid headgroups. This process is highly branched and precursors are used for several modifications. **A (starting from CdsA facing to the left of CdsA)**, First phosphatidic acid (PA) is converted by CdsA to CDP-diacylglycerol (CDP-CAG) that is used as a substrate to synthesise phosphatidylserine (PS) by PssA and is further processed to phosphatidylethanolamine (PE) through Psd. **B (starting from CdsA facing to the right of CdsA)**, PA is also used for the synthesis of phosphatidylglycerolphosphate (PG) catalysed by PgsA PG is dephosphorylated by PgpA to form phosphatidylglycerol (P), a substrate to form both, cardiolipin (CL) by Cls and lysylphosphatidylglycerol (LPG) by MprF. MprF also acts as a flippase translocating LPG to the outer leaflet of the cell. It is currently not known how other phospholipids are flipped. Figure is adapted from Zhang and Rock, 2008.

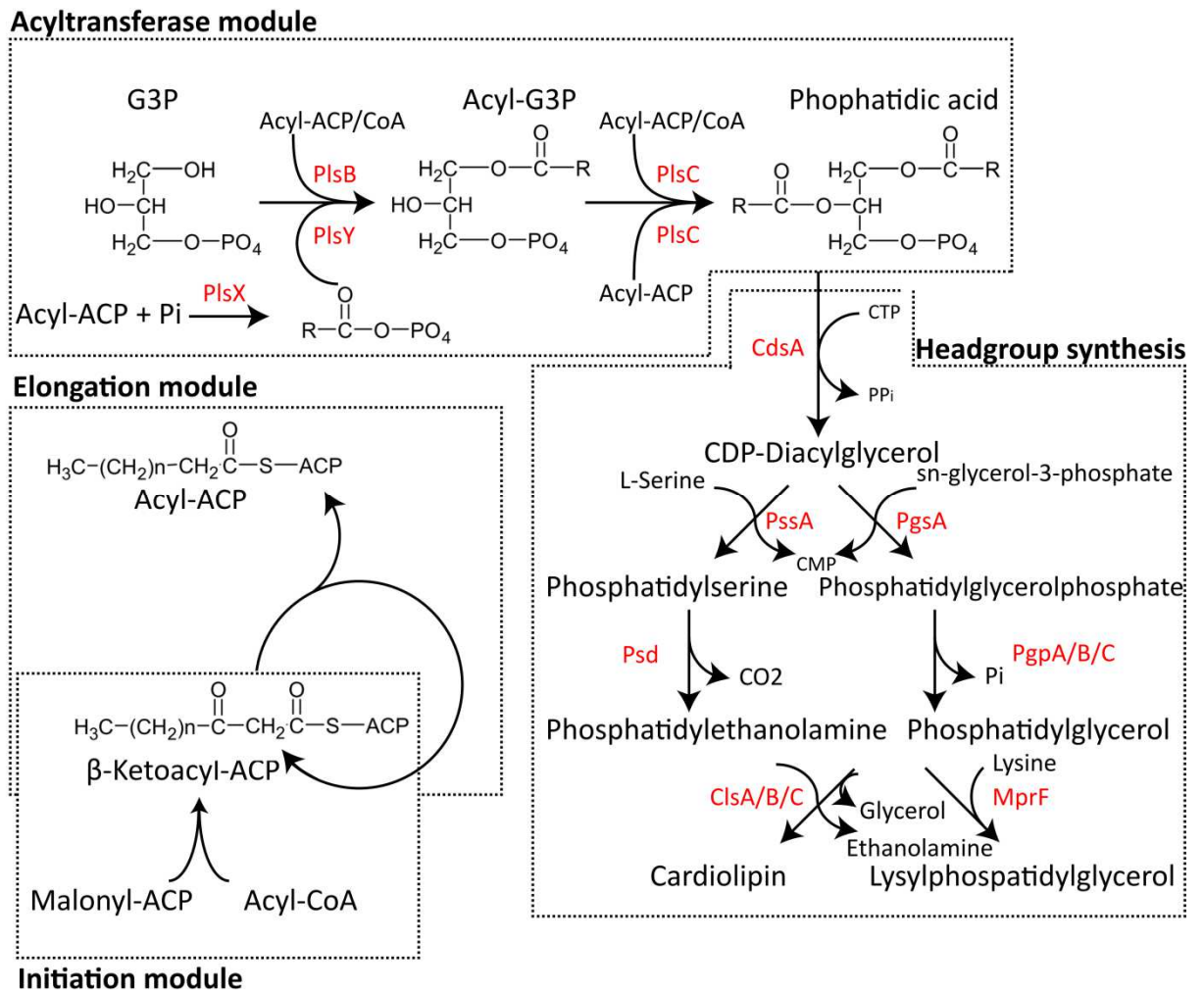


Figure 1.5 Phospholipid synthesis

Initiation module: FabH catalyses the priming reaction by condensing malonyl-ACP and Acyl-CoA to form β -Ketoacyl-ACP. **Elongation module:** The acyl-chain is extended in a cyclical process involving four enzymes acting in concert. Each turn adds two carbon atoms to the acyl chain of β -Ketoacyl-ACP. **Acyltransferase module:** Acyl-ACP is then incorporated in G3P in a species-dependent process, either by the PlsX/PlsY/PlsC system (mainly gram-positive bacteria) or the PlsB/PlsC system. **Phospholipid head group synthesis:** Phosphatidic acid gets cytidinylated to CDP-diacylglycerol by CdsA which is further processed to phosphatidylserine and eventually phosphatidylethanolamine by PssA and Psd. Alternatively, CDP-diacylglycerol is converted to phosphatidylglycerolphosphate by PgsA, followed by dephosphorylation to phosphatidylglycerol catalysed by the enzyme PgpA. Phosphatidylglycerol is then either converted to cardiolipin via ClsA/B/C or lysinylated by MprF to lysylphosphatidylglycerol. Figure is adapted from Parsons and Rock, 2013.

The by-product of this reaction, DAG, is recycled by translocation to the inner leaflet and is fed into the regular phospholipid synthesis pathway. First, the cytoplasmic enzyme DgkB phosphorylates DAG to phosphatidic acid which is converted to CDP-DAG by CdsA. PgsA catalyses the next step by adding glycerol-3-phosphate resulting in PG. PG is then dephosphorylated by a yet unknown enzyme to the precursor used by LtaS for the incorporation of GroP (Koch *et al.*, 1984, Taron *et al.*, 1983, Grundling & Schneewind, 2007b, Grundling & Schneewind, 2007a). In *S. aureus*, LTA synthesis enzymes were found to interact with many components of the cell-division machinery suggesting a coupled role of LTAs. Additionally, cells lacking LTAs exhibit severe cell-division defects. It was also demonstrated that LTA backbone synthesis takes place at the division site whereas glycolipid synthesis is found throughout the membrane (Grundling & Schneewind, 2007b, Fedtke *et al.*, 2007, Reichmann *et al.*, 2014).

1.2.4.2 Outer membrane

The outer membrane (OM) is an asymmetric bilayer only present in gram negative bacteria that is distinct in its composition from the cytoplasmic membrane as it mainly contains phospholipids on the inner leaflet and lipopolysaccharides (LPS) on the outer leaflet (Bos *et al.*, 2007). Its biogenesis requires crossing LPS and phospholipids through hydrophilic and hydrophobic parts of the cell wall making it a great energetic and organisational effort for the cell that has not yet been entirely explained. LPS is the major constituent of the outer membrane that greatly contributes to the negative charge and overall integrity of the membrane.

1.2.4.2.1 LPS synthesis and outer membrane biogenesis

LPS comprises three parts: The O-antigen, a core oligosaccharide and a lipid anchor called Lipid A. Although being part of the outer leaflet of the outer membrane, the core oligosaccharide bound to lipid A is synthesized gradually in the cytoplasm by a number of enzymes using UDP-N-acetylglucosamine (UDP-GlcNAc) as a substrate (Wang & Quinn, 2010). The final product is then flipped to the outer leaflet of the inner membrane by the ATPase driven flippase MsbA (Fig. 1.7) (Doerrler & Raetz, 2002). The O-antigen oligosaccharide is synthesised separately by glycosyltransferase enzymes using the membrane-bound undecaprenyl phosphate and UDP-GlcNAc (Raetz & Whitfield, 2002). After synthesis, it is translocated by the transporter Wzx to the periplasmic side of the inner membrane, polymerised by WzY and WzZ and connected to core-lipid A via the ligase WaaL.

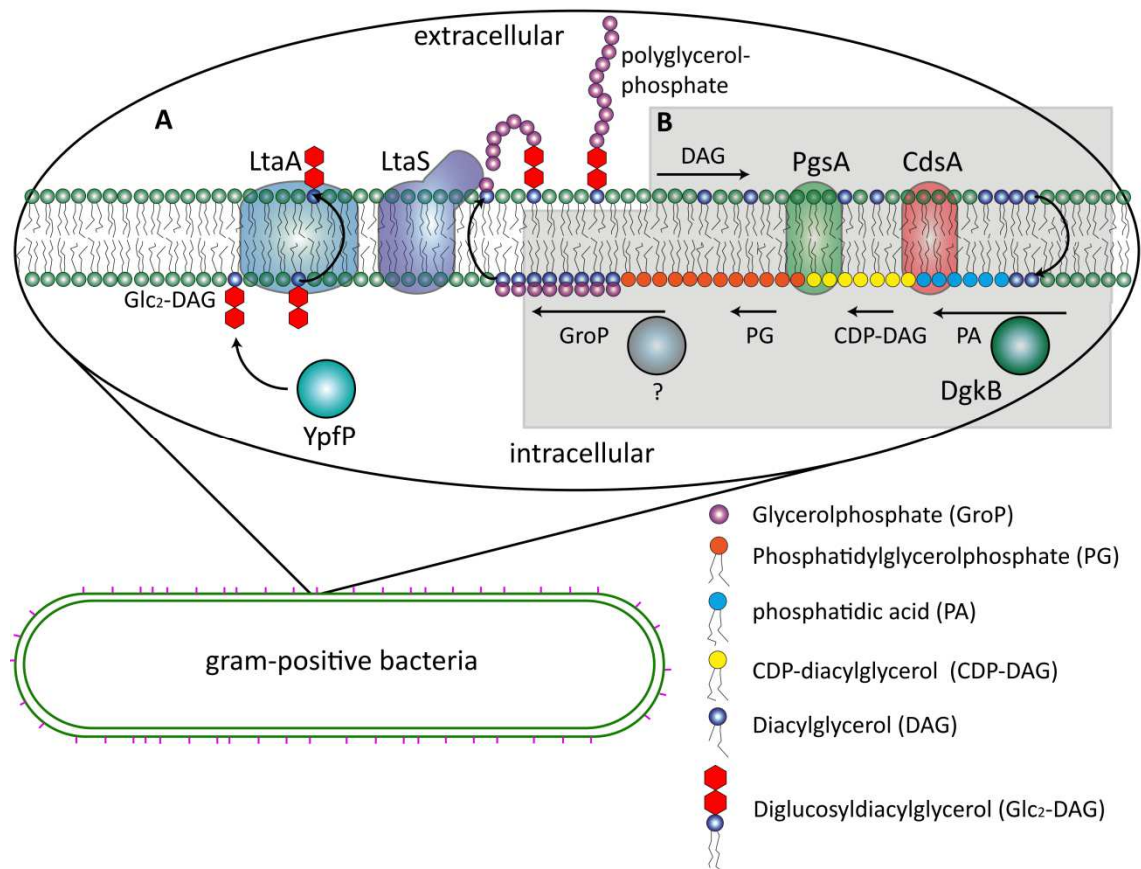


Figure 1.6 Lipoteichoic acid synthesis in gram positive bacteria

Schematic overview of lipoteichoic acid synthesis and insertion. This process is divided into two parts. **A (starting from YpfP)**, First, YpfP catalyses the synthesis of diglucosyldiacyl-glycerol (Glc₂-DAG) that is subsequently flipped to the outer leaflet by LtaA. LtaS gradually adds glycerolphosphate (GroP) from phosphatidylglycerolephosphate (PG) to the glucose end of Glc₂-DAG forming a long GroP chain. **B**, Dephosphorylated PG (DAG) is recycled through feeding to the phospholipid headgroup module. DAG gets converted to phosphatidic acid by DgkB followed by conversion to CDP-DAG by CdsA. Next, PgsA catalyses the synthesis of PG which is used as a substrate of a yet unknown enzyme that dephosphorylates PG. The final product is used by LtaS. Figure is adapted from Percy and Gründling, 2014.

to the final product LPS (Wu *et al.*, 2006, Abeyrathne *et al.*, 2005, Samuel & Reeves, 2003, Merino *et al.*, 2011). The exact mechanism of how LPS is inserted into the outer leaflet of the outer membrane is currently not fully understood. It is known that the periplasmic protein LptA binds LPS and its deletion causes the accumulation of LPS in the periplasm (Sperandeo *et al.*, 2008, Ma *et al.*, 2008, Tran *et al.*, 2008). Two competing models are currently discussed, one is based on LptA forming a bridge through the periplasm while the other relies on LptA as a chaperone guiding LPS through the periplasm (Okuda *et al.*, 2016). LptC, a membrane protein of the inner membrane and LptD, part of the outer membrane, both possess periplasmic domains that are thought to connect both membranes via LptA. The outer membrane also contains phospholipids mainly at the inner leaflet of the bilayer. It is not yet known how they are translocated to the outer membrane. However, the mechanism appears to be distinct from the LPS transport since spheroplasts treated with periplasmic extract resulted in the release of LPS but not phospholipids into the medium (Tefsen *et al.*, 2005).

1.2.5 Peptidoglycan

The cell membrane displays a first line of defence against external factors. However, due to the higher osmotic pressure of the cytoplasm, a phospholipid bilayer alone is not enough to withstand the turgor pressure. Thus, most bacteria possess and require a cell wall that also maintains cell shape and provides mechanical strength. The backbone of the cell is comprised of glycan chains cross-linked by short peptides covering the entire surface of the bacterial cell. Both gram-negative and gram-positive bacteria possess a cell-wall; however the one of gram-positive cells is thickened. The basic synthesis of peptidoglycan (PGN) is very similar between both groups and can be sub-divided into three stages: cytoplasmic generation of UDP-MurNAc and UDP-GlcNAc; anchorage to the membrane forming lipid II followed by translocation to the outer leaflet of the membrane; and finally the polymerisation via penicillin binding proteins (PBPs) (Fig. 1.8).

1.2.5.1 Synthesis of UDP-MurNAc and UDP-GlcNAc

The PGN precursors UDP-N-acetyl-muramic acid (UDP-MurNAc) and UDP-N-acetylglucosamine (UDP-GlcNAc) are synthesised in the cytoplasm. Mur ligases MurA-F sequentially add a short polypeptide chain consisting of five amino acids (usually: L-alanine, D-glutamate, m-diaminopimelate or L-lysine, and the dipeptide D-alanyl-D-alanine) to UDP-MurNAc in an ATP-dependent manner. The amino acid

composition can change depending on the bacterial species (Benson *et al.*, 1996, Brown *et al.*, 1995, Deva *et al.*, 2006, Perdih *et al.*, 2007, Boniface *et al.*, 2006, Longenecker *et al.*, 2005).

1.2.5.2 Synthesis of lipid II

The second stage of PGN synthesis takes place at the inner leaflet of the membrane where the integral membrane protein MraY anchors the UDP-MurNAc-pentapeptide to the membrane via undecaprenyl pyrophosphate (El Ghachi *et al.*, 2004, Bouhss *et al.*, 1999). The resulting product is termed lipid I. Subsequently, lipid II is formed by the addition of GlcNAc to lipid I using UDP-GlcNAc as a substrate via the membrane associated enzyme MurG (Mengin-Lecreulx *et al.*, 1991, Mohammadi *et al.*, 2007). In some bacteria such as *S. aureus*, a short peptide cross bridge is added to the third amino acid of the pentapeptide catalysed by FemXAB (Henze *et al.*, 1993, Labischinski *et al.*, 1998, Rohrer *et al.*, 1999, Seligman & Pincus, 1987, Johnson *et al.*, 1995, Benson *et al.*, 2002). In these species, the later introduced peptide cross-linking contains the cross bridge sequence instead of a direct link. The final lipid II is flipped to the outer leaflet of the bilayer by FtsW or MurJ. Many studies are currently focused on the properties of these apparent flippases (Meeske *et al.*, 2015, Sham *et al.*, 2014, Mohammadi *et al.*, 2011).

1.2.5.3 Transglycosylation and transpeptidation via PBPs

The third stage of PGN synthesis is performed by penicillin binding proteins (PBPs) in the periplasm connecting the sugar and peptide links of lipid II with each other. PBPs fulfil two major roles in PGN synthesis. The first is to connect the two sugars, MurNAc and GlcNAc via transglycosylation and the second relies on the formation of interpeptide bridges or direct connections via a transpeptidation activity. This activity requires a D-alanine dipeptide of which one is cleaved off and the other is covalently linked to the interpeptide bridge. All bacteria possess at least one transpeptidase PBP (Grandchamps *et al.*, 1995). Most bacteria however harbour a number of PBP genes and it is not fully understood whether each gene encodes a protein with a distinct function or whether there is a degree of redundancy. *B. subtilis* and *E. coli* have 16 and 12 PBPs, respectively, while *S. aureus* only possesses four PBPs and is regarded as a minimalistic system suited for the study of PBPs (Scheffers & Pinho, 2005). The *S. aureus* PBPs 1, 3 and 4 exhibit a transpeptidase (TP) activity forming the inter peptide bridge while PBP2 is a bifunctional enzyme that can perform both transglycosylation and transpeptidation (Pereira *et al.*, 2007, Pinho & Errington, 2003, Pinho & Errington, 2005).

1.2.5.2 Wall teichoic acid synthesis

Wall teichoic acids are covalently attached to peptidoglycan and major constituents of the cell wall comprising more than 60 % of the total mass (Bera *et al.*, 2007, Kojima *et al.*, 1985). Its synthesis is different from LTAs and highly species-dependent. WTAs are built from two main parts: a conserved disaccharide linker and a highly diverse chain of phosphodiester linked polyol units (Neuhaus & Baddiley, 2003). The disaccharide linker is composed of N-acetylmannosamine N-acetylglucosamine-1-phosphate linked to one or two glycerol-3-phosphate (GroP) residues and its synthesis is conserved across gram-positive bacteria. Names of enzymes involved in WTA acid are termed Tag or Tar and are used for the same protein. As a first step, TarO catalyses the transfer of N-acetyl-glucosamine from UDP-GlcNAc, a precursor shared with peptidoglycan synthesis, to the membrane anchor undecaprenylpyrophosphate (Fig. 1.9) (Rubinchik *et al.*, 2011, Soldo *et al.*, 2002). N-Acetylmannosamine from the sugar-activated UDP-ManNAc is subsequently added to GlcNAc via TarA, thereby forming the disaccharide linker part of WTAs (D'Elia *et al.*, 2009, Ginsberg *et al.*, 2006, Zhang *et al.*, 2006). The glycerolphosphotransferase TarB then adds one glycerol-phosphate unit to ManNAc (Bhavsar *et al.*, 2005, Ginsberg *et al.*, 2006). The next step in WTA synthesis extends the disaccharide linker by diverse and species-dependent polyols along with modifications mainly comprised of sugars. The mechanism to explain how the final but still membrane anchored wall teichoic acid is flipped to the outer leaflet is still unknown but it involves the membrane protein TarG and the ATPase TarH. Presumably, undecaprenylpyrophosphate is translocated and the polyol chain is following to the extracellular space through TarG driven by ATP hydrolysis via TarH (Brown *et al.*, 2013, Schirner *et al.*, 2011, Bron *et al.*, 2012). Once on the outer leaflet, WTA are disconnected from the membrane anchor and attached to the MurNAc residue of peptidoglycan via a phosphodiester bond catalysed by LytR, Cps2a, Psr in *B. subtilis* and Msr, SA0908 and SA2101 in *S. aureus*. (Kawai *et al.*, 2011, Hubscher *et al.*, 2009, Dengler *et al.*, 2012, Eberhardt *et al.*, 2012, Over *et al.*, 2011).

1.2.6 Nucleoid

The biggest polymer in bacteria based on one unit repeats is the chromosome that, together with episomal components, encodes for the entire genetic information of the bacterial cell. In eukaryotes, the chromosome also referred to as the nucleoid, is surrounded by a specialised compartment called the nucleus whereas the bacterial nucleoid apparently freely diffuses in

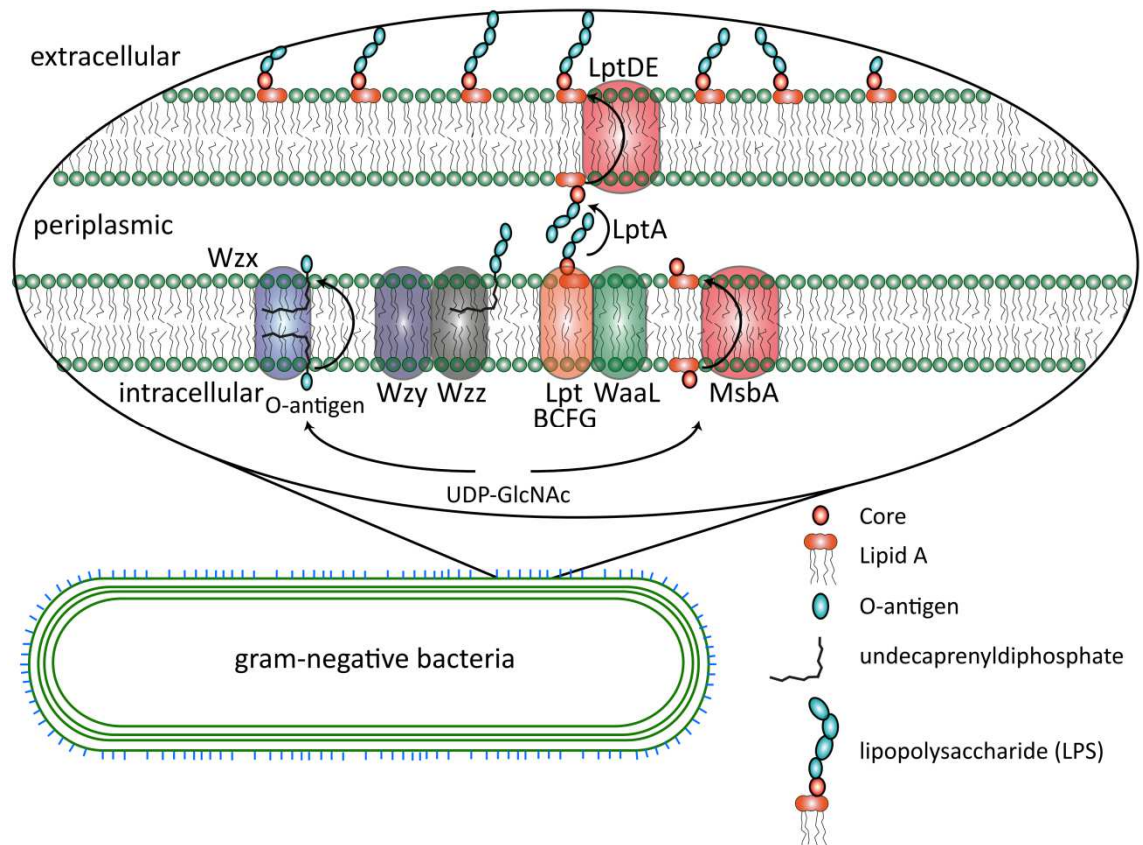


Figure 1.7 LPS synthesis and translocation in gram-negative bacteria

Schematic overview of lipopolysaccharide synthesis and insertion into the outer leaflet of the outer membrane. O-antigen and the core anchored to Lipid A are synthesised separately. The O-antigen bound to undecaprenyldiphosphate is synthesised by several cytoplasmic enzymes using UDP-GlcNAc as a substrate. Wzx translocates O-antigen to the periplasmic site where Wzy and Wzz polymerise multiple O-antigens to a long chain. The core is anchored to the membrane via Lipid A and is also synthesised from UDP-GlcNAc in the cytoplasm. MsbA flips the core-lipid A to the periplasmic leaflet and the ligase WaaL connects the O-antigen chain to core-Lipid A forming LPS. LPS is then translocated by a yet unknown mechanism through the periplasm involving LptBCFG on the inner membrane, LptA in the periplasm and LptDE in the outer membrane. The latter also acts as a flippase, translocating LPS to its destined position on the outer leaflet of the outer membrane. Figure is adapted from May *et al.*, 2016 and Bos *et al.*, 2007.

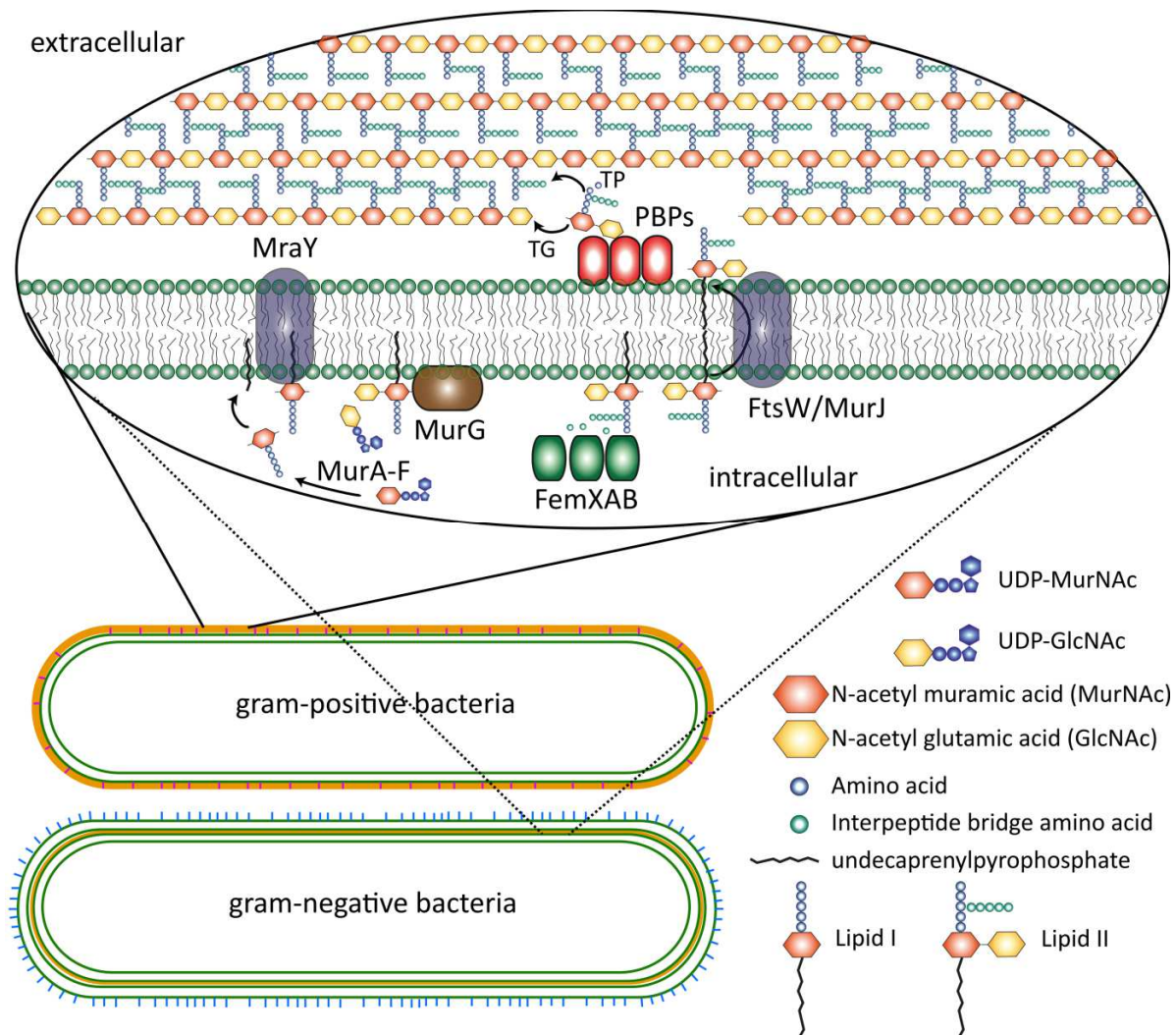


Figure 1.8 Peptidoglycan synthesis in bacteria

Schematic overview of peptidoglycan synthesis. UDP-N-acetylmuramic acid (UDP-MurNAc) is synthesised in the cytoplasm by several Mur ligases (Gomez-Baena *et al.*) and anchored to the membrane via *MraY* to an undecaprenylpyrophosphate resulting in lipid I. Lipid II formation is catalysed by *MurG* by adding N-acetylglutamic acid (GlcNAc) using UDP-GlcNAc as a substrate. In some bacteria such as *S. aureus*, a peptide bridge is added to the third amino acid via the three cytoplasmic proteins *FemXAB*. Lipid II is flipped to the periplasmic facing leaflet of the membrane and connected to existing peptidoglycan chains. The MurNAc residue is added to the GlcNAc residue via transglycosylation and the third amino acid is connected to the interpeptide bridge or fourth amino acid of pre-existing PGN. Both reactions are facilitated by penicillin binding proteins. Figure is adapted from Pinho *et al.*, 2013 and Typas *et al.*, 2012.

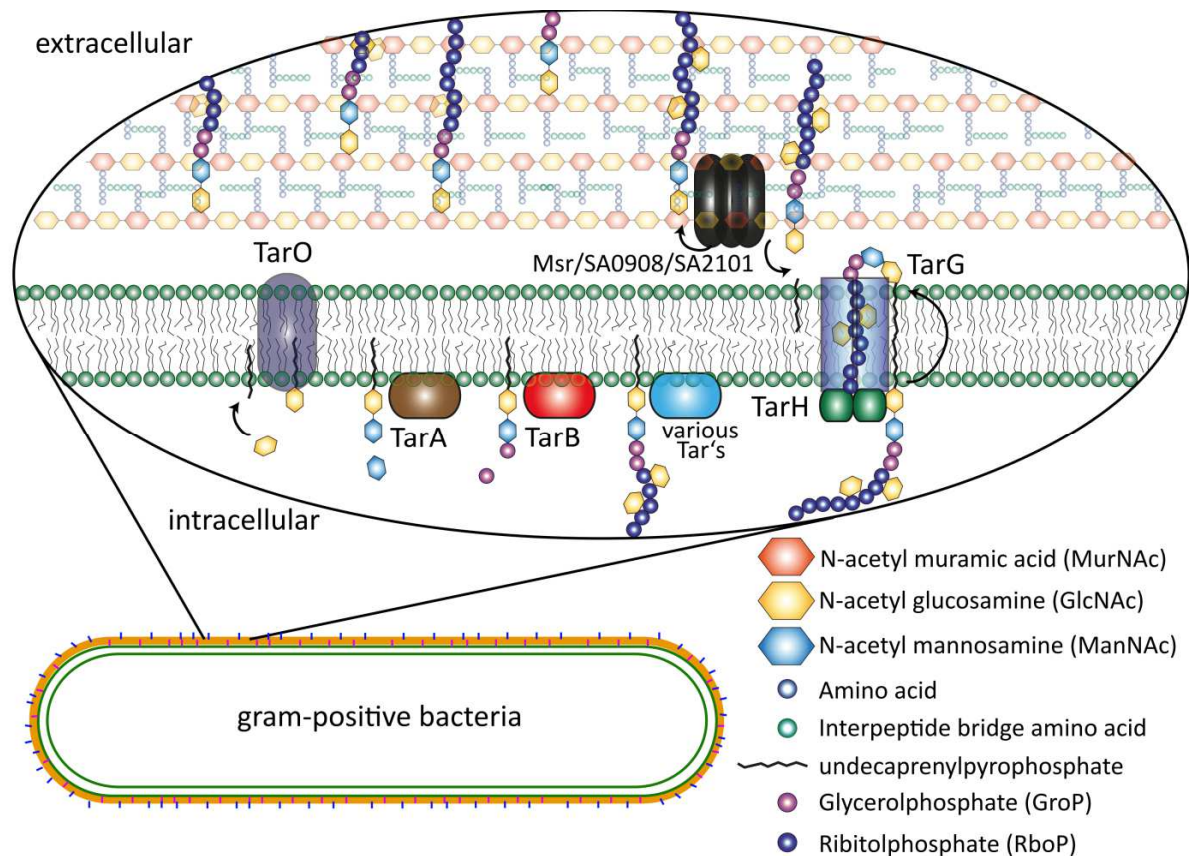


Figure 1.9 Wall teichoic acid synthesis in gram-positive bacteria

Schematic overview of wall teichoic acid synthesis. First, a membrane bound disaccharide precursor is synthesised by the membrane associated proteins TarO and TarA. This process takes place at the membrane. TarO anchors GlcNAc from UDP-GlcNAc to the membrane anchor undecaprenylpyrophosphate that is in turn extended by ManNAc which is catalysed by TarA. Next, TarB adds two GroP to the disaccharide. These reactions are conserved across gram positive bacteria whereas the following reactions, at which a decorated sugar polymer is gradually added to the linker unit, are highly species dependent. A number of Tar proteins add polyol phosphates tailored with sugars. The final product is then presumably flipped to the outer side of the membrane by the integral membrane protein TarG driven by ATP hydrolysis through a TarH dimer. Once at the extracellular side of the cell, LytR, Cps2a, Psr in *B. subtilis* and Msr, SA0908 and SA2101 in *S. aureus* catalyse the detachment of WTAs from their membrane anchor and facilitate the link to MurNAc via a phosphodiester bond. Figure is adapted from Brown *et al.*, 2013.

the cytoplasm. However, recent research revealed that also the bacterial nucleoid has a defined organisation condensed in a matrix comprised of proteins and RNAs along with organisational sequences encoded genetically on the chromosome (Thanbichler *et al.*, 2005). Furthermore, the bacterial cell contains 2-4 chromosomes during septation depending on the pace of growth. Fast growing cells begin chromosome replication prior to septation since the doubling time of certain species of bacteria, for instance *E. coli*, can be faster than the replication phase forcing cells to spatially organise their nucleoid copies (Skarstad *et al.*, 1986, Le *et al.*, 2013).

1.2.6.1 Chromosome replication

DNA synthesis requires a template from which newly synthesised DNA strands are copied in a reverse complement manner. The bacterial chromosome is highly contained and packaged by a variety of DNA condensing proteins such as SMC and MukB. These proteins, acting like eukaryotic histones, are crucial factors in chromosome condensation and partitioning (Britton *et al.*, 1998, Dervyn *et al.*, 2004, Volkov *et al.*, 2003). An overview of DNA replication is given in Figure 1.10.

1.2.7 The bacterial division machinery

The bacterial cell possesses a membrane and cell wall composed of several biopolymers. In order to proliferate and to ensure survival bacterial cells need to divide, a process that is performed mostly by binary fission in prokaryotic organisms. Bacterial cells separate into two parts that both renew into copies of the original cell. This process requires that both daughter cells receive the complete genetic information, the synthesis of cell wall and cell membrane material and the proper formation of the division ring that provides a contractile force for cytokinesis.

1.2.7.1 Temporal regulation

The polymerisation of FtsZ at the division site initiates and drives the septation of the cell (Adams & Errington, 2009). However, bacteria are exposed to a variety of quick and drastic environmental changes where cell proliferation is disadvantageous. Thus, a system to avoid cell-division initiation via FtsZ responding to the metabolic state of the cell is required. Nutrient availability is a crucial factor in cell-division initiation since proliferation in nutrient-poor conditions is disadvantageous for the survival of bacteria. This can be achieved prior to FtsZ-assembly by blocking chromosome replication

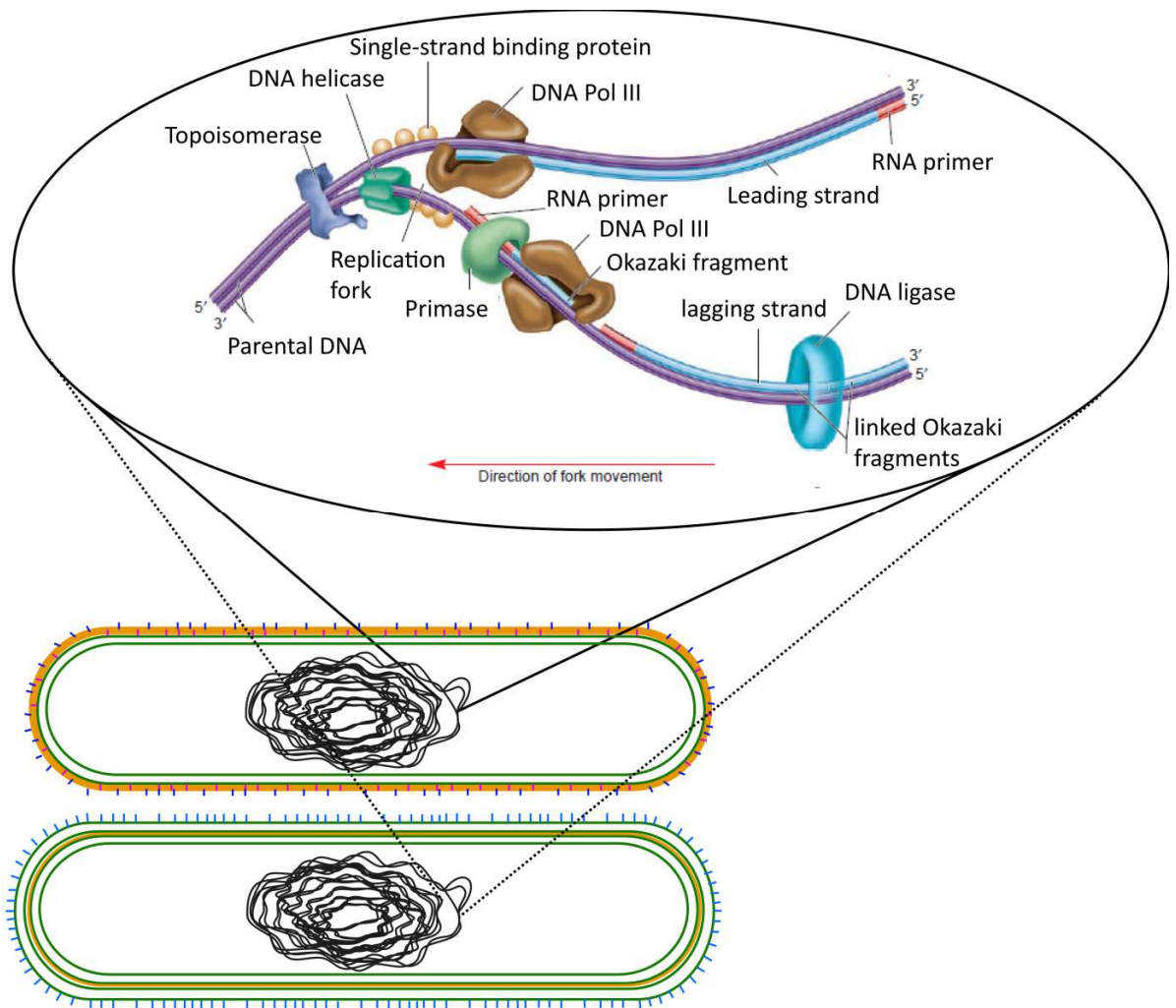


Figure 1.10 Chromosome replication

In order to disentangle the chromosome, helicases separate the two annealed DNA strands. The single strands are then stabilised by single-strand binding proteins to avoid their re-annealing. DNA is always synthesised in the 5' to 3' direction. Polymerase III adds complementary nucleotides to the leading strand whereas complementation of the lagging strand first requires primers composed of RNA which are placed by the primase. This is necessary since the replication fork opens in opposite direction to the lagging strand 5' to 3' orientation. Polymerase III then complements the lagging strand starting from RNA-primers and finishes at the next placed primer. This leaves non-annealed DNA fragments, also known as Okazaki fragments, behind. DNA fragments are finally linked via a ligase enzyme forming a phosphodiester bond. Image is adapted from:<http://reasonandscience.heavenforum.org/t1849p25-dna-replication-of-prokaryotes>.

through the synthesis of (p)ppGpp, a molecule produced in response to amino acid and carbon starvation. (p)ppGpp represses the expression of the replication initiating gene *dnaA* and interacts directly with the primase (Boutte *et al.*, 2012, Lesley & Shapiro, 2008, Potrykus & Cashel, 2008, Wang *et al.*, 2007, Denapoli *et al.*, 2013). Additionally, regulation of the FtsZ polymerisation displays a crucial factor in controlling cell-division. This control mechanism is employed in the response to the metabolic state which is linked to the recently identified enzymes UgtP in *B. subtilis* and OpgH in *E. coli* (Begg & Donachie, 1998) (Sharpe *et al.*, 1998, Weart & Levin, 2003) (Weart *et al.*, 2007) (Hill *et al.*, 2013). Both enzymes are terminal sugar transferases that use UDP-glucose for the synthesis of the diglucosyl-diacylglycerol anchor of lipoteichoic acids. UgtP and OpgH reversibly inhibit FtsZ assembly under nutrient-rich conditions where their substrate UDP-glucose is more abundant. Hence, a high level of UDP-glucose leads to increased cell length by the inhibition of Z-ring formation (Fig. 1.11) (Weart *et al.*, 2007) (Hill *et al.*, 2013).

1.2.7.2 Spatial regulation

FtsZ polymerisation can theoretically occur at any place within the cell as even *in vitro* experiments showed the formation of FtsZ bundles (Fu *et al.*, 2010)(Holden *et al.*, 2014). To prevent initiation of Z-ring formation near the cell poles or through the chromosome, bacterial cells facilitate a number of systems regulating its spatial organisation. *E. coli* has two independent mechanisms by which the formation of the dividing wall or septum is ensured to take place at the right place: The Min system and nucleoid occlusion (NO) avoid the formation of the Z-Ring at cell poles and through the chromosome (see Fig. 1.12) (Lutkenhaus, 2007) (Wu & Errington, 2012).

1.2.7.2.1 The Min system

The Min system prevents formation of the Z-ring near the cell poles. In *E. coli*, it comprises the three proteins MinCDE that oscillate between the cell poles while in *B. subtilis*, four proteins, MinCDJ and DivIVA are deployed to identify the cell poles in a non-oscillating manner (Monahan *et al.*, 2014, Rowlett & Margolin, 2015). In both systems, MinC inhibits FtsZ polymerisation and thereby prevents the formation of the cell division ring (Raskin & de Boer, 1999, Hu & Lutkenhaus, 1999). MinC is composed of two domains. The N-terminal domain inhibits the polymerisation of FtsZ while the C-terminal domain avoids interaction between FtsZ filaments and also interacts with the membrane protein MinD (Hu & Lutkenhaus, 2000).

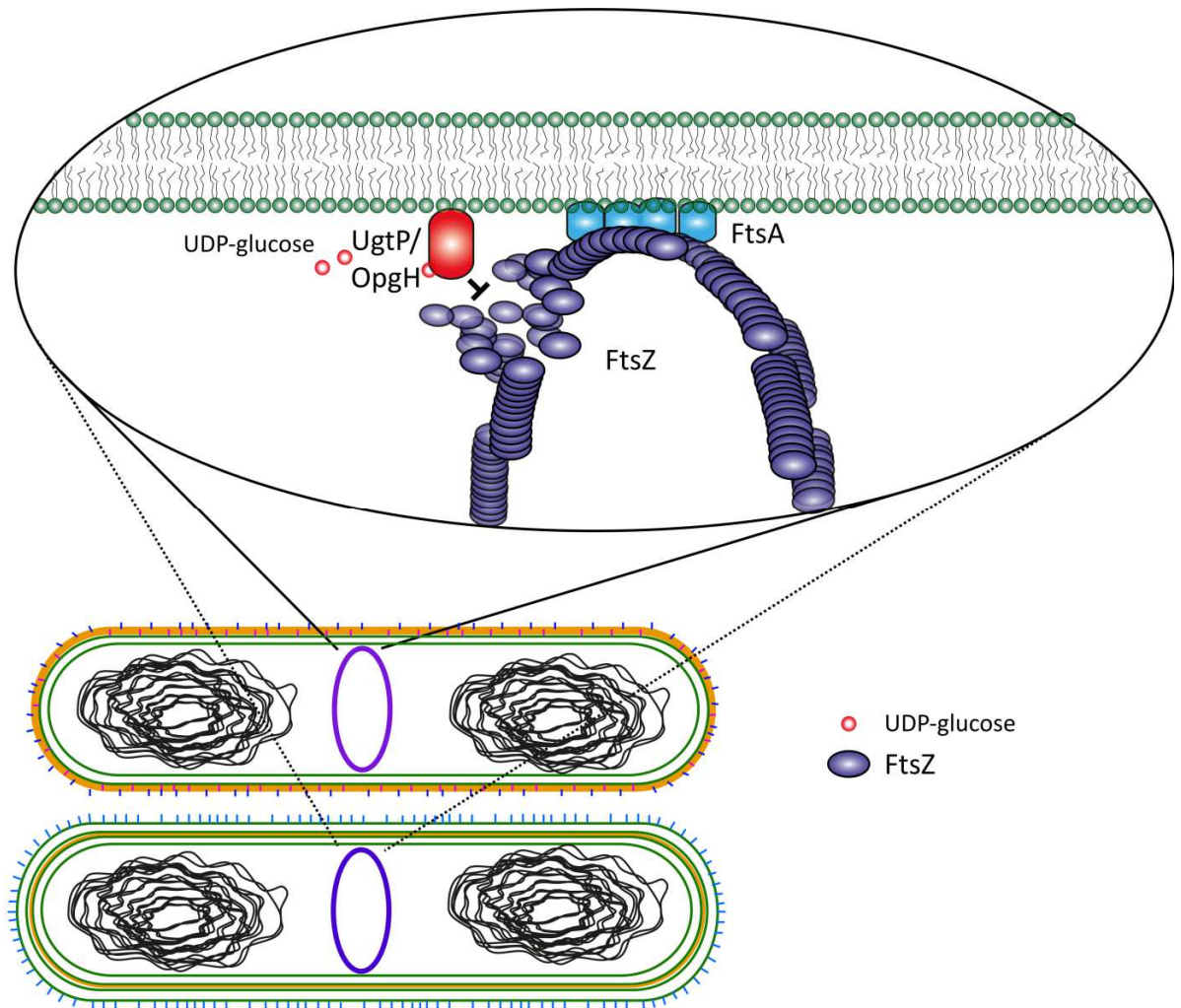


Figure 1.11 Temporal regulation of Z-ring formation

Schematic overview of cell-division initiation regulation by UgtP/OpgH. FtsZ polymerises at the cell-division site and is attached to the membrane via the membrane-associated protein FtsA. FtsZ is apparently organised in bundles of polymers that overlap each other and thereby form a discontinuous ring-like structure. Polymerisation of FtsZ is inhibited by UgtP in *B. subtilis* and OpgH in *E. coli* when induced by UDP-glucose, an abundant substrate during nutrient-rich growth conditions. Figure is adapted from (Begg & Donachie, 1998), (Sharpe et al., 1998, Weart & Levin, 2003), (Weart et al., 2007) and (Hill et al., 2013).

MinD is an ATPase that is organised as a dimer when bound to ATP and interacts with MinC forming a membrane-bound complex (Hu & Lutkenhaus, 2003, Ghosal *et al.*, 2014, Conti *et al.*, 2015, Lutkenhaus, 2008). Another member of the Min system, MinE, forms a ring-like structure that moves towards the cell poles and binds the dimer form of MinD which in turn causes the detachment of MinC (Fig. 1.12). The release of MinC triggers the ATPase activity of MinD that consecutively monomerises and dissociates from the membrane. This dynamic between MinE and MinC competing for MinD results in their oscillation between poles. Thus, a gradient of MinC is formed with its highest concentration at the cell poles and lowest concentration at the middle of the cell. Z-formation is therefore only initiated at the middle of the cell (Ma *et al.*, 2004, Lackner *et al.*, 2003, Hu *et al.*, 1999, Raskin & de Boer, 1997, Park *et al.*, 2011, Hu & Lutkenhaus, 2001, Hsieh *et al.*, 2010). The Min system in *B. subtilis* features MinCD but not a MinE homologue. Instead, DivIVA and MinJ act as localisation determinants of MinCD. DivIVA was shown to preferentially localise at negatively curved membranes and recruits MinJ to the cell poles (Lenarcic *et al.*, 2009, Eswaramoorthy *et al.*, 2011). MinJ in turn binds MinD and could replace the membrane binding properties of *E. coli* MinD (Bramkamp *et al.*, 2008, Patrick & Kearns, 2008). However, MinCD do not oscillate in *B. subtilis* but relocalise from the old cell pole to the newly formed septum after cell-division initiation to prevent the formation of multiple Z-rings near the mid-cell (Marston & Errington, 1999, Gregory *et al.*, 2008).

1.2.7.2.2 Nucleoid occlusion

The Min system ensures that the Z-ring is not formed at the cell poles; however, a second mechanism is required to guarantee that the chromosome integrity is not affected. Nucleoid occlusion (NO) factors such as Noc (*B. subtilis*) or SlmA (*E. coli*) were found through a synthetic-lethal phenotype in cells with a defective Min system. Noc binds to specific palindromic sequences that are found 70 times spread across the chromosome but are absent from the termination region (Wu *et al.*, 2009). Furthermore, Noc binds to membranes via an N-terminal amphipathic helix. Full inhibitory activity of Noc is dependent on its ability to bind DNA and membranes simultaneously which suggests the formation of a membrane-associated nucleoprotein complex that avoids polymerisation of FtsZ through the chromosome (Adams *et al.*, 2015). SlmA inhibits the polymerisation of FtsZ by a direct interaction whereas the interaction partner of Noc is still unknown (Cho *et al.*, 2011). The nucleoid occlusion in rod-shaped bacteria is

only required when major cell cycle events have been disturbed since the Min system alone is capable to position the division ring (Wu & Errington, 2004). However, in coccoid bacteria such as *S. aureus* that lack the Min system, deletion of *noc* results in division defects such as DNA breaks and multiple FtsZ rings (Veiga *et al.*, 2011).

1.2.7.2.3 Alternative mechanisms

Most work on Z-ring positioning has been done in *E. coli* and *B. subtilis* where the Min system and nucleoid occlusion play a pivotal role to ensure correct placement of the cell-division site. Recently, it has become evident that many bacteria do not possess these spatial organisers (Pinho *et al.*, 2013, Monahan *et al.*, 2014). Furthermore, although the depletion of both, the *min* genes and NO genes in *B. subtilis* and *E. coli* reduce cell viability, cells are still able to correctly place the Z-ring. Taking together, this suggests that Min and NO are not the only spatial organisers and that other systems contribute to or are able to take over Z-ring placement in *E. coli* and *B. subtilis* (Wu & Errington, 2004, Bernhardt & de Boer, 2005, Bailey *et al.*, 2014).

1.2.7.2.3.1 MipZ

Caulobacter crescentus is capable to divide properly without using the Min or NO system. MipZ, an essential ATPase protein of previously unknown function, interacts with the chromosome partitioning protein ParB forming a complex near the origin of replication at the cell poles and inhibits FtsZ polymerisation (Thanbichler & Shapiro, 2006). After replication, one copy of the chromosome moves to the other end of the cell together with MipZ. Interaction with ParB stimulates the ATPase activity of MipZ which is required for inhibition of FtsZ. ATP hydrolysis in turn causes the release of MipZ from the chromosome followed by recapturing of MipZ by ParB (Kiekebusch *et al.*, 2012). This dynamic process explains the formation of a MipZ gradient where its concentration is lowest in the midcell and highest at the cell poles, thereby preventing Z-ring formation near the cell poles.

1.2.7.2.3.2 MapZ/LocZ

Streptococcus pneumoniae is an ellipsoidal shaped gram-positive bacterium and also lacks the canonical spatial organisation systems. First evidence for a cell-division site regulatory system came from the Serine/Threonine kinase StkP. Its deletion causes elongated cells and StkP localises at the septum (Beilharz *et al.*, 2012). Later work of two groups supported the notion of an involvement of StkP in cell-division

demonstrating that MapZ, also called LocZ, is a cell-division associated protein that is phosphorylated by StkP. Both the phosphorylated as well as the non-phosphorylated form of MapZ positively affect Z-ring formation by direct protein-protein interactions with FtsZ (Fleurie *et al.*, 2014a). MapZ arrives prior to FtsZ and forms ring-like structures moving apart as the cell elongates. These rings serve as future division determinants (Fleurie *et al.*, 2014a, Holeckova *et al.*, 2015).

1.2.7.2.3.3 SsgAB

An entirely new mechanism of Z-ring regulation was found in *Streptomyces coelicolor*, another bacterium lacking all the known FtsZ-positioning proteins. SsgA-like proteins (SALP) are cell-division site determinant factors in *Streptomyces*. Cells lacking *ssgB* form long hyphae incapable of cell-division (Traag & van Wezel, 2008). *In vitro* studies showed that the membrane-associated protein SsgB positively affects FtsZ formation and interacts with FtsZ as demonstrated by FRET and BACTH studies (Willemse *et al.*, 2011). Presumably, SsgB tethers FtsZ to the membrane and induces the formation of the Z-ring. The second protein involved is SsgA that only interacts with SsgB but not FtsZ, indicating a role for SsgA in guiding SsgB to the cell-division site. Interestingly, both proteins still localise to the septum in FtsZ-depleted cells but it is currently unknown how SsgAB identify the future cell-division site. However, SsgAB proteins are only found in *Actinomycetes* (Willemse *et al.*, 2011).

1.2.7.2.3.4 PomXYZ

Myxococcus xanthus neither possesses Min proteins nor the NO system. Recently, it has been reported that cells without the ParA-like protein PomZ exhibit severe cell-division defects along with incorrectly positioned Z-rings and mini-cells lacking a chromosome (Treuner-Lange *et al.*, 2013). PomZ localises to the cell-division site prior to FtsZ and after chromosome segregation and forms a complex with PomX and PomY. PomZ interacts with FtsZ from cell extract and promotes the formation of the Z-ring upon ATP hydrolysis stimulated by PomXY and DNA binding (Schumacher, 2016). Since PomZ also localises to the future cell-division site in cells depleted of FtsZ, a role for PomZ in division-site identification has been suggested (Treuner-Lange *et al.*, 2013).

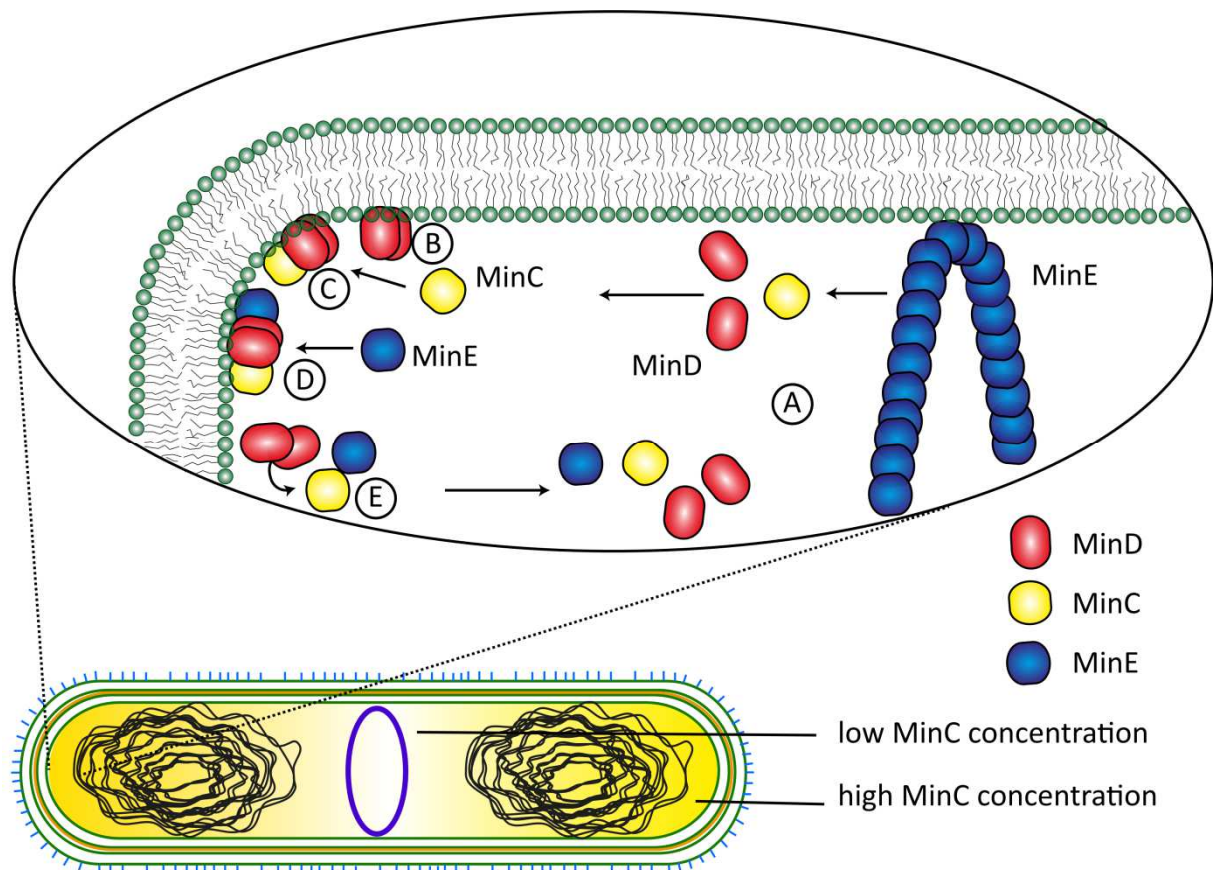


Figure 1.12 MinCDE oscillation in *E. coli*

Schematic overview of oscillation dynamics of MinCDE proteins. **A**, MinCD oscillate between cell poles. MinE forms a ring-like structure that also moves towards the cell poles following MinCD. **B**, MinD forms a dimer in the presence of ATP and binds to the membrane. **C**, MinC binds to the MinD dimer forming a membrane bound complex. **D**, MinE recognises and binds the MinD dimer and thereby causes the detachment of MinC. **E**, Released MinC activates ATPase activity of MinD which then results in the monomerisation of MinD and in return its dissociation from the membrane. Figure is adapted from Rowlett and Margolin, 2013.

1.2.7.3 Divisome assembly

After the cell-division site is determined, FtsZ polymerises and forms the Z-ring. To complete septation the following steps have to be taken into consideration:

1. FtsZ needs to be tethered to the membrane
2. Recruitment of downstream divisome proteins
3. FtsZ filament stabilisation
4. Constriction
5. Formation of a bridge between the divisome and peptidoglycan
6. Peptidoglycan synthesis
7. Membrane fusion
8. Peptidoglycan hydrolysis to release septated cells

First, FtsZ itself does not have an affinity for the membrane and needs to be tethered to the membrane via FtsA or ZipA (Pichoff & Lutkenhaus, 2005, Ma & Margolin, 1999). FtsA is highly conserved among bacteria except for Mycobacteria and Cyanobacteria whereas ZipA is only found in *E. coli* and other γ -proteobacteria. These proteins act as a scaffold recruiting a number of proteins that are required for complete septation. Recruited proteins are involved in a variety of functions of which not all are essential and overlap with each other. FtsZ assembly is regulated by EzrA, SepF, ZapA and ZapB. EzrA is only found in gram-positive bacteria with low GC content, inhibits FtsZ-assembly and limits the number of Z-rings. SepF is conserved across gram-positive and cyanobacteria and contributes to the recruitment of other cell-division-associated proteins and is capable of taking over the function of FtsA when overexpressed (Ishikawa *et al.*, 2006). Z-ring assembly is positively regulated by ZapA and ZapB by stabilising FtsZ filaments. FtsZ membrane attachment is crucial for Z-ring formation and constriction since reconstitution of FtsZ together with FtsA was enough to partially constrict liposomes *in vitro* (Osawa *et al.*, 2008, Osawa & Erickson, 2011). While the Z-ring constricts the cell, new cell material in the form of peptidoglycan and phospholipids has to be produced at the site of membrane invagination. The former has been investigated intensively and it has been demonstrated that many divisome proteins such as FtsQ (DivIB), FtsL and FtsB (DivIC) build up a link between divisome and peptidoglycan synthesis. It has been suggested that another protein, GpsB along with EzrA localises PBP1 in *B. subtilis* (Claessen *et al.*, 2008). Furthermore, DivIB interacts with PBP2B in *B. subtilis* and binds peptidoglycan in *S. aureus* (Rowland *et al.*, 2010, Bottomley *et al.*, 2014). Additionally, the integral membrane protein FtsW is a flippase translocating peptidoglycan precursors to the outer leaflet of the cell providing the substrate for PBPs in peptidoglycan synthesis (Mercer & Weiss, 2002). FtsW is also

involved in the recruitment of the peptidoglycan synthesis machinery and interacts with FtsI (PBP3), FtsL and FtsN (Di Lallo *et al.*, 2003, Fraipont *et al.*, 2011, Karimova *et al.*, 2005, Typas *et al.*, 2012). Moreover, to save septally entrapped chromosomes, FtsK, a DNA translocase, binds to specific sequences termed KOPS located throughout the chromosome and resolves chromosome dimers and moves the DNA out of the constricting septum. Although this mechanism is only crucial during stress, the deletion of the membrane part of FtsK is lethal for the cell indicating a second role for FtsK (Begg *et al.*, 1995, Bigot *et al.*, 2005, Steiner *et al.*, 1999, Fleming *et al.*, 2010). After complete cell-division, daughter cells are still attached to each other via peptidoglycan and need to be separated by hydrolases. A potential role has been demonstrated for FtsEX, an ABC transporter that recruits EnvC to the cell-division site (Schmidt *et al.*, 2004, Yang *et al.*, 2011). EnvC is a septal peptidoglycan amidase that contributes to complete septation as well as the positive regulation of the amidases AmiA, AmiB and AmiC (Uehara *et al.*, 2010). An overview of the cell-division machineries of *E. coli*, *B. subtilis* and *S. aureus* is given in Fig. 1.13.

1.2.8 Cytoplasm

All the aforementioned cellular processes follow a certain pattern. Precursors are formed in the cytoplasm, linked to the membrane and then gradually extended to polymers either at the cytoplasmic face of the membrane or after flipping to the outer leaflet of the cell. Finally, polymers are modified and anchored to their final destination. The material is provided from cytoplasmic metabolic processes whose products are transported by diffusion. Thus, not much attention has been put on the cytoplasm since it is mainly seen as an aqueous densely packed solution of polydisperse molecules (Cayley *et al.*, 1991). An early study undertaken by Elowitz *et al.* demonstrated the mobility of several cytoplasmic proteins in *E. coli* and showed that, although all proteins follow simple diffusion mechanics based on Brownian motion, a single viscosity for the cytoplasm does not explain the observed diffusion values (Elowitz *et al.*, 1999). Brownian motion is the process of random particle motion due to their collision with other particles and describes what is commonly understood as diffusion (Phillips, 2013). Recently, research has slowly moved into the physical aspects of diffusion and their biological impact on cellular processes gradually created an image to explain the observations of Elowitz *et al.* Single-particle tracking using photoactivatable fluorophores allowed the trajectories of proteins to be followed and to draw conclusions whether diffusion is homogeneous throughout the cell or regulated by intracellular structures. The photoactivatable protein Kaede was found to be

homogeneously distributed in the cytoplasm and exhibits a homogeneous diffusion. However, in longer cells, Kaede diffusion is faster within the nucleoid than in the middle of the cell (Bakshi *et al.*, 2011). Macromolecular structures such as the nucleoid are heterogeneously distributed and influence the diffusion of molecules such as the small heat shock chaperone IbpA (Coquel *et al.*, 2013). Furthermore, also protein aggregates that have to be linked to ageing in *E. coli* diffuse to and accumulate at the old cell pole that acts as a landfill (Coquel *et al.*, 2013). Single-particle tracking of the cytoplasmic photoactivatable protein mEos2 revealed geometrical aspects as an additional component that affects diffusion rates since the diffusion of mEos2 was found to be faster in the middle of the cells and slower at the cell poles where proteins are spatially more restricted (English *et al.*, 2011). Diffusion studies using fluorescently marked mRNAs further showed that diffusion of at least mRNAs is independent of cytoskeletal components such as FtsZ and MreB (Golding & Cox, 2006). FtsZ itself is localised in a stationary manner during cell-division along with a diffusive cytoplasmic form. Interestingly, although FtsZ movement follows Brownian motion, the diffusion is restricted to a helical region spanning throughout the entire cell suggesting a yet unknown diffusion barrier for FtsZ (Niu & Yu, 2008). Diffusion patterns can also be altered due to protein-protein interactions or metabolite binding. For instance, the stringent response protein RelA that binds to ribosomes shows drastically altered diffusion behaviour upon starvation and is more diffusive to reach as many ribosomes as possible (English *et al.*, 2011). A ground-breaking study undertaken by Parry *et al.*, fundamentally altered the view of the cytoplasm. The trajectories of molecules are highly dependent on their size and the metabolic state (Parry *et al.*, 2014). While small particles diffuse freely, bigger molecules are more constrained and trapped within certain areas. This leads to the formation of crowded macromolecules. However, active metabolism 'fluidises' the cytoplasm and allows bigger molecules to leave their local environment (Fig. 1.14). It is still unclear what causes the observed changes in subdiffusive motion but an explanation could be that active metabolism causes more rearrangements within macromolecules which potentially lower the hydrophobic and electrostatic interactions between macromolecule components. Thereby, molecules could leave the macromolecule and access areas further away (Parry *et al.*, 2014, Spitzer, 2011). In summary, diffusion in bacterial cells is governed by the following: geometry, molecule size that results in the formation of macromolecular structures mainly composed of 'big' molecules, the affinity to other molecules that might be stationary and the metabolic state of the cell.

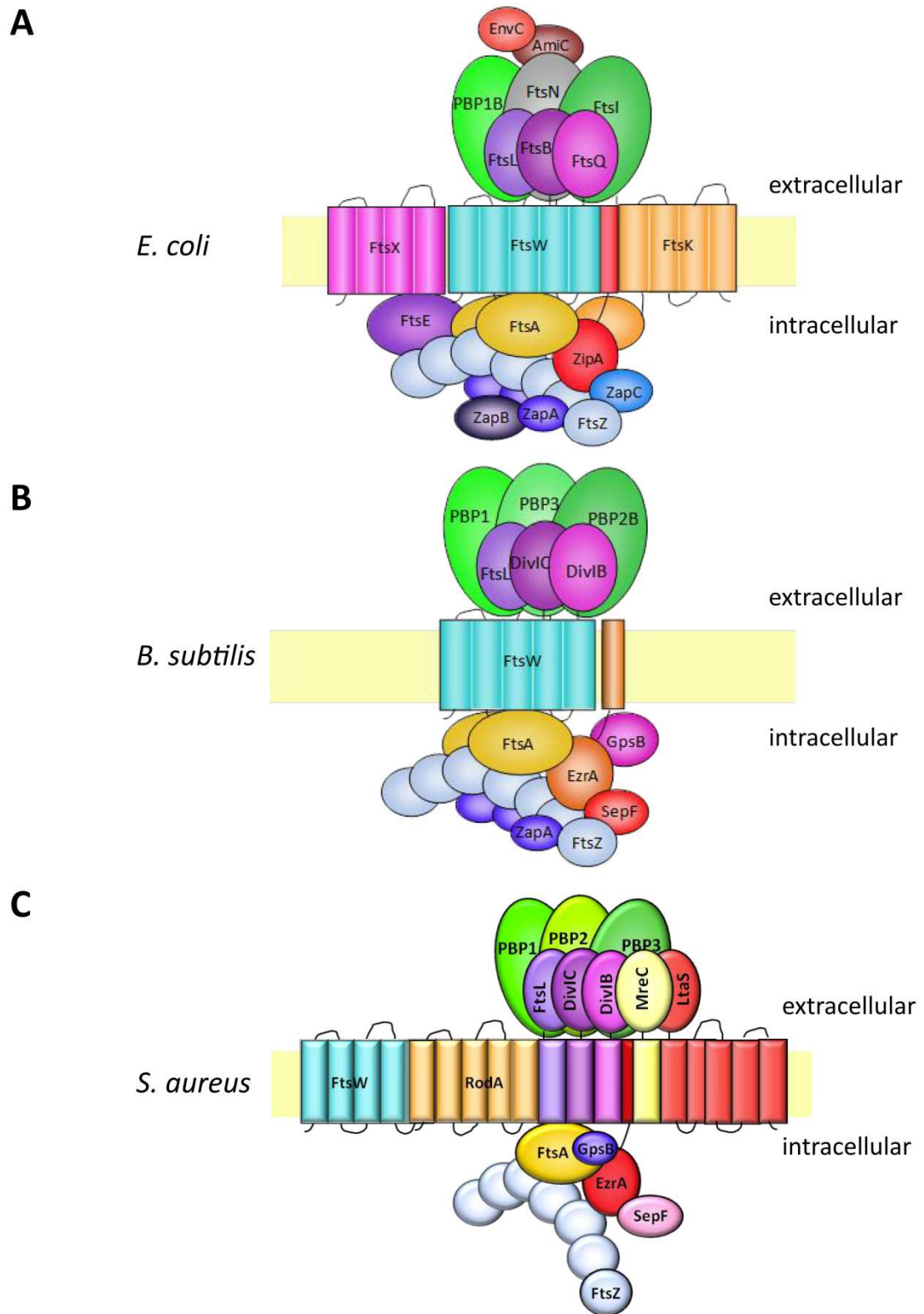


Figure 1.13 Cell-division machineries in *E. coli*, *B. subtilis* and *S. aureus*
 Schematic representation of the divisome in *E. coli* (A), *B. subtilis* (B) and *S. aureus* (C). Images are adapted from Bottomley, 2011.

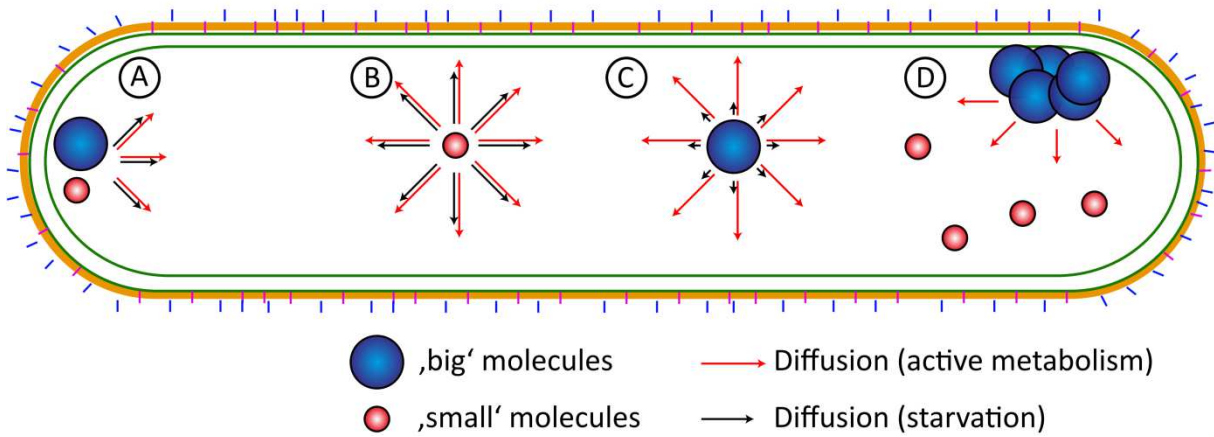


Figure 1.14 Molecule diffusion dynamics in the bacterial cytoplasm

Schematic overview of some aspects that regulate subdiffusive properties of molecules. **A**, Geometry: The cell poles spatially restrict the diffusion of molecules and can result in their polar accumulation. **B+C**, Molecule size and metabolic state: ‘Small’ molecules exhibit a faster diffusion rate compared to ‘big’ molecules (length of arrows indicates the diffusion rate). Diffusion is greatly increased during metabolism which especially affects ‘bigger’ molecules. **D**, Macromolecular crowding: Dynamics due to A-C result in crowding of ‘big’ molecules into subcellular macromolecules with low diffusion. Components of macro-molecules have increased chances to access other areas in states of active metabolism whereas ‘small’ molecules are mainly diffusive and less affected by the metabolic state. Figure is adapted from Parry *et al.*, 2014.

1.3 Localisation of membrane proteins

As discussed before, the bacterial cell is composed of a variety of biopolymers many of which are synthesised at the membrane. This process involves several synthases located in the membrane along with temporal and spatial regulatory elements. How do bacterial cells provide the structural foundation to make cellular processes as efficient as possible? Firstly, processes mostly require a complex of proteins that allow the channelling of metabolites. Secondly, these complexes are localised by protein-protein interactions within a spatial determining protein, lipid interactions or sense the curvature of the membrane (Kuriyan & Eisenberg, 2007, Bramkamp & Lopez, 2015). And lastly, synthesis has to occur at a particular place for a specific function as it would be energetically unfavourable to transport products to a far off cellular destination. In order to position membrane proteins and membrane-associated proteins, bacterial cells deploy both membrane curvature features and specific microdomains composed of certain lipids.

1.3.1 Membrane curvature as a cue for protein localisation

Ultimate cues in bacterial cells are given by their wide range of different cell shapes that can be reduced to arrangements of positively and negatively curved membranes. Polar localisation of proteins is a common feature in bacteria as seen for septal positioning mechanisms (Young, 2006). In the case of *E. coli*, the previously described tethering of MinCD to the poles gives a supramolecular foundation.

1.3.1.1 DivIVA

The cell division initiation protein DivIVA has been investigated intensively and is a bacterial topological marker. It is widely conserved among Gram-positive bacteria and mainly acts as a protein scaffold to position proteins involved in peptidoglycan synthesis, secretion or division-site selection. In *B. subtilis* and *Listeria monocytogenes*, DivIVA serves as part of the Min system and tethers MinC via MinJ to the cell poles, whereas it is required for polar growth and peptidoglycan synthesis in *Corynebacterium glutamicum*, *Streptococcus pneumoniae* and Mycobacteria (Bramkamp *et al.*, 2008, Letek *et al.*, 2008, Sieger & Bramkamp, 2014, Fleurie *et al.*, 2014b, Meniche *et al.*, 2014, Halbedel *et al.*, 2012). Yet another function of DivIVA is found in *Listeria monocytogenes* where the protein is needed for the secretion of autolysins at the poles. Cells lacking DivIVA grow as long chains that have clearly completed cell division but daughter cells are still attached (Halbedel *et al.*, 2012). Unexpectedly, a *divIVA* null

mutant of *S. aureus* shows no obvious phenotype and undergoes normal cell-division, which raises the question whether there is a homologue that takes over the function of DivIVA (Pinho & Errington, 2004). The common feature of all DivIVA proteins is that they localise at the poles or the cell division site. But it was unknown whether DivIVA is the first protein to arrive or is recruited by other factors. Two studies however clarified the picture by showing that the heterologous expression of *B. subtilis* DivIVA in *E. coli* and *Schizosaccharomyces pombe* displayed the same localisation at the poles (Edwards *et al.*, 2000). Furthermore, DivIVA that was reconstituted into liposomes was always found at locations with highly curved membranes (Lenarcic *et al.*, 2009). In spherical cells, DivIVA is homogeneously distributed, since suitable membrane areas with high curvatures are missing, which underlines its ability to discriminate between degrees of concavity (Ramamurthi & Losick, 2009). Both the heterologous expression and the reconstitution into liposomes made it clear that it is an intrinsic feature of DivIVA to bind to negatively curved membranes. DivIVA has a highly conserved N-terminus that is required for the membrane targeting (Perry & Edwards, 2004). Daptomycin-treated *B. subtilis* cells form membrane distortions that recruit DivIVA suggesting the formation of local highly curved membrane patches (Pogliano *et al.*, 2012). It forms a parallel coiled-coil that exposes hydrophobic and positively charged residues that are essential for membrane binding (Oliva *et al.*, 2010). Its C-terminus is more variable and used for interaction with proteins, however, the N-terminus of the *B. subtilis* DivIVA is needed to bind MinJ (van Baarle *et al.*, 2013). The big question however is which mechanism accounts for the polar localisation of DivIVA since lipids at strongly curved membranes are densely packed and probably prevent the insertion of the DivIVA N-terminus into the membrane? Strahl and Hamoen proposed that the answer relies in the ability of DivIVA to form oligomers. These oligomers are composed of 4-8 monomers and span half of the curvature radius of *B. subtilis* septa. Using a Monte-Carlo simulation, they could show that DivIVA likely forms stable clusters at curved membranes because of the combined interactions between each other and lipids (Fig. 1.15A) (Strahl & Hamoen, 2012). Recently, a study demonstrated that *B. subtilis* cells lacking the secretion ATPase SecA fail to properly localise DivIVA. However, it has been hypothesized that not SecA directly but a downstream effect such as potential membrane changes due to the lack of SecA are responsible for the observed DivIVA localisation (Halbedel *et al.*, 2014). Structured illumination microscopy (SIM) revealed that DivIVA forms a highly stable ring at the septum that collapses into patches at the poles (Eswaramoorthy *et al.*, 2011). Another group used photo-convertible and activatable fluorophores and proposed that DivIVA in newly divided

cells moves from the poles to the new septum. The cell-division site probably provides a higher curvature compared to the poles and is therefore favored (Bach *et al.*, 2014). The mechanism how DivIVA moves to the poles and its accompanied switch between membrane detached and soluble form remains unknown.

1.3.1.2 SpoVM

DivIVA is not the only known protein that senses curved membranes. An early study demonstrated the recruitment of a peripheral membrane protein involved in spore formation to the polar septum right after the start of spore formation. SpoVM engulfs the spore (Fig. 1.15B). However, the authors assumed that a yet unknown protein is responsible for SpoVM targeting (van Ooij & Losick, 2003). Later work clarified the picture and revealed the independent specific localisation of SpoVM to positively curved membranes that are found when the cells are forming spores (Ramamurthi *et al.*, 2009). Ramamurthy *et al.*, also observed that SpoVM localises to the outer surface of internal vesicles when expressed in *E. coli* and *Saccharomyces cerevisiae* mutants that produce vesicles or fragmented vacuoles, respectively. Additionally, purified SpoVM-GFP was found to attach to unilamellar vesicles. However, it only binds to small vesicles with diameter sizes between 1 μm and 5 μm which strongly indicates the ability of SpoVM to discriminate between the degree of positive curvature. Further studies corroborated this finding and revealed that SpoVM extensively interacts with acyl chains in membranes to sense packing differences between curved membranes leading to its preferential binding to convex membranes (Gill *et al.*, 2015).

1.3.1.3 Other curvature sensing proteins

Non-membrane proteins of the general phosphotransferase system also display a polar localisation. Enzyme I (EI) was found to be localised at the poles in *E. coli* and preferentially accumulates at sites of strong curvature in spherical *E. coli* cells (Lopian *et al.*, 2010, Govindarajan *et al.*, 2013). Co-expression with DivIVA-GFP from *B. subtilis* demonstrated that EI and DivIVA exhibit a similar localisation pattern. However, EI is a soluble protein and no membrane tethering domain could be found. Thus, it is assumed that another factor might orchestrate EI localisation (Govindarajan *et al.*, 2013).

The chemoreceptor TlpA localises at the base of the septum and at strongly curved membranes in *B. subtilis*. Structural studies of TlpA revealed its cone-shape that is required to sense negatively curved membranes (Fig. 1.15C). This localisation pattern was still seen in cell wall free cells that are also referred to as L-forms. Interestingly,

amino acid substitutions causing structural rearrangements to form a cylindrical shaped TlpA resulted in a loss of the observed localisation pattern (Strahl *et al.*, 2015).

1.3.1.4 BAR-domain containing proteins in eukaryotes

BAR domain proteins in eukaryotic organisms have been investigated intensively during the last decade. Proteins belonging to the Bin-Amphiphysin-Rvs (BAR) domain superfamily have a dimeric α -helical protein motif, which enables them to interact with membranes. Due to their curved interface they preferentially bind to positive (BAR) or negative (I-BAR) curved membranes (Fig. 1.15D) (Frost *et al.*, 2008, Saarikangas *et al.*, 2009) (Zhao *et al.*, 2011). These are found in various eukaryotic species such as yeast, *Drosophila melanogaster* or *Leishmania spec.* (Lefebvre *et al.*, 2013). Some BAR domain proteins contain an additional N-terminal amphipathic helix that inserts into the membrane and induces membrane curvature (Peter *et al.*, 2004). Furthermore, most BAR-proteins have at least one domain that enables them to interact with other proteins. Thus, BAR-proteins are scaffolding proteins that organise a variety of other proteins in a curvature-dependent manner (Mim & Unger, 2012). Creation of trusions in eukaryotic cells by these and other proteins are crucial to maintain cell fundamentals such as membrane fusion (Chamberlain *et al.*, 2001), membrane fission (Hinshaw, 2000), membrane budding (McMahon & Gallop, 2005) and endocytosis (Canton & Battaglia, 2012).

1.3.2 Driving forces for membrane curvature

Bacterial cells rely on differently curved membranes as crucial localisation cues. Consequently, this begs the question as to how curved membranes are formed. With the discovery of lipid rafts in eukaryotic cells it became evident that membranes are structured and not only composed of a disordered liquid phase (Rietveld & Simons, 1998). Using fluorescent microscopy of liposomes it was demonstrated that membranes that are formed by different lipids can laterally separate into coexisting liquid domains with distinct lipid compositions and curvatures (Baumgart *et al.*, 2003) (Parthasarathy *et al.*, 2006). These domains are enriched by cholesterol and or sphingolipids that stimulate their formation. Further studies confirmed these results and showed that even weak negative curvatures cause the enrichment of certain lipids (Nishizawa and Nishizawa, 2011).

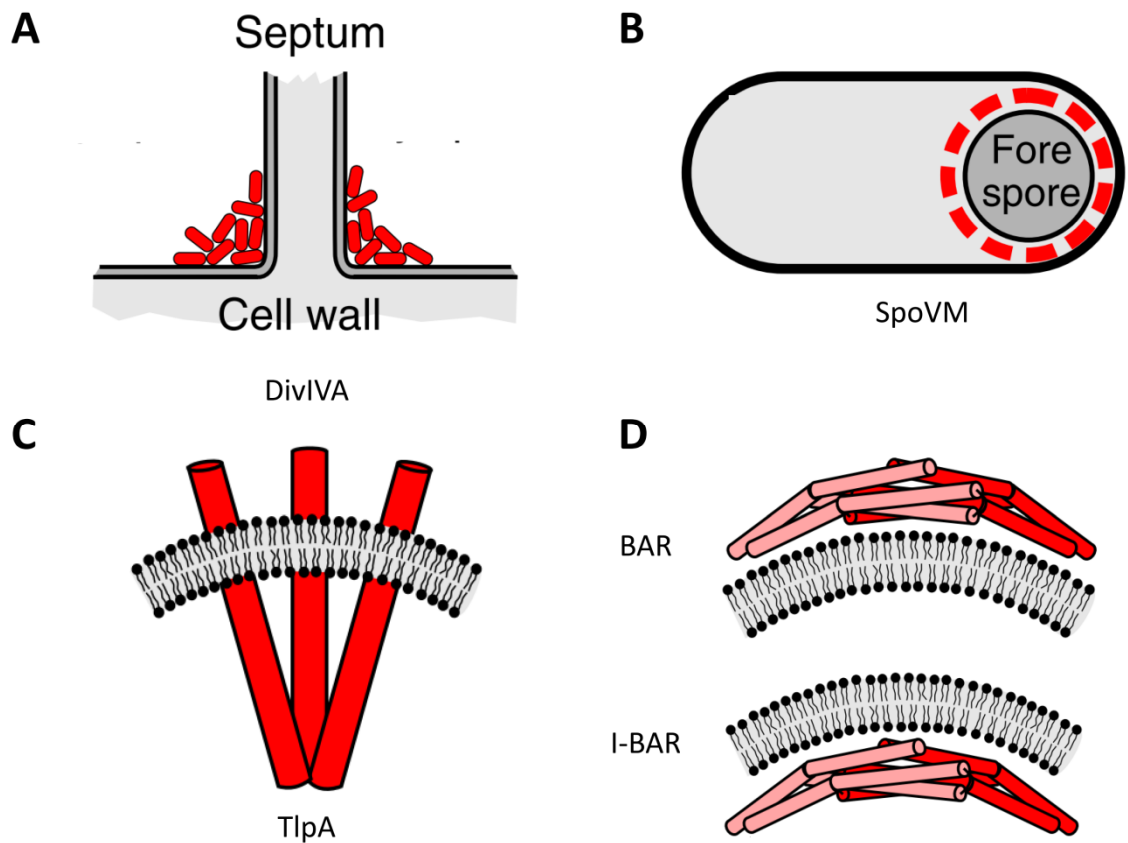


Figure 1.15 Examples of membrane curvature sensing protein mechanisms

Schematic overview of proteins and mechanisms that sense positive and negative membrane curvature. **A**, DivIVA in *B. subtilis*, accumulates to strongly negatively curved membranes by an interaction between DivIVA proteins and lipids. **B**, SpoVM in *B. subtilis* binds to the outer positively curved membranes of endospores. **C**, The cone-shaped TlpA senses negatively curved membranes in *B. subtilis*. **D**, BAR and I-BAR domain containing proteins in eukaryotes attach to positively (BAR) or negatively (I-BAR) curved membranes. Figures is adapted from Strahl *et al.*, 2015.

1.3.2.1 Lipid composition

However, not only the sorting of lipids is dependent on membrane curvature. Lipids also display an important force for the formation of curved membranes. The shape of lipids depends on the size of their headgroup and their acyl chain length, saturation and composition (Cooke & Deserno, 2006). Cylindrical lipids such as phosphatidylcholine and phosphatidylserine form flat membranes whereas conical shaped lipids such as phosphatidylethanolamine, phosphatidic acid, diacylglycerol and cardiolipin impose a negative curvature to membranes. Lipids with big headgroups forming inverted conical shapes such as lysophosphatidylcholine and phosphatidylinositol phosphates cause the generation of positive curvatures (Martens & McMahon, 2008, Chernomordik & Kozlov, 2003, Di Paolo & De Camilli, 2006, Zimmerberg & Kozlov, 2006). In principal, the ratio between the size of the acyl chain and the polar head group decide whether the lipid is likely to be a part of positively, negatively or non-curved membranes.

1.3.2.2 Shaped membrane proteins and protein crowding

Furthermore, this heterogeneity also drives the sorting of peptides and proteins. Wu and Liang, 2014, showed using MARTINI Force dynamic simulations, that proteins tend to accumulate in curved regions dependent on their intrinsic structural features (Wu & Liang, 2014). Interestingly, the simulated peptides could also further enhance the membrane curvature suggesting a complex interplay between lipids, proteins/peptides and membrane curvature that determines the organisation and shape of membranes. Proteins can insert a hydrophobic domain between lipid headgroups acting as a 'wedge' and induces local membrane curvature. The amount of these inserted motifs is crucial in the stabilisation and degree of curved membranes (Ford *et al.*, 2002, Campelo *et al.*, 2008, McMahon *et al.*, 2010). Another mechanism of how proteins induce membrane curvature is scaffolding that is seen for BAR-domain proteins or the earlier discussed crescentin (Peter *et al.*, 2004, Ausmees *et al.*, 2003). These proteins display an intrinsic shape that is imposed on the membrane through a membrane-binding interface. Additionally, in bacteria the cell-wall is a major shape and membrane curvature determining factor and both of these are affected by the insertion of new PGN material. An example is seen for MreB, that directs the PGN synthesis machinery to membrane areas of negative membrane curvature which in return results in straightening of the cells and flattened membranes (Ursell *et al.*, 2014). The shape of integral membrane proteins may also affect local membrane curvature. Transmembrane proteins such as the

ABC-transporter BmrA or the chemoreceptor protein TlpA from *B. subtilis* that form a conical or inverted conical shape can impose their intrinsic shape on the membrane (Strahl *et al.*, 2015, Fribourg *et al.*, 2014, MacKinnon, 2003, Aimon *et al.*, 2014). However, the contribution of these proteins to the overall membrane shape has not been yet fully explained.

1.3.3 Lipid microdomains in bacterial membranes

Although most simulation studies on membranes were performed using eukaryotic model membranes, it is very likely that the interplay, together with its resulting sorting of proteins and lipids also occurs in bacterial membranes. Bacterial membranes are also composed of a variety of differently shaped lipids and integral membrane proteins, but they lack cholesterol and most bacterial membranes do not contain sphingolipids. However, bacterial membranes can rarely contain hopanoids and squalene, the precursor of cholesterol. Hopanoids that are found in *Methylobacterium extorquens* have been shown to exhibit sterol-like properties *in vitro* that can order membranes and form microdomains (Saenz *et al.*, 2015, Saenz *et al.*, 2012). The first evidence that bacterial membranes possess structural heterogeneity *in vivo* came from fluorescent staining studies. Two studies showed that fluorescent lipophilic dyes are distributed heterogeneously in Mycobacteria and *E. coli* (Christensen *et al.*, 1999, Fishov & Woldringh, 1999). Using of the cardiolipin-specific 10-N-nonyl acridine orange dye led to the discovery of cardiolipin (CL) domains in *E. coli* and *B. subtilis* on the polar and septal regions (Nishizawa *et al.*, Mileykovskaya & Dowhan, 2000) (Kawai *et al.*, 2004). Another phospholipid that was found to form domains is phosphatidylethanolamine (PE). It can be visualised with the cyclic peptide probe Ro09-0198 (Ro) and it localises to septal membranes of exponentially growing cells of *B. subtilis* (Nishibori *et al.*, 2005)(Nishibori *et al.*, 2005) while it was found to be distributed uniformly in the membrane of *E. coli* and other Gram-negative bacteria such as Salmonella and Pseudomonas (Emoto & Umeda, 2001, Nishibori *et al.*, 2005). Furthermore, early work also demonstrated the heterogeneous localisation of several membrane proteins across the cytoplasmic membrane (Meile *et al.*, 2006). Eventually, a study undertaken by Lopez and Kolter revealed the existence of microdomains in bacteria as well as their association with certain proteins (Lopez & Kolter, 2010). One of them is FloT, a homologue of the well-studied eukaryotic lipid raft marker flotillin, that is found in most bacterial genomes and displays a punctate pattern in *B. subtilis* and *S. aureus* (Donovan & Bramkamp, 2009, Zhang *et al.*, 2005a, Neumann-Giesen *et al.*, 2004).

Interestingly, cells that are treated with zaragozic acid lose this pattern and are impaired in biofilm formation which is due to the delocalisation of another lipid raft associated protein, the kinase KinC. KinC is indirectly required for the inhibition of motility and activation of biofilm formation. Zaragozic acid is a known inhibitor of squalene synthases which suggests that squalene is required for the formation of microdomains in *B. subtilis* and *S. aureus* (Lopez & Kolter, 2010). STED microscopy allowed the determination of the assembly of FloT and another raft protein FloA into assemblies of 85 to 110 nm in *B. subtilis* which resemble flotillin microdomains in eukaryotic cells (Dempwolff *et al.*, 2016). The protein cargo of these microdomains include the protease FtsH, the secretion protein SecY and the signal peptidase SppA which all interact with FloT indicating a lipid raft scaffolding function for FloT (Bach & Bramkamp, 2013). A variety of other proteins were found in *B. subtilis* microdomains including proteins involved in cell-division, signaling and iron uptake (Bramkamp & Lopez, 2015).

1.4 *Staphylococcus aureus*

S. aureus is a gram-positive apparently spherically shaped bacterium that is mostly known for its virulence and the spread of antibiotic resistance (Foster, 2005, Veldkamp & van Strijp, 2009, de Lencastre *et al.*, 2007). Staphylococcal diseases in form of sepsis and abscess formation were first described by Alexander Ogston in 1880 and 1882 (Ogston, 1882, 1984) (Ogston, 1882, 1984). Nowadays, *S. aureus* is one of the major causes of nosocomial and community associated infections. Approximately 30 % of the healthy human population carry *S. aureus* in their nose and a skin puncture or break can allow *S. aureus* to enter tissues and cause infections (Kluytmans *et al.*, 1997, Lowy, 1998, Peacock *et al.*, 2001, Hennekinne *et al.*, 2012). *S. aureus* has a low GC content and can be distinguished from other staphylococcal species by DNase and coagulase tests (Lowy, 1998)(Madigan and Martinko, 2006).

1.4.1 *Staphylococcus aureus* as a model to study membrane protein localisation

Most of our knowledge about protein positioning comes from the rod-shaped model organisms *B. subtilis* and *E. coli*. These display a variety of well-studied geometrical cues such as cell poles, endospores (in *B. subtilis*) and the septum during cell-division along with several spatial organisers like the Min system or MreB. Less attention has

been given to membrane proteins that are not among the aforementioned. Some proteins are found to be distributed homogeneously throughout the cell periphery such as SecY and the ATPase subunit AtpC in *B. subtilis* whereas other proteins are found in clusters such as the respiratory protein CydB in *E. coli* and the NAD(P)H dehydrogenase NDH-1 in *Synechococcus elongatus* (Matsumoto and Matsuoka, 2012)(Lenn *et al.*, 2008b, Liu *et al.*, 2012). *S. aureus* is an apparently coccoid shaped bacterium that divides in three orthogonal planes by forming a septum in the middle of the cell generating two hemispherical daughter cells that are connected by a thin peripheral ring (Tzagoloff & Novick, 1977, Pinho *et al.*, 2013, Turner *et al.*, 2014, Turner *et al.*, 2010). The peripheral ring cracks due to circumferential stress and perforations leading to a cell ‘popping’ event where both daughter cells are separated within milliseconds and gain an apparent coccoid shape (Zhou *et al.*, 2015). Most localisation studies in *S. aureus* have been focused on proteins involved in septum formation rather than other processes taken place at the cell periphery.

1.5 A supramolecular structure in the membrane of *S. aureus*

Recent studies on the distribution of enzymes involved in lipid metabolism in *S. aureus* led to the discovery of a colocalised punctate pattern of PlsY and CdsA (Fig. 1.16AB) (Garcia-Lara *et al.*, 2015). The absence of PlsY causes severe morphological defects in division. Furthermore, the localisation of the septally located cell-division proteins EzrA and PBP2 were affected in PlsY-depleted cells which may explain the observed aberrant cell-division. It seemed unlikely that PlsY is the key protein for the localisation of this protein network and the focus was directed the MreBCD proteins that are known to function as spatial organisers. *S. aureus* lacks MreB and nearly nothing is known about the role of MreC and MreD. Deletion of *mreC* showed no effect on staphylococcal cells but *mreD* null mutants are affected in the localisation of PlsY and CdsA (Fig. 1.16C). Further studies revealed that MreD is also localised in a similar punctate pattern to PlsY and CdsA, giving first evidence that MreD might be the responsible localisation component (Fig. 1.16D). Furthermore, it was shown by a bacterial two-hybrid analysis that MreD, CdsA and PlsY interact with each other raising the question as to whether MreD forms a network of proteins anchoring them to certain spots within the cell or if there is another component that ‘arrives’ beforehand?

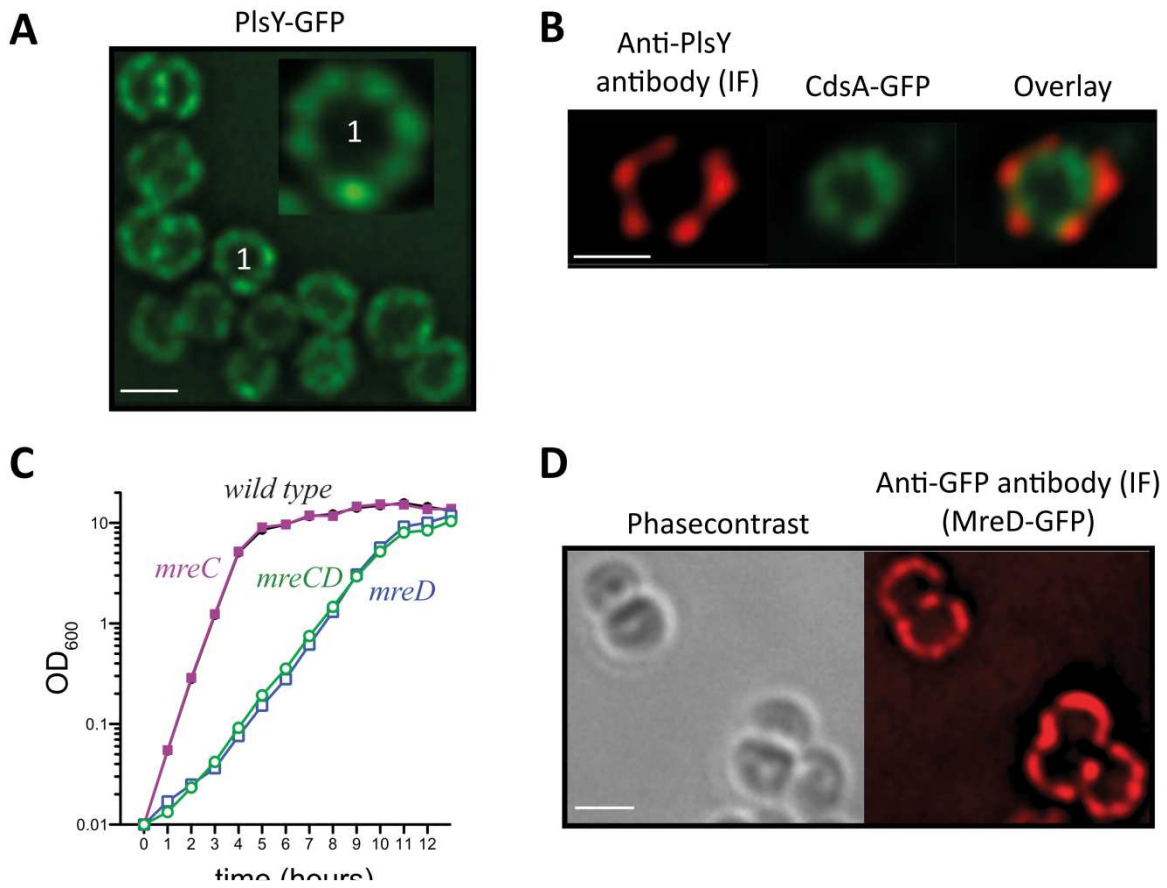


Figure 1.16 Enzymes involved in phospholipid synthesis and MreD are part of a supramolecular structure in the membrane of *S. aureus*

A, fluorescence image of PlsY-GFP in *S. aureus* SH1000. The number indicates the enlarged image of one selected cell. **B**, Immunofluorescence image of PlsY, labelled with an anti-PlsY-antibody (red) and fluorescence image of CdsA-GFP in SH1000. **C**, Growth curves of SH1000 (*wild type*), SH1000 $\Delta mreC$ (*mreC*), SH1000 $\Delta mreD$ (*mreD*) and SH1000 $\Delta mreCD$ (*mreCD*) over a time-course of 12 h. **D**, Phasecontrast and immunofluorescence image of MreD-GFP in SH1000 labelled with an anti-GFP antibody. Scale bars represent 1 μm .

1.6 Aims and summary of this study

Chapter 3: The physiological role of MreD in *S. aureus* was analysed by a functional characterisation of an *mreD* deletion mutant. This was carried by subjecting the mutant to a number of physiological stresses such as heat, anaerobic growth and varying medium composition showing that the *mreD* mutant stops growing at 42 °C. This phenotype could be restored by the addition of NaCl. A particular focus was led on the potential role of MreD on the membrane organisation of *S. aureus* which was tested by fatty acid, phospholipid and membrane fluidity analyses which demonstrated that the *mreD* mutant exhibits lower levels of CL but higher levels of PG and LPG while the fatty acid composition and membrane fluidity were not altered compared to the parental strain. Metabolome studies showed a changed metabolome between both strains and at different growth temperatures.

Chapter 4: This study also aimed to investigate the localisation of membrane proteins and specifically proteins involved in phospholipid biosynthesis in *S. aureus* using a range of fluorescent tags such as GFP, eYFP, mCherry and SNAP along with colocalisation studies. Integrative plasmids were used to express the protein of interest fused to a fluorescent marker under its native promoter. Their analysis confirmed the localisation pattern of PlsY using SNAP/eYFP/meYFP tags and further identified that its localisation is dose-dependent. Other proteins such as CydB, FloT, PlsC, PgsA, MprF and Cls2 also exhibit a non-uniform distribution in the membrane of *Staphylococcus aureus* while SecY was distributed homogeneously. A key element in this study was to investigate the underlying mechanism that determines membrane protein localisation using a variety of deletion mutants to analyse the impact of specific membrane components such as cardiolipin, lysinylated-phosphatidylglycerolphosphate and wall teichoic acids. In addition fluorescent strains were subjected to a number of inhibitors affecting fatty acid synthesis, membrane potential, Z-ring formation and the formation of squalene-dependent lipid rafts showing that FtsZ plays a crucial role in the positioning of PlsY.

Chapter 5: A novel FRET-based protein-protein interaction system was developed to confirm the interaction of PlsY with CdsA, MreD and to identify interactions with other membrane proteins demonstrating an interaction of PlsY with CdsA, MreD, PgsA and CydB, but not with SecY and MscL.

Chapter 6: To understand the basis of the punctate patterned distribution of membrane proteins, MreD-eYFP was expressed in *E. coli* where MreD was found to be distributed in patches within the membrane. As a next step, reconstitution experiments of purified MreD, labelled with Cy2, into liposomes were attempted to ask the question as to whether MreD can form the observed punctate pattern intrinsically?

Chapter 2: Materials and Methods

2.1 Media

2.1.1 Tryptic Soy Broth (TSB)

TSB (Oxoid) 30 g l⁻¹

2.1.2 Brain Heart Infusion (BHI)

BHI (Oxoid) 37 g l⁻¹

1.5 % (w/v) Oxoid agar was added to make BHI agar.

2.1.3 Lysogeny broth (LB)

Tryptone (Oxoid) 10 g l⁻¹

Yeast extract (Oxoid) 5 g l⁻¹

NaCl 10 g l⁻¹

2.1.4 LK medium

Tryptone (Oxoid) 10 g l⁻¹

Yeast extract (Oxoid) 5 g l⁻¹

KCl 7 g l⁻¹

1.5 % (w/v) Oxoid agar was added to make LK agar.

2.1.5 Lipase activity agar plates

Baird-Parker agar base (Oxoid) 63 g l⁻¹

Egg Yolk with potassium tellurite (VWR Prolabo) 50 ml l⁻¹

The Egg Yolk was added to the autoclaved Baird-Parker Agar Base after cooling down to 50-60 °C.

2.1.6 Chemically defined medium (CDM)

The recipe for CDM is based on (Hussain *et al.*, 1991).

Table 2.1 Chemically defined medium composition

Solution 1 – Dissolved in 700 ml of distilled water adjusted to pH 7.2			
Na ₂ HPO ₄ x 2H ₂ O	7 g	L-Lysine	0.1 g
KH ₂ PO ₄	3 g	L-Leucine	0.15 g
L-Aspartic Acid	0.15 g	L-Methionine	0.1 g
L-Alanine	0.1 g	L-Phenylalanine	0.1 g
L-Arginine	0.1 g	L-Proline	0.15 g
L-Cysteine	0.05 g	L-Serine	0.1 g
Glycine	0.1 g	L-Threonine	0.15 g
L-Glutamic Acid	0.15 g	L-Tryptophan	0.1 g
L-Histidine	0.1 g	L-Tyrosine	0.1 g
L-Isoleucine	0.15 g	L-Valine	0.15 g
Solution 2 – Dissolved in 140 ml of distilled water (1000x)			
Biotin	0.02 g	Pyridoxal	0.8 g
Nicotinic Acid	0.4 g	Pyridoxamine di-HCl	0.8 g
D-Panthenic Acid	0.4 g	Riboflavin	0.4 g
Thiamine HCl	0.4 g		
Solution 3 – Dissolved in 400 ml of 0.1 M HCl			
Adenine Hemisulphate	0.16 g	Guanine HCl	0.16 g
Solution 4 – Dissolved in 500 ml of 0.1 M HCl			
CaCl ₂ x 6H ₂ O	0.5 g	(NH ₄) ₂ Fe(SO ₄) ₂ x 6H ₂ O	0.3 g
Solution 5 – Dissolved in 800 ml of distilled water			
MgSO ₄ x 7H ₂ O	4 g		

Solutions 1, 3 and 4 were mixed and autoclaved together. Whereas solution 2 was filter sterilised (0.2 µm pore size) and added after cooling. Solution 5 was autoclaved separately and added after cooling.

The solutions were mixed at the following ratio:

Solution 1	Solution 2	Solution 3	Solution 4	Solution 5
7	0.0001	0.5	0.1	1

Before use, the medium was supplemented with different amounts of glucose.

2.2 Antibiotics

Antibiotics used in this study were prepared as filter-sterilised (0.2 µm pore size) stock solutions and stored at -20 °C (Tab. 1.2). For the use in liquid media, antibiotic stock solutions were added just before use whereas for the use in agar plates, stock solutions were added to media cooled below 50 °C.

Table 2.2 Antibiotics

Antibiotic	Stock conc. (mg ml ⁻¹)	<i>S. aureus</i> working conc. (µg ml ⁻¹)	<i>E. coli</i> working conc. (µg ml ⁻¹)	Dissolved in:
Ampicillin (Amp)	100	-	100	H ₂ O
Chloramphenicol (Cm)	30	30	-	100 % ethanol (v/v)
Erythromycin (Ery)	5	5	-	100 % ethanol (v/v)
Kanamycin (Kan)	50	50	50	H ₂ O
Lincomycin (Lin)	25	25	-	50 % ethanol (v/v)
Neomycin (Neo)	50	50	-	H ₂ O
Spectinomycin (Spe)	50	-	50	H ₂ O
Tetracycline (Tet)	5	5	-	100 % ethanol (v/v)

2.3 Bacterial strains and plasmids

2.3.1 *Staphylococcus aureus* strains

Table 2.3 *S. aureus* strains used in this study

Strain	Relevant genotype/Markers	Reference
RN4220	Restriction deficient transformation recipient	(Kreiswirth <i>et al.</i> , 1983)
SH1000	Derived from 8325-4, <i>rsbU</i> ⁺	(Horsburgh <i>et al.</i> , 2002)
Newman	<i>saeRS</i> constitutively expressed by SaeS T53C substitution	(Baba <i>et al.</i> , 2008, Duthie, 1952)
NewHG	Derived from Newman, repaired <i>saeS</i>	(Herbert <i>et al.</i> , 2010)
SH1000 <i>secY-gfp</i> (SJF1927)	<i>P_{secY}:secY-gfp P_{spac}:secY</i> ; Ery ^R , Lin ^R	(Garcia-Lara <i>et al.</i> , 2015)
SH1000 <i>plsY-gfp</i> (SJF1754)	<i>P_{plsY}:plsY-gfp P_{spac}:plsY</i> ; Ery ^R , Lin ^R	(Garcia-Lara <i>et al.</i> , 2015)
SH1000 <i>mreC-gfp</i> (SJF1923)	<i>P_{mreC}:mreC-gfp P_{spac}:mreC</i> ; Ery ^R , Lin ^R	(Garcia-Lara <i>et al.</i> , 2015)
SH1000 <i>mreD-gfp</i> (SJF1925)	<i>P_{mreD}:mreD-gfp P_{spac}:mreD</i> ; Ery ^R , Lin ^R	(Garcia-Lara <i>et al.</i> , 2015)
SH1000 <i>ezrA-gfp</i> (SJF2095)	<i>P_{ezrA}:ezrA-gfp P_{spac}:ezrA</i> ; Ery ^R , Lin ^R	(Steele <i>et al.</i> , 2011)
SH1000 <i>plsY-eyfp</i> (SJF4395)	<i>P_{plsY}:plsY-eyfp P_{spac}:plsY</i> ; Ery ^R , Lin ^R	This study
SH1000 <i>plsY-meyfp</i> (SJF4775)	<i>P_{plsY}:plsY-meyfp P_{spac}:plsY</i> ; Ery ^R , Lin ^R	This study
SH1000 <i>plsC-eyfp</i> (SJF4416)	<i>P_{plsC}:plsC-eyfp P_{spac}:plsC</i> ; Ery ^R , Lin ^R	This study
SH1000 <i>pgsA-eyfp</i> (SJF4414)	<i>P_{pgsA}:pgsA-eyfp P_{spac}:pgsA</i> ; Ery ^R , Lin ^R	This study
SH1000 <i>mprF-eyfp</i> (SJF4510)	<i>P_{mprF}:mprF-eyfp P_{spac}:mprF</i> ; Ery ^R , Lin ^R	This study
SH1000 <i>cydB-eyfp</i>	<i>P_{cydAB}:cydAcydB-eyfp P_{spac}:cydB</i> ;	This study

(SJF4547)	Ery ^R , Lin ^R	
SH1000 <i>floT-eyfp</i> (SJF4543)	<i>P_{floT}:floT-eyfp P_{spac}:floT</i> ; Ery ^R , Lin ^R	This study
SH1000 <i>floT-eyfp</i> + pGL485 (SJF4795)	<i>P_{floT}:floT-eyfp P_{spac}:floT</i> , pGL485; Ery ^R , Lin ^R , Cm ^R	This study
JE2 NE258	<i>Cls2::Tn</i> ; from NARSA transposon library, transposon inserted at the beginning of <i>cls2</i> ; Ery ^R	(Fey <i>et al.</i> , 2013)
RN4220 <i>plsY-gfp</i> (tet) (SJF4793)	<i>P_{plsY}:plsY-gfp P_{spac}:plsY</i> ; Tet ^R	This study
SH1000 <i>plsY-gfp</i> (tet) (SJF4794)	<i>P_{plsY}:plsY-gfp P_{spac}:plsY</i> ; Tet ^R	This study
RN4220 <i>plsY-SNAP</i> (SJF4783)	<i>P_{plsY}:plsY-SNAP P_{spac}:plsY</i> ; Tet ^R	This study
SH1000 <i>plsY-</i> <i>SNAP/secY-gfp</i> (SJF4727)	<i>P_{plsY}:plsY-SNAP P_{spac}:plsY</i> , <i>P_{secY}:secY-gfp P_{spac}:secY</i> ; Ery ^R , Lin ^R , Tet ^R	This study
RN4220 <i>pgsA-SNAP</i> (SJF4782)	<i>P_{pgsA}:pgsA-SNAP P_{spac}:pgsA</i> ; Tet ^R	This study
RN4220 <i>cydB-SNAP</i> (SJF4781)	<i>P_{cydB}:cydB-SNAP P_{spac}:cydB</i> ; Tet ^R	This study
SH1000 pGL485 (SJF2991)	pGL485; Cm ^R	(Cooper <i>et al.</i> , 2009)
SH1000 pGL621 (SJF3193)	pGL621; Cm ^R	(Garcia-Lara <i>et al.</i> , 2015)
SH1000 <i>mreD::kan</i> (SJF2976)	<i>mreD::kan</i> ; Kan ^R	(Garcia-Lara <i>et al.</i> , 2015)
SH1000 <i>mreD::kan</i> pGL621 (SJF3208)	<i>mreD::kan</i> pGL621 (<i>mreD</i>); Kan ^R , Cm ^R	(Garcia-Lara <i>et al.</i> , 2015)
SH1000 <i>mreD::kan</i> pGL631	<i>mreD::kan</i> pGL631 (<i>mreCD</i>); Kan ^R , Cm ^R	(Garcia-Lara <i>et al.</i> , 2015)
SH1000 <i>mreD::kan</i> pGL485 (SJF3210)	<i>mreD::kan</i> pGL485 ; Kan ^R , Cm ^R	(Garcia-Lara <i>et al.</i> , 2015)
SH1000 <i>mreCD::kan</i> (SJF2841)	<i>mreCD::kan</i> ; Kan ^R	(Garcia-Lara <i>et al.</i> , 2015)
SH1000 <i>mreCD::kan</i> pGL621 (SJF3202)	<i>mreCD::kan</i> pGL621 (<i>mreD</i>); Kan ^R , Cm ^R	(Garcia-Lara <i>et al.</i> , 2015)
SH1000 <i>mreCD::kan</i> pGL631 (SJF3205)	<i>mreCD::kan</i> pGL631 (<i>mreCD</i>); Kan ^R , Cm ^R	(Garcia-Lara <i>et al.</i> , 2015)
SH1000 <i>mreCD::kan</i> pGL485 (SJF3206)	<i>mreCD::kan</i> pGL485 ; Kan ^R , Cm ^R	(Garcia-Lara <i>et al.</i> , 2015)
Newman <i>mreD::kan</i> (SJF4705)	<i>mreD::kan</i> ; Kan ^R	This study
NewHG <i>mreD::kan</i>	<i>mreD::kan</i> ; Kan ^R	This study

(SJF4708)		
JE2 NE858	<i>mreD::Tn</i> ; from NARSA transposon library, transposon inserted at the beginning of <i>mreD</i> ; Ery ^R	(Fey <i>et al.</i> , 2013)
SH1000 <i>mreD::Tn</i>	<i>mreD::Tn</i> , transduced from JE NE858; Ery ^R	This study
SH1000 <i>mreD::kan</i> <i>ftsZ-eyfp</i> (SJF4711)	<i>mreD::kan</i> , pCQ11- <i>ftsZ-eyfp</i> ; Kan ^R , IPTG-inducible expression of <i>ftsZ-eyfp</i> ; Ery ^R , Lin ^R	This study
SH1000 <i>ftsZ-eyfp</i> (SJF4704)	pCQ11- <i>ftsZ-eyfp</i> , IPTG-inducible expression of <i>ftsZ-eyfp</i> ; Ery ^R , Lin ^R	(Dr.C.Walther, unpublished)
SH1000 <i>PmreCD-mreD</i> (SJF4651)	<i>geh::PmreCD-mreD</i> ; Tet ^R ,	This study
SH1000 <i>mreD::kan</i> <i>PmreCD-mreD</i> (SJF4650)	<i>mreD::kan</i> , <i>geh::PmreCD-mreD</i> ; Kan ^R , Tet ^R ,	This study
SH1000 pWhiteWalker10 (SJF4772)	pWhiteWalker10, IPTG-inducible expression of <i>plsY-gfp</i> , Ery ^R , Lin ^R	This study
SA113 <i>tarO::ermB</i> pRB- <i>tarO</i> (SJF4147)	<i>tarO::ermB</i> ; pRB- <i>tarO</i> , constitutive expression of <i>tarO</i> , Ery ^R , Cm ^R	(Peschel <i>et al.</i> , 2001)
SA113 <i>mprF::ermB</i> (SJF2207)	<i>mprF::ermB</i> ; Ery ^R	(Weidenmaier <i>et al.</i> , 2005)
SH1000 <i>mprF::ermB</i> <i>plsY-gfp</i> (SJF4767)	<i>mprF::ermB</i> , <i>PplsY:plsY-gfp</i> <i>Pspac:plsY</i> ; Ery ^R , Lin ^R , Tet ^R	This study
SH1000 Δ <i>cls1/2</i> (SJF4289)	<i>cls1::cat</i> , <i>cls2::tet</i> ; Tet ^R , Cm ^R	(Ohniwa <i>et al.</i> , 2013)
SH1000 Δ <i>cls1/2</i> <i>plsY-gfp</i> (SJF4353)	<i>cls1::cat</i> , <i>cls2::tet</i> , <i>PplsY:plsY-gfp</i> <i>Pspac:plsY</i> ; Ery ^R , Lin ^R , Tet ^R , Cm ^R	This study
SH1000 Δ <i>tarO</i> <i>plsY-gfp</i> (SJF4713)	<i>tarO::ermB</i> , <i>PplsY:plsY-gfp</i> <i>Pspac:plsY</i> ; Ery ^R , Tet ^R	This study
RN4220 <i>pgsA-mRFPmars1</i> (SJF4791)	<i>PpgsA:pgsA-mRFPmars1</i> ; <i>Pspac:pgsA</i> ; Tet ^R	This study
RN4220 <i>cdsA-mCherry</i> (SJF4792)	<i>PcdsA:cdsA-mCherry</i> ; <i>Pspac:cdsA</i> ; Tet ^R	This study
RN4220 <i>cdsA-mRFPmars1</i> (SJF4790)	<i>PcdsA:cdsA-mRFPmars1</i> ; <i>Pspac:cdsA</i> ; Tet ^R	This study
RN4220 + pWhiteWalker1 (SJF4752)	IPTG-inducible expression of <i>gfp</i> and <i>mCherry</i> ; Ery ^R , Lin ^R	(Garcia-Lara <i>et al.</i> , 2015)
RN4220 + pWhiteWalker2 (SJF4753)	IPTG-inducible expression of <i>mCherry-gfp</i> fused in tandem; Ery ^R , Lin ^R	(Garcia-Lara <i>et al.</i> , 2015)
RN4220 + pWhiteWalker3 (SJF4754)	IPTG-inducible expression of <i>mreD-mCherry</i> and <i>plsY-gfp</i> ; Ery ^R , Lin ^R	(Garcia-Lara <i>et al.</i> , 2015)
RN4220 +	IPTG-inducible expression of <i>cdsA-</i>	(Garcia-Lara <i>et al.</i> ,

pWhiteWalker4 (SJF4755)	<i>mCherry</i> and <i>plsY-gfp</i> ; Ery ^R , Lin ^R	2015)
RN4220 + pWhiteWalker7 (SJF4756)	IPTG-inducible expression of <i>cydB-mCherry</i> and <i>plsY-gfp</i> ; Ery ^R , Lin ^R	This study
RN4220 + pWhiteWalker8 (SJF4757)	IPTG-inducible expression of <i>pgsA-mCherry</i> and <i>plsY-gfp</i> ; Ery ^R , Lin ^R	This study
RN4220 + pWhiteWalker10 (SJF4758)	IPTG-inducible expression of <i>plsY-gfp</i> ; Ery ^R , Lin ^R	(Garcia-Lara <i>et al.</i> , 2015)
RN4220 + pWhiteWalker11 (SJF4759)	IPTG-inducible expression of <i>mreD-mCherry</i> and <i>plsY-gfp</i> ; Ery ^R , Lin ^R	This study
RN4220 + pWhiteWalker12 (SJF4760)	IPTG-inducible expression of <i>secY-mCherry</i> and <i>plsY-gfp</i> ; Ery ^R , Lin ^R	(Garcia-Lara <i>et al.</i> , 2015)
RN4220 + pWhiteWalker13 (SJF4761)	IPTG-inducible expression of <i>mscL-mCherry</i> and <i>plsY-gfp</i> ; Ery ^R , Lin ^R	(Garcia-Lara <i>et al.</i> , 2015)
RN4220 + pWhiteWalker14 (SJF4762)	IPTG-inducible expression of <i>fmnP-mCherry</i> and <i>plsY-gfp</i> ; Ery ^R , Lin ^R	This study
RN4220 + pWhiteWalker15 (SJF4763)	IPTG-inducible expression of <i>alsT-mCherry</i> and <i>plsY-gfp</i> ; Ery ^R , Lin ^R	This study
RN4220 + pWhiteWalker16 (SJF4764)	IPTG-inducible expression of <i>mntP-mCherry</i> and <i>plsY-gfp</i> ; Ery ^R , Lin ^R	This study
RN4220 + pWhiteWalker17 (SJF4765)	IPTG-inducible expression of <i>lspA-mCherry</i> and <i>plsY-gfp</i> ; Ery ^R , Lin ^R	This study
RN4220 + pWhiteWalker18 (SJF4766)	IPTG-inducible expression of the first transmembrane domain of PlsY fused to <i>mCherry</i> and <i>plsY-gfp</i> ; Ery ^R , Lin ^R	This study

Ery^R, erythromycin resistance; Lin^R, lincomycin resistance; Tet^R, tetracycline resistance, Cm^R, chloramphenicol resistance; Kan^R, kanamycin resistance.

2.3.2 *Escherichia coli* strains

Table 2.4 *E. coli* strains used in this study

Strain	Relevant genotype/Markers	Reference
Top10	<i>F</i> - <i>mcrA</i> Δ (<i>mrr-hsdRMS-mcrBC</i>) Φ 80 <i>lacZ</i> Δ M15 Δ <i>lacX74</i> <i>recA1</i> <i>araD139</i> Δ (<i>araleu</i>)7697 <i>galU</i> <i>galK</i> <i>rpsL</i> (<i>Str R</i>) <i>endA1</i> <i>nupG</i>	Invitrogen
NEB5 α	<i>fhuA2</i> Δ (<i>argF-lacZ</i>)U169 <i>phoA</i> <i>glnV44</i> Φ 80 Δ (<i>lacZ</i>) M15 <i>gyrA96</i> <i>recA1</i> <i>relA1</i> <i>endA1</i> <i>thi-1</i> <i>hsdR17</i>	New England Biolabs
BL21 (DE)	B F ⁻ <i>ompT</i> <i>gal</i> <i>dcm</i> <i>lon</i> <i>hsdS_B</i> (<i>r_B⁻m_B⁻) λ(DE3 [<i>lacI</i> <i>lacUV5-T7p07</i> <i>ind1</i> <i>sam7</i> <i>nin5</i>]) [<i>malB</i>⁺]_{K-12}(λ^S)</i>	New England Biolabs
C43 (DE3)	Derivative of BL21 (DE3), contains mutations in the <i>lacUV</i> promoter driving the expression of T7 RNA polymerase	(Wagner <i>et al.</i> , 2008)
C43 (DE3) pWALDO- <i>mreD-eyfp</i> (SJF4397)	pWALDO- <i>mreD-eyfp</i> ; IPTG-inducible expression of <i>mreD-eyfp</i> ; Kan ^R	This study
C43 (DE3) pWALDO- <i>mreD-6-eyfp</i> (SJF4398)	pWALDO- <i>mreD-6-eyfp</i> ; IPTG-inducible expression of <i>mreD-6-eyfp</i> ; Kan ^R	This study
C43 (DE3) pWALDO- <i>eyfp-11-mreD</i> (SJF4552)	pWALDO- <i>eyfp-11-mreD</i> ; IPTG-inducible expression of <i>eyfp-11-mreD</i> ; Kan ^R	This study
C43 (DE3) pWALDO- <i>murJ-gfp</i> (SJF4399)	pWALDO- <i>murJ-gfp</i> ; IPTG-inducible expression of <i>murJ-gfp</i> ; Kan ^R	This study

Kan^R, kanamycin resistance.

2.3.3 Plasmids

Table 2.5 Plasmids used in this study

Strain	Relevant genotype/Markers	Reference
pAISH1	Tet ^R derivative of pMUTIN4 which contains a promoterless transcriptional <i>lacZ</i> fusion, non-replicating in gram-positive bacteria; Amp ^R (<i>E. coli</i>), Tet ^R (<i>S. aureus</i>)	(Aish., 2003) (Vagner <i>et al.</i> , 1998)
pGL485	Cm ^R derivative of <i>E. coli-S. aureus</i> shuttle vector pMJ8426, containing <i>E. coli lacI</i> gene under the control of the constitutive <i>Bacillus licheniformis</i> penicillinase promoter (<i>Ppcn</i>); Spec ^R (<i>E. coli</i>), Cm ^R (<i>S. aureus</i>)	(Cooper <i>et al.</i> , 2009)
pKASBAR	Hybrid vector of pCL84 and pUC18 for integration into <i>S. aureus</i> lipase gene (<i>geh</i>) encoding the attP integration site of L54a phage; Amp ^R (<i>E. coli</i>), Tet ^R (<i>S. aureus</i>)	(Bottomley <i>et al.</i> , 2014)

pKASBAR- <i>ezrA-eyfp</i>	pKASBAR-Kan ^R ; expression of <i>ezrA-eyfp</i> under the putative promoter of <i>ezrA</i> ; Amp ^R (<i>E. coli</i>), Kan ^R (<i>S. aureus</i>)	Dr.K.Wacnik, unpublished
pKASBAR- <i>ezrA-meyfp</i>	pKASBAR-Kan ^R ; expression of <i>ezrA-meyfp</i> under the putative promoter of <i>ezrA</i> ; meYFP is the monomeric version of eYFP containing A206K; Amp ^R (<i>E. coli</i>), Kan ^R (<i>S. aureus</i>)	Dr.K.Wacnik, unpublished
pKASBAR- <i>ezrA-SNAP</i>	pKASBAR-Kan ^R ; expression of <i>ezrA-SNAP</i> under the putative promoter of <i>ezrA</i> ; Amp ^R (<i>E. coli</i>), Kan ^R (<i>S. aureus</i>)	Dr.K.Wacnik, unpublished
pCQ11-FtsZ-SNAP	<i>E. coli-S. aureus</i> shuttle vector containing the <i>lacI</i> gene and <i>ftsZ-snap</i> under control of <i>Pspac</i> ; Amp ^R (<i>E. coli</i>), Ery ^R , Lin ^R (<i>S. aureus</i>)	Dr.F.Grein, unpublished
pMUTIN- <i>gfp</i> ⁺	Contains a <i>Pspac</i> promoter regulating the expression of <i>gfp</i> ⁺ , non-replicating in gram positive bacteria; Amp ^R (<i>E. coli</i>), Ery ^R , Lin ^R (<i>S. aureus</i>)	(Kaltwasser <i>et al.</i> , 2002)
pYL112Δ19	Expression of integrase, required for integration of pKASBAR, Cm ^R (<i>S.aureus</i>)	(Luong & Lee, 2007)
pMUTIN- <i>secY-gfp</i>	Contains a translational fusion of <i>secY-gfp</i> , non-replicating in gram positive bacteria; Amp ^R (<i>E. coli</i>), Ery ^R , Lin ^R (<i>S. aureus</i>)	(Garcia-Lara <i>et al.</i> , 2015)
pMUTIN- <i>plsY-gfp</i>	Contains a translational fusion of <i>plsY-gfp</i> , non-replicating in gram positive bacteria; Amp ^R (<i>E. coli</i>), Ery ^R , Lin ^R (<i>S. aureus</i>)	This study
pMUTIN- <i>plsY-eyfp</i>	Contains a translational fusion of <i>plsY-eyfp</i> , non-replicating in gram positive bacteria; Amp ^R (<i>E. coli</i>), Ery ^R , Lin ^R (<i>S. aureus</i>)	This study
pAISH- <i>plsY-eyfp</i>	Contains a translational fusion of <i>plsY-eyfp</i> , non-replicating in gram positive bacteria; Amp ^R (<i>E. coli</i>), Tet ^R (<i>S. aureus</i>)	This study
pAISH- <i>plsY-mCherry</i>	Contains a translational fusion of <i>plsY-mCherry</i> , non-replicating in gram positive bacteria; Amp ^R (<i>E. coli</i>), Tet ^R (<i>S. aureus</i>)	This study
pAISH- <i>plsY-SNAP</i>	Contains a translational fusion of <i>plsY-SNAP</i> , non-replicating in gram positive bacteria; Amp ^R (<i>E. coli</i>), Tet ^R (<i>S. aureus</i>)	This study
pMUTIN- <i>pgsA-eyfp</i>	Contains a translational fusion of <i>pgsA-eyfp</i> , non-replicating in gram positive bacteria; Amp ^R (<i>E. coli</i>), Ery ^R , Lin ^R (<i>S. aureus</i>)	This study

pAISH- <i>pgsA-SNAP</i>	Contains a translational fusion of <i>pgsA-SNAP</i> , non-replicating in gram positive bacteria; Amp ^R (<i>E. coli</i>), Tet ^R (<i>S. aureus</i>)	This study
pAISH- <i>pgsA-mRFPmars</i>	Contains a translational fusion of <i>pgsA-mRFPmars</i> , non-replicating in gram positive bacteria; Amp ^R (<i>E. coli</i>), Tet ^R (<i>S. aureus</i>)	This study
pMUTIN- <i>plsC-eyfp</i>	Contains a translational fusion of <i>plsC-eyfp</i> , non-replicating in gram positive bacteria; Amp ^R (<i>E. coli</i>), Ery ^R , Lin ^R (<i>S. aureus</i>)	This study
pMUTIN- <i>mprF-eyfp</i>	Contains a translational fusion of <i>mprF-eyfp</i> , non-replicating in gram positive bacteria; Amp ^R (<i>E. coli</i>), Ery ^R , Lin ^R (<i>S. aureus</i>)	This study
pKASBAR- <i>cls2-eyfp</i>	pKASBAR-Kan ^R ; expression of <i>cls2-eyfp</i> under the putative promoter of <i>cls2</i> ; Amp ^R (<i>E. coli</i>), Kan ^R (<i>S. aureus</i>)	This study
pMUTIN- <i>cydB-eyfp</i>	Contains a translational fusion of <i>cydB-eyfp</i> , non-replicating in gram positive bacteria; Amp ^R (<i>E. coli</i>), Ery ^R , Lin ^R (<i>S. aureus</i>)	This study
pAISH- <i>cydB-SNAP</i>	Contains a translational fusion of <i>cydB-SNAP</i> , non-replicating in gram positive bacteria; Amp ^R (<i>E. coli</i>), Tet ^R (<i>S. aureus</i>)	This study
pMUTIN- <i>floT-eyfp</i>	Contains a translational fusion of <i>floT-eyfp</i> , non-replicating in gram positive bacteria; Amp ^R (<i>E. coli</i>), Ery ^R , Lin ^R (<i>S. aureus</i>)	This study
pAISH- <i>cdsA-mCherry</i>	Contains a translational fusion of <i>cdsA-mCherry</i> , non-replicating in gram positive bacteria; Amp ^R (<i>E. coli</i>), Tet ^R (<i>S. aureus</i>)	This study
pAISH- <i>cdsA-mRFPmars</i>	Contains a translational fusion of <i>cdsA-mRFPmars</i> , non-replicating in gram positive bacteria; Amp ^R (<i>E. coli</i>), Tet ^R (<i>S. aureus</i>)	This study
pKASBAR- <i>mreD</i>	pKASBAR-Kan ^R ; expression of <i>mreD</i> under the putative promoter of <i>mreCD</i> ; Amp ^R (<i>E. coli</i>), Kan ^R (<i>S. aureus</i>)	This study
pWALDO- <i>gfp</i>	Overexpression vector, IPTG-inducible expression of an insert tagged to <i>gfp</i> and under the control of a T7 RNA polymerase promoter, expresses <i>lacI</i> ; Kan ^R (<i>E. coli</i>)	(Waldo <i>et al.</i> , 1999)
pWALDO- <i>mreD-eyfp</i>	IPTG-inducible expression of <i>mreD-eyfp</i> ; The C-terminus of <i>eyfp</i> contains a TEV protease restriction site and a 8x His tag; Kan ^R	This study

pWALDO- <i>mreD-6-eyfp</i>	IPTG-inducible expression of <i>mreD-6-eyfp</i> ; The C-terminus of <i>eyfp</i> contains a TEV protease restriction site and a 8x His tag; Kan ^R	This study
pWALDO- <i>eyfp-11-mreD</i>	IPTG-inducible expression of <i>eyfp-11-mreD</i> ; The C-terminus of <i>mreD</i> contains a TEV protease restriction site and a 8x His tag; Kan ^R	This study
pWALDO- <i>murJ-gfp</i>	IPTG-inducible expression of <i>murJ-gfp</i> ; The C-terminus of <i>gfp</i> contains a TEV protease restriction site and a 8x His tag Kan ^R	Dr.D.Roper, unpublished
pCQ11- <i>gfp</i>	<i>E. coli-S. aureus</i> shuttle vector containing the <i>lacI</i> gene and <i>gfp</i> under control of <i>Pspac</i> ; Amp ^R (<i>E. coli</i>), Ery ^R , Lin ^R (<i>S. aureus</i>)	(Garcia-Lara <i>et al.</i> , 2015)
pWhiteWalker1	Derivative from pCQ11- <i>gfp</i> , contains <i>gfp</i> and <i>mCherry</i> under control of <i>Pspac</i> ; Amp ^R (<i>E. coli</i>), Ery ^R , Lin ^R (<i>S. aureus</i>)	(Garcia-Lara <i>et al.</i> , 2015)
pWhiteWalker2	Derivative from pCQ11- <i>gfp</i> , contains <i>gfp</i> fused <i>mCherry</i> under control of <i>Pspac</i> ; Amp ^R (<i>E. coli</i>), Ery ^R , Lin ^R (<i>S. aureus</i>)	(Garcia-Lara <i>et al.</i> , 2015)
pWhiteWalker10	Derivative from pCQ11- <i>gfp</i> , contains <i>plsY</i> fused to <i>gfp</i> under control of <i>Pspac</i> ; Amp ^R (<i>E. coli</i>), Ery ^R , Lin ^R (<i>S. aureus</i>)	(Garcia-Lara <i>et al.</i> , 2015)
pWhiteWalker3	Derivative from pCQ11- <i>gfp</i> , contains <i>plsY</i> fused to <i>gfp</i> and <i>mreD</i> fused to <i>mCherry</i> under control of <i>Pspac</i> ; Amp ^R (<i>E. coli</i>), Ery ^R , Lin ^R (<i>S. aureus</i>)	(Garcia-Lara <i>et al.</i> , 2015)
pWhiteWalker4	Derivative from pCQ11- <i>gfp</i> , contains <i>plsY</i> fused to <i>gfp</i> and <i>cdsA</i> fused to <i>mCherry</i> under control of <i>Pspac</i> ; Amp ^R (<i>E. coli</i>), Ery ^R , Lin ^R (<i>S. aureus</i>)	(Garcia-Lara <i>et al.</i> , 2015)
pWhiteWalker7	Derivative from pCQ11- <i>gfp</i> , contains <i>plsY</i> fused to <i>gfp</i> and <i>cydB</i> fused to <i>mCherry</i> under control of <i>Pspac</i> ; Amp ^R (<i>E. coli</i>), Ery ^R , Lin ^R (<i>S. aureus</i>)	(Garcia-Lara <i>et al.</i> , 2015)
pWhiteWalker8	Derivative from pCQ11- <i>gfp</i> , contains <i>plsY</i> fused to <i>gfp</i> and <i>pgsA</i> fused to <i>mCherry</i> under control of <i>Pspac</i> ; Amp ^R (<i>E. coli</i>), Ery ^R , Lin ^R (<i>S. aureus</i>)	This study
pWhiteWalker11	Derivative from pCQ11- <i>gfp</i> , contains <i>plsY</i> fused to <i>gfp</i> and <i>pheP</i> fused to <i>mCherry</i> under control of <i>Pspac</i> ; Amp ^R (<i>E. coli</i>), Ery ^R , Lin ^R (<i>S. aureus</i>)	This study
pWhiteWalker12	Derivative from pCQ11- <i>gfp</i> , contains <i>plsY</i> fused to <i>gfp</i> and <i>secY</i> fused to <i>mCherry</i> under control of <i>Pspac</i> ; Amp ^R (<i>E. coli</i>), Ery ^R , Lin ^R (<i>S. aureus</i>)	(Garcia-Lara <i>et al.</i> , 2015)

pWhiteWalker13	Derivative from pCQ11- <i>gfp</i> , contains <i>plsY</i> fused to <i>gfp</i> and <i>mscL</i> fused to <i>mCherry</i> under control of <i>Pspac</i> ; Amp ^R (<i>E. coli</i>), Ery ^R , Lin ^R (<i>S. aureus</i>)	(Garcia-Lara <i>et al.</i> , 2015)
pWhiteWalker14	Derivative from pCQ11- <i>gfp</i> , contains <i>plsY</i> fused to <i>gfp</i> and <i>fmnP</i> fused to <i>mCherry</i> under control of <i>Pspac</i> ; Amp ^R (<i>E. coli</i>), Ery ^R , Lin ^R (<i>S. aureus</i>)	This study
pWhiteWalker15	Derivative from pCQ11- <i>gfp</i> , contains <i>plsY</i> fused to <i>gfp</i> and <i>alsT</i> fused to <i>mCherry</i> under control of <i>Pspac</i> ; Amp ^R (<i>E. coli</i>), Ery ^R , Lin ^R (<i>S. aureus</i>)	This study
pWhiteWalker16	Derivative from pCQ11- <i>gfp</i> , contains <i>plsY</i> fused to <i>gfp</i> and <i>mntP</i> fused to <i>mCherry</i> under control of <i>Pspac</i> ; Amp ^R (<i>E. coli</i>), Ery ^R , Lin ^R (<i>S. aureus</i>)	This study
pWhiteWalker17	Derivative from pCQ11- <i>gfp</i> , contains <i>plsY</i> fused to <i>gfp</i> and <i>lspA</i> fused to <i>mCherry</i> under control of <i>Pspac</i> ; Amp ^R (<i>E. coli</i>), Ery ^R , Lin ^R (<i>S. aureus</i>)	This study
pWhiteWalker18	Derivative from pCQ11- <i>gfp</i> , contains <i>plsY</i> fused to <i>gfp</i> and the first transmembrane domain of PlsY fused to <i>mCherry</i> under control of <i>Pspac</i> ; Amp ^R (<i>E. coli</i>), Ery ^R , Lin ^R (<i>S. aureus</i>)	This study

Ery^R, erythromycin resistance; Lin^R, lincomycin resistance; Tet^R, tetracycline resistance, Cm^R, chloramphenicol resistance; Kan^R, kanamycin resistance; Spec^R, spectinomycin resistance; Amp^R, ampicillin resistance.

2.4 Buffers and solutions

All buffers and solutions were prepared with dH₂O, sterilised if required and stored at RT unless otherwise stated.

2.4.1 Phage buffer

MgSO ₄	1 mM
CaCl ₂	4 mM
Tris-HCl pH 7.8	50 mM
NaCl	0.6 % (w/v)
Gelatin	0.1 % (w/v)

2.4.2 Phosphate buffered saline (PBS)

NaCl	8 g l ⁻¹
Na ₂ HPO ₄	1.4 g l ⁻¹
KCl	0.2 g l ⁻¹
KH ₂ PO ₄	0.2 g l ⁻¹

The pH was adjusted to 7.4 with NaOH.

2.4.3 TAE (50x)

Tris	242 g l ⁻¹
Glacial acetic acid	5.7% (v/v)
Na ₂ EDTA pH 8.0	0.05 M

50 x stock solution was diluted 1:50 with dH₂O to produce a 1x TAE working solution.

2.4.4 Tris buffered saline (TBS)

Tris-HCl pH 7.5	50 mM
NaCl	0.1 M

EDTA-free protease inhibitor cocktail (Sigma) was added and dissolved in TBS according to the manufacturer's instructions if required.

2.4.5 QIAGEN buffers

2.4.5.1 QIAGEN Buffer P1

Tris-HCl pH 8	50 mM
EDTA	10 mM
RNase A	100 pg/ml

2.4.5.2 QIAGEN Buffer P2

NaOH	200 mM
SDS	1 % (w/v)

2.4.5.3 QIAGEN Buffer P3

Potassium acetate pH 5.5	3.0 M
--------------------------	-------

2.4.5.4 QIAGEN Buffer EB

Tris-HCl pH 8.5 10 mM

2.4.5.5 QIAGEN QBT

NaCl 0.75 M
MOPS adjusted to pH 7.0 with NaOH 50 mM
Isopropanol 15 % (v/v)
Triton X-100 0.15 % (v/v)

2.4.5.6 QIAGEN QC

NaCl 1 M
MOPS adjusted to pH 7.0 with NaOH 50 mM
Isopropanol 15 % (v/v)

2.4.5.7 QIAGEN QF

NaCl 1.25 M
MOPS adjusted to pH 8.5 with NaOH 50 mM
Isopropanol 15 % (v/v)

2.4.5.8 Buffer N3

Guanidine-HCl 4.2 M
Potassium acetate 0.9 M
Adjusted to pH 4.8 with HCl

2.4.5.9 Buffer PB

Guanidine-HCl 5 M
Isopropanol 30 % (v/v)

2.4.5.10 Buffer PE

Tris adjusted to pH 7.5 with HCl 10 mM
Ethanol 80 % (v/v)

2.4.5.11 Buffer QG

Tris adjusted to pH 6.6 with HCl	20 mM
Guanidine thiocyanate	5.5 M

2.4.5.12 Buffers AL, AW1 and AW2

Supplied in the Qiagen DNeasy Blood & Tissue Kit; details not provided.

2.4.6 Fixative

2.4.6.1 Preparation of 16 % (w/v) p-formaldehyde

2.4.6.1.1 100 mM sodium phosphate buffer

Na ₂ HPO ₄	9.36 g l ⁻¹
NaH ₂ PO ₄	3.96 g l ⁻¹

The pH was adjusted to 7 and the solution was filtered using a filter (0.2 µm pore size).

2.4.6.1.2 16 % (w/v) p-formaldehyde

8 g of p-formaldehyde were added to 40 ml of the sodium phosphate buffer followed by heating to 60 °C whilst stirring for 20 min. NaOH (≥ 5 M) were added until the solution clears. Finally the total volume was increased to 50 ml using sodium phosphate buffer.

2.4.7 SDS-PAGE solutions

2.4.7.1 SDS-PAGE reservoir buffer (10 x)

Glycine	144 g l ⁻¹
Tris	30.3 g l ⁻¹
SDS	10 g l ⁻¹

Before use, the reservoir buffer (10 x) was diluted 1:10 with dH₂O to the working solution.

2.4.7.2 SDS-PAGE loading buffer (5x)

Tris-HCl pH 6.8	250 mM
SDS	10 % (w/v)
Bromophenol blue	0.5 % (w/v)
Glycerol	50 % (v/v)
DTT	0.5 M

2.4.7.3 Coomassie Blue stain

Coomassie Blue	0.1 % (w/v)
Methanol	5 % (v/v)
Glacial acetic acid	10 % (v/v)

2.4.7.4 Coomassie destain

Methanol	5 % (v/v)
Glacial acetic acid	10 % (v/v)

2.4.8 Western blotting solutions

2.4.8.1 Blotting buffer

Tris	2.4 g l ⁻¹
Glycine	11.26 g l ⁻¹
Ethanol	20 % (v/v)

2.4.8.2 TBST (20x)

Tris	48.4 g l ⁻¹
NaCl	20 g l ⁻¹
Tween-20	2 % (v/v)

The pH was adjusted to 7.6. Before use, the TBST stock solution (20 x) was diluted 1:20 with dH₂O to give a working solution of 1 x TBST.

2.4.8.3 Blocking buffer

5 % (w/v) dried skimmed milk powder was dissolved in 1x TBST.

2.4.9 HiTrap purification buffers

2.4.9.1 0.1M Sodium phosphate buffer

NaH ₂ PO ₄ (1 M)	31.6 ml
Na ₂ HPO ₄ (1 M)	68.4 ml
dH ₂ O	900 ml

The pH was adjusted to 7.2 and the buffer was autoclaved.

2.4.9.2 START Buffer

Sodium phosphate buffer (0.1 M)	200 ml
NaCl	0.5 M
dH ₂ O	up to 1l

2.4.9.3 Elution Buffer

START buffer containing: Imidazole	0.5 M
------------------------------------	-------

2.5 Chemicals and enzymes

All chemicals and enzymes in this study were purchased from Sigma-Aldrich, Fisher Scientific, MP Biomedicals, Roche and Avanti Polar lipids unless otherwise stated. All restriction enzymes, T4 ligase, DNase, Gibson Assembly mix, PCR master mixes and appropriate buffers for DNA manipulation were purchased from New England Biolabs, Roche or Thermo-Fisher Scientific. Storage conditions and concentrations of stock solutions are listed in Table 2.6.

Table 2.6 Stock solutions used in this study

Chemical name	Storage	Concentration	Solvent
Ammonium persulfate (APS)	-20 °C	10 % (w/v)	dH ₂ O
Carbonyl cyanide 3-chlorophenylhydrazone (CCCP)	-20 °C	25 mM	DMSO
Cerulein	-20 °C	100 mM	DMSO
DNase	-20 °C	10 mg ml ⁻¹	dH ₂ O
HADA (hydroxycoumarin 3-amino-D-alanine; Department of Chemistry, University of Sheffield)	-20 °C in the dark	100 mM	DMSO
Isopropyl β -D-1-thiogalactopyranoside (IPTG)	-20 °C	1 M	dH ₂ O

Lysostaphin	-20 °C	5 mg ml ⁻¹	20 mM sodium acetate pH 5.2
PC190723 (Calbiochem)	-20 °C	10 mg ml ⁻¹	DMSO
RNase	-20 °C	2 mg ml ⁻¹	dH ₂ O
SNAP-Cell TMR-Star	-20 °C in the dark	1 mM	DMSO
Vancomycin, BODIPY® FL Conjugate	-20 °C in the dark	1 mg ml ⁻¹	DMSO
Zaragozic acid	-20 °C	100 µM	100 % Ethanol (v/v)

2.6 Centrifugation

The following centrifuges were used for harvesting cells or precipitated material. Centrifugation was carried out at room temperature unless otherwise stated.

Table 2.7 Centrifuges used in this study

Centrifuge name		Largest load capacity	Max speed
Eppendorf microcentrifuge 5418		18 x 1.5-2 ml	14,000 rpm (16,783 x g)
Sigma centrifuge 4K15C		16 x 50 ml	5,100 rpm (5,525 x g)
Avanti High Speed J25I centrifuge	JA-25.50	6 x 50 ml	25,000 rpm (75,600 x g)
	JA-10.5	6 x 400 ml	10,000 rpm (18,500 x g)
Beckman Ultracentrifuge	70.1Ti	12 x 13.5 ml	70,000 rpm (450,000 x g)
	50.2 Ti	12 x 39 ml	50,000 rpm (302,000 x g)
Optima LE-80k	SW 41	6 x 13.2 ml	41,000 rpm, (288,000 x g)

2.7 Determining bacterial cell density

2.7.1 Spectrophotometric measurement (OD₆₀₀)

The density of cell cultures was determined by measuring the optical density at a wavelength 600 nm using a Jenway 6100 spectrophotometer or a Biochrom WPA Biowave DNA spectrophotometer. Cultures were diluted to 1:10 or 1:20 in sterile appropriate medium where necessary.

2.7.2 Direct cell counts (CFU ml⁻¹)

Viable cells were estimated by direct cell counts. Thus, serial dilutions of cultures were prepared and 20 µl of dilutions 10⁻⁴ to 10⁻⁷ were spotted onto BHI agar. The number of colony forming units per 1 ml of cell culture (CFU ml⁻¹) was estimated based on visible colonies after 18 h incubation at 37 °C.

2.8 DNA purification techniques

2.8.1 Genomic DNA extraction

Genomic DNA extraction was performed using buffers provided by Qiagen Dneasy Blood & Tissue Kit (Hilden, Germany).

1 - 2 ml ml of an overnight culture of *Staphylococcus aureus* was harvested by centrifugation and resuspended in 180 μ l dH₂O. 5 μ l lysostaphin (5 mg/ml) was added and the resuspension was incubated for approximately one hour at 37 °C. Subsequently, 25 μ l proteinase K and 200 μ l buffer AL (without ethanol) were added and incubated for 30 min at 65 °C. The resuspension was mixed with 200 μ l of a 100 % ethanol (v/v) solution, vortexed and transferred to a mini spin column. The column was centrifuged for 1 min at 10,000 rpm. The column was subsequently washed with 500 μ l buffer AW1 (+ ethanol) for 1 min and 10,000 rpm, followed by an additional washing step with 500 μ l buffer AW2 (+ ethanol) for 3 min and 10,000 rpm. The column was transferred to a fresh microcentrifuge tube and 100 - 200 μ l buffer AE were added on top of the membrane. The tube was incubated at RT for 1 min the column. Finally, genomic DNA was eluted by centrifugation for 1 min at 10,000 rpm.

2.8.2 Small scale plasmid purification

Plasmid extraction of up 10 ml bacterial cultures were performed according to the manufacturer's instruction of QIAGEN Plasmid Miniprep Kit provided by Qiagen (Hilden, Germany).

1 ml of overnight culture was harvested and the pellet was resuspended in 250 μ l pre-chilled resuspension buffer (P1). If plasmids were purified from a staphylococcal culture, 8 μ l lysostaphin (5 mg/ml) was added, followed by incubation for 1 h at 37 °C. The resuspension was mixed with 250 μ l lysis buffer (P2) and inverted 5 - 7 times. 350 μ l neutralization buffer (N3) were added subsequently and the resuspension was inverted 5 - 7 times, followed by centrifugation for 10 min at 14,000 rpm at RT. The supernatant was transferred by pipetting to the provided spin column. The column was centrifuged for 1 min and washed two times with 500 μ l wash buffer. One additional centrifugation step was performed to remove residual ethanol. The column was transferred to a fresh tube and eluted with 30 - 50 μ l elution buffer (EB) that was

pipetted directly onto the column membrane. The column was incubated for 2 min at RT and DNA was eluted by centrifugation for 2 min at 12000 rpm.

2.8.3 Large scale plasmid purification

Plasmid extraction of 50 to 100 ml cultures were performed according to the manufacturer's instruction of HiSpeed plasmid midi kit provided by Qiagen (Hilden, Germany).

50 ml (high-copy plasmids) or 100 ml (low-copy plasmids) of an overnight cell culture was harvested by centrifugation at 5,000 x g for 10 min at 4 °C. Subsequently, 6 ml P2-buffer was added and mixed gently by inverting 6 - 7 times followed by incubation for 5 min at room temperature. The suspension was neutralised by addition of 6 ml P3 buffer and inverted for 6 - 7 times. The lysate was poured into the barrel of the QIAfilter Cartridge and incubated at room temperature for 10 min. In the mean time, a HiSpeed Midi Tip was equilibrated by adding 4 ml QBT buffer and allowed to empty by gravity flow. The lysate was filtered into the pre-equilibrated Tip through the QIAfilter using a plunger. After the lysate entered the resin by gravity flow, the Tip was washed with 20 ml QC buffer and eluted with 5 ml QF buffer into a 15 ml Falcon tube. The eluate was mixed with 3.5 ml 100 % Isopropanol (v/v) and incubated at RT for 5 min. Subsequently, the eluate/isopropanol mix was pushed through a QIAprecipitator using a plunger and washed with 2 ml 70 % ethanol (v/v). To remove residual ethanol, air was pressed through the QIAprecipitator several times and the nozzle was dried with absorbent paper. The QIAprecipitator was eluted with 1 ml TE buffer and the eluate was afterwards transferred back to the same filter and eluted again.

2.8.4 DNA Gel extraction and PCR purification

Gel extraction of agarose slices containing the desired DNA fragment and PCR products were purified according to the protocol of Wizard® SV Gel and PCR Clean-Up System (Promega, Madison, United States of America).

Agarose slices were pre-weighed in a 1.5 ml microcentrifuge tube and dissolved in 10 µl of membrane binding solution per 10 mg at 60 °C. PCR products were mixed with the same volume of membrane binding solution. The DNA solution was loaded onto a SV minicolumn and incubated for 1 min. The column was subsequently centrifuged for 1 min with 13,000 rpm followed by two washing steps using 700 and 500 µl membrane wash solution for 1 and 5 min at 13,000 rpm, respectively. Another

centrifugation step for 1 min was performed to remove residual ethanol. The column was finally eluted using 20 - 50 μ l nuclease-free water. The column was pre-incubated at RT for 2 - 5 min if low elution volumes were used.

2.8.5 Ethanol precipitation of DNA

DNA precipitation was carried out by mixing DNA with 0.1 volumes of 3 M sodium acetate (pH 5.2) and 3 volumes of chilled 100 % ethanol (v/v). The mixture was incubated at -80 °C for 2 h and the precipitated DNA was recovered by centrifugation at 14,000 rpm for 15 min. The supernatant was carefully removed and the pellet was washed with 1 ml 70 % ethanol (v/v). Finally, the pellet was air dried and resuspended in 10-20 μ l of pre-warmed nuclease-free dH₂O.

2.9 *In vitro* DNA manipulation techniques

2.9.1 *In vitro* DNA manipulation techniques

Primers used in this study for PCR amplification were designed as short synthetic oligonucleotides (20-40 nucleotides) that were designed according to the genomic DNA sequence of *S. aureus* 8325-4.

The predicted annealing temperature and risk of formation of secondary structural elements were identified using Clone Manager Professional Suite 8 (Sci-Ed Software, Denver, United States of America). Primers were manufactured by Eurofins Genomics (Ebersberg, Germany) and stored at -20 °C in sdH₂O as 100 pmol/ μ l stock solutions or 50 pmol/ μ l working solutions (see Tab.2.8).

2.9.2 PCR amplification

2.9.2.1 Phusion polymerase

Cloning procedures require accurate DNA sequences that were amplified using Phusion High-Fidelity PCR Master Mix with HF buffer (New England Biolabs). Unless otherwise stated, a total PCR mix volume of 50 μ l was used:

Phusion High-Fidelity PCR Master Mix (2x)	25 μ l
Forward primer (50 μ M)	2 μ l
Reverse primer (50 μ M)	2 μ l
Template DNA	50-100 ng
sdH ₂ O	up to 50 μ l

Table 2.8 Primers used in this study

Primer	Sequence (5'-> 3')	Application	Reference
Outward_gfp	GCATCACCTTCACCTCTCCACTGAC	PCR confirmation of chromosomal <i>gfp</i> integrations	This study
Outward_eyfp	GACTTGAAGAAGTCGTGCTGC	PCR confirmation of chromosomal <i>eyfp</i> integrations	This study
Outward_mCherry	ACATATGCTTTACTGCCATAC	PCR confirmation of chromosomal <i>mCherry</i> integrations	This study
Outward_SNAP	CGCTGGTGCCTTTACCCAGCAG	PCR confirmation of chromosomal <i>SNAP</i> integrations	This study
Outward_mRFPmars1	ACTGTTACAACACCACCATC	PCR confirmation of chromosomal <i>mRFPmars1</i> integrations	This study
Outward_ermB1	CACTCCTGAAGTGATTACATC	PCR confirmation of the presence of erythromycin resistance cassette <i>ermB</i>	This study
Outward_ermB2	CATCAAGCAATGAAACACGCC	PCR confirmation of the presence of erythromycin resistance cassette <i>ermB</i>	This study
5'FW14	<u>CTAGAGTCGAGGGTACATGAATCAGGAAGTTAAAAACAAAATATTTTC</u>	Amplification of <i>mprF</i> for Gibson Assembly of pMUTIN- <i>mprF-eyfp</i>	This study
3'FW14	<u>GAACCTGATTTGTGACGTATTACACGC</u>	Amplification of <i>mprF</i> for Gibson Assembly of pMUTIN- <i>mprF-eyfp</i>	This study
5'FW15	<u>CGTCACAAATCAGGTTTCAGGTTTCAGGTATG</u>	Amplification of <i>eyfp</i> for Gibson Assembly of pMUTIN- <i>mprF-eyfp</i>	This study
3'FW117	<u>ATTAGGCGGGCTGCATTACTTGTACAGCTCGTC</u>	Amplification of <i>eyfp</i> for Gibson Assembly of pMUTIN- <i>mprF-eyfp</i> , pMUTIN- <i>plsC-eyfp</i> , pMUTIN- <i>pgsA-eyfp</i> , pMUTIN- <i>floT-eyfp</i> , pMUTIN- <i>plsY-eyfp</i>	This study
5'FW10	<u>CTAGAGTCGAGGGTACATGTATTTCAGTGATTAGTAAGATTTTG</u>	Amplification of <i>eyfp</i> for Gibson Assembly of pMUTIN- <i>plsC-eyfp</i>	This study
3'FW10	<u>CTGAACCTAAACTTTTTTACAATTTTCATGCAATTC</u>	Amplification of <i>eyfp</i> for Gibson Assembly of pMUTIN- <i>plsC-eyfp</i>	This study
5'FW11	<u>GTAAAAAGTTTAGGTTTCAGGTTTCAGGTATG</u>	Amplification of <i>eyfp</i> for Gibson Assembly of pMUTIN- <i>plsC-eyfp</i>	This study

Upstream	CTCGATTCTATTAACAAGGG	Binds within the NARSA library transposon, verification of NARSA library mutants	(Fey <i>et al.</i> , 2013)
Buster	GCTTTTTCTAAATGTTTTTTAAGTAAATCAAGTAC	Binds within the NARSA library transposon, verification of NARSA library mutants	(Fey <i>et al.</i> , 2013)
5'FW16	CTAGAGTCGAGGGTACATGAATATTCCGAACCAGATT <u>AC</u>	Amplification of <i>pgsA</i> for Gibson Assembly of pMUTIN- <i>pgsA-eyfp</i>	This study
3'FW16	GAACCTGATTTTTGTTTTAAAAACATCTCTACCTTTAT <u>AAAAG</u>	Amplification of <i>pgsA</i> for Gibson Assembly of pMUTIN- <i>pgsA-eyfp</i>	This study
5'FW17	TTTAAACAAAATCAGGTTTCAGGTTTCAGGTATG	Amplification of <i>eyfp</i> for Gibson Assembly of pMUTIN- <i>pgsA-eyfp</i>	This study
5'FW07	GACTTTACAAATACATACAGGGG	Verification of $\Delta spa::tet$ and $\Delta spa::kan$	This study
3'FW07	GGTTTGGATAAAAATGATATCTATCG	Verification of $\Delta spa::tet$ and $\Delta spa::kan$	This study
5'FW08	CAATTAATAAGATATACTACTCG	Verification of $\Delta cls2::tet$	This study
3'FW08	GTTGCATTAAGTTTACTCCTC	Verification of $\Delta cls2::tet$	This study
5'FW09	CCTTTTTTTGCCCCGGCAAACATAAATTGTCATGATAT <u>TAAATTG</u>	Amplification of <i>cls2</i> and <i>tfor</i> for Gibson Assembly of pKASBAR	This study
3'FW09	GAACCTGAACCTGAGGATAAGATAGGTGACAATAATT <u>GTG</u>	Amplification of <i>pgsA</i> for Gibson Assembly of pMUTIN- <i>pgsA-eyfp</i>	This study
5'FW18	CCATATATTTATTGCTGGAACG	Sequencing of <i>mprF</i>	This study
3'FW18	CAGATGTATGCATTTCAATCG	Sequencing of <i>mprF</i>	This study
Inward_pgsA	GTGAGAAATGAGGATGTATA	PCR confirmation of chromosomal C-terminal fusions to <i>pgsA</i>	This study
Inward_plsC	TTCAGACTATCTTGTCTAG	PCR confirmation of chromosomal C-terminal fusions to <i>plsC</i>	This study
Inward_mprF	CAGAAATAATTAGAATTGATGTG	PCR confirmation of chromosomal C-terminal fusions to <i>mprF</i>	This study
Inward_plsY	CGCCTCCTGCAAACGTACGTTCCG	PCR confirmation of chromosomal C-terminal fusions to <i>plsY</i>	This study
5'FW19	CTAGAGTCGAGGGTACATGTTTAGTTTAAGTTTTATC <u>GTAATAG</u>	Amplification of <i>floT</i> for Gibson Assembly of pMUTIN- <i>floT-eyfp</i>	This study
3'FW19	GAACCTGAATGTTTCAGGTGACTCATC	Amplification of <i>floT</i> for Gibson Assembly of pMUTIN- <i>floT-eyfp</i>	This study

5'FW20	<u>CCTGAACATTCAGGTTTCAGGTTTCAGGTATG</u>	Amplification of <i>eyfp</i> for Gibson Assembly of pMUTIN- <i>floT-eyfp</i>	This study
5'FW21	<u>CTAGAGTCGAGGGTACATGATTTATGCATTTATAGGTATAACAG</u>	Amplification of <i>cydB</i> for Gibson Assembly of pMUTIN- <i>cydB-eyfp</i>	This study
3'FW21	<u>GAACCTGATGATTTCTTTCTTCAACATATTC</u>	Amplification of <i>cydB</i> for Gibson Assembly of pMUTIN- <i>cydB-eyfp</i>	This study
5'FW22	<u>A AAAGAAATCATCAGGTTTCAGGTTTCAGGTATG</u>	Amplification of <i>eyfp</i> for Gibson Assembly of pMUTIN- <i>cydB-eyfp</i>	This study
5'FW23	<u>GTGAGCGCTCACAATTAATGATGATAATCGTCATGTTAC</u>	Amplification of <i>plsY</i> for Gibson Assembly of pAISH- <i>plsY-mCherry</i> , pAISH- <i>plsY-gfp</i>	This study
3'FW23	<u>TGAACCTGACATCCATTTTATTTTAGGTTCTTC</u>	Amplification of <i>plsY</i> for Gibson Assembly of pAISH- <i>plsY-mCherry</i>	This study
5'FW24	<u>AAATGGATGTCAGGTTTCAGGTTTCAGGTATGGGCGTTAGTAAAGGC</u>	Amplification of <i>mCherry</i> for Gibson Assembly of pAISH- <i>plsY-mCherry</i>	This study
3'FW24	<u>GTATTACATATGTAAGATTTTAAAGATCTTTTATATAATTCATCCATGC</u>	Amplification of <i>mCherry</i> for Gibson Assembly of pAISH- <i>plsY-mCherry</i> , pAISH- <i>pgsA-mCherry</i> , pAISH- <i>cdsA-mCherry</i>	This study
5'FW25	<u>GTGAGCGCTCACAATTAATGAATATTCGGAACCAGATTAC</u>	Amplification of <i>pgsA</i> for Gibson Assembly of pAISH- <i>plsY-mCherry</i>	This study
3'FW25	<u>TGAACCTGATTTTTGTTTAAAAACATCTCTACCTTTATAAAAG</u>	Amplification of <i>pgsA</i> for Gibson Assembly of pAISH- <i>plsY-mCherry</i>	This study
5'FW26	<u>TTAAACAAAAATCAGGTTTCAGGTTTCAGGTATGGGCGTTAGTAAAGGC</u>	Amplification of <i>mCherry</i> for Gibson Assembly of pAISH- <i>plsY-mCherry</i>	This study
5'FW33	<u>TAACTTTAAGAAGGAGACAGGAGGAGACAATATCATGGTGAGCAAAGGTGAAG</u>	Amplification of <i>eyfp</i> for Gibson Assembly of pWALDO- <i>eyfp-8-mreD</i>	This study
3'FW33	<u>CTGGAAGTACAGGTTTTCTTTATACAGTTCATCCATACCC</u>	Amplification of <i>eyfp</i> for Gibson Assembly of pWALDO- <i>eyfp-8-mreD</i>	This study
5'FW34	<u>ACTGTATAAAGAAAACCTGTACTTCCAGGGTAGCGGTAGCGGTAGCGGTAGCGGTATGCGTACCCTGTATTATTTT</u>	Amplification of <i>mreD</i> for Gibson Assembly of pWALDO- <i>eyfp-8-mreD</i>	This study
3'FW34	<u>TGGTGATGATGATGGGCCGCACACTGACGACGTTTCAATATC</u>	Amplification of <i>mreD</i> for Gibson Assembly of pWALDO- <i>eyfp-8-mreD</i>	This study

5'FW36	TCCATAAGCCCTTGTAATATTG	Sequencing of <i>qoxA</i>	This study
3'FW36	GCCATTGTAATCATCCAGTTAC	Sequencing of <i>qoxA</i>	This study
3'FW43	CCTGAACCTGAACCTGACATCCATTTTATTTTAGGTTCTTC	Amplification of <i>plsY</i> for Gibson Assembly of pAISH- <i>plsY-gfp</i>	This study
5'FW44	AAATGGATGTCAGGTTTCAGGTTTCAGGTATGGCTAGCA AAGGAGAAG	Amplification of <i>gfp</i> for Gibson Assembly of pAISH- <i>plsY-gfp</i>	This study
3'FW44	GTATTACATATGTAAGATTTTATTTGTAGAGCTCATCCATG	Amplification of <i>gfp</i> for Gibson Assembly of pAISH- <i>plsY-gfp</i>	This study
5'FW45	GTGAGCGCTCACAATTAATGAAAGTTAGAACGCTGAC	Amplification of <i>cdsA</i> for Gibson Assembly of pAISH- <i>cdsA-mCherry</i>	This study
3'FW45	CCTGAACCTGAACCTGAAGATTGTATTAATAAAATATTTAATAATGG	Amplification of <i>cdsA</i> for Gibson Assembly of pAISH- <i>cdsA-mCherry</i>	This study
5'FW46	AATACAATCTTCAGGTTTCAGGTTTCAGGTTTCAGGTTCA GGTTCAGGTATG	Amplification of <i>mCherry</i> for Gibson Assembly of pAISH- <i>cdsA-mCherry</i>	This study
5'FW47	GTGAGCGCTCACAATTAATGAAAGTTAGAACGCTGAC	Amplification of <i>cdsA</i> for Gibson Assembly of pAISH- <i>cdsA-mRFPmars1</i>	This study
3'FW47	CCTGAACCTGAACCTGAAGATTGTATTAATAAAATATTTAATAATGGTAACAC	Amplification of <i>cdsA</i> for Gibson Assembly of pAISH- <i>cdsA-mRFPmars1</i>	This study
5'FW48	AATACAATCTTCAGGTTTCAGGTTTCAGGTATGGCATCATCAGAAGATGTTATTAAG	Amplification of <i>mRFPmars1</i> for Gibson Assembly of pAISH- <i>cdsA-mRFPmars1</i>	This study
3'FW48	GTATTACATATGTAAGATTTATTGGGATCCTGCACCTGTTG	Amplification of <i>mRFPmars1</i> for Gibson Assembly of pAISH- <i>cdsA-mRFPmars1</i> , pAISH- <i>pgsA-mRFPmars1</i>	This study
5'FW49	GTGAGCGCTCACAATTAATGAATATTC CGAACCAGAT TAC	Amplification of <i>pgsA</i> for Gibson Assembly of pAISH- <i>pgsA-mRFPmars1</i>	This study
3'FW49	CCTGAACCTGAACCTGATTTTTGTTTAAAAACATCTCTACCTTTATAAAAAG	Amplification of <i>pgsA</i> for Gibson Assembly of pAISH- <i>pgsA-mRFPmars1</i>	This study
5'FW50	TTAAACAAAAATCAGGTTTCAGGTTTCAGGTATGGCATCATCAGAAGATGTTATTAAG	Amplification of <i>mRFPmars1</i> for Gibson Assembly of pAISH- <i>pgsA-mRFPmars1</i>	This study
Inward_tarO	AAGCTATAAGATATACGTAG	PCR confirmation of $\Delta tarO::ermB$	This study
5'FW65	AAAGAATTCTTAGGAGGAAATTATTGAATGATTTATGCATTTATAGG	Amplification of <i>cydB</i> for construction of pWhiteWalker 7 (<i>cydB-mCherry+plsY-gfp</i>), extends <i>cydB</i> with an EcoRI restriction enzyme site (<i>italic</i>)	This study

3'FW65	TTTGCTAGCTGATTTCTTTCCTTCAACATA	Amplification of <i>cydB</i> for construction of pWhiteWalker 7 (<i>cydB-mCherry+plsY-gfp</i>), extends <i>cydB</i> with an <i>NheI</i> restriction enzyme site (<i>italic</i>)	This study
5'FW66	AAAGAATTCTTAGGAGGAAATTATTGAATGAATATTC CGAACCAGATTACGG	Amplification of <i>pgsA</i> for construction of pWhiteWalker 8 (<i>pgsA-mCherry+plsY-gfp</i>), extends <i>pgsA</i> with an <i>EcoRI</i> restriction enzyme site (<i>italic</i>)	This study
3'FW66	AAAGCTAGCTTTTTGTTTAAAAACATCTCTACC	Amplification of <i>pgsA</i> for construction of pWhiteWalker 8 (<i>pgsA-mCherry+plsY-gfp</i>), extends <i>pgsA</i> with an <i>NheI</i> restriction enzyme site (<i>italic</i>)	This study
5'FW73	CAATTAAGCTTGATATCGAGGAGGATGAACCGGTATG	Amplification of <i>plsY-gfp</i> for Gibson Assembly of pWhiteWalker 10 (<i>plsY-gfp</i>)	This study
3'FW73	ATTATGCATTTAGAATAGGGGCGCGCCCTATTTGTAT	Amplification of <i>plsY-gfp</i> for Gibson Assembly of pWhiteWalker 10 (<i>plsY-gfp</i>)	This study
5'FW74	CAATTAAGCTTGATATCGGAATTCTTAGGAGGAAATT ATTGAATGGAAGATAATAAATGAACCG	Amplification of <i>pheP</i> for Gibson Assembly of pWhiteWalker 11 (<i>pheP-mCherry+plsY-gfp</i>)	This study
3'FW74	ATGCTGCCGCTGCCGCCTTTTTGATTGTCATAATCGT GTG	Amplification of <i>pheP</i> for Gibson Assembly of pWhiteWalker 11 (<i>pheP-mCherry+plsY-gfp</i>)	This study
5'FW75	CAATTAAGCTTGATATCGGAATTCTTAGGAGGAAATT ATTGAATGATTCAAACCCTTGTGAAC	Amplification of <i>secY</i> for Gibson Assembly of pWhiteWalker 12 (<i>secY-mCherry+plsY-gfp</i>)	This study
3'FW75	ATGCTGCCGCTGCCGCCCTCTACCACCAAAGCCTTTAT ATTC	Amplification of <i>secY</i> for Gibson Assembly of pWhiteWalker 12 (<i>secY-mCherry+plsY-gfp</i>)	This study
5'FW76	CAATTAAGCTTGATATCGGAATTCTTAGGAGGAAATT ATTGAATGTTAAAAGAATTCAAAGAGTTCCG	Amplification of <i>mscL</i> for Gibson Assembly of pWhiteWalker 13 (<i>mscL-mCherry+plsY-gfp</i>)	This study
3'FW76	ATGCTGCCGCTGCCGCCTTTTTCTCACGTAATAAAT CTCTG	Amplification of <i>mscL</i> for Gibson Assembly of pWhiteWalker 13 (<i>mscL-mCherry+plsY-gfp</i>)	This study
5'FW77	CAATTAAGCTTGATATCGGAATTCTTAGGAGGAAATT ATTGAATGCAACAAAATAAACGTCTTATC	Amplification of <i>fmnP</i> for Gibson Assembly of pWhiteWalker 14 (<i>fmnP-mCherry+plsY-gfp</i>)	This study
3'FW77	ATGCTGCCGCTGCCGCCAATTCTTTTCAAGAAATTCG CAAG	Amplification of <i>fmnP</i> for Gibson Assembly of pWhiteWalker 14 (<i>fmnP-mCherry+plsY-gfp</i>)	This study
5'FW78	CAATTAAGCTTGATATCGGAATTCTTAGGAGGAAATT ATTGATTGAAAGATTCGATAGTTAATACC	Amplification of <i>alsT</i> for Gibson Assembly of pWhiteWalker 15 (<i>alsT-mCherry+plsY-gfp</i>)	This study

3'FW78	<u>ATGCTGCCGCTGCCGCC</u> <u>TTTATCAGAGTTCTTATATT</u> <u>TGTTAGC</u>	Amplification of <i>alsT</i> for Gibson Assembly of pWhiteWalker 15 (<i>alsT-mCherry+plsY-gfp</i>)	This study
5'FW79	<u>CAATTAAGCTTGATATCGGAATTCTTAGGAGGAAATT</u> <u>ATTGAATGTTAGAGTTTGTGCAACATTTATTTAC</u>	Amplification of <i>mntB</i> for Gibson Assembly of pWhiteWalker 16(<i>mntB-mCherry+plsY-gfp</i>)	This study
3'FW79	<u>ATGCTGCCGCTGCCGCC</u> <u>TGTTAAACTTCCTCGTTTCT</u> <u>TTC</u>	Amplification of <i>mntB</i> for Gibson Assembly of pWhiteWalker 16(<i>mntB-mCherry+plsY-gfp</i>)	This study
5'FW80	<u>CAATTAAGCTTGATATCGGAATTCTTAGGAGGAAATT</u> <u>ATTGAATGCACAAAAAATATTTTATTTGGC</u>	Amplification of <i>lspA</i> for Gibson Assembly of pWhiteWalker 17(<i>lspA-mCherry+plsY-gfp</i>)	This study
3'FW80	<u>ATGCTGCCGCTGCCGCC</u> <u>CTTAACCTCCTTCTCCTTTT</u> <u>TATTG</u>	Amplification of <i>lspA</i> for Gibson Assembly of pWhiteWalker 17(<i>lspA-mCherry+plsY-gfp</i>)	This study
5'FW81-1	<u>CTTATCGGCGCTTTC</u> <u>CCAAGTGGATTCGTAATTGGAA</u> <u>AATTATTTTTCAAAA</u> <u>AGCGGCAGCGGCAGCATGGGCG</u>	Amplification of <i>mCherry</i> . Extends <i>mCherry</i> with the nucleotide sequence encoding for the first transmembrane domain of PlsY	This study
5'FW81	<u>CAATTAAGCTTGATATCGAGGAGGAAATTATTGAATG</u> <u>ATAATCGTCATGTTACTACTAAGTTATCTTATCGGCG</u> <u>CTTTCCCA</u>	Amplification of <i>TMD(plsY)-mCherry</i> for Gibson Assembly of pWhiteWalker 18(<i>TMD(plsY)-Cherry+plsY-gfp</i>)	This study
3'FW81	<u>G TTCATCCTCCTAATCAAGATCTTTTATATAATTCAT</u> <u>CCATGCCACC</u>	Amplification of <i>TMD(plsY)-mCherry</i> for Gibson Assembly of pWhiteWalker 18(<i>TMD(plsY)-Cherry+plsY-gfp</i>)	This study
5'FW82	AGATGCGCAAGATCAAGACA	Sequencing of <i>qoxB</i>	This study
3'FW82	CGCACCATTACCCATTGTG	Sequencing of <i>qoxB</i>	This study
5'FW83	GGGCAACTGCCGGTATCGCG	Sequencing of <i>qoxB</i>	This study
3'FW83	GCCAAGCTTATTTAATTCGCC	Sequencing of <i>qoxB</i>	This study
5'FW84	GCAGAAACTGAAGCTAGATT	Sequencing of <i>qoxCD</i>	This study
3'FW84	GCTAACAAAAGTGTTAGCTGGTT	Sequencing of <i>qoxCD</i>	This study
5'FW85	<u>GTGAGCGCTCACAATTA</u> <u>ATGATGATAATCGTCATGTT</u> <u>AC</u>	Amplification of <i>plsY</i> for Gibson Assembly of pMUTIN- <i>plsY-SNAP</i>	This study
3'FW85	<u>CCTGAACCTGAACCTGACATCCATTTTATTTTAGGTT</u> <u>CTTC</u>	Amplification of <i>plsY</i> for Gibson Assembly of pMUTIN- <i>plsY-SNAP</i>	This study
5'FW86	<u>AAATGGATGTCAGGTT</u> <u>CAGGTT</u> <u>CAGGTATGGACAAAG</u> <u>ATTGCGAAATG</u>	Amplification of <i>SNAP</i> for Gibson Assembly of pMUTIN- <i>plsY-SNAP</i>	This study

3'FW86	<u>GTATTACATATGTAAGATTTTCATCCCAGACCCGTTT</u>	Amplification of <i>SNAP</i> for Gibson Assembly of pMUTIN- <i>plsY-SNAP</i> , pMUTIN- <i>pgsA-SNAP</i> , pMUTIN- <i>cydB-SNAP</i> ,	This study
5'FW87	<u>GTGAGCGCTCACAATTAATGAATATTCGGAACCAGAT</u> <u>TAC</u>	Amplification of <i>pgsA</i> for Gibson Assembly of pMUTIN- <i>pgsA-SNAP</i>	This study
3'FW87	<u>CCTGAACCTGAACCTGATTTTTGTTTAAAAACATCTC</u> <u>TACCTTTATAAAAAG</u>	Amplification of <i>pgsA</i> for Gibson Assembly of pMUTIN- <i>pgsA-SNAP</i>	This study
5'FW88	<u>TTAAACAAAAATCAGGTTTCAGGTTTCAGGTATGGACAA</u> <u>AGATTGCCGAAATG</u>	Amplification of <i>SNAP</i> for Gibson Assembly of pMUTIN- <i>pgsA-SNAP</i>	This study
5'FW89	<u>GTGAGCGCTCACAATTAATGATTTATGCATTTATAGG</u> <u>TATAACAG</u>	Amplification of <i>cydB</i> for Gibson Assembly of pMUTIN- <i>cydB-SNAP</i>	This study
3'FW89	<u>CCTGAACCTGAACCTGATGATTTCTTTCCTTCAACAT</u> <u>ATTC</u>	Amplification of <i>cydB</i> for Gibson Assembly of pMUTIN- <i>cydB-SNAP</i>	This study
5'FW90	<u>AAAGAAATCATCAGTTTCAGGTTTCAGGTATGGACAAA</u> <u>GATTGCCGAAATG</u>	Amplification of <i>SNAP</i> for Gibson Assembly of pMUTIN- <i>cydB-SNAP</i>	This study
5'FW91	GCTTCGAACATGTCTGAATCGAC	PCR confirmation of $\Delta tarO::ermB$	This study
3'FW91	CGTTAAAAGTGACTATGAAGCG	PCR confirmation of $\Delta tarO::ermB$	This study
5'FW94	<u>CCTTTTTTTGCCCCGGTTTTAACTACTAGTGACTGGA</u> <u>ATG</u>	Amplification of the <i>mreCD</i> promoter P_{mreCD} for Gibson Assembly of pKASBAR- P_{mreCD} - <i>mreD</i>	This study
3'FW94	<u>CTGCTTCTTGTATATCCTTTTCTATTTTATATTACT</u> <u>CC</u>	Amplification of the <i>mreCD</i> promoter P_{mreCD} for Gibson Assembly of pKASBAR- P_{mreCD} - <i>mreD</i>	This study
5'FW95	<u>GGATATACAAGAAAGCAGGGATAAATAATGC</u>	Amplification of <i>mreD</i> for Gibson Assembly of pKASBAR- P_{mreCD} - <i>mreD</i>	This study
3'FW95	<u>CTATGACCATGATTACGTTACCATTGACGACGTTTC</u>	Amplification of <i>mreD</i> for Gibson Assembly of pKASBAR- P_{mreCD} - <i>mreD</i>	This study
5'FW107	<u>AACAATTAAGCTTGATATCGAGGAGGAAATTATTGAG</u> <u>TGTCAAATTTAAGTCTTTGC</u>	Amplification of <i>qoxA</i> for Gibson Assembly of pCQ11- <i>qoxA</i>	This study
3'FW107	<u>ATTTATTATGCATTTAGAATAGGTTAATGTCCACCTC</u> <u>CATG</u>	Amplification of <i>qoxA</i> for Gibson Assembly of pCQ11- <i>qoxA</i>	This study
5'FW108	<u>AACAATTAAGCTTGATATCGAGGAGGAAATTATTGAA</u> <u>TGAATTTCCATGGGATCAATTAC</u>	Amplification of <i>qoxB</i> for Gibson Assembly of pCQ11- <i>qoxB</i>	This study

3'FW108	<u>ATTTATTATGCATTTAGAATAGGTCATGACTCATGAC</u> <u>TTACAG</u>	Amplification of <i>qoxB</i> for Gibson Assembly of pCQ11- <i>qoxB</i>	This study
5'FW109	<u>AACAATTAAGCTTGATATCGAGGAGGAAATTATTGAA</u> <u>TGAGTCATGATACAAACACTATTG</u>	Amplification of <i>qoxC</i> for Gibson Assembly of pCQ11- <i>qoxC</i>	This study
3'FW109	<u>ATTTATTATGCATTTAGAATAGGTCATCCGCTATACA</u> <u>CCATC</u>	Amplification of <i>qoxC</i> for Gibson Assembly of pCQ11- <i>qoxC</i>	This study
5'FW112	<u>TAACTTTAAGAAGGAGACAATAATGCGTACCCTGTAT</u> <u>TATTTC</u>	Amplification of <i>mreD</i> as a template and further for Gibson Assembly of pWALDO- <i>mreD-eyfp</i> and pWALDO- <i>mreD-6-eyfp</i> .	This study
3'FW112	<u>GAATTGACCCTGGAAGTACAGGTTTTCCCACTGACGA</u> <u>CGTTTCATATCG</u>	Amplification of <i>mreD</i> as a template and further for Gibson Assembly of pWALDO- <i>mreD-eyfp</i> and pWALDO- <i>mreD-6-eyfp</i> .	This study
3'FW113	<u>GAATTGACCCTGGAAGTACAGGTTTTCACCGCTGCCG</u> <u>CTACCGCTCCACTGACGACGTTTCATATCGATGTCG</u>	Amplification of <i>mreD</i> as a template and further for Gibson Assembly of pWALDO- <i>mreD-eyfp</i> and pWALDO- <i>mreD-6-eyfp</i> .	This study
3'FW114	<u>CTCACCATGAATTGACCCTGGAAGTAC</u>	Amplification of <i>mreD</i> as a template and further for Gibson Assembly of pWALDO- <i>mreD-eyfp</i> and pWALDO- <i>mreD-6-eyfp</i> .	This study
5'FW115	<u>TGGTGATGATGATGGGCCGCATTTTTTATACAGTTCAT</u> <u>CCATACC</u>	Amplification of <i>eyfp</i> for Gibson Assembly of pWALDO- <i>mreD-eyfp</i> and pWALDO- <i>mreD-6-eyfp</i>	This study
3'FW115	<u>GGTCAATTCATGGTGAGCAAAGGTGAAG</u>	Amplification of <i>eyfp</i> for Gibson Assembly of pWALDO- <i>mreD-eyfp</i> and pWALDO- <i>mreD-6-eyfp</i>	This study
5'FW116	<u>CTAGAGTCGAGGGTACAGGAGGTGTAATATTTATGAT</u> <u>GATAATC</u>	Amplification of <i>plsY</i> for Gibson Assembly of pMUTIN- <i>plsY-eyfp</i>	This study
3'FW116	<u>GAACCTGACATCCATTTTATTTTAGGTTCTTC</u>	Amplification of <i>plsY</i> for Gibson Assembly of pMUTIN- <i>plsY-eyfp</i> , PCR confirmation of chromosomal pMUTIN- <i>plsY-eyfp</i> and pMUTIN- <i>plsY-meyfp</i> integration	This study
5'FW117	<u>AAATGGATGTCAGGTTTCAGGTTTCAGGTATG</u>	Amplification of <i>eyfp</i> for Gibson Assembly of pMUTIN- <i>plsY-eyfp</i>	This study
5'pCQ11gfp	<u>TTTGAATTCTTAGGAGGATGATTATTTATGAGTAAAG</u> <u>GAGAAGAACT</u>	Amplification of <i>gfp</i> for construction of pCQ11- <i>gfp</i> , extends <i>gfp</i> with a EcoRI restriction enzyme site (<i>italic</i>)	(Garcia-Lara <i>et al.</i> , 2015)

3'pCQ11gfp	<u>AAAGGCGCGCCCTATTTGTATAGTTCATC</u>	Amplification of <i>gfp</i> for construction of pCQ11- <i>gfp</i> , extends <i>gfp</i> with a AscI restriction enzyme site (<i>italic</i>)	(Garcia-Lara <i>et al.</i> , 2015)
5'FL04	<u>AAAGAATTCAGGAGGATAAAACACATGGGCGTTAGTA</u> <u>AAGGCG</u>	Amplification of <i>mCherry</i> for construction of pWhiteWalker1 (<i>mCherry</i> + <i>gfp</i>), extends <i>mCherry</i> with a ribosomal binding site and a EcoRI restriction enzyme site (<i>italic</i>)	(Garcia-Lara <i>et al.</i> , 2015)
3'pWhite-Walker0 mCherryOE	<u>AAGTTCTTCTCCTTTACTCATGGTACCTCATCCTCCT</u> <u>AATCAAGATCTTTTATATAATTCATCC</u>	Amplification of <i>mCherry</i> for construction of pWhiteWalker1 (<i>mCherry</i> + <i>gfp</i>) and overlap extension PCR of pWhiteWalker2 (<i>mCherry</i> - <i>gfp</i>), extends <i>mCherry</i> with a BglII restriction enzyme site (<i>italic</i>) and a overlap sequence to <i>gfp</i> including a ribosomal binding site and a KpnI restriction enzyme site (<i>italic</i>)	(Garcia-Lara <i>et al.</i> , 2015)
5' pWhite-Walker0GFP OE	<u>GGATGAATTATATAAAAGATCTTGATTAGGAGGATGA</u> <u>GGTACCATGAGTAAAGGAGAAGAAC</u>	Amplification of <i>gfp</i> for construction of pWhiteWalker1 (<i>mCherry</i> + <i>gfp</i>), extends <i>gfp</i> with a ribosomal binding site and a KpnI restriction enzyme site (<i>italic</i>)) and a overlap sequence to <i>mCherry</i>	(Garcia-Lara <i>et al.</i> , 2015)
3'FL05	<u>AAAGGCGCGCCCTATTTGTATAGTTCATCCA</u>	Amplification of <i>gfp</i> for construction of pWhiteWalker1 (<i>mCherry</i> + <i>gfp</i>) and overlap extension PCR of pWhiteWalker2 (<i>mCherry</i> - <i>gfp</i>), extends <i>gfp</i> with a AscI restriction enzyme site (<i>italic</i>)	(Garcia-Lara <i>et al.</i> , 2015)
3'FL04OE	<u>AAGTTCTTCTCCTTTACTCATGGATCCACCAGAACCA</u> <u>GATCTTTTATATAATTCATCC</u>	Amplification of <i>mCherry</i> for overlap extension PCR of pWhiteWalker2 (<i>mCherry</i> - <i>gfp</i>), pWhiteWalker3 (<i>mreD</i> - <i>mCherry</i> + <i>plsY</i> - <i>gfp</i>) and), pWhiteWalker4 (<i>cdsA</i> - <i>mCherry</i> + <i>plsY</i> - <i>gfp</i>), extends <i>mCherry</i> with a BglII restriction enzyme site (<i>italic</i>) and a overlap sequence to <i>gfp</i> including a linker sequence	(Garcia-Lara <i>et al.</i> , 2015)
5'FL05OE	<u>GGATGAATTATATAAAAGATCTGGTTCTGGTGGATCC</u> <u>ATGAGTAAAGGAGAAGAAC</u>	Amplification of <i>gfp</i> for overlap extension PCR of pWhiteWalker2 (<i>mCherry</i> - <i>gfp</i>), extends <i>gfp</i> with a BglII restriction enzyme site (<i>italic</i>) and a overlap sequence to <i>mCherry</i> including a linker sequence	(Garcia-Lara <i>et al.</i> , 2015)

5'FL06	<u>TTTAGATCTTGATTAGGAGGATGAACCGGTATGATGATAATCGTCATG</u>	Amplification of <i>plsY</i> for construction of pWhiteWalker3 (<i>mreD-mCherry + plsY-gfp</i>), extends <i>plsY</i> with a AgeI restriction enzyme site (<i>italic</i>), a ribosomal binding site and a BglIII restriction enzyme site (<i>italic</i>)	(Garcia-Lara <i>et al.</i> , 2015)
3'FL06	AAAGGTACCCGAGCCCGAGCCCATCCATTTTATTTTAGG	Amplification of <i>plsY</i> for construction of pWhiteWalker3 (<i>mreD-mCherry + plsY-gfp</i>), extends <i>plsY</i> with a linker sequence and a KpnI restriction enzyme site (<i>italic</i>)	(Garcia-Lara <i>et al.</i> , 2015)
5'FL07	<u>TTTGAATTCTTAGGAGGAAATTATTGAATGCGTACACTGTAT</u>	Amplification of <i>mreD</i> for construction of pWhiteWalker3 (<i>mreD-mCherry + plsY-gfp</i>), extends <i>mreD</i> with a EcoRI restriction enzyme site (<i>italic</i>) and a ribosomal binding site	(Garcia-Lara <i>et al.</i> , 2015)
3'FL07OE	TCTTCGCCTTTACTAACGCCCATGCTGCCGCTGCCGTAGCCCATTTGACGACGTTT	Amplification of <i>mreD</i> for construction of pWhiteWalker3 (<i>mreD-mCherry + plsY-gfp</i>), extends <i>mreD</i> with a NheI restriction enzyme site (<i>italic</i>) and a linker sequence	(Garcia-Lara <i>et al.</i> , 2015)
5'FL08	<u>AAACGTCGTCAATGGGCTAGCGGCAGCGGCAGCATGGCGGTTAGTAAAGGCGAAGA</u>	Amplification of <i>mCherry</i> for construction of pWhiteWalker3 (<i>mreD-mCherry + plsY-gfp</i>), extends <i>mCherry</i> with a NheI restriction enzyme site (<i>italic</i>) and a linker sequence	(Garcia-Lara <i>et al.</i> , 2015)
5'FL09	<u>TTTGAATTCTTAGGAGGATGAAATTATATGAAAAGTTAGAACG</u>	Amplification of <i>cdsA</i> for construction of pWhiteWalker4 (<i>cdsA-mCherry + plsY-gfp</i>), extends <i>mCherry</i> with a EcoRI restriction enzyme site (<i>italic</i>) and a ribosomal binding site	(Garcia-Lara <i>et al.</i> , 2015)
3'FL09OE	TCTTCGCCTTTACTAACGCCCATGCTGCCGCTGCCGTAGCAGATTGTATTAATAAAATATTT	Amplification of <i>cdsA</i> for construction of pWhiteWalker4 (<i>cdsA-mCherry + plsY-gfp</i>), extends <i>cdsA</i> with a NheI restriction enzyme site (<i>italic</i>) and a linker sequence	(Garcia-Lara <i>et al.</i> , 2015)
5'FL10OE	AAATATTTTATTAATACAATCTGCTAGCGGCAGCGGCAGCATGGGCGTTAGTAAAGGCGAAGA	Amplification of <i>mCherry</i> for construction of pWhiteWalker4 (<i>cdsA-mCherry + plsY-gfp</i>), extends <i>mCherry</i> with a NheI restriction enzyme site (<i>italic</i>) and a overlap sequence to <i>cdsA</i> for overlap extension PCR	(Garcia-Lara <i>et al.</i> , 2015)

Nucleotide sequences in italic indicate added nucleotides to the original template sequence or introduced restriction enzyme sites if primers were used for non-gibson assembly cloning. Underlined nucleotides indicate homologues sequences to the template.

PCR amplifications were performed in a Veriti Thermal Cycler and the following cycle setup was employed:

1 cycle	Initial denaturation	95 °C	1 min
30 cycles	Denaturation	95 °C	30 s
	Annealing	50-60 °C	30 s
	Extension	72 °C	30 sec/kb
1 cycle	Final extension	72 °C	7 min

Following PCR, products were separated by gel electrophoresis.

2.9.2.2 Taq polymerase

Verification of chromosomal insertions where an accurate DNA amplification is not required was performed using the DreamTaq Green Master Mix (Thermo Scientific). Unless otherwise stated, a total PCR mix volume of 20 µl was used.

DreamTaq Green Master Mix (2x)	10 µl
Forward primer (50 µM)	1 µl
Reverse primer (50 µM)	1 µl
Template DNA	50-100 ng
sdH ₂ O	up to 20 µl

PCR amplifications were performed in a Veriti Thermal Cycler and the following cycle setup was employed:

1 cycle	Initial denaturation	95 °C	1 min
30 cycles	Denaturation	95 °C	30 s
	Annealing	50-60 °C	30 s
	Extension	72 °C	1 min/kb
1 cycle	Final extension	72 °C	7 min

Following PCR, products were separated by gel electrophoresis.

2.9.2.3 Colony PCR screening of *E. coli*

A sterile pipette tip was used to resuspend a single colony of *E. coli* from an agar plate into a PCR master mix containing DreamTaq Green master mix, primers and sdH_2O in a 0.2 ml thin-walled PCR tube. The PCR mix composition and PCR reaction is described described in Section 2.9.2.2.

2.9.3 Restriction endonuclease digestion

All restriction enzymes were purchased from New England Biolabs or Thermo Scientific. DNA digests were carried out according to the manufacturer's instructions. Buffers were double digest were selected using the NEB double digest finder (<https://www.neb.com/tools-and-resources/interactive-tools/double-digest-finder>) and digests were performed at the recommended incubation temperature. Digested DNA fragments were then either separated by gel electrophoresis followed by gel extraction or DNA fragments were purified by PCR purification (see section 2.8.4).

2.9.4 Ligation of DNA

Digested vector and insert DNA fragments were mixed in a molar ratio of 1:3 unless otherwise stated and the reaction was performed in a 10 μl total volume including 1 μl T4 ligase (Promega) and 1 μl T4 ligase buffer (10 x) (Promega). The ligation reaction was incubated overnight at 16 °C and subsequently used for transformation of *E. coli* cells or stored at -20 °C.

Molar ratios were calculated using the ligation calculator from the University of Düsseldorf (Germany) (http://www.insilico.uni-duesseldorf.de/Lig_Input.html).

2.9.5 Gibson Assembly

Gibson Assembly reactions were carried out according to the manufacturer's instructions (New England Biolabs).

2.9.6 Agarose gel electrophoresis

Agarose was prepared as a 0.8 % (w/v) solution in TAE buffer (1 x) and used to prepare horizontally submerged agarose gels in HU6 Mini or HU10 Mini tanks provided by Alpha Metrix (Alpha Metrix Biotech GmbH, Rödermark, Germany). After pouring the gel and before the agarose hardens, 5 μl (HU6 Mini) or 15 μl (HU10 Mini) of ethidium bromide (10 mg ml^{-1} ; Sigma-Aldrich) were mixed into the gel and appropriate combs

were inserted. DNA was mixed with 6 x DNA loading buffer (ThermoScientific) at the appropriate ratio and loaded into the wells and at least one well lane was loaded with 5 μ l GeneRuler1kb DNA ladder (see Table 2.9(ThermoScientific). Gels were for 30 – 60 min at 100 V and visualised using a transilluminator at 260 nm and photographed using the BioCoc-ItTM Imaging System (UVP, Cambridge).

Table 2.9 1kb DNA ladder (Thermo Scientific) DNA fragment sizes

Marker	DNA fragment
GeneRuler 1 kb DNA Ladder (ThermoScientific)	10,000
	8,000
	6,000
	5,000
	4,000
	3,500
	3,000
	2,500
	2,000
	1,500
	1,000
	750
	500
	250

2.9.7 Determination of DNA concentration

DNA concentrations were measured using a nanodrop ND-1000 spectrophotometer (Peqlab, Erlangen, Germany).

2.9.8 DNA sequencing

Samples were sent for Sanger DNA sequencing at GATC (GATC Biotech AG, Konstanz, Germany).

2.10 Transformation techniques

2.10.1 Transformation of *E. coli*

2.10.1.1 Preparation of electrocompetent *E. coli* cells

Overnight cultures of *E. coli* were diluted to OD₆₀₀=0.05 in 400 ml TSB or LB medium and incubated at 37 °C at 250 rpm to OD₆₀₀=0.5-0.7. Cell cultures were incubated on ice-slurry for 15 min and harvested by centrifugation for 10 min at 5000 rpm and 4 °C. Subsequently, the pellet was washed four times with ice-cold sterile sdH₂O at decreasing volumes (200 ml / 120 ml / 120 ml/ 40 ml). The resulting pellet was

resuspended in 50 % (v/v) ice-cold glycerol to reach an end concentration of approximately 10 % glycerol (v/v). Aliquots of 50 μ l were stored at -80 °C.

2.10.1.2 Electroporation of DNA into *E. coli* competent cells

Competent cells were thawed on ice for 5 min and mixed with 2-15 μ l plasmid or Gibson Assembly reaction mix. The mixture was transferred to a pre-cooled electroporation cuvette (1 mm gap). The cuvette containing the cell suspension was subsequently pulsed with 1.75 kV, 25 μ F capacity and 200 Ω resistance. 950 μ l BHI medium was added immediately after and the mixture was transferred to a 15 ml Falcon tube. Cells were incubated for 1 h at 37 °C at 250 rpm. 20 - 100 μ l were plated out on BHI agar supplemented with the respective antibiotic.

2.10.1.3 Preparation of chemically competent *E. coli* cells

2.10.1.3.1 TFBI buffer

RbCl	100 mM
MnCl ₂	50 mM
Potassium acetate	30 mM
CaCl ₂	10 mM
Glycerol	15 % (v/v)

The pH was adjusted to 6.8 with HCl and the buffer was sterile filtrated.

2.10.1.3.2 TFBII buffer

3-(<i>N</i> -morpholino) propanesulfonic acid (MOPS)	10 mM
RbCl	10 mM
CaCl ₂	75 mM
Glycerol	15 % (v/v)

The pH was adjusted to 6.8 with KOH and the buffer was sterile filtrated.

2.10.1.3.3 Preparation of chemically competent *E. coli* cells

Overnight cultures of *E.coli* were diluted to OD₆₀₀=0.1 in 100 ml LB and incubated at 37 °C to OD₆₀₀≈0.5. Cells were recovered by centrifugation for 10 min at 4 °C and 5000 rpm and resuspended in 30 ml ice-cold TFB1 buffer. The resuspended cells were incubated on ice for 90 min and again pelleted for 10 min at 4 °C and 4700 rpm. The pellet was resuspended in 4 ml ice-cold TFB2 buffer. Aliquots of 100 μ l each were stored at -80 °C.

2.10.1.4 Heat-shock transformation of DNA into *E. coli* competent cells

Competent cells were thawed on ice for 5 min and mixed with 2-15 µl plasmid or Gibson Assembly reaction mix and incubated on ice for 20 min. Cells were incubated at 42 °C for exactly 90 sec. Subsequently, 900 µl sterile BHI was added immediately and cells were incubated for 1 h at 37 °C. 200 µl were plated out on BHI agar plates supplemented with the respective antibiotic.

2.11.1 Transformation of *S. aureus*

2.11.1.1 Preparation of electrocompetent *S. aureus* RN4220 cells

Overnight cultures of *S. aureus* were diluted to OD₆₀₀=0.5 in 100 ml BHI and incubated at 37 °C at 250 rpm to OD₆₀₀≈0.6. Cell cultures were incubated on ice for 15 min and recovered by centrifugation for 10 min at 5000 rpm and 4 °C. Subsequently, the cells were washed three times with ice-cold sterile sdH₂O Water at decreasing volumes (100 ml / 50 ml / 16 ml), followed by two additional washing steps with ice-cold sterile 10 % glycerol (v/v) (2 ml / 1 ml). The resulting pellet was resuspended in 700 µl ice-cold 10 % glycerol (v/v). Aliquots of 70 µl were stored at -80 °C.

2.11.1.2 Electroporation of DNA into *S. aureus* RN4220 competent cells

Competent cells were thawed on ice for 5 min and 1 – 10 µl of DNA was added and carefully mixed by pipetting. The mixture was transferred to a pre-cooled electroporation cuvette (1 mm gap). The cuvette containing the cell suspension was subsequently pulsed with 2.5 kV, 25 µF capacity and 100 Ω resistance. The pulse-duration should be between 3.8 and 5 sec. 950 µl BHI medium was added immediately after and the mixture was transferred to a 15 ml Falcon tube. Cells were then incubated for 2 h at 37 °C and 100 - 200 µl were plated out on BHI agar supplemented with the respective antibiotic.

2.10 Phage techniques

2.10.1 Bacteriophage

Φ11 is a *S. aureus* specific phage used to transduce DNA between strains. And requires Ca²⁺ for infection maintenance (Mani *et al.*, 1993, Novick, 1991).

2.10.1 Preparation of phage lysate

150 µl of an overnight culture of *S. aureus* was mixed with 5 ml BHI medium, 5 ml phage buffer and 100 µl phage lysate in an Universal tube. The sample mixture was incubated without shaking overnight at 25 °C. Once cleared, the lysate was filter sterilised (0.2 µm pore size) and stored at 4 °C.

2.10.2 Phage transduction

The recipient *S. aureus* strain was grown overnight in 50 ml LK medium containing appropriate antibiotics. Cells were harvested by centrifugation at 5000 rpm at 4 °C for 10 min and the resulting pellet was resuspended in 1 - 3 ml LK.

The following mixtures were prepared in Universal tubes (Tab. 2.10):

Table 2.10 Phage transduction

Buffer/cells	Sample	Negative control
Recipient cells	500 µl	500 µl
LK broth	1 ml	1.5 ml
1 M CaCl ₂	10 µl	15 µl
Phage lysate	500 µl	-

These were incubated at 37 °C for 25 min without shaking, followed by an additional 37 °C incubation step at 250 rpm for 15 min. Subsequently, 1 ml ice-cold 0.02 M sodium citrate was added and the mixture was incubated on ice for 5 min. The cells were recovered by centrifugation for 10 min at 4 °C and 5000 rpm and the supernatant was removed. The pellet was resuspended in 1 ml ice-cold 0.02 M sodium citrate and incubated on ice for 45 min. 100 µl of the resuspension was spread onto LK plates containing sodium citrate and the appropriate antibiotics. The plates were then incubated at 37 °C for at least 24 hours.

2.11 Protein analysis

2.11.1 SDS-PAGE

SDS-PAGE gels consist of a resolving and a stacking gel. The resolving gel was prepared using the following components:

11 % (w/v) resolving gel

dH ₂ O	3.5 ml
1.5 M Tris-HCl (pH 8.8)	2.5 ml
10 % SDS (w/v)	100 µl
30 % Acrylamide/Bis (w/v) (37:5:1, BioRad)	4 ml
10% Ammonium persulphate (APS) (w/v)	100 µl
TEMED (N,N,N',N'-tetramethyl-ethylenediamine)	20 µl

All components were mixed in a Falcon tube and APS and TEMED were added immediately before the gel was poured into the gel casting apparatus (BioRad Mini-Protean II gel slabs). 1 ml dH₂O was loaded on top of the gel to straighten the upper edge of the gel.

Once the gel solidified, the remaining dH₂O was removed using paper and the stacking gel was prepared and poured on top of the resolving gel. A BioRad plastic comb was immediately inserted into the gel to create wells.

11 % (w/v) stacking gel

dH ₂ O	3.6 ml
1.5 M Tris-HCl (pH 8.8)	0.75 ml
10 % SDS (w/v)	50 µl
30 % Acrylamide/Bis (w/v) (37:5:1, BioRad)	0.65 ml
10% Ammonium persulphate (APS) (w/v)	50 µl
TEMED (N,N,N',N'-tetramethyl-ethylenediamine)	25 µl

After the gel solidified, the gel was transferred to a Protean II (BioRad) gel-running tank and submerged in 1x SDS PAGE reservoir buffer. The comb was removed and appropriate volumes of samples (5-20 µl) were loaded. 10 µl of prestained protein ladder broad range (New England Biolabs) were loaded into at least one lane. Proteins were separated by electrophoresis at 100 V for 100 min until the blue dye front of the sample buffer was at the base of the gel plate.

2.11.2 Coomassie staining

After electrophoresis, the gel was placed into Coomassie Blue stain for 30 min. The gel was destained using Coomassie destain solution including several solution exchanges where the last destain step was performed overnight.

2.11.3 Gel drying

The SDS gel was placed between two sheets of DryEase mini Cellophane (Invitrogen) that were soaked in Gel-Dry™ drying solution (Invitrogen). The gel and the two sheets were held together using a drying frame and base (Novex) and left (at RT) until completely dried.

2.11.4 Determination of protein concentrations

Protein concentrations were determined using a *bicinchoninic acid* assay provided by Pierce™ BCA Protein Assay Kit (Thermo Scientific). The assay was performed according to the manufacturer's instructions.

2.11.5 Western Blot

2.11.5.1 Western Blot transfer

The SDS-PAGE and Amersham™ Hybond-ECL nitrocellulose blotting membrane (GE Healthcare) were equilibrated in 25 ml blotting buffer for 15 minutes. The proteins were transferred to the nitrocellulose membrane by electrophoresis using the wet transfer system BioRad Mini-PROTEAN® Tetra for 90 minutes at 100 V with ice-cold ethanol blotting buffer.

2.11.5.2 Antibody treatment

The membrane was carefully removed from the transfer system and washed in 25 ml TBST twice for 5 min and once for 15 min at mild agitation replacing the TBST buffer between each step. Next, the membrane was incubated with 25 ml blocking buffer for 1 h at RT followed by three aforementioned washing steps. The membrane was incubated in 25 ml blocking buffer containing the appropriate primary antibody at dilution of 1:5,000 or 1:10,000 (Rabbit) for at least 2 h at RT followed by the three washing steps with TBST buffer. Subsequently, the secondary antibody was applied by incubating the membrane in 25 ml blocking buffer containing horseradish peroxidase conjugated anti-rabbit antibodies at a dilution of 1:10,000 for 1 – 2 h at RT. Finally the membrane was washed with TBST as described before.

2.11.5.2 Western blot development

The SuperSignal® West Pico (Thermo Scientific) kit was used to develop the membrane and all the following steps were performed in a dark room. The membrane was air dried on paper and covered with a mixture of 2 ml of ECL reagent 1 and 2 ml of ECL reagent 2. After a 5 min incubation, the membrane was dried and placed between two sheets of plastic foil inside a film cassette. Amersham™ Hyperfilm-ECL (GE Healthcare) was attached on top and the film cassette was closed and held together for 5 min. Next, the film was washed in developer solution until bands became visible. Immediately after the film was submerged in fixer solution and washed with dH₂O. The film was then air-dried and scanned.

2.12 Production of recombinant protein

2.12.1 Expression in *E. coli* C43 (DE3)

Recombinant protein expression and harvesting was carried out according to (Drew *et al.*, 2006).

A single colony of *E. coli* C43 (DE3) containing the plasmid pWALDO-*mreD-6-eyfp* or pWALDO-*murJ-gfp* was inoculated in LB medium supplemented with kanamycin (50 µg ml⁻¹) and grown overnight at 37 °C at 250 rpm. The culture was diluted to an OD₆₀₀=0.05 in 1 l LB medium supplemented with kanamycin (50 µg ml⁻¹) and incubated at 37 °C at 250 rpm until an OD₆₀₀≈0.5. Protein expression was induced by addition of IPTG to a final concentration of 0.4 mM to the culture followed by lowering the temperature to 25 °C. The cultures were incubated for 4 h at 25 °C at 150 rpm before cells were recovered by centrifugation for 20 min at 6000 rpm at 4 °C. Cells were washed and finally resuspended using ice-cold PBS supplemented with a protease inhibitor cocktail (PBSi) (Sigma-Aldrich).

Resuspended cells were broken in two passes through a French Press (SLM Instruments, Rochester, United States of America) at 10,000 Psi and unbroken cells were removed by centrifugation at 14,100 rpm (24,000 x g) for 12 min at 4 °C. This step was repeated and the supernatant was transferred to a fresh tube. The solution was sonicated in order to resuspend the membranes followed by centrifugation at 35,300 rpm (150,000 x g) at 4 °C for 45 min to collect the membranes containing the recombinant protein. The pellet was washed with PBSi and resuspended in 5 ml PBSi using sonication. The membranes were then solubilised by adding a 1 % DDM (w/v; in dH₂O) solution to an end concentration of 0.2 % DDM (w/v) followed by incubation at 4 °C for 1 h at mild agitation. The resuspension was centrifuged at 28,800 rpm (100,000

x g) for 45 min at 4 °C and the supernatant was transferred to a fresh micro centrifuge tube and stored at -20 °C or was immediately used for the purification via a HiTrap™ column.

2.12.2 HisTrap HP™ column for protein purification

For the purification of solubilised membranes, Elution buffer and START buffer were supplemented with 0.1 % DDM (w/v).

Both recombinant proteins contain a C-terminal 8 x His tag that was used for purification by a HisTrap HP column charged with Ni²⁺. In order to do so, a Bio-Rad Econo Gradient system and a 1 ml HisTrap HP (GE Healthcare) was used to purify the recombinant proteins. First, the column was washed with 3 ml dH₂O. Then, the column was charged with 3 ml 50 mM NiSO₄ followed by a washing step with 3 ml dH₂O to remove excess Ni²⁺ ions. Tubes and system pumps of the Bio-Rad Econo Gradient system were flushed with 20 ml sdH₂O buffer at a flow rate of 2 ml min⁻¹. The charged column was then connected to the system while the pump is running to avoid the introduction of air bubbles. The solubilised membranes were loaded at a flow rate of 0.3 ml min⁻¹. Non-specifically bound proteins were removed by a washing step using 4 % Elution buffer (v/v). Elution was performed by applying rising concentrations of the elution buffer that are mixed by the gradient pump. The elution starts at 0 % elution buffer/100 % START buffer (v/v) reaching 20 % elution buffer (v/v) /80 % START buffer (v/v) within 20 min at a flow rate of 1 ml min⁻¹. Each 1 ml fraction was collected in a separate microcentrifuge tube and analysed by SDS-PAGE.

The charged HisTrap column was washed with 10 ml 50 mM EDTA followed by 10 ml dH₂O. Finally, 10 ml of 20 % ethanol (v/v) were run through the column and stored at 4 °C.

2.13 Microscopes

Unless otherwise stated, fluorescence images were acquired using a Delta Vision deconvolution microscope (Applied precision, GE Healthcare) and images were deconvolved using SoftWoRx v.3.5.1 software. The applied filter sets are listed in Table 2.11.

Table 2.11 DeltaVision filter sets

Filter	Excitation filter/bandpass	Emission filter/bandpass	Fluorophores
DAPI	360/40	457/50	HADA
FITC	492/20	528/38	GFP, eYFP, FM1-43
RF-TR-PE	555/28	617/73	mCherry, mRFPmars1, TMR-Star
Cy5	640/20	685/40	FM4-64

2.14 Sample preparation for light-microscopy

2.14.1 Fluorescence microscopy

Overnight cultures were diluted in BHI or LB to an OD_{600} of 0.05 and grown at 37 °C on a rotary shaker until early-exponential phase ($OD_{600}=0.4-0.6$). 1 ml of cell culture was harvested by centrifugation for 3 min at 12,000 rpm and washed with 1 ml PBS. The pellet was resuspended in 500 μ l PBS μ l and 500 μ l fixative (PBS/16 % P-formaldehyde (w/v) (2:0.5)) and incubated on a shaker at RT and 90 rpm. The tubes were covered in foil if the respective strain contains fluorescent proteins or markers. Subsequently, cells were recovered by centrifugation and washed 2 times with 1 ml dH₂O. Dependent on the pellet size, the cells were resuspended in an appropriate amount of PBS or dH₂O (100 -400 μ l). 5 μ l of this solution was pipetted onto a poly-l-lysine coated slide (Polyprep, Sigma-Aldrich) and dried under a stream of nitrogen. 6 μ l sdH₂O were pipetted on top of the dried cells followed by a coverslip. The coverslip was additionally sealed with nail polish to keep the sample wet. Slide samples were either imaged immediately or stored in the dark at 4 °C.

Background of fluorescent images was subtracted and intensity values are depicted in a linear colour code.

2.14.2 Donor photobleaching FRET experiments

This section only describes the growth conditions of strains used for FRET experiments and the set-up of the microscope. FRET data analysis can be found in Section 5.2.6

Only fresh transformants of RN4220 carrying pWhiteWalker plasmids or strains streaked out from cryo cultures made from fresh transformants were used for FRET analyses. Overnight cultures were diluted to $OD_{600}=0.025$ in 50 ml BHI supplemented with erythromycin (5 μ g ml⁻¹) and lincomycin (25 μ g ml⁻¹) and grown at 37 °C and 250

rpm for 2.5 h to an $OD_{600} \approx 0.4$. Cultures were diluted again to $OD_{600} = 0.025$ in 50 ml BHI supplemented with erythromycin ($5 \mu\text{g ml}^{-1}$), erythromycin ($25 \mu\text{g ml}^{-1}$) and 0.5 mM IPTG followed by grown at 37°C and 250 rpm for 2 h to an $OD_{600} \approx 0.4$. 1 ml samples were harvested by centrifugation at 13,000 rpm for 3 min. Samples were washed with 1 ml PBS, fixed and prepared on poly-lysine slides as described previously (Section 2.13.1).

Image acquisition was carried out using a Nikon Dual Cam system and NIS elements software under a 100 x oil lens in the FITC channel. The following settings were used for imaging:

Format – Binning 2x2	Exposure – 500 ms
Readout mode – Global Shutter	Readout rate – 560 MHz
Dynamic Range – 12 bit & Gain 1	Sensor mode – Normal

Images were taken continuously over 6 min and analysed as described in Section 5.2.6.

2.14.3 Super resolution microscopy

STORM studies were performed using a system described by Dr. R.D. Turner (Turner *et al.*, 2013). An Olympus IX71 inverted optical microscope and a 60x, NA 1.4 oil immersion objective, a system was used for eYFP imaging with a 75 mW, 514 nm laser and a filter cube containing a 514 nm longpass dichroic filter and a 542/27 nm bandpass emission filter. Focus was adjusted using a piezoelectric motor (Physik Instrumente) and the image was projected onto a Hamamatsu ImagEM at 10-50 frames/sec using an image expander comprising a 35 mm and 100 mm lens.

A 1m focal length cylindrical lens was inserted between the image expander lenses to allow for compensation of drift perpendicular to the focal plane (Huang *et al.*, 2008). Focus was maintained by repeatedly localising a TetraSpeck marker and adjusting the objective position using the piezo to maintain a constant ratio of the fitted full-width half maxima (FWHM) in perpendicular directions. The camera and piezo were controlled using a custom Labview based software (Dr. R.D. Turner) and image processing was carried out according to previous studies (Huang *et al.*, 2008, Betzig *et al.*, 2006). Data were processed by fitting Gaussian functions to individual molecule fluorescence, identified by clear intrinsic blinks, using Matlab. Drift in the focal plane was corrected retrospectively by tracking a fiducial particle throughout the acquisition sequence and offsetting localisations against its position.

2.14.3.1 STORM buffers

The following stock solutions were prepared:

Tris buffer

Tris 50 mM

NaCl 10 mM

The pH was adjusted to 8 using HCl.

Catalase stock

Catalase 4 mg ml⁻¹

The catalase stock was prepared in Tris buffer.

Glucose oxidase stock

Glucose oxidase 5 mg ml⁻¹

The glucose oxidase stock was prepared in Tris buffer.

MEA stock

Mercaptoethylamine 5 mg ml⁻¹

The MEA stock was prepared in Tris buffer.

GLOX buffer (for 1 ml)

Glucose 100 mg

Tris buffer 790 µl

Glucose oxidase stock 100 µl

Catalase stock 10 µl

MEA stock 100 µl

2.14.3.2 Coverslip sample preparation

First, high-precision coverslips No.1 5H (Marienfeld-Superior, Lauda-Königshofen, Germany) were cleaned by placing the coverslips in a beaker containing 1 M KOH followed by sonication for 15 min at RT using a sonic bath. Subsequently, the coverslips were washed with dH₂O and incubated in a 0.01 % poly-L-lysine (w/v) solution (Sigma-Aldrich) for 30 min at RT. The coverslip was rinsed again with dH₂O and dried under a flow of nitrogen.

2.14.3.3 Sample application

3 μ l of cell suspension were mixed with 3 μ l of diluted Tetraspecks (1:500 in dH₂O, sonicated) used as reference points during imaging and the mixture was placed onto the cover slip. The resuspension was dried down using nitrogen followed by carefully rinsing the cover slip. Once again, the cover slip was dried using nitrogen and placed with the sample side down on a clean slide containing a drop of 5 μ l GLOX buffer. Finally, the coverslip was sealed using nail polish and the sample was ready for imaging.

2.15 Metabolite analysis

2.15.1 Harvesting samples

Metabolite samples were collected using the ethanol and sodium chloride (NaCl) method described by (Spura *et al.*, 2009).

Samples (20 ml) collected from growing cultures were transferred into a 50 ml Falcon tube containing 20 ml of quenching solution (40 % ethanol (v/v) + 0.8 % NaCl (w/v)), which had been pre-cooled to -30 °C by placing in an insulated bath containing isopropanol that had been cooled by addition of dry ice. A thermometer is used in the bath to monitor the temperature. The sample mixture was then mixed instantly by inversion, producing a cell suspension at approximately 0 °C and left to cool down to -5 °C in the -35 °C isopropanol bath over the course of 2 - 3 minutes. The cells are stirred all the time at this stage, using the thermometer. Then the cells were centrifuged at 3940 x g at -8 °C for 5 min in a pre-cooled centrifuge (Beckman Avanti HP-25I, JLA-10.500) and the supernatant was removed by aspiration and stored at -70 °C until used for metabolite extraction.

2.15.2 Metabolite extraction

The following solvents were used for the metabolite extraction. To avoid salt contamination, only LC-MS grade solvents were used. Solvents A and B were pre-cooled at -20 °C and Solvent C was put on ice before use. Furthermore, all following steps were performed on ice.

Solvent A Methanol : Chloroform : dH₂O (2.5:1:1)(v/v/v)

Solvent B Methanol : Chloroform (1:1)(v/v)

Solvent C dH₂O

The Falcon tubes containing the harvested pellets were weighed and thawed on ice. Subsequently, the pellet was resuspended in 1 ml of Solvent A by vortexing. The cells were then sonicated for 30 sec in a sonication bath containing ice slurry followed by

vortexing for 30 sec. After incubation on ice for approximately 5 min the cells were recovered by centrifugation for 2 min at 5000 rpm and 4 °C. The centrifugation separates two phases with a precipitate phase in between. The upper phase was transferred to a pre-cooled 15 ml Falcon tube whereas the bottom phase was mixed with 500 µl of Solvent B, vortexed and added to the the Falcon tube containing the upper phase. Subsequently, 350 µl Solvent C and 200 µl CHCl₃ were added and the mixture was vortexed. The phases were separated again by centrifugation for 15 min with 5000 rpm at 4 °C. The upper aqueous phase and the bottom chloroform phase were transferred carefully to separate microcentrifuge tubes and stored at - 80 °C.

2.15.3 Electro-spray induced liquid chromatography mass spectrometry

Detection of metabolites was performed by ESI-LC-MS using a QSTAR Elite liquid chromatographic system (Applied Biosystems) equipped with an autosampler. The liquid chromatography was run in electrospray negative ionisation mode and the mass range was set to 50-1000 Da. Source parameters were as follows: ionspray voltage of 3500 V, GS1 at 27, GS2 at 0 and curtain gas at 20. The data was acquired and analysed using Applied Biosystems Analyst QS 2.0 software. Prior to injection, samples were centrifuged for 10 min at 12000 rpm and equally mixed with 50:50:0.02 (Methanol:H₂O:formic acid (v/v/v)), all LC-MS grade solvents) and infused into the mass spectrometer at 0.1 ml min⁻¹.

Chapter 3: The physiological role of MreD in *S. aureus*

3.1 Introduction

3.1.1 The roles of MreC and MreD

MreC and MreD are widely conserved and thought to be shape-determinants in rod-shaped bacteria. Their genes are chromosomally located together in an operon with *mreB* and were shown to be essential, both in *E. coli* and in *B. subtilis* (Levin *et al.*, 1992) (Lee & Stewart, 2003) (Ishino *et al.*, 1986). Deletion of either *mreC* or *mreD* causes the formation of spherical cells that eventually lyse. Growth but not morphology of both mutants can be restored when grown in medium supplemented with high Mg^{2+} concentrations (Wachi *et al.*) (Leaver & Errington, 2005). MreC is a membrane bound protein with its major part facing the periplasm (Lovering & Strynadka, 2007). It is thought that MreC acts as a spatial organiser to direct PGN precursor synthesis proteins in the periplasm. (Divakaruni *et al.*, 2005) (Divakaruni *et al.*, 2007). According to this model, MreC could be the link between the intracellular cytoskeleton and periplasmic cell wall synthesis machinery. The function of MreD in rod-shaped bacteria is poorly understood. Its deletion causes the same phenotype as seen for MreC. Therefore, it is considered to act in a complex with MreB and MreC to direct peripheral PGN synthesis by control of localisation and activity of PGN synthesis proteins (Land & Winkler, 2011). Interestingly, *mreCD* are not essential in *Streptococcus pneumoniae* in strains with a suppressor mutation within the peptidoglycan synthesis gene *pbp1a* which strongly suggests an involvement of MreCD in cell wall synthesis (Land & Winkler, 2011). Another link to peptidoglycan synthesis in *S. pneumoniae* was seen in cells depleted of MreC or MreD which resulted in the formation of spherical cells connected in chains. This phenotype was also seen in *pbp2a* depletion experiments and possibly indicates that MreCD regulate PBP2a (Berg *et al.*, 2013). MreD was also shown to interact with the PGN synthesis enzymes MurG and MraY which are dependent on MreD for proper positioning in *C. crescentus* (White *et al.*, 2010). Using total internal reflection fluorescence microscopy (TIRFM), MreB in *B. subtilis* was shown to colocalise with MreC and MreD and to move in circumferential patches along the cell periphery (Garner *et al.*, 2011). These are held together by MreB and driven by peptidoglycan synthesis (Dominguez-Escobar *et al.*, 2011, Garner *et al.*, 2011). Recent research has suggested an involvement of Mre proteins in membrane organisation.

MreC and MreD were shown to be involved in the positioning of MreB which has direct effects on membrane fluidity and membrane organisation as shown by altered Nile Red staining (Strahl *et al.*, 2014). MreCD is widely conserved among ovocoid firmicutes such as Enterococci, Streptococci, Lactobacilli and Staphylococci (Pinho *et al.*, 2013). In the ellipsoid-shaped *Streptococcus pneumoniae*, MreCD are colocalised with peptidoglycan synthesis at the septa and equators and are thought to be required for cell elongation. Additionally, insertion of new PG primarily takes place at the cell-division site (Monteiro *et al.*, 2015). MreCD might be crucial for driving the elongation of cells by regulating peripheral PG synthesis and therefore their role is unclear in non-elongating coccoid bacteria such as *Staphylococcus aureus*.

During this study, Tavares *et al.*, published the characterisation of a partial *mreD* mutant in *S. aureus*. It has been reported that the deletion of full-length *mreD* was not feasible since a promoter for the downstream genes *rplU*, *ysxB* and *rpmA* is predicted to be within the end of *mreD* (Tavares *et al.*, 2015). RplU, YsxB and RpmA are putative ribosomal proteins and assumed to be essential (Chaudhuri *et al.*, 2009). Therefore only the first 374 bp of MreD (531 bp total length) were deleted and the resulting strain was used for the characterisation of an *mreD* mutant. This $\Delta mreD$ strain exhibits no growth or morphological defect and no changes in the peptidoglycan composition were observed. Furthermore, a number of stress agents such as sodium chloride, hydrogen peroxide and hydrochloric acid were tested but did not reveal any role of MreD in the response to various stresses. Also, MICs for various antibiotics remained unchanged in $\Delta mreD$.

Contradictory to that study, Garcia-Lara *et al.*, demonstrated that the construction of a full-length deletion mutant of *mreD* is achievable (Garcia-Lara *et al.*, 2015). This mutant exhibits a growth defect and shows aberrant cell-morphologies. Cells with changed shapes also exhibited a delocalisation of the phospholipid synthesis enzyme PlsY and the cell-division protein EzrA.

3.1.2 Aims of this chapter

- Investigate growth of $\Delta mreD$ in various media and incubation temperatures
- Lipidomic analysis of $\Delta mreD$: fatty acid, phospholipid composition
- Investigate the effect of MreD on membrane fluidity
- Phenotypic characterisation and whole genome sequencing of suppressors of $\Delta mreD$

3.2 Results

3.2.1 Effect of temperature on *ΔmreD*

Heat has several effects on bacterial cells. *S. aureus* cells grow faster when incubated at 42 °C rather than 37 °C, which also results in expression of heat-shock proteins that support protein folding or oxidative stress (Qoronfleh *et al.*, 1998, Qoronfleh *et al.*, 1990).

The question arises as to whether MreD is involved in adjusting to heat-stress and thereby allows faster growth? This was tested by several experiments. First, overnight cultures of SH1000 and SH1000 *ΔmreD* growth were grown on agar plates incubated at 37 °C or 42 °C (Fig. 3.1A) and CFUs were calculated based on visible colonies after 24 h (Fig. 3.1B). To test whether a short-time heat-shock affects the *mreD* mutant, stationary overnight cultures were treated at 42 °C for 10 min, subsequently plated on agar and incubated at 37 °C for 24 h (Fig. 3.1C).

The *mreD* strain exhibits a growth defect on agar plates both at 37 °C and 42 °C compared to the parental strain as seen by smaller colony size (Fig. 3.1A). However, at 42 °C, CFU counts of visible colonies after a 24 h incubation on agar were significantly ($P=0.008$) lower compared to growth on 37 °C. This effect was not achieved by a 10 min heat-shock demonstrating that 42 °C inhibits growth rather than inducing cell death. Interestingly, incubation at 42 °C revealed the formation of big colonies that are potentially suppressors of *ΔmreD* (Fig. 3.1D).

Next, growth of both strains were compared to each other in BHI broth at different temperatures. Cultures were temperature shifted by growing cells at 30 °C from an OD_{600} of 0.05 to an $OD_{600}\approx 0.2$ followed by placing the growth flask in a shaking water bath at 30, 37 or 42 °C (Fig. 3.2A). In a different approach, overnight cultures were incubated at 30, 37 or 42 °C and subsequent subcultivated cultures were incubated at the same temperature to monitor growth without a temperature shift (Fig. 3.2B).

The *mreD* strain grows worse than its parent at all temperatures tested (30, 37, 42 °C).

Comparable to the plating experiment, the *mreD* mutant exhibits a heat-sensitivity in liquid culture when temperature shifted (Fig. 3.2A). Shifting the temperature from 30 to 42 °C eventually results in growth arrest. Cells stop growing 4 h after the temperature shift. The question remains what exactly is altered during that phase until growth is entirely inhibited. Cultures that were grown at the same temperature throughout the

experiment showed a different pattern (Fig. 3.2B). The OD₆₀₀ of the *mreD* mutant grew over-night at 42 °C was very low (OD₆₀₀=1.8). Subcultured cells however were growing almost as quickly as the parent and did not exhibit any heat-sensitivity. During initial growth at 42 °C cells either adjusted to the heat-stress or suppressors likely accumulated. At 30 °C and 37 °C the *mreD* mutant still exhibited a growth defect compared to the parental strain.

Next, it was investigated what might lead to the growth inhibition at 42 °C in the *mreD* strain. Therefore, samples of SH1000, SH1000 Δ *mreD* and the complemented SH1000 Δ *mreD* Δ *geh::P_{mreCD}-mreD* (see 3.7.2 Complementation) were taken 2 h after the temperature shift, stained with fluorescent vancomycin (BODIPY) and analysed by fluorescence microscopy (Fig. 3.3AB).

Microscopic analysis of Δ *mreD* cells grown at 42 °C reveals that their cell morphology changed severely. Cells are larger and fluorescent vancomycin staining shows that septa are formed at irregular positions and appear to be bent towards the septal distal end of the cell. Many cells also exhibit excessive staining in one half of the cell (Fig. 3.3B). MreD might be involved in the placement of the septum under heat-stress or in conditions of fast growth raising the question as to whether cell-division initiation by the Z-ring formation is affected in cells lacking MreD.

In order to investigate the localisation of FtsZ in the *mreD* mutant, a plasmid expressing pCQ11-*ftsZ-eyfp* upon IPTG induction, was transduced into SH1000 and SH1000 Δ *mreD*. Strains were grown in the presence of IPTG at 30 °C and temperature shifted to 37 °C or 42 °C. As a control one group was left at 30 °C. Samples were taken 2 h post shift and analysed as previously described using fluorescence microscopy.

FtsZ localisation in the *mreD* mutant was drastically affected when grown at 42 °C. SH1000 and SH1000 Δ *mreD* grown at 30 °C exhibited a normal distribution of FtsZ at which FtsZ forms an apparent ring at the septum (Fig. 3.4AB). Cultures subjected to a temperature shift to 37 °C or 42 °C exhibited cells with unexpected FtsZ localisation patterns in both strains. FtsZ was found to be distributed in patches around the membrane of cells with increased cell size. This was observed both for SH1000 and the *mreD* mutant which might be due to overexpression of FtsZ leading to bigger cells and in turn to a delocalisation of FtsZ itself. This issue could potentially be resolved using lower IPTG inducer amounts or adding IPTG at a later time point during growth. Nevertheless, FtsZ localisation was altered in the *mreD* mutant shifted to 42 °C compared to the parent. As previously shown, cells are enlarged and the altered morphology is associated with FtsZ localised in patches and aberrant Z-ring formation at unexpected places, or multiple Z-ring formations within the same cell.

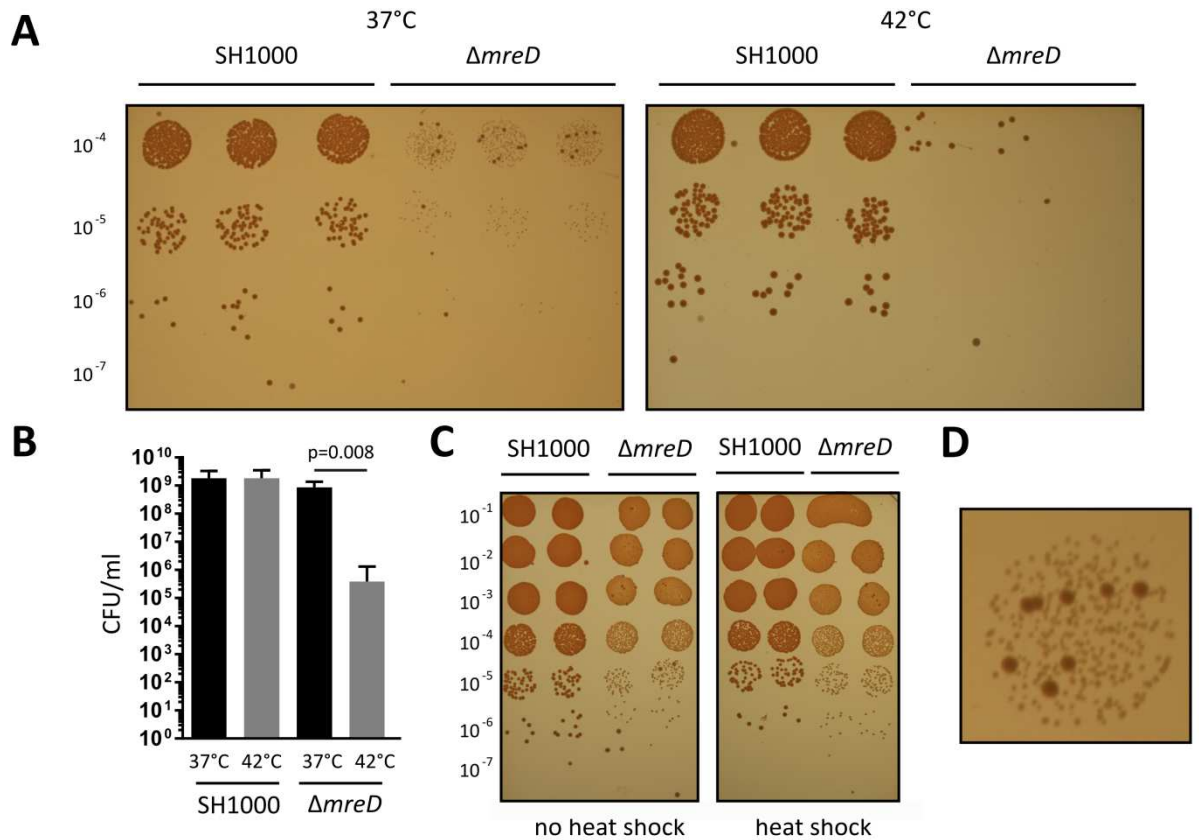
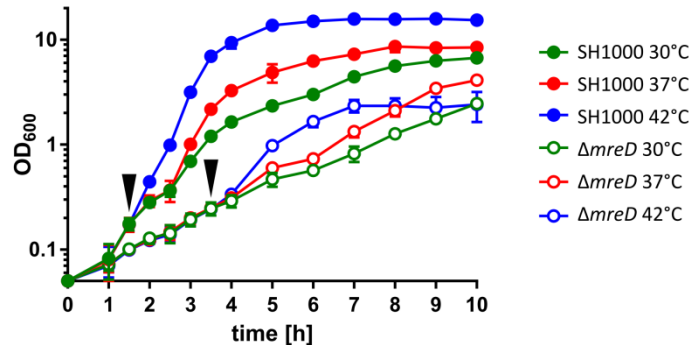


Figure 3.1 Characterization of SH1000 $\Delta mreD$ grown at 42 °C

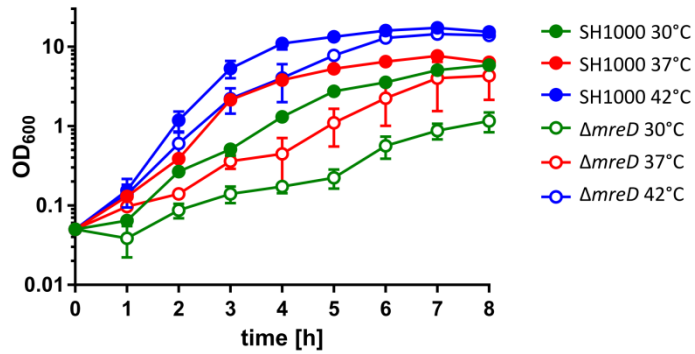
A, Growth of SH1000 and SH1000 $\Delta mreD$ on BHI agar at 37 °C or 42 °C after 24 h. **B**, CFU counts of visible colonies on agar after 24 h at 37 °C or 42 °C. At least five independent replicates were carried out. Significance value p was calculated using a paired two-tailed student's t-test **C**, Growth of SH1000 and SH1000 $\Delta mreD$ on BHI agar at 37 °C for 24 h after exposure to a 10 min 42 °C incubation. **D**, SH1000 $\Delta mreD$ shows potential suppressors restored in growth when grown at 42 °C.

A

temperature shift

**B**

no temperature shift

**Figure 3.2 Growth phenotype of SH1000 $\Delta mreD$ at various temperatures**

A, Growth curves of SH1000 and SH1000 $\Delta mreD$ grown at 30°C. The black arrows indicate a temperature shift to 30, 37 or 42 °C. Three independent replicates were carried out. **B**, Growth curves of SH1000 and SH1000 $\Delta mreD$. Pre-cultures and cultures were grown at the same temperature. Three independent replicates were carried out.

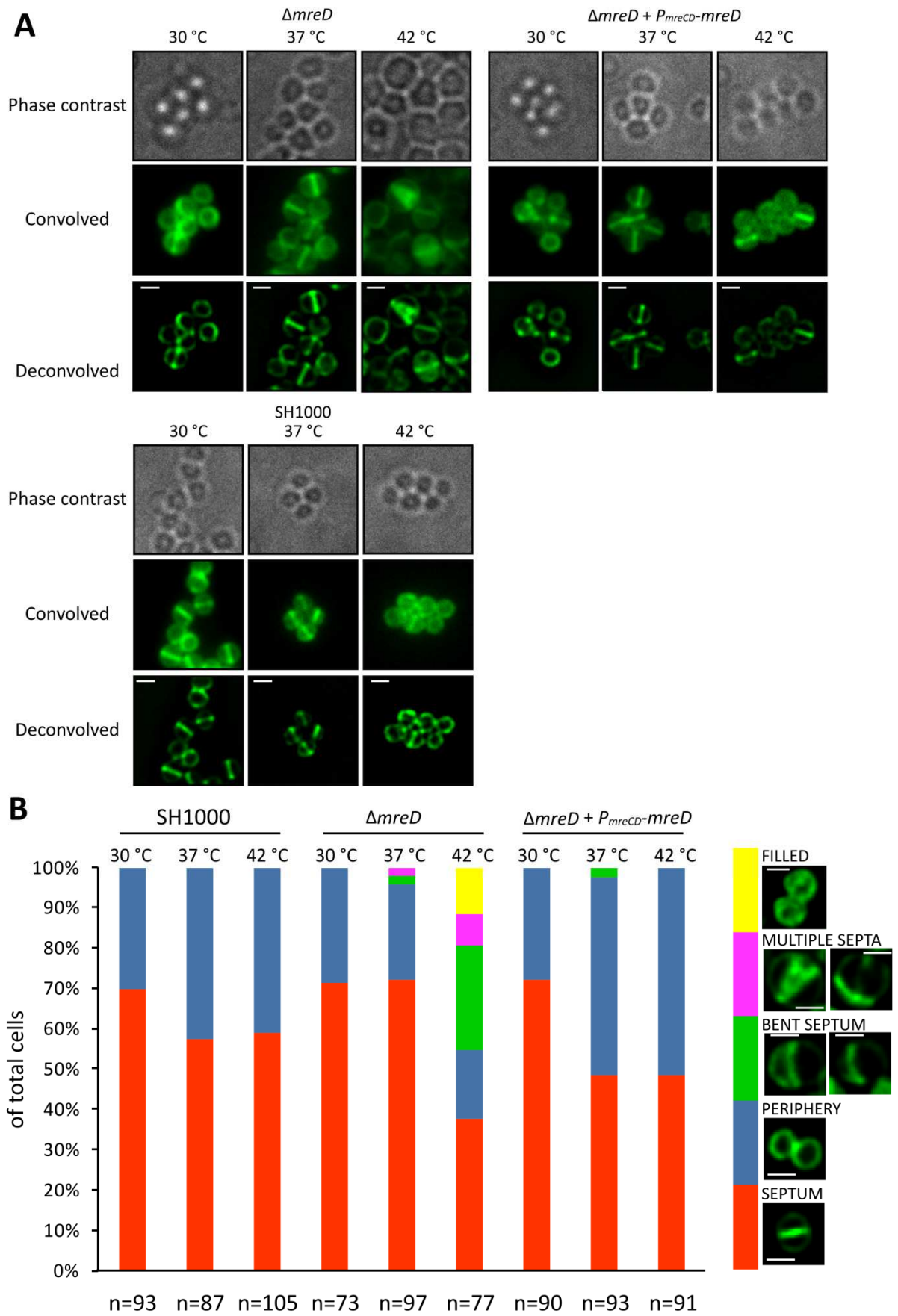


Figure 3.3 BODIPY-FL-Vancomycin labelling of SH1000 $\Delta mreD$ mutants grown at 42 °C

A, Phase contrast and fluorescence images (convolved and deconvolved) of *S. aureus* SH1000, SH1000 $\Delta mreD$ and SH1000 $\Delta mreD \Delta geh::P_{mreCD-mreD}$. Images were acquired using a Delta Vision microscope and SoftWoRx 3.5.0 software (Applied Precision). Acquisition of fluorescence images were taken using 1 sec exposure in the FITC channel. Scale bars represent 1 μm . **B**, Quantification and categorisation of BODIPY-FL-Vancomycin labelled *S. aureus* SH1000, SH1000 $\Delta mreD$ and SH1000 $\Delta mreD \Delta geh::P_{mreCD-mreD}$ grown at 30, 37 and 42 °C. Scale bars represent 1 μm .

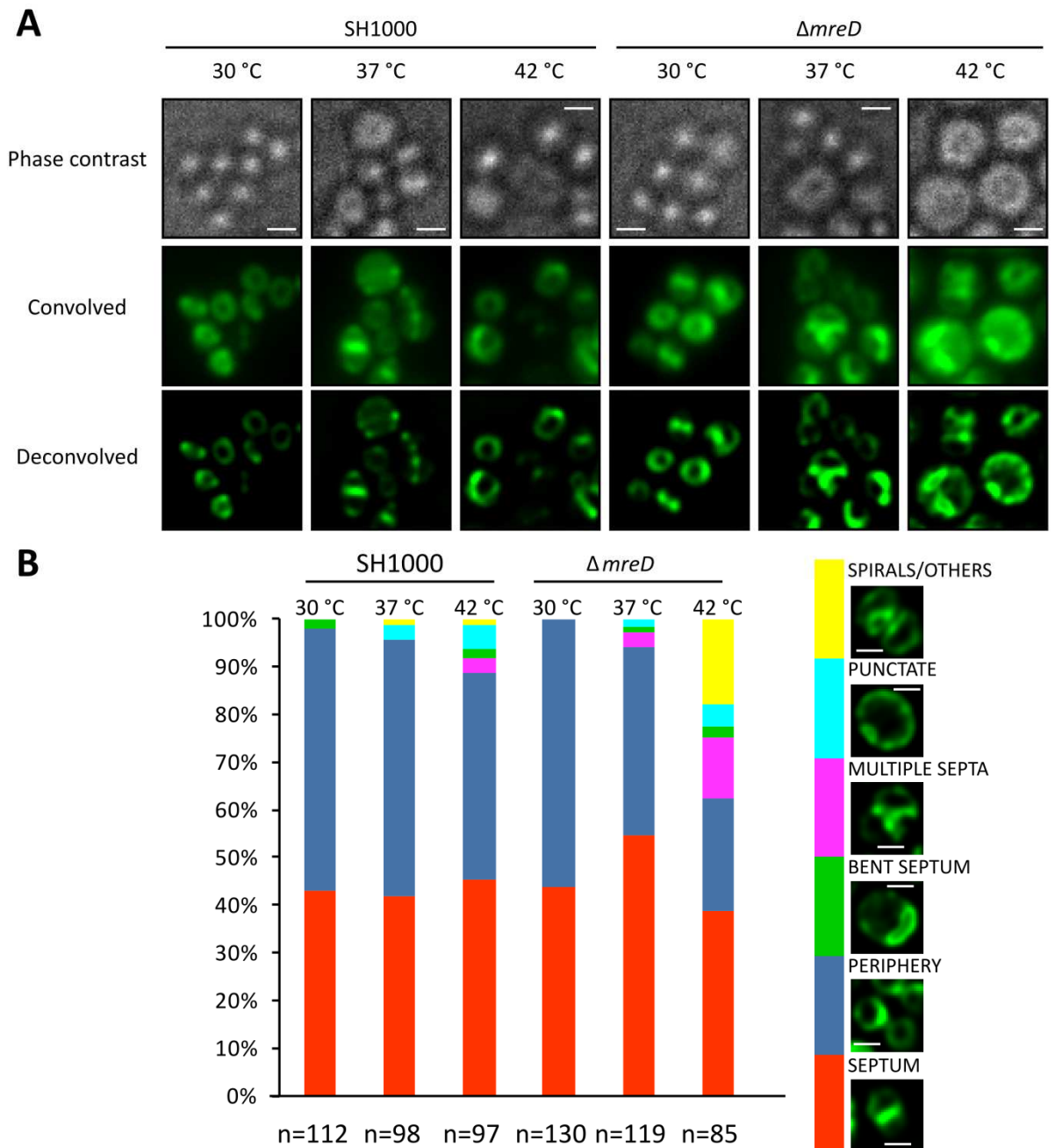


Figure 3.4 FtsZ-eYFP in SH1000 $\Delta mreD$ grown at 42 °C

A, Phase contrast and fluorescence images (convolved and deconvolved) of *S. aureus* SH1000, SH1000 $\Delta mreD$ and SH1000 $\Delta mreD \Delta geh::P_{mreCD-mreD}$. Images were acquired using a Delta Vision microscope and SoftWoRx 3.5.0 software (Applied Precision). Acquisition of fluorescence images were taken using 1 sec exposure in the FITC channel. Scale bars represent 1 μ m. **B**, Quantification and categorisation of FtsZ-eYFP in *S. aureus* SH1000, and SH1000 $\Delta mreD$ grown at 30, 37 and 42 °C. Scale bars represent 1 μ m.

3.2.2 Effect of salts on *ΔmreD* growth

Temperature sensitive mutants have been described before in *Staphylococcus aureus*. Mutations within genes involved in chromosome replication and repair, *dnaB*, *dnaI* and *dnaC* were shown to be viable but stopped growth immediately after a temperature shift from 30 °C to 43 °C (Li *et al.*, 2007, Kaito *et al.*, 2002). A similar phenotype was found for mutants harbouring mutations in peptidoglycan synthesis enzyme genes *murB* and *murC*. These mutants are able to grow until temperature shifted to 43 °C (Ishibashi *et al.*, 2007, Matsuo *et al.*, 2003). Interestingly, cell viability was restored in medium supplemented with >4 % NaCl (w/v) or >20 % sucrose (w/v). MreD itself is required for the rod-shaped morphology in *B. subtilis* mutants and for growth. The addition of 20 mM MgCl₂ to the growth medium partially restores growth of a *mreD* mutant but not morphology (Leaver & Errington, 2005).

To test whether salts or sucrose can restore the growth defect and or temperature-sensitivity of *S. aureus* SH1000 *ΔmreD*, growth curves were performed in BHI supplemented with 40 % sucrose (w/v), 20 mM MgCl₂ or 4 % NaCl (w/v). Overnight cultures were diluted to an OD₆₀₀=0.05 and grown at 37 °C or 42 °C (Fig. 3.5ABCD). Growth in 4 % NaCl (w/v) was additionally analysed by phase contrast microscopy, taking samples 2 h after the temperature shift (Fig. 3.5F). Furthermore, growth of cells plated on BHI agar supplemented with 4 % NaCl (w/v) was investigated (Fig. 3.5E).

Growth of SH1000 *ΔmreD* in BHI supplemented with 20 % sucrose (w/v) or 20 mM MgCl₂ was not altered. Nor did the supplements complement the heat-sensitivity (Fig. 3.5AB). As seen before, *mreD* mutants grow slower than SH1000 and growth at the non-permissive temperature 42 °C resulted in growth arrest after reaching a low cell-density plateau. Supplementation with 4 % NaCl (w/v) specifically relieves heat-sensitivity at 42 °C both on agar and liquid culture, but not the overall growth defect compared to the parent (Fig. 3.5CD). SH1000 *ΔmreD* cells are still enlarged grown at 42 °C in medium supplemented with NaCl but less compared to growth in non-supplemented medium (Fig. 3.5F). The heat-sensitivity could not be reversed by adding 4 % NaCl (w/v) to a *mreD* mutant culture grown at 42 °C that already reached its plateau suggesting that the inability to form correctly placed septa (Fig. 3.3) and FtsZ localisation (Fig. 3.4) is irreversible.

3.2.3 Growth of SH1000 *ΔmreD* in a chemically defined medium

Cells lacking MreD have a growth defect at 42 °C. However, it is not known whether this phenotype is due to the elevated temperature or faster growth. Faster cell propagation requires efficient cellular organisation. To test whether cell growth rate is

responsible for the observed phenotype of SH1000 $\Delta mreD$, cells were grown in a chemically defined medium (CDM) (see Chapter 2 Section 2.1.6) using different glucose concentrations to regulate the growth rate. Overnight cultures were grown in CDM and diluted to an $OD_{600}=0.05$ in CDM followed by monitoring growth at 37 °C at 250 rpm.

Growth of SH1000 and SH1000 $\Delta mreD$ in CDM was monitored under three different conditions. First, growth curves were performed in CDM and different glucose amounts were added at $OD_{600}\approx 0.2$. The *mreD* mutant exhibited a growth defect compared to the wild type (Fig. 3.6A). Growth was slower than in BHI and addition of glucose did not alter growth rate indicating that glucose is not the limiting factor in CDM. Therefore the experiment was repeated in (2x) CDM resulting in faster growth of both strains (Fig. 3.6B). Addition of glucose enhanced the growth rate of SH1000 but not of the *mreD* mutant. The same effect was seen in (2x) CDM supplemented with different glucose concentrations added from the start (Fig. 3.6C). Only very low (0.01 % glucose (w/v)) or no glucose levels affected growth of SH1000 $\Delta mreD$. This might indicate a deficiency of *mreD* to adapt to changing nutritional conditions or that the growth bottleneck is based on a metabolic process that is not addressed in this assay.

3.2.4 Membrane analysis of SH1000 $\Delta mreD$

It has been previously shown that MreD is involved in the localisation of phospholipid synthesis enzymes PlsY and CdsA (Garcia-Lara *et al.*, 2015). The delocalisation of these enzymes and potentially other proteins involved in fatty acid and phospholipid synthesis could affect their activity. Thereby the ratio between certain fatty acid species or phospholipids could be altered. The analysis of *mreB* and *mreC* mutants in *B. subtilis* revealed an increase of the overall fatty acid chain length (Strahl *et al.*, 2014). The analysis of anteiso compared to iso fatty acids however, revealed that *mreC* mutant and to a lesser extent the *mreB* mutant exhibited an increased amount of anteiso fatty acids. Interestingly, fatty acid compositions can have an effect on membrane fluidity which was shown to be a crucial factor in the organisation of bacterial membranes (Strahl *et al.*, 2014).

3.2.4.1 Phospholipid and fatty acid analysis

In order to analyse fatty acids and phospholipids, SH1000 and SH1000 $\Delta mreD$ overnight cultures were diluted in BHI to an $OD_{600}=0.05$ and grown to exponential phase of $OD_{600}\approx 0.5$ in BHI at 37 °C and 250 rpm. Pellets were washed in PBS and

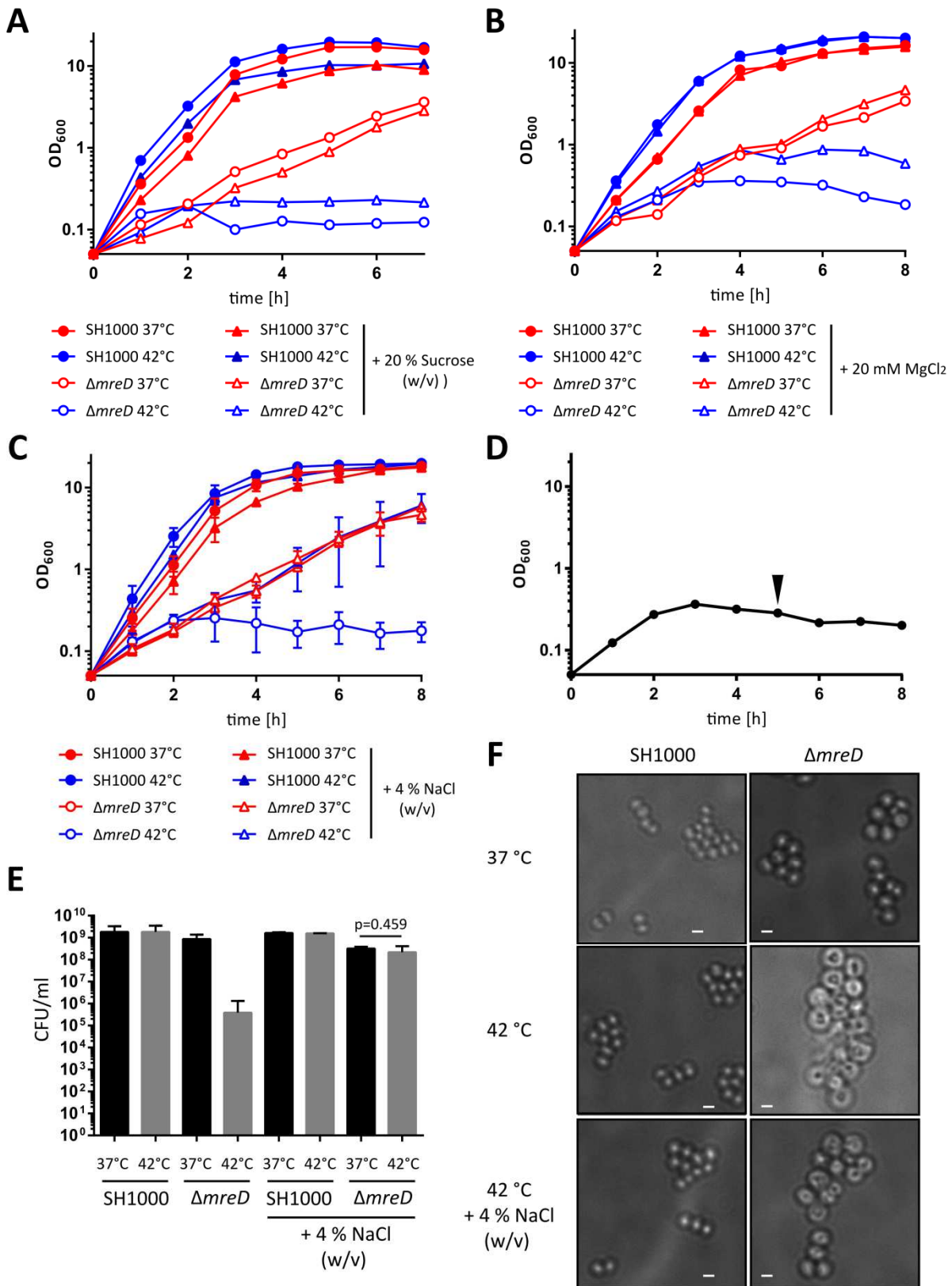


Figure 3.5 Heat-sensitivity phenotype of $\Delta mreD$ in the presence of salts or sucrose

A, Growth curves of SH1000 and SH1000 $\Delta mreD$ in BHI medium and BHI medium supplemented with 20 % sucrose (w/v). **B**, Growth curves of SH1000 and SH1000 $\Delta mreD$ in BHI medium and BHI medium supplemented with 20 mM $MgCl_2$. **C**, Growth curves of SH1000 and SH1000 $\Delta mreD$ in BHI medium and BHI medium supplemented with 4 % NaCl (w/v). Experiments were carried out in three independent replicates. **D**, Growth curve of SH1000 $\Delta mreD$ in BHI medium. Black arrow indicates addition of 4 % NaCl (w/v). **E**, CFU counts of visible colonies on agar supplemented with 4 % NaCl (w/v) after 24 h at 37 °C or 42 °C. At least three independent replicates were carried out. Significance value p was calculated using a paired two-tailed t-test. **F**, Phase contrast images of *S. aureus* SH1000, SH1000 $\Delta mreD$ and grown at 37 °C or 42 °C in regular BHI broth or supplemented with 4 % NaCl (w/v). Images were acquired using a Delta Vision microscope and SoftWoRx 3.5.0 software (Applied Precision).

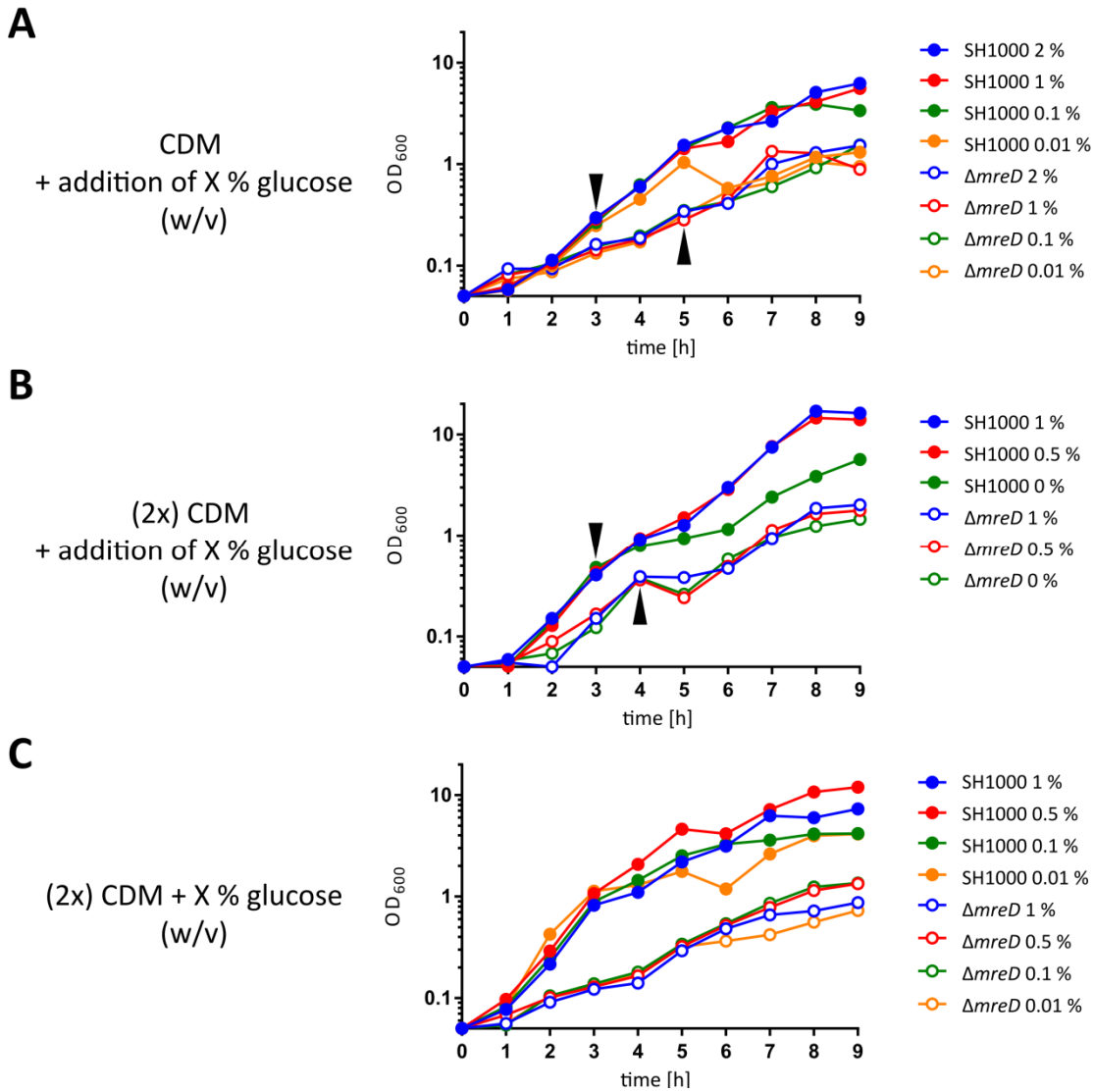


Figure 3.6 Growth of SH1000 $\Delta mreD$ in chemically defined medium (CDM)

A, Growth curves of SH1000 and SH1000 $\Delta mreD$ in CDM broth. Black arrows indicate addition of different glucose concentrations. **B**, Growth curves of SH1000 and SH1000 $\Delta mreD$ in (2x) CDM broth. Black arrows indicate addition of different glucose concentrations. **C**, Growth curves of SH1000 and SH1000 $\Delta mreD$ in (2x) CDM broth supplemented with different glucose concentrations.

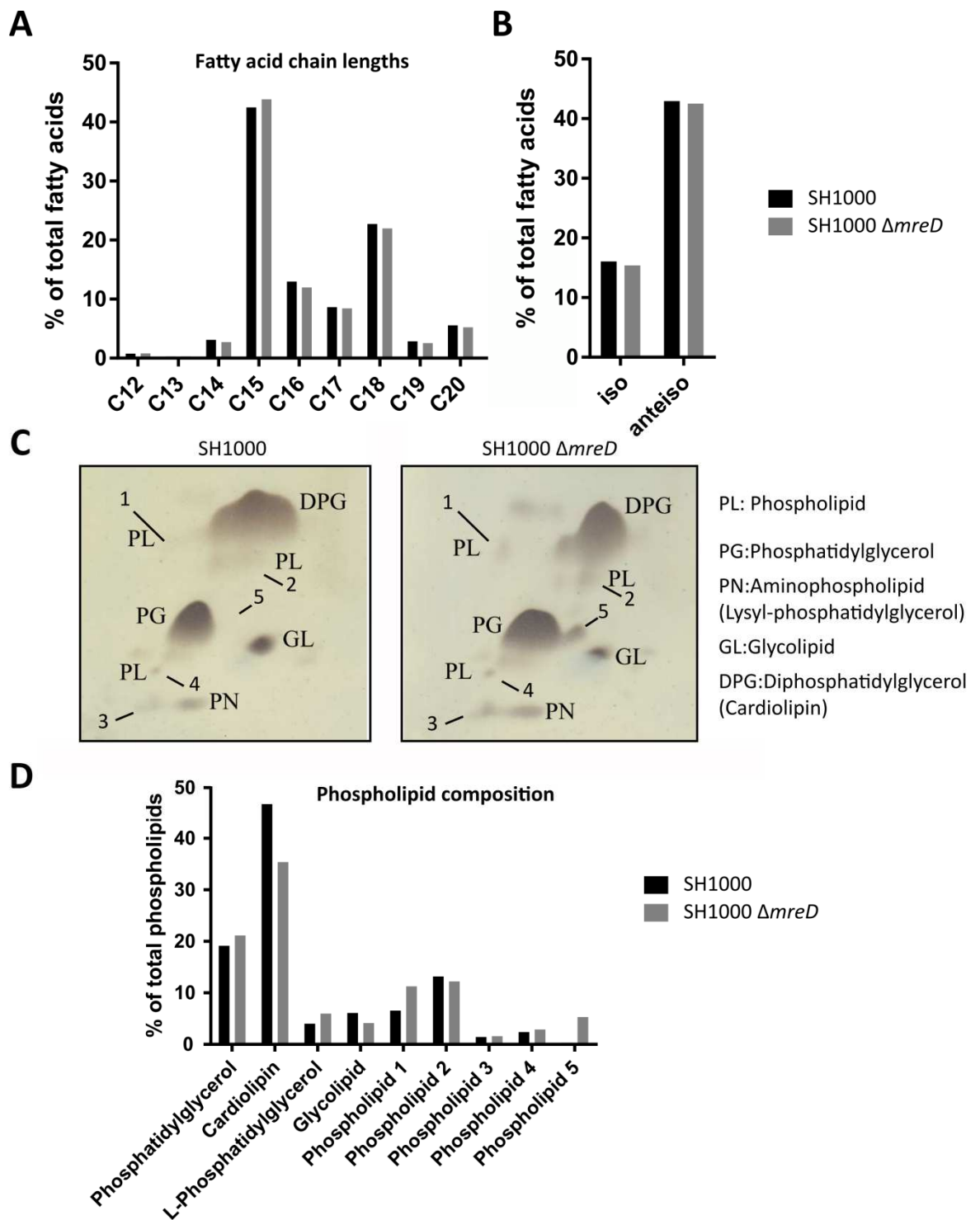


Figure 3.7 Fatty acid and phospholipid composition of SH1000 and SH1000 $\Delta mreD$
A, Fatty acid amounts relative to total fatty acids categorised into C13-C20 species. **B**, Relative amounts of iso and anteiso fatty acid species. **C**, Thin layer chromatograms of phospholipids. **D**, Phospholipid quantification based on the thin layer chromatograms (C).

snap-frozen in liquid nitrogen. Subsequently, frozen pellets were dehydrated using a freeze dryer and stored at -80 °C. Phospholipid analysis was carried out by thin layer chromatography and fatty acids were analysed as fatty acid methyl esters using gas chromatography (Fig. 3.7). Both services were provided by the DSMZ Identification Service (Braunschweig, Germany).

Fatty acid analysis results were categorised into their carbon chain length and compared to the total fatty acid amount. C15 and C18 fatty acids are the predominant species in both strains (Fig. 3.7A). C16/C17/C20 species constitute 5-13 % of the total fatty acids. Other fatty acids such as C12/C13/C14/C19 are less represented in both analysed strains under the conditions tested. SH1000 $\Delta mreD$ exhibits slightly higher amounts of C15 fatty acid species but lower long-chained species such as C16-C20 compared to the parent meaning a decrease in the overall fatty acid chain length in cells lacking MreD. Additionally, SH1000 $\Delta mreD$ has less branch-chained fatty acids as less iso and anteiso species were found compared to the parental strain (Fig. 3.7B). Both, anteiso fatty acids and short chain length fatty acids contribute to an increase of membrane fluidity (de Mendoza D *et al.*, 2002). However, this analysis did not reveal any large changes in the fatty acid composition and needs to be repeated in order to be able to draw specific conclusions about the effect of MreD on the fatty acid composition.

The phospholipid (PL) composition was analysed based on thin layer chromatograms (Fig. 3.7C). Intensity values of signal patches were measured using Fiji-ImageJ and compared to the total phospholipid amount (Fig. 3.7D). Unidentified PLs were marked with PL1-5 (Fig. 3.7C).

The *mreD* mutant exhibited more phosphatidylglycerol and more lysophosphatidyl-glycerol. Another unidentified PL, termed PL1, was also found to be more abundant in SH1000 $\Delta mreD$ compared to SH1000. Interestingly, PL5 was only found in the *mreD* mutant and cardiolipin levels were greatly (≈ 30 %) reduced. This initial analysis suggests changes in the membrane composition due to the effect of MreD.

3.2.4.2 Membrane fluidity analysis

It has been reported previously that MreB organises the bacterial membrane by creating regions of increased fluidity (RIFs) (Strahl *et al.*, 2014). These RIFs are involved in lipid homeostasis and localisation of several membrane proteins in *B. subtilis*. Furthermore, *B. subtilis* cells lacking MreD exhibited changed Nile Red staining and MreB localisation suggesting a role for MreD in the organisation of the membrane together with MreB. Changes in phospholipid composition and to a lesser degree in

fatty acid composition in SH1000 and its *mreD* mutant could have an impact on membrane fluidity.

Membrane fluidity can be measured by fluorescence polarisation using the membrane dye 1,6-diphenyl-1,3,5-hexatriene (DPH) that specifically fluoresces within hydrophobic but not within aqueous environments (Kinosita *et al.*, 1981). Movement of DPH intercalated within the membrane is dependent on the membrane fluidity (Fig. 3.8A). The more fluid the membrane the more DPH changes its orientation. This movement is analysed by exciting DPH with polarised light and measuring the intensity of emitted light parallel and perpendicular to the incident light (Fig. 3.8B) (Jovin, T. M., 1979).

Membrane fluidity analysis experiments were carried out based on a modified protocol of Bayer *et al.* (Bayer *et al.*, 2000). SH1000 and SH1000 Δ *mreD* overnight cultures were diluted in BHI to an $OD_{600}=0.05$ and grown to exponential phase of $OD_{600}\approx 0.5$. 1 ml samples were washed twice in sterile 15 mM Tris-HCl buffer (pH 7.0) and resuspended in the same buffer at an $OD_{600}=0.4$. The sample was transferred to a quartz cuvette and DPH was added to a final concentration of 4 μ M (4 mM stock solution in THF) followed by incubation for 15 min with magnetic stirring at 200 rpm in the dark at 37 °C to allow the incorporation of DPH into the membrane. Fluorescence polarisation was measured using a Spectrofluorimeter (LS50B Perkin-Elmer) equipped with a temperature-controlled cuvette holder and a magnetic cuvette stirrer. The sample was excited at 358 nm emitted light was measured at 428 nm whereas one emission polariser is oriented in the horizontal plane and the other one in the vertical plane. Measured emission intensities parallel (I_1) and perpendicular (I_2) to the plane of excitation light were used to calculate the degree of polarisation according to the following equation:

$$P = \frac{I_1 - G_2 I_2}{I_2 - G_1 I_1}$$

, where the correlation factor G is the ratio between parallel and perpendicular emitted light when the excitation light is horizontal. Lower fluorescence polarisation values indicate a higher membrane fluidity.

Fluorescence polarisation values of membrane fluidity experiments are usually within a narrow range and experiments need to be carried out multiple times to achieve significant results (Camargo *et al.*, 2008, Mishra *et al.*, 2009, Cartron *et al.*, 2014). The analysis of membrane fluidity SH1000 and the *mreD* mutant did not reveal a significant difference between both strains (Fig. 3.10C). However, experiments were only carried out three times due to limited time which is not sufficient to draw conclusions on the effect of MreD on membrane fluidity of *S. aureus*.

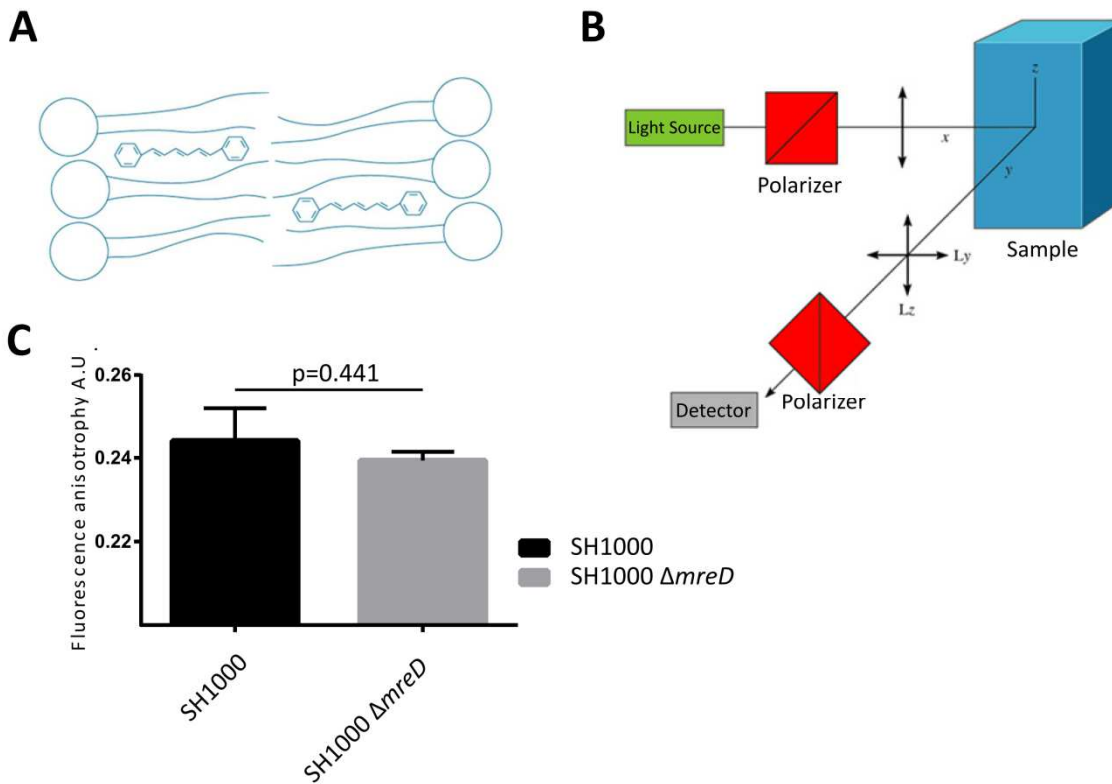


Figure 3.8 Membrane fluidity measurements

A, Schematic illustration of DPH intercalated in the membrane. **B**, Schematic illustration of fluorescence anisotropy measurements. Samples are excited by polarised light and the intensity emitted light parallel and perpendicular to the incident light is measured. **C**, Fluorescence polarisation measurements of SH1000 and SH1000 $\Delta mreD$. Experiments were performed with three independent biological replicates. P value was calculated using an unpaired student's ttest.

3.2.5 Metabolome analysis of SH1000 and SH1000 $\Delta mreD$

Cells lacking MreD were shown to be sensitive towards temperature changes (Fig. 3.1 and Fig. 3.2) and are unable to utilise different glucose amounts when added to the growth medium (Fig. 3.6). Additionally, the *mreD* mutant exhibited a growth defect at all incubation temperatures tested. Taking together this led to the assumption that MreD might act as metabolic optimiser that improves cellular processes. This hypothesis was tested by the analysis of the metabolome of SH1000 compared to SH1000 $\Delta mreD$ incubated at 37 °C and 42 °C.

3.2.5.1 Sample processing

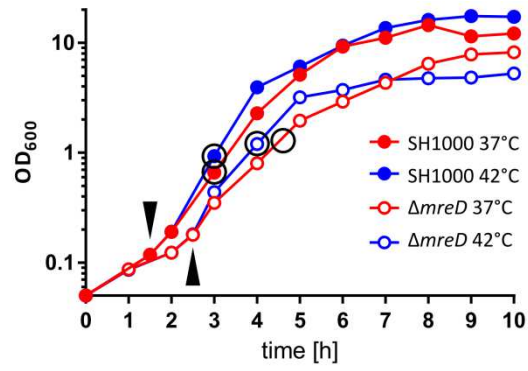
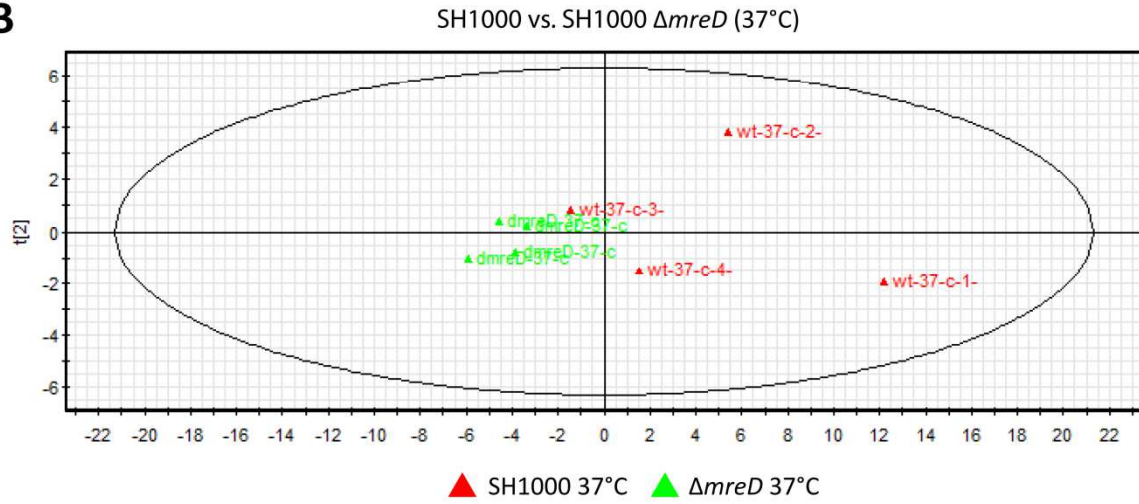
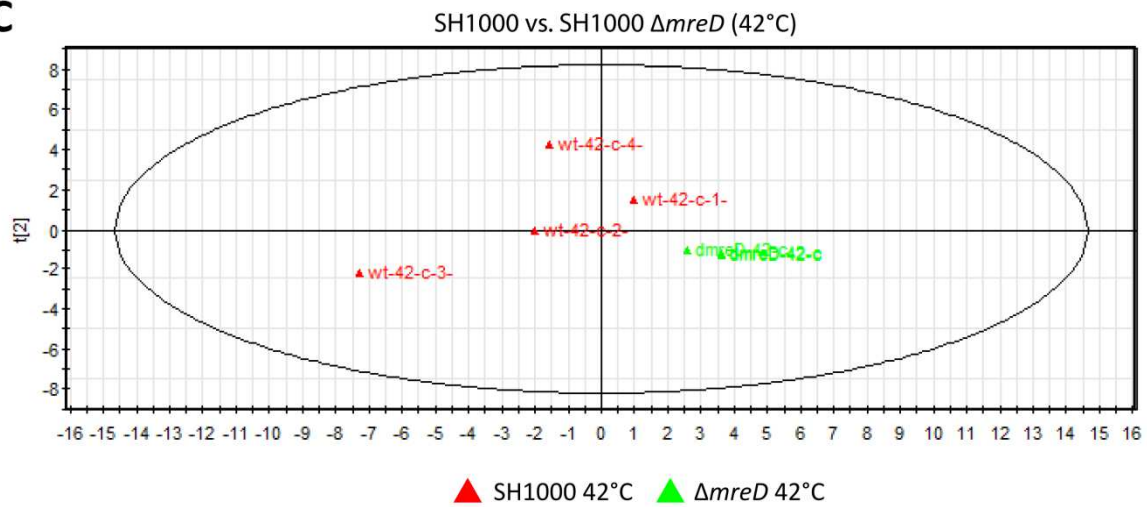
Sample preparation, metabolite extraction and metabolite analysis are described in detail in Section 2.14.

Briefly, metabolites were extracted from samples taken from a temperature-shift experiment. SH1000 and SH1000 $\Delta mreD$ were grown at 37 °C to an $OD_{600} \approx 0.2$ before cultures were either temperature shifted to 42 °C or left at 37 °C (Fig. 3.9A). Cultures were harvested at an $OD_{600} \approx 1$ and instantly mixed with the NaCl/Ethanol extraction mix pre-cooled to -30 °C. Cultures were harvested by centrifugation and the pellet was stored at -80 °C.

Metabolites were extracted using a methanol/chloroform protocol (see Section 2.14.2) and analysed by electro spray induced liquid chromatography mass spectrometry (ESI-LC-MS).

3.2.5.2 Principal component analyses between metabolome subgroups

First of all, it was tested whether the metabolomes between both strains and between growth 37 °C and 42 °C differs (Fig. 3.9BCDE). This analysis was performed by principal component analysis (PCA) using the multivariate analysis software SIMCA P+ (Umetrics SIMCA P+, Umeå, Sweden). PCA identifies groups of variables that are related to each other between multiple multivariate datasets and visualises them on a PCA plot (Trivedi *et al.*, 2012). This plot shows possible groups of similar or unrelated datasets at which the distance between data points indicate how closely both datasets are related to each other.

A**B****C**

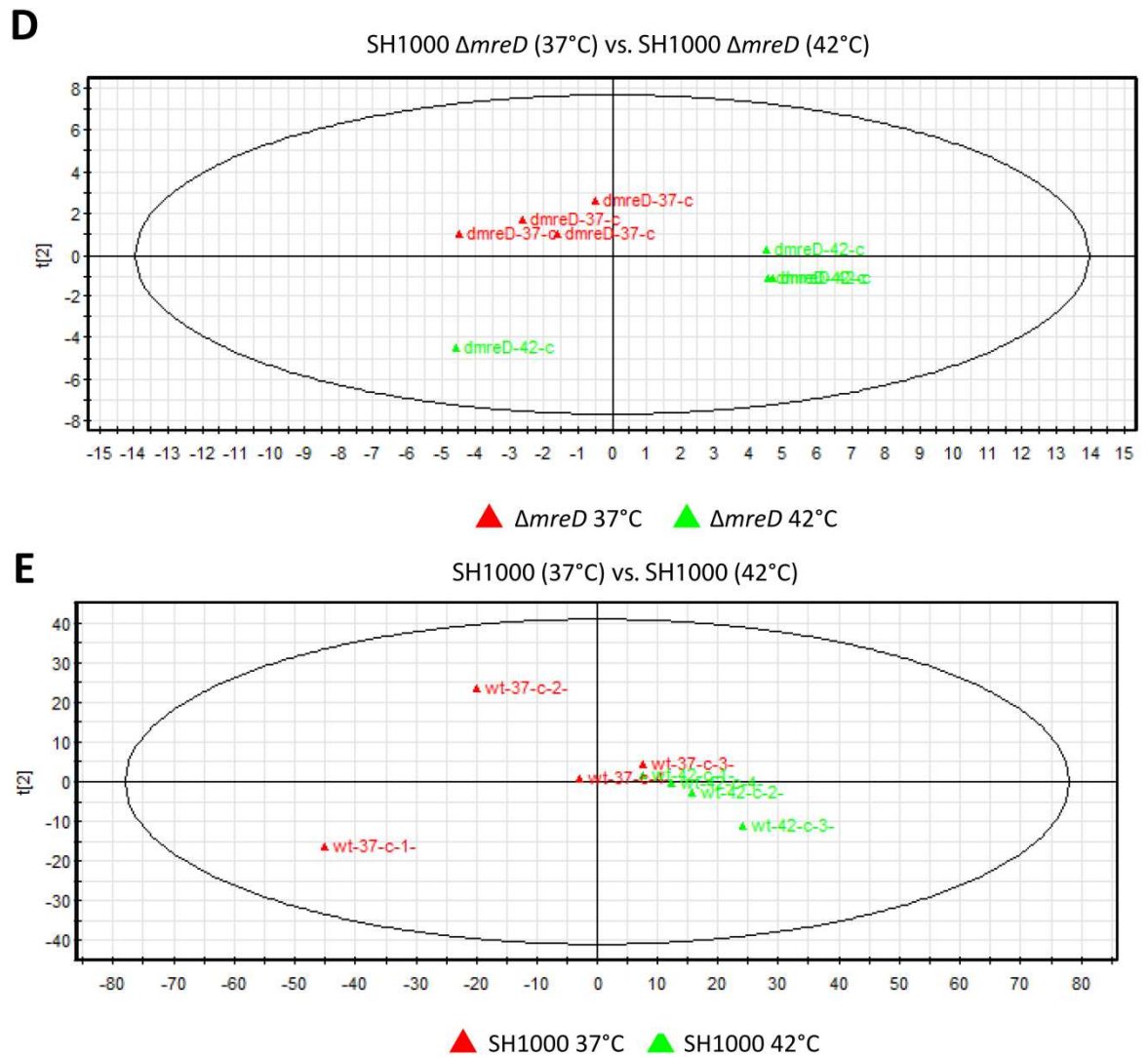


Figure 3.9 Metabolome principal component analyses

Individual triangles represent metabolomes for SH1000 (red triangle) and SH1000 $\Delta mreD$ (green triangle). Overlapping points indicate ‘similar’ or matching metabolomes. **A**, Growth curve of SH1000 and SH1000 $\Delta mreD$. Black arrows indicate a temperature shift. Black circles indicate sampling points for metabolite extraction. **B**, PCA of four metabolome biological replicates of SH1000 and SH1000 $\Delta mreD$ grown at 37 °C. **C**, PCA of four metabolome biological replicates of SH1000 and SH1000 $\Delta mreD$ grown at 42 °C. **D**, PCA of four metabolome biological replicates of SH1000 $\Delta mreD$ grown at 37 °C or 42 °C. **E**, PCA of four metabolome biological replicates of SH1000 grown at 37 °C or 42 °C.

The principal component analysis between four biological replicates of SH1000 and SH1000 $\Delta mreD$ metabolomes from cultures grown at 37 °C identifies a cluster of $\Delta mreD$ metabolomes that are closely related to each other (Fig. 3.9B). Metabolomes of SH1000 are more spread but rather unrelated to the $\Delta mreD$ metabolome cluster. This means that the metabolome of SH1000 $\Delta mreD$ is different from its parental strain when grown at 37 °C. However, the metabolomes between different replicates of SH1000 grown at 37 °C were also found to exhibit variations compared to each other which could be explained by an extreme variability of metabolites due to small changes in their growth phase. Potentially, samples of SH1000 metabolomes were harvested at slightly different time points and thus exhibit differing metabolite compositions. Yet, the PCA does not show a random unrelated distribution of all metabolome datasets indicating that the metabolite extraction and analysis reveals real changes and is reproducible.

The same analysis was carried out between both strains grown at 42 °C (Fig. 3.9C) and gives a similar picture. Metabolomes of SH1000 $\Delta mreD$ are strongly clustered and different from the ones of SH1000 showing that the metabolome of the $mreD$ mutant grown at 42 °C is different from SH1000 grown at the same temperature.

Next, the effect of a temperature shift on SH1000 $\Delta mreD$ was tested by comparing metabolomes of the $mreD$ mutant grown at 37 °C against growth at 42 °C (Fig. 3.9D). The PCA identifies two clusters where the metabolomes of SH1000 $\Delta mreD$ grown at 37 °C are similar to each other. The other cluster is composed with all $\Delta mreD$ samples grown at 42 °C with the exception of one outlier. This suggests that SH1000 $\Delta mreD$ temperature shifted from 37 °C to 42 °C exhibits a change in its metabolite composition.

No clear cluster formation can be seen comparing metabolomes of SH1000 grown at 37 °C and 42 °C (Fig. 3.9E). All datasets apart from two samples grown at 37 °C are located within the same cluster. It is therefore likely that the temperature switch in SH1000 did not cause large metabolome alteration.

3.2.5.3 Identification of altered metabolites

It has been shown that the metabolome between SH1000 and its $mreD$ mutant is altered and the logical next step is to identify which metabolites are changed. Even small differences in metabolite levels can indicate changes in metabolic processes. Some metabolites are very abundant whereas others are rarely found but no less important. Therefore, the comparison of absolute metabolite levels can lead to wrong conclusions and oversee changes of low level metabolites. Hence, metabolites that were found to be significantly different (two-tailed paired ttest, $p < 0.005$) between SH1000 and SH1000 $\Delta mreD$ grown at 37 °C independent of absolute numbers were picked and further

investigated. Since the identity of metabolites is unknown they are referred to their mass/charge in the following analyses.

A number of metabolites were found to be significantly up or down-regulated comparing the metabolomes from SH1000 $\Delta mreD$ with SH1000 grown at 37 °C (Fig. 3.10A). Some metabolites were up to 250 % up and 90 % down-regulated in the *mreD* mutant.

Next it was analysed how the same investigated metabolites are altered in SH1000 $\Delta mreD$ grown at 42 °C (Fig. 3.10B). Thus, the same analysis was performed comparing the same metabolites between SH1000 $\Delta mreD$ grown at 42 °C compared to growth at 37 °C. This reveals that metabolites being up-regulated at 37 °C are down-regulated at 42 °C and vice versa. The metabolome of SH1000 $\Delta mreD$ at 42 °C is therefore more similar to SH1000 grown at 37 °C.

The first step in the identification of altered metabolite levels is to study which molecule masses could correspond to the mass found by mass spectrometry. It has to be noted that electro spray induced mass spectrometry signals indicate the mass of protonated molecules at which molecules can be protonated with H^+ , Na^+ , K^+ or NH_4^+ . The signal output of mass data is stated as mass/charge since molecules could be protonated more than once in case of a normality of >1 .

These information were taken together and a list of potential metabolites was collected (see Table 3.1). Most masses, however, correspond to several different metabolites and it is therefore not possible to identify a molecule solely based on its mass. This requires further analysis to collect more information of the mass signal (Table 3.1).

3.2.5.4 Metabolite identification by tandem mass spectrometry

Tandem mass spectrometry is a technique that separates a signal based on its mass to charge ratio. Thus, it is possible to fragment the isolated mass by electron capture (EC) ionisation (Leis *et al.*, 2004). This results in the separation of certain groups that indicate whether the molecule of interest contains certain functional groups and thus gives more information about its identity. Tandem mass spectrometry with EC induced fragmentation was performed on signal peaks 100.2/142.2/211.2/242.2/ 244.2/258.2 /267.1 and 473.2. One example of this fragmentation process is shown in Fig. 3.11.

The additional information gathered by fragmentation analyses was not enough to identify the metabolites of interest since none of the observed fragmentation patterns corresponded to the potential metabolite candidates. This might be explained by choosing the wrong candidates or too strong fragmentation settings that might have resulted in unexpected fragmentation patterns. The analysis of the metabolome was not continued since it would have been difficult to identify a range of metabolites.

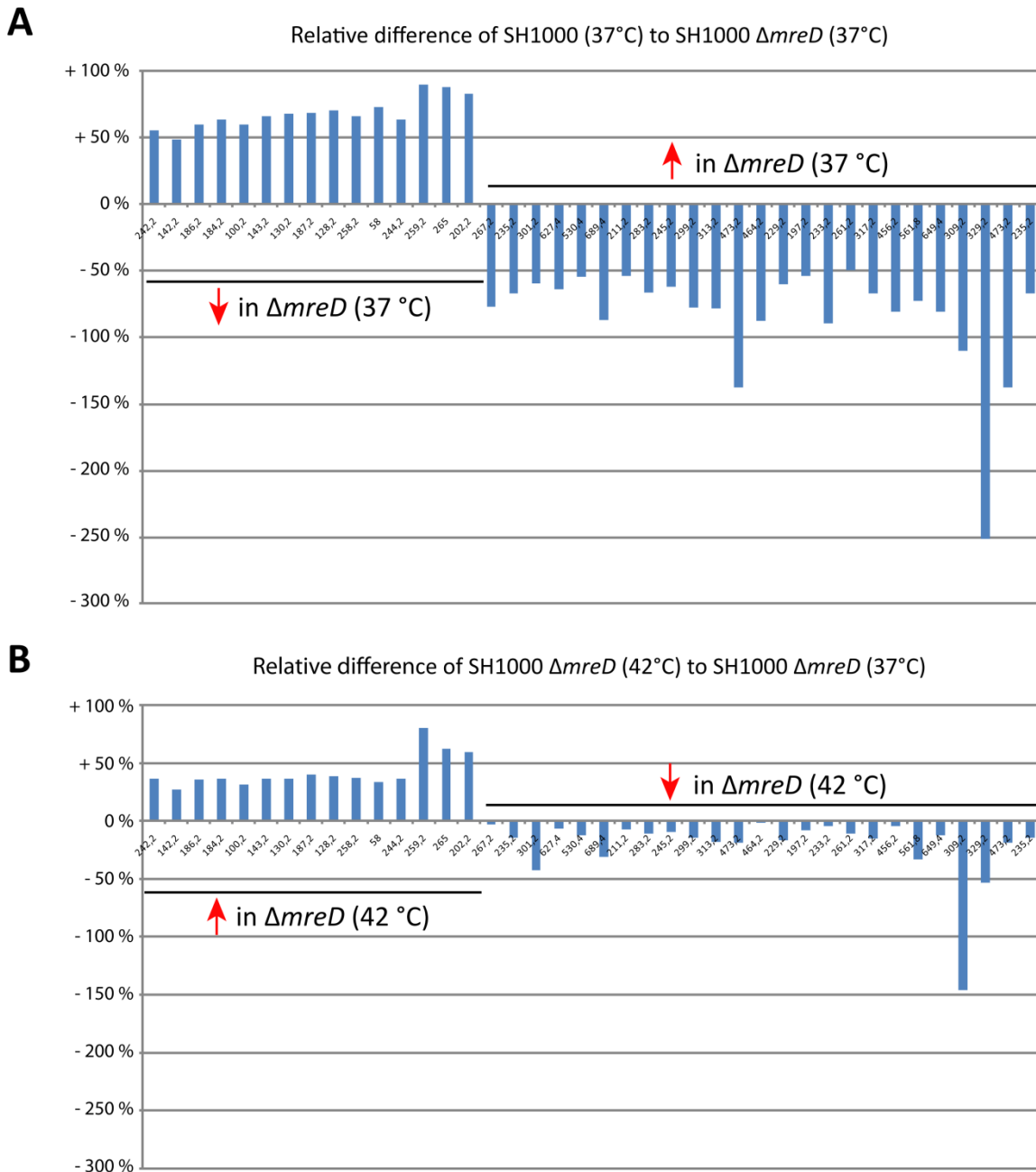


Figure 3.10 Relative changes of metabolite levels

A, Relative changes in metabolite levels from SH1000 compared to SH1000 $\Delta mreD$ grown at 37 °C. Metabolites were chosen since they were found to be significantly altered between both strains. Red arrows indicate whether metabolite levels are lower or higher in $\Delta mreD$ strain compared to its parent. **B**, Relative changes in metabolite levels from SH1000 $\Delta mreD$ grown at 42 °C compared to SH1000 $\Delta mreD$ grown at 37 °C. Metabolites analysed from SH1000 $\Delta mreD$ compared to SH1000 were chosen. Red arrows indicate whether metabolite levels are lower or higher in the $\Delta mreD$ strain grown at 42 °C compared to growth at 37 °C.

Table 3.1 Analysed metabolite masses and potential candidates

Mass	Metabolite candidates
↓ 242.2	O-succinyl-L-homoserine, pantothenic acid, oxaloglutarate, 4-amino-2-methyl-5-phosphomethylpyrimidine
↓ 142.2	ethanolamine phosphate, histidinol, hygrine, homoserine, threonine, 3-amino-2-methylpropanoate, 4-aminobutanoate, malonate, urea-1-carboxylate
↓ 186.2	3-phosphoserine, 2-amino-3-carboxymuconate semialdehyde, glutamic acid, O-acetyl-L-serine, L-2-aminoadipate
↓ 184.2	2-oxoglutarate, 2-aminoadipic acid, O-acetyl-L-homoserine, 3-phosphonoxypropionate, choline phosphate
↓ 100.2	ethanolamine, cysteamine
↓ 143.2	no candidates could be found
↓ 130.2	5-oxoproline, pyrroline-hydroxy-carboxylate, L-pipecolate
↓ 187.2	no candidates could be found
↓ 128.2	2-aminomuconate-6-semialdehyde, serine, diethanolamine, alanine, oxalic acid, dihydroxyacetone, lactic acid
↓ 258.2	4-amino-2-methyl-5-phosphomethylpyrimidine, O-succinyl-L-homoserine, pantothenic acid, 3-(imidazol-4-yl)-2-oxopropyl phosphate
↓ 58	no candidates could be found
↓ 244.2	cytidine, histidinol phosphate, N-acetyl-D-galactosamine, N-acetyl-D-glucosamine, N-acetyl-D-mannosamine
↓ 259.2	no candidates could be found
↓ 265	4-amino-4-deoxychorismate
↓ 202.2	glucosamine
↑ 267.2	uridine, biotin, (R)-5-phosphomevalonate, deoxyuridine, myristic acid
↑ 235.2	4-phospho-L-aspartate, galactonate, gluconic acid
↑ 301.2	linolenic acid, mannitol-1-phosphate
↑ 627.4	tetrahydropteroyltri-L-glutamate
↑ 530.4	Inositide Triphosphate
↑ 689.4	glycogen
↑ 211.2	saccharic acid, 5-hydroxy-ferulic acid, sedoheptulose, sinapyl-alcohol, jasmonic acid, 7,8-diaminononanoate, 3-dehydroshikimate, capric acid
↑ 283.2	dimethoxybenzoic acid, mannitol, sorbitol, uridine, biotin, 1L-myo-inositol-1-phosphate, fructose-1/6-phosphate, galactose-1-phosphate
↑ 245.2	uridine, biotin, cystathionine, flavone, 4-methyl-5-(2-phosphoethyl)-thiazole, homoisocitrate, lipoic acid
↑ 299.2	6-phosphogluconate, 2-[3-carboxy-3-(methylammonio)propyl]-L-histidine
↑ 313.2	icosanoic acid, sedoheptulose-7-phosphate, catechin, N-(L-arginino)succinate
↑ 473.2	copalyl diphosphate, geranylgeranyl-PP
↑ 464.2	thiamine
↑ 229.2	arginine, Gramine, isopropylmaleate, 2-isopropyl-3-oxosuccinate, N-formimino-L-glutamate, Ethyl (E,Z)-decadienoate, D-gluconate, cis-still
↑ 197.2	D-galacturonate, D-glucuronate, jasmonic acid, 4-(glutamylamino), N2-succinyl-L-ornithine, melatonin
↑ 233.2	no candidates could be found
↑ 261.2	L-γ-glutamyl-L-hypoglycin, D-erythro-imidazole-glycerol-phosphate, alpha;-D-galactose, alpha;-D-mannose, beta;-D-glucose-6-phosphate, I
↑ 317.2	cinchonine, linolenic acid, alpha-Eleostearic acid, Punicic acid, Sterculic acid, 9,10-Dihydroxystearic acid, alpha;-ribazole
↑ 456.2	no candidates could be found
↑ 561.8	no candidates could be found
↑ 649.4	no candidates could be found
↑ 309.2	mevalonate-5-PP, 14-Dihydroxycornestine, 5-phospho-ribosyl-glycineamide, retinol
↑ 329.2	docosahexaenoic acid, 2',3'-cyclic UMP
↑ 473.2	no candidates could be found
↑ 235.2	4-phospho-L-aspartate, galactonate, gluconic acid, sedoheptulose-7-phosphate, N-(L-arginino)succinate

This table contains all analysed metabolites based on their mass and their corresponding potential molecule. Importantly, candidate molecules do not possess the mass shown here, but their protonated mass correlating with the mass detected by ESI-LC-MS. Red arrows indicate whether metabolite levels are lower or higher in SH1000 *ΔmreD* compared to SH1000.

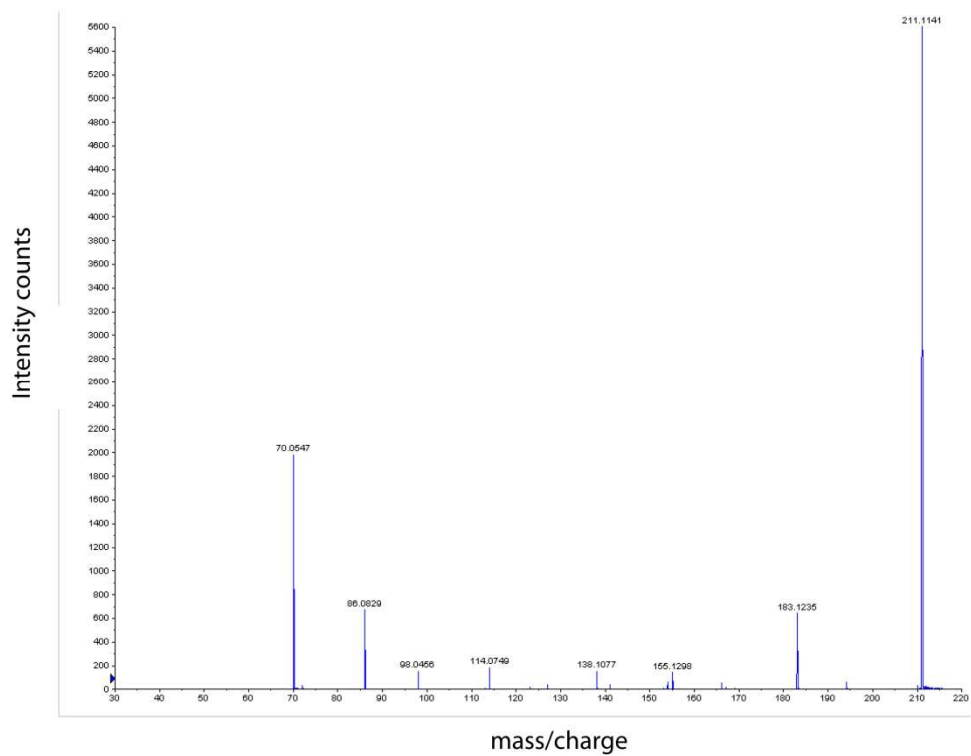


Figure 3.11 Tandem mass spectrometry electron capture induced fragmentation of peak 211.2 da

3.2.6 Suppressors of $\Delta mreD$

3.2.6.1 Phenotypic characterisation of $\Delta mreD$ suppressors

SH1000 $\Delta mreD$ forms big colony variants that potentially contain suppressors of *mreD*. These suppressors are especially pronounced when the *mreD* mutant was streaked on agar at 42 °C. Most cells are unable to grow due to the heat-sensitivity of SH1000 $\Delta mreD$ as shown in Fig. 3.2 and Fig. 3.3. The suppressors however, are not affected by heat and when restreaked, it is revealed that these variants are growing faster than their parental strain (Fig. 3.12AC). PCR and whole genome sequencing confirmed that these strains are *mreD* mutants and suppressors are still resistant towards kanamycin since *mreD* is replaced by a kanamycin resistance cassette (Fig. 3.12A). Plating of suppressors at 37 °C and 42 °C shows that suppressors lost their heat-sensitivity (Fig. 3.12D).

To test whether the suppressors exhibit mutations in *mreC*, the double *mreCD* mutant was checked for the formation of suppressor mutants grown at 42 °C (Fig. 3.12B).

Suppressor mutants could be found both for the *mreD* as well as for the *mreCD* mutant when strains are grown on BHI agar incubated at 42 °C (Fig. 3.12). This also reveals that the *mreCD* mutant exhibits a heat-sensitivity.

Next, it was determined whether these variants contain suppressors. This would mean that the suppressors are stable and growth should be restored when strains are restreaked. In order to test this, $\Delta mreD$ suppressed clones were streaked next to their parental strain and plates were incubated for 24 h at 37 °C. Subsequently, single colonies of the suppressed strain were restreaked and the procedure was repeated twice. For comparison, the parental $\Delta mreD$ strain, was streaked next to the potential suppressed strains.

Suppressed clones always grew faster than their parental strain (Fig. 3.13) and are likely to be mutants since the restored growth was stably inherited after continued restreaking .

3.2.6.2 Whole genomes sequencing of $\Delta mreD$ suppressors

To identify potential suppressor mutations of $\Delta mreD$, genomic DNA of SH1000 $\Delta mreD$ and seven SH1000 $\Delta mreD$ suppressed clones were sent for whole genome sequencing (paired end, 50 bp reads) (GATC, Konstanz, Germany). Whole genome sequencing

coverage was > 300x and therefore more than enough for the identification of single nucleotide polymorphisms (SNPs). The SH1000 sequence was used as a template to compare whole genome sequences and to identify SNPs between SH1000 *ΔmreD*, its suppressed derivatives and the original sequence. In the following analysis, only SNPs between SH1000 *ΔmreD* and suppressed derivatives were taken into account (Table 3.2). A complete analysis including all sequences can be found online using the following link: <http://lin5.shef.ac.uk/saureus2/>

Whole genome sequencing revealed up to three non-silent mutations in each *ΔmreD* suppressed strain compared to the parental SH1000 *ΔmreD* (Table 3.2). Out of seven sequenced suppressor strains, four (No. 5, 15, 16 and 23) showed mutations in ‘*qox*’ genes that encode for subunits of the protein complex cytochrome aa3. Cytochrome aa3 is one of the terminal oxidases in staphylococci and contributes to the last step of respiration by transferring electrons to oxygen (Tynecka *et al.*, 1999, Clements *et al.*, 1999). The mutations found include stop codons at the beginning of *qoxB* and *qoxC* and amino acid exchanges within the N-terminus of QoxA and QoxC.

Furthermore, whole genome sequencing revealed that two strains (No.12 and 15) harbouring mutations in genes involved in the phosphotransferase system (PTS). PTS is a multicomponent protein system that facilitates the uptake of sugars in bacteria (Bramley & Kornberg, 1987).

One suppressor strain (No.9) harbours an amino acid exchange within the global regulator CodY as the only found SNP (Ledala *et al.*, 2014, Majerczyk *et al.*, 2010). CodY is a repressor that regulates various aspects of metabolism and virulence factors. CodY has also been shown to regulate oxidative stress related proteins by inhibiting expression of *katA* (catalase) and *sodM* (superoxide dismutase) (Pohl *et al.*, 2009).

Whole genome sequencing of suppressor No.10 additionally revealed a SNP within the gene *sbi* that is encoding the immunoglobulin G binding protein. Since its major role is during host infection specifically in the evasion of the immune response (Smith *et al.*, 2011), it seems unlikely that *sbi* is involved in suppression of a lack of MreD.

Many of the SNPs found point to the *qoxABCD* operon as being involved in the suppression of *ΔmreD*. Confirmation of the SNPs was carried out by PCR amplification and sequencing of *qoxA* (5’FW36/3’FW36), *qoxB* (5’FW82/3’FW83) and *qoxCD* (5’FW84/3’FW84) from suppressed strains No. 5, 15, 16 and 23. Additionally, *qoxABCD* genes of 5 additional suppressed strains (No.17, 18, 19, 21 and 22) were sent for sequencing. SNPs in *qox* genes revealed by whole genome sequencing were

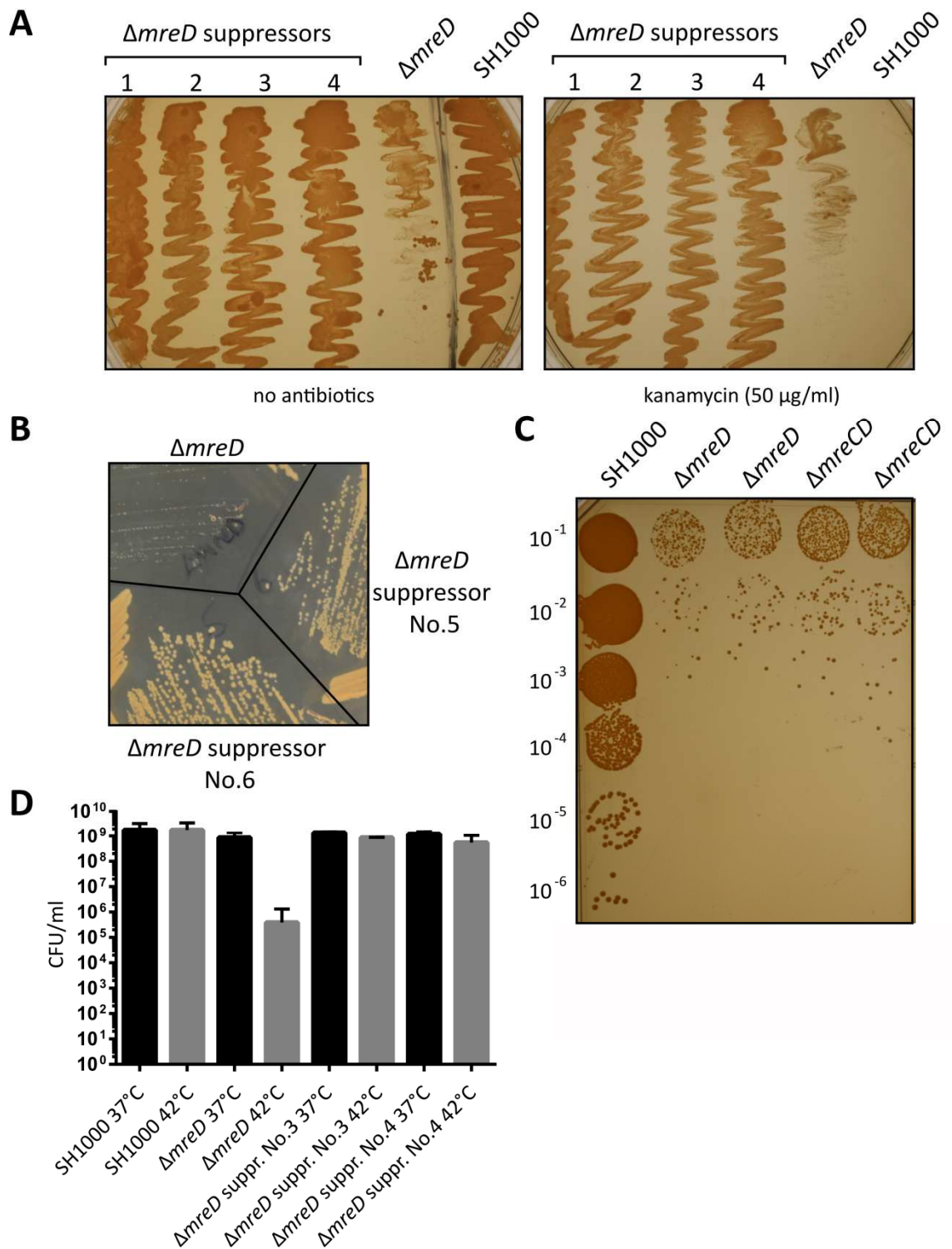


Figure 3.12 SH1000 $\Delta mreD$ suppressor growth on plate

A, Growth of SH1000, SH1000 $\Delta mreD$ and $\Delta mreD$ suppressors on BHI agar plates without or with kanamycin at 37 °C for 24 h. **B**, Plating of SH1000, SH1000 $\Delta mreD$ and SH1000 $\Delta mreCD$ BHI agar plates incubated at 42 °C for 24 h. **C**, Growth of SH1000 $\Delta mreD$ and $\Delta mreD$ suppressors on BHI agar incubated at 37 °C for 24 h. **D**, Plating CFU counts on BHI agar of SH1000, SH1000 $\Delta mreD$ and $\Delta mreD$ suppressors at 37 °C and 42 °C.

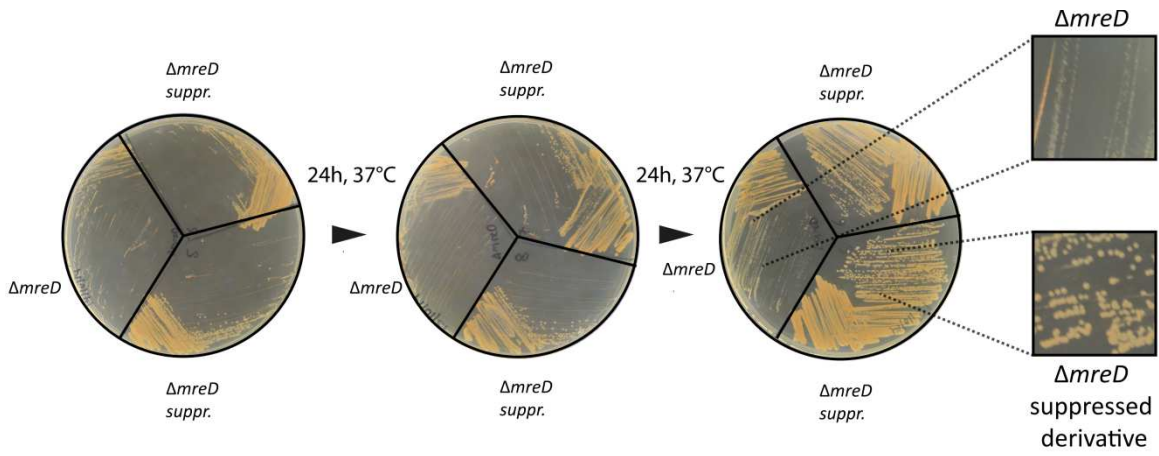


Figure 3.13 Restreaking of SH1000 $\Delta mreD$ suppressed derivatives

SH1000 $\Delta mreD$ suppressed derivatives were streaked on BHI supplemented with kanamycin (50 $\mu\text{g/ml}$). SH1000 $\Delta mreD$ streaks were performed from the same plate. Right images show magnified plate areas.

Table 3.2 Single nucleotide polymorphisms of SH1000 Δ *mreD* suppressor strains

Strain Number	Gene	Mutation	Function
5	SAOUHSC_01002 (<i>qoxA</i>)	S43L	Quinol oxidase AA3, subunit II
10	SAOUHSC_02660	M250I	Hypothetical protein, putative Mg transporter
	SAOUHSC_02706 (<i>sbi</i>)	A266V	Immunoglobulin G-binding protein Sbi (Smith <i>et al.</i> , 2011)
	SAOUHSC_02790	K718I	Hypothetical protein, putative helicase
11	SAOUHSC_01228 (<i>codY</i>)	N11K	transcriptional repressor CodY, GTP-binding protein that senses the intracellular GTP concentration as an indicator of nutritional limitations (Pohl <i>et al.</i> , 2009)
12	SAOUHSC_00524 (<i>rpoB</i>)	R825I	RNA polymerase beta chain
	SAOUHSC_01979	P75L	Hypothetical protein, Cro/C1 family transcriptional regulator
	SAOUHSC_02661 (<i>ptsG1</i>)	G6A	PTS system sucrose-specific transporter subunit IIBC
15	SAOUHSC_00749	V276L	Hypothetical protein, domains of FepB (ABC-type Fe ³⁺ -hydroxamate transport system) and FatB (Siderophore binding protein)
	SAOUHSC_01029 (<i>ptsA</i>)	R138H	Phosphoenolpyruvate-protein Phosphotransferase (Bramley & Kornberg, 1987)
	SAOUHSC_01000 (<i>qoxC</i>)	L70Stop (201 amino acid total length)	Cytochrome c oxidase subunit III
16	SAOUHSC_01001 (<i>qoxB</i>)	Q190Stop (662 amino acid total length)	quinol oxidase, subunit I
	SAOUHSC_A00526	R64L	Hypothetical protein
23	SAOUHSC_01000 (<i>qoxC</i>)	E29K	Cytochrome c oxidase subunit III

Amino acid exchanges are stated in the amino acid one letter code. If a mutation leads to a stop codon, the original total amino acid sequence length is stated in brackets.

confirmed by re-sequencing (not shown). Furthermore, sequencing of additional suppressed strains showed that 2 out of 5 sequenced strains also harboured mutations in *qox* genes. Sequencing revealed a mutation at the beginning of *qoxB* leading to a frameshift and following stop codon (after 5 aa) in strain No.21. Another mutation was found in *qoxA* of strain No.18 causing a stop codon after the 148th codon (total length of QoxA is 320 amino acids). All mutations found in *qoxABCD* genes are summarised in Fig. 3.14.

In summary, many mutations were found in *qox* genes and two suppressed strains (No. 5 and 23) were shown to only harbour mutations in these genes. This strongly suggests an involvement of the terminal oxidase in suppression of $\Delta mreD$. Potentially, all mutations lead to a non functional cytochrome aa3 that has a positive effect on cells lacking MreD.

If respiration has a harmful effect on the *mreD* mutant, growth at anaerobic conditions could relieve the growth defect. This was tested by growing the *mreD* mutant and its parent on agar plates incubated at 37 or 42 °C in a sealed box containing AnaeroGen sachets (ANAEROGENTM, Thermo Scientific) and in liquid culture in BHI filled universal tube incubated without shaking. However, no differences to aerobic growth were observed (not shown).

3.2.7 Complementation of $\Delta mreD$

Phenotypes observed after mutation of a gene of interest have to be confirmed by complementation experiments to exclude the influence of polar effects and spontaneous mutations.

Former complementation was performed by constitutive expression of *mreD* or *mreC* together with *mreD* using a plasmid-based system (Ma, 2016). However, the growth defect on agar was not complemented and growth in liquid was only complemented when *mreD* was expressed in $\Delta mreCD$ but no complementation was seen when *mreD* is expressed in $\Delta mreD$. Expression of *mreD* together with *mreC* in $\Delta mreCD$ only partially complemented growth in liquid culture.

3.2.7.1 Plasmid-based complementation of $\Delta mreD$

To reproduce these experiments plasmids pGL485 (empty vector expressing *lacI*) (Cooper *et al.*, 2009), pGL621 (*mreD* expression) and pGL631 (*mreCD* expression)

were transduced into SH1000, $\Delta mreD$ and $\Delta mreCD$ and growth in BHI medium supplemented with chloramphenicol (10 $\mu\text{g/ml}$) was investigated.

As seen in Fig. 3.15, previous results could not be reproduced and expression of *mreD* alone led to slightly impaired growth of SH1000 and both the *mreD* and *mreCD* mutant. Expression of *mreCD* in the *mreD* mutant but not in the double mutant partially restored growth (Fig. 3.15).

3.2.7.2 Single-copy-expression of *mreD* complementation of $\Delta mreD$

The plasmid-based complementation of the growth phenotype is therefore not conclusive. Using a promoter prediction software ([http://www.softberry.com/berry.phtml?topic=bprom &group=programs&subgroup=gfindb](http://www.softberry.com/berry.phtml?topic=bprom&group=programs&subgroup=gfindb);) suggests that *mreC* and *mreD* expression is driven by a promoter upstream of *mreC*. However, there might also be a promoter within the last 80 bp of *mreD* driving the expression of a downstream DNA fragment encoding for the ribosomal proteins *rplU*, *ysxB* and *rpmA* (see Fig. 3.16). Using the neural network promoter prediction (http://www.fruitfly.org/seq_tools/promoter.html) on the other hand proposes two promoters in the intergenic region of *mreD* and *rplU*. Thus, this suggests that expression of downstream genes might not be affected by the deletion of *mreD*.

3.2.7.2.1 Construction of complementation vector pKASBAR- P_{mreCD} -*mreD*

To ensure that the observed phenotypes of the *mreD* mutant are not due to downstream effects, a single copy of *mreD* integrated ectopically on the chromosome expressed by the promoter of *mreCD* was constructed.

This was facilitated using pKASBAR, a derivative of pCL84 (Kabli, 2013))(Lee *et al.*, 1991). pKASBAR is a non-replicating plasmid in *S. aureus* that integrates into the lipase gene via site-specific recombination with help of an integrase expressed from plasmid pYL112 Δ 19.

A DNA fragment upstream of *mreC* (5'FW94/3'FW94) and the gene encoding *mreD* (5'FW95/3'FW93) were amplified from SH1000 genomic DNA and both fragments were cloned into the *Bam*HI/*Eco*RI site of pKASBAR-*ezrA-eyfp* using Gibson Assembly replacing *ezrA-eyfp* (see Fig. 3.17). Recombinant plasmids were tested by PCR using primer pair 5'FW94/3'FW93 resulting amplification of a 732 bp fragment (Fig. 3.17B) and validated by DNA sequencing (GATC Biotech AG, Konstanz, Germany). The resulting plasmid, pKASBAR- P_{mreCD} -*mreD*, was electroporated into a RN4220 strain containing the helper

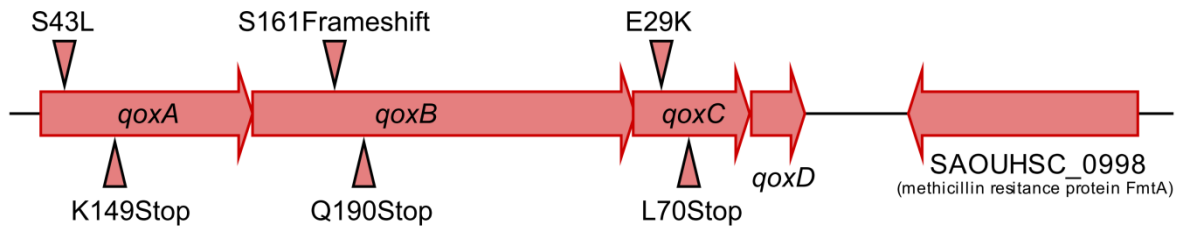


Figure 3.14 SNPs found in SH1000 $\Delta mreD$ suppressed strains

Schematic representation of the *qoxABCD* operon and SNPs found in $\Delta mreD$ suppressors. No.5 (*qoxA*:S43L), No.18 (*qoxA*:K149Stop), No.21 (*qoxB*:S161Frameshift), No.16 (*qoxB*:Q190Stop), No.23 (*qoxC*:E29K), No.15 (*qoxC*:L70Stop).

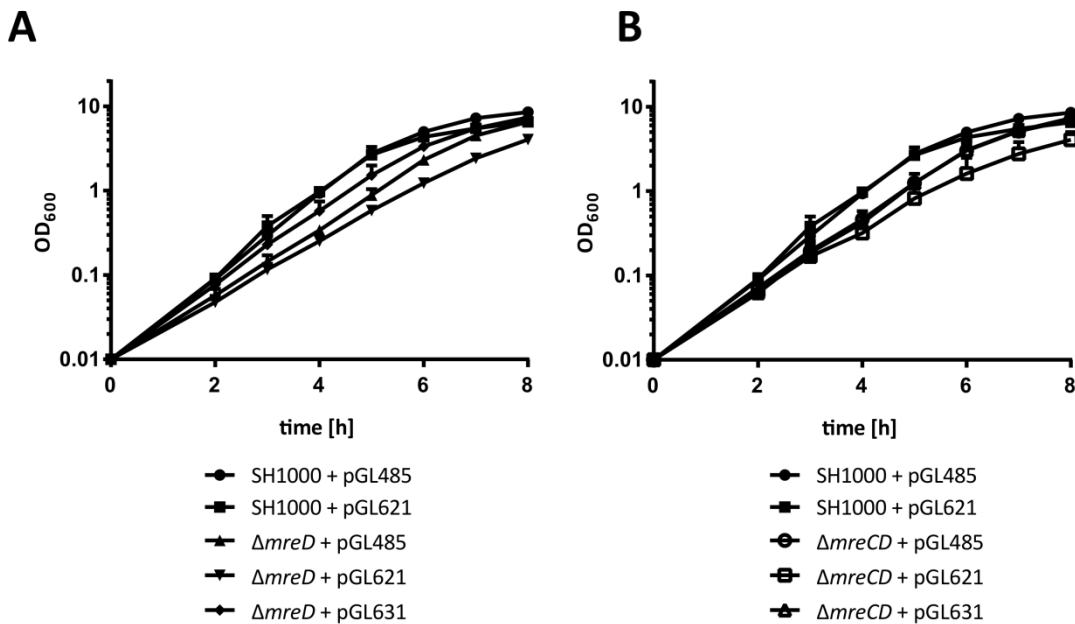


Figure 3.15 Plasmid-based complementation of the growth phenotype of SH1000 $\Delta mreD$ and SH1000 $\Delta mreCD$

A, Growth curves of SH1000 and SH1000 $\Delta mreD$ with pGL485 (*lacI*), pGL621 (*mreD*) and pGL631 (*mreCD*) in BHI broth. Three independent experiments were carried out. **B**, Growth curves of SH1000 and SH1000 $\Delta mreCD$ with pGL485 (*lacI*), pGL621 (*mreD*) and pGL631 (*mreCD*) in BHI broth. Three independent experiments were carried out.

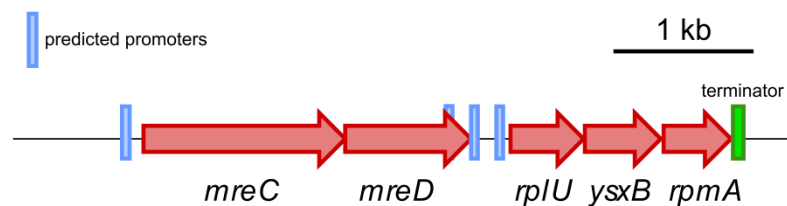


Figure 3.16 Schematic overview of the native genomic region of *mreCD*

Predicted promoters (Softberry and Neural network promoter prediction) are indicated by blue bars and the terminator is indicated by a green bar.

plasmid pYL112 Δ 19 that expresses an integrase needed for the chromosomal integration of pKASBAR (Luong & Lee, 2007, Lee *et al.*, 1991) and from there transduced into the *mreD* deletion strain and SH1000 wild type strain. Integration into the lipase gene was confirmed by streaking candidates on a Baird-Parker agar plate supplemented with Egg-Yolk (Fig. 3.17D). Positive candidates lost their halo indicating the loss of lipase activity. Additionally, integration of the plasmid was tested by PCR using primers 5'FW94/3'FW93 for the presence of the promoter P_{mreCD} next to *mreD* and primer pair Fwd_mreD_EcoRI/3'FW12 for verification of $\Delta mreD::kan$. (Fig. 3.17CE).

3.2.7.2.2 Analysis of single-copy *mreD* expression complementation of SH1000

$\Delta mreD$

Constructed strains were analysed for morphology as follows. Overnight cultures were subcultivated to an $OD_{600}=0.05$ and grown to exponential phase. Samples were harvested and treated with FM1-43 to visualise membranes and allow cell-size measurements, followed by analysis using a Nikon Dual Cam epifluorescence microscope (Fig. 3.18AB).

Growth phenotypes were investigated on agar plates (Fig. 3.18D) and in BHI broth (Fig. 3.18C). To analyse whether the single-copy complementation vector complements the previously described heat-sensitivity, over-night cultures were plated on BHI agar using drop spreading and plates were then incubated at 37 or 42 °C (Fig. 3.18E).

The *mreD* mutant expressing an ectopically integrated single-copy of *mreD* in the lipase gene was analysed regarding morphology phenotype as well as growth in liquid and on BHI agar plates. Cells lacking MreD exhibited a high proportion of cells with increased cell sizes (Fig. 3.18 AB). Expression of *mreD* in the *mreD* mutant led to smaller cells than the wild type and the non-complemented mutant. Both, growth in liquid and on agar plates were partially restored in the complemented $\Delta mreD$ strain and as seen in Fig. 3.18E the growth at 42 °C on BHI agar was also restored.

3.2.7.3 Transduction of $\Delta mreD$ into pre-complemented SH1000

As shown in Section 3.2.1, suppressor mutations arising in the complemented strains is possible. To circumvent the risk of suppressor formation, the $\Delta mreD::kan$ mutation was transduced into SH1000 carrying the P_{mreCD} -*mreD* complementation or the empty pKASBAR construct. Strains were restreaked on BHI plates supplemented with appropriate antibiotics after transduction and subsequently streaked on BHI plates without antibiotics (Fig. 3.19).

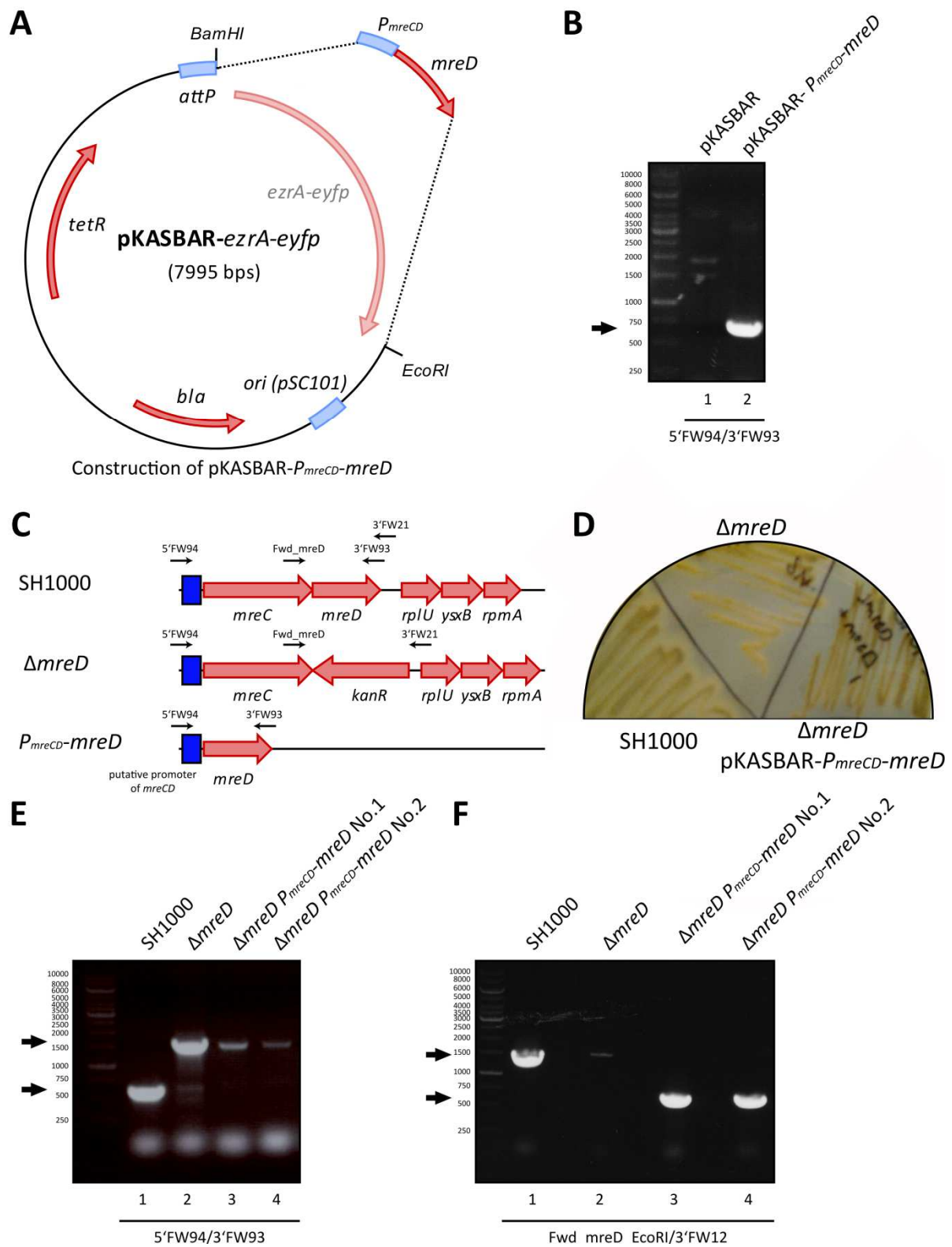


Figure 3.17 Construction of a single-copy chromosomal complementation plasmid for $\Delta mreD$

A, Diagram illustrating the construction of pKASBAR-*P_{mreCD}-mreD*. **B**, Verification of pKASBAR-*P_{mreCD}-mreD* (Lane 2) by PCR using primer pair 5'FW94/3'FW93 which results in amplification of 732 bp fragment, marked by a black arrow. PCR products were separated by 1% (w/v) TAE agarose gel electrophoresis. No DNA amplification is seen using pKASBAR as a negative control template (Lane 1). **C**, Schematic overview of the native genomic region of *mreCD*, *mreCΔmreD* and integrated pKASBAR-*P_{mreCD}-mreD*. Black arrows indicate primer binding sites. **D**, Lipase activity test. SH1000, SH1000 $\Delta mreD$ and SH1000 $\Delta mreD \Delta geh::P_{mreCD}-mreD$ growth on Baird-Parker agar supplemented with egg yolk. The halo around colonies indicates lipase activity. **E**, Verification of $\Delta mreD ::kan$ by PCR using primer pair Fwd_mreD_EcoRI/3'FW12. PCR products were separated by 1% (w/v) TAE agarose gel electrophoresis. A band of approximately 1600 bp, marked by a black arrow, indicates replacement of *mreD* by the kanamycin resistance cassette (Lanes 3-4). A band of approximately 600 bp, marked by a black arrow, indicates the presence of the native *mreD*. Genomic DNA from SH1000 was used as a negative control template (Lane 1) and genomic DNA from SH1000 $\Delta mreD::kan$ was used as a positive control template (Lane 2). **F**, Verification of chromosomal integration of *P_{mreCD}-mreD* by PCR using primer pair 5'FW94/3'FW93. PCR products were separated by 1% (w/v) TAE agarose gel electrophoresis. A band of approximately 600 bp, marked by a black arrow, indicates chromosomal integration of *P_{mreCD}-mreD* (Lanes 3-4). A band of approximately 1500 bp, marked by a black arrow, indicates the native *P_{mreCD}-mreCD* locus. Genomic DNA from SH1000 and from SH1000 $\Delta mreD::kan$ were used as negative control templates resulting in the native *P_{mreCD}-mreCD* for SH1000 genomic DNA (Lane 1) and no DNA amplification for SH1000 $\Delta mreD::kan$ genomic DNA (Lane 2).

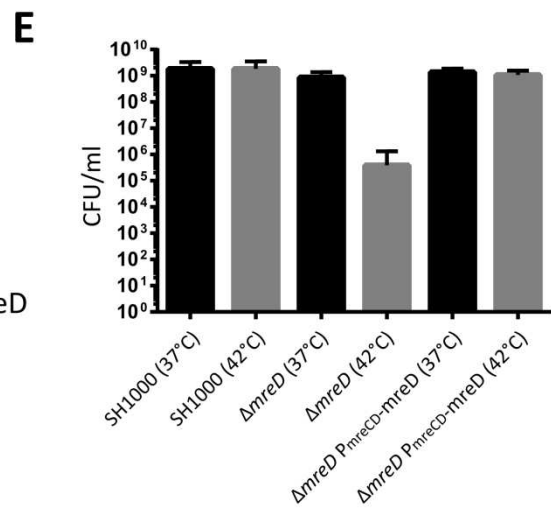
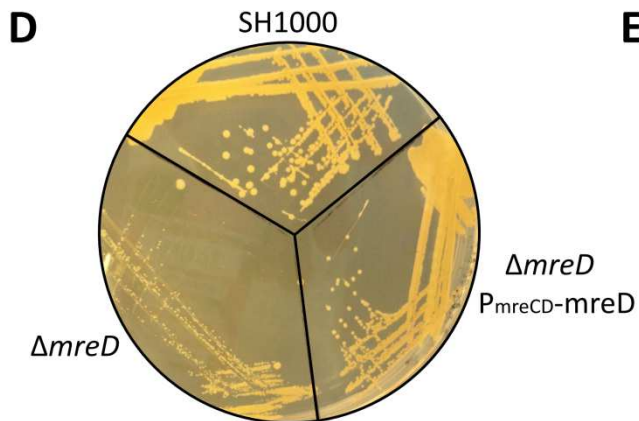
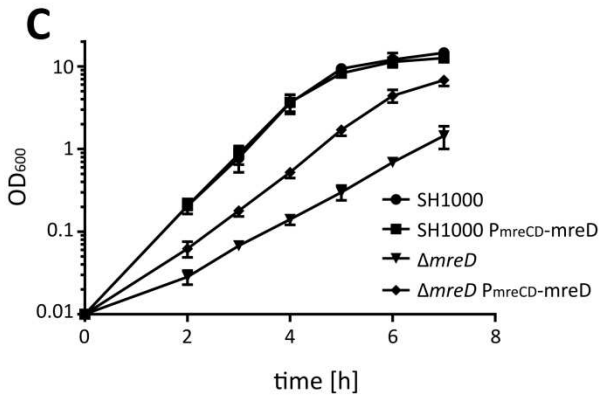
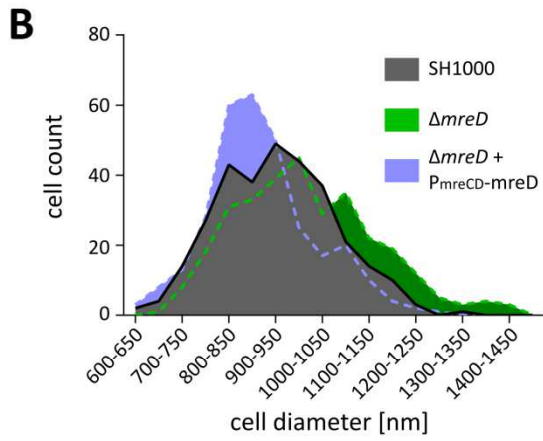
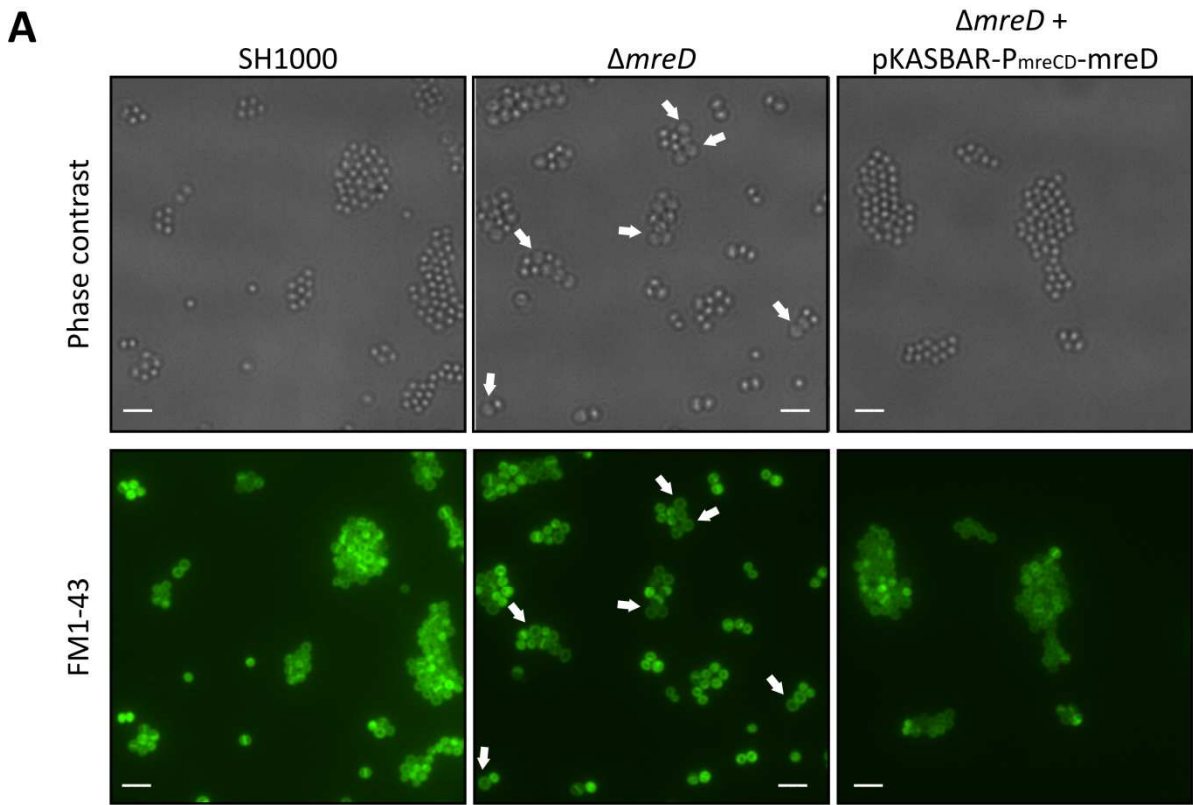


Figure 3.18 Complementation of SH1000 $\Delta mreD$ by single-copy $mreD$ expression

A, Phase contrast and convolved fluorescence images of *S. aureus* SH1000, SH1000 $\Delta mreD$ and SH1000 $\Delta mreD \Delta geh::P_{mreCD-mreD}$ stained with FM1-43. Images were acquired using a Nikon Dual Cam microscope and NIS elements software (Nikon Instruments). White arrows indicate abnormally sized cells. Scale bars represent 3 μm . **B**, Cell counts categorized by cell diameter. **C**, Growth curves of *S. aureus* SH1000, SH1000 $\Delta mreD$ and SH1000 $\Delta mreD \Delta geh::P_{mreCD-mreD}$ in BHI broth. **D**, Growth curves of *S. aureus* SH1000, SH1000 $\Delta mreD$ and SH1000 $\Delta mreD \Delta geh::P_{mreCD-mreD}$ on BHI agar plates. **E**, CFU/ml counts of *S. aureus* SH1000, SH1000 $\Delta mreD$ and SH1000 $\Delta mreD \Delta geh::P_{mreCD-mreD}$ plated on BHI agar incubated at 37 and 42 °C.

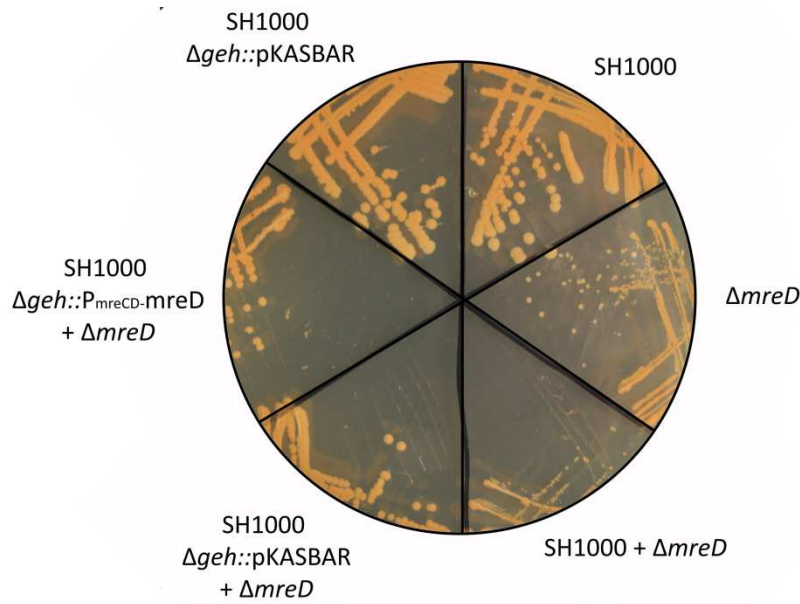


Figure 3.19 Growth on BHI agar of precomplemented SH1000 $\Delta mreD$

Growth on BHI agar of various complemented and non-complemented *mreD* mutants and SH1000 wild type strains. Plates were incubated for 36 h at 37 °C. The ‘+ $\Delta mreD$ ’ indicates that this mutation was transduced into the strain.

The original and a fresh SH1000 $\Delta mreD$ both show a growth defect on plate although the fresh mutant appears to exhibit a more pronounced growth defect as colonies are found throughout the streak for the original mutant but not the fresh mutant (Fig. 3.19). The empty plasmid, pKASBAR, has no effect on growth on SH1000. A pre-complemented SH1000 that got transduced by $\Delta mreD$ is partially restored in growth and colony sizes are bigger as for the parental *mreD* strain but colonies are not found throughout the entire streak. However, the empty pKASBAR plasmid also seems to confer partially restored growth in $\Delta mreD$. These observations were reproducible as other transformants exhibited the same growth phenotypes. It seems unlikely that the knockout of the lipase gene *geh* or the resistance marker of pKASBAR are responsible for the growth complementation since growth of SH1000 containing pKASBAR was not affected.

3.2.7.4 $\Delta mreD$ in other strain backgrounds

In order to investigate whether the lack of MreD results in a growth defect in other strain backgrounds $\Delta mreD::kan$ was transduced into Newman and NewHG and growth curves were performed. The replacement of *mreD* by the kanamycin resistance cassette was confirmed by PCR with primers Fwd_mreD_EcoRI/3'FW12 that are binding upstream and at the end of *mreD* using genomic DNA. Amplification of an approximately 1500 bp fragment indicates $\Delta mreD::kan$ whereas amplification of a 600 bp fragment shows the original *mreD* gene. There was always an amplification of a 600 bp fragment in all PCR reactions which is probably due to nonspecific amplification of a DNA fragment of similar size or a low frequent recombination event may be taking place.

Newman $\Delta mreD$ and NewHG $\Delta mreD$ exhibited a growth defect compared to their parental counterparts suggesting that the previously observed growth defect phenotype in SH1000 is not a strain-specific effect (Fig. 3.20).

The NARSA library is a collection of transposon mutants in a plasmid-cured USA300 strain (Fey *et al.*, 2013). It was tested whether a transposon integrated at the beginning of *mreD* (insertion within the first 5 amino acids) (see Fig. 3.21A) has an effect on growth. In order to do so, $\Delta mreD::Tn$ from USA300 NE858 was transduced into SH1000 and the resulting strain was tested for growth in BHI broth.

The insertion of a transposon at the beginning of *mreD* does not affect growth in liquid broth (Fig. 3.21B). The *mreD* gene contains several alternative start codons at the beginning and *mreD* expression could be driven by an alternative RBS within the beginning of *mreD* or at the end of the transposon. Another explanation could also be that *mreD* has no effect on growth and the observed growth phenotype of $\Delta mreD::kan$ is due to polar effects meaning that the deletion of *mreD* reduced expression of its downstream genes that are required for growth.

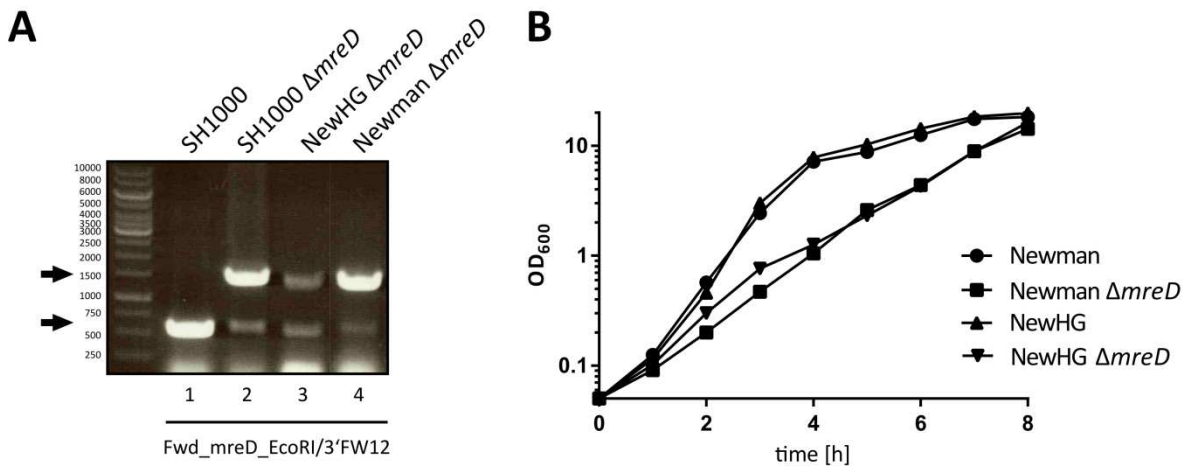


Figure 3.20 Growth phenotype of Newman $\Delta mreD$ and NewHG $\Delta mreD$

A, Verification of $\Delta mreD::kan$ by PCR using primer pair Fwd_mreD_EcoRI/3'FW12. PCR products were separated by 1% (w/v) TAE agarose gel electrophoresis. A band of approximately 1500 bp, marked by a black arrow, indicates replacement of *mreD* by a *kanR*. A band of approximately 600 bp, marked by a black arrow, indicates the presence of *mreD*. **B**, Growth curve of Newman, NewHG and their $\Delta mreD$ mutant, respectively.

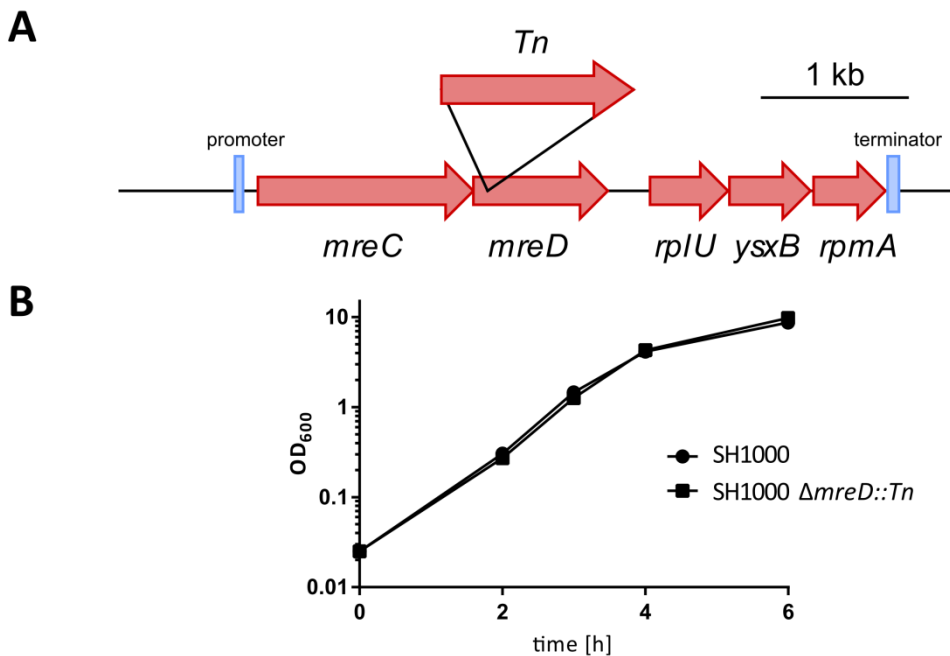


Figure 3.21 Growth phenotype of the *mreD* transposon mutant SH1000 NE858

A, Schematic overview of the native genomic region of *mreCD* and transposon insertion site of NE858. **B**, Growth curve of SH1000 and SH1000 $\Delta mreD::Tn$ (NE858).

3.3 Discussion

3.3.1 Is MreD required for cell viability?

A previous study by Tavares *et al.*, demonstrated that a partial mutant of *mreD* is not affected in growth, morphology, peptidoglycan composition and did not exhibit any sensitivity towards various stresses (Tavares *et al.*, 2015). It was therefore hypothesised that MreD has no effect on cell viability which strongly contradicts the findings in this study.

The key experiment to prove the involvement of a gene of interest in the observed phenotype is complementation. A plasmid-based complementation, using expression of *mreD* or *mreCD* revealed that the growth deficiency of SH1000 $\Delta mreD$ in liquid culture was only partially restored expressing *mreC* and *mreD* together. Expression of *mreD* alone worsened growth both in the mutant as well as the wild type strain which might show a ratio dependent effect at which a naturally occurring ratio between MreC and MreD is required for MreD function. However, the *mreC* mutant also possesses a different ratio and did not exhibit a growth defect (Garcia-Lara *et al.*, 2015). Therefore, this effect might only be seen using a plasmid-based *mreD* expression which likely results in a higher expression of *mreD* than in the native cell.

Chromosomal integration into the lipase gene locus of *mreD* under control of the putative promoter of *mreCD* partially complemented growth on agar and in liquid culture and completely restored the morphology phenotype (Fig. 3.18). Partial growth complementation might be due to non-wild type expression levels. Although the native promoter of *mreCD* was employed, the complementation construct was still different from the wild type setting. First, expression within the lipase gene might be different than at the *mreCD* locus, Second, *mreD* expression levels are likely to be higher since the *mreD* gene follows the promoter immediately instead of being transcribed after *mreC*. In conclusion, the partial complementation at this point is convincing.

A problem arises however regarding SH1000 $\Delta mreD$ with the integrated empty plasmid pKASBAR(tet) which also exhibited restored growth similar to the complemented strain (Fig. 3.19). This phenomenon was reproducible and growth was restored when pKASBAR was transduced into the *mreD* mutant and vice versa, transducing *mreD* into SH1000 harbouring the integrated pKASBAR(tet) plasmid. This questions the complementation by *mreD*. Complementation might be either achieved by the knockout of the lipase gene or the plasmid itself, e.g. the resistance marker. Both scenarios seem unlikely. Additionally, the formation of suppressors might explain the

apparent growth restoration. However, in this case both small and big colony variants should have been observable after transduction. However, a difference was observed when analysing growth on agar of the original *mreD* strain compared to a fresh *mreD* mutant (Fig. 3.19). The freshly constructed strain exhibited a more pronounced growth defect compared to the original strain which could point to spontaneous mutations. Furthermore, it also shows that the *mreD* mutant is not stable and exhibits altered phenotypes after restreaking.

Investigating whether the resistance marker has an influence on growth restoration could be resolved by using an erythromycin resistance marker version of pKASBAR. Also an inducible copy of *mreD* could be investigated to titrate levels of *mreD* expression.

It must be taken into account, that *mreD* might not be required for growth and that the observed phenotypes are due to polar effects. All downstream genes *rplU*, *ysxB* and *rpmA* are proposed to be essential (Chaudhuri *et al.*, 2009) and are likely to be encoded in one operon based on promoter and terminator predictions. Several putative promoters are found in between *mreD* and *rplU* and one was found within the end of *mreD* (Fig. 3.16). A putative terminator was only found downstream of *rpmA*. This possibility that the observed effect is based on a down-regulation of *rplU-ysxB-rpmA* is supported by a study in *E. coli* showing that a *rplU-rpmA* deletion mutant stops growth at high (43 °C) and low (25 °C) temperatures (Wower *et al.*, 1998). At 37 °C, the mutant was still viable and able to grow but also exhibited a severe growth defect. This phenotype is reminiscent of that observed for SH1000 $\Delta mreD$ suggesting that the growth defect and heat-sensitivity might be due to lower transcript levels of *rplU-ysxB-rpmA*. The mRNA levels of the downstream genes could be measured using RT-PCR. Additionally, 5'RACE-PCR could be applied to identify whether the predicted promoter within *mreD* is functional.

3.3.2 Effect of MreD on membrane organisation

MreB was shown to functionally organise the membrane of *B. subtilis* by creating membrane domain regions of increased fluidity (Strahl *et al.*, 2014). These lipid domains are involved in membrane compartmentalisation and membrane protein localisation. In *B. subtilis*, MreD does not have an effect on membrane fluidity (Strahl *et al.*, 2014). The coccoid bacterium *S. aureus* however, lacks MreB and MreD could overtake functions of MreB and replace its role as a spatial organiser. Cells lacking MreD fail to localise phospholipid synthesis enzymes PlsY and CdsA and exhibit an

altered phospholipid composition (Garcia-Lara *et al.*, 2015) (Fig. 3.7C). MreD could act as a glue to bring together and thereby optimise phospholipid enzyme activity by protein interactions or by generating lipid domains. These domains could favour the localisation of phospholipid synthesis enzymes and bring proteins that belong together in close proximity to each other. The lack of MreD does not abolish phospholipid synthesis, since that would lead to immediate growth arrest, but it potentially reveals bottlenecks in the process. The loss of MreD might shift the reaction equilibrium of certain steps within phospholipid synthesis and thereby slowing it down and altering the composition.

However, fatty acid analyses of a *mreD* mutant compared to its parent did not reveal massive changes. SH1000 Δ *mreD* was found to exhibit a slightly decreased amount of longer fatty acids that contribute to higher fluidity (Fig. 3.7). Yet, anteiso fatty acid species, that were shown to significantly increase membrane fluidity, were not found to be different to the wild type (de Mendoza D *et al.*, 2012). It is therefore not surprising that the membrane fluidity when tested directly by fluorescence polarisation was not significantly altered (Fig. 3.8). In summary, MreD is unlikely to be involved in regulating membrane fluidity but might have an impact on phospholipid synthesis.

SH1000 Δ *mreD* exhibits a heat-sensitivity when grown at 42 °C both on agar as well as in liquid culture (Fig. 3.1). Growth in medium supplemented with 4 % NaCl (w/v) restored the heat sensitivity but not the impaired growth rate (Fig. 3.5). The membrane composition of *Lactobacillus casei* and *Bifidobacterium bifidum* subjected to various NaCl concentrations was reported to be significantly altered (Gandhi & Shah, 2016). Saturated fatty acid content was increased along with an increase in cardiolipin and decrease in phosphatidylglycerol upon NaCl-induced salt stress. Another study reported that growth of *Pseudomonas halosaccharolytica* at high temperatures is enhanced by NaCl which also increases cardiolipin amounts along with a decrease of phosphatidylglycerol (Ohno *et al.*, 1979). Furthermore, *Staphylococcus aureus* cells incubated in medium supplemented with various NaCl concentrations also exhibits similar alterations. Cardiolipin increases whereas phosphatidylglycerol and lysylphosphatidylglycerol diminishes dependent on the amount of NaCl (Kanemasa *et al.*, 1972). Importantly, this study shows that the *mreD* mutant in *S. aureus* exhibits the opposite effect of what was reported for NaCl stressed cells.

SH1000 Δ *mreD* exhibits decreased levels of cardiolipin and increased levels of phosphatidylglycerol and lysylphosphatidylglycerol (Fig. 3.7BC). Possibly, NaCl

reverses the phospholipid composition and thereby restores cardiolipin, PG and lys-PG to wild type levels which could be required for growth at high temperatures.

3.3.4 Suppressors of $\Delta mreD$

Suppressor mutations can infer the role and function of the genes. The analysis of a lipoteichoic acid deficient mutant ($\Delta ltaS$) which normally exhibits increased cell size, misplaced septa and eventually lyses revealed that suppressors in *gdpP* restored cell viability (Corrigan *et al.*, 2011). GdpP is a phosphodiesterase that degrades the bacterial second messenger c-di-AMP. It later turned out that c-di-AMP amongst others regulate potassium uptake suggesting a role of lipoteichoic acids in ion-homeostasis (Corrigan *et al.*, 2013). Another example is found for MreD itself. MreD is essential in *S. pneumoniae* but a mutation in *pbp1a* relieved the essentiality of *mreD* and indicated a role of MreD in peptidoglycan synthesis (Land & Winkler, 2011).

Suppressors also revealed an important aspect of cell wall free forms of *B. subtilis*, also referred to as L-forms. *B. subtilis* is able to grow without a cell wall but requires to be stabilised in a hyperosmotic medium (Mercier *et al.*, 2014). This transition requires the synthesis of excess membrane synthesis (Mercier *et al.*, 2013) and suppressors in *ispA*. IspA catalyses the formation of a precursor required for the synthesis of menaquinone that is involved in the electron transport chain (ETC). Thereby it could be shown that reduced ETC activity leading to reduced oxidative stress increased the cell viability of *B. subtilis* L-forms (Kawai *et al.*, 2015).

Suppressor formation of SH1000 $\Delta mreD$ was predominantly observed when cells were grown at 42 °C (Fig. 3.1). These suppressors were found to be heat-resistant and exhibited partially restored growth on agar (Fig. 3.12). Whole genome sequencing revealed a number of mutations including stop codons in genes encoding for the terminal oxidase Cytochrome aa3 (Fig. 3.14 and Tab. 3.2). *Staphylococcus aureus* harbours at least two terminal oxidases, Cytochrome aa3 (*qoxABCD*) and Cytochrome bd (*cydAB*) (Clements *et al.*, 1999, Gotz & Mayer, 2013) (Tynecka *et al.*, 1999). Aerobic growth in a single mutant of either the *qox* genes or *cyd* genes is barely affected suggesting that one system is able to take over the other. A double mutant however, is completely inhibited in aerobic respiration (Hammer *et al.*, 2013).

Interestingly, SNPs in suppressors of SH1000 $\Delta mreD$ were only found in *qox* but not *cyd* genes which might implicate a specific role of MreD connected to Cytochrome aa3. The fact that deletion of one terminal oxidase normally has no effect

on aerobic growth also shows that Cytochrome aa3 could produce toxic by-products in the absence of MreD.

MreD could help to localise or assemble Cytochrome aa3. Without MreD, Cytochrome aa3 function could be disturbed and also inhibit its electron donors NADH-dehydrogenase and menaquinone which could cause an electron reflux and oxidative damage. These could be responsible for the growth defect and heat-sensitivity of SH1000 $\Delta mreD$.

3.4 Main findings in this chapter

- Replacement of the *mreD* gene with a kanamycin cassette results in a severe growth defect and heat-sensitivity.
- The phospholipid composition in SH1000 $\Delta mreD$ is altered. Less CL but more PG and lys-PG was found compared to SH1000.
- Cells growing at 42 °C stop growing and exhibit misplaced septa, FtsZ localisation and aberrant cell morphologies. This heat sensitivity is relieved by high amounts of NaCl.
- The *mreD* mutant forms suppressors that are partially restored in growth on agar and do not possess a heat-sensitivity.
- Suppressors harbour mutations in a variety of genes but mainly in genes encoding for Cytochrome aa3.

3.5 Contributions

Fatty acid and phospholipid extraction and analysis shown in Fig. 3.7 were provided by the DSMZ identification service (Braunschweig, Germany). The analysis of whole genome sequencing data of *mreD* suppressor strains shown in Table 3.2 was performed by Dr. Roy Chaudhuri (University of Sheffield). Membrane fluidity experiments shown in Fig. 3.8 were performed by me and Dr. Helena Rosado (Imperial College London). All other experiments in this chapter were carried out by me

Chapter 4: Localisation of membrane proteins in *S. aureus*

4.1 Introduction

4.1.1 Membrane heterogeneity and localisation of phospholipid synthesis enzymes

Bacterial membranes are primarily composed of proteins embedded in a lipid bilayer. The lipids consist of a hydrophilic phospholipid headgroup carrying a hydrophobic tail that is usually composed of two fatty acids. Both components are variable and serve different functions.

The major phospholipids in bacteria are phosphatidylglycerol (PG), cardiolipin (CL) and phosphatidylethanolamine (PE) (de Mendoza *et al.*, 2003)(Fischer *et al.*, 1978). The phospholipid composition is highly dependent on the species and is altered due to various environmental changes. *E. coli* membranes are composed of 5 % CL, 20–25 % PG and 70–80 % PE whereas *S. aureus* exhibits mainly PG (43 %) , lysinylated PG (30 %) and CL (20 %) but no PE (Hayami *et al.*, 1979, Dowhan, 1997). Anionic phospholipids such as CL, phosphatidic acid (PA) and PE have been found to be preferentially located at negatively curved regions of the cell membrane such as the septum and poles in *E. coli* (Renner *et al.*, 2013, Ramamurthi, 2010, Jouhet, 2013, Renner & Weibel, 2011). Conversely, PG, stained with FM4-64, was found in the whole membrane or in a helical pattern along the long axis of the cell in *B. subtilis* (Barak *et al.*, 2008). The helical organisation of FM4-64 stained lipids was missing in cells depleted of MurG, an enzyme involved in peptidoglycan precursor synthesis, indicating a connection between membrane organisation and peptidoglycan synthesis (Muchova *et al.*, 2011). However, the helical arrangement could not be observed in *E. coli* (Fishov & Woldringh, 1999) and no unambiguous evidence could be shown apart from that FM4-64 specifically stains PG (Strahl *et al.*, 2014). Nevertheless, these studies indicate a heterogeneity in the bacterial membrane that could be explained by the subcellular localisation of lipid synthesis enzymes.

In *B. subtilis*, translational fusions of lipid synthesis enzymes with GFP have been used to study their localisation. Fusions revealed that the cardiolipin synthase, ClsA, colocalises with its product and therefore plays an important role in the localisation of CL (Nishibori *et al.*, 2005). A number of other metabolism associated membrane proteins were also found to localise to the septum including PgsA, PssA ,

Psd, CdsA, MprF and UgtP (functions are described in Section 1.2.4.1) (Nishibori *et al.*, 2005). UgtP exhibits a septal, as well as a peripheral, heterogeneous punctate pattern which corresponds to its role in the synthesis of glucolipids and in the regulation of FtsZ-assembly (Shiomi & Margolin, 2007, Weart *et al.*, 2007). The question arises as to how these enzymes are targeted to the septum? A well conserved amphipathic α -helix was found near the C-terminus of cardiolipin synthases in *E. coli*, *B. subtilis*, *S. aureus* and a number of other bacterial species (Kusaka *et al.*, 2016). The deletion of this motif results in the loss of septal localisation indicating that this amphipathic helix is required for the septal localisation of cardiolipin synthases. Yet, no amphipathic helices were found for PgsA and other phospholipid synthesis enzymes suggesting a different mode of localisation.

The enzymes PlsY and PlsX link fatty acid with phospholipid synthesis. PlsY is localised at the cell periphery and at the septum in *B. subtilis* shown by using a xylose-inducible chromosomal expression system (Hunt *et al.*, 2006). The localisation of PlsX was unexpected as although it also localises at the cell-division site, it arrives prior to other proteins colocalised with the FtsZ-anchoring protein FtsA, and remains at the cell-division site after septation. It could therefore act as cell-division marker before the Z-ring forms. Its depletion results in aberrant Z-ring formation and suggests a connection between fatty acid synthesis and cell-division (Takada *et al.*, 2014). Furthermore, protein-protein interaction studies also revealed an interaction between PlsX and FtsA as well as several other cell-division associated proteins, metabolic enzymes and cytoskeletal proteins (Takada *et al.*, 2014).

4.1.2 Aims of this chapter

- The general localisation of membrane proteins within the membrane was investigated. Specifically, integral membrane proteins involved in phospholipid synthesis such as PlsY and other membrane proteins were analysed utilising several reporter protein fusions.
- Colocalisation approaches were used to identify coordination in protein patterns.
- What are the molecular processes that lead to membrane protein localisation? Employing PlsY-GFP as a marker protein, a variety of inhibitors and gene mutations were used to analyse their impact on the localisation of membrane proteins.

4.2 Results

4.2.1 Localisation of PlsY

PlsY was shown to localise in a punctate pattern throughout the membrane. Localisation studies were performed using a GFP fusion and immunolocalisation with an antibody targeting an extracellular peptide loop of PlsY (Garcia-Lara *et al.*, 2015).

The following PlsY localisation studies were performed using a strain that expresses the native *plsY* gene translationally fused to *gfp* under control of its native promoter ensuring native levels of PlsY-GFP. This was carried out with an derivative of the integrative plasmid pMUTIN (Kaltwasser *et al.*, 2002). pMUTIN-*plsY-gfp* integrates by homologous recombination into the native locus of *plsY* and thereby places a *plsY-gfp* fusion under control of the native promoter of *plsY* while the original *plsY* gene is placed under control of the IPTG-inducible promoter Pspac. Repression of the original *plsY* gene is facilitated by LacI which is expressed from the integrated pMUTIN plasmid.

4.2.1.1 Growth phase dependent localisation of PlsY

The subcellular localisation of PlsY-GFP in SH1000 was studied at different growth phases by comparing early-, late exponential and stationary phase cells using fluorescence microscopy of fixed cells.

An overnight culture of SH1000 *plsY-gfp* was precultured to an $OD_{600}=0.05$ in BHI and incubated at 37 °C at 250 rpm in the presence of erythromycin (5 µg/ml) and lincomycine (25 µg/ml). Samples were taken at early exponential phase (after 2 or 3 h), late exponential (after 4 or 5 h) and stationary phase (7 h), fixed using p-formaldehyde and analysed by fluorescence microscopy.

Cells taken from exponential phase exhibit a punctate localisation pattern of PlsY-GFP that is especially distinctive during early exponential phase (Fig. 4.1AB). This pattern lessens in stationary phase. However, cells also appear smaller and have less overall fluorescent signal and thus a diminished signal to noise ratio. A Z-stack of two cells from early-exponential phase reveals the three-dimensional non-homogeneous distribution of PlsY-GFP in the membrane (Fig. 4.1C). Since the diffraction limit of about 250 nm pushes light-microscopy to its limits to see structures within the 1 µm diameter *Staphylococcus aureus* it is required to deconvolve acquired images. Nonetheless, the localisation pattern can be seen in convolved pictures even though with less clarity. Additionally, another algorithm called super resolution radial fluctuations (SRRF) (Gustafsson *et al.*, 2016) that assumes that signals are formed of a point spread function with a higher degree of symmetry than the background which can be applied to

improve the resolution and showed similar results compared to deconvolution (Fig. 4.2AB). This analysis was undertaken using a Nikon confocal microscope and data analysis was performed with the NanoJ-SRRF software package for Fiji-ImageJ.

4.2.1.2 Cell-cycle dependent localisation of PlsY

The localisation of PlsY during the cell cycle was studied by co-labelling using HADA. HADA is a fluorescent D-amino acid that is incorporated into the peptidoglycan and can be used to indicate the cell cycle status (Kuru *et al.*, 2012).

An overnight culture of SH1000 *plsY-gfp* was precultured to an $OD_{600}=0.05$ in BHI and incubated at 37 °C at 250 rpm in the presence of erythromycin (5 µg/ml) and lincomycin (25 µg/ml). Samples were taken at an $OD_{600}\approx 0.5$ and cells were labelled with 5 µl HADA (100 mM stock solution) in PBS for 5 min at 37 °C on a rotary wheel. Labelled cells were washed with PBS, fixed and analysed by fluorescence microscopy.

PlsY-GFP localises in a cell-phase dependent manner (Fig. 4.3AB). The fusion goes to the septum during cell division and it appears that two dots are formed at the septum base during early-division phase that merge or redistribute to form a single dot at the cell-division site after the fission is almost finished. However, the fusion is also distributed in a punctate pattern both during cell-division and in non-dividing cells. Cell counts show that a punctate pattern is common and that PlsY-GFP is predominantly localised at the septum during late cell-division (Fig. 4.3B).

4.2.1.3 Dose dependent localisation of PlsY

The question arises as to whether the number of PlsY-GFP molecules affects its localisation pattern. In order to test this, IPTG controlled *plsY-gfp* expression from a plasmid (pWW10, see Section 5.2.4) was carried out using 50 and 500 µM IPTG. Fluorescence of samples was measured using a Tecan Plate reader with 100 µl cells adjusted to an $OD_{600}=5$ that were washed and resuspended in PBS. Fluorescence measurements were taken by exposure for 1 sec at 485 nm and Emission at 535 nm. Samples were taken every 30 min after addition of IPTG, fixed with p-formaldehyde and visualised by fluorescence microscopy.

The fluorescence of the samples increased over time upon IPTG addition and was dependent on the amount of IPTG whereby higher IPTG concentrations led to higher fluorescence (Fig. 4.4A). One sample was taken before and one at the time of IPTG addition which resulted in no measurable fluorescence counts. This shows that the IPTG-inducible expression of *plsY-gfp* is tightly repressed without the inducer in the tested framework.

A higher expression level of *plsY-gfp* has no effect on growth, indicating that high amounts of the fusion are not harmful for the cell. The signal-to-noise ratio of

acquired fluorescence images improved in correlation to the measured values (Fig. 4.4AB). Cells exhibit an obvious punctate distribution of PlsY-GFP at low expression levels of *plsY-gfp*. This pattern however gets lost at later stages (500 μ M IPTG, 120 min past IPTG addition) and the PlsY-GFP fusion is located throughout the whole membrane. The septal localisation of PlsY-GFP during cell-division however, is independent of the expression levels (Fig. 4.4B).

4.2.1.4 Verification of the punctate localisation pattern of PlsY

It has been suggested recently that the helical bundles seen for an YFP-MreB fusion were formed due to an artefact of the fluorescent protein tag that are potentially created by the multimerisation of YFP (Margolin, 2012, Swulius & Jensen, 2012).

To investigate whether the observed localisation pattern is due to the multimerisation of the GFP-tag, the localisation of PlsY was investigated with eYFP and its monomeric version. meYFP was generated by replacing alanine at position 206 with lysine (Fig. 4.5) which disrupts the hydrophobic interaction at the dimeric interface. This mutation also creates a monomeric version of GFP (von Stetten *et al.*, 2012).

4.2.1.4.1 Construction of a PlsY-eYFP and PlsY-meYFP fusion in *S. aureus*

In order to construct pMUTIN-*plsY-(m)eyfp*, *plsY* (5'FW116/3'FW116) was amplified using SH1000 genomic DNA as a template and *eyfp* (5'FW117/3'FW117) was amplified using plasmids pKASBAR-*ezrA-eyfp* or pKASBAR-*ezrA-meyfp* (Wacnik, 2016) as templates. DNA fragments were cloned into the *KpnI/SpeI* site of pMUTIN-*gfp+* using Gibson Assembly (Fig. 4.6A) and transformed into *E. coli* NEB5 α . Recombinant plasmids were tested by restriction digest with HindIII and SpeI resulting in 6388 and 394 bp fragments (Fig. 4.6C) and validated by DNA sequencing (GATC Biotech AG, Konstanz, Germany). The resulting plasmids, pMUTIN-*plsY-eyfp* and pMUTIN-*plsY-meyfp*, were electroporated into RN4220 and from there transduced into SH1000. Genomic integration at the *plsY* locus was confirmed by PCR amplification of a 1077 bp fragment using one primer that binds in the genome upstream of *plsY* and one primer within the *eyfp* gene (Inward_plsY/Outward_eyfp) (Fig. 4.6D). No amplification of a 1077 bp fragment was seen using SH1000 genomic DNA as a template. The whole *plsY* gene was amplified with the use of primers Inward_plsY/3'FW116 resulting in a 807 bp fragment to confirm the PCR and template.

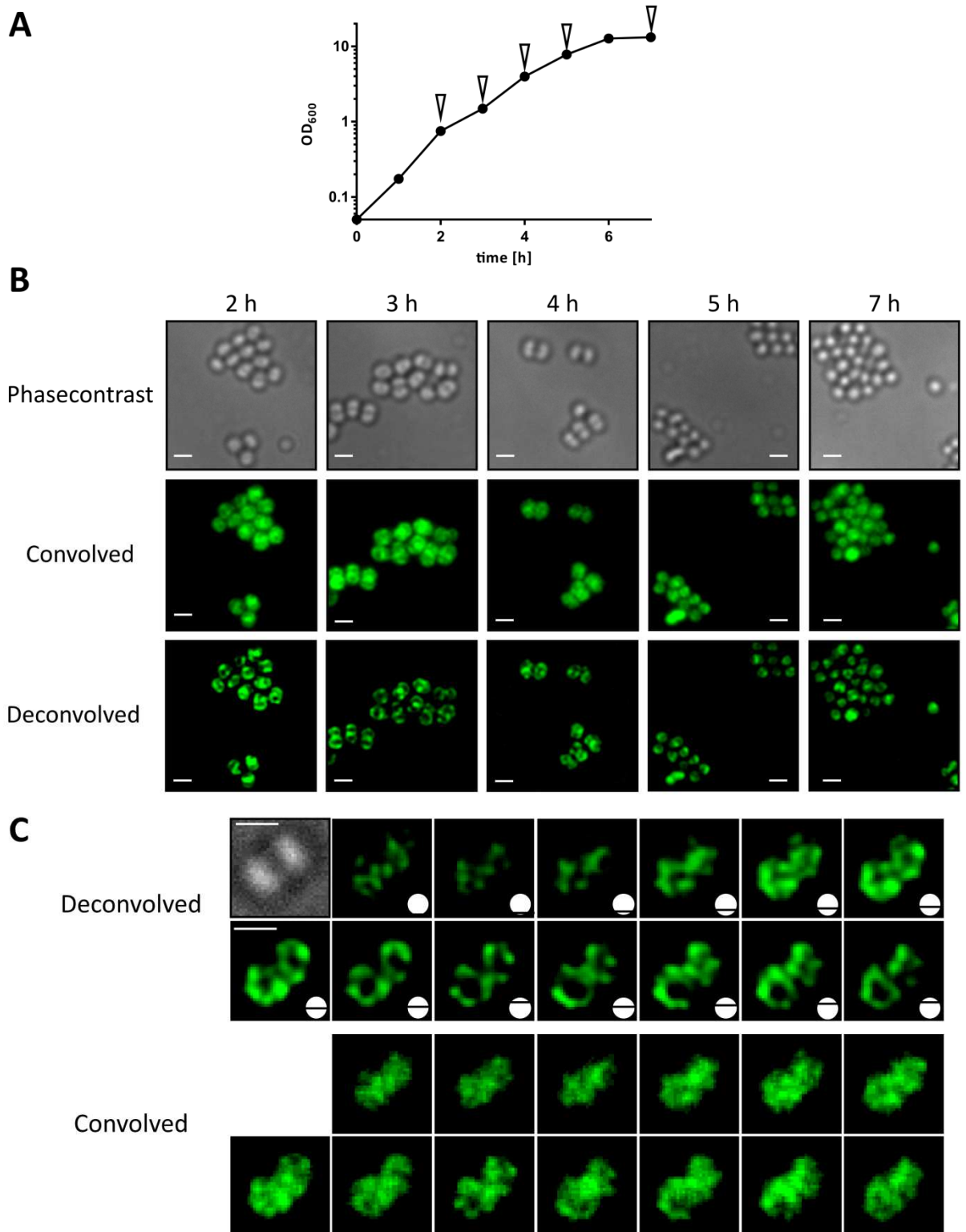
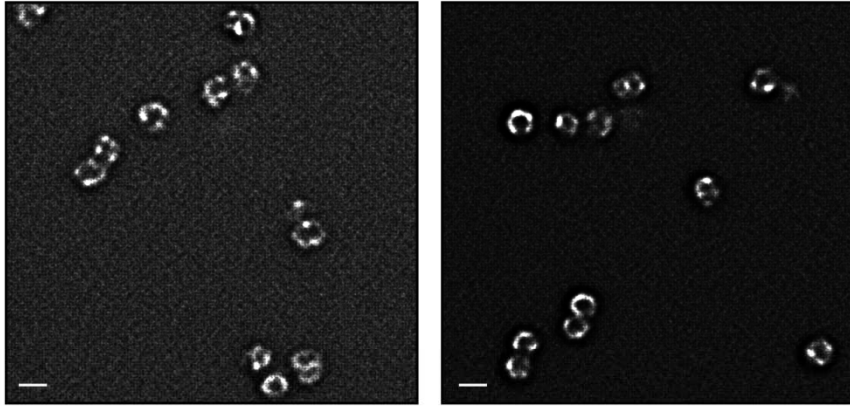


Figure 4.1 Growth phase dependent localisation of PlsY-GFP

A, Growth of SH1000 *plsY-gfp*. Imaging sampling points are indicated by white arrows.

B, Phase contrast and fluorescence images (convolved and deconvolved) of *S. aureus* SH1000 *plsY-gfp*. Images were acquired using a Delta Vision microscope and SoftWoRx 3.5.0 software (Applied Precision). Acquisition of fluorescence images were taken using 2.5sec exposure in the FITC channel. Scale bars represent 2 μ m. **C**, Z-stack images of selected cells from early-exponential growth phase. Scale bars represent 1 μ m.

A



B

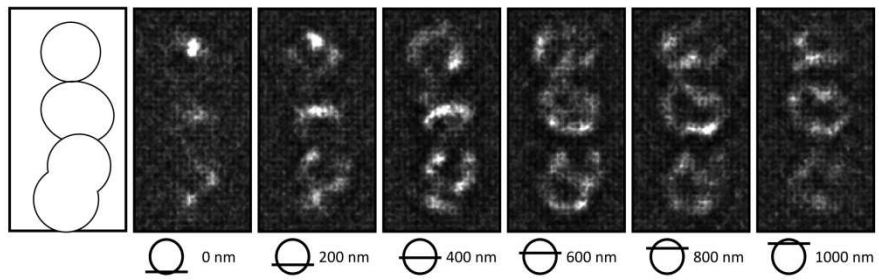


Figure 4.2 SRRF analysis of PlsY-GFP

A, SRRF analysis of exponentially grown SH1000 *plsY-gfp* cells. Scale bars represent 1 μm . **B**, SRRF analysis of exponentially grown SH1000 *plsY-gfp* cells Z-stack images of selected cells.

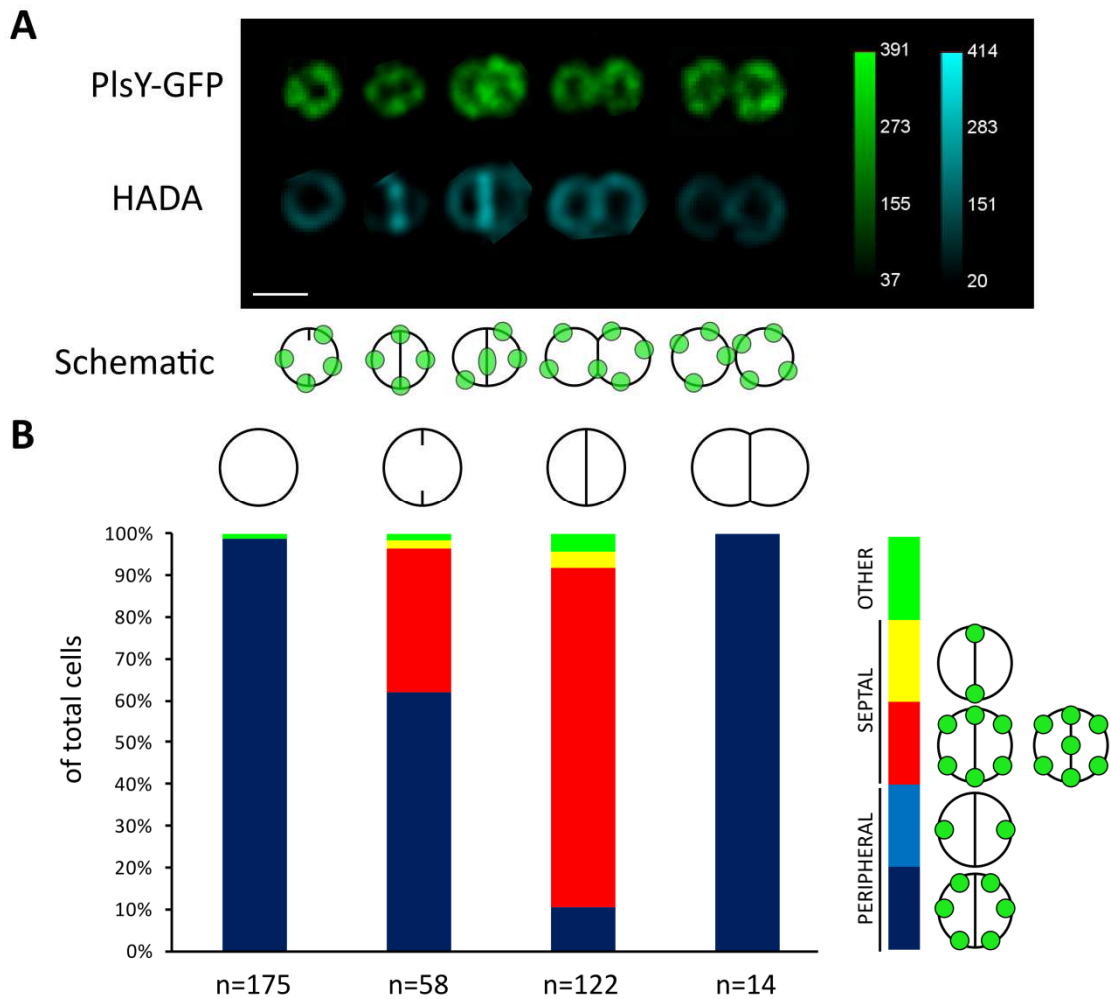


Figure 4.3 Cell-cycle dependent localisation of PlsY-GFP

A, Deconvolved fluorescence images of selected cells representing different cell-cycle stages of *S. aureus* SH1000 *plsY-gfp* labelled with HADA. Images were acquired using a Delta Vision microscope and SoftWoRx 3.5.0 software (Applied Precision). Acquisition of fluorescence images were taken using 1.5 sec exposure in the DAPI channel and 2.5sec exposure in the FITC channel. Scale bar represents 1 μ m. Fluorescent signal intensities are depicted in a linear colour code and saturated pixels are highlighted in red. **B**, Cell counts categorized depending on PlsY-GFP localisation and cell-cycle stage indicated by HADA labelling. Value n indicates counted cells for each group. Red and yellow bars indicate septal and blue bars indicate peripheral PlsY-GFP localisation. The green coloured bar indicates random PlsY-GFP localisation.

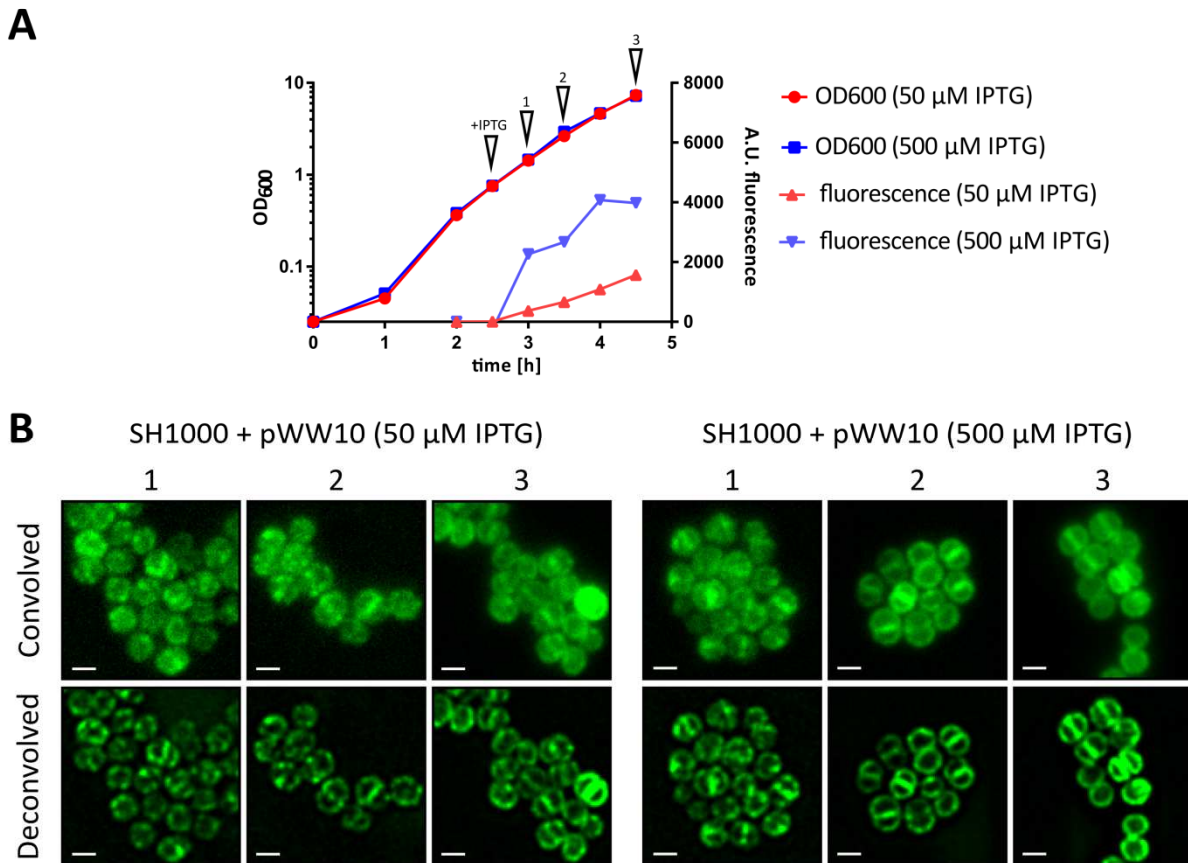


Figure 4.4 Dose-dependent localisation of PlsY-GFP

A, Growth curve of SH1000 + pWhiteWalker10 (IPTG-inducible *plsY-gfp* expression) grown in the presence of 50 or 500 μM IPTG. Left Y-axis shows OD₆₀₀ and right Y-axis shows A.U. fluorescence values, white arrows indicate imaging sampling points and IPTG addition. **B**, Fluorescence images (convolved and deconvolved) of *S. aureus* SH1000 + pWhiteWalker10 1, 2 or 3 h post addition of IPTG. Images were acquired using a Delta Vision microscope and SoftWoRx 3.5.0 software (Applied Precision). Acquisition of fluorescence images was taken using 1 sec exposure in the FITC channel. Scale bars represents 1 μm.

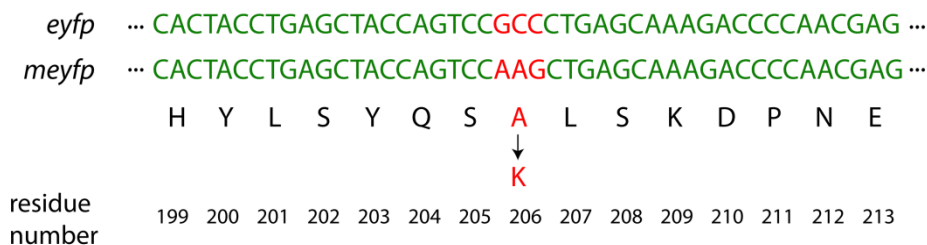


Figure 4.5 Nucleotide and amino acid sequence of *eyfp* compared to *meyfp*

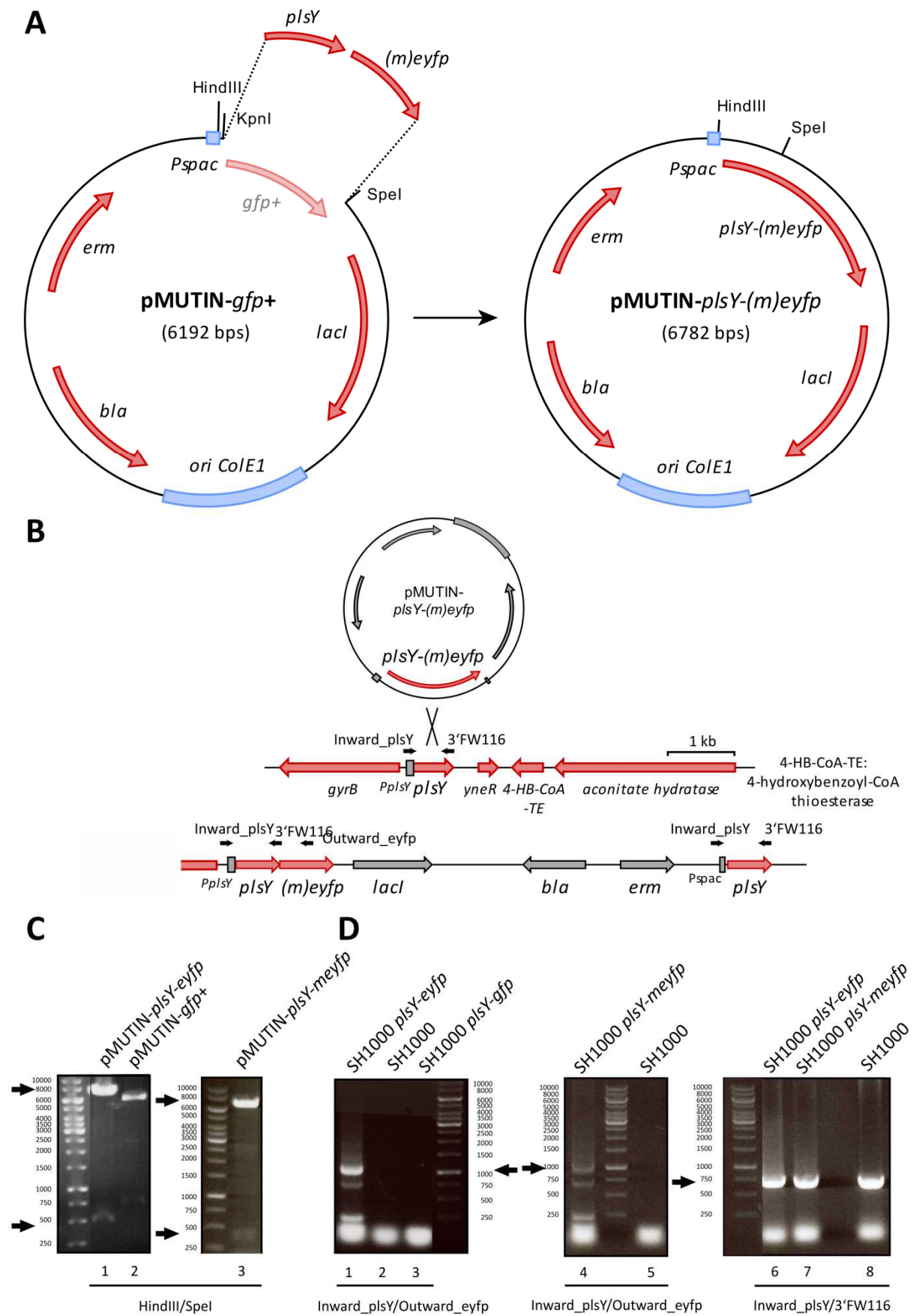


Figure 4.6 Construction of a chromosomal *plsY*-(*m*)*eyfp* fusion in *S. aureus* SH1000

A, Diagram illustrating the construction of pMUTIN-*plsY*-(*m*)*eyfp*. **B**, Schematic overview of the native genomic region of *plsY* and post integration of pMUTIN-*plsY*-(*m*)*eyfp*. Black arrows indicate primer binding sites. **C**, pMUTIN-*plsY*-*eyfp* p (Lane 1), pMUTIN-*plsY*-*meyfp* (Lane 3), and pMUTIN-*gfp*+ (Lane 2) were digested with HindIII and SpeI and separated by 1 % (w/v) TAE agarose gel electrophoresis. Bands of 6388 bp and 394 bp, corresponding to pMUTIN-*plsY*-*eyfp* (Lane 1) and pMUTIN-*plsY*-*meyfp* (Lane 3), respectively, are marked by black arrows. Bands of 5394 bp and 608 bp (and 190 bp) correspond to pMUTIN-*gfp*+ (Lane 2). **D**, Verification of pMUTIN-*plsY*-*eyfp* and pMUTIN-*plsY*-*meyfp* integration by PCR using primer pair Inward_*plsY*/Outward_*eyfp*. PCR products were separated by 1 % (w/v) TAE agarose gel electrophoresis. A band of 1077 bp, marked by a black arrow, indicates pMUTIN-*plsY*-*eyfp* chromosomal integration (Lane 1) and pMUTIN-*plsY*-*meyfp* chromosomal integration (Lane 4). No DNA amplification is seen using genomic DNA from SH1000 (Lanes 2 and 5) or SH1000 *plsY*-*gfp* (Lane 3). PCR amplification of the whole *plsY* gene using primer pair Inward_*plsY*/3'FW116 results in a band of 807 bp using genomic DNA from pMUTIN-*plsY*-*eyfp* and pMUTIN-*plsY*-*meyfp* chromosomally integrated into the genome of SH1000 and the parental SH1000 as templates (Lanes 6-7).

4.2.1.4.2 Localisation of PlsY-eYFP

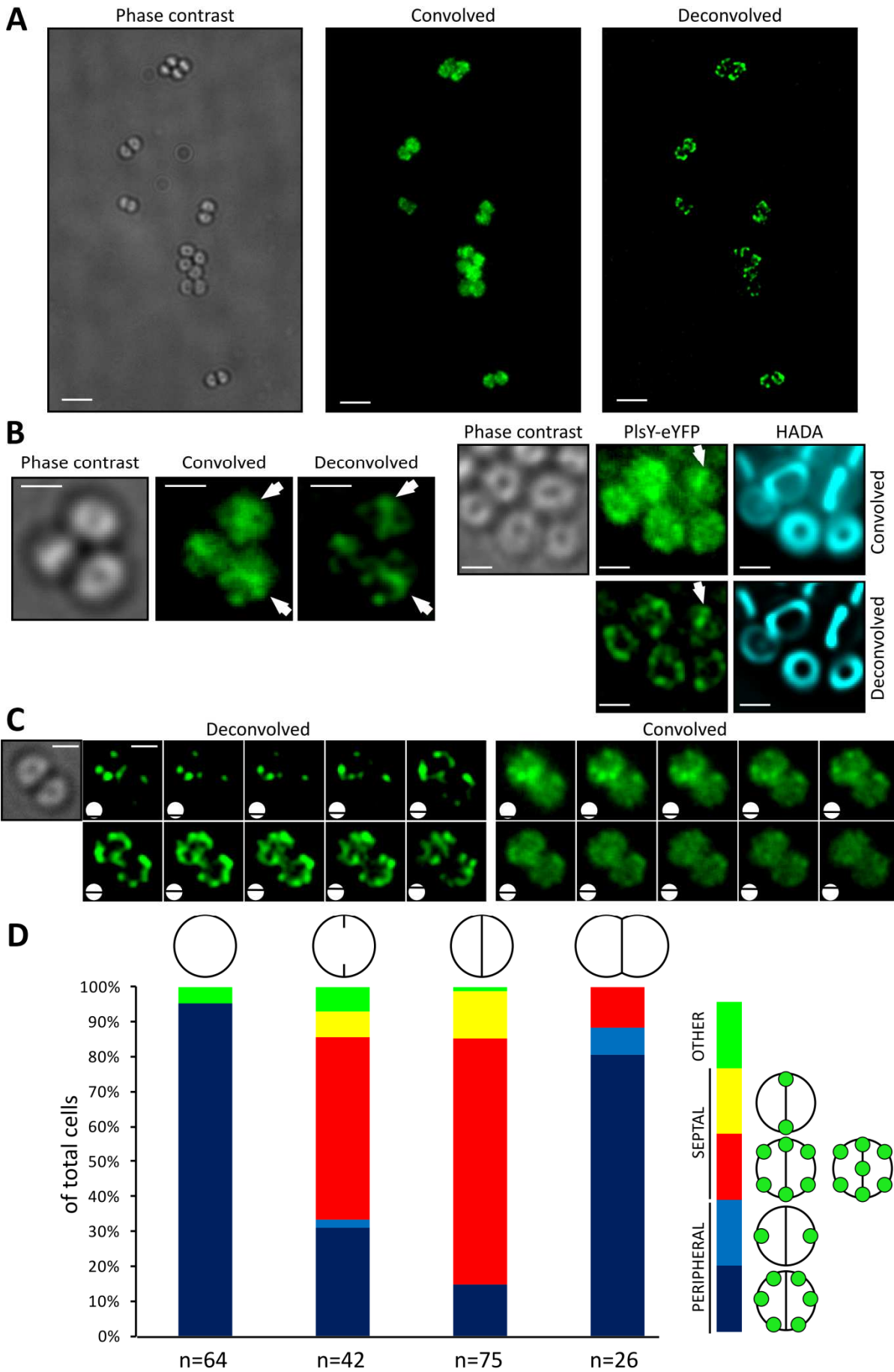
First of all, the localisation of PlsY-eYFP was investigated to confirm that the fusion localises the same as PlsY-GFP to exclude that eYFP alters the properties of PlsY. Thus, overnight cultures of SH1000 *plsY-eyfp* and SH1000 *plsY-meyfp* were diluted to an $OD_{600}=0.05$ and grown at 37 °C for 2 h at 250 rpm. 1 ml samples were harvested, fixed using p-formaldehyde and imaged by fluorescence microscopy.

PlsY-GFP and PlsY-eYFP exhibit a similar distribution pattern (compare Fig. 4.3B with Fig. 4.7D). Both fusions are localised in a heterogeneous fashion and the majority of the cells show a septal localisation of both fusions in cells during early and late-cell division stages. The GFP tagged PlsY fusion however was easier to image due to a higher fluorescence signal. Furthermore, detected fluorescence signals for the PlsY-eYFP fusion varied between cells whereas fluorescence of PlsY-GFP was more consistent. PlsY fused to the monomeric version of eYFP, meYFP, was not expressed or fluorescent in the majority of cells (Fig. 4.8). Cells that exhibit a fluorescent signal however, show a punctate patterned distribution of PlsY-meYFP along with a septal localisation. It is not known why the fusion is not expressed in every cell but the monomeric property of meYFP has no influence on the localisation pattern observed for PlsY-eYFP.

4.2.2 Localisation of other phospholipid synthesis enzymes

4.2.2.1 Genes selected for investigation

It has been shown that PlsY is distributed heterogeneously and forms a punctate localisation pattern. The question arises whether other enzymes of the phospholipid synthesis pathway are localised in a similar fashion or even colocalised. In order to investigate other fusions, enzymes involved in phospholipid synthesis (see Fig. 1.5) were bioinformatically analysed in terms of their genetic organisation and topology to choose suitable candidates for localisation studies (Tab. 4.1).



Phase contrast and fluorescence images (convolved and deconvolved) of *S. aureus* SH1000 *plsY-eyfp*. Images were acquired using a Delta Vision microscope and SoftWoRx 3.5.0 software (Applied Precision). Acquisition of fluorescence images were taken using 2.5 sec exposure in the FITC channel. **A**, Scale bars represent 3 μm . **B**, Selected cells showing the localisation of PlsY-eYFP and HADA. White arrows indicate septal localisation. Scale bars represent 1 μm . **C**, Z-stack images of selected cells. Scale bars represent 1 μm . **D**, Cell counts categorized depending on PlsY-eYFP localisation and cell-cycle stage indicated by HADA labelling. Value n indicates counted cells for each group. Red and yellow bars indicate septal and blue bars indicate peripheral PlsY-eYFP localisation. The green coloured bar indicates random PlsY-eYFP localisation.

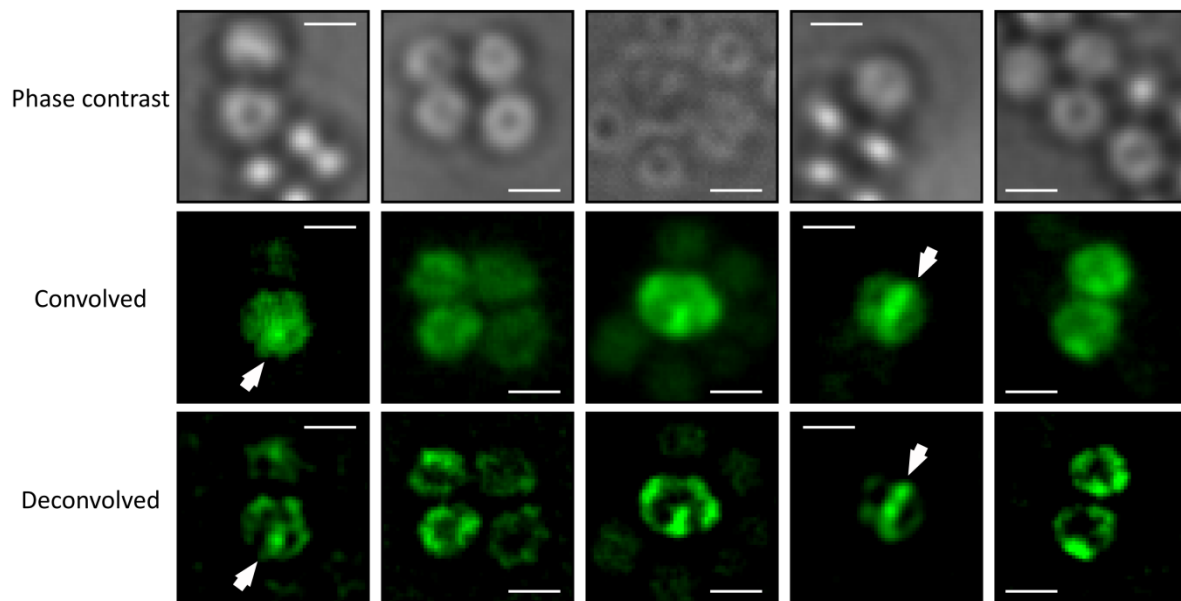
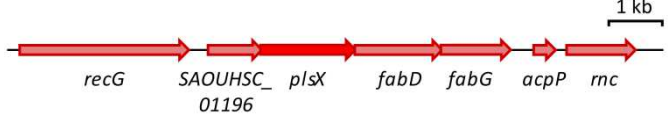
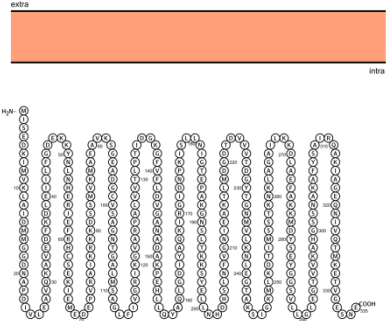
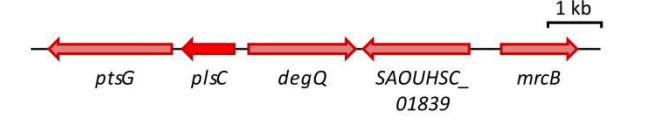
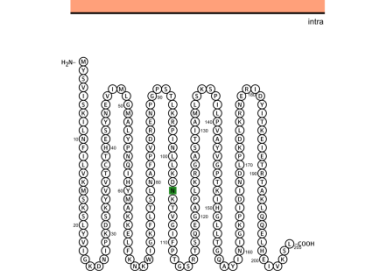
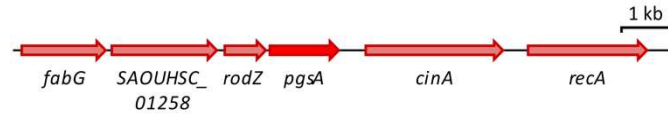
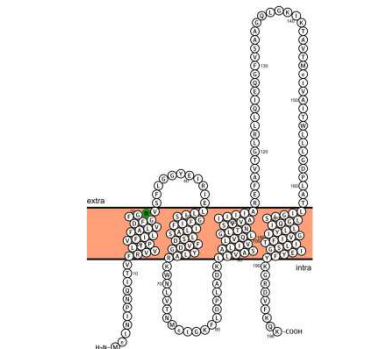
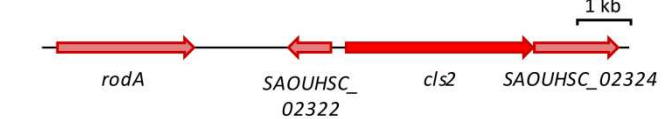
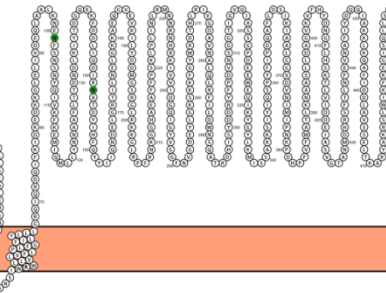
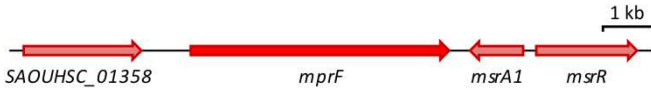
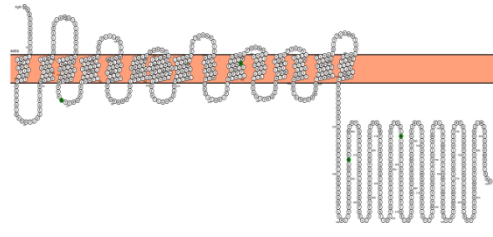


Figure 4.8 Localisation of PlsY-meYFP in *S. aureus* SH1000

Phase contrast and fluorescence images (convolved and deconvolved) of *S. aureus* SH1000 *plsY-meyfp*. Images were acquired using a Delta Vision microscope and SoftWoRx 3.5.0 software (Applied Precision). Acquisition of fluorescence images were taken using 2.5 sec exposure in the FITC channel.

Table 4.1 Bioinformatic analysis of phospholipid synthesis enzymes

Gene name	GeneID (<i>Staphylococcus aureus</i> NCTC8325)	Function (protein length in amino acids) and topology Prediction (http://wlab.ethz.ch/protter/#)
PlsX	SAOUHSC_01197	glycerol-3-phosphate acyltransferase (336)
 <p><i>recG</i>: ATP-dependent DNA helicase <i>SAOUHSC_01196</i>: fatty acid biosynthesis transcriptional regulator, potentially <i>fabA</i> <i>fabD</i>: malonyl CoA-acyl carrier protein transacylase <i>dabG</i>: 3-oxoacyl-(acyl-carrier-protein) reductase <i>acpP</i>: acyl carrier protein <i>rnc</i>: ribonuclease III</p>		
PlsC	SAOUHSC_01837	1-acyl-sn-glycerol-3-phosphate acyltransferase (206)
 <p><i>ptsG</i>: Phosphotransferase system IIC components <i>degQ</i>: putative Periplasmic serine protease <i>SAOUHSC_01839</i>: tyrosyl-tRNA synthase <i>mrcB</i>: Membrane carboxypeptidase, Transglycosylase</p>		
PgsA	SAOUHSC_01260	CDP-diacylglycerol-glycerol-3-phosphate 3-phosphatidyltransferase (193)
 <p><i>fabG</i>: 3-ketoacyl-(acyl-carrier-protein) reductase <i>SAOUHSC_01258</i>: hypothetical protein <i>rodZ</i>: Cytoskeletal protein, Helix-turn-helix motif <i>cinA</i>: competence-damage inducible protein <i>recA</i>: recombinase A</p>		
Cls2	SAOUHSC_02323	major cardiolipin synthase (495)
 <p><i>rodA</i>: rod shape-determining protein RodA <i>SAOUHSC_02322</i>: putative <i>Staphylococcus aureus</i> copper-sensitive operon repressor (CsoR) <i>SAOUHSC_02324</i>: putative RnaY; HD superfamily phosphodiesterase</p>		

MprF	SAOUHSC_01359	lysylphosphatidyl-glycerol synthetase (841)
 <p data-bbox="151 347 805 481"> <i>SAOUHSC_01358</i>: predicted PurR-regulated permease PerM <i>mprF</i>: methionine sulfoxide reductase A <i>msrR</i>: Cps2a, transcriptional regulator </p>		

Transmembrane domains were found for proteins PgsA, Cls2 and MprF but not for PlsC and PlsX. However, PlsX has been described as a membrane associated protein in *B.subtilis* (Takada *et al.*, 2014). PgsA and MprF are predicted to have cytoplasmic C-termini that could be used for protein fusions. Additionally, both proteins together with PlsC are likely to be monocistronic or the last gene of their operon which makes a C-terminal fusion using pMUTIN feasible. Although PlsC was not identified as an integral membrane protein by Protter it was included to analyse how an allegedly non-membrane protein of the same pathway is localised. Therefore, PgsA, MprF and PlsC were chosen for localisation studies using single-copy chromosomally integrated *eyfp* tagged protein fusions under control of their native promoters.

Another phospholipid synthesis enzyme, the major cardiolipin synthase Cls2, was chosen to be investigated using a slightly different approach. The gene *cls2* was found to be located within a potential operon including a downstream gene that might be expressed together with *cls2*. Thus, a *cls2-eyfp* fusion was chromosomally integrated into the lipase gene under control of its native promoter in a *cls2* deficient strain.

The gene encoding for PlsX is likely to be the middle of an operon and was therefore not considered for localisation studies as well as the phosphatidylserine decarboxylase Psd since it could not be found in the genome of *S. aureus* NCTC8325 or has not been annotated.

4.2.2.2 Construction of single-copy integrative plasmids for phospholipid synthesis enzyme fusions with eYFP

eYFP was chosen to determine the localisation of phospholipid synthesis enzymes since it has been shown to be useful for STORM studies (Dr. R. D. Turner, personal communication) and can be imaged with the filter set available for the Delta Vision deconvolution microscope (Applied precision, GE Healthcare).

4.2.2.2.1 Construction of a PlsC-eYFP fusion in *S. aureus*

In order to construct pMUTIN-*plsC-eyfp*, *plsC* (5'FW10/3'FW10) from SH1000 genomic DNA and *eyfp* (5'FW11/3'FW117) from plasmid pKASBAR-*ezrA-eyfp* were amplified, cloned into the *KpnI/SpeI* site of pMUTIN-*gfp+* using Gibson Assembly (Fig. 4.9) and transformed into *E. coli* NEB5 α . Recombinant plasmids were tested by restriction digest with EcoRI and ClaI resulting in 5626, 814, 287 and 45 bp fragments. (Fig. 4.9C) and validated by DNA sequencing (GATC Biotech AG, Konstanz, Germany). The resulting plasmid, pMUTIN-*plsC-eyfp*, was electroporated into RN4220 and from there transduced into SH1000. Genomic integration at the *plsC* locus was confirmed by PCR amplification of a 906 bp fragment using one primer that binds at the beginning of *plsC* and one primer within the *eyfp* gene (5'FW10/Outward_eyfp) (Fig. 4.9D). No DNA amplification was seen using SH1000 genomic DNA as a negative control template. The whole *plsC* gene was amplified with the use of primers 5'FW10/3'FW10 resulting in a 638 bp fragment to confirm the PCR and template.

4.2.2.2.2 Construction of a PgsA-eYFP fusion in *S. aureus*

In order to construct pMUTIN-*pgsA-eyfp*, *pgsA* (5'FW16/3'FW16) from SH1000 genomic DNA and *eyfp* (5'FW17/3'FW117) from plasmid pKASBAR-*ezrA-eyfp* were amplified, cloned into the *KpnI/SpeI* site of pMUTIN-*gfp+* using Gibson Assembly (Fig. 4.10) and transformed into *E. coli* NEB5 α . Recombinant plasmids were tested by restriction digest with PstI resulting in 3284, 2000 and 1452 bp fragments (Fig. 4.10C) and validated by DNA sequencing (GATC Biotech AG, Konstanz, Germany). The resulting plasmid, pMUTIN-*pgsA-eyfp*, was electroporated into RN4220 and from there transduced into SH1000. Genomic integration at the *pgsA* locus was confirmed by PCR amplification of a 870 bp fragment using one primer that binds at the beginning of *pgsA* and one primer within the *eyfp* gene (5'FW16/Outward_eyfp) (Fig. 4.10D). No DNA amplification was seen using SH1000 genomic DNA as a negative control template. The whole *pgsA* gene was amplified with the use of primers 5'FW16/3'FW16 resulting in a 600 bp fragment to confirm the PCR and template.

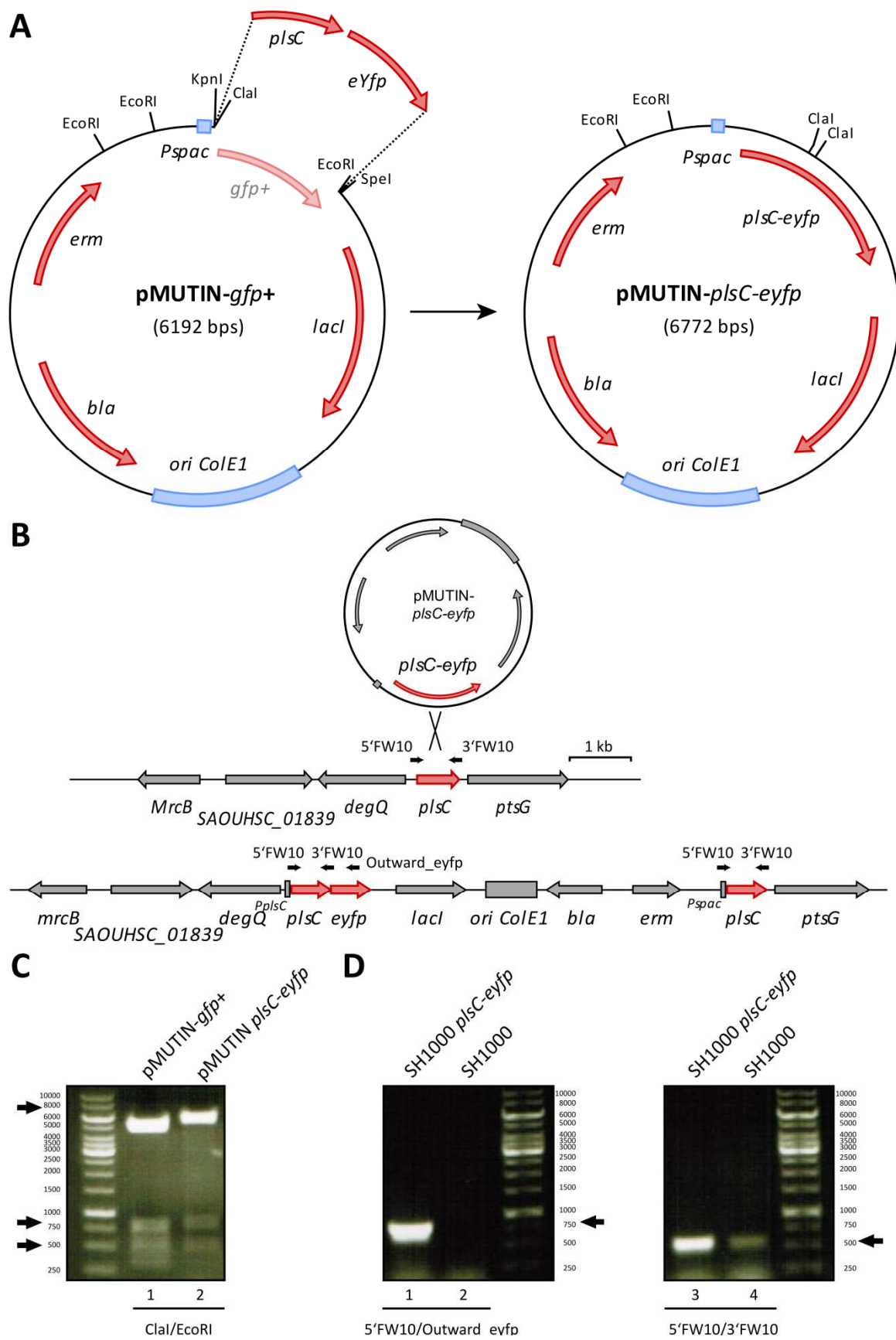


Figure 4.9 Construction of a chromosomal *plsC-eyfp* fusion in *S. aureus* SH1000

A, Diagram illustrating the construction of pMUTIN-*plsC-eyfp*. **B**, Schematic overview of the native genomic region of *plsC* and post integration of pMUTIN-*plsC-eyfp*. Black arrows indicate primer binding sites. **C**, pMUTIN-*plsC-eyfp* (Lane 2) and pMUTIN-*gfp+* (Lane 1) were digested with ClaI and EcoRI and separated by 1 % (w/v) TAE agarose gel electrophoresis. Bands of 5626, 814, 287 and 45 bp, corresponding to pMUTIN-*plsC-eyfp*, respectively, are marked by black arrows. Bands of 4829, 747, 329 and 287 bp correspond to pMUTIN-*gfp+*. **D**, Verification of pMUTIN-*plsC-eyfp* integration by PCR using primer pair 5'FW10/Outward_eyfp. PCR products were separated by 1 % (w/v) TAE agarose gel electrophoresis. A band of 906 bp, marked by a black arrow, indicates pMUTIN-*plsC-eyfp* chromosomal integration (Lane 1). No DNA amplification is seen using SH1000 genomic DNA (Lane 2). PCR amplification of the whole *plsC* gene using primer pair 5'FW10/3'FW10 results in a band of 638 bp, marked by a black arrow (Lanes 3-4).

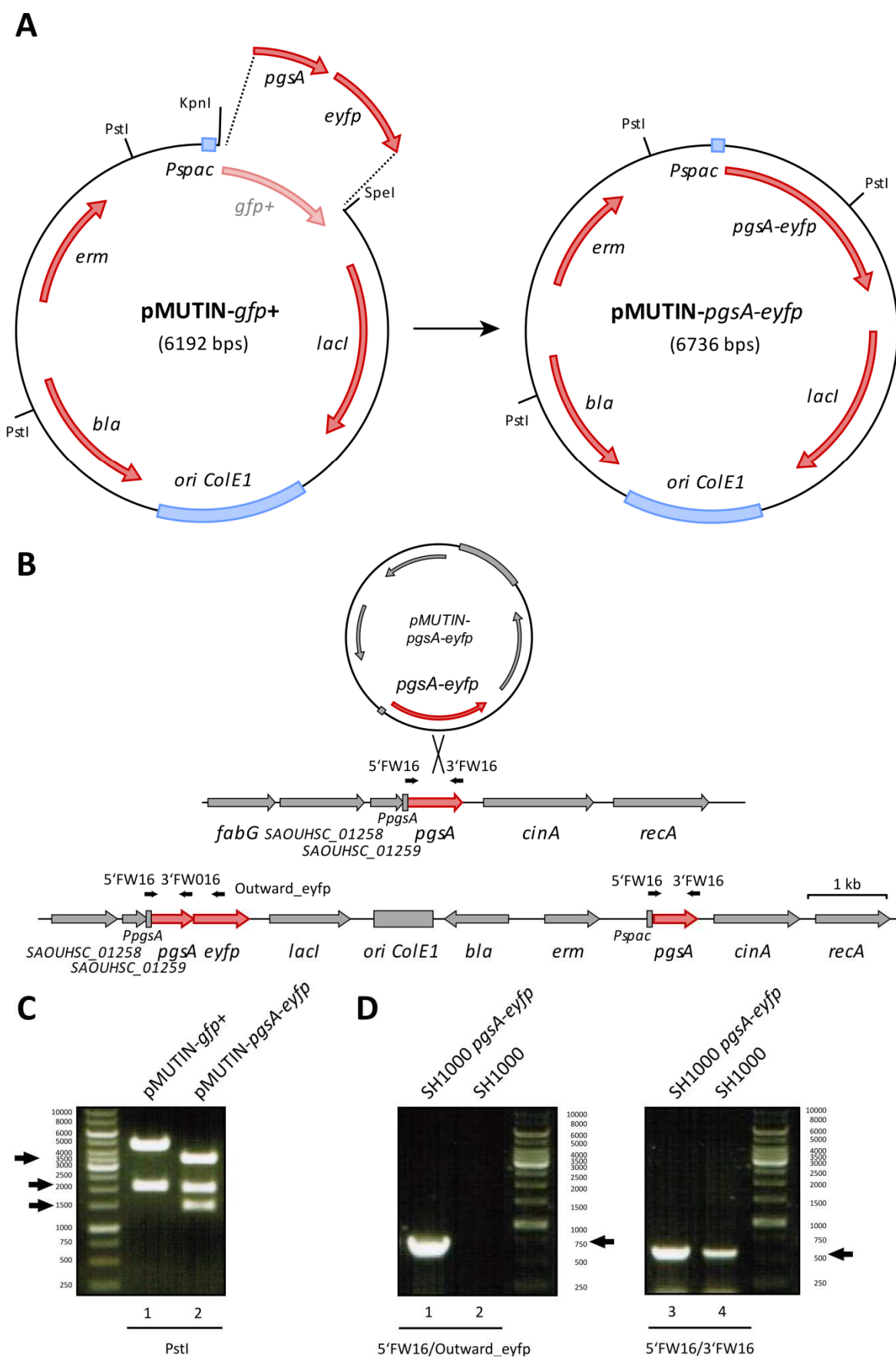


Figure 4.10 Construction of a chromosomal *pgsA-eyfp* fusion in *S. aureus* SH1000

A, Diagram illustrating the construction of pMUTIN-*pgsA-eyfp*. **B**, Schematic overview of the native genomic region of *pgsA* and post integration of pMUTIN-*pgsA-eyfp*. Black arrows indicate primer binding sites. **C**, pMUTIN-*pgsA-eyfp* (Lane 2) and pMUTIN-*gfp+* (Lane 1) were digested with PstI and separated by 1 % (w/v) TAE agarose gel electrophoresis. Bands of 3284, 2000 and 1452 bp, corresponding to pMUTIN-*pgsA-eyfp*, respectively, are marked by black arrows. Bands of 4192 and 2000 bp correspond to pMUTIN-*gfp+*. **D**, Verification of pMUTIN-*pgsA-eyfp* integration by PCR using primer pair 5'FW05/Outward_eyfp. PCR products were separated by 1 % (w/v) TAE agarose gel electrophoresis. A band of 870 bp, marked by a black arrow, indicates pMUTIN-*pgsA-eyfp* chromosomal integration (Lane 1) . No DNA amplification is seen using SH1000 genomic DNA (Lane 2). PCR amplification of the whole *pgsA* gene (Lanes 3-4) using primer pair 5'FW05/3'FW05 results in a band of 600 bp, marked by a black arrow, indicating the functionality of the PCR.

4.2.2.2.3 Construction of an MprF-eYFP fusion in *S. aureus*

In order to construct pMUTIN-*mprF-eyfp*, *mprF* (5'FW14/3'FW14) from SH1000 genomic DNA and *eyfp* (5'FW14/3'FW117) from plasmid pKASBAR-*ezrA-eyfp* were amplified, cloned into the *KpnI/SpeI* site of pMUTIN-*gfp+* using Gibson Assembly (Fig. 4.11) and transformed into *E. coli* NEB5 α . Recombinant plasmids were tested by restriction digest with EcoRI and SpeI which should result in 6944, 1449 and 287 bp fragments (Fig. 4.11C) and validated by DNA sequencing (GATC Biotech AG, Konstanz, Germany). The resulting plasmid was electroporated into RN4220 and from there transduced into SH1000. Genomic integration at the *mprF* locus was confirmed by PCR amplification of a 2813 bp fragment using one primer that binds at the beginning of *mprF* and one primer within the *eyfp* gene (5'FW01/Outward_eyfp) (Fig. 4.11D). No DNA was seen using SH1000 genomic DNA as a negative control template. The whole *mprF* gene was amplified with the use of primers 5'FW01/3'FW14 resulting in a 2543 bp fragment to confirm the PCR and template.

4.2.2.2.4 Construction of a Cls2-eYFP fusion in *S. aureus*

The gene encoding for the major cardiolipin synthase *cls2* is likely to be organised in an operon since its downstream gene, SAOUHSC_02324 (hypothetical protein), begins immediately after the stop codon of *cls2* (see Tab. 4.1). The use of pMUTIN could therefore affect the expression of SAOUHSC_02324. pKASBAR is a pCL84 derivative that is non-replicative in gram positive bacteria and integrates into the lipase gene *geh* (Lee *et al.*, 1991) (Kabli, 2013). This integration is facilitated by site specific recombination via help of an integrase between an *attB* site located within the lipase gene and an *attP* site located on pKASBAR (Fig. 4.12B). A promoter prediction suggests (<http://www.fruitfly.org/>) that the promoter of *cls2* is localised within 100 bp upstream of the start codon.

Single-copy expression of *cls2* under its native promoter was achieved via integration of a pKASBAR plasmid carrying *cls2* and its promoter into the genome of a *cls2* negative RN4220 strain. The *cls2* gene from RN4220 was knocked out by transduction of a JE2 NARSA transposon library strain containing a transposon at the beginning of *cls2* (JE NE258). In order to construct pKASBAR-*P_{cls2}-cls2-eyfp*, *cls2* and its upstream sequence (5'FW09/3'FW09) were amplified from SH1000 genomic DNA, cloned into the *BamHI/AscI* site of pKASBAR-*ezrA-eyfp* using Gibson Assembly (Fig. 4.12A). This led to the exchange of *ezrA* by *cls2* and its promoter in frame with *eyfp*. The resulting plasmid was transformed into *E. coli* NEB5 α . Recombinant plasmids were tested by restriction digest with EcoRI resulting in 6347 and 1357 bp fragments (Fig. 4.12E) and validated by DNA sequencing (GATC Biotech AG, Konstanz, Germany). The resulting plasmid, pKASBAR-*P_{cls2}-cls2-eyfp*, was electroporated into RN4220

expressing an integrase from plasmid pYL112 Δ 19 and from there transduced into RN4220 Δ *cls2::Tn*. The loss of lipase activity was tested on Baird-Parker agar supplemented with egg yolk (Fig. 4.12D). The presence of a chromosomal *cls2-eyfp* fusion was confirmed by PCR amplification of a 1831 bp fragment using one primer that binds at the beginning of *cls2* and one primer within the *eyfp* gene (5'FW08/Outward_eyfp) (Fig. 4.12F). No DNA amplification was seen using SH1000 genomic DNA as a negative control template. The knock-out of the original *cls2* gene via transposon insertion was also confirmed by PCR. According to the NARSA library information (<http://app1.unmc.edu/fgx/index.html>), the transposon inserted in reverse into *cls2* (Fig. 4.12C). Based on this, transposon integration was tested twice using two primer combinations (5'FW08/Upstream and Buster/3'FW08, see Fig. 4.10C for primer binding sites) that should result in approximately 1500 bp (5'FW08/Upstream) and 600 bp (Buster/3'FW08) fragments whereas no DNA was amplified using SH1000 genomic DNA as a template (Fig. 4.12F).

4.2.2.3 Localisation studies of phospholipid synthesis enzyme fusions with *eyfp*

The constructed strains expressing *eyfp* fusions of phospholipid synthesis enzymes were used for localisation studies by fluorescence microscopy. Hence, overnight cultures were diluted to an OD₆₀₀=0.05 and grown at 37 °C for 2 h at 250 rpm. 1 ml samples were harvested, fixed using p-formaldehyde and imaged by fluorescence microscopy.

The phospholipid synthesis enzyme fusions, PlsC-eYFP, PgsA-eYFP, MprF-eYFP and Cls2-eYFP, were found to localise in a punctate pattern and at the septum in cells undergoing cell division (Fig. 4.13 - 4.16). All fusions except for PgsA-eYFP showed a punctate distribution at the septum along with peripherally localised fusions. Fluorescence levels of PgsA-eYFP were lower compared to the other fusions and thus, the fusion protein appears to only localise at the septum in cells undergoing cell-division.

Interestingly, the analysis of Cls2-eYFP localisation by comparing eYFP fluorescence with HADA signals throughout the Z-stack reveals that Cls2-eYFP appears to be localised at the base of the septum during cell-division (Fig. 4.16C). This potentially indicates that Cls2-eYFP localises to the site of highest membrane curvature within the cell during cell-division.

In summary, all proteins involved in phospholipid synthesis were found not to distribute homogeneously throughout the membrane but to be localised in a punctate pattern and to display septal localisation in dividing cells. However, at this stage more experiments are required to conclude whether these proteins are colocalised.

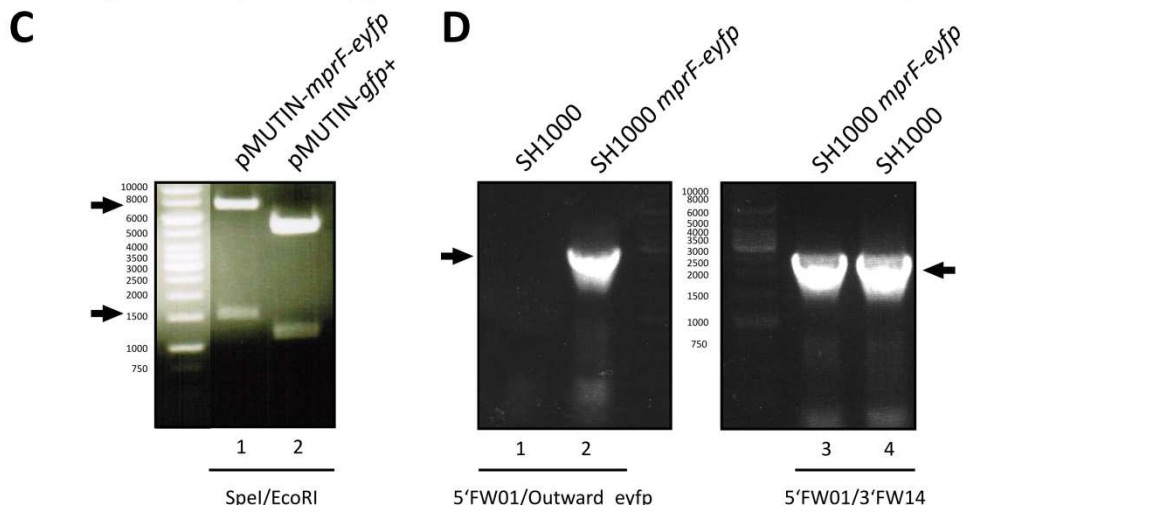
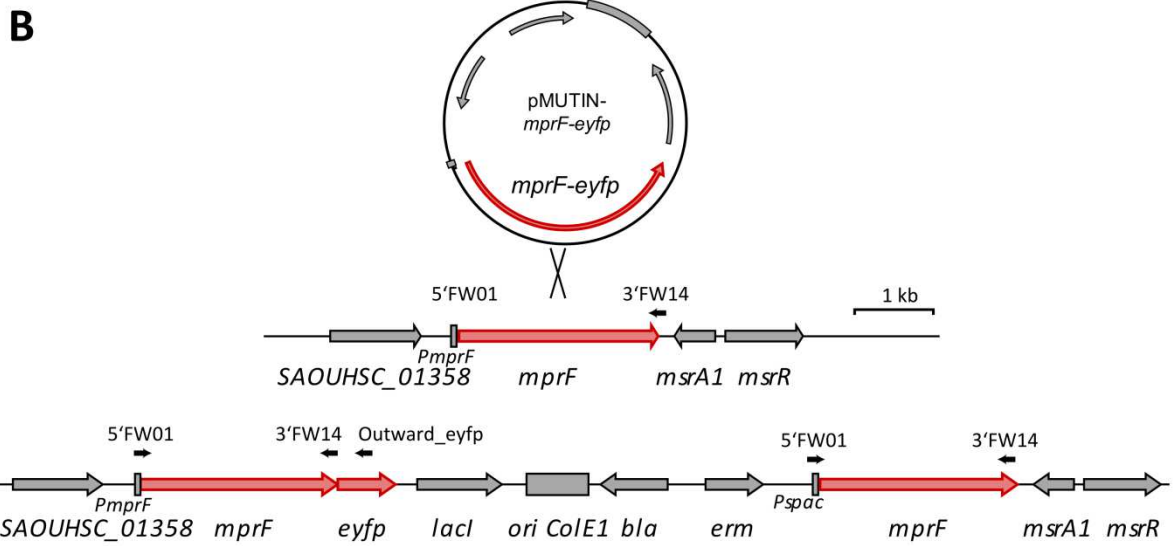
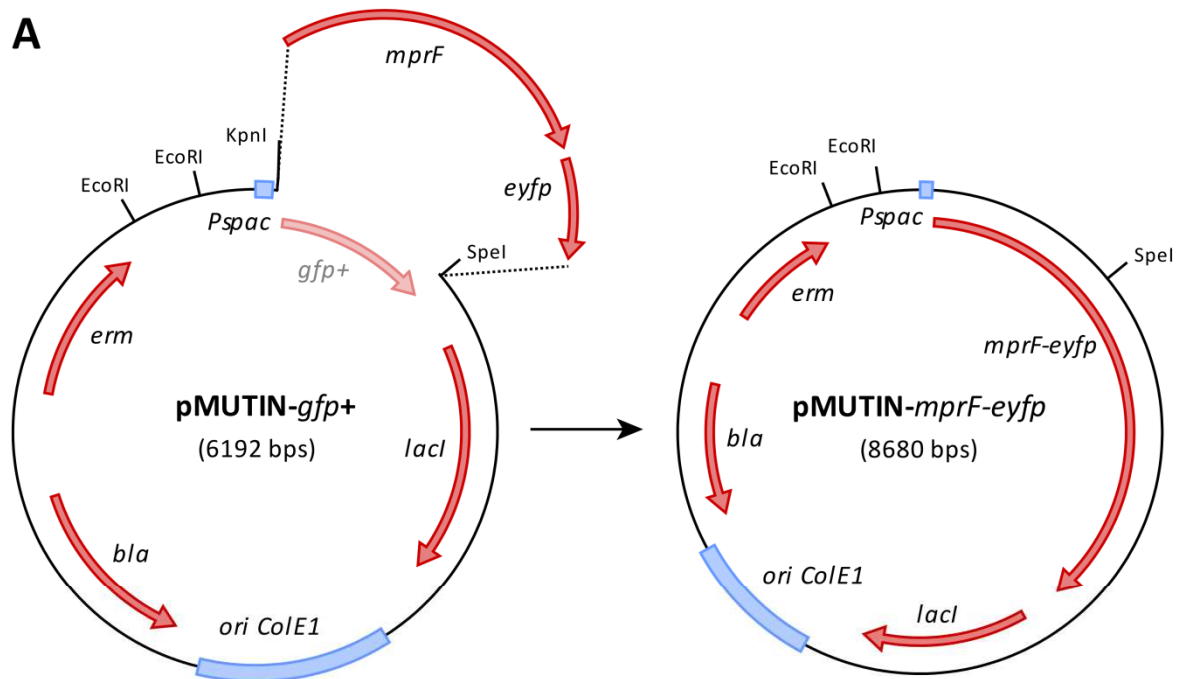
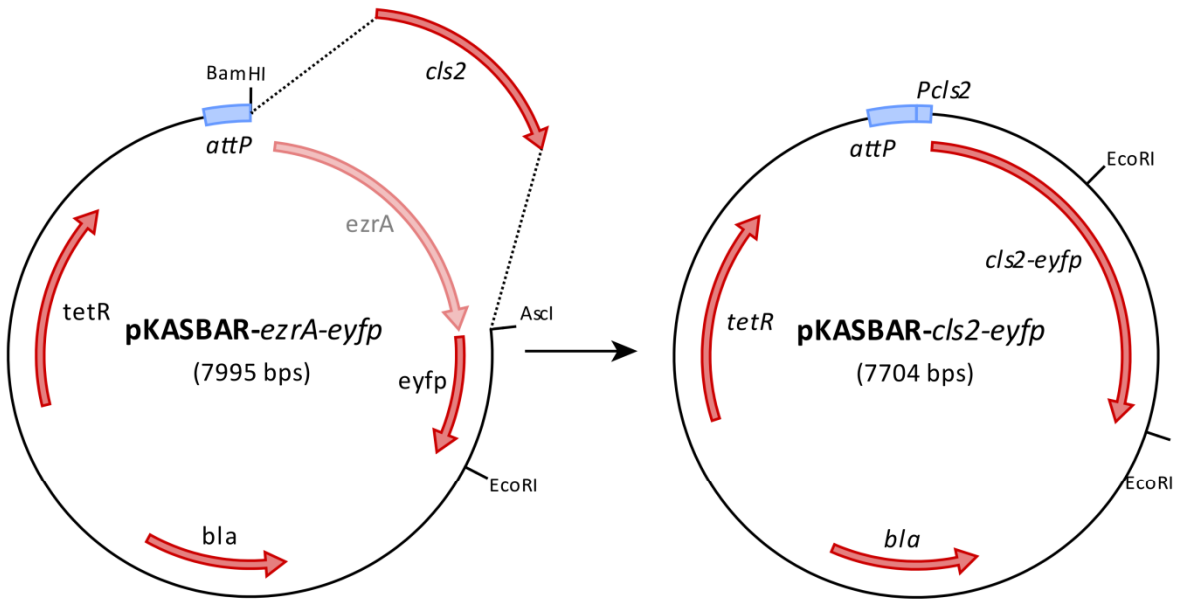
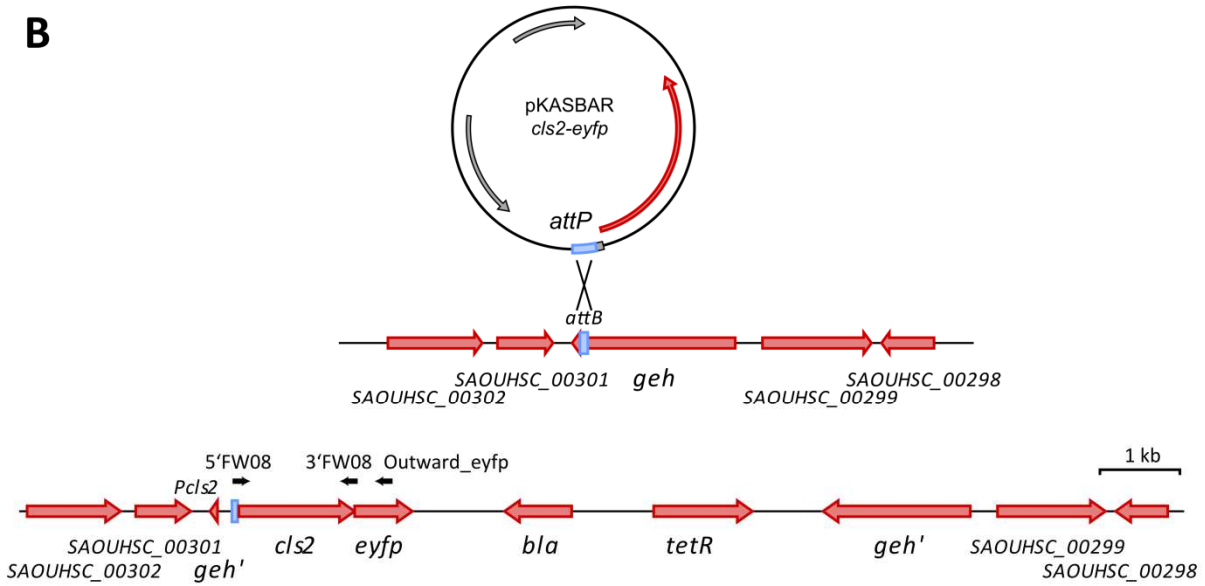
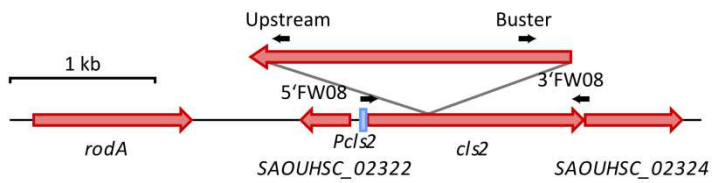


Figure 4.11 Construction of a chromosomal *mprF-eyfp* fusion in *S. aureus* SH1000

A, Diagram illustrating the construction of pMUTIN-*mprF-eyfp*. **B**, Schematic overview of the native genomic region of *mprF* and post integration of pMUTIN-*mprF-eyfp*. Black arrows indicate primer binding sites. **C**, pMUTIN-*mprF-eyfp* (Lane 1) and pMUTIN-*gfp+* (Lane 2) were digested with SpeI/EcoRI and separated by 1 % (w/v) TAE agarose gel electrophoresis. Bands of 6944 and 1449 (and 287 bp), corresponding to pMUTIN-*mprF-eyfp*, respectively, are marked by black arrows. Bands of 4819 and 1076 (and 287 and 10 bp) correspond to pMUTIN-*gfp+*. **D**, Verification of pMUTIN-*mprF-eyfp* integration by PCR using primer pair 5'FW01/Outward_eyfp. PCR products were separated by 1 % (w/v) TAE agarose gel electrophoresis. A band of 2813 bp, marked by a black arrow, indicates pMUTIN-*mprF-eyfp* chromosomal integration (Lane 2). No DNA amplification is seen using SH1000 genomic DNA (Lane 1). PCR amplification of the whole *mprF* gene (Lanes 3-4) using primer pair 5'FW01/3'FW14 results in a band of 2543 bp, marked by a black arrow.

A**B****C****D**

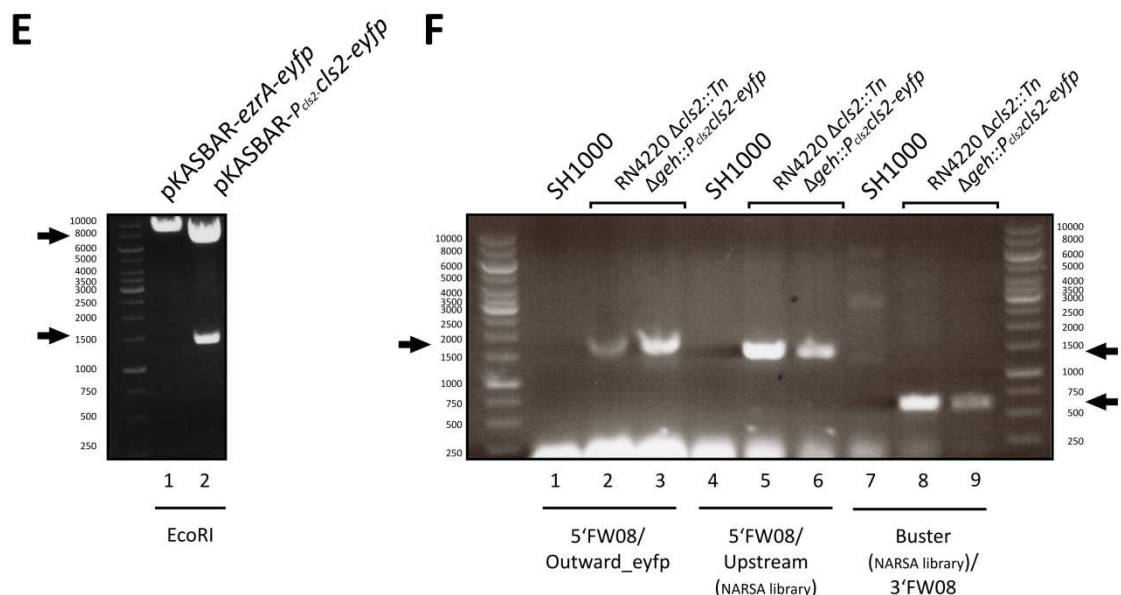


Figure 4.12 Construction of a chromosomal *cls2-eyfp* fusion in *S. aureus* RN4220 *cls2::Tn*

A, Diagram illustrating the construction of pKASBAR-*P_{cls2}-cls2-eyfp*. **B**, Schematic overview of the native genomic region of *geh* and post integration of pKASBAR-*P_{cls2}-cls2-eyfp*. Black arrows indicate primer binding sites. **C**, Schematic overview of the native genomic region of *cls2* and transposon integration site. Black arrows indicate primer binding sites. **D**, Lipase activity test. RN4220 and RN4220 *cls2::Tn Δgeh::cls2-eyfp* growth on Baird-Parker agar supplemented with egg yolk. The halo around RN4220 colonies indicates lipase activity. **E**, pKASBAR-*P_{cls2}-cls2-eyfp* (Lane 2) and pKASBAR-*ezrA-eyfp* (Lane 1) were digested with EcoRI and separated by 1 % (w/v) TAE agarose gel electrophoresis. Bands of 6347 and 1357 bp, corresponding to pKASBAR-*P_{cls2}-cls2-eyfp* (Lane 2), respectively, are marked by black arrows. A band of 7995 bp corresponds to linearized pKASBAR-*ezrA-eyfp* (Lane 1). **F**, Verification of pKASBAR-*P_{cls2}-cls2-eyfp* integration by PCR amplification using primer pair 5'FW08/Outward_eyfp. PCR products were separated by 1 % (w/v) TAE agarose gel electrophoresis. A band of 1831 bp, marked by a black arrow, indicates pKASBAR-*P_{cls2}-cls2-eyfp* chromosomal integration (Lanes 2-3). No DNA amplification is seen using SH1000 genomic DNA (Lane 1). Verification of $\Delta cls2::Tn$ by PCR amplification using primer pair 5'FW08/Upstream and Buster/3'FW08. Bands of approximately 1500 bp (Lanes 5-6) and 600 bp (Lanes 8-9), respectively, marked by black arrows, indicate transposon integration into *cls2*. No DNA amplification is seen for both primer pairs using SH1000 genomic DNA (Lanes 4 and 7).

4.2.2.3.1 Localisation of PlsC-eYFP

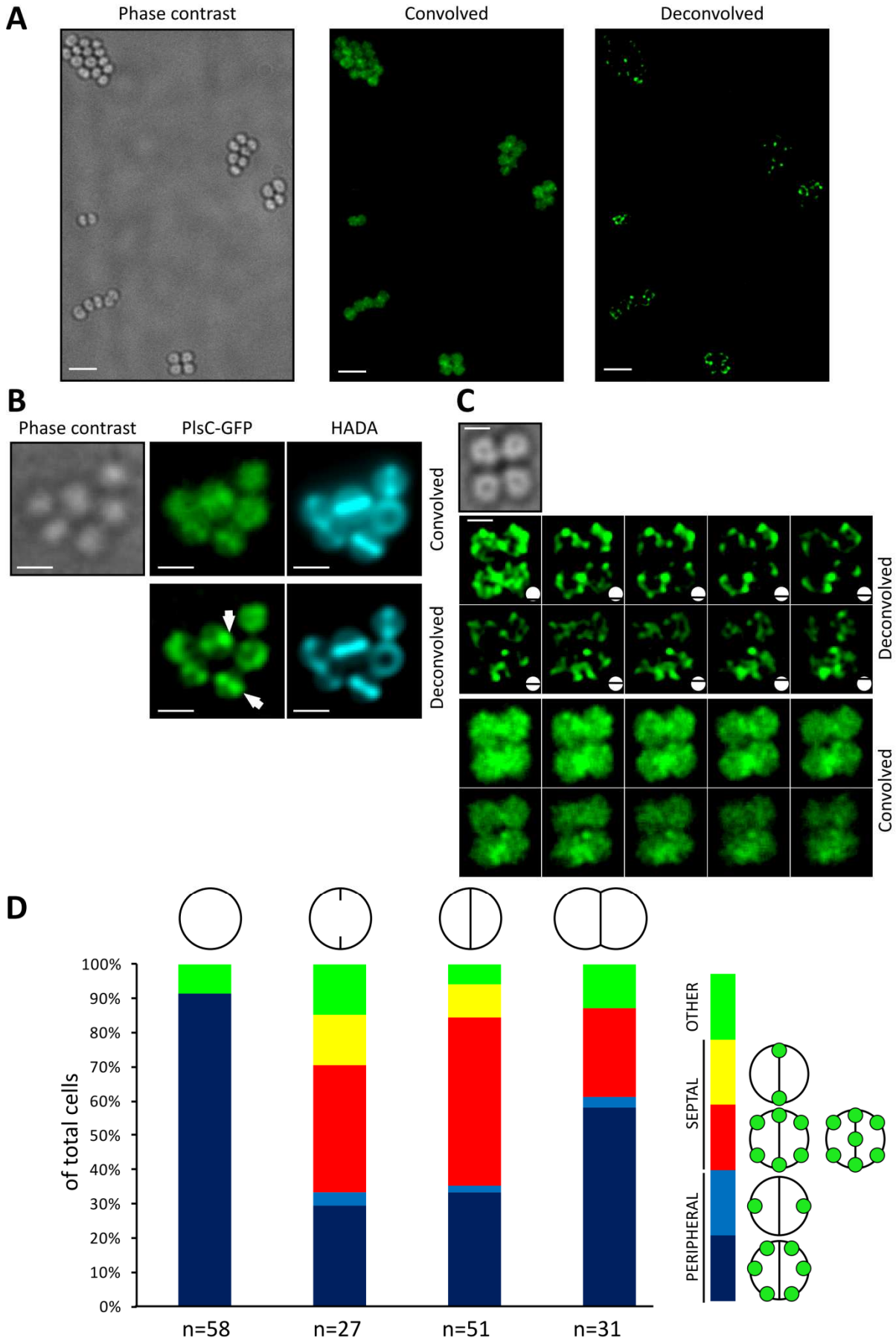
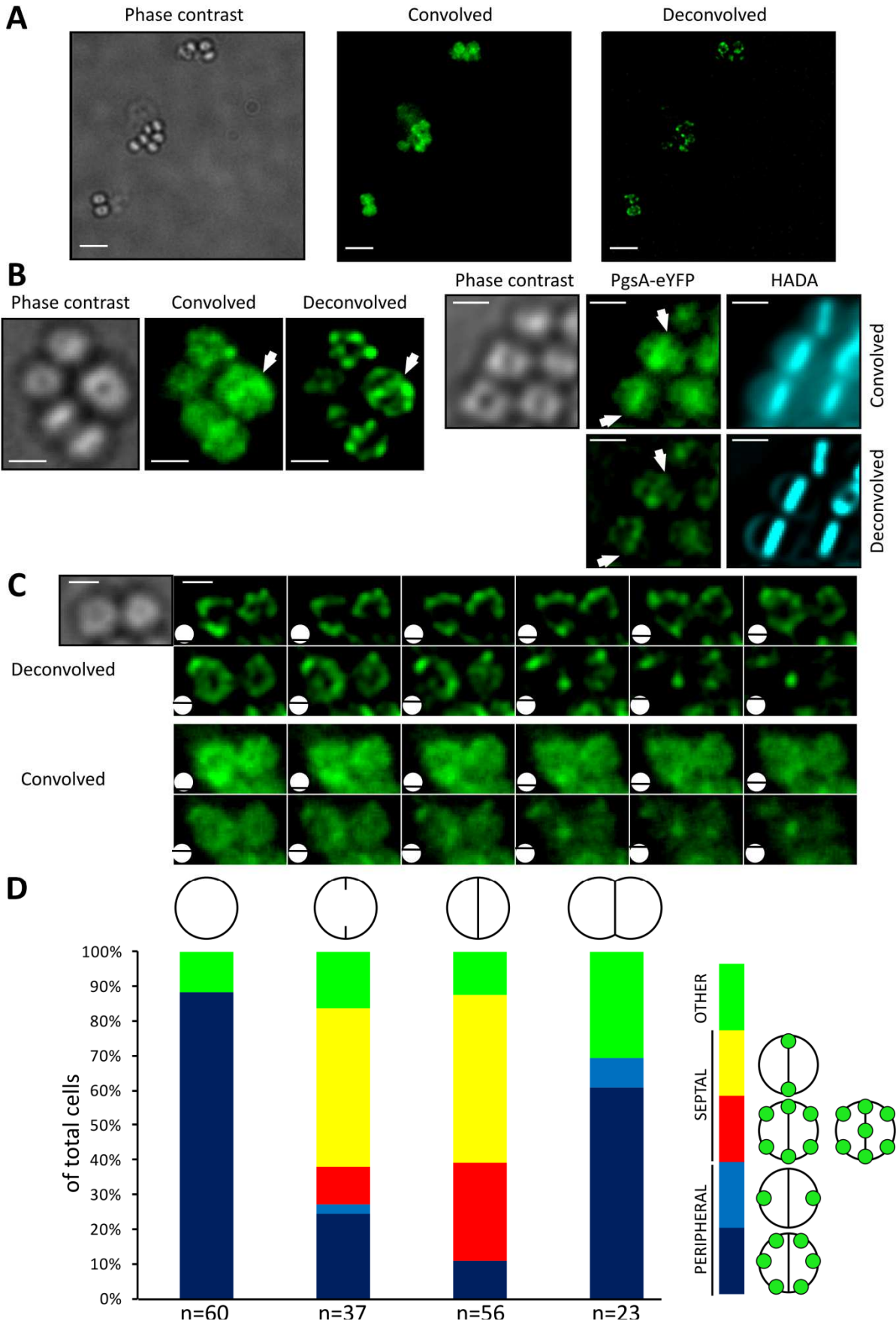


Figure 4.13 Localisation of PlsC-eYFP in *S. aureus* SH1000

Phase contrast and fluorescence images (convolved and deconvolved) of *S. aureus* SH1000 *plsC-eyfp*. Images were acquired using a Delta Vision microscope and SoftWoRx 3.5.0 software (Applied Precision). Acquisition of fluorescence images were taken using 2.5 sec exposure in the FITC channel and 1 sec exposure in the DAPI channel. **A**, Scale bars represent 3 μm . **B**, Selected cells showing the localisation of PlsC-eYFP and HADA. The white arrows indicate septal localisation. Scale bars represent 1 μm . **C**, Z-stack images of selected cells. Scale bars represent 1 μm . **D**, Cell counts categorized depending on PlsC-eYFP localisation and cell-cycle stage indicated by HADA labelling. Value n indicates counted cells for each group. Red and yellow bars indicate septal and blue bars indicate peripheral PlsC-eYFP localisation. The green coloured bar indicates random PlsC-eYFP localisation.

4.2.2.3.2 Localisation of PgsA-eYFP



Phase contrast and fluorescence images (convolved and deconvolved) of *S. aureus* SH1000 *pgsA-eyfp*. Images were acquired using a Delta Vision microscope and SoftWoRx 3.5.0 software (Applied Precision). Acquisition of fluorescence images were taken using 2.5 sec exposure in the FITC channel and 1 sec exposure in the DAPI channel. **A**, Scale bars represent 3 μm . **B**, Selected cells showing the localisation of PgsA-eYFP and HADA. The white arrows indicate septal localisation. Scale bars represent 1 μm . **C**, Z-stack images of selected cells. Scale bars represent 1 μm . **D**, Cell counts categorized depending on PgsA-eYFP localisation and cell-cycle stage indicated by HADA labelling. Value n indicates counted cells for each group. Red and yellow bars indicate septal and blue bars indicate peripheral PgsA-eYFP localisation. The green coloured bar indicates random PgsA-eYFP localisation.

4.2.2.3.3 Localisation of MprF-eYFP

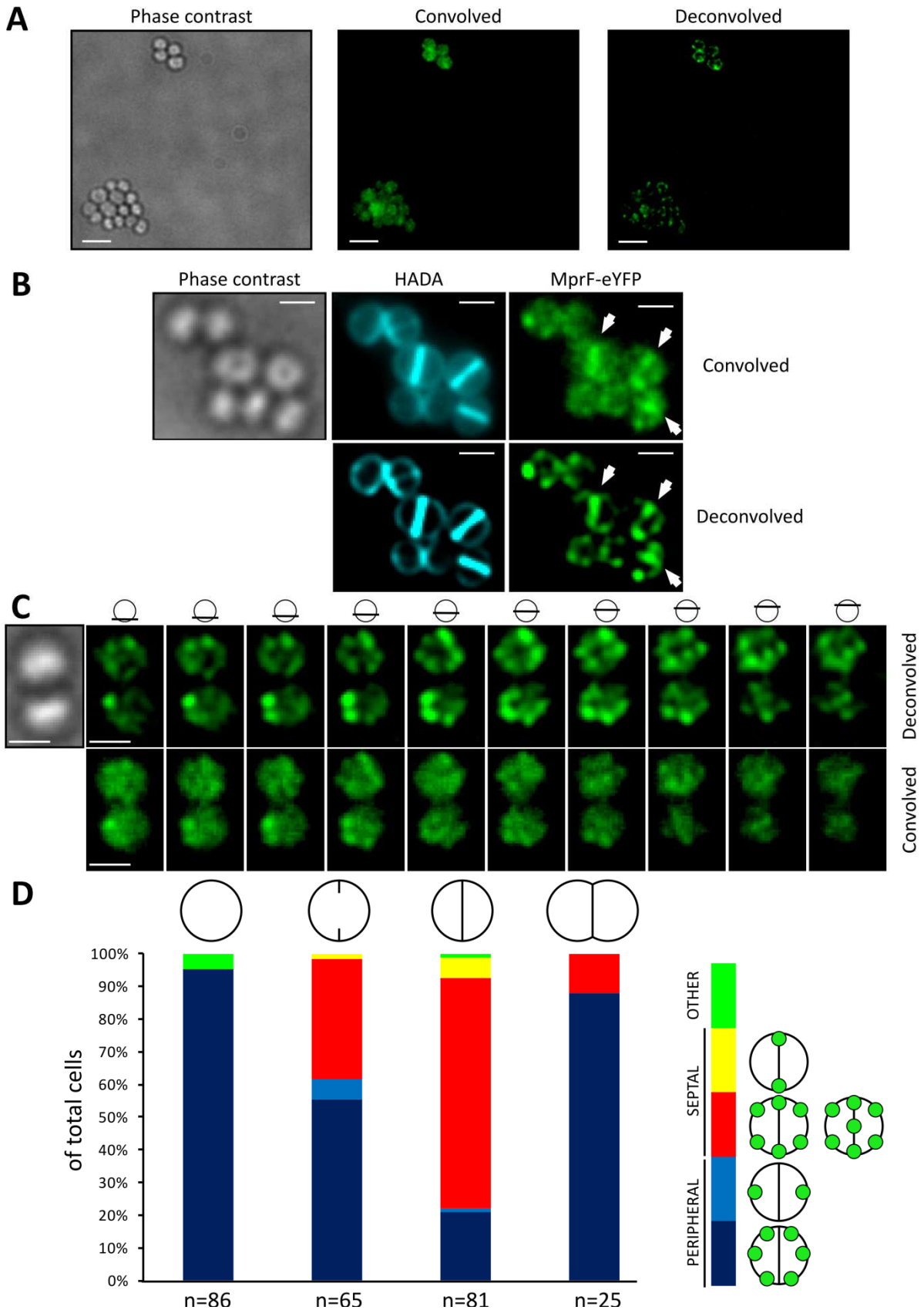


Figure 4.15 Localisation of MprF-eYFP in *S. aureus* SH1000

Phase contrast and fluorescence images (convolved and deconvolved) of *S. aureus* SH1000 *mprF-eyfp*. Images were acquired using a Delta Vision microscope and SoftWoRx 3.5.0 software (Applied Precision). Acquisition of fluorescence images were taken using 2.5 sec exposure in the FITC channel. **A**, Scale bars represent 3 μm . **B**, Selected cells showing the localisation of MprF-eYFP. The white arrows indicate septal localisation. Scale bars represent 1 μm . **C**, Z-stack images of selected cells. Scale bars represent 1 μm . **D**, Cell counts categorized depending on MprF-eYFP localisation and cell-cycle stage indicated by HADA labelling. Value n indicates counted cells for each group. Red and yellow bars indicate septal and blue bars indicate peripheral MprF-eYFP localisation. The green coloured bar indicates random MprF-eYFP localisation.

4.2.2.3.4 Localisation of Cls2-eYFP

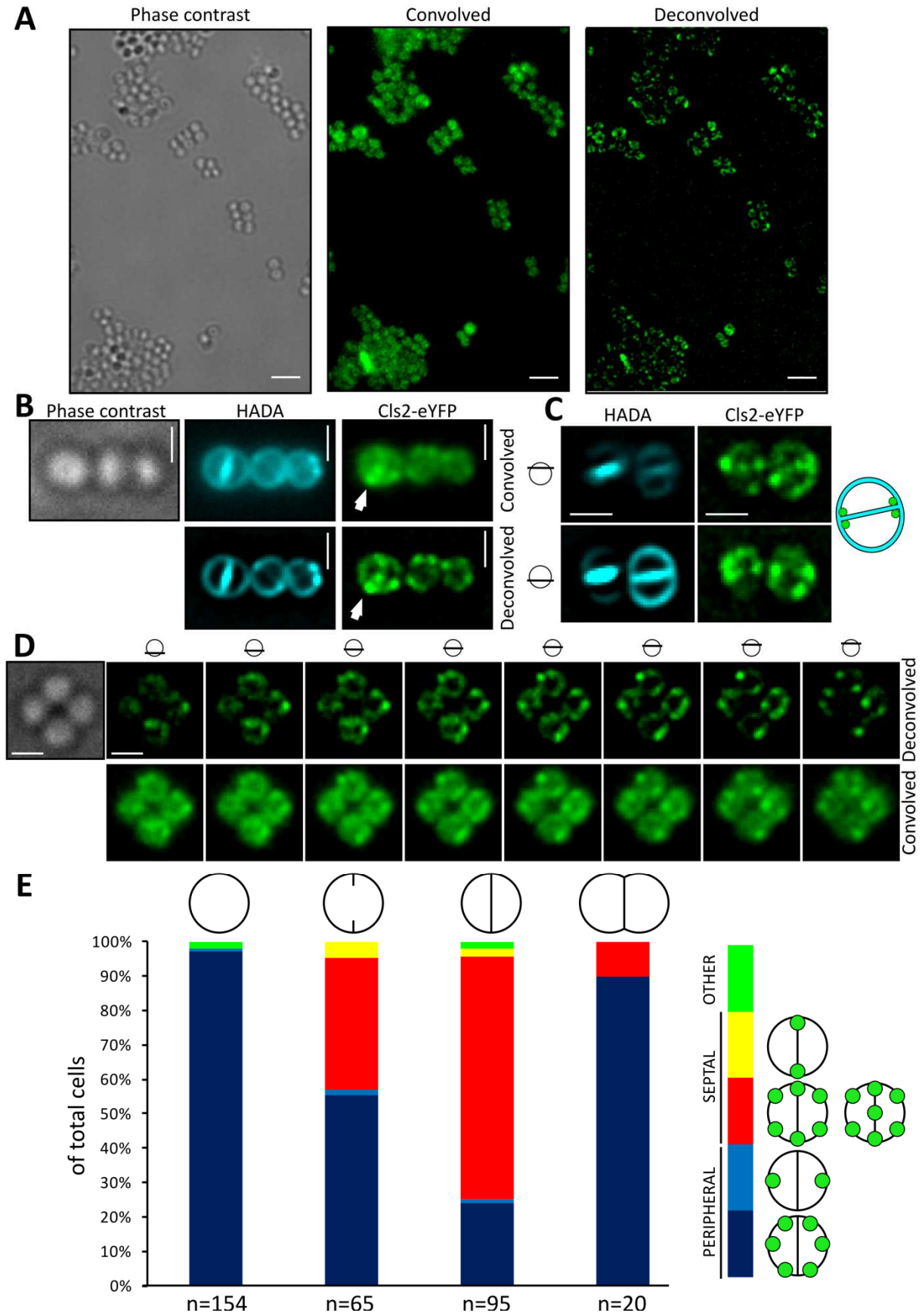


Figure 4.16 Localisation of Cls2-eYFP in *S. aureus* RN4220

Phase contrast and fluorescence images (convolved and deconvolved) of *S. aureus* RN4220 $\Delta_{geh}::P_{cls2-cls2-eyfp} \Delta_{cls2}$. Images were acquired using a Delta Vision microscope and SoftWoRx 3.5.0 software (Applied Precision). Acquisition of fluorescence images were taken using 2.5 sec exposure in the FITC channel. **A**, Scale bars represent 3 μm . **B**, Selected cells showing the localisation of Cls2-eYFP. The white arrow indicates septal localisation. Scale bars represent 1 μm . **C**, Selected cells at the upper and lower Z-level of the cells showing the localisation of Cls2-eYFP. Scale bars represent 1 μm . **D**, Z-stack images of selected cells. Scale bars represent 1 μm . **E**, Cell counts categorized depending on Cls2-eYFP localisation and cell-cycle stage indicated by HADA labelling. Value n indicates counted cells for each group. Red and yellow bars indicate septal and blue bars indicate peripheral Cls2-eYFP localisation. The green coloured bar indicates random Cls2-eYFP localisation.

4.2.2.4 Localisation studies of non-phospholipid synthesis proteins

The previous localisation studies were focused on enzymes involved in phospholipid synthesis and revealed that all of them show a similar punctate heterogeneous distribution. This raises several questions whether this localisation pattern is unique to phospholipid synthesis enzymes and how membrane proteins from unrelated pathways are distributed.

4.2.2.5 Cytochrome B subunit (CydB)

CydB is a subunit of cytochrome BD, a quinol oxidoreductase, one of two terminal oxidases in *S. aureus*. Its main function is the production of a proton motive force through a transfer of protons during respiration. It has been shown previously that a C-terminal CydB-GFP fusion in *E. coli* is functional and localises in mobile membrane patches within the plasma membrane (Lenn *et al.*, 2008b). These mobile patches could coincide with the punctate localisation pattern of the analysed staphylococcal membrane proteins.

4.2.2.5.1 Construction of a CydB-eYFP fusion in *S. aureus*

pMUTIN-*cydB-eyfp* was constructed by amplification of, genes *cydB* (5'FW21/3'FW21) from SH1000 genomic DNA and *eyfp* (5'FW22/3'FW117) from plasmid pKASBAR-*ezrA-eyfp* were amplified, cloned into the *KpnI/SpeI* site of pMUTIN-*gfp+* using Gibson Assembly (Fig. 4.17) and transformed into *E. coli* NEB5 α . Recombinant plasmids were tested by restriction digest with PstI which should result in 6944, 1449 and 287 bp fragments (Fig. 4.17C). However, neither the digest of pMUTIN-*gfp+* which should result in DNA fragments of 5394, 608 and 190 bp nor of pMUTIN-*cydB-eyfp* resulted in the expected digestion pattern. This might be explained due to star activity of PstI or that the plasmid sequence of pMUTIN-*gfp+* used for analysis is incorrect. Sequencing showed that the insert is correct and harbours no mutations. The resulting plasmid, pMUTIN-*cydB-eyfp*, was electroporated into RN4220 and from there transduced into SH1000. Genomic integration at the *cydB* locus was confirmed by PCR amplification of a 1311 bp fragment using one primer that binds at the beginning of *cydB* and one primer within the *eyfp* gene (5'FW21/Outward_eyfp) (Fig. 4.17D). No DNA amplification was seen using SH1000 genomic DNA as a negative control template. The whole *cydB* gene was amplified with the use of primers 5'FW21/3'FW21 resulting in a 1040 bp fragment confirming the PCR and template.

4.2.2.5.2 Localisation of CydB-eYFP

In order to study the localisation of CydB-eYFP in *S. aureus* SH1000, an overnight culture was diluted to an $OD_{600}=0.05$ and grown at 37 °C to an $OD_{600}\approx 0.5$. Cells were labelled with 5 μ l HADA (100 mM stock solution) in PBS for 5 min and subsequently washed with PBS followed by fixing with para-formaldehyde before analysis by fluorescence microscopy.

CydB-eYFP distributes non-homogeneously in the membrane (Fig. 4.18). Fluorescence can be seen in punctate patches around the cell periphery but not at the cell-division site (Fig. 4.18BD). This is confirmed by cell counts showing that CydB-eYFP is only septally localised in around 20-30 % of cells undergoing cell-division. These counts however, could be miscategorised due to the limited resolution that could lead to an apparent septal localisation. Notably, the fluorescence levels between cells differed and could be explained that the fusion is not expressed in every single cell at the same level.

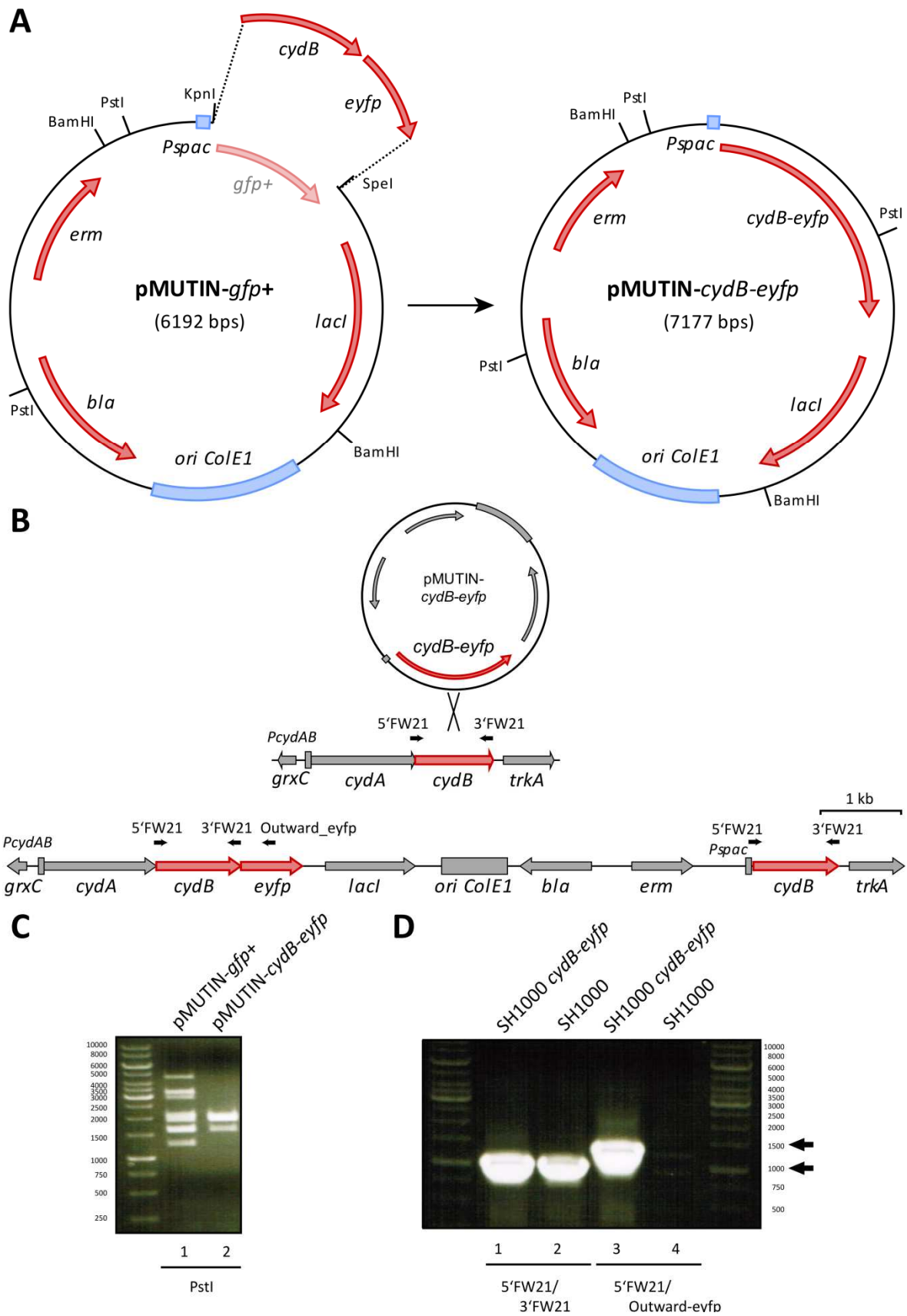


Figure 4.17 Construction of a chromosomal *cydB-eyfp* fusion in *S. aureus* SH1000

A, Diagram illustrating the construction of pMUTIN-*cydB-eyfp*. **B**, Schematic overview of the native genomic region of *cydB* and post integration of pMUTIN-*cydB-eyfp*. Black arrows indicate primer binding sites. **C**, pMUTIN-*cydB-eyfp* (Lane 2) and pMUTIN-*gfp+* (Lane 1) were digested with PstI and separated by 1 % (w/v) TAE agarose gel electrophoresis. Bands of 6388 bp and 394 bp, corresponding to pMUTIN-*cydB-eyfp*, respectively, are marked by black arrows. Bands of 5394 bp and 608 bp (and 190 bp) correspond to pMUTIN-*gfp+*. **D**, Verification of pMUTIN-*cydB-eyfp* integration by PCR using primer pair 5'FW21/Outward_eyfp. PCR products were separated by 1 % (w/v) TAE agarose gel electrophoresis. A band of 1311 bp, marked by a black arrow, indicates pMUTIN-*cydB-eyfp* chromosomal integration (Lane 3). No DNA amplification is seen using genomic DNA from SH1000 (Lane 4). PCR amplification of the whole *cydB* gene using primer pair 5'FW21/3'FW21 results in a band of 1040 bp (Lanes 1-2), marked by a black arrow, indicating the functionality of the PCR.

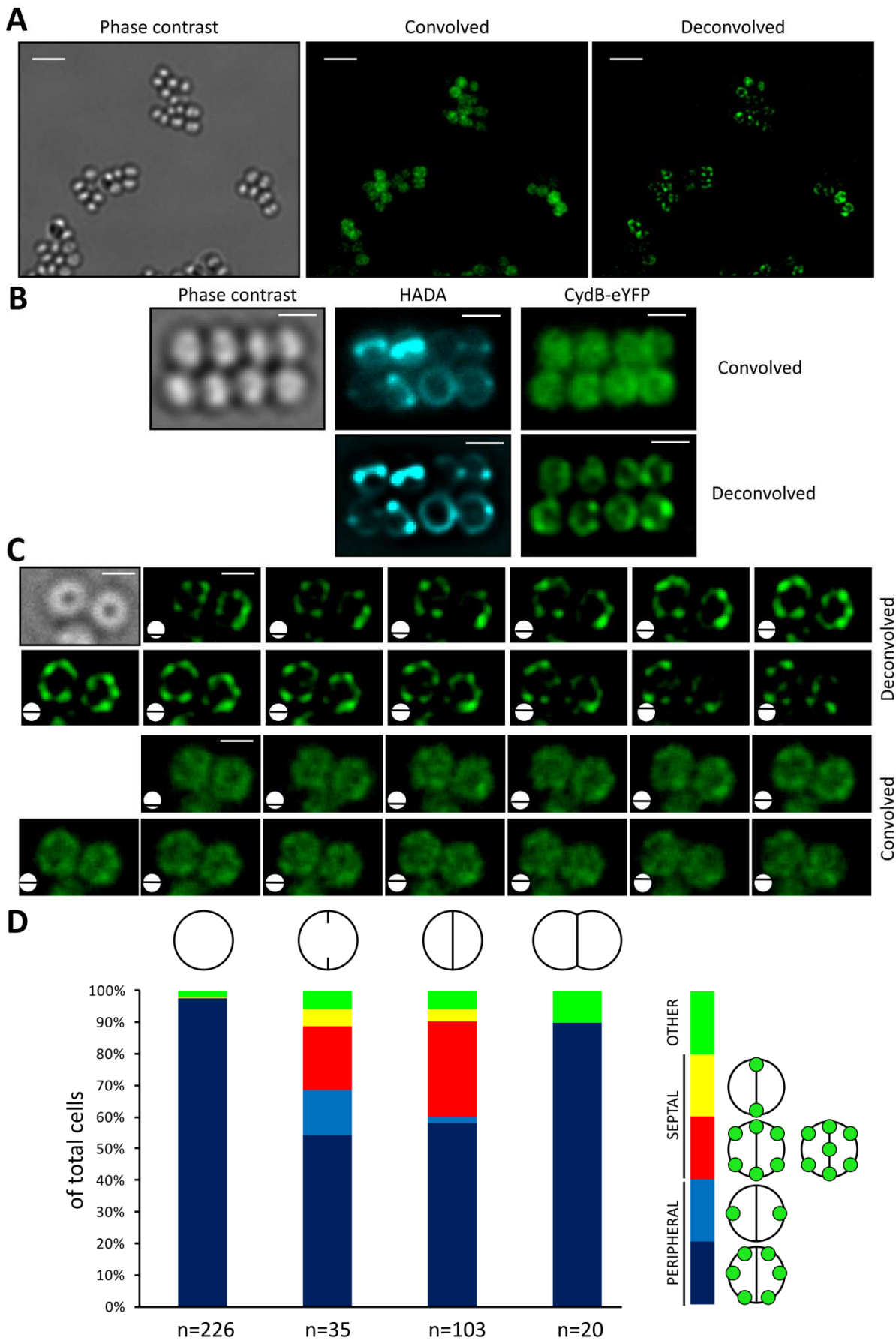


Figure 4.18 Localisation of CydB-eYFP in *S. aureus* SH1000

Phase contrast and fluorescence images (convolved and deconvolved) of *S. aureus* SH1000 *cydB-eyfp*. Images were acquired using a Delta Vision microscope and SoftWoRx 3.5.0 software (Applied Precision). Acquisition of fluorescence images were taken using 2.5 sec exposure in the FITC channel. **A**, Scale bars represent 3 μm . **B**, Selected cells showing the localisation of CydB-eYFP and HADA. Scale bars represent 1 μm . **C**, Z-stack images of selected cells. Scale bars represent 1 μm . **D**, Cell counts categorized depending on CydB-eYFP localisation and cell-cycle stage indicated by HADA labelling. n indicates counted cells for each group. Red and yellow bars indicate septal and blue bars indicate peripheral CydB-eYFP localisation. The green coloured bar indicates random CydB-eYFP localisation.

4.2.2.6 Flotillin

The first evidence for the existence of lipid rafts in *S. aureus* has been published recently (Lopez & Kolter, 2010). Lopez *et al.*, showed that the bacterial homologue of Flotillin-1 (FloT) a lipid raft marker in eukaryotes, localises at a single spot in the membrane of *S. aureus* (Fig. 4.19) (Lopez & Kolter, 2010). This localisation is dependent on the cholesterol precursor squalene. Cells treated with zaragozic acid, an inhibitor of the squalene synthase, exhibit a loss of FloT localisation which eventually leads to its degradation. In order to allow comparison of FloT localisation to PlsY, the localisation of FloT was investigated followed by a zaragozic acid assay.

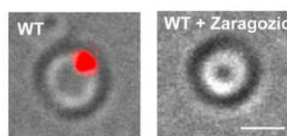


Figure 4.19 Localisation of FloT-eYFP in *S. aureus* UAMS-1

Image is taken from (Lopez & Kolter, 2010).

4.2.2.6.1 Construction of a FloT-eYFP fusion in *S. aureus*

pMUTIN-*floT-eyfp* was constructed by amplification of, genes *floT* (5'FW19/3'FW19) from SH1000 genomic DNA and *eyfp* (5'FW20/3'FW117) from plasmid pKASBAR-*ezrA-eyfp* were amplified, cloned into the *KpnI/SpeI* site of pMUTIN-*gfp+* using Gibson Assembly (Fig. 4.20) and transformed into *E. coli* NEB5 α . Recombinant plasmids were tested by restriction digest with PacI and BamHI resulting in 3435, 2926, 619 and 167 bp fragments (Fig. 4.20C) and further validated by DNA sequencing (GATC Biotech AG, Konstanz, Germany). The resulting plasmid, pMUTIN-*floT-eyfp*, was electroporated into RN4220 and from there transduced into SH1000. Genomic integration at the *floT* locus was confirmed by PCR amplification of a 1281 bp fragment using one primer that binds at the beginning of *floT* and one primer within the *eyfp* gene (5'FW21/Outward_eyfp) (Fig. 4.20D). No DNA amplification was seen using SH1000 genomic DNA as a negative control template. The whole *floT* gene was amplified with the use of primers 5'FW19/3'FW19 resulting in a 1011 bp fragment confirming the PCR and template.

4.2.2.6.2 Localisation of FloT-eYFP

In order to study the localisation of FloT-eYFP in *S. aureus* SH1000, an overnight culture was diluted to an $OD_{600}=0.05$ and grown at 37 °C to an $OD_{600}\approx 0.5$. Cells were harvested, washed with PBS followed by fixing with para-formaldehyde and analysed by fluorescence microscopy.

As reported previously, FloT-eYFP is expected to localise in a single patch in the membrane (Lopez & Kolter, 2010). Conversely, the majority of cells were found to show a heterogeneous punctate distribution (Fig. 4.21AB) similar to the ones observed for phospholipid synthesis enzymes (Fig. 4.7 and Fig. 4.13 - Fig. 4.16).

To determine if the integration of pMUTIN affected the localisation, the multicopy *lacI* expressing plasmid pGL485 was transduced to SH1000 *floT-eyfp* to create strain SH1000 *floT-eyfp* + pGL485. pMUTIN integration results in the original untagged *floT* gene under control of the IPTG inducible promoter *Pspac*. It also expresses one copy of *lacI*, the repressor of *Pspac*. This could potentially constitute an issue since one copy might not be enough to tightly repress the expression of untagged *floT* and it could thereby affect the localisation of FloT-eYFP.

The expression of the original gene upon IPTG addition nor a tighter regulation through pGL485 alters the localisation of FloT-eYFP inferring that the original gene does not affect the localisation of FloT-eYFP (Fig. 4.22). Yet it may be possible that the integration of pMUTIN affects the downstream gene (SAOUHSC_01675, putative DNA translocase) and that it is linked to *floT* localisation. However, it seems unlikely that a helicase is involved in the localisation of a membrane protein. On the other hand, the localisation of FloT-eYFP that has been published recently might be an artefact due to overexpression (Lopez & Kolter, 2010). The paper does not state clearly whether a single-copy expression or overexpression of *floT-eyfp* was applied for the study.

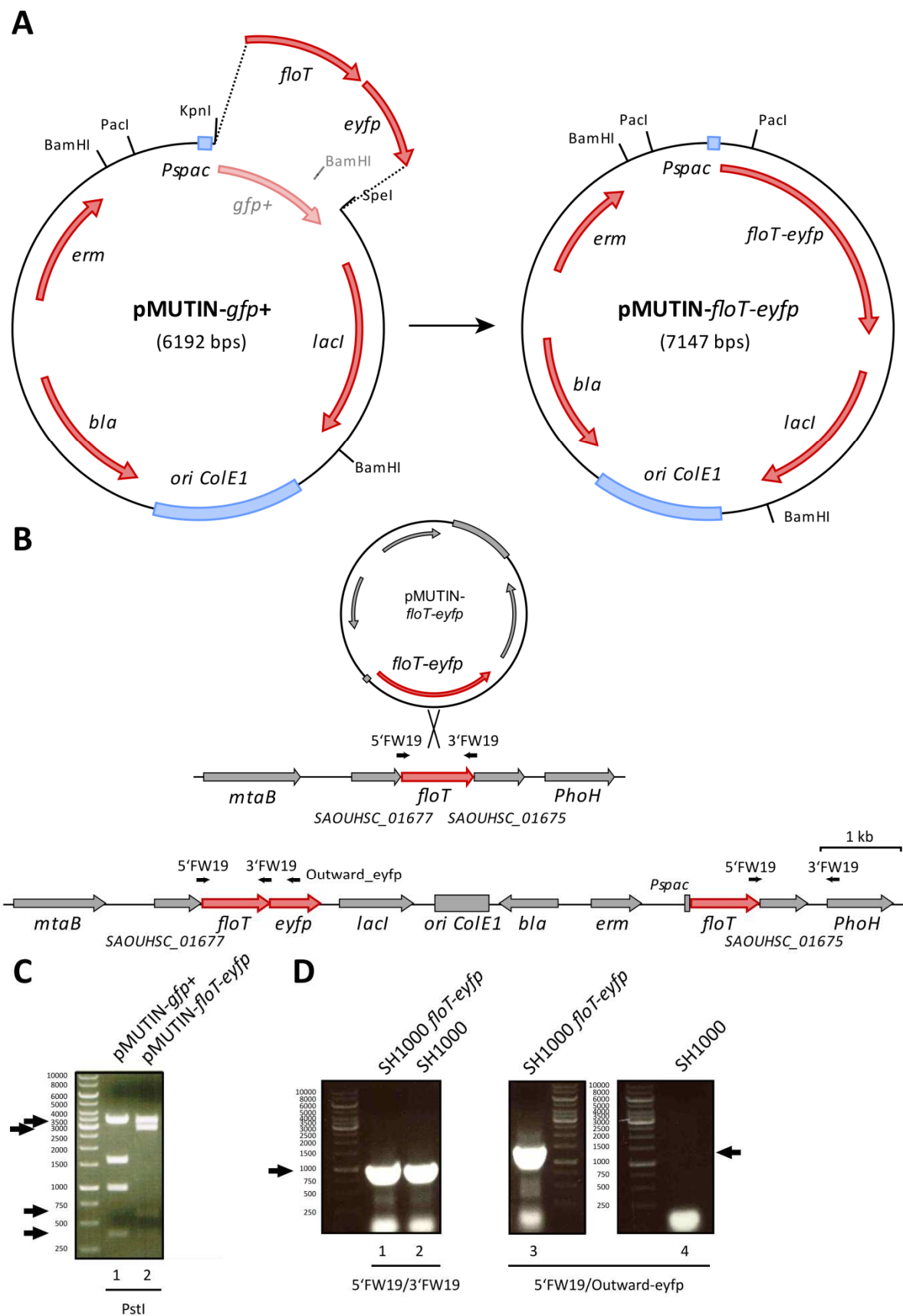


Figure 4.20 Construction of a chromosomal *floT-eyfp* fusion in *S. aureus* SH1000

A, Diagram illustrating the construction of pMUTIN-*floT-eyfp*. **B**, Schematic overview of the native genomic region of *floT* and post integration of pMUTIN-*floT-eyfp*. Black arrows indicate primer binding sites. **C**, pMUTIN-*floT-eyfp* (Lanes 2-4) and pMUTIN-*gfp+* (Lane 1) were digested with PacI and BamHI and separated by 1 % (w/v) TAE agarose gel electrophoresis. Bands of 3435, 2926, 619 and 167 bp, corresponding to pMUTIN-*floT-eyfp* (Lane 2), respectively, are marked by black arrows. Bands of 343, 1599, 991 and 167 bp correspond to pMUTIN-*gfp+* (Lane 1). **D**, Verification of pMUTIN-*floT-eyfp* integration by PCR using primer pair 5'FW19/Outward_eyfp. PCR products were separated by 1 % (w/v) TAE agarose gel electrophoresis. A band of 1281 bp, marked by a black arrow, indicates pMUTIN-*floT-eyfp* chromosomal integration (Lane 3). No DNA amplification is seen using genomic DNA from SH1000 (Lane 4). PCR amplification of the whole *floT* gene using primer pair 5'FW19/3'FW19 results in a band of 1011 bp) (Lanes 1-2).

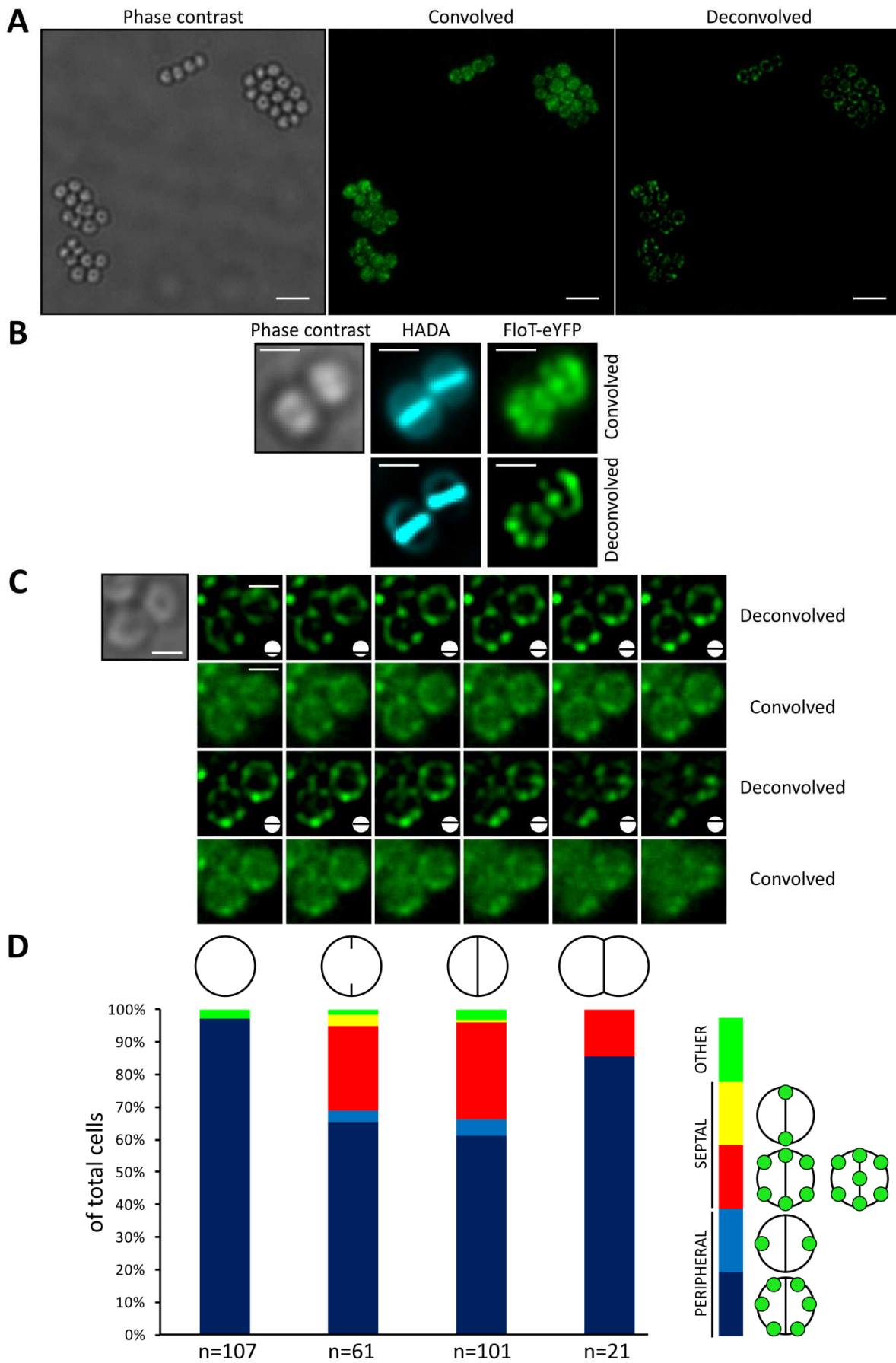


Figure 4.21 Localisation of FloT-eYFP in *S. aureus* SH1000

Phase contrast and fluorescence images (convolved and deconvolved) of *S. aureus* SH1000 *floT-eyfp*. Images were acquired using a Delta Vision microscope and SoftWoRx 3.5.0 software (Applied Precision). Acquisition of fluorescence images were taken using 1.5 sec exposure in the FITC channel. **A**, Scale bars represent 3 μm . **B**, Selected cells showing the localisation of FloT-eYFP and HADA. Scale bars represent 1 μm . **C**, Z-stack images of selected cells. Scale bars represent 1 μm . **D**, Cell counts categorized depending on FloT-eYFP localisation and cell-cycle stage indicated by HADA labelling. n indicates counted cells for each group. Red and yellow bars indicate septal and blue bars indicate peripheral peripheral FloT-eYFP localisation. The green coloured bar indicates random FloT-eYFP localisation.

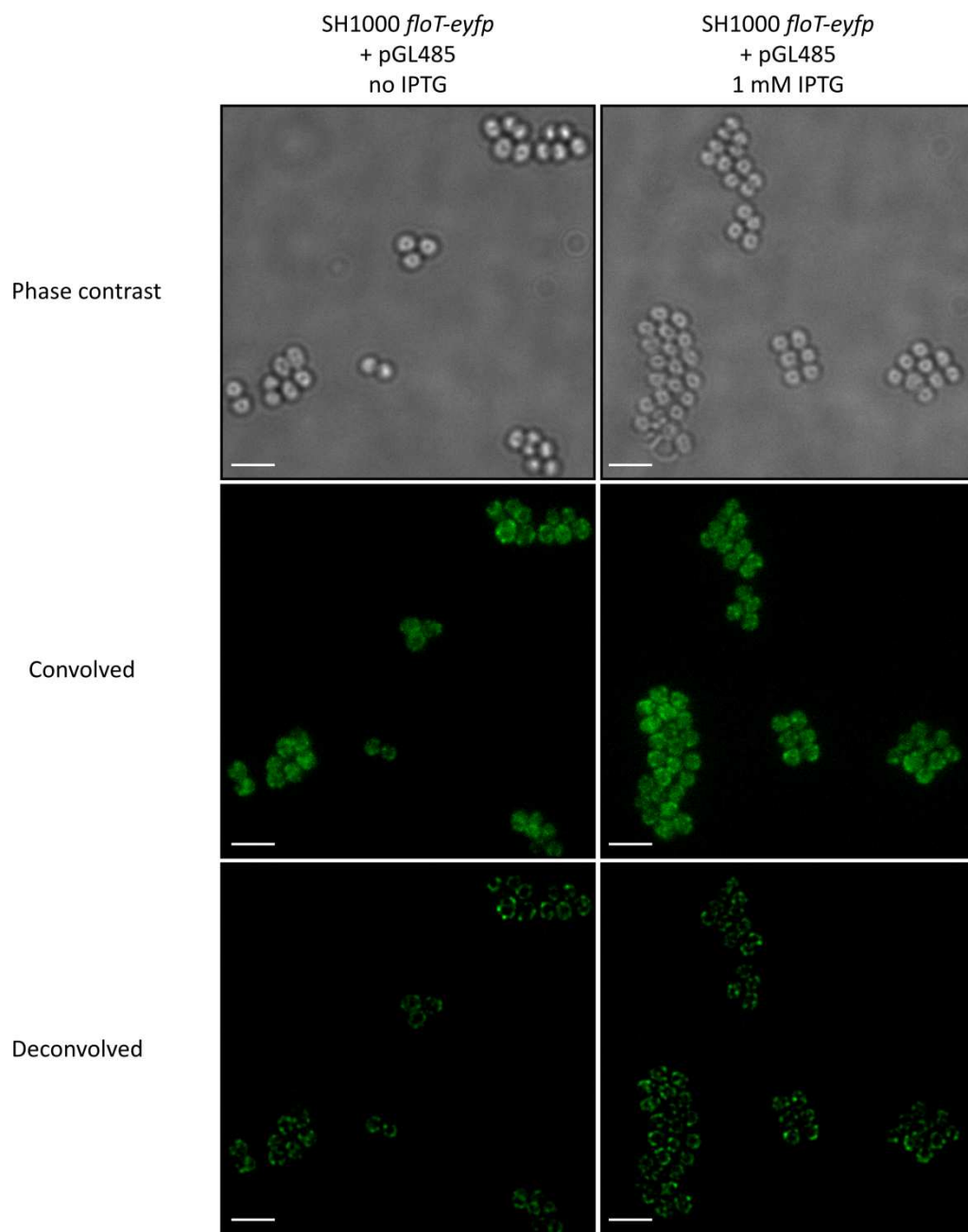


Figure 4.22 Localisation of FloT-eYFP in *S. aureus* SH1000

Phase contrast and fluorescence images (convolved and deconvolved) of *S. aureus* SH1000 *floT-eyfp* + pGL485 grown in the presence of no (left) or 1 mM IPTG (right). Images were acquired using a Delta Vision microscope and SoftWoRx 3.5.0 software (Applied Precision). Acquisition of fluorescence images were taken using 1.5 sec exposure in the FITC channel. Scale bars represent 3 μ m.

4.2.2.7 Secretion ATPase (SecY)

SecY is part of the bacterial Sec secretion machinery. It is composed of three integral membrane proteins, SecYEG, that form a channel pore driven by the peripheral cytoplasmic ATPase SecA (Wickner *et al.*, 1991, Driessen *et al.*, 2001). It has been shown previously that SecY is homogeneously distributed in *B. subtilis* (Matsumoto *et al.*, 2015) and was therefore chosen for localisation studies in *S. aureus* to compare its localisation pattern with PlsY.

4.2.2.7.1 Construction of a SecY-GFP fusion in *S. aureus*

Construction of pMUTIN-secY-gfp was carried out by Jagath Kasturiarachchi (Garcia-Lara *et al.*, 2015) by replacing *plsY* with *secY* from pMUTIN-*plsY-gfp*. *secY* was amplified from SH1000 template DNA.

4.2.2.7.2 Localisation of SecY-GFP

In order to study the localisation of SecY-GFP in *S. aureus* SH1000, an overnight culture was diluted to an OD₆₀₀=0.05 and grown at 37 °C to an OD₆₀₀≈0.5. Cells were harvested, washed with PBS followed by fixing with para-formaldehyde and analysed by fluorescence microscopy.

SecY-GFP appears to be localised homogeneously throughout the membrane (Fig. 4.23AB). 60-70 % of the cells exhibit homogeneous distribution of SecY-GFP and additionally, SecY-GFP barely localises at the cell-division site (Fig. 4.23). It is therefore the first investigated membrane protein in this study showing a non-punctate localisation pattern. This observation has to be treated cautiously though. Due to the light diffraction limit it is not possible from these images to conclude whether proteins are distributed homogeneously or in a punctate pattern of more and smaller 'dots'. Therefore it is inevitably possible that SecY is more abundant than PlsY and thus appears to be localised homogeneously. Dose-dependent experiments with PlsY-GFP expression (Fig. 4.4AB) gave the first evidence that the concentration of proteins affect their localisation which might also be the case for SecY-GFP. It has to be noted that SecY-GFP distribution is not perfectly homogeneous and some dot-like distribution can be seen. Nevertheless, its localisation is distinctly different from the other investigated membrane proteins.

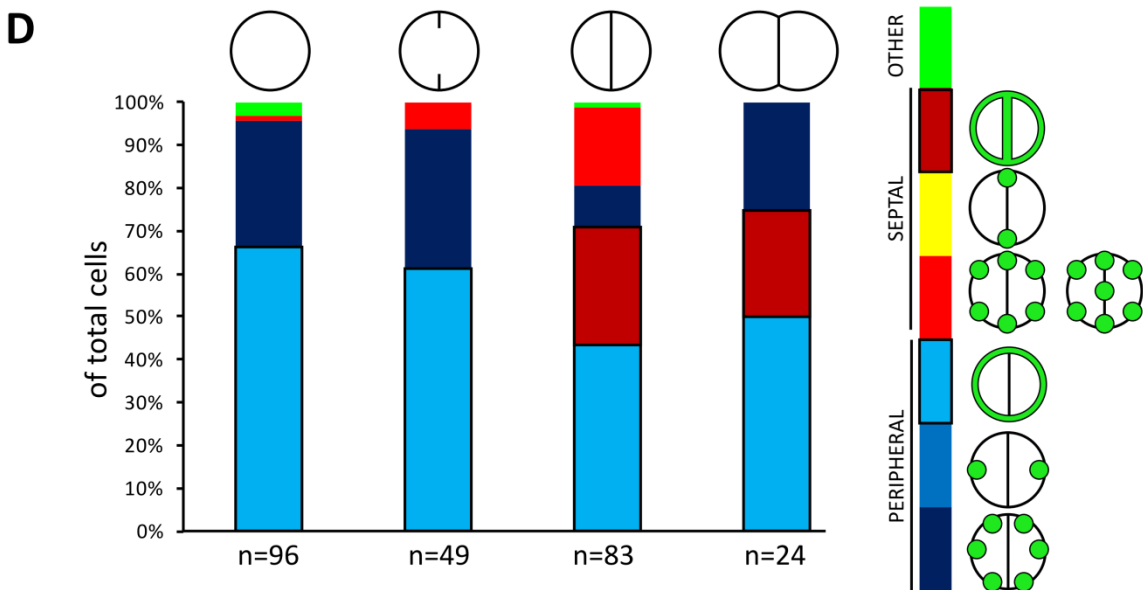
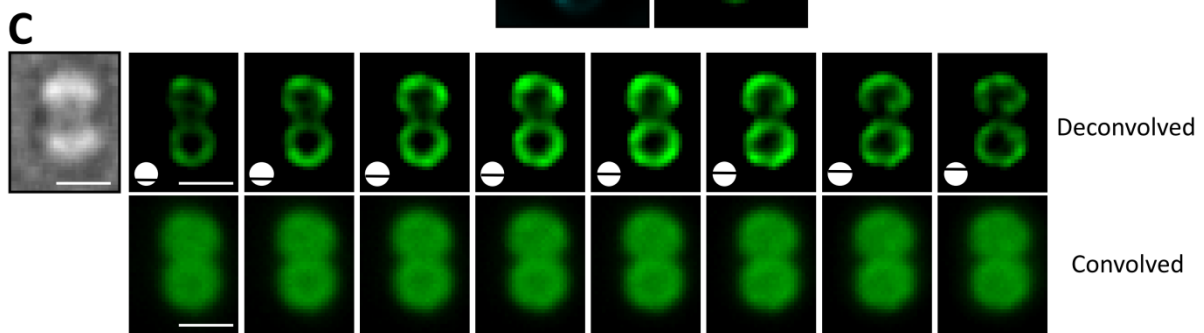
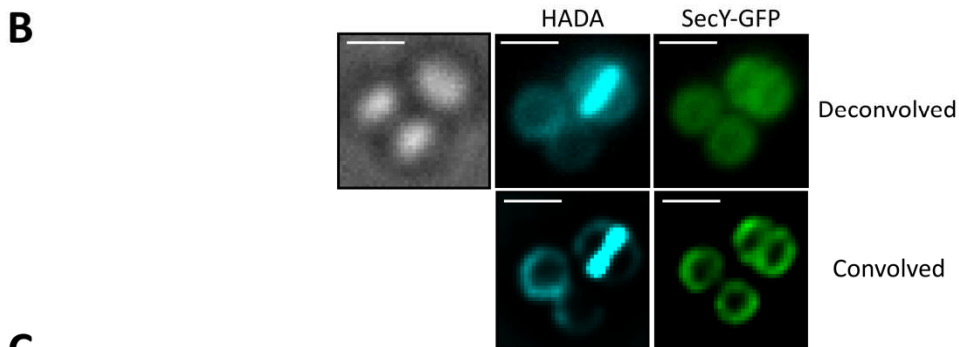
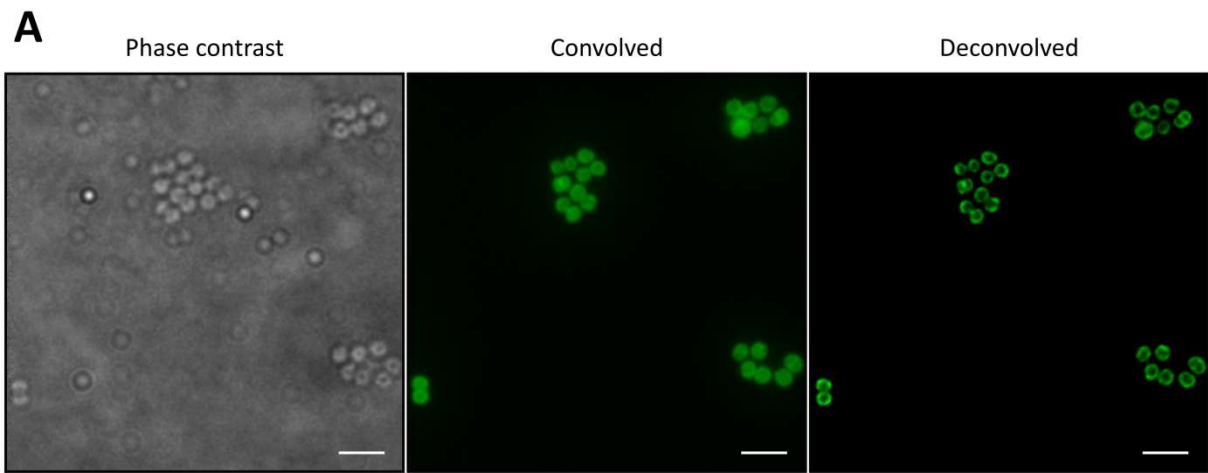


Figure 4.23 Localisation of SecY-GFP in *S. aureus* SH1000

Phase contrast and fluorescence images (convolved and deconvolved) of *S. aureus* SH1000 *secY-gfp*. Images were acquired using a Delta Vision microscope and SoftWoRx 3.5.0 software (Applied Precision). Acquisition of fluorescence images were taken using 2 sec exposure in the FITC channel. **A**, Scale bars represent 3 μm . **B**, Selected cells showing the localisation of SecY-GFP and HADA. Scale bars represent 1 μm . **C**, Z-stack images of selected cells. Scale bars represent 1 μm . **D**, Cell counts categorized depending on SecY-GFP localisation and cell-cycle stage indicated by HADA labelling. n indicates counted cells for each group. Red and yellow bars indicate septal and blue bars indicate peripheral SecY-GFP localisation. Black framed bars indicate a homogeneous distribution of SecY-GFP. The green coloured bar indicates random SecY-GFP localisation.

4.2.3 Homogeneity Distribution measurements

To calculate whether SecY-GFP is less heterogeneously distributed in the membrane compared to PlsY-GFP, a new measurement was introduced to analyse the variation of fluorescence signal within the membrane. First, the polar transformer plug-in for Fiji-ImageJ was employed to convert images to polar coordinates where the y-value represents the angle and the x-value stands for the distance from the centre of the image (<https://imagej.nih.gov/ij/plugins/polar-transformer.html>). An intensity profile of this image was then created and plotted. The intensity values were used to calculate the standard deviation as an indicator for heterogeneity. The standard deviation is both influenced by the variation of fluorescence as well as the intensity. To remove the latter effect, the coefficient of variation (CV) was calculated as follows:

$$\text{CV-factor} = \text{STDEV}/\text{Mean intensity value} \times 100$$

An example using the logo of the Sheffield United football club is given in Figure 4.24. A high CV indicates a more heterogeneous distribution of fluorescence signal, while low values indicate a more homogeneous distribution. Since cytoplasmic signals affect the CV (see the two swords and the rose in Fig. 4.24) the measurements were further optimised by removing the cytoplasm. This was performed by deleting approximately 20 % of the cell volume from the cell centre. However, this procedure was not carried out for deconvolved images since deconvolution already reduces cytoplasmic signals.

The CV measurement was performed using fluorescence images (convolved and deconvolved) of PlsY-GFP and SecY-GFP in SH1000. As a control for a homogeneous distribution of fluorescence, fluorescence images of cytoplasmic GFP in RN4220 + pWhiteWalker1 (*gfp* and *mCherry* expression) was analysed.

SH1000 *plsY-gfp* cells exhibit a CV factor of 18.2 (convolved) and 18.3 (deconvolved) while the CV-factor of SH1000 *secY-gfp* cells was found to be significantly lower at 12.2 (convolved) and 11.8 (deconvolved) ($p = 0.0130$ between convolved images and $p = 0.0014$ between deconvolved images). Thus, SecY-GFP is more homogeneously distributed in the membrane compared to PlsY-GFP. Cytoplasmic GFP was found to be distributed more homogeneously than SecY-GFP and PlsY-GFP as CV values were 8.7 (convolved) and 8.1 (deconvolved).

Moreover, deconvolution does not significantly alter the CV-factor ($p > 0.69$ for all analysed groups).

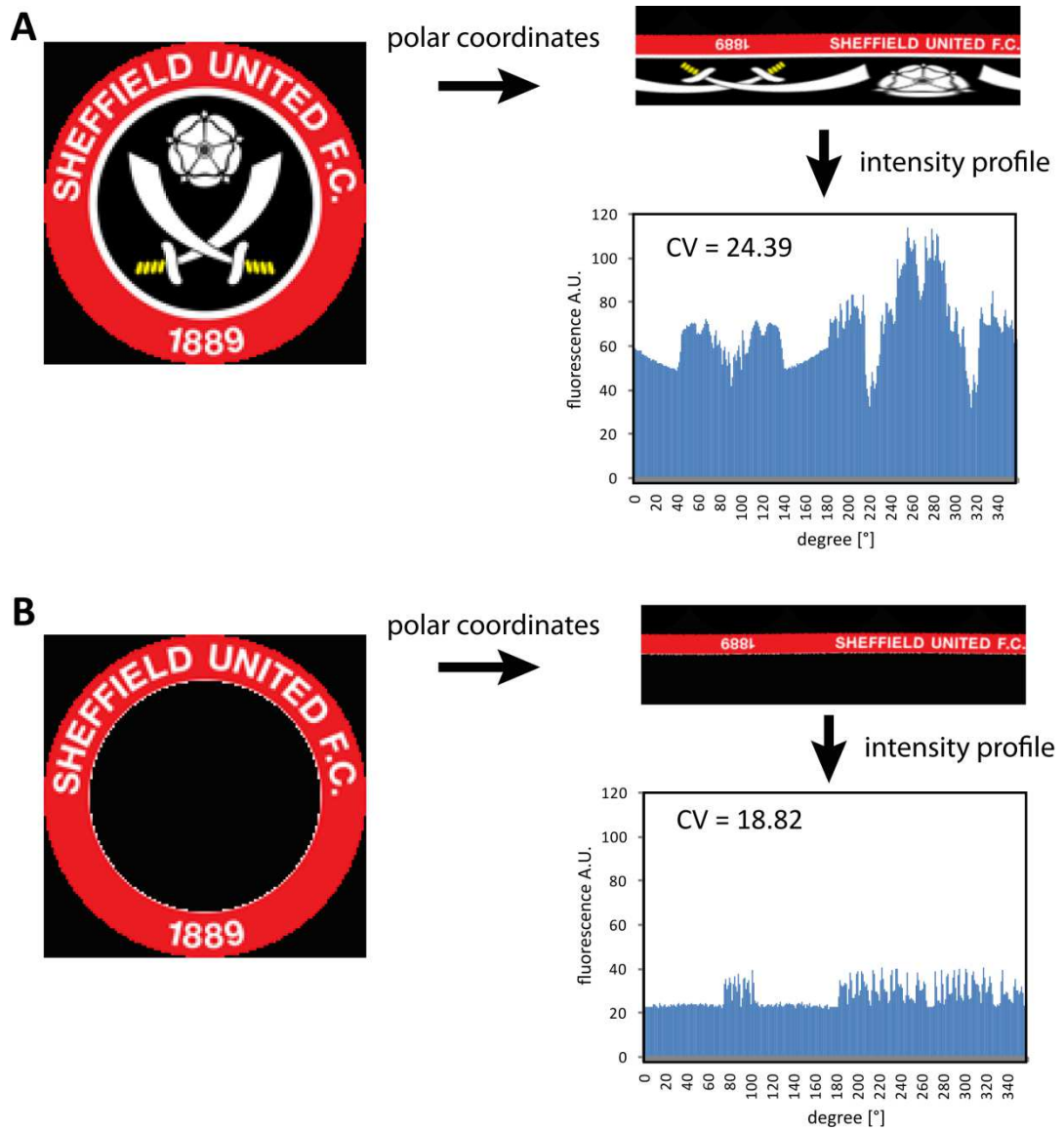


Figure 4.24 Example for the calculation of the coefficient of variation factor

The logo of Sheffield United with (A) or without (B) the inner part as a representative of the bacterial cytoplasm, was converted to polar coordinates. These were then used to plot an intensity profile and calculate the coefficient of variation (CV).

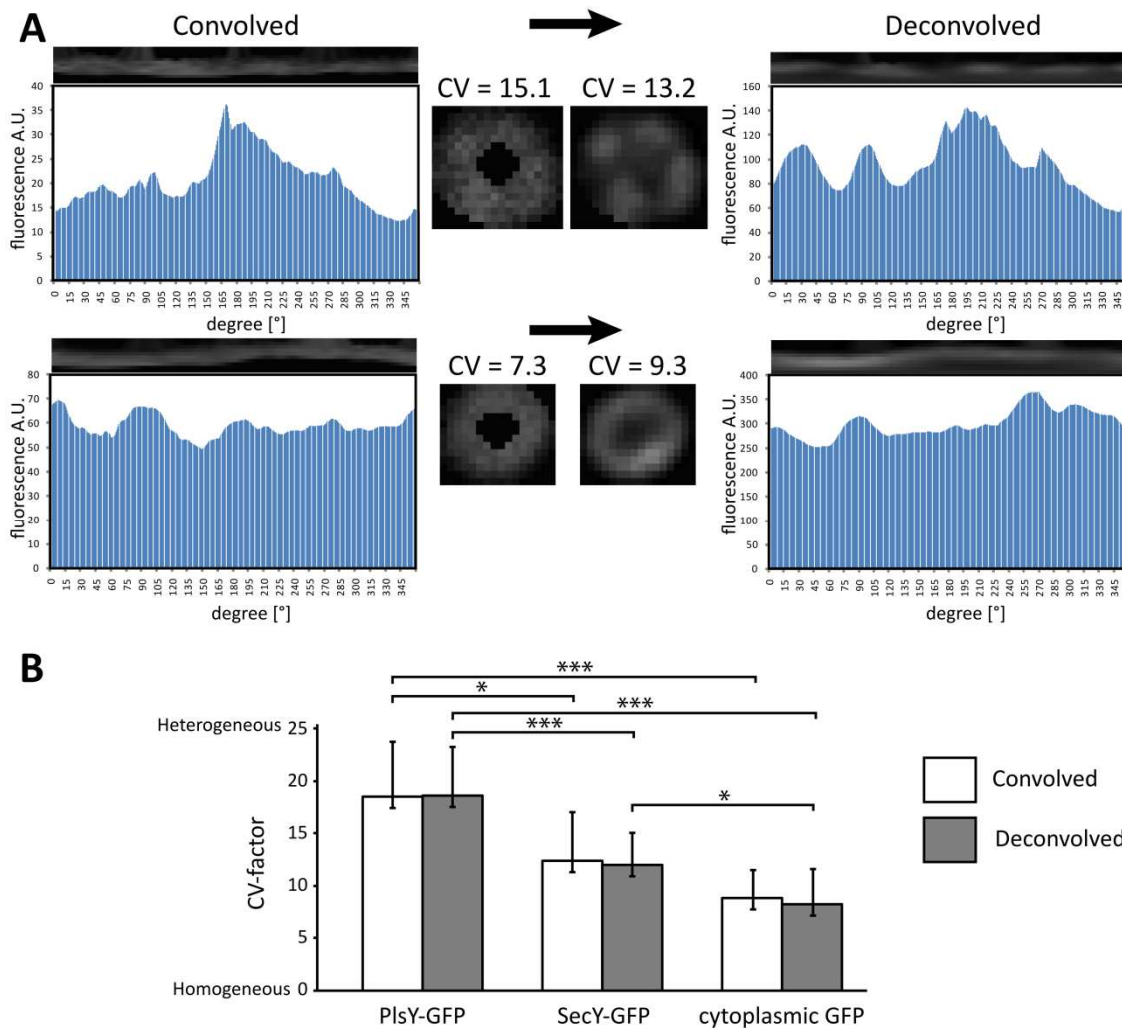


Figure 4.25 CV factor calculation for PlsY-GFP and SecY-GFP in *S. aureus*

A, Convolved and deconvolved images of SH1000 *plsY-gfp* and SH1000 *secY-gfp* were converted into polar coordinates (bars atop of plot profiles) and their intensity profile was plotted. The CV-factor indicates the heterogeneity of fluorescence signal and is calculated based on the intensity values derived from the polar coordinate image. The cytoplasm was removed by deleting approximately 20 % of the cell volume starting from the cell centre. **B**, The CV-factor for 10 cells using convolved and deconvolved images of SH1000 *plsY-gfp* and SH1000 *secY-gfp* were calculated. Additionally, a control using cytoplasmic GFP from strain RN4220 + pWhiteWalker 1 (*gfp* and *mCherry* expression) was employed. P-values were calculated using a two-tailed two-sample equal variance ttest. No significance was found between SecY-GFP and cytoplasmic GFP. Asterisks indicate the following p-values: *: $p < 0.05$; **: $0.01 < p < 0.05$; ***: $p < 0.01$.

4.2.4 Colocalisation studies of membrane proteins

The previous experiments showed that membrane proteins have a tendency to be organised in a punctate non-uniform pattern. Consequently, the next step is to study the localisation of several membrane proteins in the same cell. Evidently, a second fluorophore is required to carry out colocalisation studies.

GFP is an excellent fluorophore in terms of folding or brightness but it cannot be used in combination with eYFP due to their overlap of excitation/emission spectra (Fig. 4.26). This puts the blue and red light spectrum into focus. eCFP and mCherry are commonly used in localisation studies. However, eCFP exhibits a clear deficiency in its properties. The Excitation/Emission of CFP lies within the auto fluorescence range of bacterial cells and possesses a low brightness which all together makes it a bad fluorophore especially for the study of low abundance proteins. (http://nic.ucsf.edu/dokuwiki/doku.php?id=fluorescent_proteins). Additionally, both its excitation and emission spectra overlap with that of GFP. At the other end of the range, 'red' proteins suffer from long maturation times and low brightness levels making it difficult to choose an appropriate protein. mCherry and mRFPmars1 have both been used before for localisation studies in *S. aureus* (Fischer *et al.*, 2004, Brzoska & Firth, 2013), and offer non-overlapping spectra with GFP. Despite their low brightness properties, mCherry and mRFPmars1 were chosen for co-localisation studies in combination with GFP simply because of a lack of good alternatives.

A similar approach than the previously shown single-copy tagged genes was used in order to construct mCherry or mRFPmars1 tagged proteins. pAISH1 is a pMUTIN derivative that contains a tetracycline resistance marker instead of a erythromycin resistance marker (Aish, 2003) making the application of both plasmids in concert possible. Unfortunately, single-copy expression of PlsY-mCherry, PgsA-mRFPmars1, CdsA-mCherry and CdsA-mRFPmars1, did not yield sufficient fluorescence signals (not shown)(construction of plasmids can be found in the Appendix: Section 9.1.1 - 9.1.4). Most cells either did not express the fusions, showed severe growth defects or only a small subset of cells express the fusions (not shown). This could be explained by slow folding of mCherry and mRFPmars1 or low fluorescence signal.

Table 4.2 Fluorescence properties of selected fluorescent proteins

Protein	λ_{ex}	λ_{em}	EC	QY	Brightness	Aggregation	Relative brightness to eGFP [%]	Notes
eCFP	433	475	32500	0.4	13.0	Monomer	39	
superfolder GFP	485	510	83300	0.65	54.1	Monomer	160	Fast folding, highly stable
mNeonGreen	506	517	116000	0.80	92.8	Monomer	276	
eGFP	488	507	56000	0.6	33.6	Monomer	100	
eYFP	513	527	83400	0.61	50.9	Monomer	151	
Citrine	516	529	77000	0.76	58.5	Monomer	174	
mKO	548	559	51600	0.6	31.0	Monomer	92	
mOrange	548	562	71000	0.69	49.0	Monomer	146	~2.5 hr maturation time
mCherry	587	610	72000	0.22	15.8	Monomer	47	~15 min maturation time
mRFP	584	607	50,000	0.25		Monomer	37	~15 min maturation time
tdTomato	554	581	138000	0.69	95.2	Monomer	283	~1 hr maturation time

λ_{ex} : Excitation wavelength, λ_{em} : Emission wavelength, EC: The extinction coefficient determines the amount of absorbed light. QY: The quantum yield describes the efficiency of molecules to convert absorbed photons into emitted photons. This table is adapted from the following websites: <http://nic.ucsf.edu/FPvisualization/> and <http://www.microscopyu.com/articles/livecellimaging/fpintro.html>

4.2.4.1 Colocalisation studies using overexpression plasmids

In order to measure the protein-interaction between various membrane proteins and PlsY, overexpression plasmids expressing *plsY-gfp* together with a membrane protein of interest translationally fused to *mCherry* were constructed. Plasmid construction, bioinformatic analyses and function of selected membrane proteins are described in Section 5.2.3.

Protein-interaction plasmids were also used to investigate the localisation of PlsY together with other membrane proteins either related to phospholipid synthesis such as CdsA or PgsA or proteins of other metabolic processes that are expected not to be colocalised with PlsY (Tab. 4.3). These include the formerly described respiratory protein CydB, the secretion ATPase SecY, the phenyl-alanine transporter PheP, the mechanosensitive channel MscL and the lipoprotein signal peptidase LspA (Tab. 4.3). Furthermore, localisation of PlsY was compared with that of MreD which was reported to interact with PlsY in a bacterial-two-hybrid assay (Garcia-Lara *et al.*, 2015).

These plasmids were used to overcome the issues encountered for single-copy expression of mCherry-membrane protein fusions and analyse the localisation of PlsY-GFP compared to other membrane proteins of interest.

RN4220 strains containing the plasmids pWhiteWalker3 (*mreD*), 4 (*cdsA*), 7 (*cydB*), 8 (*pgsA*), 11 (*pheP*), 12 (*secY*), 13 (*mscL*) or 17 (*lspA*) were precultured from an overnight culture to an OD₆₀₀ of 0.05 and grown for 2 h at 37°C supplemented with 50 µM IPTG to an OD₆₀₀≈0.7-0.9. 1 ml samples were taken, fixed and prepared for fluorescence microscopy.

All fusions, both *plsY-gfp* and the membrane proteins fused to *mCherry*, were expressed at high levels since short exposure times (0.7 sec (FITC), 1 sec (RFP)) compared to 2.5 sec for single-copy *plsY-gfp* expression were sufficient for their visualisation. Although with less clarity, punctate patterns can still be seen for PlsY-GFP and the other fusions. Fig. 4.27 shows their localisation and arrows indicate whether proteins appear to be colocalised (white arrows) or non-colocalised (red arrows). This analysis reveals several interesting observations.

First of all, using PlsY-GFP as an indicator for cells that are undergoing cell-division (Fig. 4.28), MreD and CdsA almost always localise at the septum of cells in early and late cell-division stage. PgsA and LspA are septally colocalised during late cell-division. Membrane proteins CydB, PheP and more conspicuously SecY and MscL, do not exhibit septal colocalisation with PlsY-GFP in the majority of cells (Fig. 4.28).

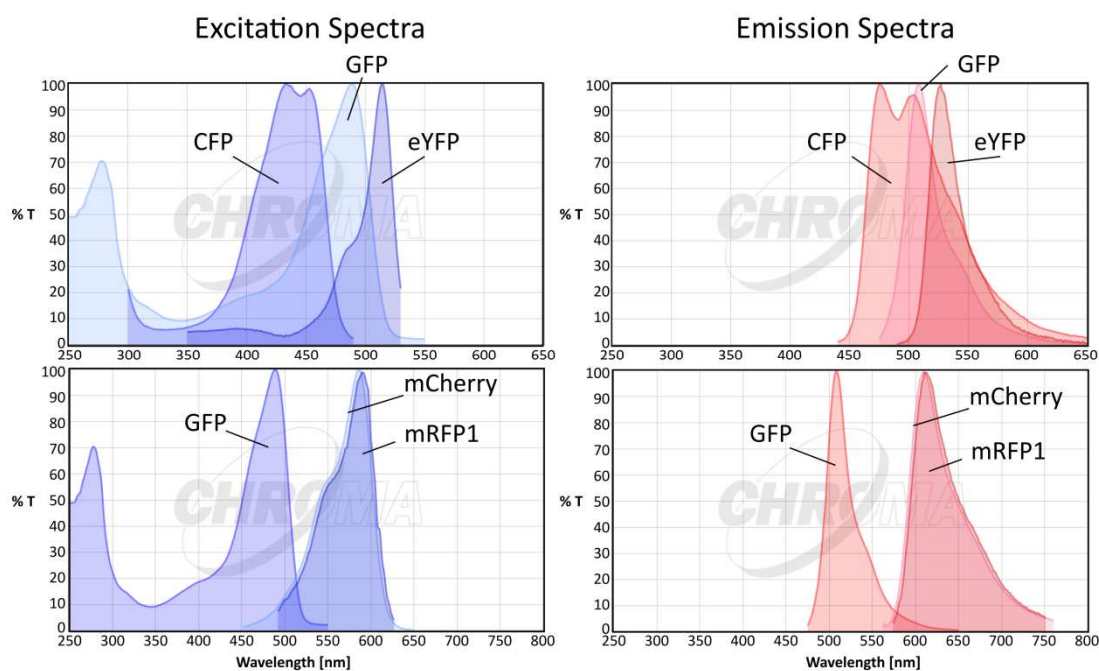
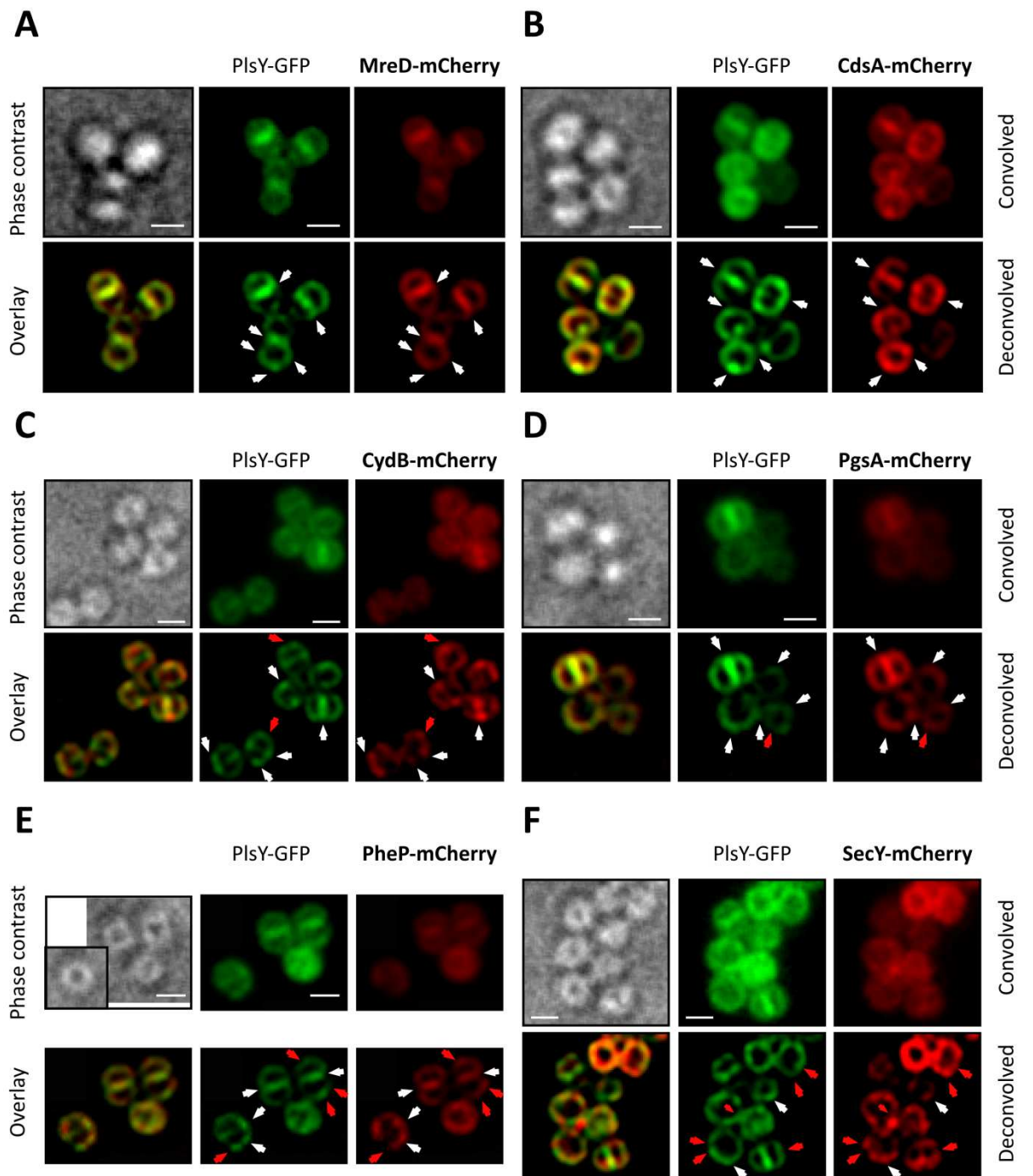


Figure 4.26 Excitation and emission spectra of selected fluorescent proteins compared to GFP

Excitation and emission spectra of CFP and eYFP compared to GFP (upper panel) and mCherry and mRFP1 compared to GFP (lower panel). %T stands for the transmission efficiency indicating the proportion of light exciting the fluorophore and light emission.

Table 4.3 Selected proteins used for colocalisation studies with PlsY-GFP

Protein name	Function
CdsA	CDP-diacylglycerol synthase, catalyses the conversion of phosphatidic acid to CDP-diacylglycerol (Garcia-Lara <i>et al.</i> , 2015)
PgsA	Phosphatidylglycerol synthase (Garcia-Lara <i>et al.</i> , 2015)
MreD	Cytoskeletal protein, potentially involved in the localisation of phospholipid synthesis enzymes (Garcia-Lara <i>et al.</i> , 2015)
CydB	Respiration (4.2.2.5 Cytochrome B subunit (CydB))
SecY	ATPase, drives secretion of the Sec system (4.2.2.7 Secretion ATPase (SecY))
PheP	Phenyl-alanine transporter (Horsburgh <i>et al.</i> , 2004)
MscL	Large-conductance mechanosensitive channel, pressure sensor (Haswell <i>et al.</i> , 2011)
LspA	Lipoprotein signal peptidase, lipoprotein processing (Tjalsma <i>et al.</i> , 1999)



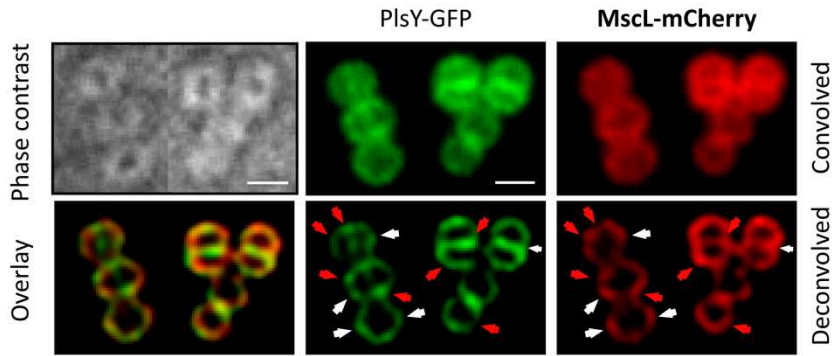
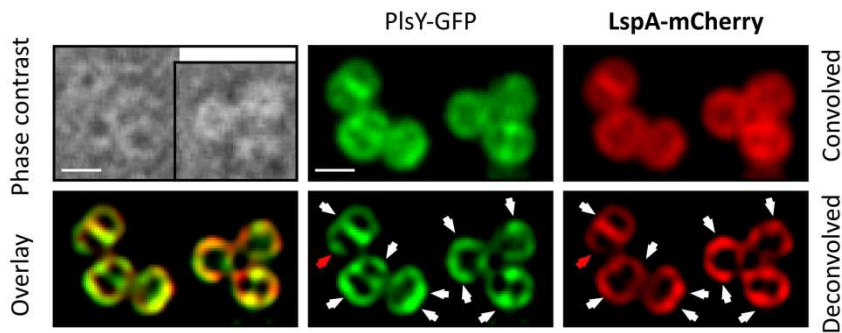
G**H**

Figure 4.27 Localisation of PlsY-GFP and various membrane proteins fused to mCherry in *S. aureus* SH1000

Phase contrast and fluorescence images (convolved and deconvolved) of *S. aureus* RN4220 *plsY-gfp* and various proteins fused to mCherry. Images were acquired using a Delta Vision microscope and SoftWoRx 3.5.0 software (Applied Precision). Acquisition of fluorescence images were taken using 0.7 sec exposure in the FITC channel and 1 sec exposure in the RFP channel. **A-H**, White arrows indicate matching fluorescence signals in FITC and RFP channel. Red arrows indicate mismatching punctate fluorescence signals. Scale bars represent 1 μm .

The colocalisation of punctate fluorescence signals is more common for PlsY-GFP with MreD, CdsA, PgsA and LspA (see white and red arrows in Fig. 4.27ABDH) and a mixture of matching and non-matching punctate signals is seen for CydB, PheP, SecY and MscL (Fig. 4.27CEFG). To quantify this observation a pixel-by-pixel analysis was applied using Fiji ImageJ.

This analysis was carried out for strains expressing *plsY-gfp* together with MreD (pWW3), CdsA (pWW4), CydB (pWW7), PgsA (pWW8), SecY (pWW12) and MscL (pWW13) fused to mCherry. A strain only expressing *plsY-gfp* (pWW10) was used as a control. These proteins were selected as representatives of proteins that appear to be colocalised, partially colocalised or not-colocalised with PlsY-GFP according to Fig. 4.27.

The overlap coefficient according to Manders was chosen to calculate colocalisation. Manders indicates an overlap of signals of two channels (Zinchuk *et al.*, 2007)(Manders *et al.*, 1993). It is composed of two values named M1 and M2. M1 describes whether a signal in channel 1 for example the FITC channel, is correlated with a signal in channel 2 for example the RFP channel. In other words, if a pixel is green and red, M1 has a value of 1. If a pixel is green but not red, the value of M1 is 0. Manders M2 describes the opposite comparing a signal in channel 2 with channel 1.

Samples were prepared and imaged the same way as described before and three image fields with comparable amounts of cells per strain were taken. Images were deconvolved and both convolved and deconvolved images were analysed to identify whether deconvolution alters results of colocalisation. Channels were separated and the background of fluorescence images was subtracted (Rolling Ball radius: 50 pixels). The threshold of the FITC channel image was auto adjusted and a selection of pixels within the threshold was created. Colocalisation was analysed using the Coloc2 Plugin in Fiji ImageJ using the threshold selection for both images. This procedure was repeated for all three replicates.

Colocalisation analysis according to Manders shows that a pixel-by-pixel analysis of two fluorescence images can be applied to measure colocalisation of two membrane proteins, however with one drawback that will be explained later. The negative control of sole expression of *plsY-gfp* without a mCherry fusion results in a low M1 value meaning that a 'green' signal is not correlated with a 'red' signal. Comparing M1 values of convolved with deconvolved images does not alter results (Fig. 4.29).

Regarding the colocalisation of PlsY with the membrane proteins of interest, colocalisation of PlsY with MreD, CdsA, CydB and PgsA can be seen. SecY and MscL however also show colocalisation to a certain degree but less than the other membrane proteins. This might be explained by a general problem with this analysis. It has to be taken into account that the comparison of two membrane proteins will always result in high false-positive values because both proteins are localised in the membrane and the light-diffraction limits to resolve most structures. Thus, this kind of colocalisation measurement is not very sensitive.

Nevertheless, the previous observation that PlsY is colocalised with MreD, CdsA and PgsA and non-colocalisation of PlsY with SecY and MscL (Fig. 4.27A-H) can be confirmed. According to Fig. 4.27C, CydB is partially colocalised with PlsY but using Manders overlay coefficient results in a high M1 value. Hence, colocalisation of PlsY with CydB remains unclear.

4.2.4.2 Localisation studies of SNAP-tagged membrane proteins

However, the amount of membrane proteins in the cell clearly affects their localisation as shown previously by the dose-dependent *plsY-gfp* expression meaning the shown distribution patterns are not necessarily conclusive. First, proteins are likely to be overexpressed which directly affects their localisation and second, these localisation studies were performed with non-native levels. The expression system of pWhiteWalker theoretically results in equal amounts of both fusions, which does not represent a native cell.

An alternative approach is required to verify and further analyse the localisation of these proteins. SNAP tags are self-labelling enzymes that can be translationally fused to a gene of interest and fluorescently labelled with suitable substrates (Keppler *et al.*, 2004a, Keppler *et al.*, 2004b). To overcome the potential folding issues of mCherry and mRFPmars1, single copy expression of C-terminal fusions of CydB, PlsY and PgsA with SNAP were constructed. The C-terminus of all proteins is predicted to be at the inside of the cell. Therefore the SNAP tag substrate has to be capable of diffusing through the membrane. Additionally, its excitation and emission wavelengths should be compatible with GFP or eYFP. TMR-Star (SNAP-Cell® TMR-Star) meets the criteria. It diffuses through the membrane of *S. aureus* (Dr.C.Walther, personal communication) and its ex/em wavelengths are suitable for colocalisation studies with GFP and eYFP (Fig. 4.30).

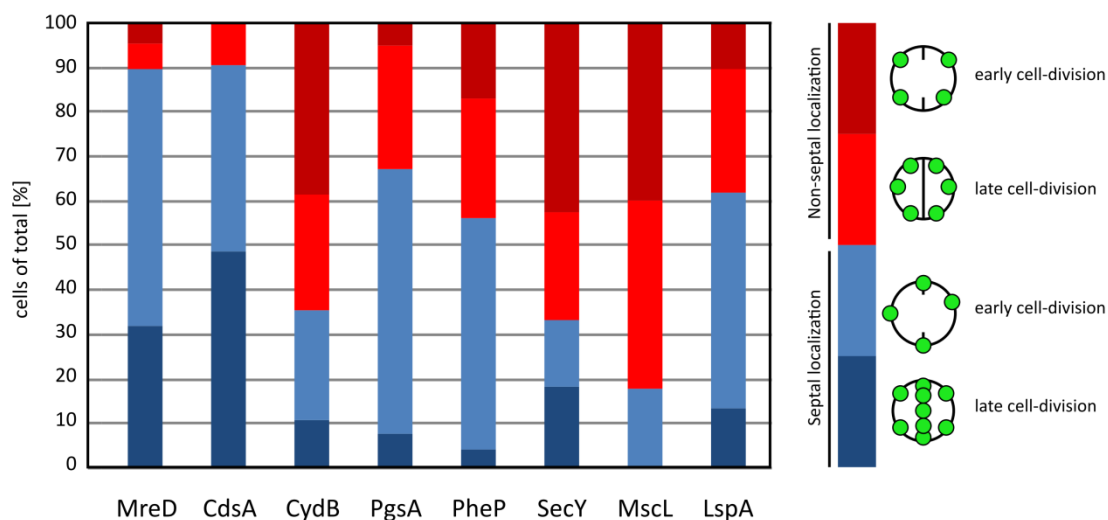


Figure 4.28 Septal colocalisation of various membrane proteins fused to mCherry with PlsY-GFP

Fluorescence signals in the RFP channel were counted and categorized. Each count includes at least 60 cells undergoing cell-division taking the localisation of PlsY-GFP as an indicator for cell-division. At least 50 cells undergoing cell-division were counted and categorised for each strain.

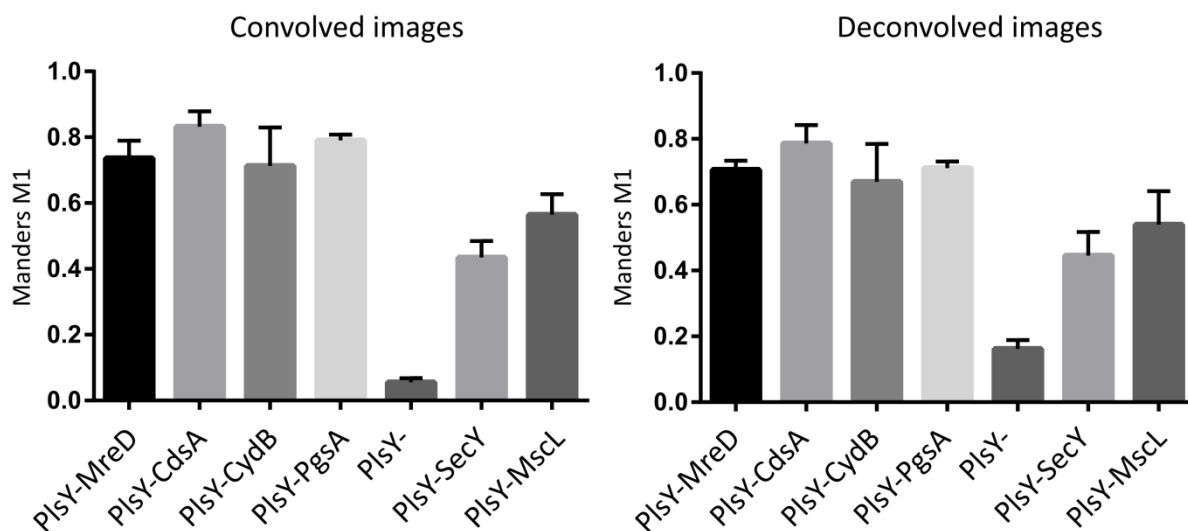


Figure 4.29 Overlap coefficient according to Manders using convolved and deconvolved images

Three images of strains expressing PlsY-GFP and a membrane protein of interest fused to mCherry were analysed using Fiji ImageJ Coloc2 Plugin. Images were acquired using a Delta Vision microscope and SoftWoRx 3.5.0 software (Applied Precision). Acquisition of fluorescence images were taken using 0.7 sec exposure in the FITC channel and 1 sec exposure in the RFP channel. Analysis was carried out in triplicate on three image fields.

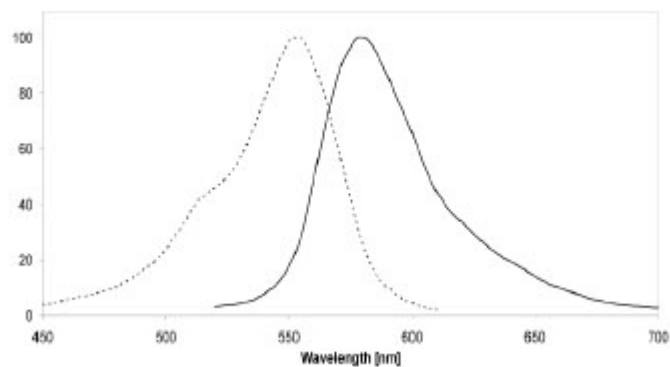


Figure 4.30 Excitation and emission spectra of TMRStar

Excitation maximum: 554 nm Emission maximum 580 nm. Image was taken from NEB (<https://www.neb.com/products/s9105-snap-cell-tmr-star>).

4.2.4.2.1 Construction of a PlsY-SNAP fusion in *S. aureus*

Single-copy expression of *plsY-SNAP* regulated by its native promoter was achieved using pAISH1 (Aish, 2003). Construction of pAISH-*plsY-SNAP* was facilitated by amplification of *plsY* (5'FW85/3'FW85) from SH1000 genomic DNA and amplification of the gene encoding for SNAP (5'FW86/3'FW86) from plasmid pCQ11-*ftsZ-SNAP*. Both fragments were then cloned into the *HindIII/SwaI* site of pAISH1 using Gibson Assembly (Fig. 4.31A) and transformed into *E. coli* NEB5 α . Recombinant plasmids were tested by restriction digest with EcoRV and PstI. (Fig. 4.31C) resulting in approximately 2000, 1400 and 1100 bp fragments and validated by DNA sequencing (GATC Biotech AG, Konstanz, Germany). The resulting plasmid, pAISH-*plsY-SNAP*, was electroporated into RN4220 and from there transduced into SH1000. Genomic integration at the *plsY* locus was confirmed by PCR amplification of an approximately 800 bp fragment using one primer that binds in the genome upstream of *plsY* and one primer within the *SNAP* gene (Inward_*plsY*/Outward_*SNAP*) (Fig. 4.31D).

4.2.4.2.2 Localisation of PlsY-SNAP (TMR-Star)

SH1000 *plsY-SNAP* was precultured from an over-night culture to an OD₆₀₀=0.05 and grown to exponential phase of OD₆₀₀≈0.6 at 37°C and 250 rpm without antibiotics. 1 ml samples were harvested by centrifugation and washed with PBS. The pellet was resuspended in 1 ml PBS and 600 nM TMR-Star (SNAP-Cell® TMR-Star) was added. The tube was covered in foil and incubated at 37 °C for 10 min on a rotary wheel. Subsequently, cells were recovered by centrifugation, washed with PBS and the pellet was resuspended in 1 ml BHI. The tube was covered again in foil and incubated at 37 °C for 15 min on a rotary wheel. Cells were harvested, fixed with para-formaldehyde and analysed by fluorescence microscopy.

The localisation of PlsY-SNAP was analysed by addition of TMR-Star, a SNAP substrate fluorescent in the RFP channel. The fluorescence was brighter than the GFP tagged PlsY since an exposure time of 1.5 sec instead of 2.5 sec was enough to visualise the fusion. The SNAP tag PlsY fusion localises in a punctate pattern throughout the membrane and at the cell septum (Fig. 4.32AB) which is in accordance with the localisation seen for the PlsY-GFP and PlsY-eYFP fusions.

4.2.4.3.1 Construction of a CydB-SNAP fusion in *S. aureus*

Construction of pAISH-*cydB-SNAP* was facilitated by amplification of *cydB* (5'FW89/3'FW89) from SH1000 genomic DNA and amplification of the gene encoding for SNAP (5'FW90/3'FW86) from plasmid pCQ11-*ftsZ-SNAP*. Both fragments were

then cloned into the *HindIII/SwaI* site of pAISH1 using Gibson Assembly (Fig. 4.33A) and transformed into *E. coli* NEB5 α . Recombinant plasmids were tested by restriction digest with EcoRV resulting in approximately 4500, 2500, 1000 and 400 bp fragments, (Fig. 4.33C) and validated by DNA sequencing (GATC Biotech AG, Konstanz, Germany). The resulting plasmid, pAISH-*cydB-SNAP*, was electroporated into RN4220 and from there transduced into SH1000. Genomic integration at the *cydB* locus was confirmed by PCR amplification of an approximately 1169 bp fragment using one primer that binds in the genome upstream of *cydB* and one primer within the *SNAP* gene (5'FW21/Outward_SNAP) (Fig. 4.33D).

4.2.4.3.2 Localisation of CydB-SNAP (TMR-Star)

Localisation of CydB-SNAP in SH1000 was investigated as shown for PlsY-SNAP (Section 4.2.4.2.2). Briefly, an overnight culture was diluted and grown to exponential phase. Samples were harvested and labelled using TMRStar (SNAP-Cell® TMR-Star). Subsequently, cells were fixed and analysed by fluorescence microscopy (Fig. 4.34).

CydB-SNAP (TMR-Star) localises in the same way as CydB-eYFP showing that its heterogeneous localisation pattern is not an artefact of the eYFP-tag (Fig. 4.18). Some of the cells show septal localisation of CydB-SNAP which was also seen for earlier localisation studies using a mCherry or eYFP fusions.

4.2.4.4.1 Construction of a PgsA-SNAP fusion in *S. aureus*

Construction of pAISH-*cydB-SNAP* was facilitated by amplification of *pgsA* (5'FW87/3'FW87) from SH1000 genomic DNA and amplification of the gene encoding for SNAP (5'FW88/3'FW86) from plasmid pCQ11-*ftsZ-SNAP*. Both fragments were then cloned into the *HindIII/SwaI* site of pAISH using Gibson Assembly (Fig. 4.35) and transformed into *E. coli* NEB5 α . Recombinant plasmids were tested by restriction digest with EcoRV (Fig. 4.35B) and validated by DNA sequencing (GATC Biotech AG, Konstanz, Germany). The resulting plasmid, pAISH-*pgsA-SNAP*, was electroporated into RN4220 and from there transduced into SH1000. Genomic integration at the *pgsA* locus was confirmed by PCR amplification of an approximately 1169 bp fragment using one primer that binds in the genomic part upstream of *pgsA* and one primer within the *SNAP* gene (5'FW21/Outward_SNAP) (Fig. 4.35D).

4.2.4.4.2 Localisation of PgsA-SNAP (TMR-Star)

Localisation of PgsA-SNAP in SH1000 was investigated as shown for PlsY-SNAP (Section 4.2.4.2.2). Briefly, an overnight culture was diluted and grown to exponential

phase. Samples were labelled using TMRStar (SNAP-Cell® TMR-Star), fixed using para-formaldehyde and analysed by fluorescence microscopy.

The microscopic analysis demonstrates that PgsA-SNAP is found to be localised similar as PgsA-eYFP in heterogeneous punctate distribution pattern and is localised at the septum during cell-division (Fig. 4.36).

4.2.4.5 Colocalisation of SecY-GFP and PlsY-SNAP (TMRStar)

4.2.4.5.1 Construction of a double tagged SecY-GFP and PlsY-SNAP strain

In order to construct a double-tagged strain expressing *secY-gfp* and *plsY-SNAP*, phage lysate of RN4200 *plsY-SNAP* was transduced to SH1000 *secY-gfp*. Integration of *plsY-SNAP* at the *plsY* locus was confirmed by PCR using genomic DNA as a template and primer pair Inward_plsY/Outward_SNAP. Amplification of an approximately 800 bp fragment indicated integration of *plsY-SNAP* (Fig. 4.37C). Integration of *secY-gfp* was also confirmed by PCR amplification of an approximately 1400 bp fragment using a primer binding at the beginning of *secY* and one primer binding within *gfp* (5'FW75/Outward_gfp) (Fig. 4.37D).

4.2.4.5.1 Colocalisation of SecY-GFP and PlsY-SNAP (TMRStar)

Localisation of SecY-GFP and PlsY-SNAP in SH1000 was investigated as shown for PlsY-SNAP (Section 4.2.4.2.2). Briefly, an overnight culture was diluted and grown to exponential phase. Samples were washed with PBS and subsequently the PlsY-SNAP fusion was labelled using 600 nM TMRStar (SNAP-Cell® TMR-Star). The tube was covered in foil and incubated at 37 °C for 10 min on a rotary wheel. Labelled samples were washed in PBS and incubated in BHI for 15 min followed by an additional washing step with PBS before being fixed and analysed by fluorescence microscopy (Fig. 4.38).

PlsY-SNAP and SecY-GFP are not colocalised. PlsY-SNAP localisation was unchanged in a double tagged strain and SecY-GFP appears to be localised homogeneously (Fig. 4.23). As shown before, PlsY localises to the septum early during cell-division and remains there until cells are divided. SecY however, does only go to the septum during late-cell division as the full septum is formed as indicated by the PlsY localisation showing that both proteins are localised by different mechanisms.

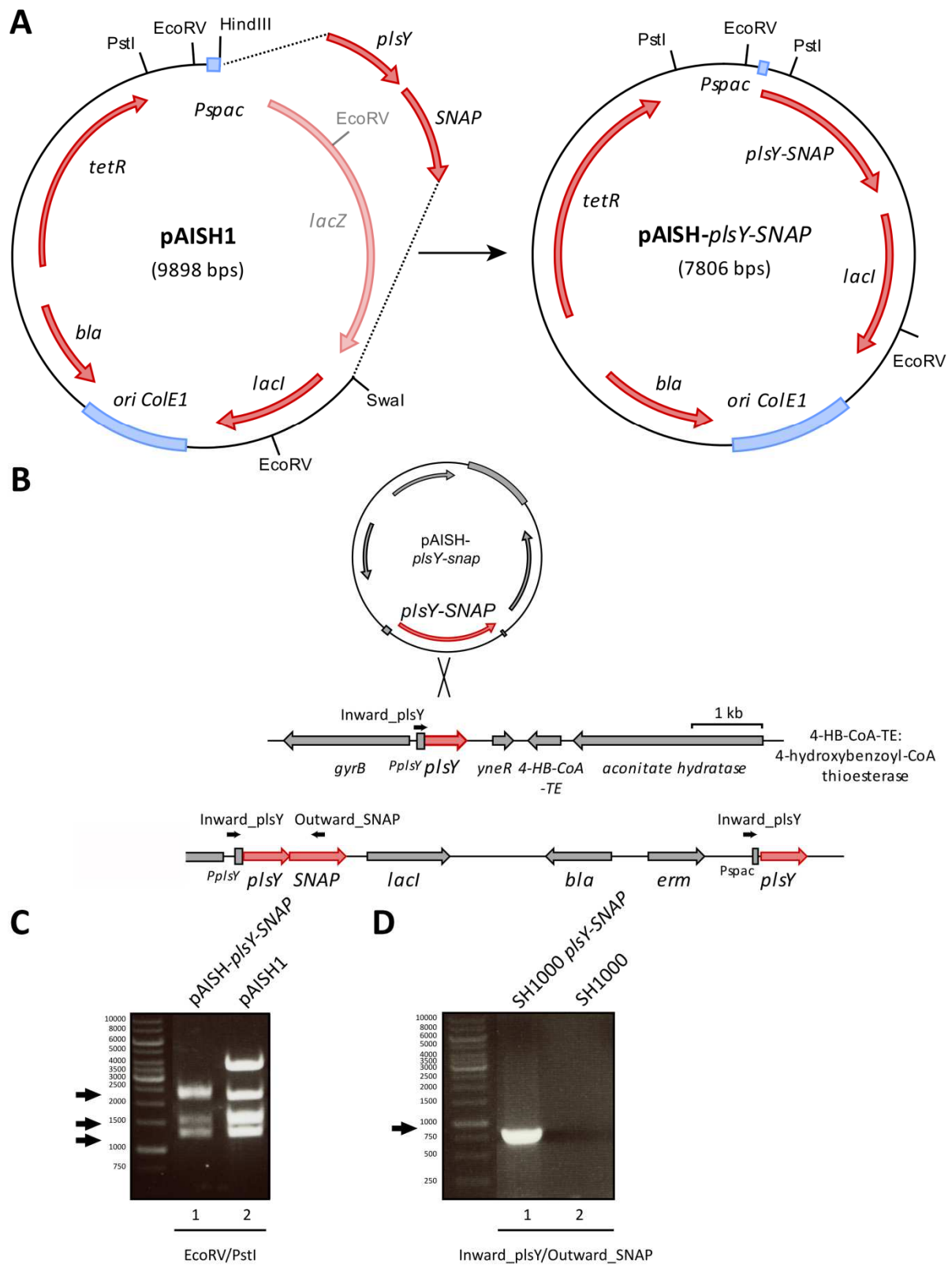


Figure 4.31 Construction of a chromosomal *plsY-SNAP* fusion in *S. aureus* SH1000

A, Diagram illustrating the construction of pAISH-*plsY*-SNAP. **B**, Schematic overview of the native genomic region of *plsY* and post integration of pAISH-*plsY*-SNAP. Black arrows indicate primer binding sites. **C**, pAISH-*plsY*-SNAP (Lane 1) and pAISH1 (Lane 2) were digested with EcoRI and PstI and separated by 1% (w/v) TAE agarose gel electrophoresis. Bands of approximately 2000, 1400 and 1100 bp, corresponding to pAISH-*plsY*-SNAP (Lane 1), respectively, are marked by black arrows. Bands of approximately 5000, 2000, 1400 and 1100 bp correspond to pAISH1 (Lane 2). **D**, Verification of pAISH-*plsY*-SNAP integration by PCR using primer pair Inward_*plsY*/Outward_SNAP. PCR products were separated by 1% (w/v) TAE agarose gel electrophoresis. A band of 800 bp, marked by a black arrow, indicates chromosomal integration of pAISH-*plsY*-SNAP (Lane 1). No DNA amplification can be seen using SH1000 genomic DNA as a template (Lane 2).

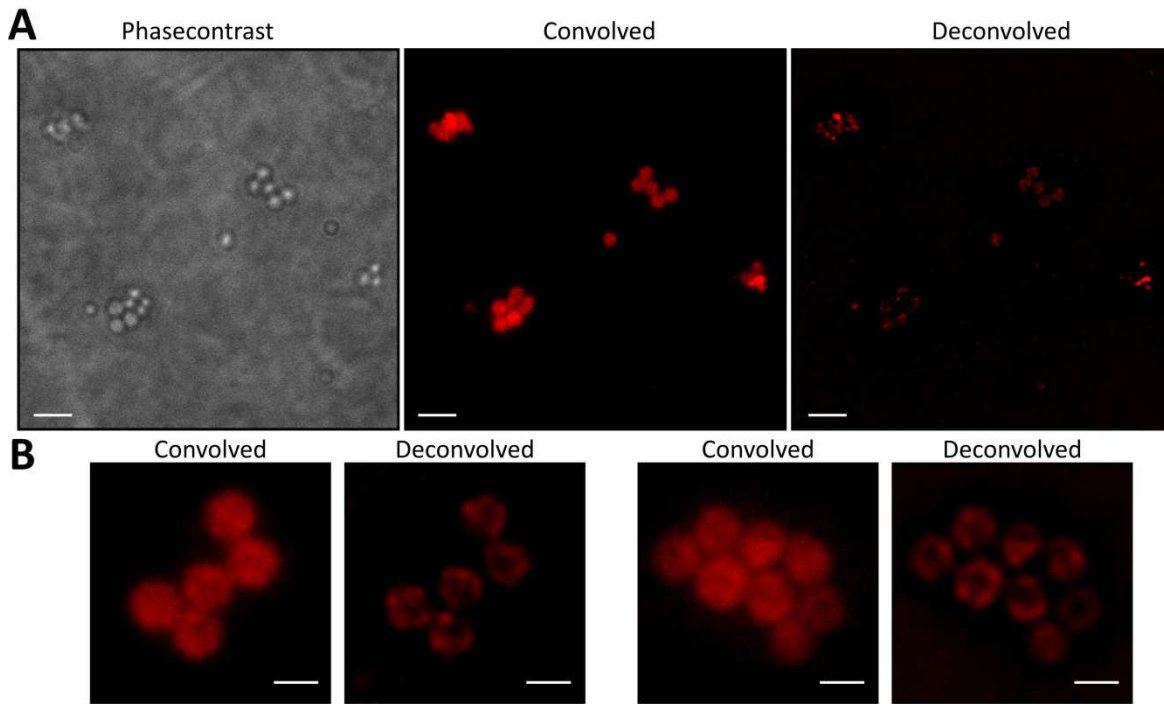


Figure 4.32 Localisation of PlsY-SNAP in *S. aureus* SH1000

Phase contrast and fluorescence images (convolved and deconvolved) of *S. aureus* SH1000 *plsY-SNAP* using TMR-Star as a SNAP-substrate. Images were acquired using a Delta Vision microscope and SoftWoRx 3.5.0 software (Applied Precision). Acquisition of fluorescence images were taken using 1.5 sec exposure in the RFP channel. **A**, Scale bars represent 3 μm . **B**, Images of selected cells. Scale bars represent 1 μm .

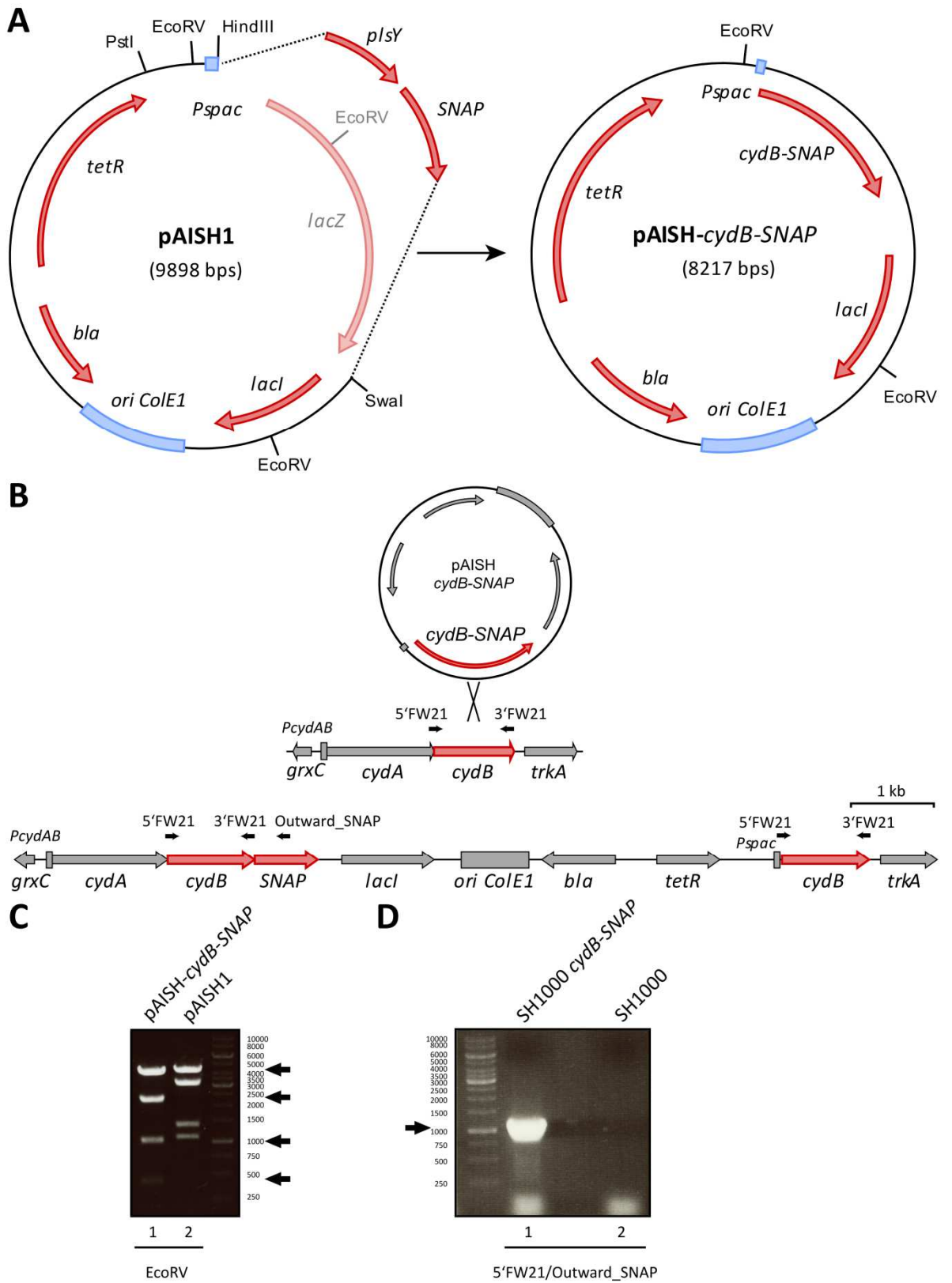


Figure 4.33 Construction of a chromosomal *cydB-SNAP* fusion in *S. aureus* SH1000

A, Diagram illustrating the construction of pAISH-*cydB*-SNAP. **B**, Schematic overview of the native genomic region of *cydB* and post integration of pAISH-*cydB*-SNAP. Black arrows indicate primer binding sites. **C**, pAISH-*cydB*-SNAP (Lane 1) and pAISH1 (Lane 2) were digested with EcoRV and separated by 1 % (w/v) TAE agarose gel electrophoresis. Bands of approximately 4500, 2500 , 1000 and 400 bp, corresponding to pAISH-*cydB*-SNAP (Lanes 1-4), respectively, are marked by black arrows. Bands of approximately 4500, 3000, 1300 and 1100 bp correspond to pAISH1 (Lane 5). **D**, Verification of pAISH-*cydB*-SNAP integration by PCR using primer pair 5'FW21/Outward_SNAP. PCR products were separated by 1 % (w/v) TAE agarose gel electrophoresis. A band of 1169 bp, marked by a black arrow, indicates chromosomal integration of pAISH-*cydB*-SNAP (Lane 1). No DNA amplification can be seen using SH1000 genomic DNA as a template (Lane 2).

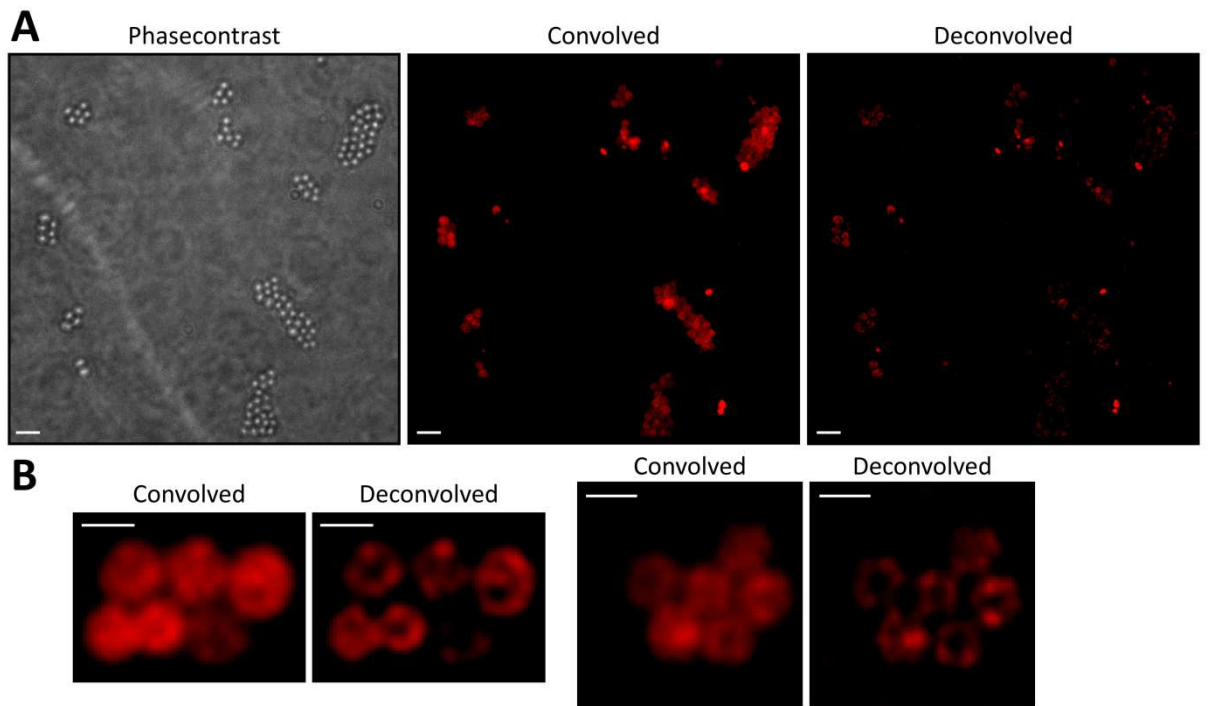


Figure 4.34 Localisation of CydB-SNAP in *S. aureus* SH1000

Phase contrast and fluorescence images (convolved and deconvolved) of *S. aureus* SH1000 *cydB-SNAP* using TMR-Star as a SNAP-substrate. Images were acquired using a Delta Vision microscope and SoftWoRx 3.5.0 software (Applied Precision). Acquisition of fluorescence images were taken using 1.5 sec exposure in the RFP channel. **A**, Scale bars represent 3 μm . **B**, Images of selected cells. Scale bars represent 1 μm .

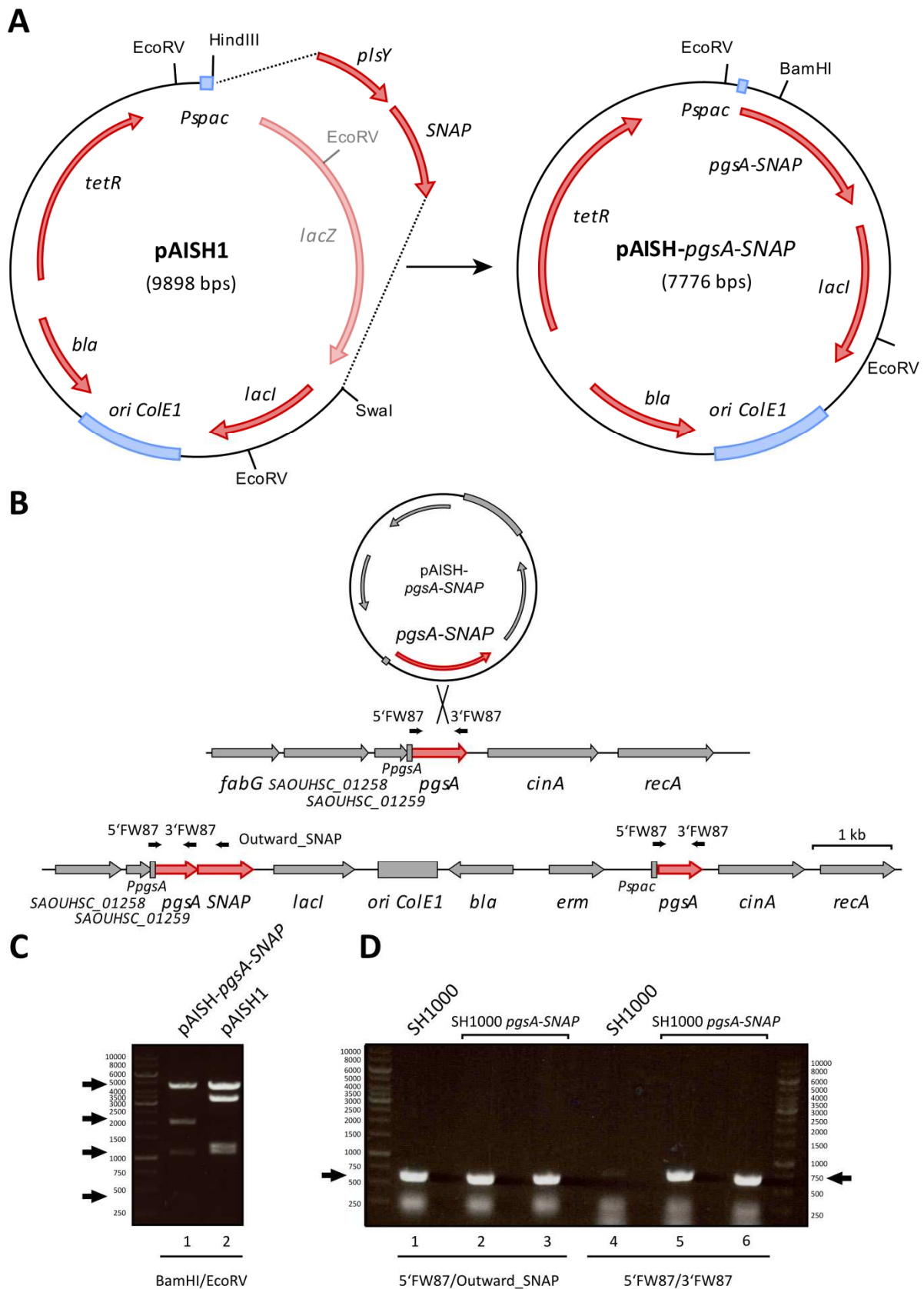


Figure 4.35 Construction of a chromosomal *pgsA-SNAP* fusion in *S. aureus* SH1000

A, Diagram illustrating the construction of pAISH-*pgsA*-SNAP. **B**, Schematic overview of the native genomic region of *pgsA* and post integration of pAISH-*pgsA*-SNAP. Black arrows indicate primer binding sites. **C**, pAISH-*pgsA*-SNAP (Lane 1) and pAISH1 (Lane 2) were digested with BamHI and EcoRV and separated by 1 % (w/v) TAE agarose gel electrophoresis. Bands of approximately 4200, 2000 , 1100 and 400 bp, corresponding to pAISH-*pgsA*-SNAP (Lane 1), respectively, are marked by black arrows. Bands of approximately 4200, 3500, 1200 and 1100 bp correspond to pAISH1 (Lane 2). **D**, Verification of pAISH-*pgsA*-SNAP integration by PCR using primer pair 5'FW87/Outward_SNAP. PCR products were separated by 1 % (w/v) TAE agarose gel electrophoresis. A band of 729 bp, marked by a black arrow, indicates chromosomal integration of pAISH-*pgsA*-SNAP (Lanes 5-6). No DNA amplification is seen using SH1000 genomic DNA (Lane 4). PCR amplification of the whole *pgsA* gene using primer pair 5'FW87/3'FW87 results in a band of 610 bp (Lanes 1-3).

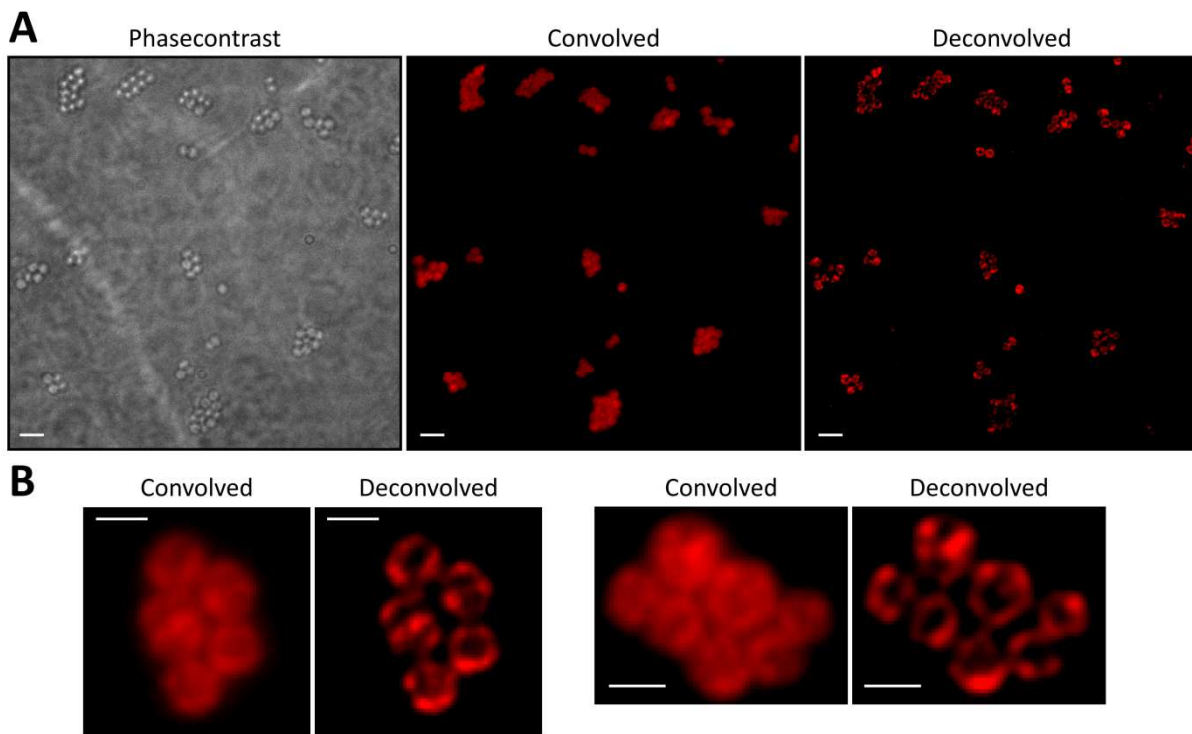


Figure 4.36 Localisation of PgsA-SNAP in *S. aureus* SH1000

Phase contrast and fluorescence images (convolved and deconvolved) of *S. aureus* SH1000 *pgsA-SNAP* using TMR-Star as a SNAP-substrate. Images were acquired using a Delta Vision microscope and SoftWoRx 3.5.0 software (Applied Precision). Acquisition of fluorescence images were taken using 1.5 sec exposure in the RFP channel. **A**, Scale bars represent 3 μm . **B**, Images of selected cells. Scale bars represent 1 μm .

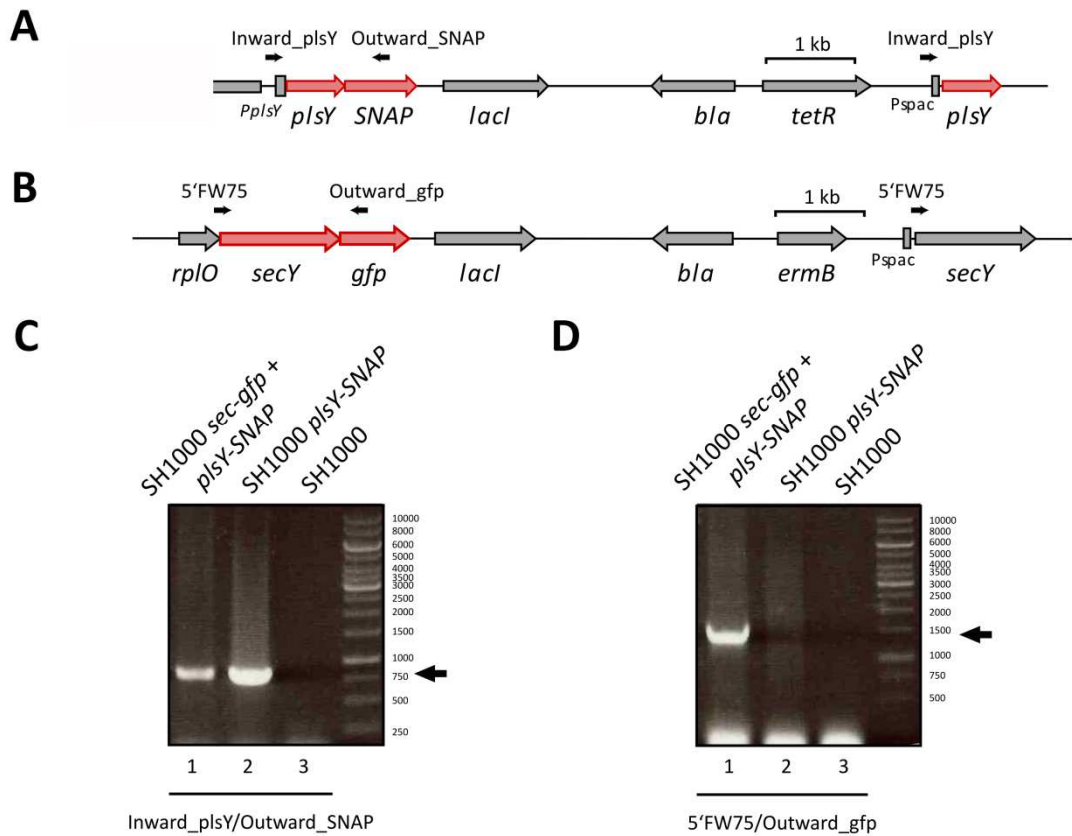


Figure 4.37 Construction of SH1000 *secY-gfp plsY-SNAP*

A, Schematic representation of the genomic region of pAISH-*plsY-SNAP* chromosomally integrated into the *plsY* locus. Primer binding sites are indicated by black arrows. **B**, Schematic representation of the genomic region of pMUTIN-*secY-gfp* chromosomally integrated into the *secY* locus. Primer binding sites are indicated by black arrows. **C**, Verification of pAISH-*plsY-SNAP* integration by PCR using primer pair Inward_*plsY*/Outward_*SNAP*. PCR products were separated by 1 % (w/v) TAE agarose gel electrophoresis. A band of approximately 800 bp, marked by a black arrow, indicates integration of pAISH-*plsY-SNAP* (Lane 1). Genomic DNA of SH1000 *plsY-SNAP* was used as a positive control template (Lane 2). No DNA amplification was seen for SH1000 genomic DNA (Lane 3). **D**, Verification of pMUTIN-*secY-gfp* integration by PCR using primer pair 5'FW75/Outward_*gfp*. PCR products were separated by 1 % (w/v) TAE agarose gel electrophoresis. A band of approximately 1400 bp, marked by a black arrow, indicates integration of pMUTIN-*secY-gfp* (Lane 1). No DNA amplification was seen for SH1000 genomic or SH1000 *plsY-SNAP* DNA (Lane 2-3).

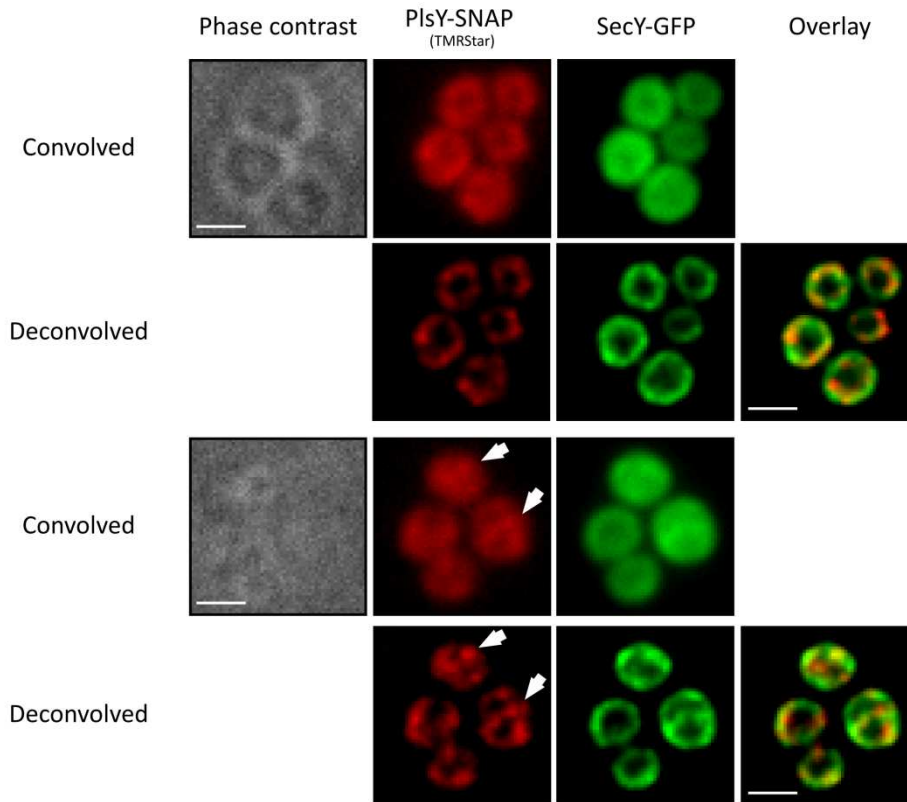


Figure 4.38 Colocalisation of SecY-GFP and PlsY-SNAP in *S. aureus* SH1000

Phase contrast and fluorescence images (convolved and deconvolved) of *S. aureus* SH1000 *secY-gfp plsY-SNAP* using TMR-Star as a SNAP-substrate. Images were acquired using a Delta Vision microscope and SoftWoRx 3.5.0 software (Applied Precision). Acquisition of fluorescence images were taken using 1.5 sec exposure in the FITC channel and 1.5 sec exposure in the RFP channel. Scale bars represent 1 μm .

4.2.5 Role of membrane components in PlsY-GFP localisation

My work has illustrated the heterogeneous localisation of many membrane proteins in *S. aureus*. At least for PlsY-GFP the heterogeneous localisation is dose-dependent and overexpression of PlsY-GFP leads to a loss of this pattern to an apparent homogeneous distribution. How these patterns are generated, maintained and the role of specific components of the bacterial membrane is investigated in the following studies.

4.2.5.1 Inhibition of squalene synthesis

The existence of lipid rafts in bacteria has been previously reported (Lopez & Kolter, 2010, LaRocca *et al.*, 2013, Toledo *et al.*, 2014). Lipid rafts are described as microdomains within the membrane enriched in cholesterol, glycolipids and sphingolipids. Lopez *et al.*, revealed lipid rafts in *S. aureus* that contain a number of signalling proteins and FloT, a homologue of flotillin that is known as a lipid raft marker in eukaryotic cells. Interestingly, these structures are localised in a single position in the membrane of *S. aureus* and are dependent on squalene. Squalene is a precursor of cholesterol although cholesterol is not produced in Staphylococci (Fig. 4.39). Fortunately, zaragozic acid (ZA), an inhibitor of the squalene synthase was already known and was used to show that cells that lack squalene lost FloT localisation. It is hypothesised that FloT requires squalene for its localisation and gets degraded if it is not placed properly.

Since FloT exhibits a non-homogeneous distribution comparable to PlsY, it was tested whether squalene is involved in the placement of PlsY. In order to investigate this, cells were grown in the presence of zaragozic acid at various concentrations.

Zaragozic acid inhibits the activity of the squalene synthase. Squalene, as well as being required for the formation of lipid rafts, is also a precursor of staphyloxanthin (Fig. 4.39A). Since staphyloxanthin is responsible for the distinct golden coloration of *S. aureus*, the pellet of cultures treated with either 1 μ M, 10 μ M or no ZA was analysed to confirm the activity of ZA and to test which concentration is needed for following localisation studies. Although a slight change of colour can be observed, complete inhibition was only seen for cells treated with 10 μ M ZA (Fig. 4.39). To test whether zaragozic acid has any effect on localisation of PlsY-GFP, cells were treated with 1 μ M, 10 μ M or no zaragozic acid for 2 h or 5 h, respectively, and analysed by fluorescence microscopy. The application of 10 μ M zaragozic acid led to a obvious loss of localisation and decrease in fluorescence signal of FloT-eYFP (Fig. 4.40). However, no

effect on the localisation or fluorescence on PlsY-GFP was seen. Therefore, it is likely that squalene is not involved in the localisation of PlsY.

4.2.5.2 PlsY-GFP localisation in a cardiolipin (*cls1/cls2*) deletion mutant

Cardiolipin, also called diphosphatidylglycerol, is a cone-shaped phospholipid. Due to its structure, its hydrophilic head group is smaller in cross-section than its hydrophobic tail (Huang *et al.*, 2006, Mukhopadhyay *et al.*, 2008) making it preferentially localise to negatively curved membranes that are found at the cell poles and the septum. Its intrinsic ability to sense negatively curved membranes makes CL interesting for protein localisation studies since proteins could use CL as a prior localisation cue. Some proteins like the osmosensory transporter ProP were shown to require cardiolipin for their polar localisation (Romantsov *et al.*, 2007, Mileykovskaya, 2007).

In order to study PlsY-GFP localisation in a strain lacking cardiolipin, chromosomally integrated pMUTIN-*plsY-gfp* was transduced to SH1000 Δ *cls1* Δ *cls2*. This strain lacks both known cardiolipin synthases in *S. aureus*. Integration of pMUTIN-*plsY-gfp* at the native locus of *plsY* was confirmed via PCR amplification using one primer binding upstream of *plsY* and one primer binding within *gfp* resulting in amplification of an approximately 900 bp fragment (Fig. 4.41B).

The localisation of PlsY-GFP was investigated as previously shown. Overnight cultures were subcultured to an OD₆₀₀=0.05 and grown to exponential phase of an OD₆₀₀≈0.5 in BHI medium supplemented with erythromycin (5 µg/ml), tetracycline (5 µg/ml) and chloramphenicol (1 µg/ml) incubated at 37 °C at 250 rpm. Samples were fixed and analysed by fluorescence microscopy.

No growth defect could be observed (not shown) and PlsY-GFP localisation was unchanged in a mutant lacking both cardiolipin synthases (Fig. 4.42). Fluorescence is seen as a punctate pattern and at the septum during cell-division which suggests that cardiolipin is not involved in the placement of PlsY.

4.2.5.3 PlsY-GFP localisation in a lys-PG (*mprF*) deletion mutant

MprF is a phospholipid modifying enzyme that alters the net charge of phosphatidylglycerol (Andra *et al.*, 2011) and could therefore have an impact on membrane organisation and potentially the localisation of membrane proteins like PlsY. MprF catalyses an enzymatic transfer of a lysine residue to PG which converts a positive net charge that was shown to confer resistance to antimicrobial peptides (Ernst *et al.*, 2015).

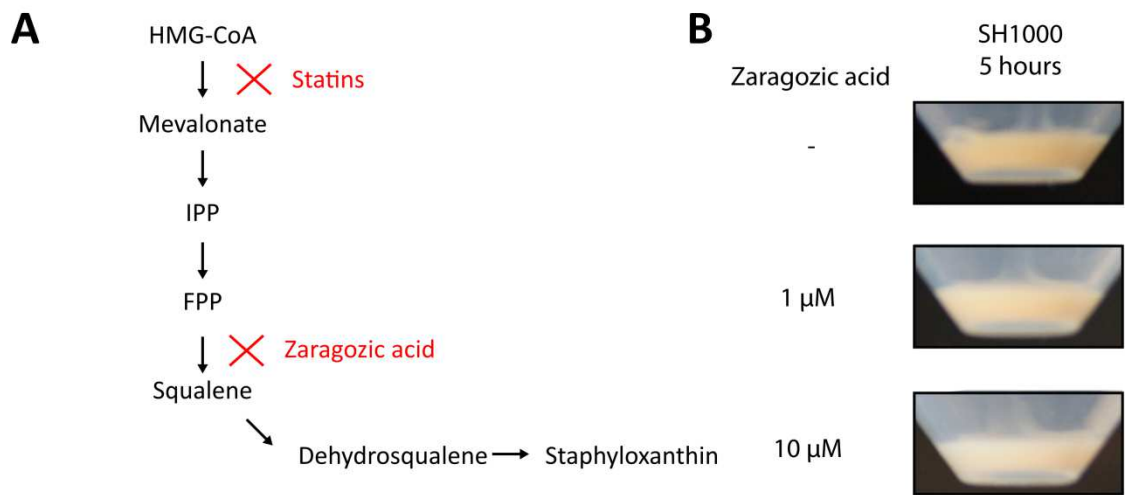


Figure 4.39 Inhibitory effect of zaragozic acid on squalene and staphyloxanthin production

A, schematic presentation of the biochemical pathway to produce squalene in *S. aureus*. The full names of the intermediates are as follows: HMG-CoA (3-Hydroxy-3-methylglutaryl-CoA), IPP (Isopentenylpyrophosphat), FPP (Farnesyl-diphosphate farnesyltransferase). **B**, Pellet of *S. aureus* SH1000 *floT-eyfp* cells treated with zaragozic acid at different concentrations and untreated after 5 h growth.

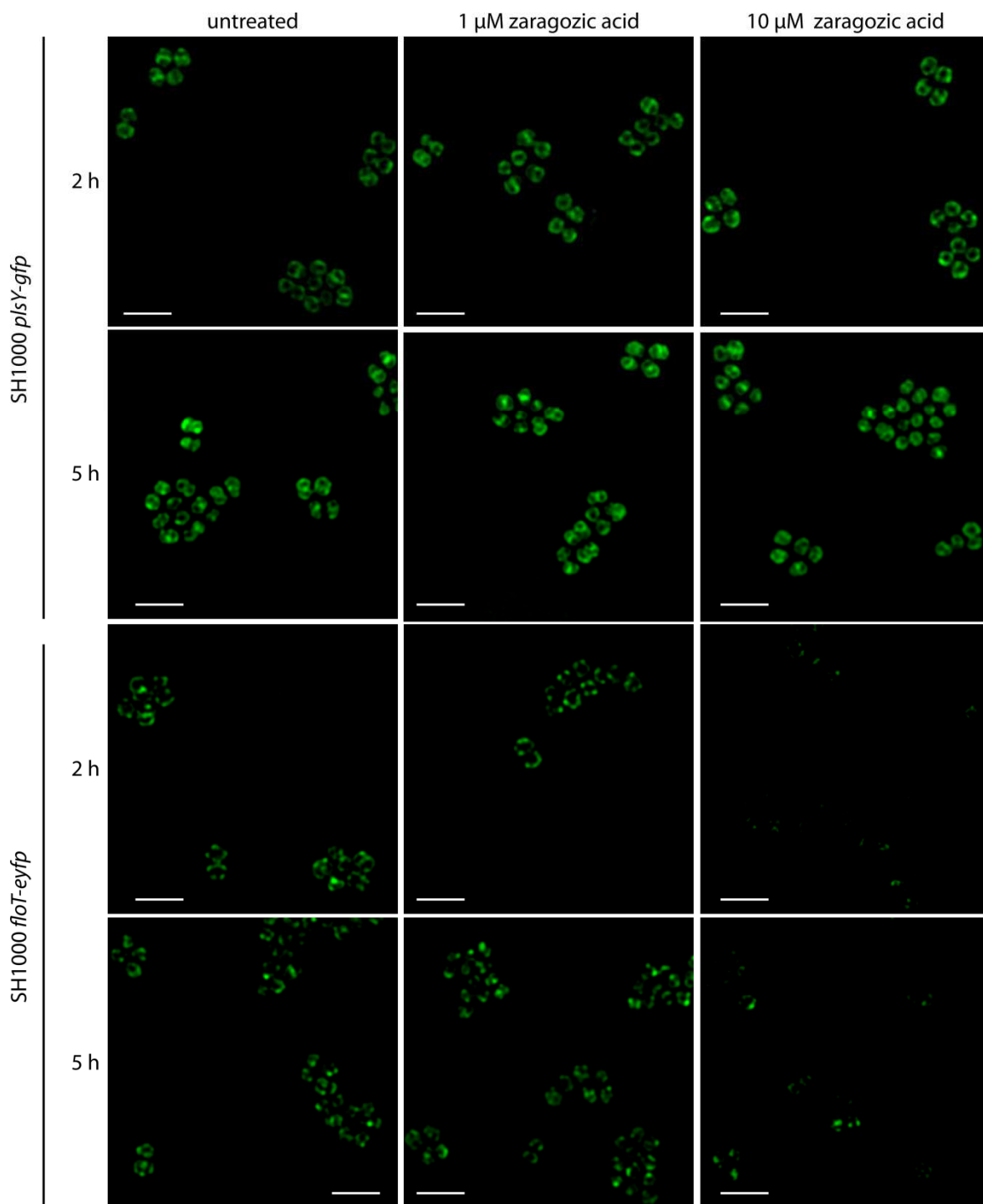


Figure 4.40 Effect of zaragozic acid on localisation of PlsY-GFP and FloT-eYFP
 Fluorescence images of *S. aureus* SH1000 *floT-eyfp* and SH1000 *plsY-gfp* after 2 and 5 h treatment with zaragozic acid. Images were acquired using a Delta Vision microscope and SoftWoRx 3.5.0 software (Applied Precision). Acquisition of fluorescence images were taken using 2.5 sec exposure in the FITC channel for PlsY-GFP and 1.5 sec exposure in the FITC channel for FloT-eYFP. Scale bars represent 3 μ m.

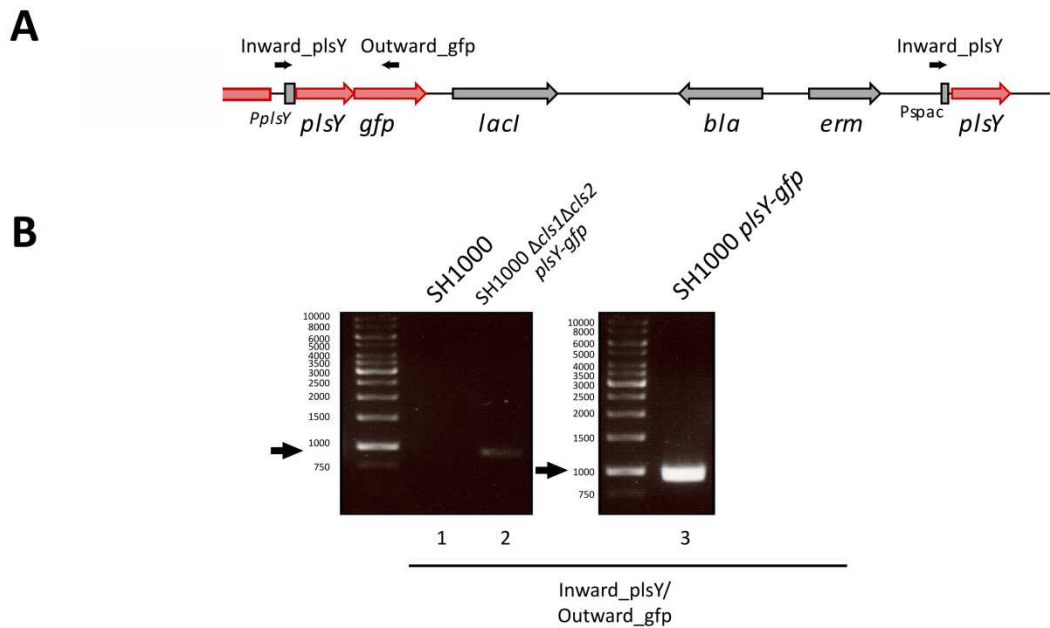


Figure 4.41 Construction of SH1000 $\Delta cls1\Delta cls2 plsY-gfp$

A, Schematic representation of the genomic region of pMUTIN-*plsY-gfp* chromosomally integrated into the *plsY* locus. Primer binding sites are indicated by black arrows. **B**, Verification of pMUTIN-*plsY-gfp* integration by PCR using primer pair Inward_plsY/Outward_gfp. PCR products were separated by 1 % (w/v) TAE agarose gel electrophoresis. A band of approximately 900 bp, marked by a black arrow, indicates pMUTIN-*plsY-gfp* chromosomal integration (Lane 2). No DNA amplification is seen using SH1000 genomic DNA (Lane 1). Genomic DNA of SH1000 *plsY-gfp* was used as a positive control template (Lane 3).

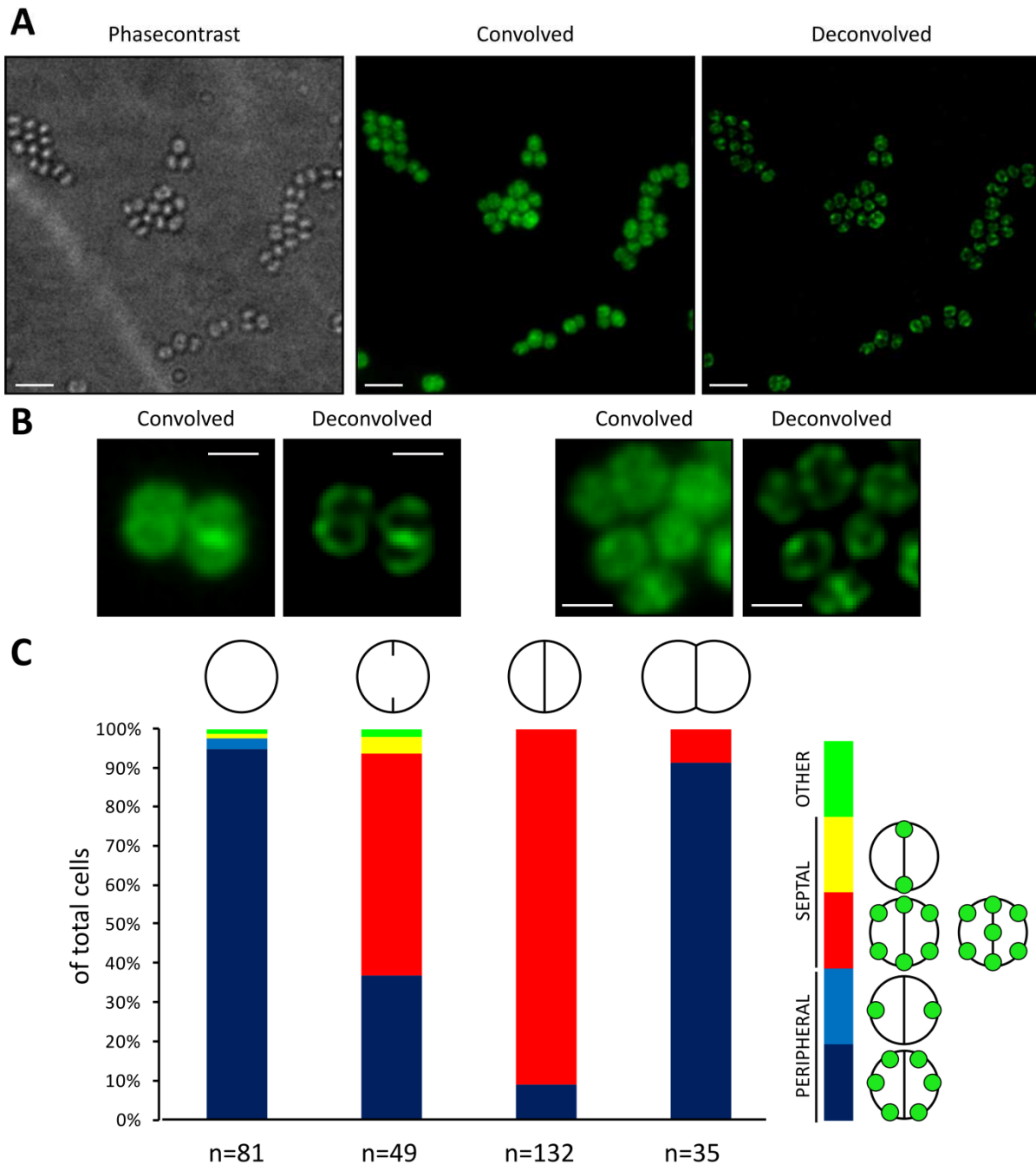


Figure 4.42 PIsY-GFP localisation in a $\Delta cls1\Delta cls2$ mutant

Phase contrast and fluorescence images (convolved and deconvolved) of *S. aureus* SH1000 $\Delta cls1\Delta cls2$ *plsY-gfp*. Images were acquired using a Delta Vision microscope and SoftWoRx 3.5.0 software (Applied Precision). Acquisition of fluorescence images were taken using 2.5 sec exposure in the FITC channel. **A**, Scale bars represent 3 μm . **B**, Images of selected cells. Scale bars represent 1 μm . **C**, Cell counts categorized depending on PIsY-GFP localisation and cell-cycle stage indicated by HADA labelling. Value n indicates counted cells for each group. Red and yellow bars indicate septal and blue bars indicate peripheral PIsY-GFP localisation. The green coloured bar indicates a random PIsY-GFP localisation.

So the question arises as to whether an altered charge of PG has an influence on membrane domains and/or membrane protein localisation which was investigated localisation studies of PlsY-GFP in a strain lacking *mprF*.

Replacing the gene *mprF* by an erythromycin resistance cassette was achieved by transduction of $\Delta mprF::ermB$ from strain SA113 $\Delta mprF::ermB$ (Peschel *et al.*, 2001) to SH1000 *plsY-gfp*. The $\Delta mprF::ermB$ was transduced to the tetracycline resistant version of SH1000 *plsY-gfp* (see Appendix Fig. 9.5 for construction of pAISH-*plsY-gfp*) due to selection marker purposes. The replacement of *mprF* by *ermB* was verified by PCR using primer pair Inward_mprF-N/Outward_ermB1 (see Fig. 4.43B for primer binding sites) and genomic DNA as a template resulting in the amplification of an approximately 800 bp fragment for strains containing the $\Delta mprF::ermB$ mutation and no DNA amplification for the wild type SH1000 strain and SH1000 *plsY-gfp* (Fig. 4.43C). SH1000 $\Delta mprF::ermB$ genomic DNA was used as a positive control. The chromosomal fusion of *plsY* to *gfp* was verified by primer pair 5'FW23/Outward_gfp (see Fig. 4.43A for primer binding sites) that amplifies an approximately 800 bp fragment and results in no amplification for wild type SH1000 genomic DNA (Fig. 4.43E). The whole *plsY* gene was amplified using primers 5'FW23/3'FW23 resulting in a 632 bp to confirm both the PCR and template (Fig. 4.43D).

Localisation of PlsY-GFP in strain SH1000 $\Delta mprF::ermB$ *plsY-gfp* was then investigated as previously described and samples from early-exponential phase were harvested, fixed and analysed by fluorescence microscopy.

The deletion of *mprF* results in the loss of lysinylation of phosphatidylglycerol phosphate (LPG). No growth defect could be observed (not shown) and the localisation of PlsY-GFP was not affected by the lack of LPG. PlsY-GFP exhibits a septal localisation during cell-division along with a heterogeneous punctate pattern at the cell membrane periphery (Fig. 4.44). Therefore, MprF and LPG do not appear to be involved in the localisation of PlsY.

4.2.5.4 PlsY-GFP localisation in a wall teichoic acid (*tarO*) deletion mutant

Wall teichoic acids are a crucial multifunctional component of gram positive cells that are involved in the localisation of a number of enzymes. They are thought to regulate ion homeostasis by binding extracellular metal cations and protons which has direct effects on the positioning of autolysins and their activity (Kern *et al.*, 2010).

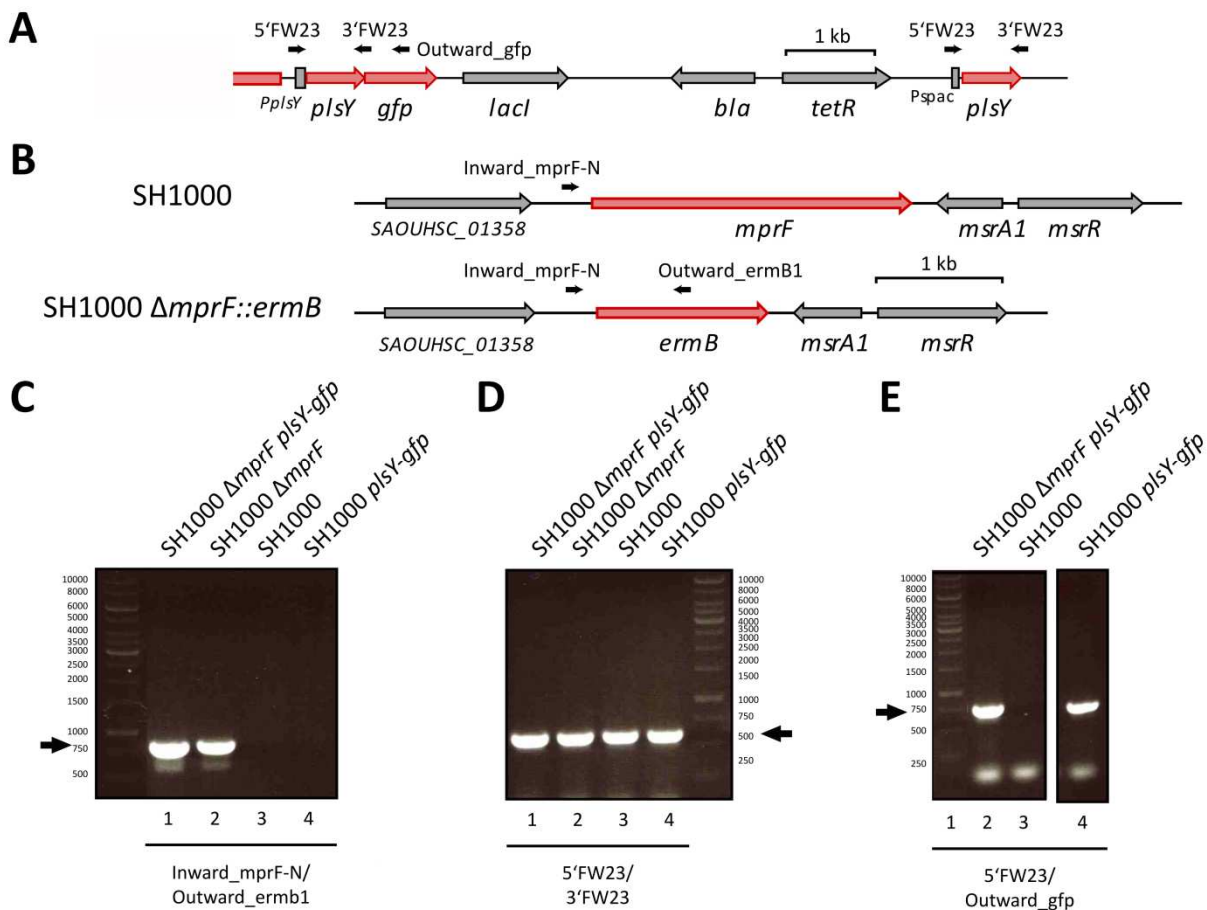


Figure 4.43 Construction of SH1000 Δ *mprF::ermB* *plsY-gfp*

A, Schematic representation of the genomic region of pAISH-*plsY-gfp* chromosomally integrated into the *plsY* locus. Primer binding sites are indicated by black arrows. **B**, Schematic representation of the genomic region of *mprF* and Δ *mprF::ermB*. Primer binding sites are indicated by black arrows. **C**, Verification of *mprF* replacement by PCR using primer pair Inward_mprF-N/Outward_ermB1. PCR products were separated by 1 % (w/v) TAE agarose gel electrophoresis. A band of approximately 800 bp, marked by a black arrow, indicates replacement of *mprF* by an erythromycin resistance cassette (Lanes 1-2). No DNA amplification is seen using SH1000 and SH1000 *plsY-gfp* genomic DNA as negative control templates (Lanes 3-4). **D**, PCR amplification of the whole *plsY* gene using primer pair 5'FW23/3'FW23 resulting in a band of 638 bp, marked by a black arrow (Lanes 1-4). PCR products were separated by 1 % (w/v) TAE agarose gel electrophoresis. **E**, Verification of pAISH-*plsY-gfp* integration by PCR using primer pair 5'FW23/Outward_gfp. PCR products were separated by 1 % (w/v) TAE agarose gel electrophoresis. A band of approximately 800 bp, marked by a black arrow, indicates pMUTIN-*plsY-gfp* chromosomal integration (Lane 1). No DNA amplification is seen using SH1000 genomic DNA as negative control template (Lanes 2). Genomic DNA from SH1000 *plsY-gfp* was used as positive control template (Lane 3).

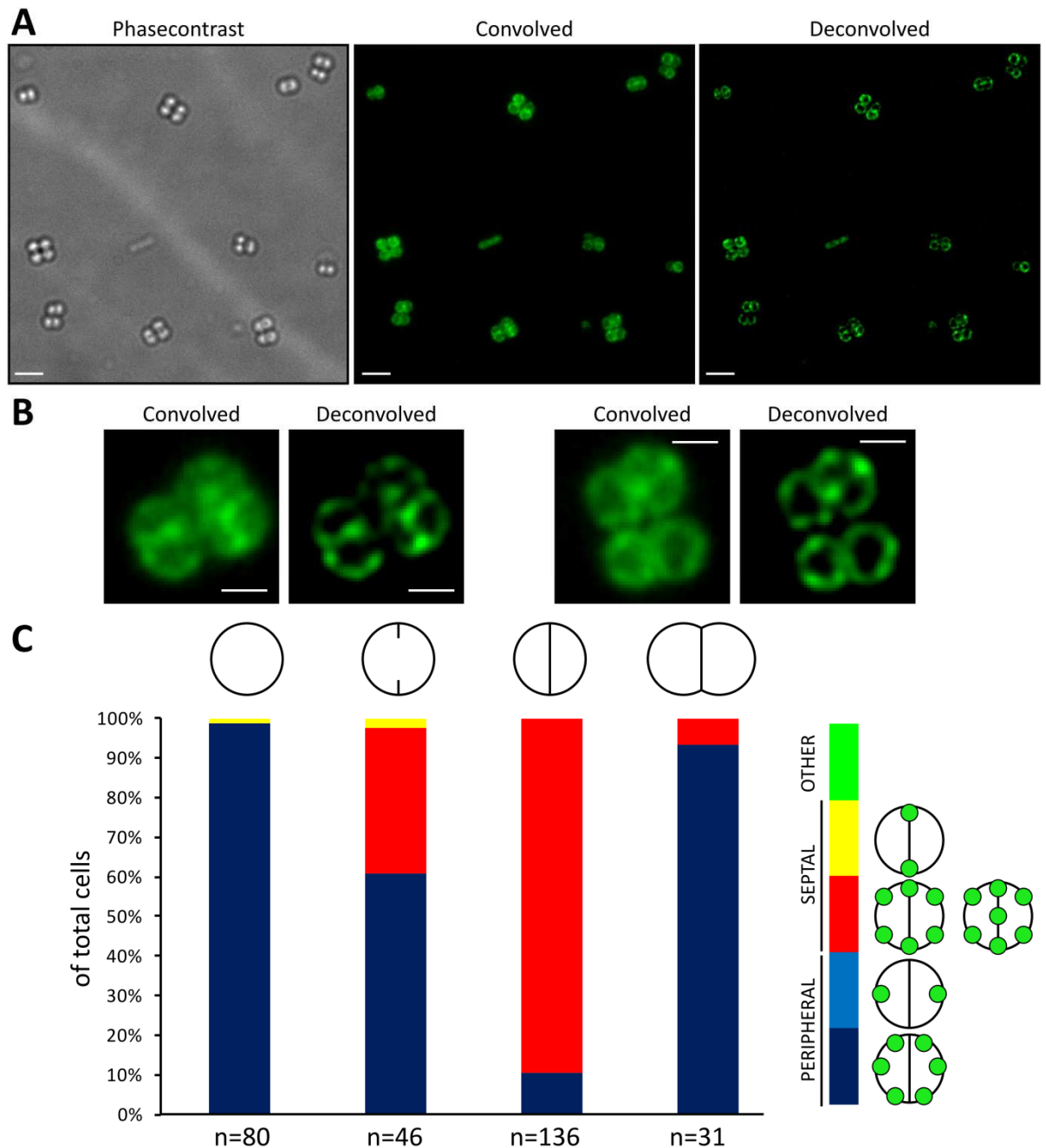


Figure 4.44 PlsY-GFP localisation in a $\Delta mprF$ mutant

Phase contrast and fluorescence images (convolved and deconvolved) of *S. aureus* SH1000 $\Delta mprF$ *plsY-gfp*. Images were acquired using a Delta Vision microscope and SoftWoRx 3.5.0 software (Applied Precision). Acquisition of fluorescence images were taken using 2.5 sec exposure in the FITC channel. **A**, Scale bars represent 3 μm . **B**, Images of selected cells. Scale bars represent 1 μm . **C**, Cell counts categorized depending on PlsY-GFP localisation and cell-cycle stage indicated by HADA labelling. Value n indicates counted cells for each group. Red and yellow bars indicate septal and blue bars indicate peripheral PlsY-GFP localisation. The green coloured bar indicates random PlsY-GFP localisation.

Many studies identified an interaction between WTAs and the PG machinery showing that WTAs are involved in the proper placement of cross-linking enzymes PBP4 and Fmt (Atilano *et al.*, 2010, Qamar & Golemi-Kotra, 2012). Cells lacking WTAs through the deletion of *tarO* (*tarO*), a gene required for the first step of WTA synthesis, also showed a decrease in PG cross-linking (Schlag *et al.*, 2010). The localisation of WTAs themselves is controversially discussed. Some studies suggest that WTAs attach to nascent PG at the septum since fluorescent TarO fusions exhibit septal localisation (Atilano *et al.*, 2010, Bhavsar *et al.*, 2005). However, other studies using fluorescently labelled concavalin, a lectin being reported to bind WTAs, suggest the opposite since fluorescence could only be observed at non-septal PG (Schlag *et al.*, 2010, Andre *et al.*, 2011). Nevertheless, WTAs are an interesting component in protein localisation that could be also involved in the localisation of PlsY.

The knockout of WTAs was facilitated by transduction of a $\Delta tarO::ermB$ to SH1000 *plsY-gfp* mutation resulting in a complete loss of WTA synthesis. A complemented *tarO* mutant (SA113 $\Delta tarO::ermB$ + pRB-*tarO*) (Weidenmaier *et al.*, 2005) was used for phage transduction since phages require WTA to infect cells. The $\Delta tarO::ermB$ was transduced to the tetracycline resistant version of SH1000 *plsY-gfp* (see Appendix Fig. 9.5 for construction of pAISH-*plsY-gfp*) due to selection marker purposes. The replacement of *tarO* by *ermB* was verified by PCR using primer pair Fwd_*tarO*/Rev_*tarO* (see Fig. 4.45B for primer binding sites) and genomic DNA as a template which results in the amplification of an approximately 1600 bp fragment for strains containing the $\Delta tarO::ermB$ mutation and an approximately 1100 bp fragment for the wild type SH1000 strain (Fig. 4.45C). The chromosomal fusion of *plsY* to *gfp* was confirmed by primer pair Inward_*plsY*/Outward_*gfp* (see Fig. 4.45A for primer binding sites) that amplifies a approximately 950 bp fragment and results in no amplification using wild type SH1000 genomic DNA (Fig. 4.45D).

SH1000 $\Delta tarO::ermB$ *plsY-gfp* showed an unexpected growth defect on agar plates. When streaking out this strain, only a few colonies appeared at the beginning of the streak. These colonies however were not visibly affected in growth and exhibited no obvious growth defect in liquid culture (Fig. 4.46A). Restreaking the colonies resulted in the same effect of single colonies at the beginning of the streak. This might be due to improper cell-division and proliferation leading to clumping and therefore do not spread easily or indicating the generation of suppressors.

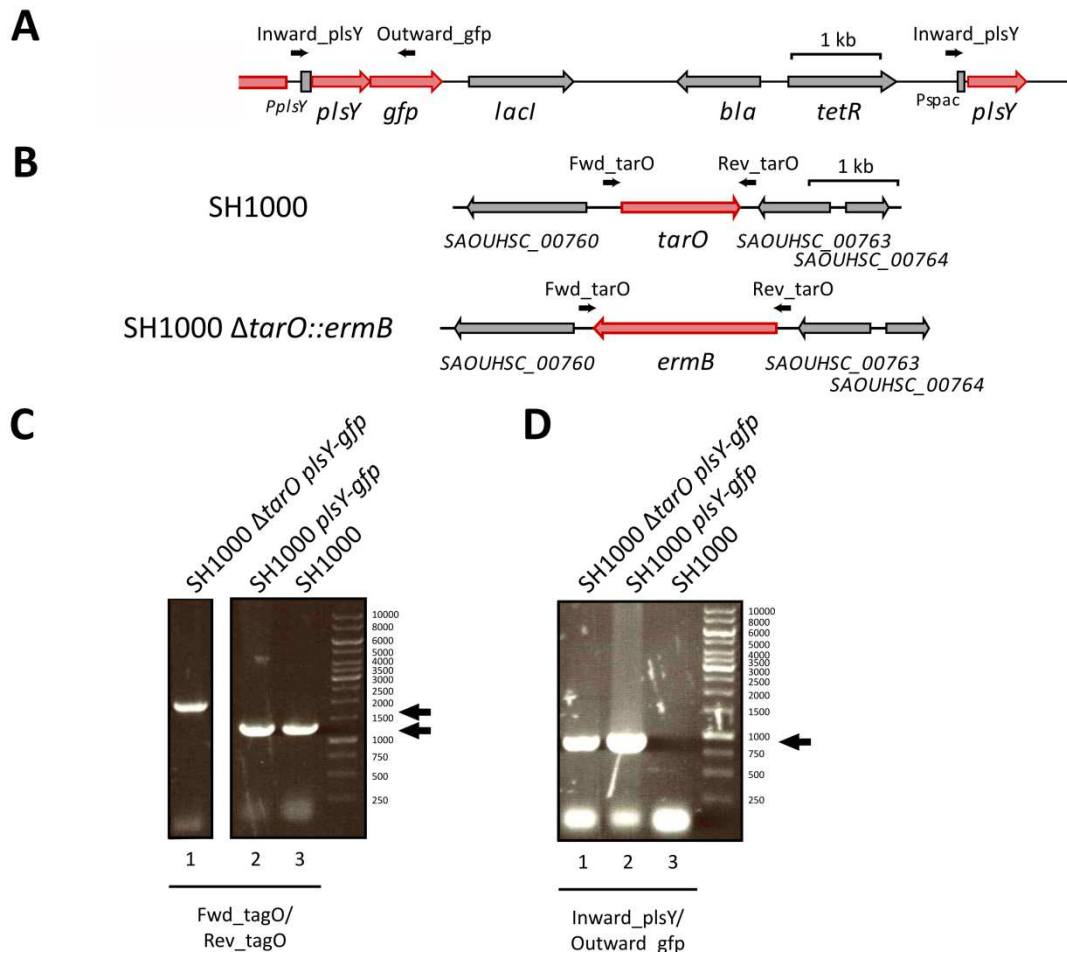


Figure 4.45 Construction of SH1000 $\Delta tarO::ermB$ *plsY-gfp*

A, Schematic representation of the genomic region of pAISH-*plsY-gfp* chromosomally integrated into the *plsY* locus. Primer binding sites are indicated by a black arrow. **B**, Schematic representation of the genomic region of *tarO* and $\Delta tarO::erm$. Primer binding sites are indicated by a black arrow. **C**, Verification of replacement of *tarO* by *ermB* by PCR using primer pair Inward_plsY/Outward_gfp. PCR products were separated by 1 % (w/v) TAE agarose gel electrophoresis. A band of approximately 1600 bp, marked by a black arrow, indicates pMUTIN-*plsY-gfp* chromosomal integration (Lane 1). Genomic DNA from SH1000 and SH1000 *plsY-gfp* were used as negative control templates and resulted in amplification of an approximately 1100 bp fragment (Lanes 2-3). **D**, Verification of pAISH-*plsY-gfp* integration by PCR using primer pair Inward_plsY/Outward_gfp. PCR products were separated by 1 % (w/v) TAE agarose gel electrophoresis. A band of approximately 900 bp, marked by a black arrow, indicates pMUTIN-*plsY-gfp* chromosomal integration (Lane 1). Genomic DNA from SH1000 *plsY-gfp* was used as a positive control template (Lane 2). No DNA amplification is seen using SH1000 genomic DNA as a negative control template (Lane 3).

The localisation of PlsY-GFP in *ΔtarO* was investigated as previously described. Samples were taken 2, 3 and 4 h after subcultivation (see Fig. 4.46A for sampling points). Samples were then fixed and analysed by fluorescence microscopy.

Although SH1000 *ΔtarO plsY-gfp* exhibits no growth defect in liquid culture, the microscopical analysis reveals severe morphological aberrations (Fig. 4.46AB). Cells are heavily enlarged, especially during exponential growth phase (Fig. 4.46B and Fig. 4.45B). Parental PlsY-GFP localisation is seen in most cells (Fig. 4.47A). PlsY-GFP is heterogeneously distributed and localises at the septum of dividing cells (see white arrows in enlarged images). At sample point 3 h, the septal localisation cannot be clearly observed or is lost which might be due to a further changed morphology. Furthermore, due to enlarged cells, the punctate pattern of PlsY-GFP becomes more obvious which is probably based on a better resolution of fluorescence signal.

In summary, it is likely, that WTAs are not directly involved in the positioning of PlsY which is still non-homogeneously localised. The altered cell morphology on the other hand affects its septal localisation whereas the underlying punctate pattern of PlsY though, remains unaffected by the lack of WTAs.

4.2.5.5 Effect of fatty acid synthesis inhibition on PlsY-GFP localisation

Cerulenin is an antibiotic that inhibits fatty acid synthesis in bacteria (Goldberg *et al.*, 1973). It binds to one of the seven fatty acid synthase moieties (β -ketoacyl-acyl-ACP synthase) and thereby inhibits fatty acid synthesis (Fig. 4.48) (Price *et al.*, 2001). It is thought that this inhibition perturbs the membrane function and it was specifically found to alter protein secretion (Jacques, 1983). This makes cerulenin interesting in two aspects. First, the perturbation of the membrane might affect membrane protein localisation. Second, PlsY connects fatty acids via PlsX with glycerol-3-phosphate and the removal of its substrate could have a direct effect on PlsY-localisation by interrupting the reaction chain.

Localisation of PlsY-GFP was studied in presence of various concentrations of cerulenin. SH1000 *plsY-gfp* was subcultured from an over-night culture to an $OD_{600}=0.05$ and grown in BHI medium supplemented with 0, 5, 25, 50 or 100 μ M cerulenin. Additionally, for one culture, cerulenin was added at a concentration of 500 μ M after 2 h of growth at an $OD_{600}\approx 0.7$. Samples were taken 2, 3 or 4 h post subcultivation. One sample was taken at 4 h for the culture with addition of 500 μ M cerulenin. Cells were fixed and analysed by fluorescence microscopy.

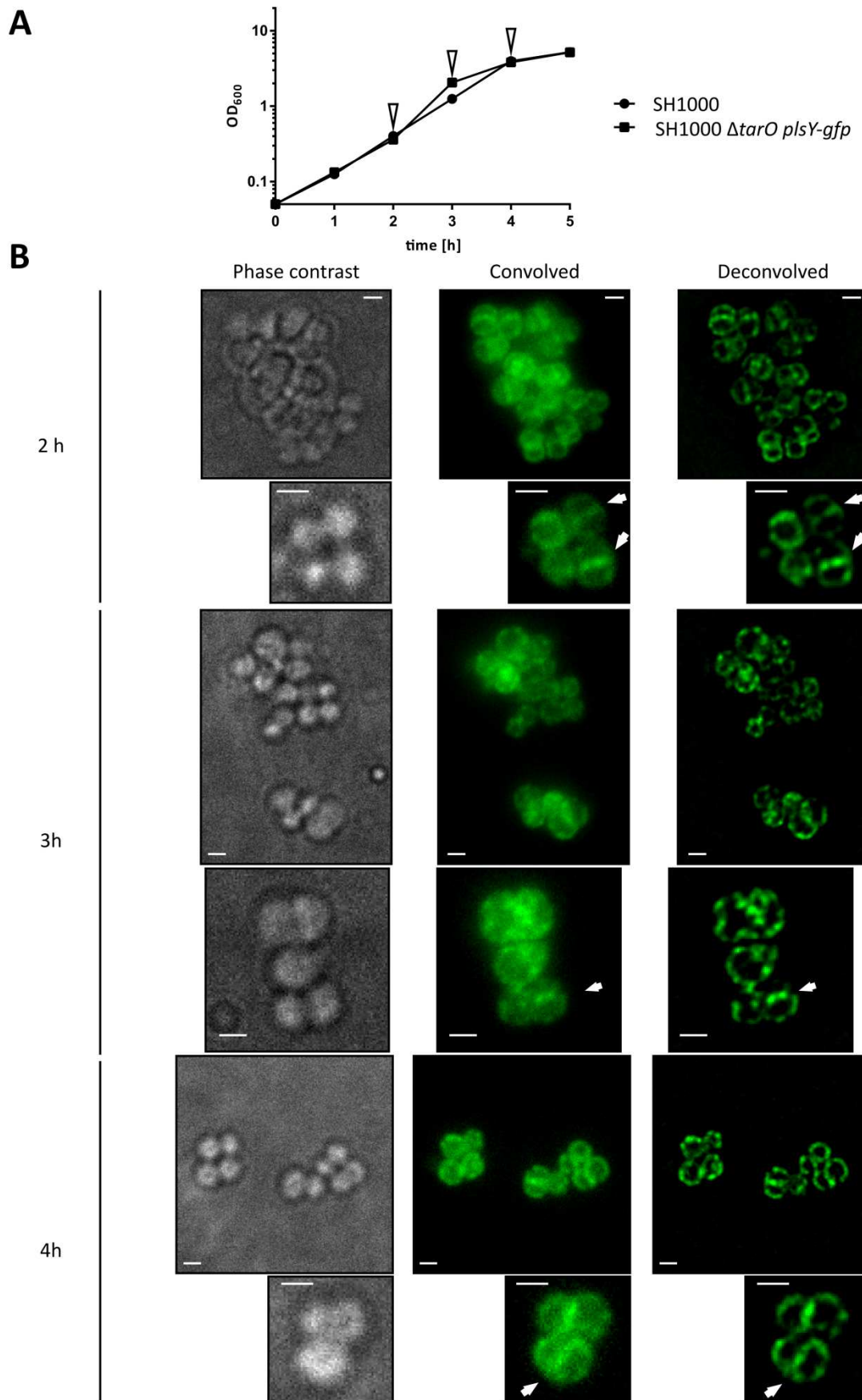


Figure 4.46 PlsY-GFP localisation in a $\Delta tarO$ mutant

A, Growth curve of SH1000 and SH1000 $\Delta tarO$ *plsY-GFP*. Arrows indicate sampling points. **B**, Phase contrast and fluorescence images (convolved and deconvolved) of *S. aureus* SH1000 $\Delta tarO$ *plsY-gfp* samples taken 2, 3 and 4 h past subcultivation. Images were acquired using a Delta Vision microscope and SoftWoRx 3.5.0 software (Applied Precision). Acquisition of fluorescence images were taken using 2.5 sec exposure in the FITC channel. The second row of images for each sampling point shows enlarged selected cells. White arrows indicate septal localisation of PlsY-GFP. Scale bars represent 1 μ m.

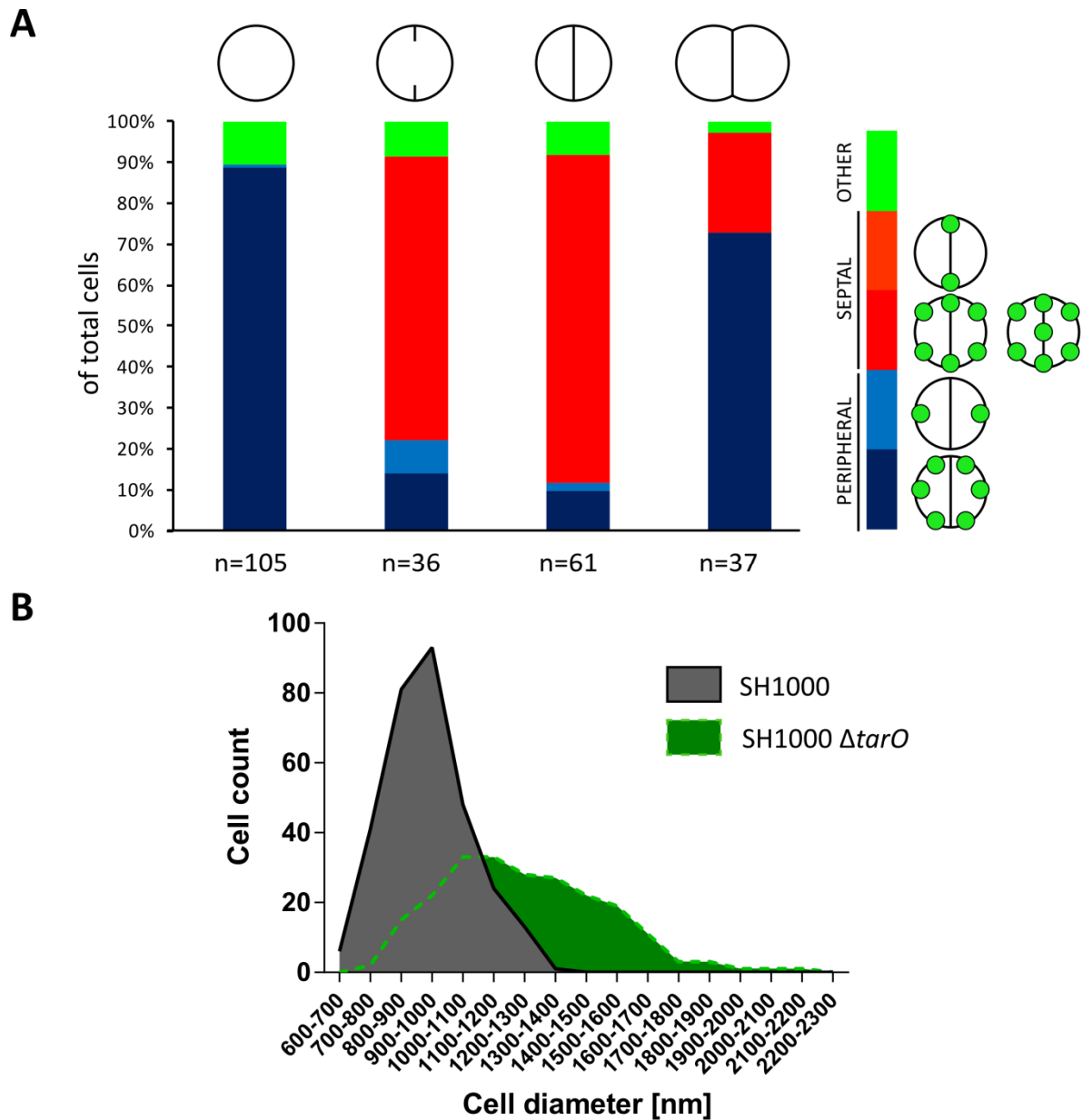


Figure 4.47 PIsY-GFP localisation in a $\Delta tarO$ mutant and morphology of $\Delta tarO$
A, Cell counts categorized depending on PIsY-GFP localisation and cell-cycle stage indicated by HADA labelling. Value n indicates counted cells for each group. Red bars indicate septal and blue bars indicate peripheral PIsY-GFP localisation. The green coloured bar indicates random PIsY-GFP localisation. **B**, Cell counts of exponentially growing cells, categorised into their cell diameter.

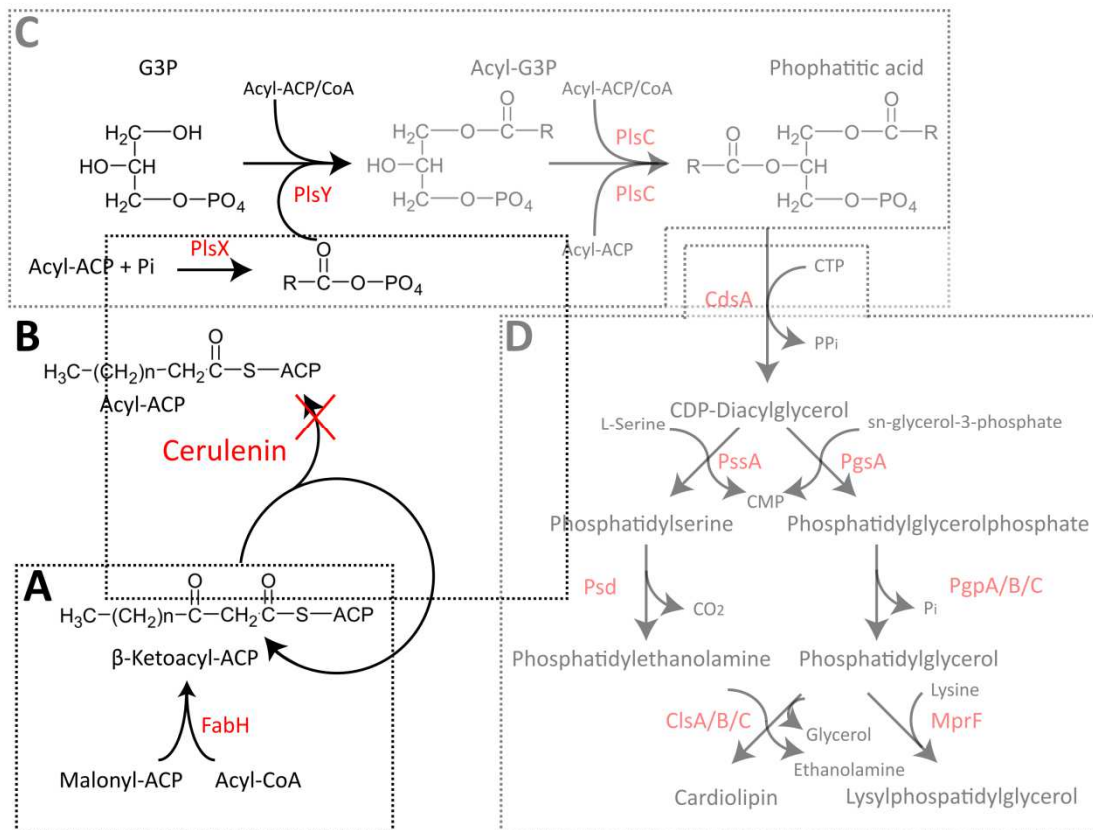


Figure 4.48 Cerulenin inhibits fatty acid synthesis

Schematic overview of fatty acid synthesis linked to phospholipid synthesis and the effect of cerulenin. A more detailed description of the enzymatic processes are described in Section 1.2.5.1.4 and Fig. 1.5. Cerulenin inhibits the β -ketoacyl-acyl-ACP synthase activity and therefore fatty acid synthesis.

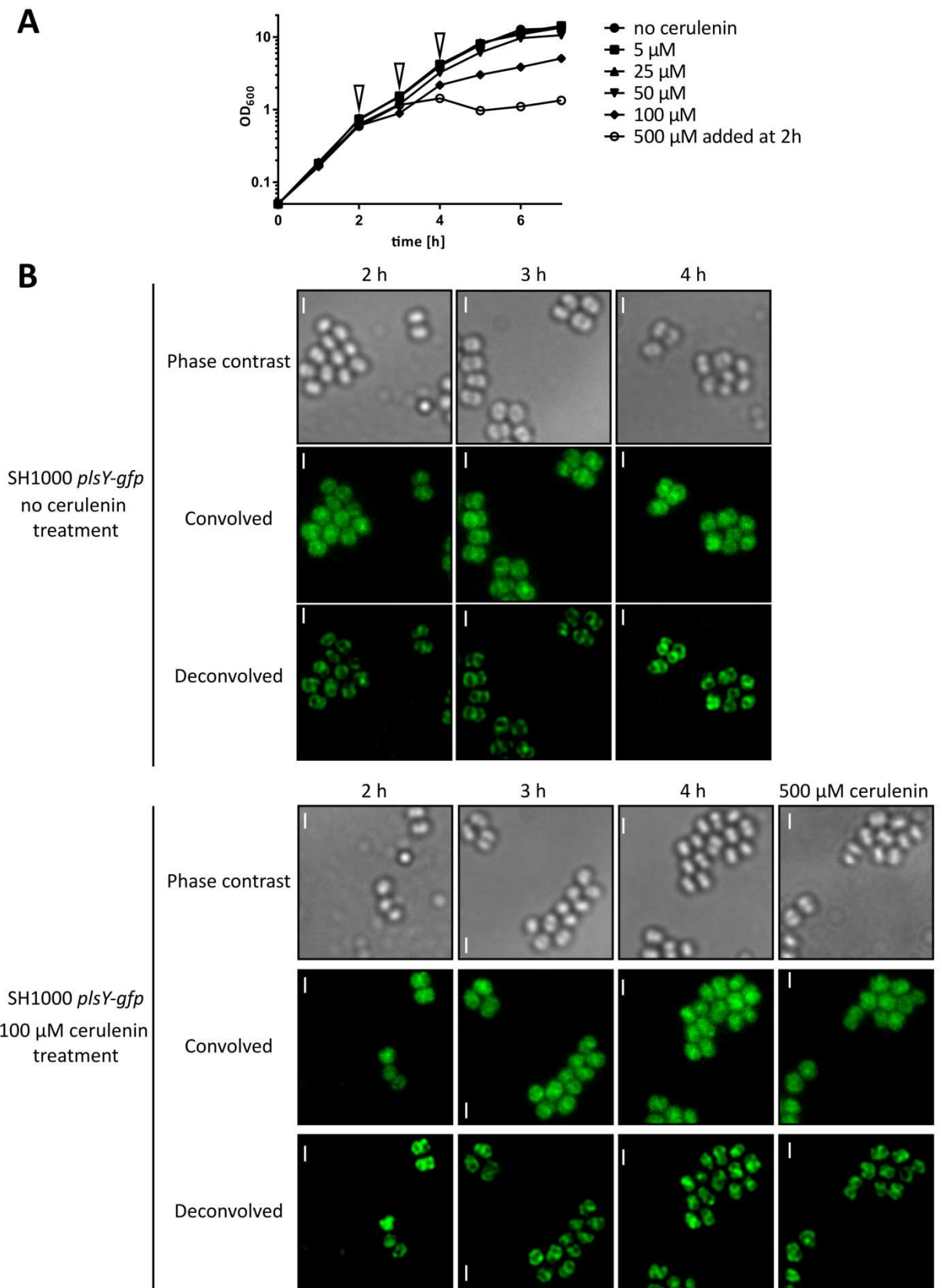


Figure 4.49 Effect of fatty acid inhibition on PlsY-GFP localisation

A, Growth curve of SH1000 *plsY-gfp* grown in the presence of different concentrations of cerulenin. Arrows indicate sampling points. **B**, Phase contrast and fluorescence images (convolved and deconvolved) of *S. aureus* SH1000 *plsY-gfp* samples taken 2, 3 and 4 h past subcultivation. Images were acquired using a Delta Vision microscope and SoftWoRx 3.5.0 software (Applied Precision). Acquisition of fluorescence images were taken using 2.5 sec exposure in the FITC channel. Scale bars represent 1 μm .

Cerulenin affects growth of *S. aureus* (Fig. 4.49). Strains grown in the presence of 100 μM cerulenin, but not 5-50 μM , exhibited impaired growth. The late addition of 500 μM cerulenin to exponentially growing cells stopped growth entirely. However, samples taken to investigate the localisation of PlsY-GFP in these strains did not show any changes. PlsY-GFP localises to the septum and in heterogeneous patches. Images taken 4 h post subcultivation of strains grown in the presence of 100 or 500 μM cerulenin show a slightly altered localisation pattern of PlsY-GFP that lacks a punctate distribution in many cells and appears to be focused at one spot within some cells. This effect however, is not very clear due to the limited resolution and makes it hard to draw conclusions on the effect of cerulenin on PlsY-GFP localisation. Nevertheless, cerulenin might have an effect on membrane protein localisation.

4.2.5.6 Effect of membrane potential inhibition on PlsY-GFP localisation

The previous experiments focused on directly affecting the integrity of membranes to reveal potential localisation cues of PlsY. But what if other membrane processes may be involved such as respiration and membrane potential? It has been reported before that respiratory complexes form punctate patches in the membrane that can be spatially redistributed in response to light (Liu *et al.*, 2012).

To test whether respiration or membrane potential has an influence on the localisation of PlsY-GFP, cells were treated with the uncoupling agent carbonyl cyanide *m*-chlorophenyl hydrazone (CCCP). CCCP inhibits the terminal oxidase that exports protons by acting as an ionophore along with the inhibition of the ATP synthase (Diez-Gonzalez & Russell, 1997). This destroys the membrane potential by increasing intracellular protons along with reduced ATP which eventually leads to cell death (Diez-Gonzalez & Russell, 1997). MreB was shown to require an intact membrane potential and delocalised in *B. subtilis* cells treated with CCCP (Strahl & Hamoen, 2010).

The localisation of PlsY-GFP was studied in the presence of various concentrations of CCCP. SH1000 *plsY-gfp* was subcultured from an overnight culture to an $\text{OD}_{600}=0.05$ and grown in BHI medium supplemented with 0, 0.5, 2.5 or 25 μM CCCP. Additionally, for one culture, CCCP was added at a concentration of 25 μM after 2 h of growth at an $\text{OD}_{600}\approx 0.8$. Samples were taken 3 h post subcultivation or 1 h after addition of 25 μM CCCP. Cells were fixed and analysed by fluorescence microscopy.

CCCP has a strong effect on growth of *S. aureus* cells. Low concentrations (0.5 - 2.5 μM) of CCCP were sufficient to inhibit growth entirely (Fig. 4.50A). Cells almost immediately stopped growth after addition of CCCP. However, localisation was not affected and a punctate distribution pattern along with septal localisation could still be observed which leads to the conclusion that the membrane potential does not effect the localisation of PlsY-GFP (Fig. 4.50B).

4.2.5.7 Effect of FtsZ-polymerisation inhibition

Localisation studies of phospholipid synthesis enzymes in *B. subtilis* revealed that their septal localisation is dependent on FtsZ in a conditional, IPTG-inducible *ftsZ* mutant. Upon depletion of FtsZ cells fail to divide and grow filamentously. PssA and ClsA lost septal localisation and distributed in random patches dispersed in the membrane indicating that septal localisation is dependent on FtsZ ring formation (Nishibori *et al.*, 2005). Z-ring formation is mediated by a GTPase driven polymerisation of FtsZ. This polymerisation can be inhibited using the small molecule PC190723 that binds to the GTP-binding site of FtsZ and stabilises its monomeric state (Elsen *et al.*, 2012, Haydon *et al.*, 2008). Thereby FtsZ stops polymerising and cells keep growing without division.

The use of PC190723 to study the localisation of PlsY is interesting in two ways. First, it allows the investigation of PlsY localisation in enlarged cells and second, the determination of the role of FtsZ polymerisation in PlsY positioning.

SH1000 *plsY-gfp* was grown as previously described. Overnight cultures were subcultivated in BHI to an $\text{OD}_{600}=0.05$ and grown in the presence of erythromycin (5 $\mu\text{g}/\text{ml}$) and lincomycin (25 $\mu\text{g}/\text{ml}$). Samples were taken before addition of 10 μl of PC190723 stock solution and after incubation for further 30, 60, 90, 120 and 150 min. To indicate septum formation, samples were labelled with 5 μl HADA (100 mM stock solution) for 30 min at 37 °C before fixing and analysis by fluorescence microscopy.

Treatment with PC190723 has no immediate effect on cell-growth using optical density measurements as treated cultures grew identically to the control up to 2 h post addition followed by growth arrest (Fig. 4.51A). Microscopic analysis reveals that cell size enlarges depending on the duration of treatment with PC190723 as the cells enlarge, no septal localisation of PlsY-GFP can be observed as most cells appear to have stopped cell-division (Fig. 4.51C). Some cells appear to attempt cell-division resulting in sandwich-like deformed cells where PlsY-GFP is localised at the presumptive beginning of septum formation (see 3 h treatment). Cells treated for 210 min were excluded from the following analysis since cells did not label with HADA

anymore and many cells lacked any fluorescence of PlsY-GFP suggesting that cells were dying.

PlsY-GFP localisation appears to be more homogeneously distributed in cells treated with PC190723 compared to untreated cells. This was quantified by calculating the coefficient of variation (CV-factor) as described in Section 4.2.3 (Fig. 4.51B and Fig. 4.52).

Quantification of PlsY-GFP localisation dependent on cell-size reveals a significant correlation between PC190723 treated cells and a lower CV-factor ($p < 0.001$ for all treated groups) which indicates a more homogeneous distribution of PlsY-GFP (Fig. 4.51B). However, as cells grow larger, the CV-factor remains at the same low level.

In conclusion, septal localisation of PlsY is dependent on FtsZ-polymerisation. The heterogeneous punctate pattern is lost in cells treated with PC190723 independent of the duration of PC190723 treatment (Fig. 4.51B and Fig. 4.52).

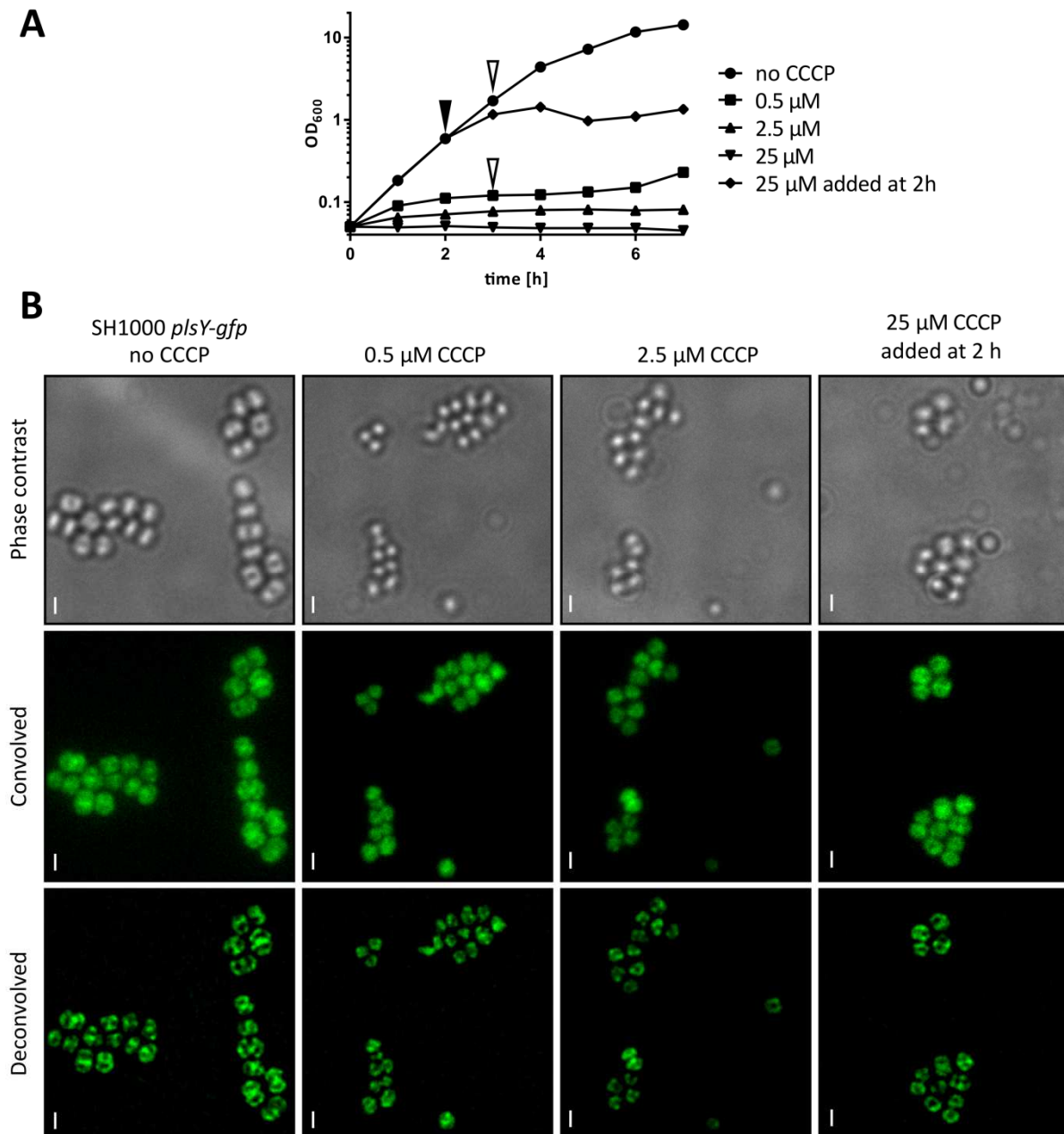


Figure 4.50 Effect of membrane potential inhibition on PlsY-GFP localisation

A, Growth curve of SH1000 *plsY-gfp* grown in the presence of different concentrations of carbonyl cyanide *m*-chlorophenyl hydrazone (CCCP). White arrows indicate sampling points. The black arrow indicates the addition of 25 μM CCCP. **B**, Phase contrast and fluorescence images (convolved and deconvolved) of *S. aureus* SH1000 *plsY-GFP* in the presence of different amounts of CCCP. Images were acquired using a Delta Vision microscope and SoftWoRx 3.5.0 software (Applied Precision). Acquisition of fluorescence images were taken using 2.5 sec exposure in the FITC channel. Scale bars represent 1 μm .

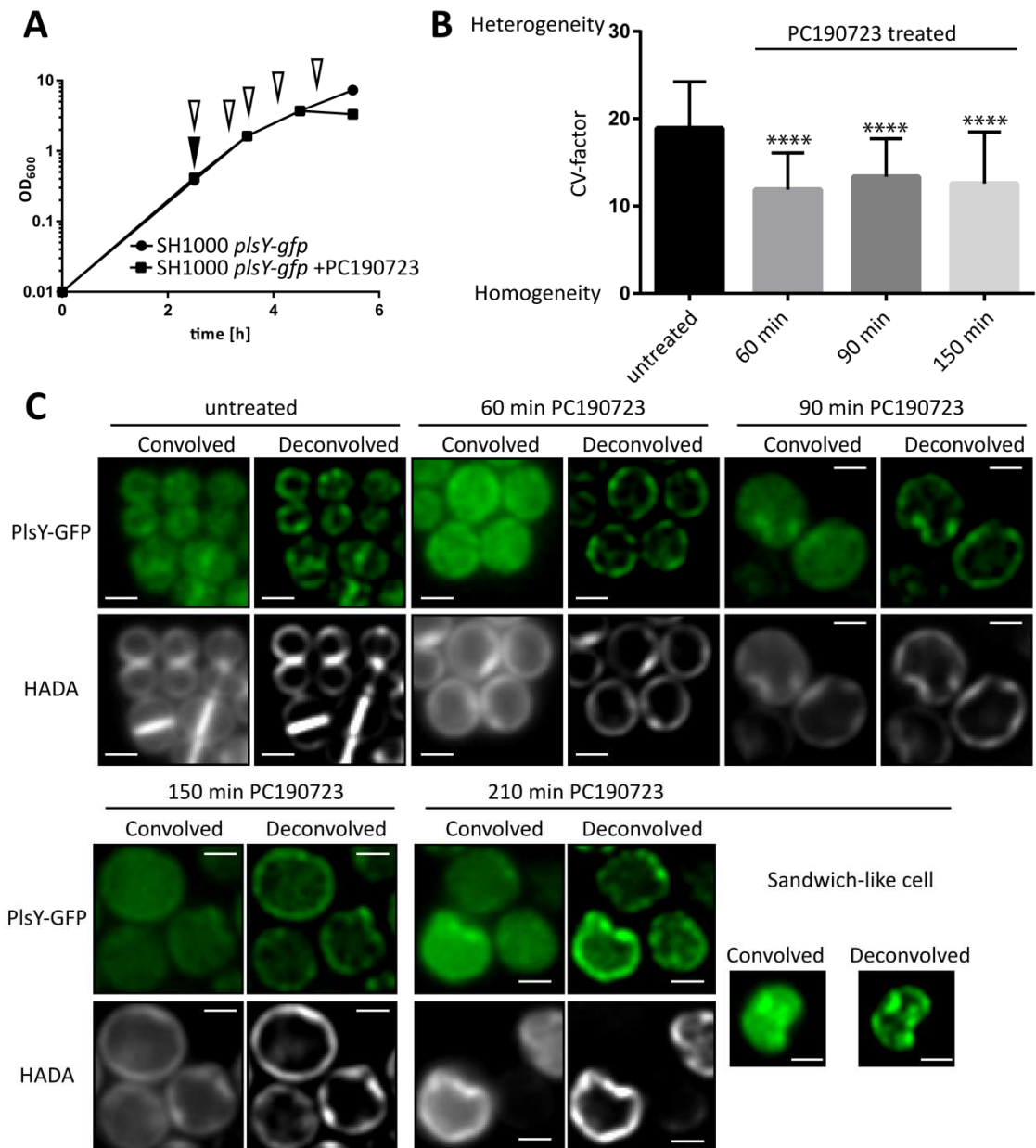


Figure 4.51 Quantification of PlsY-GFP localisation in PC190723 treated cells

A, Growth curves of SH1000 *plsY-gfp*. Black arrow indicates addition of PC190723. White arrows indicate sampling points. **B**, CV-factor calculation of deconvolved images of SH1000 *plsY-gfp* untreated and treated with PC190723 for 60, 90 or 150 min. 40 cells were measured for each group and significance values against the untreated group were calculated using a two-tailed unpaired t test. **C**, Fluorescence images (convolved and deconvolved) of *S. aureus* SH1000 *plsY-gfp* samples treated or untreated with PC190723. Samples were taken before or 60, 90, 150 and 210 min after addition of PC190723 with HADA labelling for the final 30 min. Images were acquired using a Delta Vision microscope and SoftWoRx 3.5.0 software (Applied Precision). Acquisition of fluorescence images were taken using 1 sec exposure in the DAPI channel and 2.5 sec exposure in the FITC channel. Scale bars represent 1 μ m.

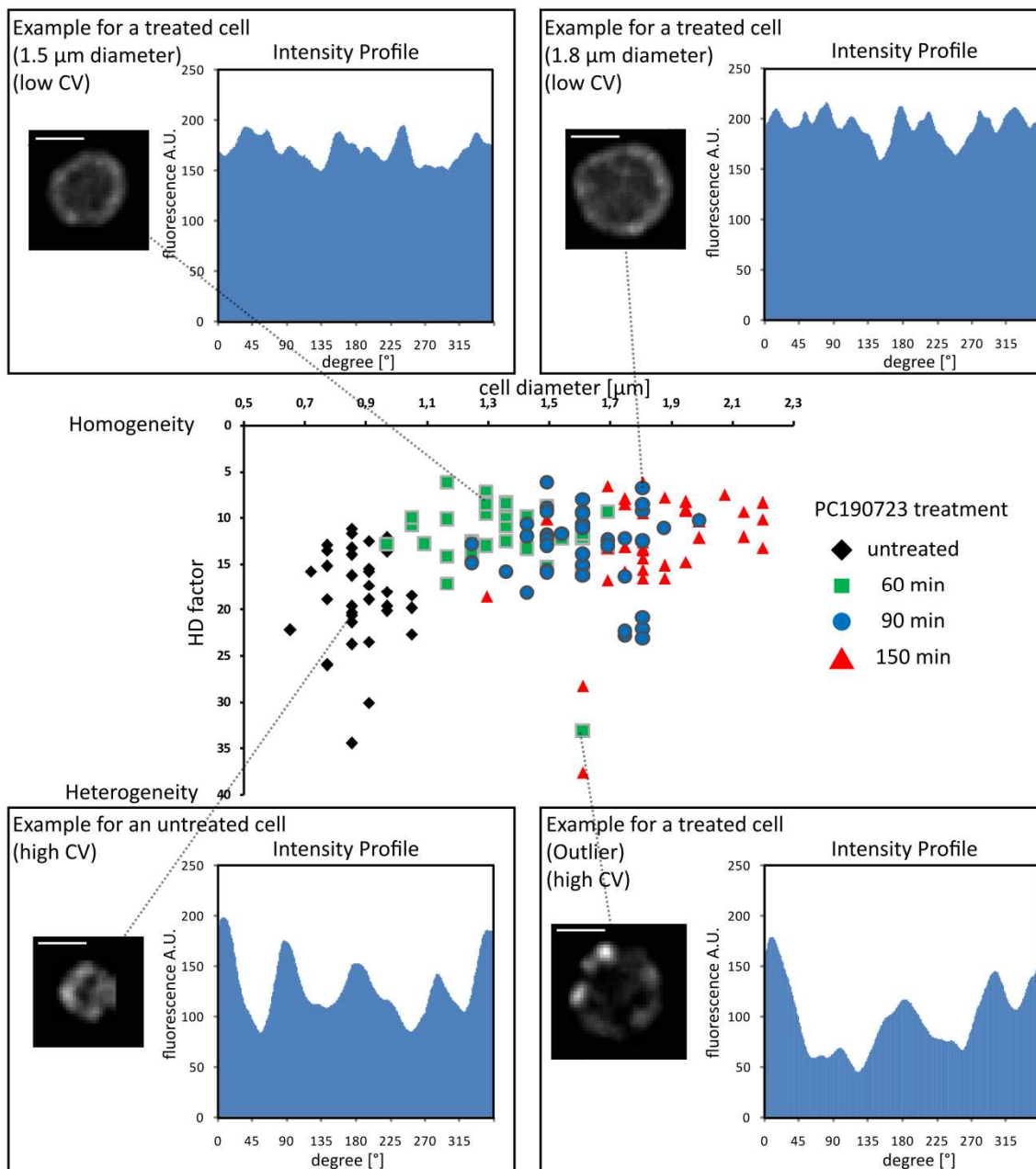


Figure 4.52 Correlation between cell size, PC19072 treatment and coefficient of variation

Fluorescence images (deconvolved) of SH1000 *plsY-gfp* cells untreated (diamonds) or treated with PC190723 for 60 min (green squares), 90 min (blue circles) or 150 min (red triangles) were measured in diameter (X-axis) and CV-factor (Y-axis) and plotted. Each data point represents a single cell. Four cell examples including a deconvolved image and their intensity profile are shown to illustrate the correlation between CV-factor, image and intensity profile.

4.2.5.8 PlsY-GFP localisation in protoplasts

The cell wall is a multifunctional essential component of bacteria. Besides its main function to counteract cell turgor pressure and to act as a physical barrier against exterior factors it is one of the key players in protein localisation. In gram positive cells, many proteins are known to be anchored to peptidoglycan via the LPXTG motif that is recognized by the enzyme sortase A that cleaves off the sorting signal and covalently links the target protein via transpeptidation to the cell wall (Mazmanian *et al.*, 1999). These cell-wall associated proteins include a number of virulence factors such as clumping factor A (McDevitt *et al.*, 1994) fibronectin binding proteins (Flock *et al.*, 1987) iron-regulated surface protein B (IsdB) (Mazmanian *et al.*, 2003) or staphylococcal protein A (DeDent *et al.*, 2007). A variety of proteins possess transmembrane domains or are integral membrane proteins that act on the outside of the membrane at the cell wall. Examples of these proteins are PBPs that are linked to the membrane through a single transmembrane domain but present their enzymatic active domains on the outside of the cell to catalyse the transglycosylation and transpeptidation of peptidoglycan precursors (Zapun *et al.*, 2008).

The question arises as to whether membrane proteins that exhibit a heterogeneous punctate localisation pattern, specifically PlsY, are anchored via extracellular cell-wall associated factors which can be determined by the enzymatic removal of the cell-wall using lysostaphin? To avoid cell lysis of protoplasts due to osmotic pressure, cells were stabilised in a hyperosmotic medium.

SH1000 *plsY-gfp* was subcultured from an over-night culture to an $OD_{600}=0.05$ and grown in BHI medium for 3 h to an $OD_{600}\approx 1.5$. Cells were recovered by centrifugation and resuspended in SMM-BHI medium (50 % BHI (v/v) , 50 % SMM (v/v) (1 M sucrose, 0.04 M maleic acid, 0.04 M $MgCl_2 \times 6 H_2O$, pH 6.5)). The culture was then split into two 500 μ l fractions. One fraction was treated with 5 μ l lysostaphin (5 mg/ml stock solution) for 10 min at RT on a rotary wheel whereas the other fraction was treated the same way without lysostaphin. The generation of protoplasts was monitored by turbidity in 1 % SDS and CFU counts (not shown). 50 μ l of cells were recovered by centrifugation and 100 μ l of a 1 % SDS (w/v) solution was added on top of the pellet. The disappearance of the pellet within 1 min indicated the disruption of protoplasts. Protoplasts were placed on a non-coated slide and analysed by fluorescence microscopy.

Protoplasts could be stabilised using a sucrose rich medium that prevents cell lysis. Cells do not appear to be enlarged compared to non-treated cells due to osmotic pressure showing BHI-SMM medium successfully creates isoosmotic conditions that

maintain cell integrity of protoplasts (Fig. 4.53A). The underlying localisation behaviour of PlsY is not altered in protoplasts (Fig. 4.53AB). PlsY-GFP still localises in patches around the cell periphery. No septal localisation can be seen simply because there are no septa without peptidoglycan in protoplasts (Fig. 4.53AB).

In conclusion, apart from septal localisation, the punctate PlsY-GFP localisation pattern is neither dependent, nor affected by, lysostaphin-mediated removal of the cell wall.

4.2.5.9 Effect of SDS treatment on PlsY-GFP localisation

Previous results indicated so far that PlsY localisation is solely dependent on the membrane and FtsZ polymerisation. Specific non-essential phospholipid species are not required for its proper placement as well as the cell wall. However, the geometry of the membrane could have an impact on the localisation of PlsY. Therefore it was of interest to see whether the disruption of the membrane via detergents alters the localisation of PlsY-GFP.

Sodium dodecyl sulfate (SDS) possesses a long hydrophobic tail combined with a polar head group that imitates phospholipids and integrates into and disrupts the membrane. Cells were treated with SDS up to the the critical micelle concentration of 8 mM.

SH1000 *plsY-gfp* was grown as previously described. A 1 ml sample of exponentially growing cells was harvested, resuspended in PBS supplemented with various concentrations of SDS (0, 0.125, 0.25, 0.5, and 2 mM) and incubated covered in foil for 10 min at RT on a rotary wheel. These cultures were used for CFU counts and the rest were harvested by centrifugation, fixed and prepared for light-microscopy as previously described.

PlsY-GFP localisation in cells treated with SDS is altered in a dose-dependent manner. Instead of its punctate pattern around the cell membrane it is aberrantly localised in one or two patches (Fig. 4.54AB). This occurred dependent on the concentration of SDS (Fig. 4.54AB) whereby the use of >2 mM SDS resulted in an altered localisation pattern of at least 50 % of the cells. It has to be noted, that the signal-to-noise ratio deteriorated which could be explained by protein degradation due to the SDS treatment. CFU counts reveal that changed PlsY-GFP localisation correlates with reduced CFUs meaning that cells with an altered localisation pattern might be dead. Nevertheless, this shows that there was a pattern beforehand that requires an intact membrane. SDS disrupts the membrane and the localisation of PlsY-GFP.

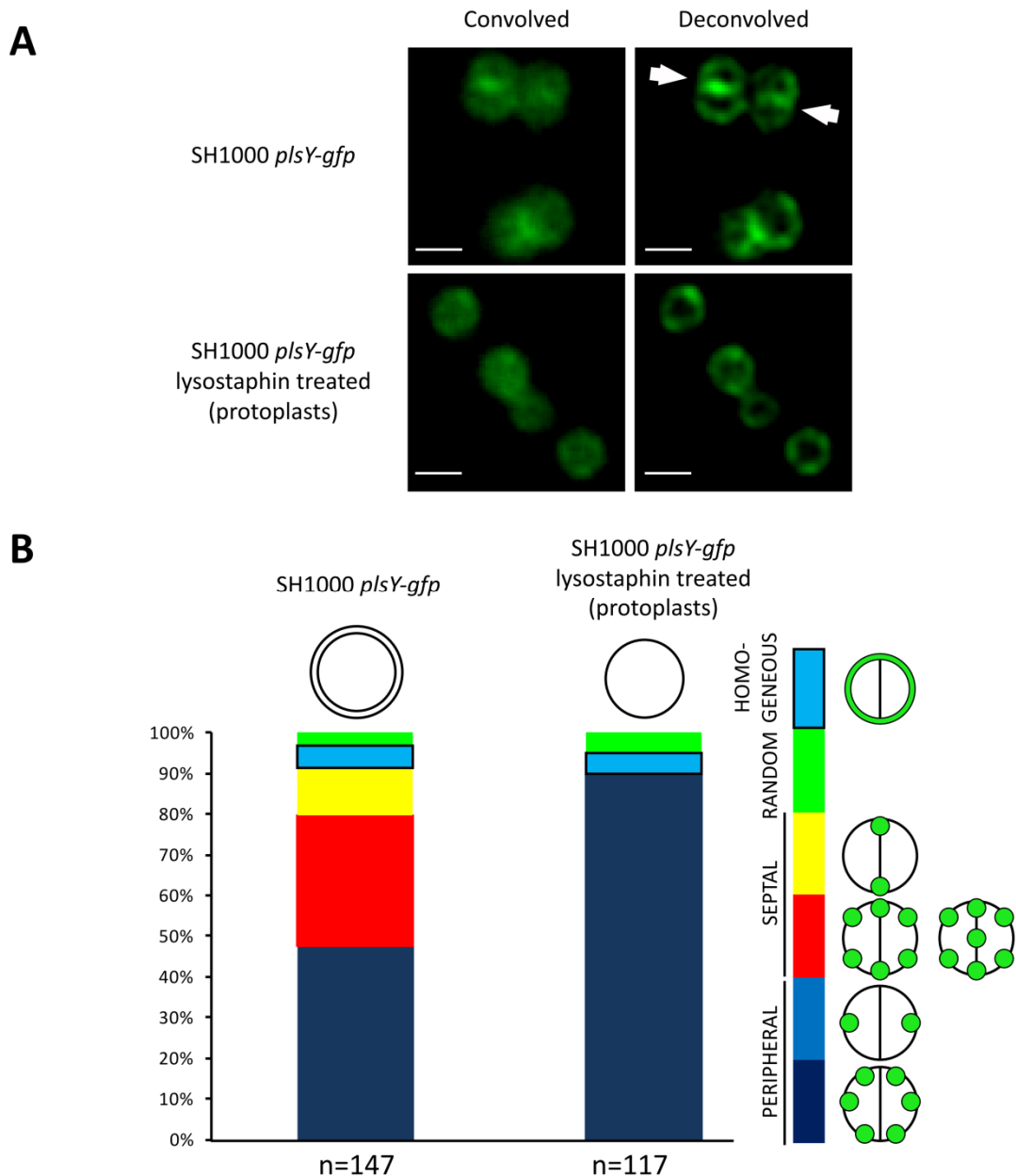


Figure 4.53 Localisation of PlsY-GFP in protoplasts

Phase contrast and fluorescence images (convolved and deconvolved) of *S. aureus* SH1000 *plsY-gfp* samples treated or untreated with lysostaphin stabilised in a sucrose-rich medium. Images were acquired using a Delta Vision microscope and SoftWoRx 3.5.0 software (Applied Precision). Acquisition of fluorescence images were taken using 2.5 sec exposure in the FITC channel. **A**, Scale bars represent 1 μm . **B**, Cell counts categorized depending on PlsY-GFP. Value n indicates counted cells for each group. Red and yellow bars indicate septal and blue bars indicate peripheral PlsY-GFP localisation. The green coloured bar indicates random or homogeneous PlsY-GFP localisation and the black frames blue bar indicates a peripheral homogeneous distribution.

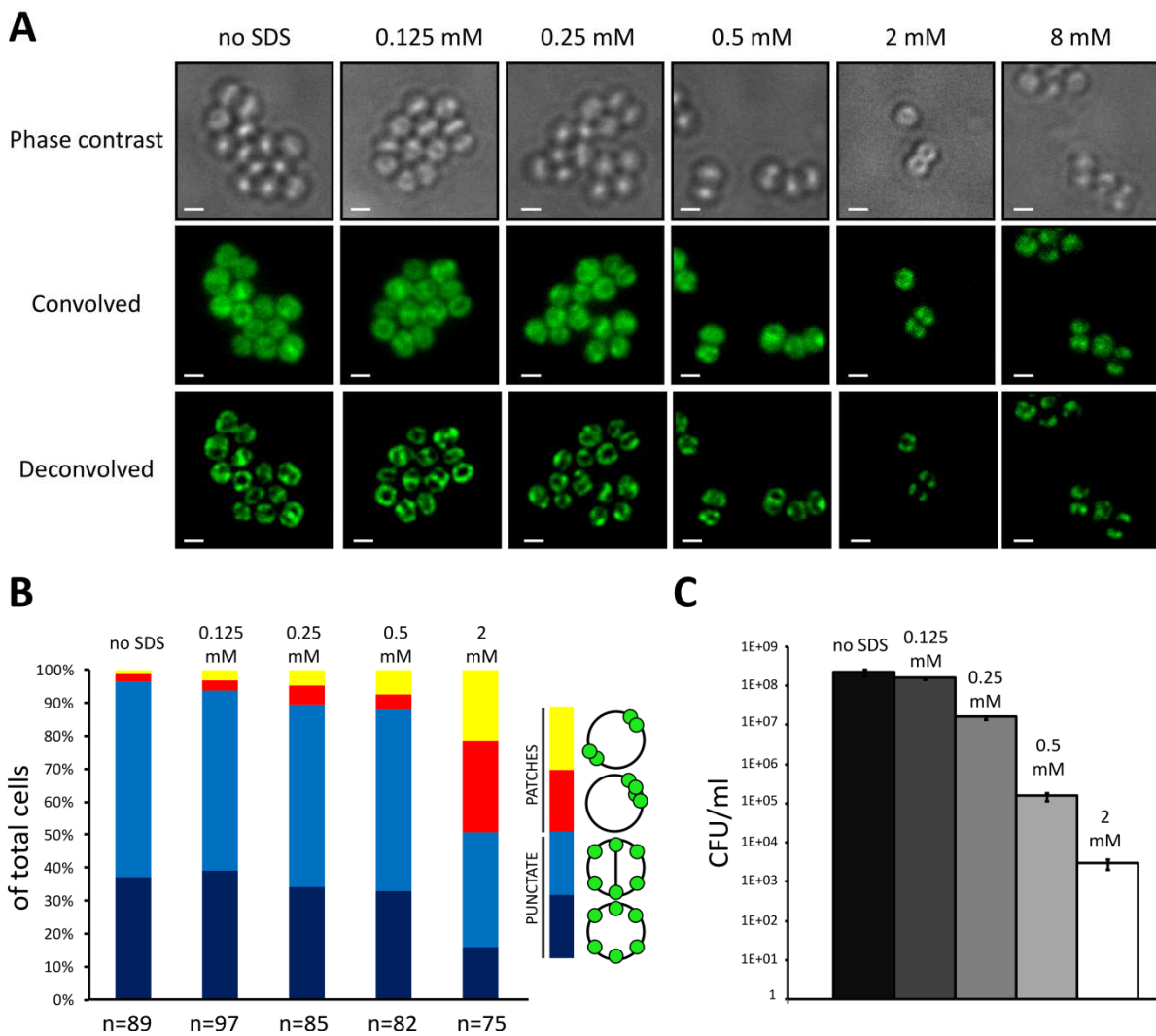


Figure 4.54 Effect of SDS on PlsY-GFP localisation

A, Phase contrast and fluorescence images (convolved and deconvolved) of *S. aureus* SH1000 *plsY-gfp* samples treated with different SDS concentrations. Images were acquired using a Delta Vision microscope and SoftWoRx 3.5.0 software (Applied Precision). Acquisition of fluorescence images were taken using 2.5 sec exposure in the FITC channel. Scale bars represent 1 μ m. **B**, Cell counts of PlsY-GFP localisation categorized in 4 groups. Red and yellow bars indicate localisation of PlsY-GFP in one or two patches in the membrane. Blue bars indicate PlsY-GFP localisation in a punctate heterogeneous pattern and at the septum in dividing cells. N indicates number of cells counted for each group. **C**, CFU counts for cultures treated with different SDS concentrations in PBS for 10 min. Cultures were plated on BHI agar and incubated at 37 $^{\circ}$ C for 24 h.

4.3 Discussion

4.3.1 Localisation of PlsY in *S. aureus*

In *B. subtilis*, the phospholipid synthesis enzyme YneS (PlsY) was found to localise at the cell periphery and at the cell-division site (Hunt *et al.*, 2006). PlsY in *S. aureus* is strongly associated with the septum as well as the cell-periphery in a heterogeneous punctate pattern during cell-division. Non-dividing cells exhibit an even clearer punctate distribution of PlsY. This localisation pattern suggests a manifold role of PlsY. The cell-division protein EzrA was found at unexpected division planes in the absence of PlsY in a conditional knockout strain (Garcia-Lara *et al.*, 2015) giving the first evidence for a role of PlsY in cell-division and the link between phospholipid synthesis and the divisome in *S. aureus*.

Interestingly, localisation studies in *B. subtilis* on PlsX, an enzyme that catalyses the first step in phospholipid synthesis, revealed a heterogeneous punctate distribution of PlsX (Takada *et al.*, 2014). PlsX was also shown to interact with various cell-division associated proteins such as the FtsZ-anchoring protein FtsA and EzrA or cytoskeletal proteins such as MreB. Further studies focused on its role on cell-division showed that PlsX localises to potential cell-division sites and affects the Z-ring formation which again indicates a connection between phospholipid synthesis and cell-division.

PlsY might very likely be involved in a similar role together with PlsX and mark future cell-division sites. The absence or misplacement of these ‘road signs’ might then lead the divisome to the wrong place resulting in misplaced septa. The big questions however remain unsolved: Which protein arrives first and how do they know where to go? It seems unlikely that PlsY is the first to arrive and be the key to position Z-ring formation, since its overexpression did not affect cell viability and cell-division (Fig. 4.4B). Additionally, cells lacking MreD exhibit aberrant cell morphologies along with the delocalisation of PlsY (Garcia Lara *et al.*, 2015). This might indicate a role of MreD further up the line of command than PlsY in the organisation of a punctate protein localisation pattern in the membrane

4.3.2 FtsZ dependent localisation of PlsY

Phospholipid synthesis enzymes in *B. subtilis* are localised at the septum (Nishibori *et al.*, 2005). This localisation was shown to be FtsZ dependent, as the depletion of FtsZ in a conditional mutant resulted in the loss of septal localisation of Pss and ClsA. Both

proteins dispersed in random patches in the peripheral membrane (Nishibori *et al.*, 2005).

In contrast to *B. subtilis*, phospholipid synthesis enzymes in *S. aureus* are not solely septally localised but also exhibit a punctate pattern throughout the membrane. The septal localisation of PlsY-GFP is lost in cells with non-polymerising FtsZ as shown by a homogeneous distribution of PlsY-GFP. The depletion of FtsZ in *B. subtilis* causes filamentous growth since Z-ring formation is impeded. It might be that phospholipid synthesis enzymes are then localised by a second cell-division associated protein or mechanism that is not present in *S. aureus*.

In respect to *S. aureus*, this potentially reveals two localisation mechanisms. The first one is the positioning to the cell-division site that is dependent on FtsZ and peptidoglycan as shown with localisation studies in protoplasts (Fig. 4.53AB and Fig. 4.51) and the second one is based on the ability of FtsZ to polymerise which is required for the heterogeneous distribution of PlsY-GFP (Fig. 4.51 and Fig. 4.52). Importantly, the heterogeneous distribution is independent on the cell size since the duration of FtsZ-polymerisation inhibition which is correlated to the cell size does not affect the localisation of PlsY (Fig. 4.52). Additionally, PlsY localisation in a strain lacking WTAs which also results in larger cells was unaffected (Fig. 4.47).

4.3.3 The role of lipid domains in the localisation of membrane proteins

PlsY is an essential part of phospholipid synthesis by linking fatty acids to glycerol-3-phosphate. It is thought that phospholipid synthesis mainly takes place the septum since all phospholipid synthesis enzymes in *B. subtilis* like ClsA, CdsA, Psd, MprF and YhdO (PlsC) were found to go to the septum (Nishibori *et al.*, 2005). However, only CL and PE are localised to the septum or cell poles in rod-shaped bacteria whereas PG is found at the septum and cell periphery. The mechanism whereby certain lipids (CL and PE) are being kept from diffusing to the cell periphery whereas PG is free to go remains unclear. The distinct localisation of CL and PE led to the assumption that these lipid domains are required for the localisation of polar and septal membrane proteins. This was found for the osmosensory ProP in *E. coli* that failed to localise to the cell poles in a CL deletion mutant (Mileykovskaya, 2007, Romantsov *et al.*, 2007). In *S. aureus* it is only possible to delete CL and LPG since other lipids are required for cell viability (Martin *et al.*, 1999). Both lipids were shown not be required for the septal or peripheral

localisation of PlsY (Fig. 4.42, Fig. 4.44 and Fig. 4.55) leaving only PG as a phospholipid as a localisation cue for PlsY. Furthermore, the deletion of *tarO*, resulting in the loss of wall teichoic acids, increases the septal localisation of PlsY-GFP in cells beginning the septum formation but only slightly increased the heterogeneous localisation pattern of PlsY-GFP (Fig. 4.55). The role of lipoteichoic acids in the placement of PlsY was not studied since its deletion is lethal.

FM dyes stain negatively charged lipids such as CL and PG (Brumback *et al.*, 2004) and revealed a striking helical pattern in *B. subtilis* (Barak *et al.*, 2008). It was suggested that this pattern is dependent on the synthesis of peptidoglycan and its insertion directed by MreB (Daniel & Errington, 2003, Wang *et al.*, 2012). Other proteins like MinD or SecA were shown to colocalise with the helical arrangement stained by FM dyes (Barak *et al.*, 2008, Campo *et al.*, 2004). Importantly, this pattern was lost in protoplasts and cells depleted of MurG, providing strong evidence for a link between peptidoglycan and lipid organisation (Muchova *et al.*, 2011). PlsY localisation however, was not affected in protoplasts suggesting that PG/CL are not specifically required for the placement of PlsY (Fig. 4.53). Yet, SDS treated cells exhibit a changed PlsY localisation where the original punctate pattern is disrupted and PlsY localises to one or two dots per cell (Fig. 4.54). This points out that while specific lipids might not be required, the membrane integrity as a whole is crucial for the positioning of PlsY.

4.3.4 Dose-dependent localisation of membrane proteins

One of the most studied and most controversial localisation of a bacterial protein is MreB. It has been shown in several publications that MreB localises in a helical pattern throughout the the whole cell and thereby navigates a number of proteins including components of the cell division synthesis apparatus (Shih *et al.*, 2005, Vats & Rothfield, 2007, Vats *et al.*, 2009, Wang *et al.*, 2012). It turned out that the helical pattern was due to the YFP tag and overexpressed MreB (Swulius *et al.*, 2011, Garner *et al.*, 2011, Dominguez-Escobar *et al.*, 2011). This example shows that protein localisation studies have to be carefully examined.

Localisation of wild type levels of PlsY has been validated thoroughly using a variety of localisation methods including different fluorescent protein fusions (GFP, eYFP) (Fig. 4.3 and Fig. 4.7), a monomeric eYFP version (Fig. 4.8), SNAP tag (Fig. 4.32) and immunofluorescence microscopy (Garcia-Lara *et al.*, 2015).

However, two proteins in this study, PlsY and SecY, showed varying localisation patterns depending on their expression levels (Fig. 4.4 and comparing Fig. 4.23 with

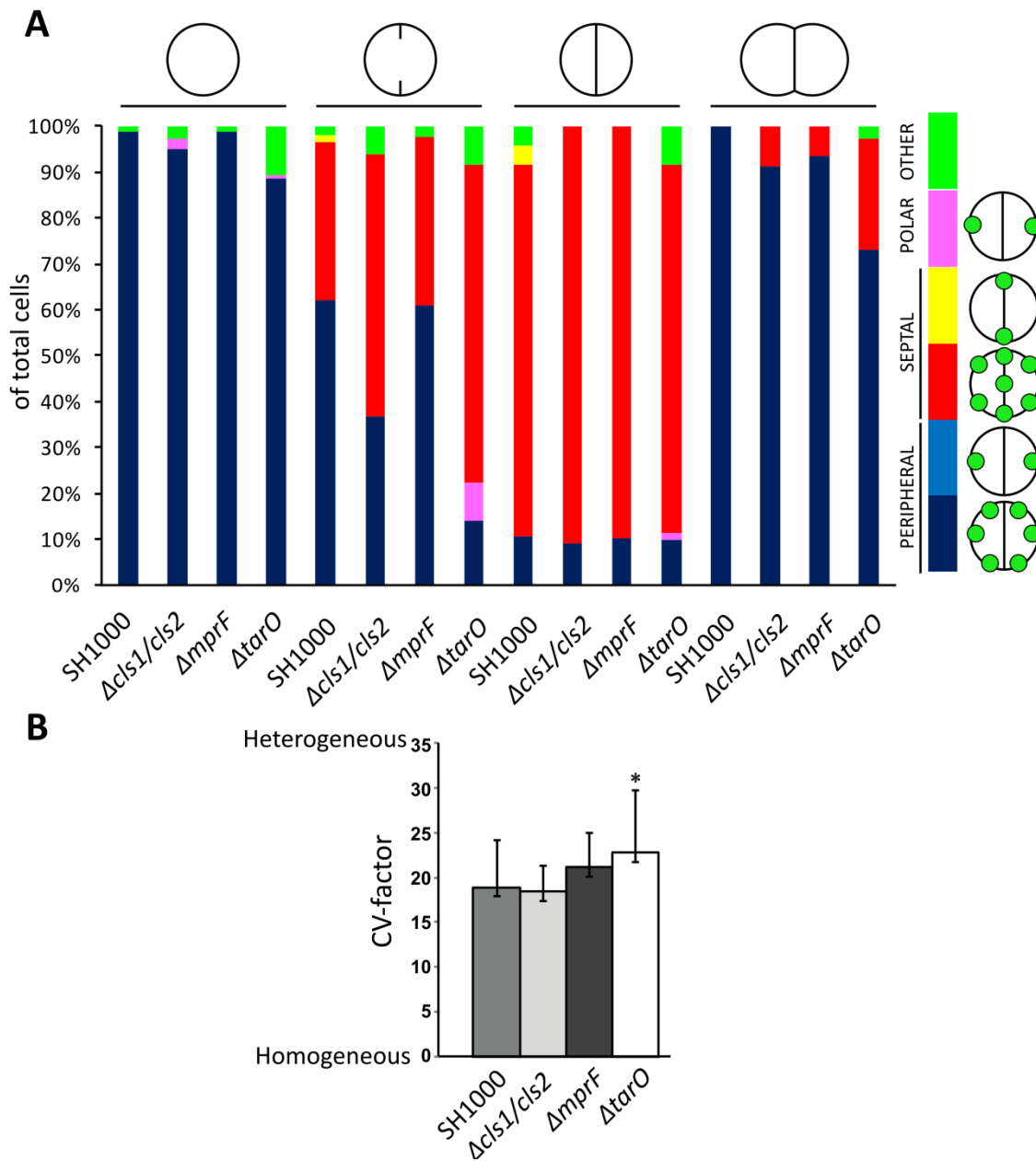


Figure 4.55 Summary of the effect of cardiolipin and lysinylated phosphatidylglycerolphosphate on the localisation of PlsY

A, Cell counts categorized depending on PlsY-GFP localisation in SH1000, SH1000 $\Delta cls1/2$ and SH1000 $\Delta mprF$ dependent on the cell-cycle stage indicated by HADA labelling. Red and yellow bars indicate septal and blue bars indicate peripheral PlsY-GFP localisation. The green coloured bar indicates random PlsY-GFP localisation. Data was taken from Fig. 4.1, Fig. 4.42 and Fig. 4.44. **B**, CV-factor calculation of 20 cells of deconvolved images of PlsY-GFP in SH1000, SH1000 $\Delta cls1/cls2$, SH1000 $\Delta mprF$ and SH1000 $\Delta tarO$. Significance values against SH1000 were calculated using a two-tailed unpaired student's ttest.

4.27F). PlsY is localised in a heterogeneous fashion at wild type levels but distributes homogeneously when overexpressed on a plasmid (Fig. 4.4). A higher number of PlsY molecules might lead to a higher number of dots that are eventually not distinguishable using fluorescence based microscopy limited by light-diffraction. SecY on the other hand, is localised throughout the whole membrane but appeared to form a dot like distribution expressed from an IPTG-inducible plasmid after a short IPTG induction (Fig. 4.27F). This potentially resulted in a lower expression level compared to its wild type level. The cell might use the regulation of membrane protein expression levels as a mechanism to regulate protein localisation and thereby their activity and function.

4.3.5 Subcellular localisation of other membrane proteins

The localisation of a number of proteins were analysed in this study. First and foremost, membrane proteins tend to distribute heterogeneously in random patches. Proteins involved in phospholipid synthesis appear to be colocalised with PlsY whereas others are positioned in a similar fashion but do not localise at the same spots as PlsY. Another important localisation marker is whether a protein is going to the septum indicating a possible role in cell-division.

Proteins found to be septally localised were enzymes involved in phospholipid synthesis such as PlsY, CdsA, PgsA, MprF, PlsC and Cls2 (Fig. 4.7 and Fig. 4.13-Fig. 4.16). Their septal localisation suggests that phospholipid synthesis in *S. aureus* mainly takes place at the septum. However, all these proteins were also shown to additionally localise at the cell-periphery in a punctate pattern, potentially demonstrating that phospholipid synthesis also takes place at the cell periphery or that these proteins have a second so far unknown role. MreD was recently shown to affect localisation of PlsY and showed a weak interaction with PlsY using BACTH (Garcia-Lara *et al.*, 2015).

Some proteins such as the phenylalanine transporter PheP and the lipoprotein signal peptidase LspA also exhibit a septal localisation in the majority of dividing cells (Fig. 4.28). Both proteins do not seem to share roles with PlsY as LspA is involved in the maturation of lipoproteins (Zhao & Wu, 1992) and PheP is an amino acid transporter PheP (Horsburgh *et al.*, 2004). However, it remains unclear whether lipoprotein maturation takes place at the septum suggesting that lipoproteins are integrated into the membrane during septation along with the synthesis of peptidoglycan and phospholipids. The role of phenylalanine transport at the septum remains unclear. Proteins SecY, MscL and CydB only show septal localisation in a minority of cells, mainly during early cell-division (Fig. 4.28). These counts however, might be due to the

limited resolution and localisation patches could have been near the septum start and misinterpreted as septum associated localisation. Homogeneous non-septal localisation of SecY has been described for *E. coli* (Brandon *et al.*, 2003) and *B. subtilis* (Matsumoto *et al.*, 2015) and this study in *S. aureus* confirms these findings suggesting that secretion seems to be a process required throughout the cell membrane but not at the septum (Fig. 4.23). The large mechanosensitive channel (MscL) is responsible for turgor regulation upon activation by osmotic pressure (Perozo & Rees, 2003, Sukharev *et al.*, 1994). MscL needs to be exposed to external pressure rather than pressure induced by the daughter cell during septation which could lead to an unwanted induction during cell-division. Therefore, it makes sense to find MscL at the cell-periphery rather than at the septum. It would be of interest to investigate whether MscL is naturally localised in a punctate or homogeneous pattern since a homogeneous distribution would be favourable to sense the overall pressure on the cell surface.

Cytochrome BD subunit II CydB was found to be localised in patches mainly at the cell-periphery (Fig. 4.18, Fig. 4.27C and Fig. 4.28). This is consistent with findings in *E. coli* describing CydB to be concentrated in mobile domains (Lenn *et al.*, 2008b). Other studies on respiratory proteins such as the succinate dehydrogenase (SDH) and ATP synthase in *B. subtilis* or the SDH and the NADPH dehydrogenase in *Synechococcus elongatus* revealed a localisation pattern in discrete spots in the membrane (Johnson *et al.*, 2004, Liu *et al.*, 2012).

Lenn *et al.*, hypothesised the formation of so-called ‘respirazones’ that concentrate respiration components in specialised microdomains. Respirazones would allow the cell to optimise the efficiency of electron and proton circuits resulting in a higher output of ATP for the cell and reduction of oxidative stress (Lenn *et al.*, 2008a). Finding CydB to exhibit a similar distribution pattern in the membrane of *S. aureus* is a first indicator for the existence of respirazones in *S. aureus*.

4.3.6 Conclusion

Membrane proteins in *S. aureus* tend to form punctate patterns at the cell periphery. Phospholipid biosynthetic enzymes also exhibit a septal localisation providing evidence for a link between lipid synthesis and cell-division. Interestingly, no specific membrane or cell wall components such as cardiolipin, LPG or WTAs are required for the localisation of PlsY. However, level of PlsY and FtsZ-polymerisation are crucial for the pattern formation.

4.4 Main findings in this chapters

- The phospholipid synthesis enzyme PlsY is localised in a heterogeneous punctate pattern at the cell periphery and at the septum during cell-division as shown with an eYFP, a GFP and a SNAP fusion with PlsY.
- Most investigated membrane proteins also exhibit a punctate localisation pattern using native expression levels including phospholipid synthesis enzymes PgsA, PlsC, MprF, Cls2, the eukaryotic lipid raft marker, FloT and the respiratory protein CydB.
- The secretion protein SecY is homogeneously distributed in the membrane.
- The localisation of PlsY and SecY are dose-dependent.
- The localisation of PlsY is independent of lys-PG, cardiolipin, WTAs, membrane potential, is not disturbed by fatty acid synthesis inhibition and does not require peptidoglycan.
- Inhibition of FtsZ polymerisation redistributes PlsY.
- Cells treated with SDS exhibit an altered PlsY localisation.

4.5 Contributions

I performed all experiments in this chapter with the exception of the NanoJ-SRRF analysis shown in Fig. 4.2, which was carried out by Dr. Sian Culley (University College London).

Chapter 5: Membrane protein interaction studies in *S. aureus*

5.1 Introduction

5.1.1 Protein-interaction analysis methods in bacteria

Cellular functions rely on the interplay between proteins. To understand what role a specific protein plays, it is crucial to consider its place within its local environment since most biological processes are executed by groups of proteins rather than a single protein. The discovery of genetically encoded fluorophores has enabled the study of the localisation of a wide range of proteins. However, due to the diffraction limit, it is not possible to conclude the colocalisation at the molecular level or interactions between proteins which requires the application of resolution-independent or indirect methods. Relatively few bacteria have been comprehensively studied for protein-protein interactions. Most of these interactions have never been verified by a second method and therefore have to be considered of potentially limited biological relevance.

There are two main approaches for protein-interaction studies: complementation assays such as yeast 2-hybrid and bacterial 2-hybrid and immunoprecipitation based methods. The yeast 2-hybrid assay was first shown by Fields and Song in 1989 and relies on the reconstitution properties of the transcription regulator GAL4 from *Saccharomyces cerevisiae* (Fields & Song, 1989). The DNA binding domain and the activation domain of GAL4 can be fused separately to proteins of interest. If both proteins interact with each other, both GAL4 domains are reconstituted and enable the expression of reporter genes. Yeast 2-hybrid has been used early to identify interactions between cell-division proteins in various bacteria (Wang *et al.*, 1997, Yan *et al.*, 2000, Din *et al.*, 1998, Liu *et al.*, 1999). However, heterologous host interaction studies of bacterial proteins in yeast might be inaccurate and Y2H is known to produce a high number of false positive results since many proteins were demonstrated to induce GAL4 without an interaction with the activation domain. It even has been estimated that 50 % of all Y2H results are unreliable (Deane *et al.*, 2002). These major flaws were resolved with the introduction of the bacterial adenylate cyclase two hybrid system (BACTH). BACTH facilitates a similar mechanism as Y2H by restoring the activity of two domains of the *Bordetella pertussis* adenylate cyclase to proteins of interest in an adenylate cyclase negative (*cyA*⁻) strain of *E. coli* (Karimova *et al.*, 1998). A positive interaction activates the adenylate cyclase to convert ATP to cAMP. cAMP triggers the transcriptional activation of the *lac* operon containing *lacZ*. Expression of *lacZ* results in the hydrolysis of X-Gal to galactose and 5-bromo-4-chloro-3-hydroxyindole. The

latter product exhibits an intense blue colour that can be detected as an indicator for positive protein-protein-interaction. Unlike Y2H, the transcriptional activation of a reporter gene is uncoupled from the protein-protein-interaction and thus allows the investigation of membrane and as well as cytoplasmic proteins and produces less false positive results. BACTH has been used intensively to study protein interactions of cell-division proteins in many bacteria. In *S. aureus* BACTH was used to map the interactome between cell-division related proteins (Steele *et al.*, 2011) and showed the interaction between Fem proteins involved in peptidoglycan synthesis (Rohrer & Berger-Bachi, 2003). Another study used BACTH to demonstrate that RNases in *S. aureus* form a protein complex termed the 'Degradosome' (Roux *et al.*, 2011). Although being superior to Y2H in the analysis of bacterial proteins, BACTH exhibits many problems that can cause false-negative and false-positive results. Proteins fused to the adenylate cyclase domains may not be folded properly which might be especially problematic for multimerising proteins for their interaction properties. Also, both studied proteins might never be expressed together or their interaction is dependent on a third protein or condition that is not present in *E. coli*. Y2H and BACTH are easy to carry out and allow the screening for possible interaction partners with a protein of interest or even the generation of an entire interactome. However, due to a variety of problems, positive interactions have to be confirmed by another method such as co-purification via an affinity tag. Immunoprecipitation relies on the pull-down of protein complexes using an antibody that binds the native protein of interest or a protein translationally fused to an affinity tag. Pulled-down proteins can be then identified by Western blot or mass spectrometry. Co-immunoprecipitation was used to show protein interactions between components of the type 3 secretion system of *Pseudomonas aeruginosa* by enhancing the cytoplasmic secretion regulator PcrG with an affinity tag that was used for a pull-down assay (Lee *et al.*, 2010). Furthermore, this method demonstrated interactions within the Z-ring of FtsZ with FtsW and ClpX in *M. tuberculosis* and between penicillin binding proteins in *Caulobacter crescentus* (Datta *et al.*, 2002, Sureka *et al.*, 2010, Figge *et al.*, 2004). Although Co-IP is a reliable method to show protein complexes it misses the detection of weak or transient interactions.

A series of other approaches have been used to reveal protein-protein-interactions such as Plasmon Surface Resonance (Ishino *et al.*) which is based on the changing refractive index of a medium on a gold film with absorbed proteins in response to interactions with added proteins (Patching, 2014). Moreover, phage display and affinity gel electrophoresis were successfully applied to study protein interactions. An overview of commonly applied protein-protein interaction methods in bacteria is listed in Table 5.1.

Table 5.1 Protein-protein interaction methods

	Protein-protein interaction method	Advantages and Disadvantages	First described in and application examples
Complementation assays	Yeast-2-Hybrid (Y2H)	<ul style="list-style-type: none"> ▪ easy to carry out ▪ high number of false positives, ▪ fusions are hybrids ▪ requires overexpression ▪ heterologous host 	(Fields & Song, 1989)(first described) (Chien <i>et al.</i> , 1991, Wang <i>et al.</i> , 1997) (Yan <i>et al.</i> , 2000, Din <i>et al.</i> , 1998, Liu <i>et al.</i> , 1999)
	Bacterial adenylate cyclase two-hybrid system (BACTH)	<ul style="list-style-type: none"> ▪ easy to carry out ▪ high number of false positives ▪ fusions are hybrids, ▪ non native environment if not <i>E. coli</i> ▪ requires overexpression 	(Karimova <i>et al.</i> , 1998) (first described)(Claessen <i>et al.</i> , 2008, Daniel <i>et al.</i> , 2006, Datta <i>et al.</i> , 2006, Ebersbach <i>et al.</i> , 2008, Fraipont <i>et al.</i> , 2011, Galli & Gerdes, 2010, Karimova <i>et al.</i> , 2005, Marbouty <i>et al.</i> , 2009, Mazouni <i>et al.</i> , 2004, Muller <i>et al.</i> , 2007, Patrick & Kearns, 2008)
	Bimolecular fluorescence/luminescence complementation (BiFC/BiLC)	<ul style="list-style-type: none"> ▪ <i>in vivo</i> ▪ native environment 	(Ghosh <i>et al.</i> , 2000) (first described)(Morell <i>et al.</i> , 2008)
Spectroscopic analysis	Surface Plasmon resonance	<ul style="list-style-type: none"> ▪ low-throughput ▪ requires purified proteins ▪ non-native environment 	(Liedberg <i>et al.</i> , 1995) (first described)(Bertsche <i>et al.</i> , 2006)
Biochemical approaches	Farwestern	<ul style="list-style-type: none"> ▪ requires purified proteins ▪ proteins are denatured ▪ non-native environment 	(Reddy & Kumar, 2000, Sato <i>et al.</i> , 2011)
	Phage display	<ul style="list-style-type: none"> ▪ Non-native environment 	(Smith, 1985) (first described)(Rosander <i>et al.</i> , 2002, Wall <i>et al.</i> , 2003)
	Affinity purification	<ul style="list-style-type: none"> ▪ potential protein degradation or modification during sample preparation, ▪ results dependent on antibody binding efficiency ▪ nonspecific binding to beads 	(Bertsche <i>et al.</i> , 2006, Corbin <i>et al.</i> , 2007, de Leeuw <i>et al.</i> , 1999, Espeli <i>et al.</i> , 2003, Buddelmeijer & Beckwith, 2004, Noirclerc-Savoie <i>et al.</i> , 2005, Butland <i>et al.</i> , 2005)
Fluorescence-based measurements	FRET/FRAP/FLIM	<ul style="list-style-type: none"> ▪ real-time analysis of dynamic processes ▪ capable of detecting transient interactions ▪ low sensitivity ▪ native environment ▪ extremely sensitive to small distance changes 	(Forster, 2012)(first described)(Sourjik <i>et al.</i> , 2007, Berg <i>et al.</i> , 2013, Hu & Lutkenhaus, 1999, Okuno <i>et al.</i> , 2009, Shen & Lutkenhaus, 2010, Szeto <i>et al.</i> , 2001, Fraipont <i>et al.</i> , 2011, Broussard <i>et al.</i> , 2013)

5.1.2 Förster Resonance Energy Transfer

The Förster-resonance energy transfer is a non-radiative energy transfer between two light-sensitive molecules. A well known example of FRET in nature is seen in photosynthesis. Light-harvesting complexes focus energy by a gradual transfer of energy of carotenoids to phycobiline to Chlorophyll b and a (van Thor & Hellingwerf, 2002). Energy is only transferred upon excitation of a donor fluorophore if its emission spectrum overlaps with the excitation spectrum of an acceptor fluorophore (see Fig. 5.1).

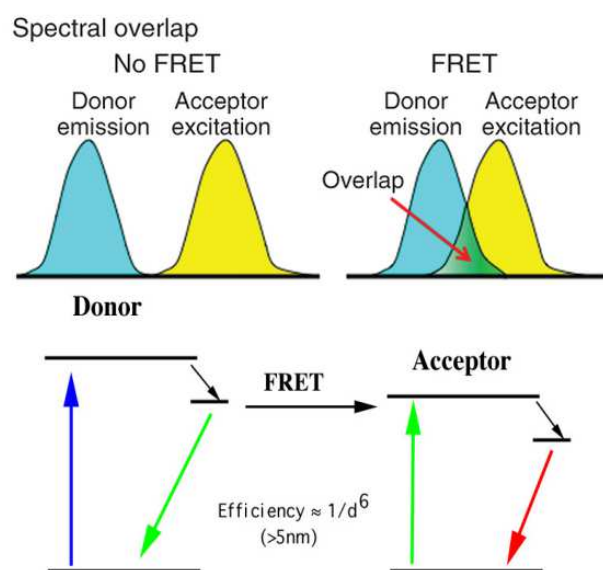


Figure 5.1 Schematic overview of FRET

A, FRET only occurs if the emission spectrum of a donor fluorophore overlaps with the excitation spectrum of an acceptor fluorophore. Image is taken from (Broussard et al., 2013). **B**, FRET itself describes the transfer of energy from an excited state of the donor to the ground state of the acceptor fluorophore. Image is taken from <https://de.wikipedia.org/wiki/Förster-Resonanzenergietransfer>.

Since the efficiency of FRET is inversely proportional to the sixth power of the distance between donor and acceptor, it makes it a powerful tool to investigate small changes in distance between 1 and 10 nm of fluorophores (Stryer, 1978). Thus, the fusion of appropriate fluorophores to molecules of interest allows making conclusions on their potential colocalisation and interaction (Harris, 2010).

FRET based interaction systems are the leading approach to study protein interactions *in vivo*, for instance to investigate the interaction between the chemotaxis

response regulator CheY and its phosphatase CheZ in *E. coli* which later led to the first interactome revealed by FRET (Sourjik *et al.*, 2007, Vaknin & Berg, 2004, Sourjik & Berg, 2002). FRET has also been applied to study the redox state by using genetically modified fused fluorescent proteins that carry reactive cysteine residues. The cysteine residues form a disulfide bond in an oxidised state which brings both fluorophores closer to each other and thereby increases the FRET efficiency (Abraham *et al.*, 2014).

FRET also provided the experimental framework to reveal protein interactions within the divisome and peptidoglycan synthesis enzymes in *E. coli*. Van der Ploeg *et al.*, revealed the interaction between MreB with other cytoskeletal proteins such as RodZ and RodA together with the peptidoglycan synthesis enzyme PBP2. These interactions were abolished using the MreB polymerization inhibitor A22 (van der Ploeg *et al.*, 2015). A FRET system using near endogenous levels of the investigated proteins unveiled the interaction of FtsZ with itself and ZapA. Additionally it allowed the study of the interaction between various other Z-ring associated proteins such as FtsN, FtsI, FtsW and FtsQ (Alexeeva *et al.*, 2010). Furthermore, this system could show the interaction of PBP2 with PBP3 at the cell division site (van der Ploeg *et al.*, 2013). Other studies involved the design of biosensors to screen colonies for calcium uptake or the validation of protein interactions between magnetosome associated proteins in magnetotactic bacteria (Litzlbauer *et al.*, 2015, Carillo *et al.*, 2013).

5.1.3 Measurement techniques

Since FRET is a non-radiative process, it is not possible to directly detect and quantify FRET. However, FRET affects the emission intensity of acceptor and donor as well as the lifetime of the donor fluorophore which can be measured with the appropriate instruments.

5.1.3.1 Sensitized emission

FRET results in a decreased donor emission and increased acceptor due to the energy transfer from the donor to the acceptor (Clegg, 2009). Thus, FRET efficiency can be inferred from the variation of emission intensities since excitation of the donor also results in excitation of the acceptor which is known as sensitized FRET. However, an issue can be an emission crosstalk leading to a direct excitation of the acceptor. This effect can be corrected by acquisition of fluorescence images of samples with donor-only, acceptor-only or both fluorophores using different filter settings.

5.1.3.2 Fluorescence Lifetime Imaging Microscopy (FLIM)

FLIM measures how long in average a fluorophore remains in its excited state. These time constants lie in a range of pico to nano seconds and therefore require very fast image acquisition. Since the fluorescence lifetime is influenced by a number of environmental changes such as pH, ion, oxygen or FRET partners it can be a useful tool for a variety of applications (Gadella, 2009)(George Abraham *et al.*, 2015).

5.1.3.3 Acceptor bleaching

Presently, the most prevalent measurement method for FRET is acceptor photobleaching. The principle idea is to unquench the donor fluorophore by bleaching the acceptor. This avoids the energy transfer and concomitantly increases the emission intensity of the donor. A gradual acceptor bleach can thereby help to find the optimal bleaching settings (Van Munster *et al.*, 2005).

5.1.3.4 Donor Photobleaching (pbFRET)

Fluorophores are only sensitive to photodamage in their excited state. Since FRET decreases their fluorescence lifetime they are also less sensitive to photodamage and hence have longer photobleaching times. Consequently, the FRET efficiency can be inferred from photo-bleaching over time (see Fig. 5.2)

pbFRET was introduced by Jovin *et al.*, in 1989 and used to show clustering of lectin receptors and conformational changes of major histocompatibility complex molecules (Young *et al.*, 1994, Szollosi *et al.*, 2002). However, pbFRET has never been applied in prokaryotic cells. Both acceptor- and donor photobleaching require long time-frames and are therefore most applicable to fixed samples where cell function is not affected by the bleaching and the measurement is not affected by potential specimen movements.

5.1.4 Aims of this chapter

- Establishment of a donor photo bleaching based protein-interaction system in *S. aureus*
- Confirmation of protein interactions between PlsY and CdsA and PlsY and MreD
- Analysis of protein interaction of PlsY with other membrane proteins

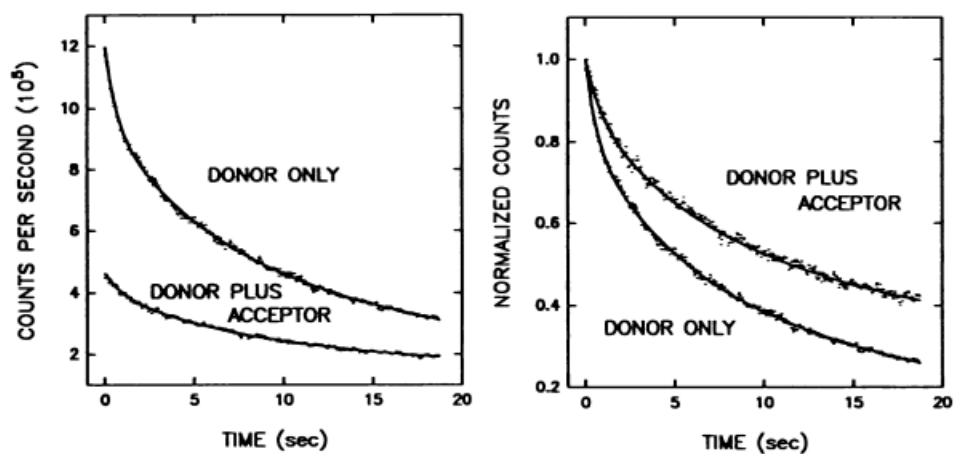


Figure 5.2 Examples for donor photobleaching decay rates

pbFRET measures the photobleaching decay rates of a donor fluorophore in presence and absence of an acceptor fluorophore. The donor bleaches slower in the presence of an acceptor due its reduced energy excitation. Image is taken from (Young et al., 1994).

5.2 Results

5.2.1 Genetic and experimental setup

Donor photobleaching was chosen as the measurement technique due to its simplicity in terms of image acquisition. This method can be performed with a standard equipped wide field microscope. In this study, a Nikon Dual Cam System was used to carry out FRET experiments. Proteins of interest were translationally fused to GFP or mCherry encoded on the shuttle-vector pCQ11. This pair was chosen based on good expression levels in *S. aureus* as seen in previous experiments and low unwanted photosensitivity in case other measurement techniques like FLIM or acceptor photobleaching should be applied (Tramier *et al.*, 2006).

pWhiteWalker, a derivative of pCQ11 designed in this study, is a shuttle-vector and fusions are expressed in *E. coli* and gram-positive bacteria such as *S. aureus*. Both fusions are expressed under control of the IPTG-inducible promoter *Pspac* (Yansura & Henner, 1984). This allows the controlled expression of proteins in the experimental host. The emission spectrum of GFP and the excitation spectrum of mCherry overlap (see Fig. 5.3A) making them a suitable FRET pair. However, their spectral overlap is less favourable compared to other commonly applied FRET pairs like eYFP/mCherry or CFP/eYFP (see Fig. 5.3BC).

Fig. 5.4 shows the genetic setup of the pCQ11 based pWhiteWalker experimental plasmids. Both fluorophores and genes of interest can be replaced by restriction digest. Additionally, proteins of interest are fused to mCherry or GFP via a five amino acid glycine-serine linker (GGSGS) to decrease the risk of steric hindrance between protein of interest and the fluorescent protein.

5.2.2 Selected controls

Donor photobleaching analyses the bleaching behaviour of a donor, in this case GFP, over time. The FRET efficiency is calculated comparing bleaching time constants of a donor in the presence of an acceptor compared to the time constant of the donor in the absence of an acceptor. In this study, protein-interactions between PlsY and various other membrane proteins were tested. This requires expression of PlsY-GFP only as a control for the donor in absence of an acceptor. Since donor photobleaching has not been used in *S. aureus*, or other bacteria before it is not known what to expect. In order to introduce a positive control, GFP and mCherry were translationally fused in tandem linked by the same Glycine-Serine linker used for the experimental plasmids. In this case, both fluorophores are forced to stay in close proximity and therefore to show FRET.

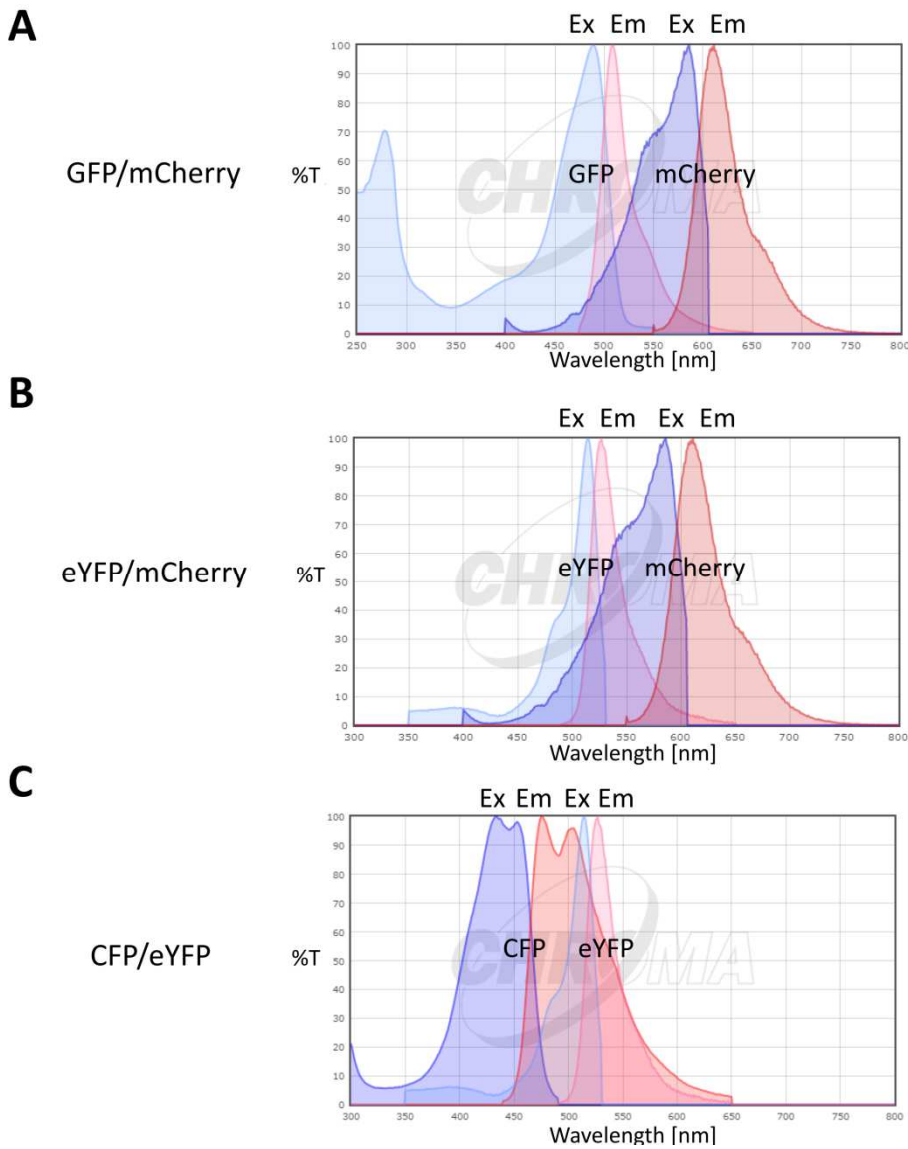


Figure 5.3 Excitation and emission spectra of selected fluorophores

Spectra were generated using Chroma Spectra Viewer (<https://www.chroma.com/spectra-viewer>). **A**, Excitation (blue) and emission (red) spectra of GFP and mCherry. **B**, Excitation (blue) and emission (red) spectra of eYFP and mCherry. **C**, Excitation (blue) and emission (red) spectra of CFP and eYFP.

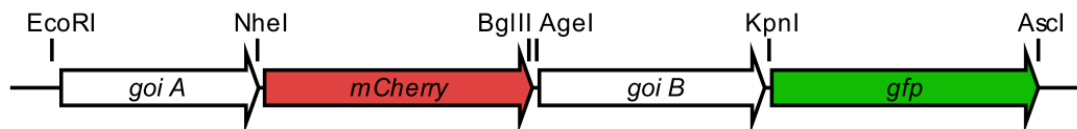


Figure 5.4 Schematic presentation of the genetic constructs used for FRET experiments

Genes are indicated by arrows. The gene of interest A (*goi A*) is translated in frame with *mCherry* whereas the gene of interest B (*goi B*) is translated in frame with *gfp*. Every part of the system can be replaced by restriction digest and cloning.

5.2.3 Genes selected for investigation

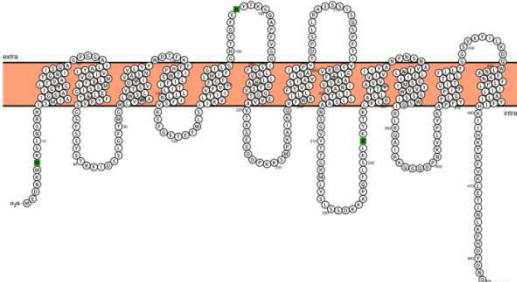
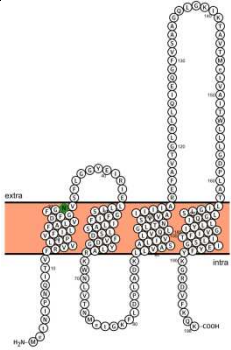
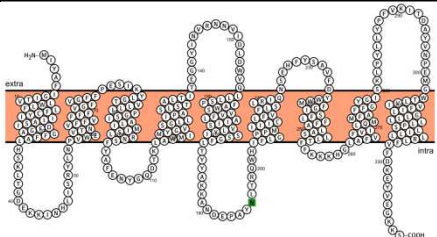
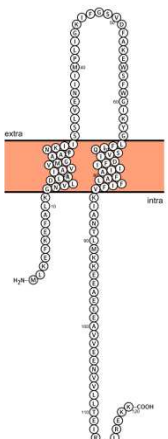
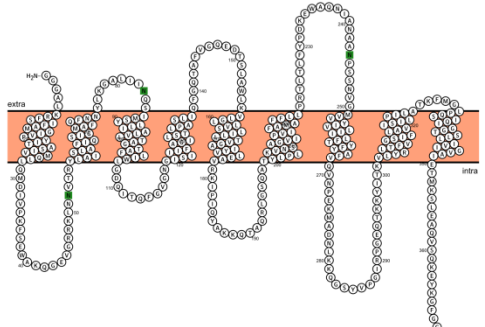
The primary aim was to confirm protein-interaction results obtained by BACTH. Therefore a PlsY-GFP fusion was investigated in the presence of CdsA- or MreD-mCherry fusions. Additionally, membrane proteins of various metabolic or physiological functions were tested for interaction with PlsY. For this purpose integral membrane proteins were chosen based on their topology and size. GFP was translationally fused to the C-terminus of PlsY since this configuration has been shown to be functional and the C-terminus is likely to be on the inside of the cell. Thus, only membrane proteins with a cytoplasmic C-terminus were chosen for interaction studies to make sure the fluorescent protein fusion is in the inside of the cell and to maintain the overall structure of the overexpression plasmid. Additionally, only proteins with a maximum size of 500 amino acids were chosen to avoid the construction of massively large plasmids (>13000bp).

5.2.4 Construction of FRET plasmids

Plasmids pWhiteWalker1-4 and pCQ11-*gfp* were constructed in cooperation with Lucas Walker (Walker, 2015). Some of these plasmids were renamed and the updated name is shown in Table 5.3.

The plasmid pWhiteWalker1 was constructed as follows: codon-optimised forms of the genes *mCherry* (Uniprot X5DSL3-1) and *gfp* (eGFP; Uniprot Q8GHE2-1) containing their own ribosomal binding sites were separately amplified by PCR (oligonucleotide primers: 5'FL04/3'pWhiteWalker0mCherryOE and 5'pWhiteWalker0GFPOE/3'FL05, respectively), fused by overlap extension PCR and cloned at the *EcoRI/AscI* site of shuttle-vector pCQ11 (Fig. 5.5). A translational fusion of *mCherry-gfp* linked by a sequence encoding a Serine/Glycine linker was constructed by PCR amplification of *mCherry* and *gfp* (oligonucleotide primers: 5'FL04/3'FL04OE and 5'FL05OE/3'FL05, respectively), fusion of the fragments using overlap extension PCR and cloning of the final fragment at the *EcoRI/AscI* site of pCQ11. This resulted in plasmid pWhiteWalker2. In the following constructs *S. aureus* SH1000 genomic DNA was used as a template for amplification of all investigated genes. Construction of pWhiteWalker3 was carried out by amplification and cloning the gene coding for *S. aureus plsY* (5'FL06/3'FL06) at the *BglIII/KpnI* site of pWhiteWalker1 in lieu of *gfp*. Additionally, a tandem fusion of *mreD* (5'FL07/3'FL07OE) and *mCherry* (5'FL08OE/3'FL04) was created by overlap extension PCR. This fragment contained a ribosome-binding site and is flanked by *BglIII* and *EcoRI* sites that were used for

Table 5.2 Bioinformatic analysis of selected integral membrane proteins chosen for protein interaction studies with PlsY

Gene name	GeneID	Function (protein length in amino acids)	Topology Prediction (http://wlab.ethz.ch/protter/#)
<i>pheP</i>	SAOUHS C_01326	Phenylalaninetransporter (484)	
<i>pgsA</i>	SAOUHS C_01260	CDP-diacylglycerol--glycerol-3-phosphate 3-phosphatidyltransferase, involved in phospholipid synthesis, processes the CdsA product CDP-diacylglycerol into Phosphatidylglycerolphosphate that is required for Phosphatidylglycerol (PG) synthesis (193)	
<i>cydB</i>	SAOUHS C_01032	Cytochrome B subunit, component of the terminal oxidase Cytochrome bd (339)	
<i>mscL</i>	SAOUHS C_1342a	Large-Conductance Mechanosensitive Channel, translates physical forces applied to the membrane into electro-physiochemical signals (120)	
<i>secY</i>	SAOUHS C_02989	Main transmembrane subunit of the Sec secretion pathway, ATPase (430)	

<i>alsT</i>	SAOUHS C_01354	Sodium-Alanine Symporter (486)	
<i>lspA</i>	SAOUHS C_01162	Lipoprotein signal peptidase (163)	
<i>fmnP</i>	SAOUHS C_01505	Riboflavin Symporter (181)	
<i>mntP</i>	SAOUHS C_00636	Manganese transporter (278)	

Table 5.3 Nomenclature of FRET plasmids and their features

Plasmid name	Features	Purpose
pCQ11- <i>gfp</i>	Expression of cytoplasmic <i>gfp</i>	Intermediate plasmid used for the construction of other pWhiteWalker's
pWhiteWalker1	Expression of cytoplasmic <i>gfp</i> and <i>mCherry</i>	Negative control
pWhiteWalker2	Expression of cytoplasmic <i>gfp</i> and <i>mCherry</i> fused in tandem	Positive control
pWhiteWalker10	Expression <i>plsY-gfp</i>	Negative control, used for FRET efficiency calculation
pWhiteWalker3	Expression <i>plsY-gfp</i> and <i>mreD-mCherry</i>	Confirmation of PlsY-MreD interaction
pWhiteWalker4	Expression <i>plsY-gfp</i> and <i>mreD-mCherry</i>	Confirmation of PlsY-CdsA interaction
pWhiteWalker7	Expression <i>plsY-gfp</i> and <i>cydB-mCherry</i>	Investigation of potential interactions of PlsY with other membrane proteins
pWhiteWalker8	Expression <i>plsY-gfp</i> and <i>pgsA-mCherry</i>	Investigation of potential interactions of PlsY with other membrane proteins
pWhiteWalker11	Expression <i>plsY-gfp</i> and <i>pheP-mCherry</i>	Investigation of potential interactions of PlsY with other membrane proteins
pWhiteWalker12	Expression <i>plsY-gfp</i> and <i>secY-mCherry</i>	Investigation of potential interactions of PlsY with other membrane proteins
pWhiteWalker13	Expression <i>plsY-gfp</i> and <i>mscL-mCherry</i>	Investigation of potential interactions of PlsY with other membrane proteins
pWhiteWalker14	Expression <i>plsY-gfp</i> and <i>fmnP-mCherry</i>	Investigation of potential interactions of PlsY with other membrane proteins
pWhiteWalker15	Expression <i>plsY-gfp</i> and <i>alsT-mCherry</i>	Investigation of potential interactions of PlsY with other membrane proteins
pWhiteWalker16	Expression <i>plsY-gfp</i> and <i>mntP-mCherry</i>	Investigation of potential interactions of PlsY with other membrane proteins
pWhiteWalker17	Expression <i>plsY-gfp</i> and <i>lspA-mCherry</i>	Investigation of potential interactions of PlsY with other membrane proteins
pWhiteWalker18	Expression <i>plsY-gfp</i> and TMD(<i>plsY</i>)- <i>mCherry</i>	Investigation of PlsY interaction with an artificially membrane bound mCherry

A more detailed description of plasmids used in this chapter can be found in Section 2.3.3 Table 2.5.

cloning into the *EcoRI/BglIII* site of the modified pWhiteWalker1 containing *plsY*. This resulted in the final construct pWhiteWalker3 containing tandem fusions of *mreD-mCherry* and *plsY-gfp*. pWhiteWalker 4 was constructed in the same manner as for pWhiteWalker3, using a gene encoding *cdsA* (5'FL09/3'FL09OE) fused by overlap extension PCR to *mCherry* (5'FL10OE/3'FL04) in lieu of *mreD*. The resulting construct contained tandem fusions of *cdsA-mCherry* and *plsY-gfp*.

Construction of pCQ11-*gfp* was carried out by amplification of *gfp* using primers 5'pCQ11gfp/3'CQ11gfp followed by restriction digest with *EcoRI/AscI*. The digested DNA fragment was then ligated into *EcoRI/AscI* cut pCQ11 resulting in pCQ11-*gfp*.

In order to construct pWhiteWalker7 and 8, genes encoding for *cydB* and *pgsA* were amplified using primer pairs 5'FW65/3'FW65 and 5'FW66/3'FW66 respectively. These fragments were then cut with *EcoRI* and *NheI* and ligated into pWhiteWalker3 that was cut with the same enzymes replacing *mreD* with *cydB* or *pgsA*. A schematic cloning overview of the construction of pWhiteWalker's 7,8 and 10-18 is depicted in Figures 5.6 and 5.7.

Plasmids pWhiteWalker10-18 were constructed using Gibson Assembly (New England Biolabs, Hitchin, United Kingdom). pWhiteWalker3 was used as a template to amplify a tandem fusion of *plsY-gfp* (5'FW73/3'FW73) that was subsequently cloned into the *EcoRI/AscI* site of pCQ11-*gfp* replacing *gfp* by *plsY-gfp* resulting in pWhiteWalker10. In order to construct pWhiteWalker11-17, genes encoding *pheP*, *secY*, *mscL*, *fmnP*, *alsT*, *mntP* and *lspA* were amplified using primer pairs 5'FW74/3'FW74 (*pheP*), 5'FW75/3'FW75 (*secY*), 5'FW76/3'FW76 (*mscL*), 5'FW77/3'FW77 (*fmnP*), 5'FW78/3'FW78 (*alsT*), 5'FW79/3'FW79 (*mntP*) and 5'FW80/3'FW80 (*lspA*), respectively. These DNA fragments were then cloned into *NheI/EcoRI* cut pWhiteWalker3 replacing *mreD*. This resulted in plasmids containing tandem fusions of the cloned genes with *mCherry* together with *plsY-gfp*.

pWhiteWalker18 containing a tandem fusion of *plsY-gfp* together with the first transmembrane domain of PlsY fused to the C-terminus of *mCherry* was constructed by amplifying *mCherry* through two amplification rounds. First, *mCherry* was amplified using primer pair 5'FW81-1/3'FW81. The product was subsequently used as a template for another PCR amplification round using primers 5'FW81/3'FW81, thus resulting in an enhanced *mCherry* containing a nucleotide sequence that encodes for the first 27 amino acids of PlsY on the C-terminus. This DNA fragment was cloned into the *EcoRI/BglIII* site of pWhiteWalker3, thus replacing *mreD-mCherry* (Fig. 5.7).

All plasmids were transformed into *E. coli* NEB5 α by Heat-Shock transformation and correct transformants were checked by restriction digest (see Fig. 5.5B-E, 5.6C-G and Fig. 5.7B) followed by DNA sequencing (GATC Biotech AG, Konstanz, Germany). Recombinant plasmids containing the correct insert without mutations were purified, concentrated and electroporated into *S. aureus* RN4220.

Restriction digest of pCQ11-*gfp* and pWhiteWalker10 candidate plasmids resulted in unexpected DNA fragment sizes using the restriction enzymes *SpeI* and *AscI*. Sequencing however showed the right DNA sequence for the inserts. *AscI* was used before and cuts once within the plasmid backbone suggesting an additional *SpeI* restriction site within the plasmid backbone that was not indicated in the plasmid sequence used for cloning.

5.2.5 Analysis of functionality

To test the functionality of the constructed plasmids in RN4220, overnight cultures were diluted to an OD₆₀₀=0.05 and grown for 2 h at 37 °C in the presence of erythromycin (5 μ g / ml) and lincomycin (25 μ g / ml) and 500 mM IPTG. Cultures were harvested, washed with PBS and analysed by fluorescence microscopy using a Nikon Dual Cam epifluorescence microscope.

Both strains expressing *gfp* and *mCherry* from pWhiteWalker1 or 2 show cytoplasmic fluorescence signals in the FITC and RFP channel (TexasRed) (see Fig. 5.8AB). The control plasmid pWhiteWalker10 only expresses a *plsY-gfp* fusions that is localised at the membrane and the septum during cell-division (Fig. 5.8G). Importantly, there is no cross-bleed through the RFP (TexasRed) channel using the excitation and emission settings applied for image acquisition of all strains (Fig. 5.8G). All the other pWhiteWalkers express a *plsY-gfp* fusion together with a gene of interest fused to *mCherry*. *mCherry*-fusions with *mreD*, *cdsA*, *cydB*, *pgsA*, *pheP*, *secY*, *mscL*, *fmnP*, *mntB* and *lspA* are expressed and membrane-associated (Fig. 5.8C-F and H-K and M-N). An *alsT-mCherry* fusion was barely expressed in most cells and expressed fusions do not appear to be membrane-associated (Fig. 5.8L). The expression of *mCherry* fused to the first transmembrane domain of PlsY also does not express well, but the fusion appears to be located at the membrane (Fig. 5.8O).

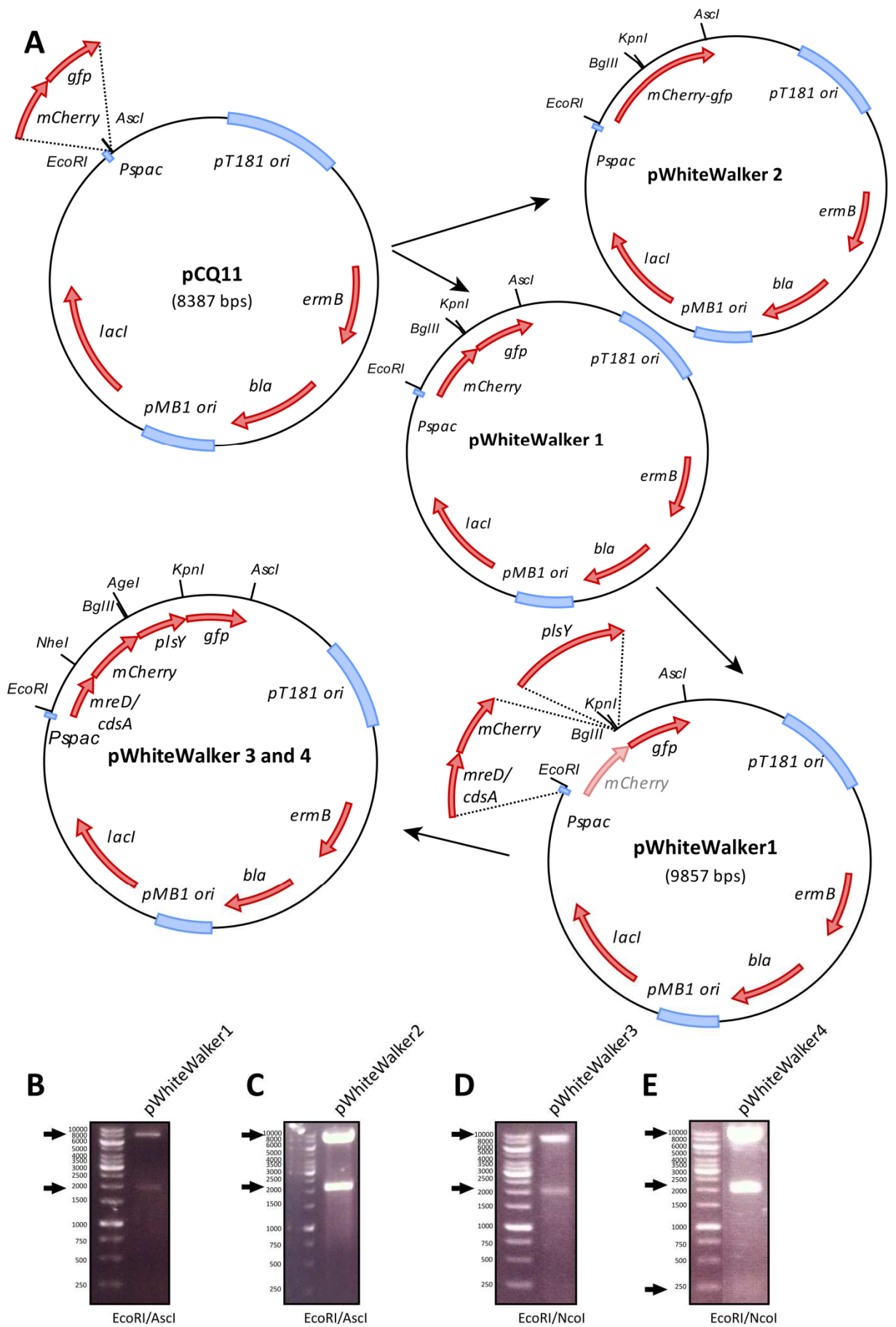


Figure 5.5 Construction of pWhiteWalker 1-4

A, Diagram illustrating the construction of pWhiteWalker 1-4. pCQ11 was used as the backbone for the integration of *mCherry* inframe with *gfp* (pWhiteWalker2) or *mCherry* separately expressed from *gfp* (pWhiteWalker1). *mCherry* of pWhiteWalker1 was then replaced by a translational fusion of *mreD* (pWhiteWalker 3) or *cdsA* (pWhiteWalker 4) with *mCherry* and *plsY* was inserted upstream and inframe of *gfp* resulting in plasmids pWhiteWalker 3 and 4. **B**, pWhiteWalker1 candidate plasmids (Lanes 1-4) were digested with EcoRI/AscI and separated by 1 % (w/v) TAE agarose gel electrophoresis. Bands of 8380 and 1477 bp corresponding to pWhiteWalker1, respectively, are marked by black arrows. **C**, pWhiteWalker2 candidate plasmids (Lanes 1-4) were digested with EcoRI/AscI and separated by 1 % (w/v) TAE agarose gel electrophoresis. Bands of 8380 and 1471 bp corresponding to pWhiteWalker2, respectively, are marked by black arrows. **D**, pWhiteWalker3 candidate plasmids (Lanes 1-2) were digested with EcoRI/NcoI and separated by 1 % (w/v) TAE agarose gel electrophoresis. Bands of 8933 and 2097 bp corresponding to pWhiteWalker3, respectively, are marked by black arrows. **E**, pWhiteWalker4 candidate plasmids (Lanes 1-3) were digested with EcoRI/NcoI and separated by 1 % (w/v) TAE agarose gel electrophoresis. Bands of 8933, 2112 and 237 bp corresponding to pWhiteWalker4, respectively, are marked by black arrows. A list of plasmids used in this chapter and their nomenclature can be found in Table 5.3.

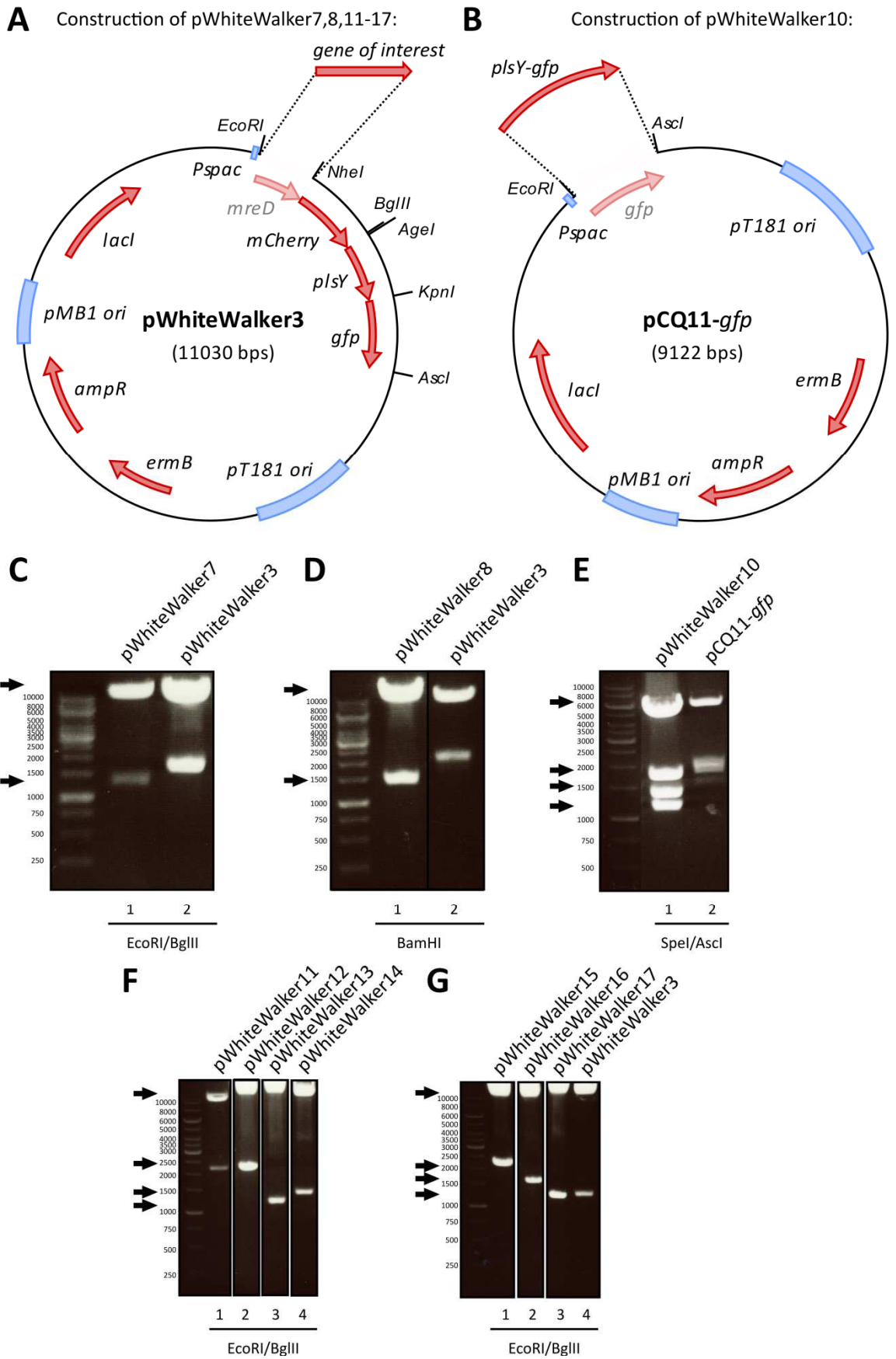


Figure 5.6 Construction of pWhiteWalker 7, 8, 10-17

A, Diagram illustrating the construction of pWhiteWalker 7,8 and 11-17. pWhiteWalker3 was used as the backbone for the replacement of *mreD* with the gene of interest resulting in a translational fusion of the gene of interest with *mCherry* along with the separate expression of a translational fusion of *plsY* with *gfp*. **B**, Diagram illustrating the construction of pWhiteWalker10. pCQ11-*gfp* was used as a backbone for the construction of pWhiteWalker 10 by replacing *gfp* with *plsY-gfp*. **C**, pWhiteWalker7 (Lane 1) and pWhiteWalker3 (Lane 2) were digested with EcoRI/BglII and separated by 1 % (w/v) TAE agarose gel electrophoresis. Bands of 9749 and 1329 bp corresponding to pWhiteWalker7, respectively, are marked by black arrows. **D**, pWhiteWalker8 (Lane 1) and pWhiteWalker3 (Lane 2) were digested with BamHI and separated by 1 % (w/v) TAE agarose gel electrophoresis. Bands of 9626 and 1452 bp corresponding to pWhiteWalker8, respectively, are marked by black arrows. **E**, pWhiteWalker10 (Lane 1) and pCQ11-*gfp* (Lane 2) were digested with AscI/SpeI and separated by 1 % (w/v) TAE agarose gel electrophoresis. Bands of approximately 5000, 2000, 1500 and 1200 bp corresponding to pWhiteWalker10 (Lane 1), respectively, are marked by black arrows. **F**, pWhiteWalker11 (Lanes 1), pWhiteWalker12 (Lane 2), pWhiteWalker13 (Lane 3) and pWhiteWalker14 (Lane 4) were digested with EcoRI/BglII and separated by 1 % (w/v) TAE agarose gel electrophoresis. Bands of 9750 and 2202 bp corresponding to pWhiteWalker11, respectively, are marked by black arrows. Bands of 9750 and 2040 bp corresponding to pWhiteWalker12, respectively, are marked by black arrows. Bands of 9750, 1077 bp (and 33 bp) corresponding to pWhiteWalker13, respectively, are marked by black arrows. Bands of 9750 and 1293 bp corresponding to pWhiteWalker14, respectively, are marked by black arrows. **G**, pWhiteWalker15 (Lane 1), pWhiteWalker16 (Lane 2), pWhiteWalker17 (Lane 3) and pWhiteWalker3 (Lane 4) were digested with EcoRI/BglII and separated by 1 % (w/v) TAE agarose gel electrophoresis. Bands of 9750 and 2208 bp corresponding to pWhiteWalker15, respectively, are marked by black arrows. Bands of 9750 and 1584 bp corresponding to pWhiteWalker16, respectively, are marked by black arrows. Bands of 9750 and 1239 bp corresponding to pWhiteWalker17, respectively, are marked by black arrows. Bands of 9749 and 1281bp corresponding to pWhiteWalker3, respectively, are marked by black arrows. A list of plasmids used in this chapter and their nomenclature can be found in Table 5.3.

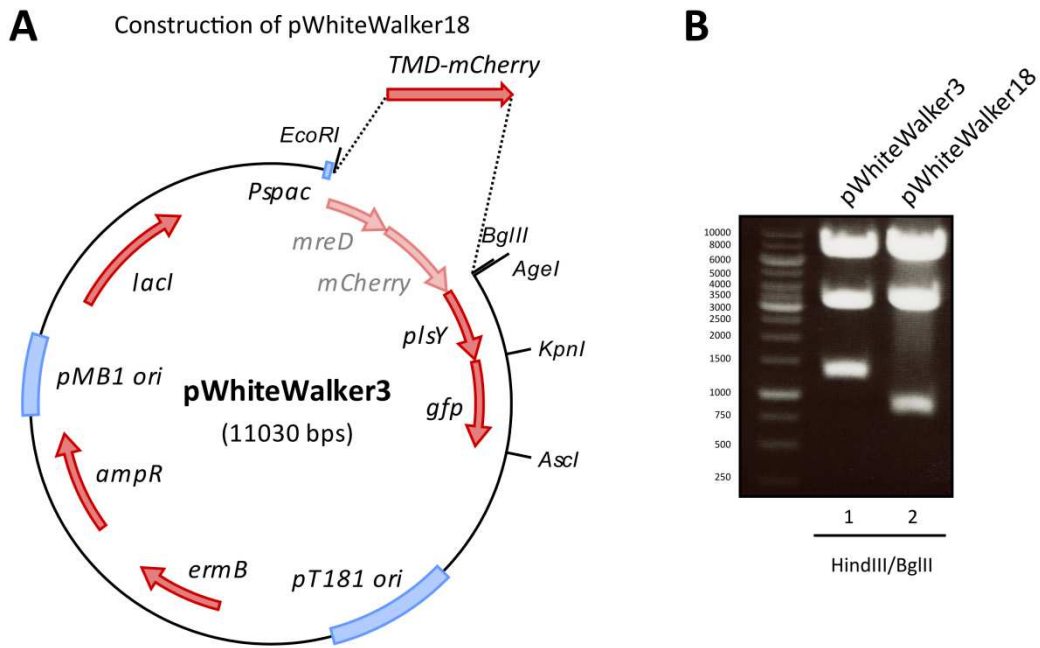
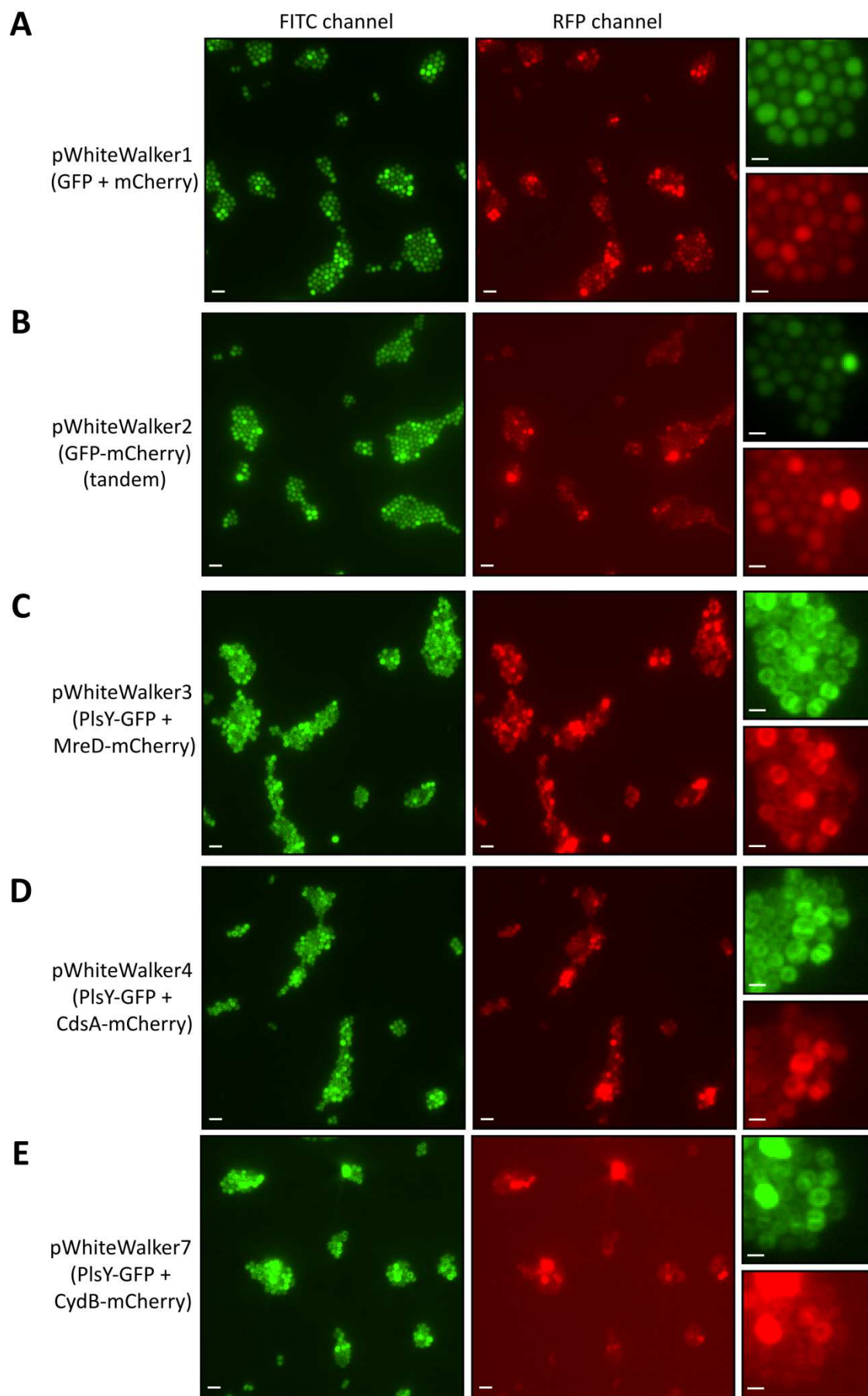
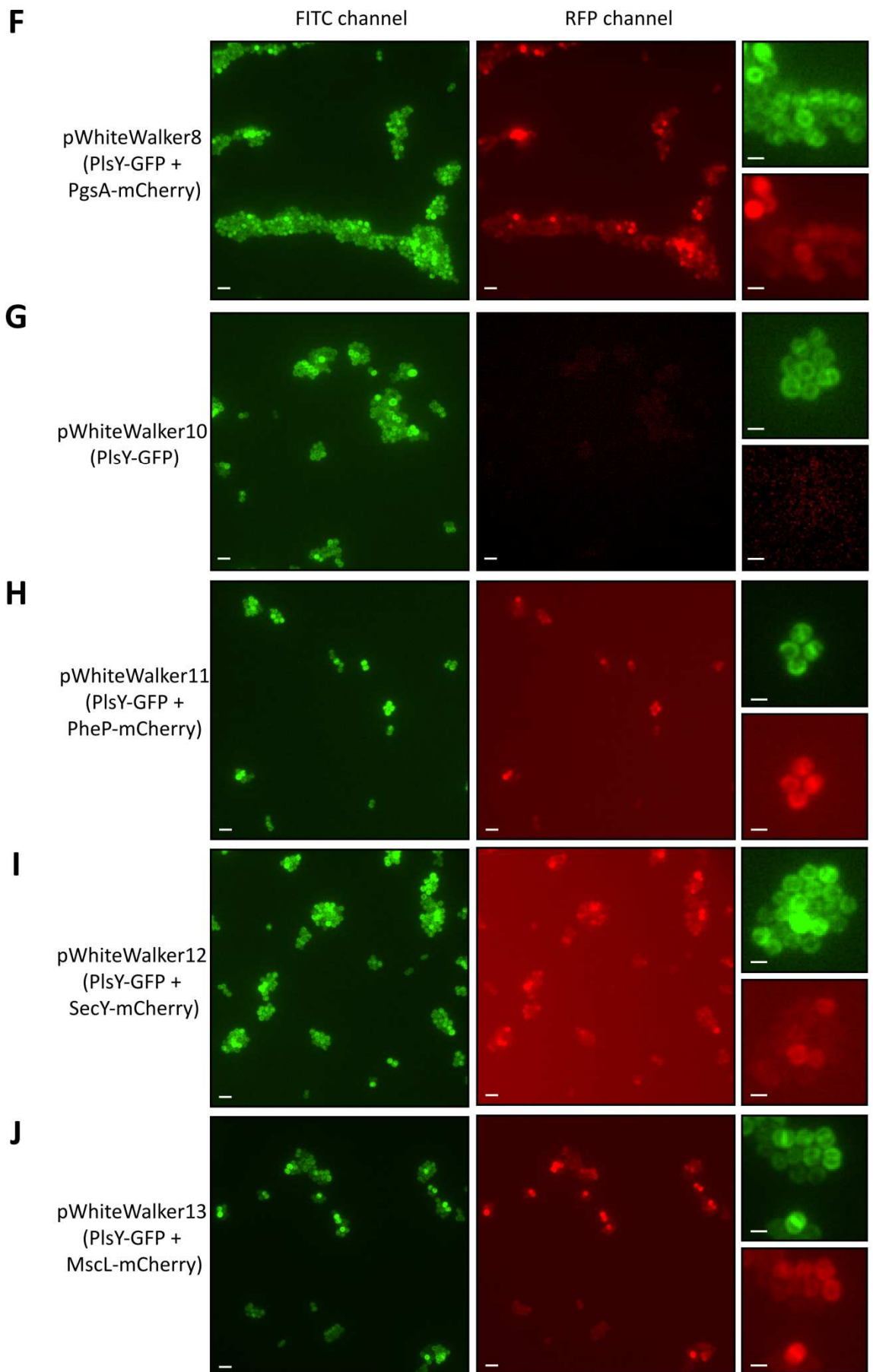


Figure 5.7 Construction of pWhiteWalker 18

A, Diagram illustrating the construction of pWhiteWalker 18. pWhiteWalker3 was used as a backbone replacing *mreD-mCherry* with an enhanced *mCherry* containing the sequence encoding for the first transmembrane domain of PlsY at its N-terminus. **B**, pWhiteWalker18 (Lane 2) and pWhiteWalker3 (Lane 1) were digested with HindIII/BglII and separated by 1% (w/v) TAE agarose gel electrophoresis. Bands of 6583, 3154 and 836 bp corresponding to pWhiteWalker18 (Lane 2), respectively, are marked by black arrows. Restriction digest of pWhiteWalker3 results in bands of 6583, 3154 and 1293 bp (Lane 1). A list of plasmids used in this chapter and their nomenclature can be found in Table 5.3.





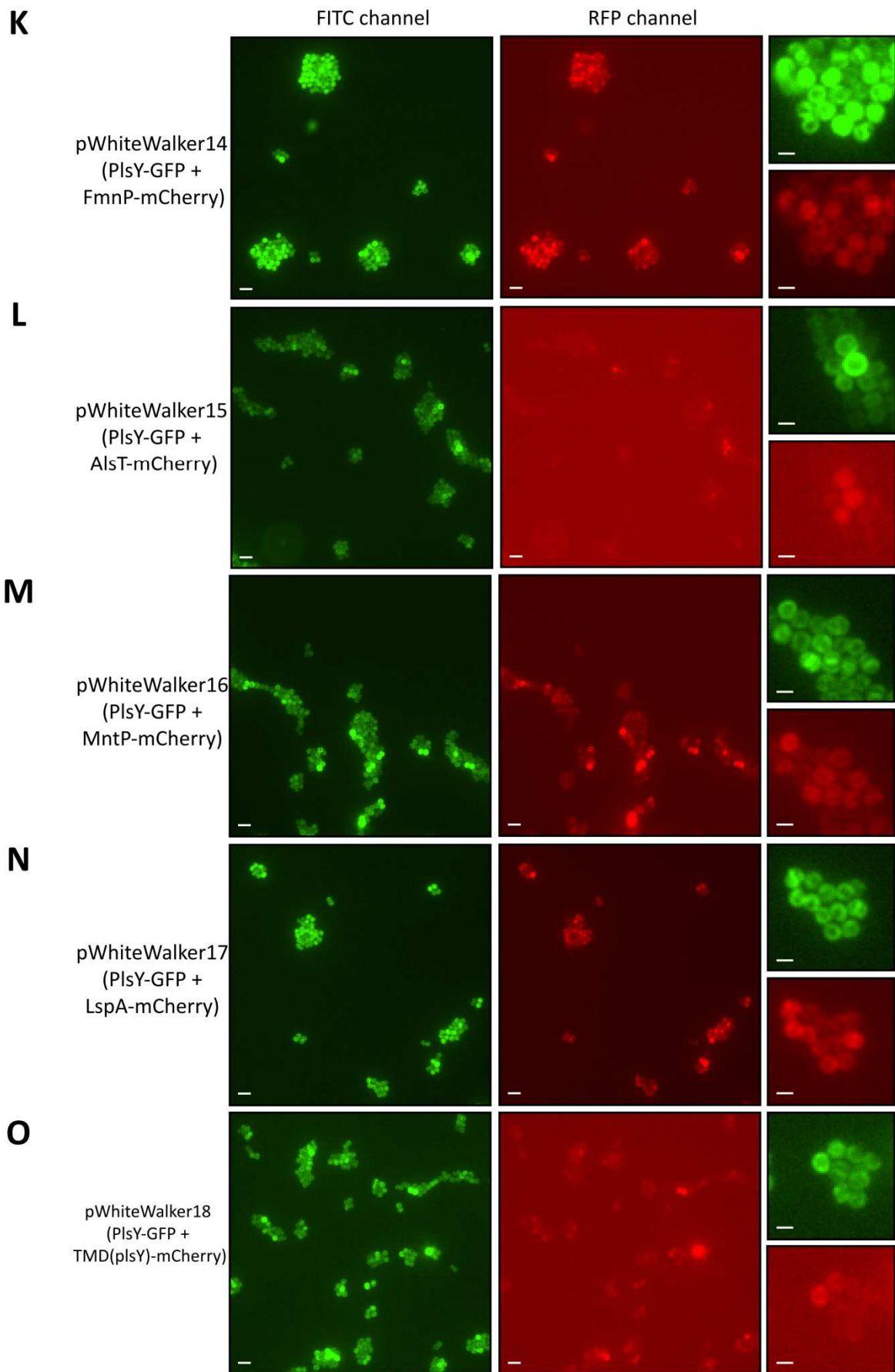


Figure 5.8 Localisation of PlsY-GFP and various membrane proteins fused to mCherry in *S. aureus* RN4220

Fluorescence images (convolved) of *S. aureus* RN4220 + pWhiteWalkers incubated in the presence of antibiotics and 500 μ M IPTG for 2 h. Images were acquired using a Nikon Dual Cam system and NIS elements software (Nikon Instruments). Acquisition of fluorescence images were taken using 500 ms exposure in both channels. Scale bars on the left panel represent 3 μ m and scale bars on the right represent 1 μ m. **A**, Fluorescence images of RN4220 + pWhiteWalker1 (*mCherry* + *gfp*). **B**, Fluorescence images of RN4220 + pWhiteWalker2 (*mCherry-gfp*, fused in tandem). **C**, Fluorescence images of RN4220 + pWhiteWalker3 (*mreD-mCherry* + *plsY-gfp*). **D**, Fluorescence images of RN4220 + pWhiteWalker4 (*mreD-mCherry* + *plsY-gfp*). **E**, Fluorescence images of RN4220 + pWhiteWalker7 (*cydB-mCherry* + *plsY-gfp*). **F**, Fluorescence images of RN4220 + pWhiteWalker8 (*pgsA-mCherry* + *plsY-gfp*). **G**, Fluorescence images of RN4220 + pWhiteWalker10 (*plsY-gfp*). **H**, Fluorescence images of RN4220 + pWhiteWalker11 (*pheP-mCherry* + *plsY-gfp*). **I**, Fluorescence images of RN4220 + pWhiteWalker12 (*secY-mCherry* + *plsY-gfp*). **J**, Fluorescence images of RN4220 + pWhiteWalker13 (*mscL-mCherry* + *plsY-gfp*). **K**, Fluorescence images of RN4220 + pWhiteWalker14 (*fmntP-mCherry* + *plsY-gfp*). **L**, Fluorescence images of RN4220 + pWhiteWalker15 (*alsT-mCherry* + *plsY-gfp*). **M**, Fluorescence images of RN4220 + pWhiteWalker16 (*mntP-mCherry* + *plsY-gfp*). **N**, Fluorescence images of RN4220 + pWhiteWalker17 (*lspA-mCherry* + *plsY-gfp*). **O**, Fluorescence images of RN4220 + pWhiteWalker18 (*TMD(plsY)mCherry* + *plsY-gfp*).

5.2.6 FRET measurements

Protein interactions using FRET are measured by their FRET efficiency. This value describes the amount of transferred energy between donor and acceptor. As described in the introduction, this energy transfer only occurs in close proximity between both fluorophores. A detailed protocol of sample preparation, image acquisition and analysis can be found in the Methods section. Briefly, cells were continuously bleached for 5 min at wavelength 488 nm and fluorescence intensity over time was used to determine the photobleaching decay rate in arbitrary units/frame. Table 5.4 lists the photobleaching time constants for all carried out FRET strains. These values were used to calculate the FRET efficiency using the following formula:

$$E=1-\tau_{PB}/\tau'_{PB}$$

where τ_{PB} is the time constant of PlsY-GFP in the absence of an acceptor and τ'_{PB} is the time constant of PlsY-GFP in presence of the investigated fusion. In other words, expression of *plsY-gfp* from pWhiteWalker10 was used for determination of τ_{PB} . FRET efficiencies were only calculated between strains that were analysed on the same day to minimise experimental variations. Therefore, time constant summaries cannot draw conclusions on FRET efficiencies.

This study demonstrates a donor-photobleaching FRET approach for the first time in *S. aureus* to identify protein interactions between PlsY fused to GFP and various other membrane proteins fused to mCherry. All values were calculated based of the photobleaching decay rate of GFP compared to the one of a strain only expressing *plsY-gfp*. Since this system is novel, a positive control using a cytoplasmic tandem fusion of mCherry-GFP, was required to get an idea of a positive FRET result. mCherry-GFP (pWW2) exhibits an efficiency value of 19.9% \pm 9.9 % whereas a strain expressing cytoplasmic non-fused *mCherry* and *gfp* (pWW1) shows an efficiency of 6.5% \pm 10.1 % (Fig. 5.9AB). These values are not significantly different but exhibit a relatively low p-value of 0.076 (Fig. 5.9C). Expression of cytoplasmic GFP and mCherry might result in too high levels of both proteins and thereby cause random FRET events in the cytoplasm. However, the analysis of FRET efficiencies between PlsY and MreD (pWW3) or CdsA (pWW4) or PgsA (pWW8) shows high efficiency levels of 20 – 23 % that are not significantly different from each other (p-values range from 0.06 to 0.99) (Fig. 5.9ABC). Furthermore, the interaction between CydB and PlsY (pWW7) also exhibits a high FRET efficiency value of 13.0% \pm 4.6 % that is not significantly different from MreD (p = 0.074), CdsA (p = 0.500) and PgsA (p = 0.152). Two proteins showed a low FRET efficiency. SecY-PlsY (pWW12) and MscL-PlsY (pWW13) interaction

measurements demonstrate FRET efficiencies of $-0.4 \% \pm 4.8 \%$ and $-4.1 \% \pm 5.3 \%$, respectively (Fig. 5.9AB). Both data sets are significantly different to the mCherry-GFP fusion, MreD ($p = 0.0024$ for pWW12 and $p = 0.0041$ for pWW13), CydB ($p = 0.0174$ for pWW12 and $p = 0.0456$ for pWW13) and PgsA studies ($p = 0.0179$ for pWW12 and $p = 0.0316$ for pWW13) (Fig. 5.9C). The analysis of interaction between PlsY and the artificially membrane bound mCherry protein (pWW18) containing a N-terminal transmembrane domain exhibits a negative FRET efficiency. This could be explained that this protein has a negative effect on PlsY-GFP and potentially decreases its fluorescence lifetime. FRET interaction studies between PlsY and PheP, FmnP and LspA were only carried out once and showed FRET efficiency values in between the negative and positive values seen for other groups. These studies have to be repeated in order to draw conclusions. Furthermore, although the interaction between PlsY and CdsA (pWW4) exhibit a high FRET efficiency value, it is not significantly different from any other group (p values range between 0.1659 and 0.9998) since this group has only been carried out twice.

In conclusion, a donor photo bleaching approach to reveal interactions between membrane proteins in *S. aureus* is viable and identified the interaction of PlsY with MreD and PgsA. Additionally, CdsA and CydB are potential interaction partners but need to be clarified since significance values (for CdsA) or FRET efficiency (for CydB) are different from the other positively tested proteins.

Table 5.4 Donor photobleaching times

Plasmid name	pWhiteWalker1	pWhiteWalker2	pWhiteWalker10	pWhiteWalker3
Time constant [A.U./frame]	99.2±6.8	118.6±9.9	94.6±8.6	124.2±7.5
Sample size	4	6	6	5

Plasmid name	pWhiteWalker4	pWhiteWalker7	pWhiteWalker8	pWhiteWalker11
Time constant [A.U./frame]	112.8±6.5	108.4±12.3	118.2±8.3	93.4
Sample size	2	4	3	1

Plasmid name	pWhiteWalker12	pWhiteWalker13	pWhiteWalker14	pWhiteWalker15
Time constant [A.U./frame]	94.1±11.5	98.8±12.0	104.2	-
Sample size	3	4	1	0

Plasmid name	pWhiteWalker16	pWhiteWalker17	pWhiteWalker18
Time constant [A.U./frame]	-	92.5	85.8±14.4
Sample size	0	1	2

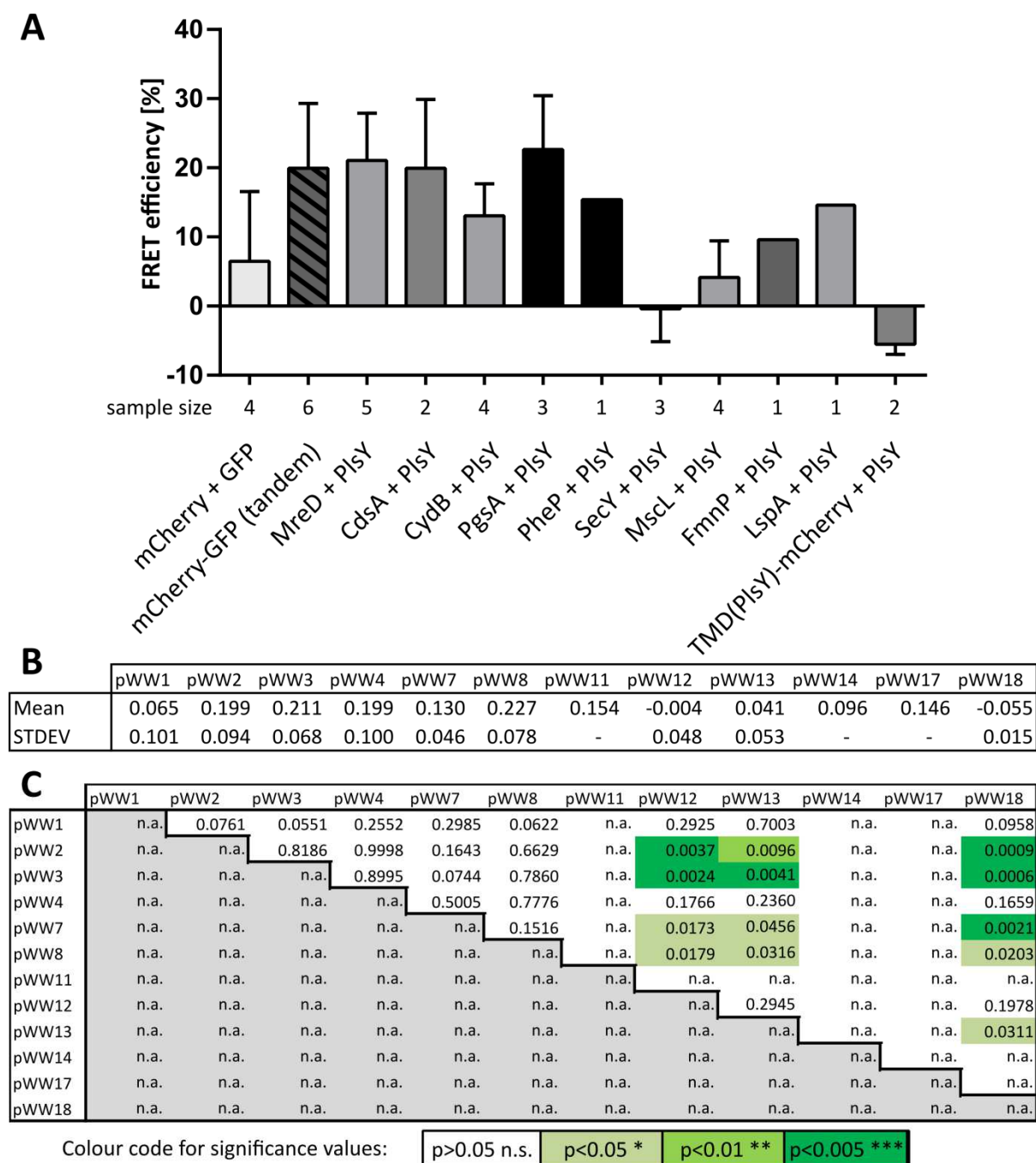


Figure 5.9 Protein-protein-interactions between PlsY-GFP and various membrane proteins fused to mCherry

A, FRET efficiencies calculated based on donor photo bleaching decay rates of GFP compared with the decay rate of a strain expressing *plsY-gfp* (pWhiteWalker10) alone. Sample size indicates the biological replicate of each group. **B**, Mean and standard deviation values of FRET efficiencies used for **A**. **C**, Cross-table of significance values calculated between all groups that were investigated in duplicate or more repeats (no pWhiteWalkers11,14 and 17). Significance was calculated using a student's t-test, two-tailed unequal variance. Green bars indicate significance whereas non-coloured bars (n.s.) indicate no significance.

5.2.7 FRET measurements in presence the of Daptomycin

Daptomycin is a lipopeptide antibiotic used to treat gram positive bacteria. Its mode of action has not been entirely elucidated but it is thought that daptomycin acts on the cell membrane causing local changes in membrane curvature that eventually result in the delocalisation of cell-division proteins in a Ca^{2+} ion dependent manner (Pogliano *et al.*, 2012). In order to investigate whether this delocalisation has an effect on the interaction between the previously shown membrane proteins, FRET studies were carried out comparing the interaction of PlsY with MreD, CydB, SecY and MscL. Additionally, the translational fusion of mCherry-GFP was used as a positive control since its FRET activity is based on a interaction in the cytoplasm and not in the membrane. Therefore, if daptomycin affects the interaction between membrane proteins, no effect should be seen on the cytoplasmic mCherry-GFP fusion.

In order to determine the minimal inhibitory concentration of daptomycin, an overnight culture of *S. aureus* SH1000 was diluted to an $\text{OD}_{600}=0.025$ in 25 ml BHI supplemented with CaCl_2 (5 μg / ml) and grown at 37 °C at 250 rpm to $\text{OD}_{600}\approx 1.4$ followed by addition of daptomycin (1, 10 or 50 μg / ml). 50 μg / ml daptomycin was the only concentration causing a growth defect and therefore chosen for the following FRET interaction studies. (Fig. 5.10A).

The interaction between membrane proteins in the presence of FRET was carried out as described in Section 5.2.6 with the modification that the second subculture was supplemented with CaCl_2 (5 μg / ml) and grown for 1.5 h before adding daptomycin to a final concentration of 50 μg / ml. The cultures were then incubated for another 30 min before cells were fixed and analysed by fluorescence microscopy (Fig. 5.10B).

All FRET efficiency values except for the positive control, mCherry-GFP, decreased in the presence of daptomycin (Fig. 5.10B). The interaction of PlsY with CydB is completely abolished whereas the interaction values between SecY and MscL with PlsY even reached negative levels of $\approx -7\%$. The FRET efficiency of MreD-PlsY however remains high and only exhibits a decrease of around 3 %. Interestingly, the translational fusion of mCherry-GFP was not affected by daptomycin and even increased by $\approx 9\%$. These changes might be explained that the interaction of all fusions except for mCherry-GFP is affected by daptomycin and that the reference strain expressing *plsY-gfp* alone that was used to calculate the FRET efficiency values might also have been affected. However, this study was only carried out once since it requires high amounts of daptomycin and thus is not conclusive regarding the effect of daptomycin on the interaction of membrane proteins in *S. aureus*.

5.2.8 Single cell subcellular FRET measurements

The application of FRET revealed an interaction between PlsY and MreD but no interaction between PlsY and SecY. Furthermore, PlsY might interact with CydB. This protein-protein interaction system is capable of determining where, on a subcellular level, the interaction takes place. Usual measurements were carried out by analysing the fluorescence intensity of GFP of a whole image field over time. Repeating the analysis of selected cells that are either undergoing cell-division or do not show cell-division was studied to reveal a potential difference (Fig. 5.11A). Additionally, cells undergoing cell-division were further subdivided into septa and peripheral membranes to investigate whether protein interactions mainly occur at the septum.

In order to achieve this, 10 cells or subcellular areas per image field of strains RN4220 + pWhiteWalker3 (MreD), pWhiteWalker7 (CydB), pWhiteWalker10 (PlsY-GFP only) and pWhiteWalker12 (SecY), were selected and analysed (Fig. 5.11B).

Using a single-cell donor-bleaching analysis results in similar values compared to the whole image method applied to the initial FRET efficiency calculation (Fig. 5.11B). PlsY-MreD displays a high FRET value for all investigated subcellular areas. However, the FRET efficiency is higher for cells undergoing cell-division indicating that these cells might exhibit more protein interaction between PlsY and MreD. Interaction between PlsY and SecY is low or even negative in all studied areas. Interestingly, CydB-PlsY interaction is more pronounced in cells undergoing cell-division and dissecting these cells further reveals an interaction at the cell periphery rather than the septum. However, the standard deviation is high and the difference is not significant.

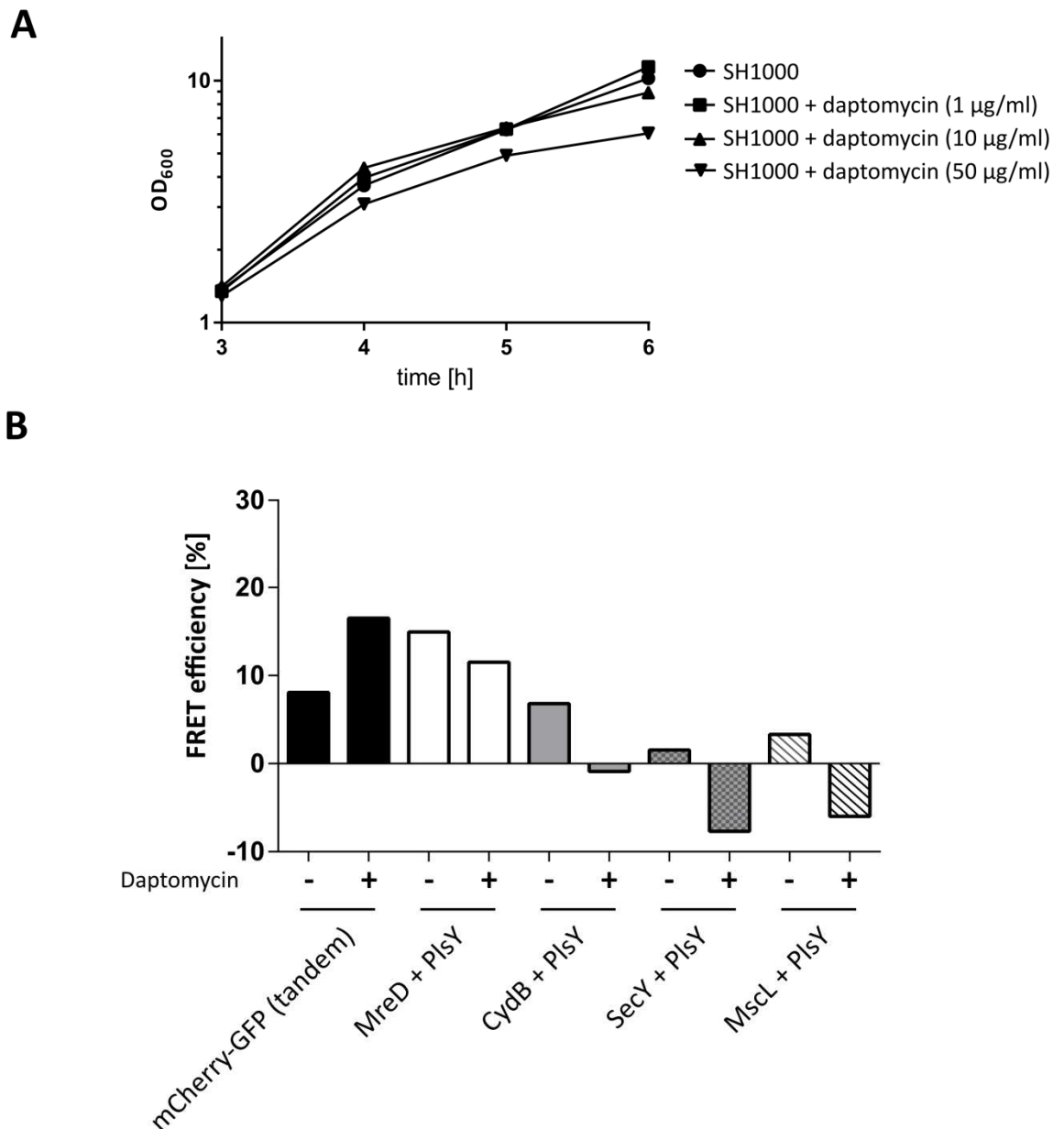


Figure 5.10 Protein-protein-interactions between PlsY-GFP and various membrane proteins fused to mCherry in the presence and absence of daptomycin

A, Growth curves of SH1000 in the presence of CaCl_2 ($5 \mu\text{g} / \text{ml}$) and daptomycin. Strains were grown to an $\text{OD}_{600} \approx 1.4$ followed by addition of daptomycin. Only OD_{600} values after addition of daptomycin are shown to clarify the growth defect. **B**, FRET efficiencies calculated based on donor photo bleaching decay rates of GFP compared with the decay rate of a strain expressing *plsY-gfp* (pWhiteWalker10) alone in the presence of CaCl_2 ($5 \mu\text{g} / \text{ml}$) and daptomycin ($50 \mu\text{g} / \text{ml}$). ‘-’ indicates no addition of daptomycin whereas ‘+’ indicates the addition of daptomycin.

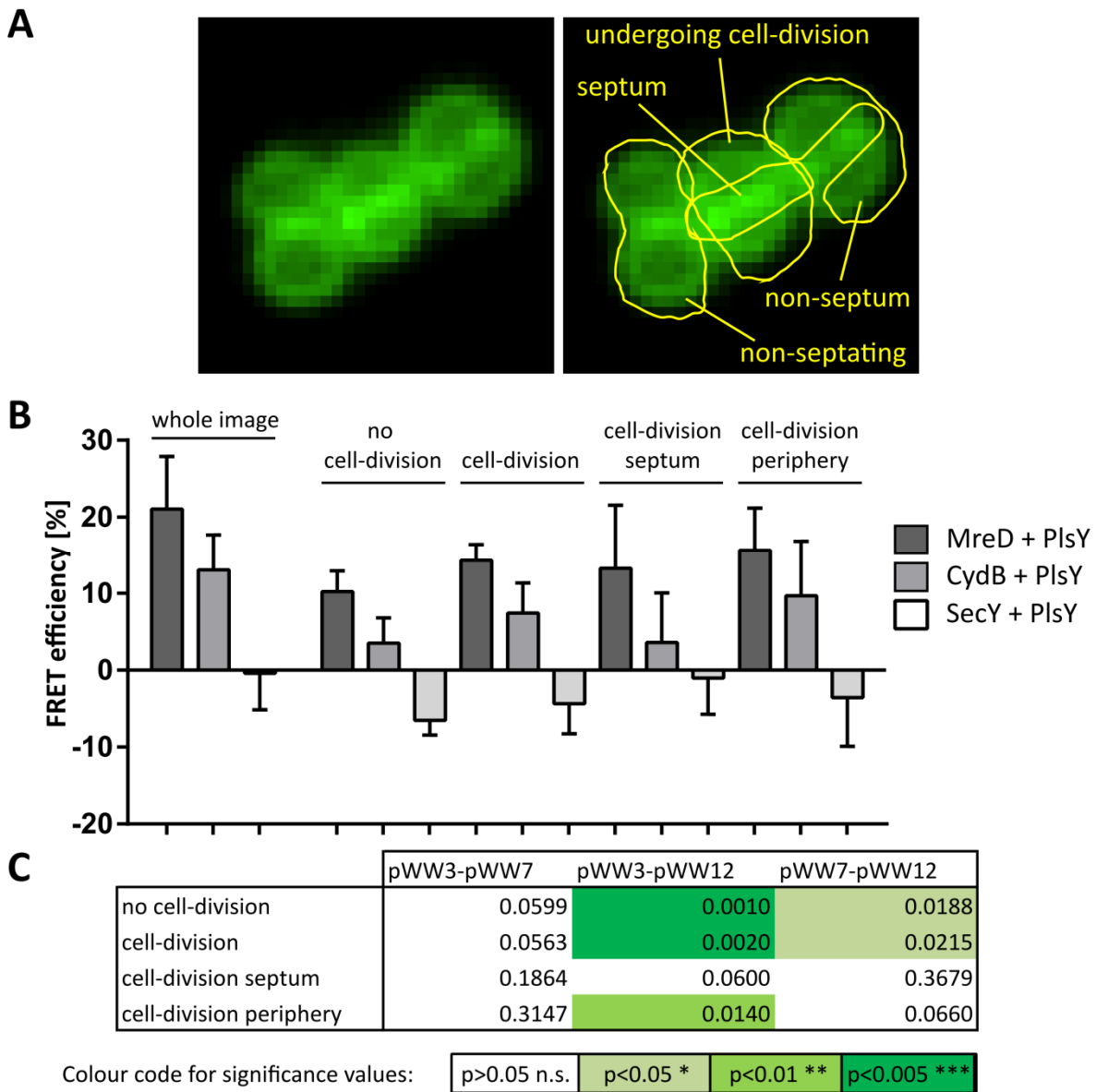


Figure 5.11 Subcellular single-cell FRET analysis of protein-interactions of PlsY-GFP and MreD, CydB and SecY fused to mCherry

A, Schematic presentation of the data analysis in terms of selected subcellular areas used for FRET efficiency measurements. **B**, FRET efficiencies of protein interactions of PlsY with MreD, CydB or SecY. Whole image values were taken from Fig. 5.9B. **C**, Significance values calculated between all three groups within the subcellular area of measurement. Significance was calculated using a two-tailed equal variance student's t-test. Green bars indicate significance whereas non-coloured bars (n.s.) indicates no significance.

5.3 Discussion

5.3.1 A novel system to study protein-protein-interactions in *S. aureus*

This study introduced a novel method to study protein-protein interactions in *S. aureus*. A donor photobleaching approach allows investigating protein interactions *in vivo* in its native host. This can have great benefits compared to bacterial-two hybrid studies in *E. coli* since heterogeneous expression can result in delocalised and misfolded proteins that exhibit altered properties. The measurements are reproducible but require at least three independent replicates to produce significant data. However, this assay is time consuming and not suitable to screen for protein interactions in between a group of proteins. The protein interaction assay here was used with exponentially growing cells to investigate protein interactions between fast growth where cellular processes have to be efficient. Since photobleaching rates are theoretically dose-independent, it should be possible to use this system to analyse protein interactions over time to study the relation between two proteins dependent on the growth phase. This study also demonstrates that the analysis of subcellular areas is feasible which could be a powerful tool to study protein-interactions dependent on the cell-cycle stage. Furthermore, it would be of great interest to elucidate the mode of action of membrane targeting antibiotics by analysing their effect on the interaction between membrane proteins. Preliminary results using daptomycin demonstrated that protein-interactions between PlsY and MreD decreased and the interaction between PlsY and CydB was entirely abolished. Importantly, daptomycin had no negative effect on the cytoplasmic control comprised of a tandem fusion of mCherry-GFP. Further studies could investigate the effects of telomycin or lysocin E, two cytoplasmic membrane targeting antibiotics that are active in gram positive bacteria (Fu *et al.*, 2015, Hamamoto *et al.*, 2015). Interestingly, daptomycin, telomycin and lysocin intercalate between specific lipids. Daptomycin targets phosphatidyl-glycerolphosphate, telomycin intercalates between cardiolipin and lysocin exhibits an affinity to menaquinones (Epanand *et al.*, 2016). In case the membrane proteins investigated in this study preferentially localise in a local microenvironment of specific lipids, the use and comparison of these antibiotics could identify these lipids. The treatment should specifically only inhibit interactions of membrane proteins localised in these lipid domains.

To deploy better controls than the cytoplasmic expression of mCherry and GFP, either separately expressed or in tandem, it would of interest to construct membrane bound fluorophore fusions. A first attempt was undertaken by fusing the first transmembrane domain of the integral membrane protein PlsY to the N-terminus of mCherry termed TMD(PlsY)-mCherry. Although the fusion appears to be located at the

cell periphery, it did not express or fluoresce well (Fig. 5.8) and also exhibits a lower photobleaching rate than the negative control of PlsY-GFP alone (Fig. 5.9A). This could be explained due to a detrimental effect of TMD(PlsY)-mCherry on PlsY-GFP. To repeat the experiment using a different transmembrane domain fused to mCherry and or GFP would further corroborate the protein-interaction system. Additionally, the analysis of protein levels using Western blots with anti-GFP and anti-mCherry antibodies could be used to ensure that both protein fusions are expressed at the same level.

5.3.2 PlsY is part of a complex protein-interaction network

Bacterial two-hybrid studies revealed the interaction between PlsY, CdsA and MreD (Fig. 1.19). The donor photobleaching system used here confirms the interactions between PlsY/CdsA and between PlsY/MreD (Fig. 5.9) which further indicates that the cytoskeletal protein MreD could be involved in the localisation of PlsY and indirectly of CdsA. Furthermore, it has been demonstrated that PlsY interacts with PgsA, another component of the phospholipid biosynthesis pathway (Fig. 5.9). These findings along with the localisation studies using fluorescent protein fusions point to a protein cluster composed of phospholipid synthesis enzymes and MreD. This cluster could improve the synthesis of phospholipid head groups through metabolic channelling. No enzymatic activity is known for MreD so far suggesting that MreD might act as a glue to keep phospholipid synthesis enzymes together.

Additionally, the interaction of PlsY with other membrane proteins was investigated and showed that PlsY potentially interacts with the respiratory enzyme CydB. A FRET efficiency of 13 % was found between PlsY and CydB which is lower than that of other studied interactions. CydB is one of at least two terminal oxidases in *S. aureus* that facilitate the last step in respiration that transfers an electron to O₂ forming H₂O and thereby pumping a proton to the outside of the cell. This step is required to drive the ATP synthase to generate ATP (Miller & Gennis, 1983, Kita *et al.*, 1984, Clements *et al.*, 1999). The synthesis of phosphatidic acid, the substrate for CdsA can either be performed by the acetyltransferase module by PlsX/Y/C or by a recycling process catalysed by DgkB (Fig. 1.5 and Fig. 1.6) (Miller *et al.*, 2008). The latter is ATP dependent and it might be advantageous for the cell to keep respiration and phospholipid synthesis close to each other to improve cellular processes.

In Section 4.2.2.7, fusions of the secretion protein SecY with GFP showed that SecY homogeneously distributes in the membrane unlike phospholipid synthesis enzymes that exhibit a heterogeneous punctate distribution. The analysis of PlsY and SecY shows no interaction, suggesting that both proteins are likely to be independent of each other. Thus, secretion might be a process that is required throughout the cell periphery but not

at specific places. Moreover, no interaction between PlsY and MscL is found and it would of interest to study the localisation of MscL expressed at native levels.

This study further corroborates a link between cell-division and lipid synthesis. The cytoskeletal protein MreD that is thought to be involved in peptidoglycan synthesis in other species interacts with the phospholipid biosynthesis enzyme PlsY. Depletion studies of PlsY revealed the delocalisation of the cell-division proteins EzrA and PBP2 (Garcia-Lara *et al.*, 2015). A similar link is seen in *B. subtilis* where PlsX has been shown to interact with several cell-division proteins including DivIB, DivIC, FtsL and FtsA together with cytoskeletal proteins such as MreB, Mbl and RodZ (Takada *et al.*, 2014). PlsX arrives prior to FtsA and FtsZ at the cell-division site and its localisation is stabilised by the Z-ring. Additionally it localises to the cell poles (Takada *et al.*, 2014). PlsY might have the same properties as PlsX and it would be of great interest to study their interaction. Furthermore, a bacterial two-hybrid assay did not identify an interaction between PlsY and FtsA in *S. aureus* in preliminary experiments (Bottomley, 2011). This could either mean that the interaction has to be tested under different conditions or that not PlsY but PlsX or MreD are the key interaction partners that facilitate the link between cell-division and phospholipid biosynthesis.

5.3.3 Main findings in this chapter

- Establishment of a FRET donor photobleaching system to study protein-protein interactions in *S. aureus*.
- Confirmation of the interaction between PlsY and MreD and between PlsY and CdsA
- PlsY also interacts with the phospholipid synthesis enzyme PgsA and the respiratory protein CydB.
- Daptomycin treatment decreases the protein interaction of membrane proteins such as between PlsY and MreD and between PlsY and CydB.

3.5 Contributions

The construction and analysis of pWhiteWalkers 1-4 was carried out by me and Lucas Walker as part of his Master thesis. The software used for the analysis of photobleaching decay rates was provided by Dr. Robert Turner (University of Sheffield). All other experiments in this chapter were performed by me.

Chapter 6: *In vitro* studies of MreD

6.1 Introduction

6.1.1 Reconstitution of bacterial proteins *in vitro*

The study of protein functions *in vivo* can be misleading. The bacterial cell is composed of a variety of proteins acting independently and in concert with each other. Removing one protein can result in pleiotropic phenotypes that might only be indirectly linked to the protein of interest and thus makes it hard to draw conclusions. In order to comprehend how proteins function, it is required to gradually remove parts of the system to study a protein in a well-defined and controlled environment which can range from expression in a heterologous host to proteins bound to microbeads or membrane nanodiscs (see Fig. 1 for an overview of *in vivo* and *in vitro* study systems).

6.1.2 Subcellular localisation and *in vitro* study examples

6.1.2.1 DivIVA

DivIVA localises to the septum and/or cell poles in *B. subtilis* (Edwards & Errington, 1997, Marston *et al.*, 1998). However, it was unclear how DivIVA targets membranes and finds its way to the cell-division site and poles. Expression of DivIVA in *B. subtilis* mutants exhibiting aberrant cell morphologies showed that DivIVA preferentially binds to highly curved membranes (Lenarcic *et al.*, 2009). This observation was confirmed expressing DivIVA in constrained *E. coli* cells. Confining *E. coli* spheroplasts in agarose micro chambers allowed bending of cells and adjustment of their shape to the chambers (Renner *et al.*, 2013). Experiments using DivIVA in liposomes also revealed that the N-terminus containing an amphipathic helix is required for membrane binding (Lenarcic *et al.*, 2009). DivIVA lost its localisation pattern in lysozyme induced spheroplasts where it was found to distribute uniformly around the cell (Ramamurthi & Losick, 2009).

6.1.2.2 SpoVM

SpoVM expressed in the non-sporulating bacterium *E. coli* showed that it binds to convex shaped membranes (Ramamurthi *et al.*, 2009). Interestingly, an *E. coli* $\Delta mreB$ strain forming internal vesicles revealed that SpoVM binds to the surface of the vesicles which mimic forespores. This observation was also seen expressing SpoVM in a mutant of *Saccharomyces cerevisiae* that produces internal vacuoles. Additionally, the use of GUVs and spherical supported lipid bilayers at which a lipid bilayer is coated around

silica beads with defined sizes revealed that SpoVM binds to the surface of curved membranes dependent on the degree of positive curvature (Ramamurthi *et al.*, 2009, Gill *et al.*, 2015).

6.1.2.3 MinCDE

To understand the underlying mechanism of how Min protein oscillation works required *in vitro* studies. Reconstitution of fluorescently labelled MinCDE on a supported lipid bilayer that mimicks the inner membrane of *E. coli* showed that MinCDE proteins self-organise and propagate in waves (Loose *et al.*, 2008). This movement lasted for several micrometers and only required a lipid membrane and ATP for the activity of MinD. The wave lengths were 10 fold longer than the length of *E. coli* which could be explained by missing boundaries in a cell-free environment or higher reaction rates in the tested *in vitro* system in comparison to *E. coli* (Loose *et al.*, 2011). A similar observation was made by reconstitution of MinCDE on the surface of GUV which resulted in circular and spiral waves of MinCDE (Martos *et al.*, 2013). The analysis of Min protein propagation in a controlled environment such as GUVs also allowed the identification of other physiochemical factors influencing Min proteins. It was also demonstrated that lipid composition can alter Min protein movement since MinD and MinE preferentially bind to anionic lipids (Vecchiarelli *et al.*, 2014).

6.1.2.4 FtsZ-FtsA

FtsZ is the first protein moving to the cell-division site forming the Z-ring that initiates cell septation but it is not a membrane bound protein and relies on FtsA to be tethered to the membrane (Bi & Lutkenhaus, 1991). Isolation of FtsA into a nanodisc containing lipids proved to be a powerful tool to study its membrane binding properties and revealed its affinity for the inner membrane. Interestingly, FtsA was shown to exhibit a 10 fold higher affinity to native *E. coli* inner membranes containing membrane proteins than to *E. coli* lipids without proteins which indicates that other cell-division proteins could support the membrane targeting of FtsA (Martos *et al.*, 2012b). Cloning the membrane targeting sequence of FtsA to the C-terminus of FtsZ (FtsZ-mts) allowed studying the activity of FtsZ *in vitro*. This demonstrated that FtsZ alone can form Z-rings that move laterally along tubular vesicles. These rings generate a force and can constrict but not divide vesicles (Osawa *et al.*, 2008). Later studies using co-reconstitution of fluorescently tagged FtsZ and FtsA in GUVs showed that vesicle-division can be achieved suggesting that FtsA plays a critical role in membrane division (Osawa & Erickson, 2013). FtsZ and FtsA were found to be homogeneously distributed but started to form dense spots and fibres upon GTP addition (Jimenez *et al.*, 2011).

Finally, the combination of both FtsZ and the Min system demonstrated impressively what can be achieved with a simple *in vitro* system. The reconstitution of oscillating MinCDE proteins in a membrane-clad soft-polymer compartment, mimicking a rod-shaped cell, together with FtsZ-mts revealed that FtsZ only formed a Z-ring at the middle of the compartment (Zieske & Schwille, 2014, Arumugam *et al.*, 2012).

6.1.2.5 Other examples of protein reconstitutions

Reconstitution experiments aim to understand how proteins work under defined conditions and also work towards a bottom-up reconstitution of an artificial cell to address general questions how life can be created and maintained. This includes several other aspects of cell maintenance and division like chromosome partitioning and cytoskeletal features.

The actin homologue MreB was shown to bind directly to membranes and is capable of self-assembly to double protofilaments when reconstituted on lipid bilayers (Salje *et al.*, 2011, van den Ent *et al.*, 2014). Due to its crucial role as a shape-determinant and in peptidoglycan synthesis (Kawai *et al.*, 2009, Kruse *et al.*, 2005, White *et al.*, 2010, Vats & Rothfield, 2007) MreB is considered a key component of bacterial cells and its implementation with FtsZ and Min proteins into an *in vitro* system would be of great interest. Furthermore, cells require to segregate their genetic material in order to propagate. The ParABS system is a key player in a mitosis-like partitioning of low-copy plasmids in bacteria. ParB bound to specific *parS* DNA sites present on the plasmid is capable to bind ParA and thereby activates its ATPase activity. ParA in return loses its affinity for DNA. This results in ParB pulling the DNA and chasing after ParA (Rodionov *et al.*, 1999, Hirano *et al.*, 1998, Erdmann *et al.*, 1999). An *in vitro* system where ParA was reconstituted inside a DNA-carpeted flow cell demonstrated the detachment of DNA upon ParB-stimulated ATPase activity (Hwang *et al.*, 2013).

The combination of these described systems that work in isolated *in vitro* systems could be a powerful tool towards a bottom-up reconstitution of an artificial cell.

6.1.7 Aims of this chapter

- Expression and localisation studies of *S. aureus* MreD in *E. coli*
- Overexpression and purification of *S. aureus* MreD
- Reconstitution of purified MreD into liposomes
- Localisation studies of membrane proteins in cytoplasmic membrane vesicles derived from *S. aureus* membranes

6.2 Results

6.1.1 Heterologous expression of *mreD-eyfp* in *E. coli*

MreD was shown to interact with PlsY and CdsA (Garcia-Lara *et al.*, 2015). The deletion of *mreD* causes the delocalisation of PlsY and MreD itself was shown to localise in a punctate pattern. As a first step in determining how MreD is able to form a heterogeneous punctate distribution it was investigated how *S. aureus* MreD localises in the heterologous expression host *E. coli*. Since *E. coli* preferentially uses different codons as *S. aureus*, the genes encoding for *mreD* and *eyfp* were codon-optimised to the use in *E. coli* (DNA and amino acid sequence can be found in the Appendix: Fig. 9.6 and Fig. 9.7) (GeneArt™, Thermo Fisher Scientific, Waltham, United States of America).

An *eyfp* translational fusion to *mreD* was chosen as eYFP can be used for super resolution microscopy studies (Dr.R.D.Turner, personal communication). The fusion was expressed from the IPTG-inducible overexpression plasmid pWALDO. The insert in this plasmid is tagged with 8 histidines and can therefore also be used for protein purification purposes (Waldo *et al.*, 1999).

Three constructs were designed to analyse whether a C-terminal or N-terminal fusion of MreD with eYFP or a linker sequence in between both proteins is more suitable for expression or affects the localisation properties of MreD (see Fig. 6.2 for an overview of expression constructs). Additionally, a TEV protease recognition site was cloned in between MreD and eYFP to be able to cut off eYFP post purification. Expression of all constructs is driven by a T7-RNA polymerase promoter that is repressed by LacI and therefore requires an *E. coli* strain expressing the T7-RNA polymerase and medium supplemented with IPTG. The plasmids were expressed in *E. coli* C43 (DE3), a derivative from BL21 that was selected for better overexpression of membrane proteins (Miroux & Walker, 1996). Strain C43 harbours a mutation in the promoter driving the expression of T7 RNA polymerase, *lacUV*, resulting indirectly in a slower expression of the gene of interest (Wagner *et al.*, 2008). This can have a positive effect on the cell since it is not overwhelmed by high expression of potentially toxic proteins.

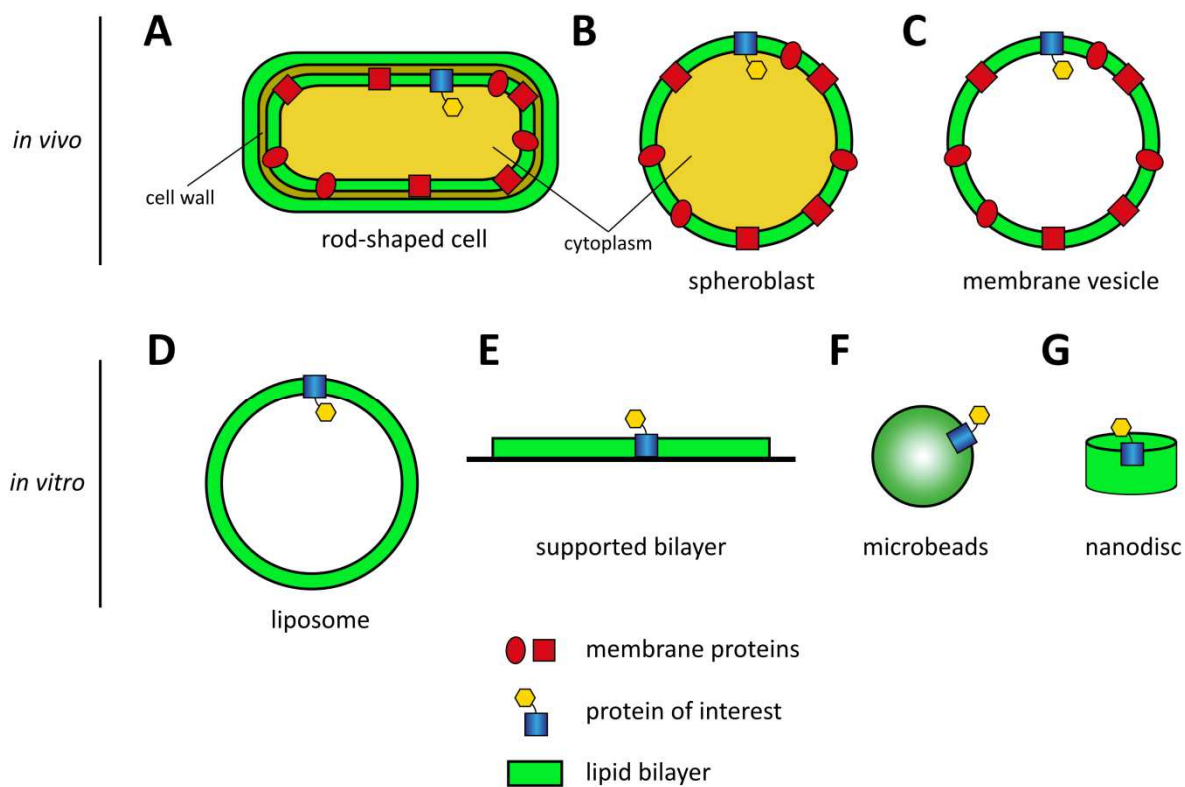


Figure 6.1 Schematic overview of *in vivo* and *in vitro* protein study systems

Adapted and extended from (Martos *et al.*, 2012a, Salje *et al.*, 2011).

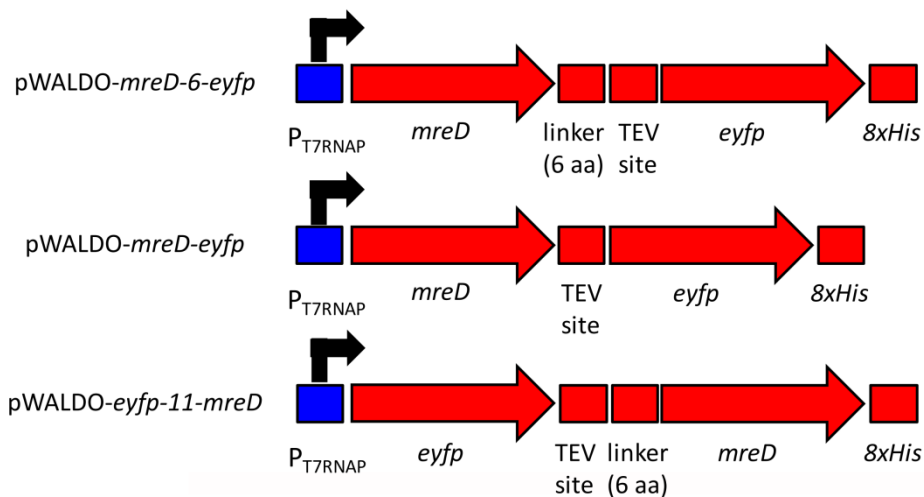


Figure 6.2 Schematic overview of *mreD-eyfp* fusion expression constructs

The blue bar indicates the IPTG-inducible T7RNA promoter. The red bars and arrows are translated in frame and encode for a single protein.

6.1.1.1 Construction of an IPTG-inducible MreD-eYFP fusion in *E. coli*

First, *mreD* was amplified by either extending the gene with a TEV protease restriction site (primer pair: 5'FW112/3'FW112) or a TEV site including a six amino acid linker sequence (SGSGSG) (primer pair: 5'FW112/3'FW113) at the N-terminus of *mreD* using the codon-optimised *mreD* gene provided by GeneArt™ (Thermo Fisher Scientific, Waltham, United States of America) as a template. The PCR products were purified and served as templates for further PCR amplification using primer pair 5'FW112/3'FW114. The gene encoding for *eyfp* was amplified with primers 5'FW115/3'FW115 using codon optimised linear DNA fragments provided by GeneArt™ (Thermo Fisher Scientific, Waltham, United States of America) as a template. All DNA fragments were gel purified and two combinations (*mreD-TEVsite* + *eyfp* or *mreD-TEVsite-linker* + *eyfp*) were cloned into the *XhoI/HindIII* site of pWALDO-*gfp*-E using Gibson Assembly (see Fig. 6.3 for an overview), followed by transformation into *E. coli* NEB5 α . Recombinant plasmids were tested by restriction digest with *ClaI* resulting in 4325, 1753 and 453 bp fragments for pWALDO-*mreD*-6-*eyfp* and 4325, 1753 and 435 bp fragments for pWALDO-*mreD*-*eyfp*. Plasmids were validated by DNA sequencing (GATC Biotech AG, Konstanz, Germany) and electroporated into *E. coli* C43 (DE3).

Additionally, for an N-terminal *eyfp-mreD* fusion, *mreD* was amplified with primers 5'FW34/3'FW34 and *eyfp* was amplified with primers 5'FW33/3'FW33 using their codon optimised gene templates. In this configuration, *eyfp* was extended by a TEV site and an 11 amino acid linker (GSGSGSGSGSG) at the N-terminus. Both DNA fragments were gel purified and cloned into the *XhoI/HindIII* site of pWALDO-*gfp*-E (Waldo *et al.*, 1999) using Gibson Assembly (Fig. 6.3) followed by transformation into *E. coli* NEB5 α . Recombinant plasmids were tested by restriction digest with *EcoRV* and *PstI* resulting in 5092 and 1494 bp fragments (Fig. 6.3B) and were further validated by DNA sequencing (GATC Biotech AG, Konstanz, Germany). All recombinant plasmids were then electroporated into *E. coli* C43 (DE3).

6.1.1.2 Localisation of MreD-eYFP and MurJ-GFP in *E. coli*

In order to investigate the localisation of MreD-eYFP, MreD-6-eYFP and eYFP-11-MreD in *E. coli*, overnight cultures were diluted to an OD₆₀₀=0.05 in BHI and grown at 25 °C for 5 h in the presence of kanamycin (50 μ g/ml) and 1 mM IPTG. Cells were harvested, washed with PBS and analysed by fluorescence microscopy.

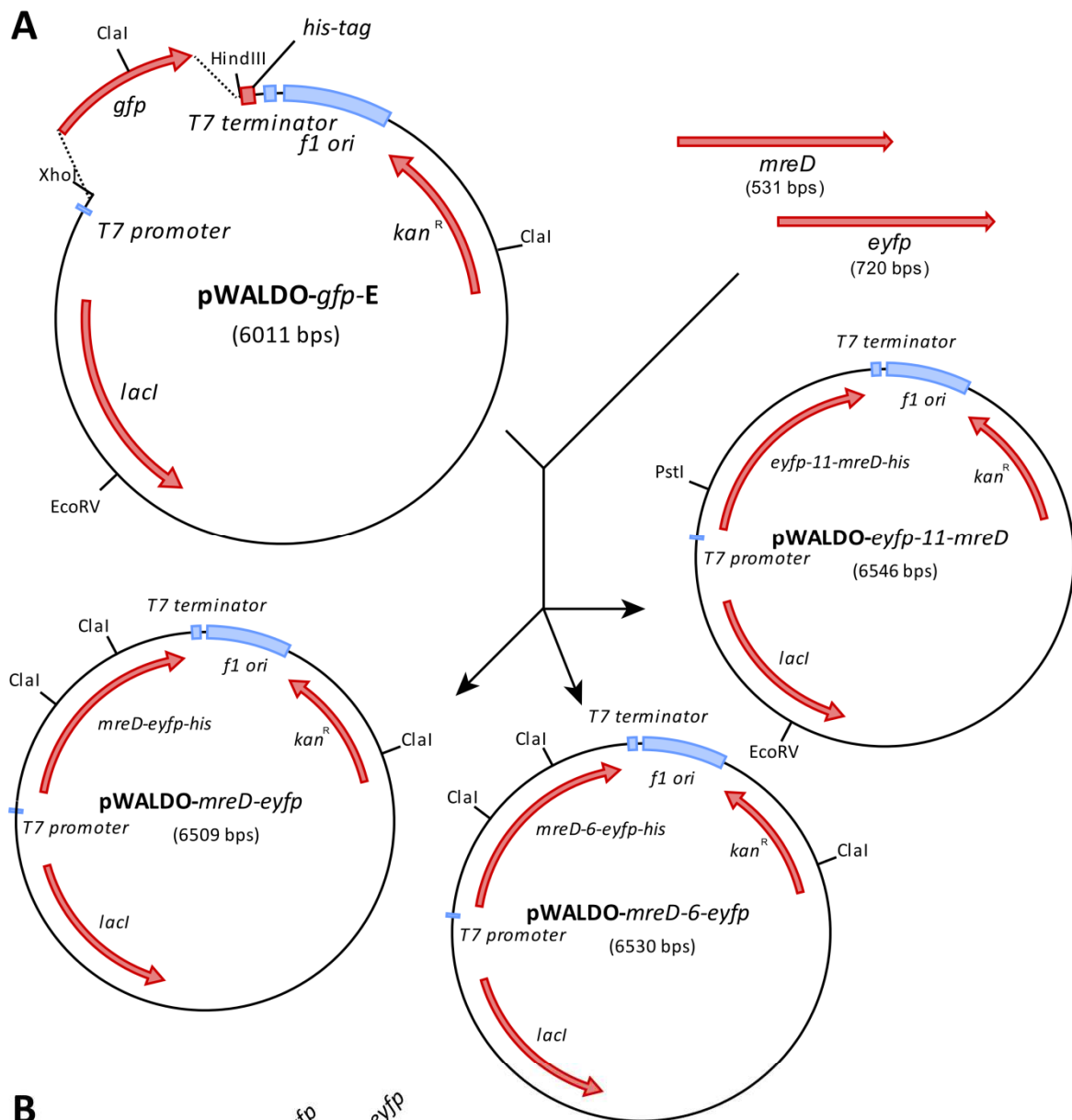


Figure 6.3 Construction of IPTG-inducible *mreD-eyfp* fusion constructs in *E. coli*

A, Diagram illustrating the construction of pWALDO-*mreD-eyfp*/ pWALDO-*mreD-6-eyfp* and pWALDO-*eyfp-11-mreD*. **B**, pWALDO-*mreD-eyfp* (Lanes 1-2) and pWALDO-*mreD-6-eyfp* (Lanes 3-4) candidate plasmids and pWALDO-*gfp-E* (Lane 5) were digested with *Cla*I. WALDO-*eyfp-11-mreD* (Lanes 6-8) candidate plasmids and pWALDO-*gfp-E* (Lane 9) were digested with *Eco*RV and *Pst*I. All digest products were separated by 1 % (w/v) TAE agarose gel electrophoresis. Bands of 4325, 1753 and 435 bp, corresponding to pWALDO-*mreD-eyfp* (Lanes 1-2), respectively, are marked by black arrows. Bands of 4325, 1753 and 453 bp, corresponding to pWALDO-*mreD-6-eyfp* (Lanes 3-4), respectively, are marked by black arrows. Bands of 4325 and 1753 bp correspond to pWALDO-*gfp-E* (Lane 5). Bands of 5092 bp and 1494 bp, corresponding to pWALDO-*eyfp-11-mreD* (Lanes 6-8), respectively, are marked by black arrows. A band of 6011 bp corresponds to pWALDO-*gfp-E* (Lane 9).

As a control strain to analyse the localisation of a membrane protein unrelated to MreD, pWALDO-*murJ-gfp* (gift from Dr.D.Roper, University of Warwick) was electroporated into *E. coli* C43 (DE3) and prepared as described for the MreD-eYFP fusion strains. MurJ flips lipid-linked precursors for peptidoglycan synthesis (lipid II) from the inside to the outside of the cell (Sham *et al.*, 2014).

All fusions were expressed in *E. coli* C43 (DE3) (Fig. 6.4). Both the C-terminal as well as the N-terminal fusion of MreD and eYFP are localised at the cell periphery as well as the cell poles. However, they do not exhibit a preference for the poles since no increased polar fluorescence can be observed. The fluorescence is not equally distributed throughout the membrane and appears to form a punctate pattern. In contrast to the MreD-eYFP fusion, MurJ-GFP localises preferentially at the cell pole and to a lesser extent to the cell periphery.

Since the MreD-eYFP fusions are likely to be highly expressed, it was tested next whether the distribution pattern is maintained at lower expression levels. Thus, overnight-cultures were diluted in BHI to an OD₆₀₀=0.05 and grown at 37 °C for 1 h in the presence of kanamycin (50 µg/ml) at 250 rpm. Subsequently, 0.6 mM IPTG was added and cultures were grown for another 2 h at 37 °C. Cells were harvested, washed with PBS and analysed by fluorescence microscopy (Fig. 6.5AB). Additionally, MreD-6-eYFP localisation was analysed using stochastic optical reconstruction microscopy (Fig. 6.6).

Low expression of MreD-6-eYFP and eYFP-11-MreD clarifies the protein localisation pattern in *E. coli*. Both fusions localise in a punctate pattern and do not exhibit a preference for the cell poles (Fig. 6.5AB). C-terminal or N-terminal tagging with eYFP to MreD does not alter its localisation properties. However, it is not known whether the tag itself affects the localisation. STORM studies of MreD-6-eYFP in *E. coli* also confirm its non homogeneous distribution (Fig. 6.6). However, due to the overexpression of the fusion protein, the localisation pattern appears messier compared to deconvolved epifluorescence images and the fusion seems to be localised at the whole cell periphery. This might show that deconvolution oversimplifies the localisation pattern and that MreD-6-eYFP in *E. coli* is rather localised in a gradient than in clearly separated areas. Nevertheless, the fusion does not localise homogeneously.

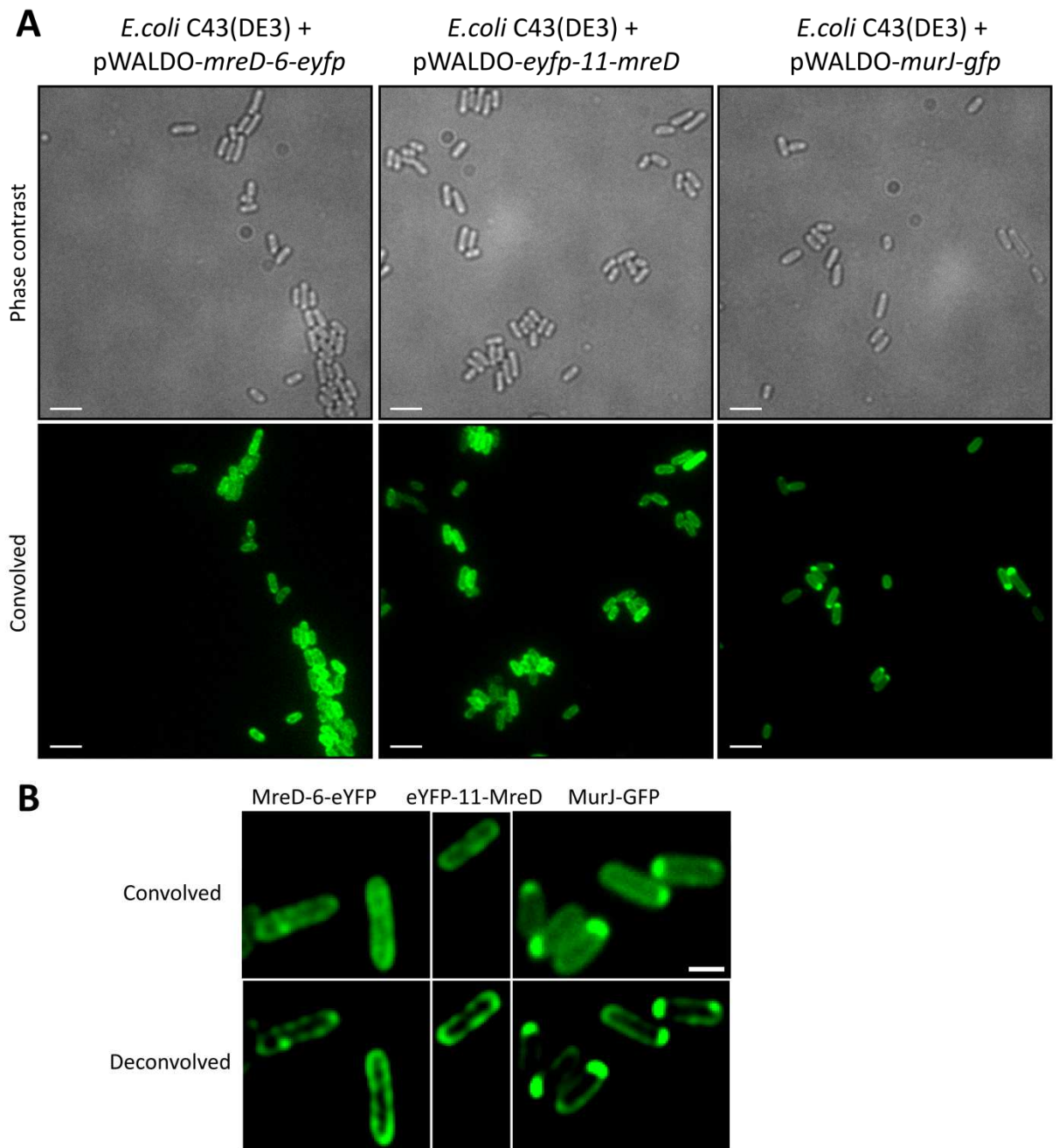


Figure 6.4 Localisation of MreD-eYFP fusions and MurJ-GFP in *E. coli*

A, Phase contrast and fluorescence images (convolved and deconvolved) of *E. coli* C43 (DE3) + pWALDO-*mreD-6-eyfp*, pWALDO-*eyfp-11-mreD* and pWALDO-*murJ-gfp* grown in the presence of 1 mM IPTG for 5 h. Images were acquired using a Delta Vision microscope and SoftWoRx 3.5.0 software (Applied Precision). Acquisition of fluorescence images were taken using 1 sec exposure in the FITC channel. Scale bars represent 3 μm . **B**, Images of selected cells. Scale bar represents 1 μm .

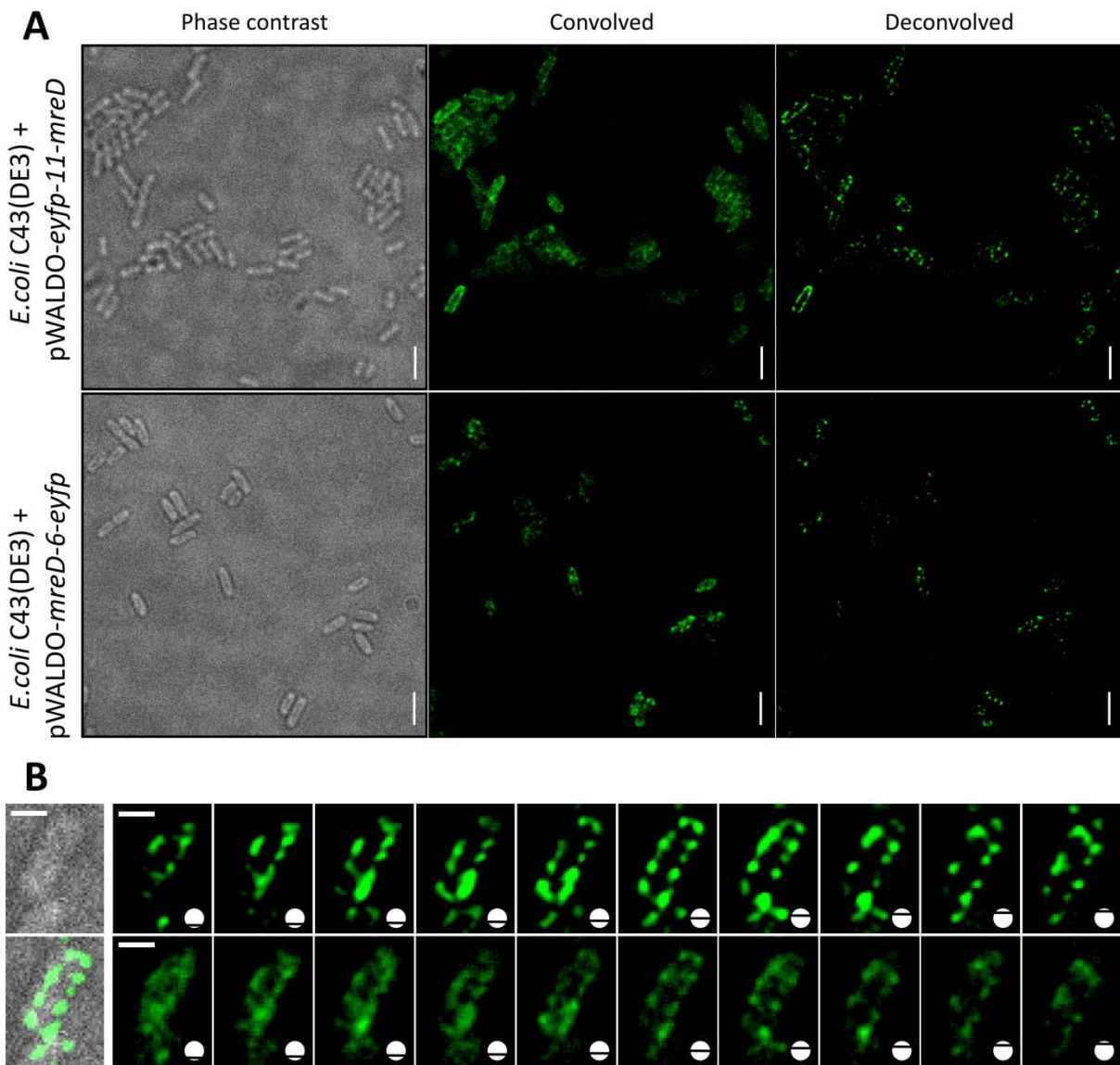


Figure 6.5 Localisation of MreD-eYFP fusions in *E. coli* at low expression levels

A, Phase contrast and fluorescence images (convolved and deconvolved) of *E. coli* C43 (DE3) + pWALDO-*mreD-6-eyfp*, pWALDO-*eyfp-11-mreD* and pWALDO-*murJ-gfp* grown in the presence of 0.4 mM IPTG for 2.5 h. Images were acquired using a Delta Vision microscope and SoftWoRx 3.5.0 software (Applied Precision). Acquisition of fluorescence images were taken using 1 sec exposure in the FITC channel. Scale bars represent 3 μ m. **B**, Z-stack images of selected *E. coli* + pWALDO-*mreD-6-eyfp* cells. Scale bar represents 1 μ m.

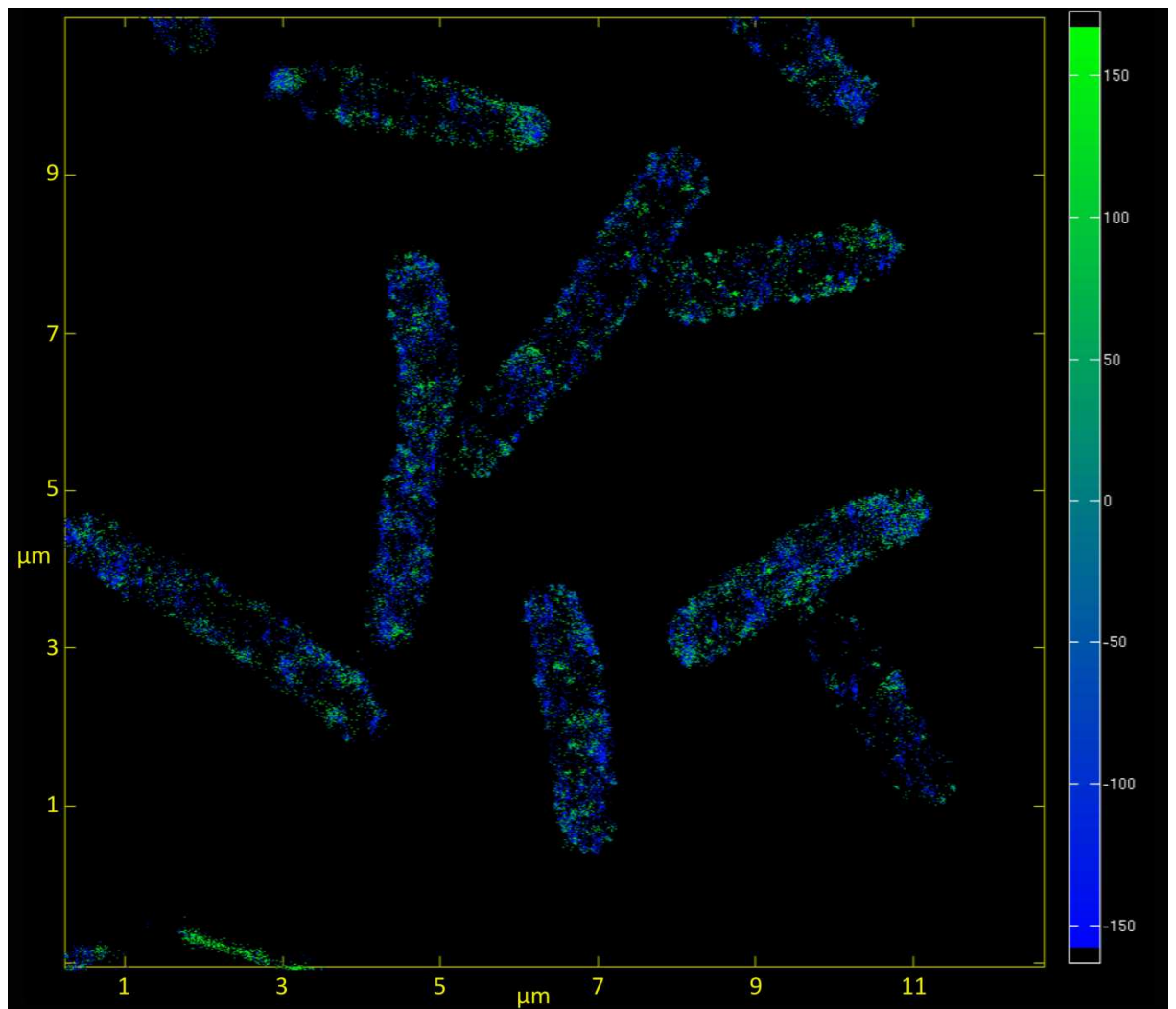


Figure 6.6 3D-STORM imaging of MreD-6-eYFP in *E. coli*

3D-STORM reconstruction images of MreD-eYFP localisation in *E. coli* C43 (DE3) + pWALDO-*mreD-6-eyfp*. Imaging was performed in GLOX -MEA. The colour scale represents the z-axis (nm).

Next it was asked as to whether the rod-shape of *E. coli* is required for the heterogeneous localisation pattern of MreD-eYFP. Cells were prepared as shown for the previous experiment (Fig. 6.5). Cells were harvested and washed with ice-cold Tris-HCl (10 mM, pH 7.5) and the pellet was resuspended to an OD₆₀₀=0.6 in sucrose buffer (33 mM Tris-HCl (pH 8.0), 20 % sucrose (w/v)). 80 µl of EDTA (0.1 M) and 400 µl lysozyme (1 mg/ml) were added to 1 ml of resuspended cells and the tube was covered in foil and incubated at 4 °C on a rotary wheel for 30 min. Cells were then washed with and resuspended in ice-cold sucrose buffer. Prepared spheroplasts were placed on non-coated slides and analysed by fluorescence microscopy.

MreD-eYFP localises in a heterogeneous fashion in *E. coli* spheroplasts (Fig. 6.7). Therefore the rod-shape is not the determinant for MreD positioning in terms of its heterogeneous distribution.

6.1.2 Localisation of membrane proteins in cytoplasmic vesicles

As a next step, the localisation properties of *S. aureus* membrane proteins were investigated in isolated protoplast membranes that are also referred to as cytoplasmic membrane vesicles. In *B. subtilis* and *E. coli*, cytoplasmic membrane vesicles are generated by the enzymatic removal of the cell wall using lysozyme in a hypotonic medium which causes the cells to burst. In an alternative gradual approach, the cell wall is removed first in a stabilising hypertonic medium followed by the transfer to a hypotonic medium (see Fig. 6.8). Cytoplasmic membrane vesicles still contain all the native membrane proteins and components.

Since MreD at its native levels is not abundant enough for visualisation, an EzrA-GFP fusion, that was shown to be very bright under the microscope, was used to establish the cytoplasmic membrane vesicle protocol. *S. aureus* is lysozyme resistant due to an O-acetyl group on its N-acetylmuramic acid residue sterically hindering the access for lysozyme (Bera *et al.*, 2005). Therefore, lysostaphin was used instead of lysozyme in the following protocols. A new protocol for the creation of cytoplasmic membrane vesicles was designed based on Kim *et al.* and Alcayaga *et al.* including modifications (Kim *et al.*, 2009, Alcayaga *et al.*, 1992).

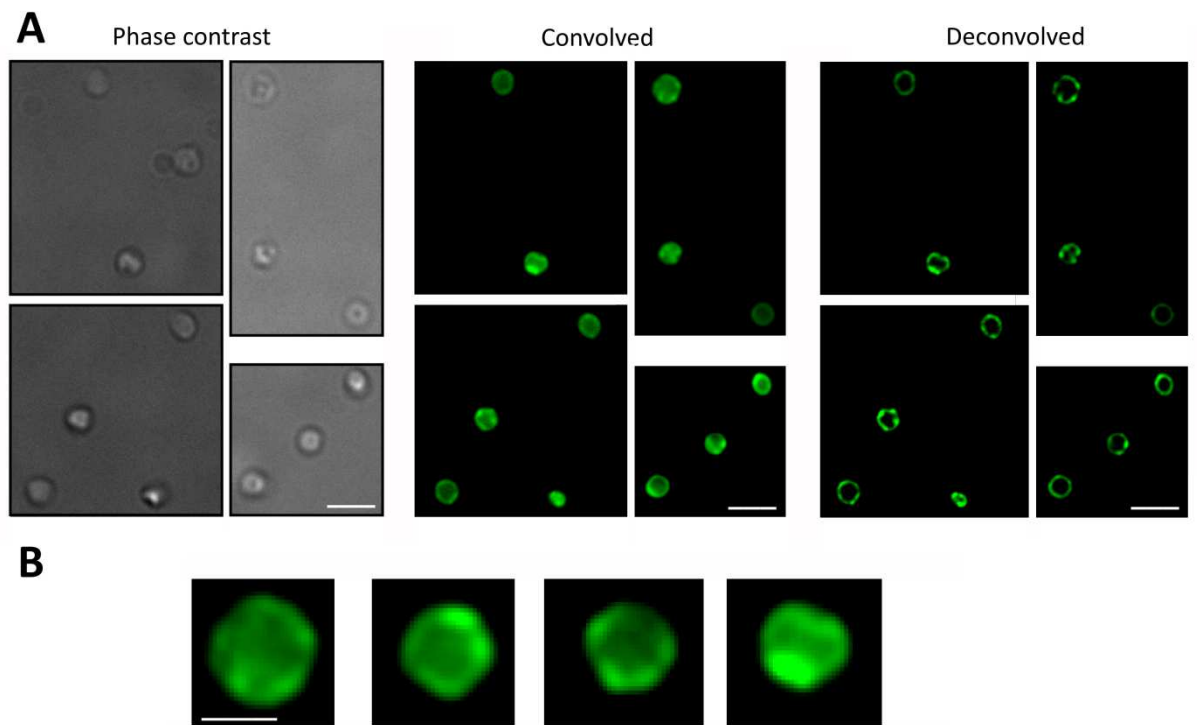


Figure 6.7 Localisation of MreD-eYFP in *E. coli* spheroplasts

A, Phase contrast and fluorescence images (convolved and deconvolved) of *E. coli* C43 (DE3) + pWALDO-*mreD-6-eyfp* spheroplasts. Images were acquired using a Delta Vision microscope and SoftWoRx 3.5.0 software (Applied Precision). Acquisition of fluorescence images were taken using 1 sec exposure in the FITC channel. Scale bars represent 3 μm . **B**, Selected convolved fluorescence images. Scale bar represents 1 μm .

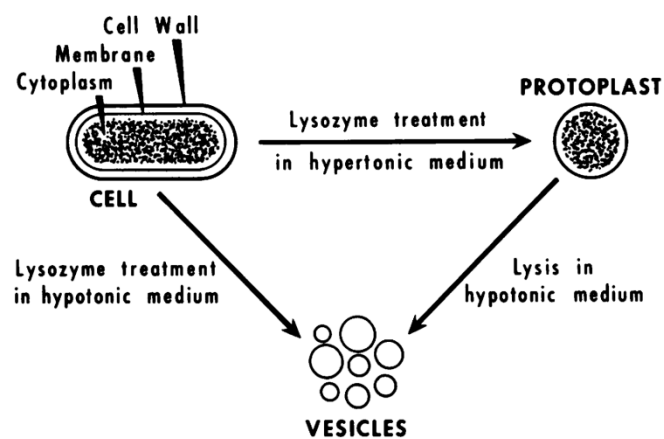


Figure 6.8 Schematic overview of the preparation of membrane vesicles
Image is adapted from Konings *et al.*, 1973.

Overnight cultures of SH1000 and SH1000 *ezrA-gfp* (Steele *et al.*, 2011) were diluted in 1 l to an $OD_{600}=0.05$ in a HCl-washed 3 l flask. Cultures were grown to an $OD_{600}\approx 2$ at 37 °C and 200 rpm. Cells were harvested by centrifugation at 6000 x g for 20 min at 4 °C and subsequently washed with Tris-HCl (50 mM, pH7.5). The pellet was resuspended in 40 ml hypertonic resuspension buffer (1 M sucrose, 50 mM Tris-HCl, pH 7.5, protease inhibitor cocktail (Sigma-Aldrich, St.Louis, United States)). Lysostaphin and DNase were added to a final concentration of 75 µg/ml and 20 µg/ml, respectively. The tubes were covered in foil and incubated at 37 °C with mild agitation at 40 rpm for 2.5 h. Formation of protoplasts was monitored on a microscope placing a sample of protoplasts on a non-coated slide without sealing the coverslip. Cells were put on focus before adding a drop of a 10 % SDS (w/v) solution at the edge of the coverslip. The disappearance of cells straight after adding SDS indicated the presence of protoplasts. Protoplasts were recovered by centrifugation at 5000 x g at 4 °C for 15 min and resuspended in 40 ml hypotonic resuspension buffer (50 mM Tris-HCl, pH 7.5, protease inhibitor cocktail (Sigma-Aldrich, St.Louis, United States)) supplemented with RNase (10 µg/ml) and DNase (10 µg/ml). The resuspension was incubated at RT for 1 h at mild agitation covered in foil. Subsequently, unbroken cell debris was removed by centrifugation at 2000 x g for 10 min at 4 °C and the supernatant was centrifuged at 25 000 rpm (38 000 x g; Beckman Ti50.2 rotor) for 30 min at 4 °C. The pellet was carefully resuspended in sucrose buffer (300 mM sucrose, 50 mM Tris-HCl, pH 7.5) and loaded on top of a sucrose gradient in a SW41 polycarbonate tube. The gradient was built up as follows: 3.5 ml 50 % sucrose (w/v), 3.5 ml 30 % sucrose (w/v), 3.5 ml 20 % sucrose (w/v) and 1-1.5 ml sample. The gradient was run for 10 h at 4 °C and 36400 rpm (100 000 x g) and fractions at the interphases to 20 %, 30 %, 50 % and near the bottom of the tube were carefully collected. Samples were mixed with a 2 % agarose (w/v) solution and placed on a non-coated slide followed by analysis using fluorescence microscopy.

Vesicle formation is a rare event since not many membrane vesicles could be observed even though the initial culture volume was very high. Membrane vesicles reached sizes of 2-10 µm and were mostly connected to other vesicles and smaller undefined potential membrane particles.

First, vesicles derived from SH1000 expressing *ezrA-gfp* were analysed (Fig. 6.9A) using a vesicle-agarose suspension supplemented with FM4-64. Vesicles were successfully stained with the membrane dye, FM4-64, as a fluorescent signal could be seen in the Cy5 channel. Furthermore, the Ezra-GFP fusion appears to be present in the

vesicles and fluoresces. However, using two controls, one with SH1000 derived vesicles stained with FM4-64 and the other without the addition of FM4-64, questions the observation seen for SH1000 EzrA-GFP vesicles (Fig. 6.9B). Vesicles prepared in agarose supplemented with FM4-64 exhibit fluorescence in both the Cy5 and the FITC channel which shows that the fluorescence seen for SH1000 EzrA-GFP vesicles is unlikely to be due to the EzrA fusion (Fig. 6.9B). Furthermore, using no membrane dye still results in fluorescence signals in both channels even though the signal strength is weaker. In conclusion, FM4-64 could cross-bleed to the FITC channel and membrane vesicles may exhibit auto-fluorescence in both channels.

6.1.3 Localisation of membrane proteins in liposomes

6.1.3.1 Liposome formation by lipid emulsion

Cytoplasmic membrane vesicles are not suitable for membrane protein localisation studies since the autofluorescence hinders the application of fluorescently tagged membrane proteins in the FITC channel.

The use of liposomes could circumvent this issue if the observed autofluorescence of vesicles is due to fluorescent components in the membrane of *S. aureus*. In order to do so, a lipid emulsion protocol adapted from (Osawa *et al.*, 2008) was applied using DMPC lipids. This method is based on layering a lipid emulsion on top of an aqueous phase followed by centrifugation resulting in the formation of vesicles as the lipid emulsion enters the aqueous phase.

25 μ l of a DMPC stock solution (10 mg/ml in 100 % methanol (v/v))(Avanti Polar lipids, Alabaster, United States of America) was dried under air-flow in an eppendorf tube at RT. The lipid pellet was resuspended in 250 μ l mineral oil (Affymetrix, Santa Clara, United States of America) followed by 20 x 2 sec sonication cycles at maximal amplitude (Equipment). The resuspension was incubated at RT for 5 h and subsequently 130 μ l of the resuspension were layered on top of 50 μ l dH₂O in an eppendorf tube followed by centrifugation at 2000 x g for 3 min. The bottom phase containing a mix of vesicles and dH₂O was carefully removed without mixing both phases and 40 μ l of this phase were gently and quickly mixed with 20 μ l agarose (2 %, (w/v), low gelling agarose) supplemented with FM 4-64 (1 μ g/ml) or FM1-43 (1 μ g/ml). 20 μ l of this mix were placed on a non-coated slide and analysed by fluorescence microscopy.

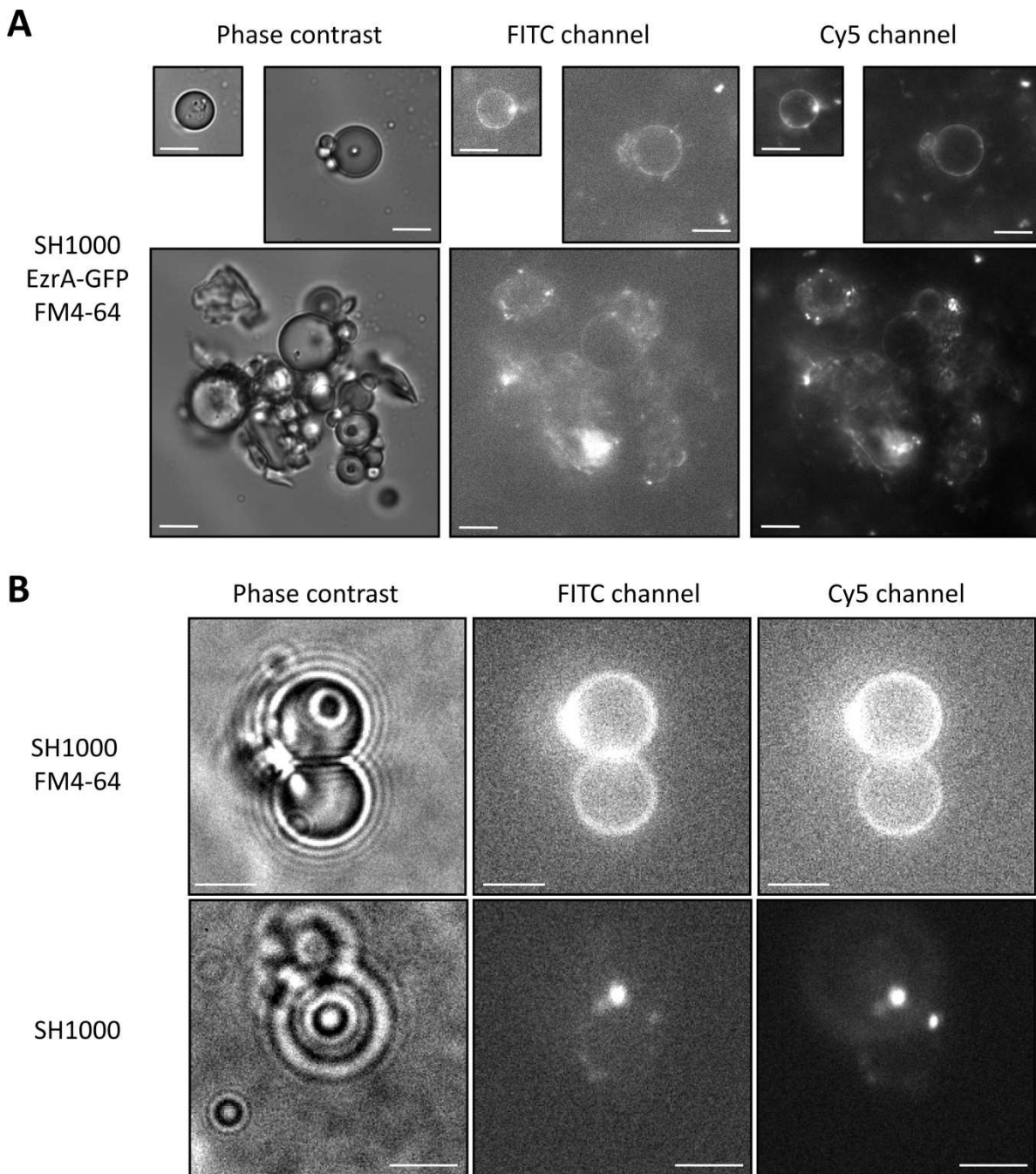


Figure 6.9 Cytoplasmic membrane vesicles of *S. aureus*

A, Phase contrast and fluorescence images (convolved and deconvolved) of cytoplasmic membrane vesicles derived from *S. aureus* SH1000 *ezrA-gfp* and prepared in agarose supplemented with FM4-64. Images were acquired using a Delta Vision microscope and SoftWoRx 3.5.0 software (Applied Precision). Acquisition of fluorescence images were taken using 1 sec exposure in the FITC channel and 1 sec exposure in the Cy5 Channel. Scale bars represent 5 μm . **B**, Cytoplasmic membrane vesicles of *S. aureus* SH1000 prepared in agarose with and without the addition of FM4-64. Scale bar represents 5 μm .

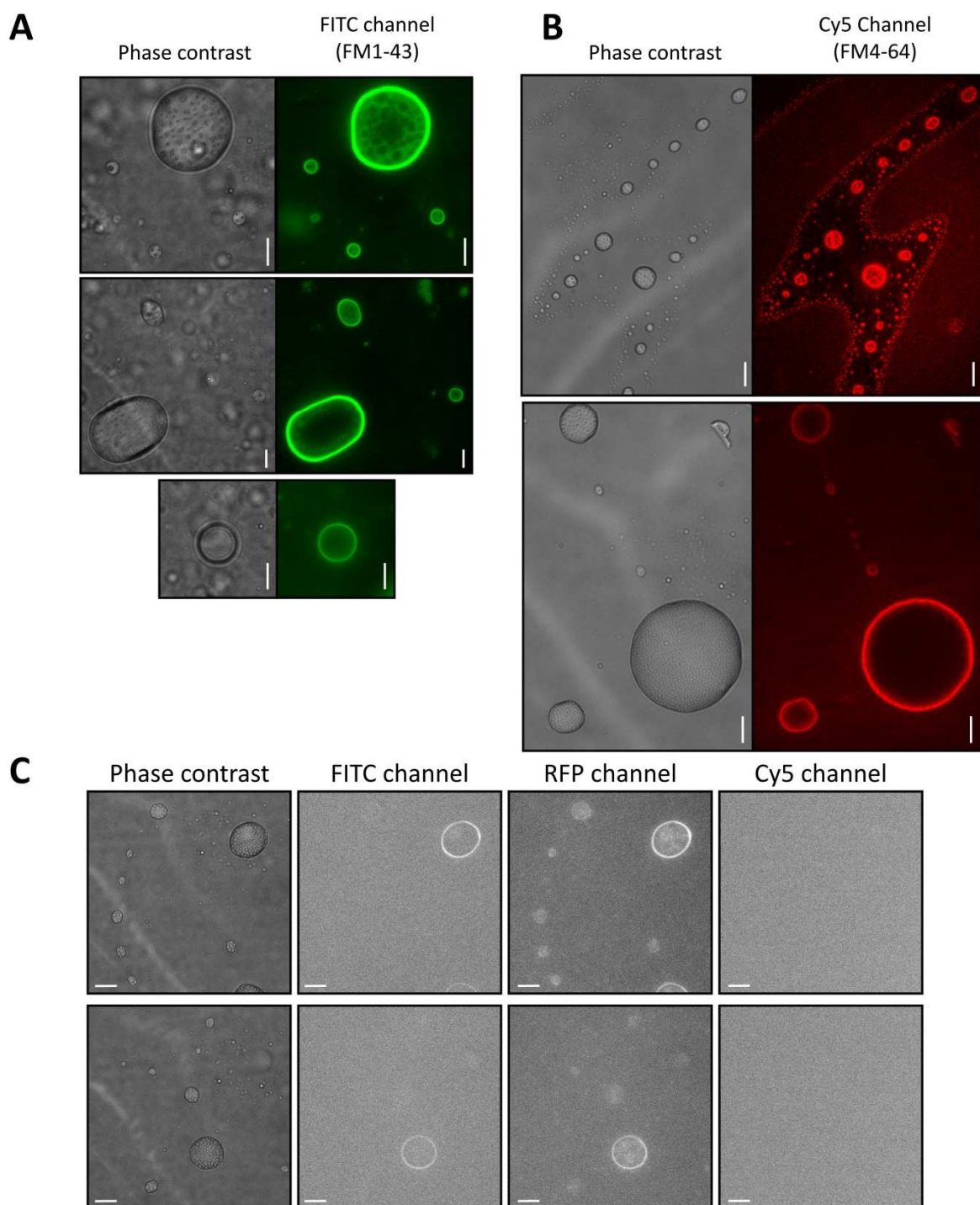


Figure 6.10 Liposome generation using the emulsion method

Images were acquired using a Delta Vision microscope and SoftWoRx 3.5.0 software (Applied Precision). Acquisition of fluorescence images were taken using 1 sec exposure in the FITC channel, 1 sec in the RFP channel and 1 sec exposure in the Cy5 channel. Scale bars represent 5 μm . **A**, Phase contrast and fluorescence images (convolved) of liposomes derived from DMPC lipids and prepared in agarose supplemented with FM1-43. **B**, Phase contrast and fluorescence images (convolved) of liposomes derived from DMPC lipids and prepared in agarose supplemented with FM4-64. **C**, Phase contrast and fluorescence images (convolved) of liposomes derived from DMPC lipids and prepared in agarose without membrane dyes.

Liposomes could be successfully formed using the lipid emulsion method. Liposomes were stained by stabilising the vesicles in agarose supplemented with membrane dyes FM1-43 and FM4-64 resulting in bright vesicles in the FITC channel (FM1-43) and Cy5 (FM4-64) channel (Fig. 6.10AB). Observed vesicle sizes were in the range between a 1 to 30 μm in diameter. However, fluorescence analyses of unstained vesicles revealed an autofluorescence in the FITC and RFP channel but not in the Cy5 channel (Fig. 6.10C) which could potentially be an issue for localisation studies with reconstituted proteins that are labelled with dyes fluorescent at these wavelengths.

6.1.3.2 Reconstitution of MreD into liposomes

6.1.3.2.1 Overexpression and purification of MreD-6-eYFP

MreD-6-eYFP purification was performed according to a protocol based on the purification of GFP-tagged membrane proteins (Drew *et al.*, 2006). As a control to establish the purification protocol, MurJ-GFP was also overexpressed and purified.

Protein overexpression and purification is described in detail in Section 2.12. Briefly, recombinant proteins were overexpressed by growing *E. coli* C43 (DE3) + pWALDO-*mreD-6-eyfp* or pWALDO-*murJ-gfp* to exponential phase at 37 °C, followed by induction with 1 mM IPTG and shifting the incubation temperature to 25 °C for 4 h. Cultures were harvested and broken by a French press. Membranes were purified by ultracentrifugation and solubilised using DDM. The proteins were then purified by passage over a HiTrapTM affinity column (GE Healthcare), that was preloaded with Ni SepharoseTM and charged with Ni²⁺. The column was washed with 5 % (w/v) imidazole and finally eluted by increasing imidazole concentrations. Eluted 1 ml fractions were collected, separated by 15 % (w/v) SDS-PAGE and purified MreD-6-eYFP and MurJ-GFP were visualised by western blotting using anti-GFP antibodies (Rabbit) (Thermo Fisher Scientific, Waltham, United States of America) as primary antibodies and anti-Rabbit peroxidase (Goat, horseradish peroxidase conjugate) as secondary antibodies (Thermo Fisher Scientific, Waltham, United States of America). The western blot was developed by enhanced chemiluminescence using the PierceTM ECL Western Blotting Substrates (Thermo Fisher Scientific, Waltham, United States of America).

Purification of MreD-6-eYFP was unsuccessful since the fusion did not bind properly to the HiTrap column and was washed out with low imidazole amounts (see

Fig. 6.11A, Lanes 3-4). Separation of the initial membranes used for purification also did not show any signal indicating that the amount of MreD-6-eYFP fusions in the overexpression might not be sufficient for purification (Fig. 6.11A, Lane 1). The band corresponding to MreD-6-eYFP runs between 32 and 46 kDa which is lower than expected since the calculated weight of MreD-6-eYFP is 54.6 kDa (<http://www.sciencegateway.org/tools/proteinmw.htm>).

Purification of MurJ-GFP could be achieved since a strong signal of a protein band can be seen of elution fractions (Fig. 6.11B, Lanes 6-8) and MurJ-GFP fusions could also be visualised in purified membranes (Fig. 6.11B, Lane 1).

Overexpression and purification of MreD-6-eYFP with plasmid pWALDO-*mreD-6-eyfp* was also attempted by A.Szewczak (Cambridge) but expression yields were not sufficient and the fusion could not be purified via a Nickel column (personal communication A.Szewczak). Therefore, purified non-fluorescent MreD including a C-terminal His-tag was used for reconstitution studies (gift from Prof. J. Löwe, University of Cambridge).

6.1.3.2.2 FITC-labelling of purified MreD

In order to visualise MreD, purified MreD proteins were labelled with Fluorescein Isothiocyanate (FITC). FITC is a derivative of Fluorescein that reacts with amine groups and can be used to label proteins. 2 mg of purified MreD proteins were mixed in 1 ml labelling buffer (200 mM sodium bicarbonate, 0.04 % n-dodecyl β -d-maltoside (DDM) (w/v), pH 9) and 50 μ l FITC (10 mg/ml stock solution in DMSO) was added. The tube was covered in foil and incubated at RT for 6 h on a rotary wheel. Unbound FITC was removed using an equilibrated PD MidiTrap G-25 desalting column (equilibration buffer: 20 ml of 20 mM Tris-HCl, 100 mM NaCl, 0.03 % DDM (w/v) pH 7) (GE Healthcare, Little Chalfont, United Kingdom). The concentration of the desalted MreD-FITC solution was determined by Pierce™ BCA Protein Assay Kit (Thermo Fisher Scientific, Waltham, United States of America) and stored at -70 °C.

6.1.3.2.3 Reconstitution of FITC-labelled MreD into liposomes

Liposomes were created as previously described in Section 6.1.3.1. Briefly, DMPCs were dried under air-flow and the lipid pellet was resuspended in 250 μ l mineral oil followed by sonication. The resuspension was incubated at RT for 5 h. Labelled MreD was added and the mixture was vigorously vortexed before 130 μ l of the resuspension

was layered on top of 50 μl dH_2O in an Eppendorf tube followed by centrifugation at 2000 x g for 3 min. The bottom phase was removed and 40 μl was mixed with 20 μl agarose (2 % (w/v), low gelling agarose) supplemented with FM 4-64 (1 $\mu\text{g}/\text{ml}$). 20 μl of this mix were placed on a non-coated slide and analysed by fluorescence microscopy.

MreD reconstitution into liposomes was attempted using several combinations to explore how the membrane dye or different protein concentrations affect the liposomes. First, liposomes were generated using 0.5 μM MreD-FITC without FM4-64 to investigate whether the FITC-labelled protein exhibits a cross-bleed to the Cy5 channel. As seen in Fig. 6.12A, no fluorescence signal can be observed in the Cy5 channel, but a liposome with a fluorescent signal in the FITC channel can be observed. Next, various MreD-FITC concentrations ranging from 0.5 to 7 μM protein were employed. Protein concentrations higher than 2 μM resulted in a massive fluorescent signal (not shown). Using 2 μM MreD-FITC shows that the labelled protein binds to liposomes (Fig. 6.12B). However, the background signal is very high and no signal can be observed for FM4-64 that was used to stain the liposomes. Potentially, the amount of MreD-FITC is too abundant and blocks the incorporation of FM4-64. Using 0.5 μM resulted in the best results showing liposomes stained with FM4-64 and MreD-FITC (Fig. 6.12D). The background signal is still very high and probably indicates that the unbound FITC was not removed enough by the desalting column. Interestingly, liposomes appear to be deformed. This might indicate a potential effect of MreD on the liposome structure by bending the membranes or that the detergent used to keep the purified MreD proteins soluble affects the liposomes. The fluorescent signal in the FITC channel is distributed homogeneously and no detailed features can be observed. As a control, only FM4-64 without using MreD-FITC was used to investigate whether FM4-64 causes a fluorescent signal in the FITC channel (Fig. 6.12C). Unfortunately, a clear signal could be seen even though no MreD-FITC was used. This signal was weaker compared to the MreD-FITC reconstitution experiments and might be due to the autofluorescence of the liposomes (see Fig. 6.10) or due to a fluorescence cross-bleed from FM4-64.

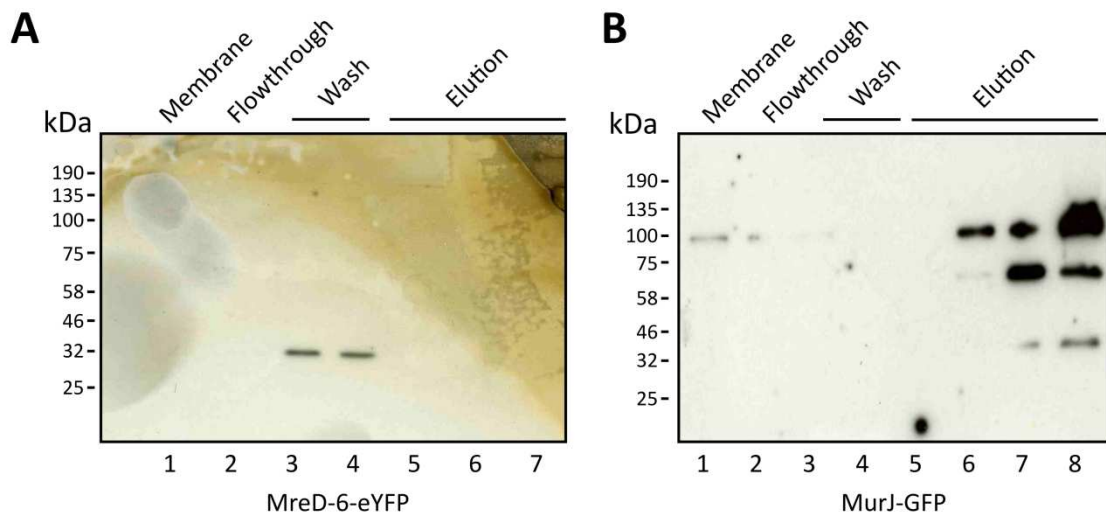


Figure 6.11 Purification of MreD-6-eYFP and MurJ-GFP

Western Blot of various purification steps of MreD-6-eYFP and MurJ-GFP. Western blots were performed using a 1:2000 dilution of Anti-GFP (Rabbit) antibodies as a primary and 1:10000 Anti-Rabbit (Goat) peroxidase as a secondary antibody. Blots were developed by enhanced chemiluminescence. Western Blot of purification fractions of MreD-6-eYFP (**A**) and MurJ-GFP (**B**). The following fractions were analysed: purified membranes (Lane 1), flowthrough of membranes passaged through the HiTrap column (Lane 2), Wash fractions (Lanes 3-4) and elution fractions (Lanes 5-7 for MreD-6-eYFP and lanes 5-8 for MurJ-GFP).

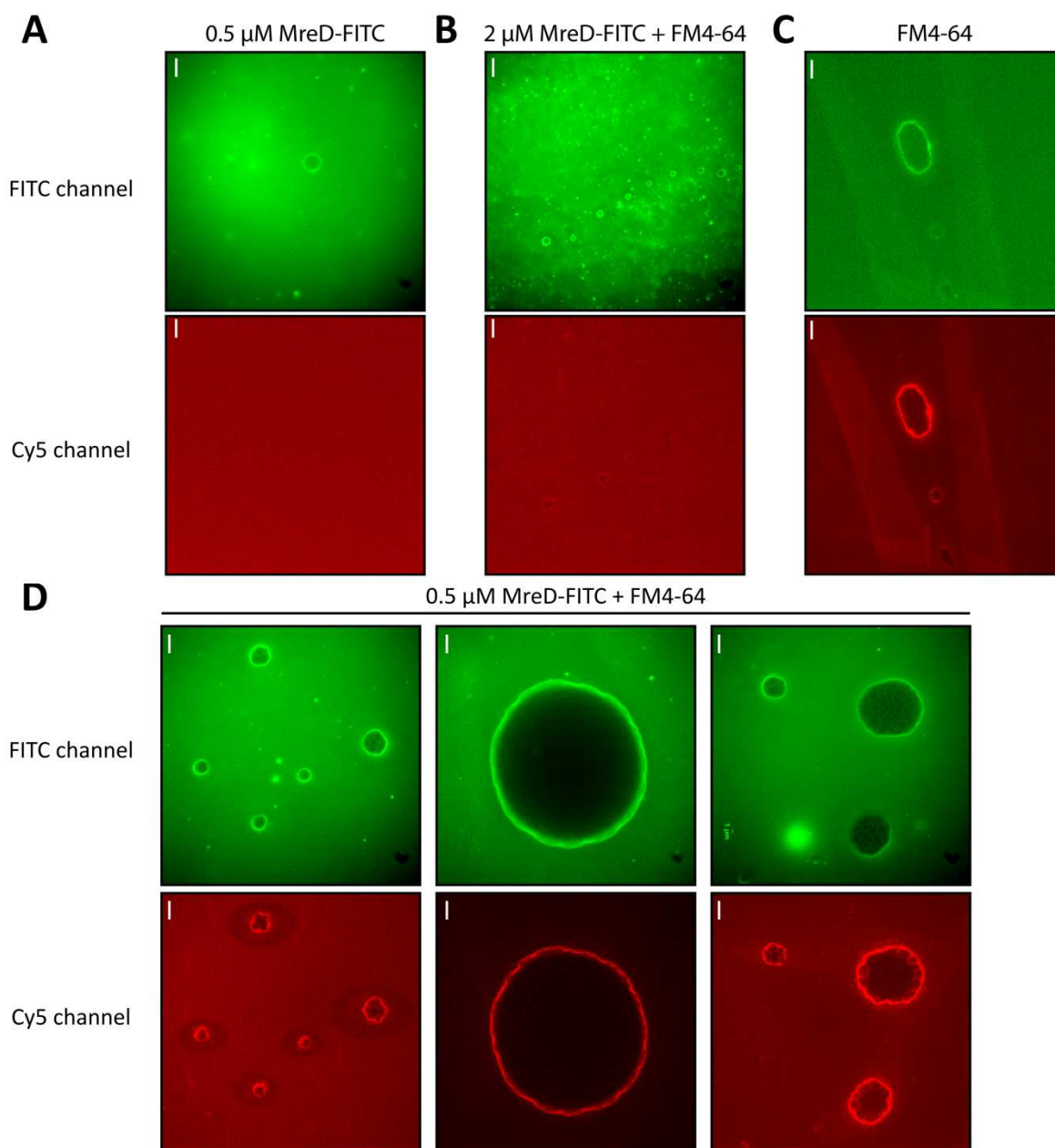


Figure 6.12 MreD-FITC reconstitution into liposomes

Fluorescence images (convolved) of different concentrations of reconstituted FITC-labelled MreD into liposomes derived from DMPC in agarose with or without FM4-64. Images were acquired using a DeltaVision microscope and SoftWoRx 3.5.0 software (Applied Precision). Acquisition of fluorescence images were taken using 0.2 sec exposure at 50 % intensity in the FITC channel and 1 sec exposure in the Cy5 channel. Scale bars represent 5 μm. **A**, Fluorescence images (convolved) of liposomes derived from DMPC lipids with 0.5 μM FITC-labelled MreD and prepared in agarose. **B**, Fluorescence images (convolved) of liposomes derived from DMPC lipids with 2 μM FITC-labelled MreD and prepared in agarose supplemented with FM4-64. **C**, Fluorescence images (convolved) of liposomes derived from DMPC lipids and prepared in agarose supplemented with FM4-64. **D**, Fluorescence images (convolved) of liposomes derived from DMPC lipids with 0.5 μM FITC-labelled MreD and prepared in agarose supplemented with FM4-64.

6.3 Discussion

6.3.1 Punctate patterned distribution of membrane proteins in rod-shaped bacteria

MreD-eYFP expressed in *E. coli* localises in a heterogeneous punctate pattern (Fig. 6.5). This localisation is dose-dependent since higher expression resulted in a more homogeneous distribution at the cell-periphery (Fig. 6.4). Importantly, although MreD does not avoid the cell poles, no increased polar fluorescence could be observed unlike for other membrane proteins such as MurJ (Fig. 6.4), the lactose transporter LacY, the chemotaxis protein CheR or the phosphotransferase system protein E1 (Romantsov *et al.*, 2010, Santos *et al.*, 2014, Govindarajan *et al.*, 2013).

There are two possibilities as to how MreD localises in a punctate pattern: First, the heterogeneous punctate localisation pattern might be an intrinsic property of MreD by sensing membrane domains or membrane curvature. *E. coli* poles are enriched in cardiolipin and phosphatidylethanolamine and MreD might avoid these lipids (Kawai *et al.*, 2004, Nishibori *et al.*, 2005). Furthermore, the degree of membrane curvature could be the critical parameter determining the localisation of MreD. The radius of the *E. coli* cylinder is $0.37 \pm 0.05 \mu\text{m}$ and the radius of *E. coli* spheroplasts $0.61 \pm 0.09 \mu\text{m}$ whereas the *S. aureus* exhibits also a similar cell size radius of $0.46 \pm 0.04 \mu\text{m}$ (the average cell size of 76 cells was measured from exponentially growing cells using MreD-eYFP in *E. coli* and PlsY-GFP in *S. aureus* as membrane markers). Hence, *E. coli* rods and spheroplast membranes offer similar degrees of membrane curvature compared to *S. aureus* membranes.

The second explanation for the punctate localisation of *S. aureus* MreD in *E. coli* could be that the protein is positioned by MreB. MreBCD interact with each other in *E. coli* and form a membrane bound complex (Kruse *et al.*, 2005). MreB localises either in a helical pattern throughout the cell or in patches at the cell-periphery (Errington, 2015). In either way, if MreB positions MreD, the localisation of MreD could appear as a punctate pattern. In *B. subtilis*, MreD localises similarly to *E. coli* in a banded pattern along with MreB and MreC (Leaver & Errington, 2005). Therefore, a punctate pattern of MreD in the rod-shaped bacterium *E. coli* is not surprising and might facilitate pre-existing localisation cues.

Also other membrane proteins in rod-shaped bacteria were found to exhibit a punctate localisation pattern. The succinate dehydrogenase Sdh, the ATPase AtpA as

well as the phage protein p16.7 localise in discrete patches along the cell periphery of *B. subtilis* and form a pattern reminiscent of MreD-eYFP in *E. coli* (Johnson *et al.*, 2004). Recently, KinC, a histidine kinase involved in sporulation, and FloT were shown to be localised in lipid rafts in *B. subtilis* (Meile *et al.*, 2006, Lopez & Kolter, 2010). These rafts also form discrete patches in the membrane. It is not known yet whether these lipid rafts are connected to the positioning of other punctate patterned membrane proteins such as Sdh, AtpA or p16.7. Another membrane protein localised heterogeneously is the FtsZ-associated protein UgtP (Nishibori *et al.*, 2005). UgtP is a division inhibitor that stops FtsZ assembly under nutrient rich-conditions and colocalises with FtsZ (Shiomi & Margolin, 2007, Weart *et al.*, 2007).

In conclusion, several mechanisms can be responsible for a punctate patterned distribution of membrane proteins in rod-shaped bacteria and specifically for MreD in *E. coli* as shown in this study. These encompass cytoskeletal components such as MreB, membrane domains or FtsZ. However, it can not be excluded that MreD self-organises based on a specific degree of membrane curvature.

6.3.2 Reconstitution of MreD into liposomes

The overexpression and purification of MreD-eYFP in *E. coli* was not successful which could be explained in several ways. MreD-eYFP containing a C-terminal His-tag might not bind properly to the HiTrap column. MreD is an integral membrane protein and likely to be insoluble. Therefore it might be covered in a mix of lipids and detergents and the His-tag might not be exposed and thus useless in terms of purification. MreD containing a C-terminal His-tag but without eYFP, however, could be purified indicating that the eYFP tag might be an issue which could be resolved with the use of different detergents, an N-terminal His-tag of MreD-eYFP or the use of other affinity tags such as the streptavidin tag.

Labelling of membrane proteins might also exhibit a problem regarding their micro environment. In this study, amine-labelling with FITC was used to visualise purified MreD. Since proteins are likely to be covered in lipids or detergents, FITC might not reach amine residues of MreD resulting in incomplete labelling. Additionally, protein reconstitution experiments revealed a high background fluorescence that is either due to labelled MreD not being incorporated into liposomes or due to unbound FITC. In the latter case, a desalting column is not enough to remove unbound FITC which could be resolved by an additional purification step via gel filtration.

Reconstituted MreD appears to be localised homogeneously in liposomes. No detailed features such as a punctate localisation pattern could be observed. Potentially, too much MreD was used for reconstitution experiments or if MreD is capable of self-organisation and requires a specific membrane curvature, the liposomes generated in this study were probably too large. Vesicles were 5 μm in diameter and thus substantially larger than *S. aureus* or *E. coli* cells. Another explanation could be that the punctate heterogeneous localisation pattern of MreD is based on a different underlying mechanism that is not present in liposomes such as membrane domains or other proteins.

6.3.3 Conclusion

MreD-eYFP localises non-homogeneously in a punctate pattern in *E. coli*. This pattern is maintained in spheroplasts and therefore, the rod-shape, cell wall and the outer membrane are not required for the localisation pattern. Purification of MreD-eYFP failed but MreD without an eYFP tag could be purified. Purified proteins were attempted to be reconstituted into liposomes and appear to be localised homogeneously in liposomes. However, autofluorescence of liposomes and high background fluorescence potentially due to unbound label exhibit major problems with this method.

6.4 Main findings in this chapters

- MreD with a C-terminal or N-terminal fusion with eYFP localises in a punctate pattern in *E. coli*
- The punctate pattern of MreD-eYFP is maintained in *E. coli* spheroplasts
- MreD labelled with FITC distributes homogeneously in liposomes but more experiments are required to draw conclusions of the properties of MreD in liposomes

3.5 Contributions

Purified MreD was provided by the laboratory of Prof. Jan Löwe (Andrzej Szewczak, University of Cambridge). I performed all experiments in this chapter.

Chapter 7: General Discussion

All life demands the temporal and spatial control of essential biological functions. However, cellular organisation in the prokaryote kingdom is poorly understood. Bacteria lack many of the known organisers as well as the compartmentalisation of eukaryotic cells and have to count on the cell wall and the membrane as anchoring sites for fundamental processes. Furthermore, these membrane-associated processes are driven by proteins organised in complexes that have to be positioned at certain subcellular locations. The discrimination between subcellular cues is vital and much research over recent years has been focused on determining how proteins identify where to locate, be it the cell poles, division site etc. An important role for sensing membrane curvature has begun to be established. Studies have focused on regions of greatest membrane curvature but the question remains as to how proteins are organised throughout the cell membrane? In addressing fundamental questions that can lead to a better understanding of biological systems it is inevitable to apply a reductionist approach. The removal and dissection of individual components allows the identification of novel mechanisms contributing to the whole system. In this respect, the study of membrane protein localisation in the apparently spherical bacterium *S. aureus* seems a logical approach. *S. aureus* lacks many of the known spatial organisers such as MreB and the Min system (Pinho *et al.*, 2013) and does not have highly curved cell poles. It therefore represents a simplified model for the study of membrane protein organisation.

Recently, a novel protein localisation pattern and supramolecular structure was found in the membranes of *S. aureus* (Garcia-Lara *et al.*, 2015). This structure is composed of the phospholipid synthesis enzymes PlsY and CdsA being localised in a heterogeneous punctate pattern that is stabilised by the cytoskeletal protein MreD. This study focused on the identification of how this pattern is maintained and whether other membrane proteins exhibit a similar localisation as seen for PlsY and CdsA.

7.1 Pattern maintenance

Cells lacking MreD exhibit delocalised PlsY. This study also demonstrated that a *mreD* mutant grown at 42 °C shows severe morphological changes along with the delocalisation of FtsZ and aberrant placement of the septum (Fig. 3.3 and Fig. 3.4) while the majority of cells, when grown at 37 °C, do not exhibit delocalisation effects.

MreD might therefore act as a spatial stabiliser required for fast growth when cellular processes have to be efficient.

Previous studies revealed the importance of membrane domains and thus specific lipids on the placement of membrane proteins. In particular, cardiolipin and phosphatidylethanolamine were shown to be localised at the cell poles or the septum and to be required for localisation of many proteins such as the osmosensory transporter ProP in *E. coli* (Romantsov *et al.*, 2007, Mileykovskaya, 2007), or the cholera toxin export system in *Vibrio cholerae* (Camberg *et al.*, 2007). Since membrane proteins could have an affinity for certain lipids it would be possible to also observe lipid-dependent patterns for PlsY. The three major phospholipids in *S. aureus* are cardiolipin, phosphatidyl-glycerolphosphate and lysinylated phosphatidylglycerolphosphate (de Mendoza *et al.*, 2003)(Fischer *et al.*, 1978). Surprisingly, PlsY localisation was unaffected in strains lacking either CL or LPG (Fig. 4.40 and Fig. 4.42). The enzyme catalysing the synthesis of PG, PgsA, is essential in *S. aureus* (Chaudhuri *et al.*, 2009) making localisation studies of PlsY in a mutant lacking PG not feasible. Additionally, wall teichoic acids, squalene and peptidoglycan are not required for the punctate pattern of PlsY (Fig. 4.44, Fig. 4.38 and Fig. 4.51.). It is therefore possible that the observed localisation pattern solely relies on the existence of a membrane.

So how can PlsY, CdsA and MreD adopt the observed pattern in a uniformly curved membrane (in non-septating cells), in the absence of cytoskeletal components and without an impact through the cell-wall or the investigated membrane constituents?

A mathematical approach considering the basic features of the staphylococcal cell was used to analyse the distribution of PlsY (Garcia-Lara *et al.*, 2015). If integral membrane protein complexes inflict a sufficiently large local curvature on the membrane, protein complexes can themselves spontaneously form the observed patterns (see Fig. 7.1 for a graphical simplified representation of the model). A homogeneous or random distribution would be accompanied with high energy costs to counteract the intrinsic locally induced membrane curvature imposed by the protein complexes. This model is robust in respect to altering parameters since changing single variables of the system over a broad range does not change the formation of protein patterns. However, the intrinsic properties of the protein complexes play a crucial role in their own localisation. Changing the degree of membrane bending leads to the decay of the localisation pattern. Therefore the composition of the protein complex is pivotal, which is where MreD and other proteins come into play.

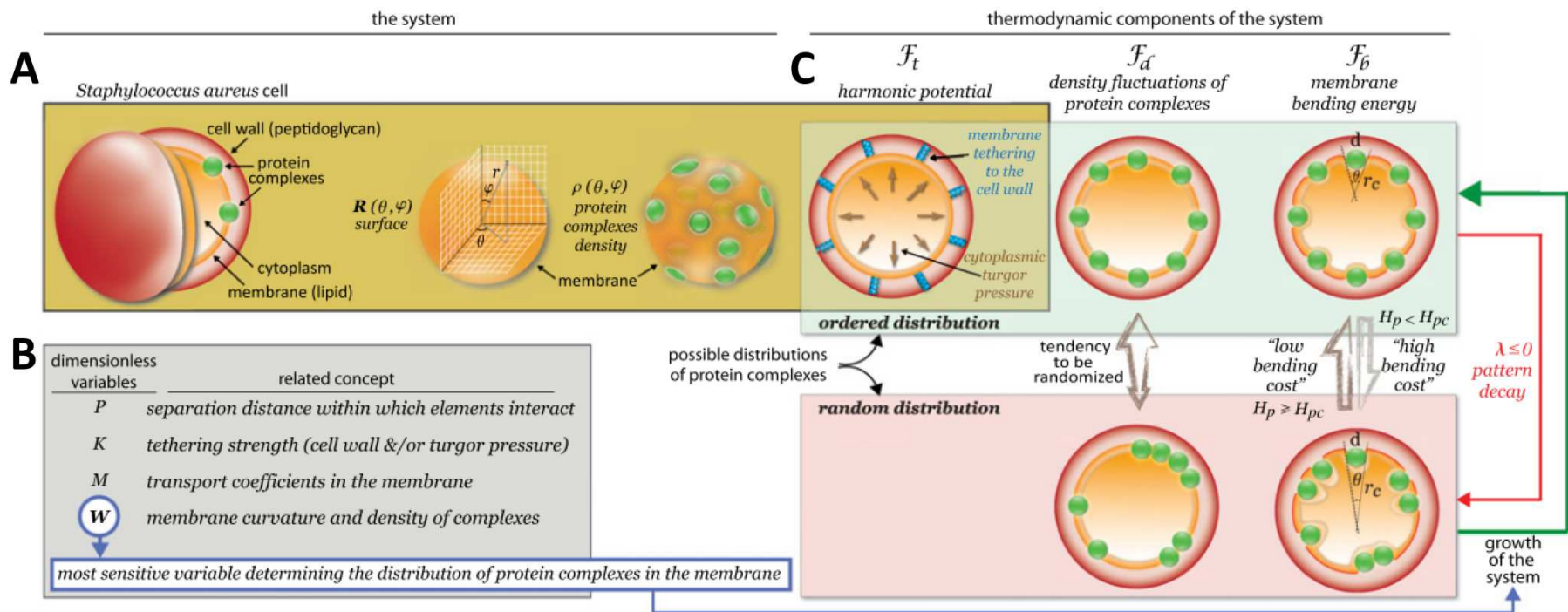


Figure 7.1 A mathematical explanation for the punctate patterned distribution of membrane proteins in *S. aureus*

A, The bacterial membrane is a lipid-based surface, under cytoplasm-induced turgor pressure and tethered to the cell wall, which contains protein complexes whose distribution is a 3D phenomenon that can be defined by a mathematical function. **B**, The latter depends on multiple independent variables that can be grouped into dimensionless variables (P , K , M , and W). This enables one to solve the differential equations corresponding to the various components and overall free energy of the system. The solutions to the equation are two functions $\lambda +$ and $\lambda -$, representing the growth ($\lambda > 0$; pattern formation of protein complexes) or decay ($\lambda < 0$ and $\lambda = 0$; random distribution of protein complexes) in the membrane. **C**, A linear analysis reveals W as the key variable determining the distribution of protein complexes. Hence, the presence of a protein complex in the membrane induces a membrane deformation that results in localised membrane curvature (H_p) and will entail a bending cost. If the curvature is larger than a critical threshold (H_{pc}), it will result in a system that will enable the growth of patterns. If $H_p < H_{pc}$, the resulting system will lead to the decay of patterns. A more detailed explanation and the respective calculations can be found in Garcia-Lara *et al.*, 2015.

7.2 A metabolic perspective

This study revealed that a number of proteins exhibit a heterogeneous distribution pattern. Other proteins involved in phospholipid synthesis such as PgsA, MprF, PlsC and the cardiolipin synthase Cls2 exhibit a similar localisation pattern to PlsY and CdsA. Also proteins from non-related metabolic processes were found not to be homogeneously distributed but to be localised in certain spots throughout the cell-periphery. These proteins include the respiratory protein CydB and the lipid raft marker FloT. Additionally, PlsY was shown to interact with PgsA and CdsA using a novel FRET-based protein-interaction system giving further evidence for a phospholipid synthesis protein complex. Importantly, PlsY does not interact with other membrane proteins such as the homogeneously distributed SecY and shows less interaction with CydB. These interactions not only take place at the septum, where many metabolic processes (such as the majority of peptidoglycan synthesis) are localised, but also at the cell-periphery (Fig. 5.11) (Monteiro *et al.*, 2015). In summary, this shows that the membrane of *S. aureus* is highly organised and not a random fluid cell compartment that only exhibits organisation at the septum.

These observations are in agreement with the ‘compartmentalised fluid’ or ‘partitioned’ model of biological membranes (Engelman, 2005, Kusumi *et al.*, 2005, Marguet *et al.*, 2006) that replaced the out-of-date traditional fluid mosaic model (Singer & Nicolson, 1972). According to the new membrane paradigm, a random membrane protein distribution must be regarded as the exception rather than the rule. But why do these protein patterns and thus the intrinsic properties of membrane proteins evolve? This is important since it shows that there may exist an underlying organisational pattern that conducts proteins of the same metabolic processes to be where they are supposed to be. Thus, the bacterial cell reduces energy costs by avoiding the active transport of metabolic intermediates to the next enzyme or avoiding time-loss and inefficiency due to the transport via diffusion over a long range. Metabolic channelling through the formation of protein complexes anchored to the membrane through the bending imposed by the complexes themselves could be a common mechanism applied in all organisms that does not require prior curvature of membranes.

7.3 A link between phospholipid synthesis and cell-division?

It is currently unknown as to how *S. aureus* divides in three planes which requires a system to create cell polarity in the absence of known polarity determinants such as the Min system (Pinho *et al.*, 2013). Moreover, a *divIVA* null mutant shows no apparent

phenotype (Pinho & Errington, 2004). Another polarity determinant, TipN, identifies the new cell pole, but is only found in *C. crescentus* (Lam *et al.*, 2006). It is therefore likely that the future cell-division sites are marked through an epigenetic inheritance system in *S. aureus*. An AFM analysis demonstrated that cells exhibit an altered peptidoglycan architecture at the newly formed septum with a ‘piecrust’ ring, remnants of which are inherited over generations and might facilitate a cue used to divide in orthogonal planes (Turner *et al.*, 2010). However, it is not known whether this structure is recognised by the membrane proteins involved in the placement of the Z-ring.

Some of the findings in my study point towards the involvement of the observed localisation patterns in the placement of the Z-ring. Cells depleted in PlsY exhibit incorrectly placed Z-rings and a severe growth defect but it seems unlikely that PlsY is a spatial organiser (Garcia-Lara *et al.*, 2015). Additionally, cells lacking MreD have a similar phenotype compared to PlsY depleted cells (Garcia-Lara *et al.*, 2015). Bacterial-two-hybrid analyses also identified the interaction between PlsY, PBP4 and putative wall teichoic acid ligases SA1195 and SA0908 (Kent, 2013).

A link with FtsZ is present for PlsX in *B. subtilis* which exhibits a punctate pattern reminiscent of PlsY and interacts with the FtsZ-anchoring protein FtsA (Takada *et al.*, 2014). PlsX localises at the future cell-division site prior to and independent of FtsZ. Deletion of *plsX* also results in a severe growth defect along with misplaced septa.

7.4 Future work

Future studies will work towards a better understanding of the supramolecular structure described here, in a biological context and to elucidate their physical properties. This can be done on several levels. Studies of membrane proteins in *S. aureus* are crucial for a basic understanding that can be transferred and tested in other bacterial species and their properties can be examined in cell-free systems such as liposomes.

7.4.1 *In vivo* and *Ex vivo*

Epifluorescence microscopy allowed an initial analysis of the supramolecular organisation of membrane proteins but ultimately, super resolution techniques such as STORM/PALM are required to get further insights of the nature of the investigated membrane proteins. Preliminary attempts to achieve high-resolution images of PlsY-eYFP at native levels in *S. aureus* were unsuccessful (not shown) and may require more suitable fluorescent fusions. These could also be used for single molecule tracking to

investigate whether the protein complexes are mobile and how they behave in respect to other potentially non-colocalised proteins such as MscL and CydB.

Furthermore, the investigation of the localisation of a range of membrane proteins at native levels combined with quantitative image analysis would allow mapping of the membrane of *S. aureus*. This analysis could be transferred to the ellipsoidal shaped *Enterococcus faecalis* or *Streptococcus pneumoniae* to investigate whether altered membrane curvature features found in these bacteria are enough to fundamentally effect the localisation of membrane proteins. Alternatively, membrane proteins taken from *S. aureus* could be expressed in ellipsoidal and rod-shaped bacteria as shown for MreD in this study (Section 6.1.1.2) and compared to their native homologues. This would direct future work as to how membrane protein properties, independent of their metabolic function, evolved dependent on cell shape. In this respect, it is crucial to determine whether the monomeric version of eYFP in a MreD-meYFP fusion expressed in *E. coli* still localises in a punctate pattern.

Additionally, a role for protein complexes might lie in a connection to cell-division which could be further analysed by protein-interactions studies using co-immunoprecipitation of PlsY-GFP with anti-GFP antibodies. BACTH studies with PlsX and cell-division components could show whether PlsX is the linking factor. The heterogeneous distribution of PlsY was found to be dependent on the ability of FtsZ to polymerise. It would be interesting to extend this observation with the FRET assay to analyse whether protein-interactions between PlsY and CdsA or MreD require the punctate patterned distribution of PlsY, by combination of PC190723 treated cells with FRET.

7.4.2 *In vitro*

Ultimately the aim is to analyse purified proteins in an *in vitro* system to have a ‘filter’ free view on the properties of membrane proteins. It has been shown before that proteins reconstituted into liposomes can self-assemble and form patterns as seen for FtsA, ZipA and FtsZ (Osawa *et al.*, 2008, Osawa & Erickson, 2013, Martos *et al.*, 2012a). In this study, a preliminary attempt was undertaken using MreD. Future work should be directed to the purification of a range of membrane proteins followed by their reconstitution using a different liposome generation method that yields more vesicles than the one employed in my work. These could be prepared using the hydration method followed by the use of a lipid extruder (<https://avantilipids.com/tech-support/liposome-preparation>). Moreover, various lipid compositions could shed light

on the influence of lipids in the observed patterns. These techniques could also be used to study membrane protein localisation in non-curved membranes such as supported lipid bilayers.

The protruding nature of membrane proteins in membranes could be facilitated using atomic force microscopy (AFM). This tool could show whether PlsY and Co. are forming protein complexes on a molecular level. Using the vesicle purification protocol described in Section 6.1.2 coupled to fluorescence microscopy and AFM would allow to identify the position of the PlsY-GFP fusion and to study their supramolecular architecture in native *S. aureus* membranes.

7.5 Conclusion

My study highlights a simple mechanism that potentially controls physiological processes within a complex system. While bacteria were once thought of as being simple life forms, the last decade have provided unexpected insights, drawing the picture of an intricate cell composed of simple mechanisms. It is these ‘hidden’ mechanisms that constitute the framework for the development of cellular life forms. The discovery of a supramolecular organisation of membrane proteins in *S. aureus* could be a common feature and apply across all biology.

My work illustrates a glimpse into future avenues for research. These will be technically challenging but their outcome will help to unravel the fundamentals of life.

Chapter 8: References

- (1984) Classics in infectious diseases. "On abscesses". Alexander Ogston (1844-1929). *Reviews of infectious diseases* **6**: 122-128.
- Abeyrathne, P. D., C. Daniels, K. K. Poon, M. J. Matewish & J. S. Lam, (2005) Functional characterization of WaaL, a ligase associated with linking O-antigen polysaccharide to the core of *Pseudomonas aeruginosa* lipopolysaccharide. *Journal of bacteriology* **187**: 3002-3012.
- Abraham, B. G., V. Santala, N. V. Tkachenko & M. Karp, (2014) Fluorescent protein-based FRET sensor for intracellular monitoring of redox status in bacteria at single cell level. *Analytical and bioanalytical chemistry* **406**: 7195-7204.
- Adams, D. W. & J. Errington, (2009) Bacterial cell division: assembly, maintenance and disassembly of the Z ring. *Nature reviews. Microbiology* **7**: 642-653.
- Adams, D. W., L. J. Wu & J. Errington, (2015) Nucleoid occlusion protein Noc recruits DNA to the bacterial cell membrane. *The EMBO journal* **34**: 491-501.
- Aimon, S., A. Callan-Jones, A. Berthaud, M. Pinot, G. E. Toombes & P. Bassereau, (2014) Membrane shape modulates transmembrane protein distribution. *Developmental cell* **28**: 212-218.
- Alcayaga, C., R. Venegas, A. Carrasco & D. Wolff, (1992) Ion channels from the *Bacillus subtilis* plasma membrane incorporated into planar lipid bilayers. *FEBS letters* **311**: 246-250.
- Alexeeva, S., T. W. Gadella, Jr., J. Verheul, G. S. Verhoeven & T. den Blaauwen, (2010) Direct interactions of early and late assembling division proteins in *Escherichia coli* cells resolved by FRET. *Molecular microbiology* **77**: 384-398.
- Alhamadsheh, M. M., F. Musayev, A. A. Komissarov, S. Sachdeva, H. T. Wright, N. Scarsdale, G. Florova & K. A. Reynolds, (2007) Alkyl-CoA disulfides as inhibitors and mechanistic probes for FabH enzymes. *Chemistry & biology* **14**: 513-524.
- Ames, G. F., (1968) Lipids of *Salmonella typhimurium* and *Escherichia coli*: structure and metabolism. *Journal of bacteriology* **95**: 833-843.
- Anderson, D. E., F. J. Gueiros-Filho & H. P. Erickson, (2004) Assembly dynamics of FtsZ rings in *Bacillus subtilis* and *Escherichia coli* and effects of FtsZ-regulating proteins. *Journal of bacteriology* **186**: 5775-5781.
- Andra, J., T. Goldmann, C. M. Ernst, A. Peschel & T. Gutschmann, (2011) Multiple peptide resistance factor (MprF)-mediated Resistance of *Staphylococcus aureus* against antimicrobial peptides coincides with a modulated peptide interaction with artificial membranes comprising lysyl-phosphatidylglycerol. *The Journal of biological chemistry* **286**: 18692-18700.
- Andre, G., M. Deghorain, P. A. Bron, S. van, II, M. Kleerebezem, P. Hols & Y. F. Dufrene, (2011) Fluorescence and atomic force microscopy imaging of wall teichoic acids in *Lactobacillus plantarum*. *ACS chemical biology* **6**: 366-376.
- Arumugam, S., G. Chwastek, E. Fischer-Friedrich, C. Ehrig, I. Monch & P. Schwille, (2012) Surface topology engineering of membranes for the mechanical investigation of the tubulin homologue FtsZ. *Angew Chem Int Ed Engl* **51**: 11858-11862.
- Atilano, M. L., P. M. Pereira, J. Yates, P. Reed, H. Veiga, M. G. Pinho & S. R. Filipe, (2010) Teichoic acids are temporal and spatial regulators of peptidoglycan cross-linking in *Staphylococcus aureus*. *Proceedings of the National Academy of Sciences of the United States of America* **107**: 18991-18996.
- Ausmees, N., J. R. Kuhn & C. Jacobs-Wagner, (2003) The bacterial cytoskeleton: an intermediate filament-like function in cell shape. *Cell* **115**: 705-713.

- Baba, T., T. Bae, O. Schneewind, F. Takeuchi & K. Hiramatsu, (2008) Genome sequence of *Staphylococcus aureus* strain Newman and comparative analysis of staphylococcal genomes: polymorphism and evolution of two major pathogenicity islands. *Journal of bacteriology* **190**: 300-310.
- Bach, J. N., N. Albrecht & M. Bramkamp, (2014) Imaging DivIVA dynamics using photo-convertible and activatable fluorophores in *Bacillus subtilis*. *Frontiers in microbiology* **5**: 59.
- Bach, J. N. & M. Bramkamp, (2013) Flotillins functionally organize the bacterial membrane. *Molecular microbiology* **88**: 1205-1217.
- Bagchi, S., H. Tomenius, L. M. Belova & N. Ausmees, (2008) Intermediate filament-like proteins in bacteria and a cytoskeletal function in *Streptomyces*. *Molecular microbiology* **70**: 1037-1050.
- Bailey, M. W., P. Bisicchia, B. T. Warren, D. J. Sherratt & J. Mannik, (2014) Evidence for divisome localization mechanisms independent of the Min system and SlmA in *Escherichia coli*. *PLoS genetics* **10**: e1004504.
- Bakshi, S., B. P. Bratton & J. C. Weisshaar, (2011) Subdiffraction-limit study of Kaede diffusion and spatial distribution in live *Escherichia coli*. *Biophysical journal* **101**: 2535-2544.
- Barak, I., K. Muchova, A. J. Wilkinson, P. J. O'Toole & N. Pavlendova, (2008) Lipid spirals in *Bacillus subtilis* and their role in cell division. *Molecular microbiology* **68**: 1315-1327.
- Baumgart, T., S. T. Hess & W. W. Webb, (2003) Imaging coexisting fluid domains in biomembrane models coupling curvature and line tension. *Nature* **425**: 821-824.
- Bayer, A. S., R. Prasad, J. Chandra, A. Koul, M. Smriti, A. Varma, R. A. Skurray, N. Firth, M. H. Brown, S. P. Koo & M. R. Yeaman, (2000) In vitro resistance of *Staphylococcus aureus* to thrombin-induced platelet microbicidal protein is associated with alterations in cytoplasmic membrane fluidity. *Infection and immunity* **68**: 3548-3553.
- Beall, B. & J. Lutkenhaus, (1991) FtsZ in *Bacillus subtilis* is required for vegetative septation and for asymmetric septation during sporulation. *Genes & development* **5**: 447-455.
- Begg, K. J., S. J. Dewar & W. D. Donachie, (1995) A new *Escherichia coli* cell division gene, ftsK. *Journal of bacteriology* **177**: 6211-6222.
- Begg, K. J. & W. D. Donachie, (1998) Division planes alternate in spherical cells of *Escherichia coli*. *Journal of bacteriology* **180**: 2564-2567.
- Beilharz, K., L. Novakova, D. Fadda, P. Branny, O. Massidda & J. W. Veening, (2012) Control of cell division in *Streptococcus pneumoniae* by the conserved Ser/Thr protein kinase StkP. *Proceedings of the National Academy of Sciences of the United States of America* **109**: E905-913.
- Bell, R. M., (1975) Mutants of *Escherichia coli* defective in membrane phospholipid synthesis. Properties of wild type and Km defective sn-glycerol-3-phosphate acyltransferase activities. *The Journal of biological chemistry* **250**: 7147-7152.
- Benson, T. E., D. B. Prince, V. T. Mutchler, K. A. Curry, A. M. Ho, R. W. Sarver, J. C. Hagadorn, G. H. Choi & R. L. Garlick, (2002) X-ray crystal structure of *Staphylococcus aureus* FemA. *Structure* **10**: 1107-1115.
- Benson, T. E., C. T. Walsh & J. M. Hogle, (1996) The structure of the substrate-free form of MurB, an essential enzyme for the synthesis of bacterial cell walls. *Structure* **4**: 47-54.
- Bera, A., R. Biswas, S. Herbert, E. Kulauzovic, C. Weidenmaier, A. Peschel & F. Gotz, (2007) Influence of wall teichoic acid on lysozyme resistance in *Staphylococcus aureus*. *Journal of bacteriology* **189**: 280-283.

- Bera, A., S. Herbert, A. Jakob, W. Vollmer & F. Gotz, (2005) Why are pathogenic staphylococci so lysozyme resistant? The peptidoglycan O-acetyltransferase OatA is the major determinant for lysozyme resistance of *Staphylococcus aureus*. *Molecular microbiology* **55**: 778-787.
- Berg, K. H., G. A. Stamsas, D. Straume & L. S. Havarstein, (2013) Effects of low PBP2b levels on cell morphology and peptidoglycan composition in *Streptococcus pneumoniae* R6. *Journal of bacteriology* **195**: 4342-4354.
- Bernhardt, T. G. & P. A. de Boer, (2005) SlmA, a nucleoid-associated, FtsZ binding protein required for blocking septal ring assembly over Chromosomes in *E. coli*. *Molecular cell* **18**: 555-564.
- Bertsche, U., T. Kast, B. Wolf, C. Fraipont, M. E. Aarsman, K. Kannenberg, M. von Rechenberg, M. Nguyen-Disteche, T. den Blaauwen, J. V. Holtje & W. Vollmer, (2006) Interaction between two murein (peptidoglycan) synthases, PBP3 and PBP1B, in *Escherichia coli*. *Molecular microbiology* **61**: 675-690.
- Betzig, E., G. H. Patterson, R. Sougrat, O. W. Lindwasser, S. Olenych, J. S. Bonifacino, M. W. Davidson, J. Lippincott-Schwartz & H. F. Hess, (2006) Imaging intracellular fluorescent proteins at nanometer resolution. *Science* **313**: 1642-1645.
- Bharat, T. A., G. N. Murshudov, C. Sachse & J. Lowe, (2015) Structures of actin-like ParM filaments show architecture of plasmid-segregating spindles. *Nature* **523**: 106-110.
- Bhavsar, A. P., R. Truant & E. D. Brown, (2005) The TagB protein in *Bacillus subtilis* 168 is an intracellular peripheral membrane protein that can incorporate glycerol phosphate onto a membrane-bound acceptor in vitro. *The Journal of biological chemistry* **280**: 36691-36700.
- Bi, E. F. & J. Lutkenhaus, (1991) FtsZ ring structure associated with division in *Escherichia coli*. *Nature* **354**: 161-164.
- Bigot, S., O. A. Saleh, C. Lesterlin, C. Pages, M. El Karoui, C. Dennis, M. Grigoriev, J. F. Allemand, F. X. Barre & F. Cornet, (2005) KOPS: DNA motifs that control *E. coli* chromosome segregation by orienting the FtsK translocase. *The EMBO journal* **24**: 3770-3780.
- Boniface, A., A. Bouhss, D. Mengin-Lecreulx & D. Blanot, (2006) The MurE synthetase from *Thermotoga maritima* is endowed with an unusual D-lysine adding activity. *The Journal of biological chemistry* **281**: 15680-15686.
- Bork, P., C. Sander & A. Valencia, (1992) An ATPase domain common to prokaryotic cell cycle proteins, sugar kinases, actin, and hsp70 heat shock proteins. *Proceedings of the National Academy of Sciences of the United States of America* **89**: 7290-7294.
- Bos, M. P., V. Robert & J. Tommassen, (2007) Biogenesis of the gram-negative bacterial outer membrane. *Annual review of microbiology* **61**: 191-214.
- Bottomley, A. L., A. F. Kabli, A. F. Hurd, R. D. Turner, J. Garcia-Lara & S. J. Foster, (2014) *Staphylococcus aureus* DivIB is a peptidoglycan-binding protein that is required for a morphological checkpoint in cell division. *Molecular microbiology*.
- Bouhss, A., D. Mengin-Lecreulx, D. Le Beller & J. Van Heijenoort, (1999) Topological analysis of the MraY protein catalysing the first membrane step of peptidoglycan synthesis. *Molecular microbiology* **34**: 576-585.
- Boutte, C. C., J. T. Henry & S. Crosson, (2012) ppGpp and polyphosphate modulate cell cycle progression in *Caulobacter crescentus*. *Journal of bacteriology* **194**: 28-35.
- Bramkamp, M., R. Emmins, L. Weston, C. Donovan, R. A. Daniel & J. Errington, (2008) A novel component of the division-site selection system of *Bacillus*

- subtilis and a new mode of action for the division inhibitor MinCD. *Molecular microbiology* **70**: 1556-1569.
- Bramkamp, M. & D. Lopez, (2015) Exploring the existence of lipid rafts in bacteria. *Microbiology and molecular biology reviews : MMBR* **79**: 81-100.
- Bramley, H. F. & H. L. Kornberg, (1987) Sequence homologies between proteins of bacterial phosphoenolpyruvate-dependent sugar phosphotransferase systems: identification of possible phosphate-carrying histidine residues. *Proceedings of the National Academy of Sciences of the United States of America* **84**: 4777-4780.
- Brandon, L. D., N. Goehring, A. Janakiraman, A. W. Yan, T. Wu, J. Beckwith & M. B. Goldberg, (2003) IcsA, a polarly localized autotransporter with an atypical signal peptide, uses the Sec apparatus for secretion, although the Sec apparatus is circumferentially distributed. *Molecular microbiology* **50**: 45-60.
- Braun, T., A. Orlova, K. Valegard, A. C. Lindas, G. F. Schroder & E. H. Egelman, (2015) Archaeal actin from a hyperthermophile forms a single-stranded filament. *Proceedings of the National Academy of Sciences of the United States of America* **112**: 9340-9345.
- Britton, R. A., D. C. Lin & A. D. Grossman, (1998) Characterization of a prokaryotic SMC protein involved in chromosome partitioning. *Genes & development* **12**: 1254-1259.
- Bron, P. A., S. Tomita, S. van, II, D. M. Remus, M. Meijerink, M. Wels, S. Okada, J. M. Wells & M. Kleerebezem, (2012) *Lactobacillus plantarum* possesses the capability for wall teichoic acid backbone alditol switching. *Microbial cell factories* **11**: 123.
- Broussard, J. A., B. Rappaz, D. J. Webb & C. M. Brown, (2013) Fluorescence resonance energy transfer microscopy as demonstrated by measuring the activation of the serine/threonine kinase Akt. *Nature protocols* **8**: 265-281.
- Brown, E. D., E. I. Vivas, C. T. Walsh & R. Kolter, (1995) MurA (MurZ), the enzyme that catalyzes the first committed step in peptidoglycan biosynthesis, is essential in *Escherichia coli*. *Journal of bacteriology* **177**: 4194-4197.
- Brown, S., J. P. Santa Maria, Jr. & S. Walker, (2013) Wall teichoic acids of gram-positive bacteria. *Annual review of microbiology* **67**: 313-336.
- Brumback, A. C., J. L. Lieber, J. K. Angleson & W. J. Betz, (2004) Using FM1-43 to study neuropeptide granule dynamics and exocytosis. *Methods* **33**: 287-294.
- Brzoska, A. J. & N. Firth, (2013) Two-plasmid vector system for independently controlled expression of green and red fluorescent fusion proteins in *Staphylococcus aureus*. *Applied and environmental microbiology* **79**: 3133-3136.
- Buddelmeijer, N. & J. Beckwith, (2004) A complex of the *Escherichia coli* cell division proteins FtsL, FtsB and FtsQ forms independently of its localization to the septal region. *Molecular microbiology* **52**: 1315-1327.
- Butland, G., J. M. Peregrin-Alvarez, J. Li, W. Yang, X. Yang, V. Canadien, A. Starostine, D. Richards, B. Beattie, N. Krogan, M. Davey, J. Parkinson, J. Greenblatt & A. Emili, (2005) Interaction network containing conserved and essential protein complexes in *Escherichia coli*. *Nature* **433**: 531-537.
- Cabeen, M. T., H. Herrmann & C. Jacobs-Wagner, (2011) The domain organization of the bacterial intermediate filament-like protein crescentin is important for assembly and function. *Cytoskeleton (Hoboken)* **68**: 205-219.
- Camargo, I. L., H. M. Neoh, L. Cui & K. Hiramatsu, (2008) Serial daptomycin selection generates daptomycin-nonsusceptible *Staphylococcus aureus* strains with a heterogeneous vancomycin-intermediate phenotype. *Antimicrobial agents and chemotherapy* **52**: 4289-4299.

- Camberg, J. L., T. L. Johnson, M. Patrick, J. Abendroth, W. G. Hol & M. Sandkvist, (2007) Synergistic stimulation of EpsE ATP hydrolysis by EpsL and acidic phospholipids. *The EMBO journal* **26**: 19-27.
- Campelo, F., H. T. McMahon & M. M. Kozlov, (2008) The hydrophobic insertion mechanism of membrane curvature generation by proteins. *Biophysical journal* **95**: 2325-2339.
- Campo, N., H. Tjalsma, G. Buist, D. Stepniak, M. Meijer, M. Veenhuis, M. Westermann, J. P. Muller, S. Bron, J. Kok, O. P. Kuipers & J. D. Jongbloed, (2004) Subcellular sites for bacterial protein export. *Molecular microbiology* **53**: 1583-1599.
- Canton, I. & G. Battaglia, (2012) Endocytosis at the nanoscale. *Chemical Society reviews* **41**: 2718-2739.
- Carillo, M. A., M. Bennet & D. Faivre, (2013) Interaction of proteins associated with the magnetosome assembly in magnetotactic bacteria as revealed by two-hybrid two-photon excitation fluorescence lifetime imaging microscopy Förster resonance energy transfer. *The journal of physical chemistry. B* **117**: 14642-14648.
- Cartron, M. L., S. R. England, A. I. Chiriac, M. Josten, R. Turner, Y. Rauter, A. Hurd, H. G. Sahl, S. Jones & S. J. Foster, (2014) Bactericidal activity of the human skin fatty acid cis-6-hexadecanoic acid on *Staphylococcus aureus*. *Antimicrobial agents and chemotherapy* **58**: 3599-3609.
- Cayley, S., B. A. Lewis, H. J. Guttman & M. T. Record, Jr., (1991) Characterization of the cytoplasm of *Escherichia coli* K-12 as a function of external osmolarity. Implications for protein-DNA interactions in vivo. *Journal of molecular biology* **222**: 281-300.
- Chamberlain, L. H., R. D. Burgoyne & G. W. Gould, (2001) SNARE proteins are highly enriched in lipid rafts in PC12 cells: implications for the spatial control of exocytosis. *Proceedings of the National Academy of Sciences of the United States of America* **98**: 5619-5624.
- Charbon, G., M. T. Cabeen & C. Jacobs-Wagner, (2009) Bacterial intermediate filaments: in vivo assembly, organization, and dynamics of crescentin. *Genes & development* **23**: 1131-1144.
- Chaudhuri, R. R., A. G. Allen, P. J. Owen, G. Shalom, K. Stone, M. Harrison, T. A. Burgis, M. Lockyer, J. Garcia-Lara, S. J. Foster, S. J. Pleasance, S. E. Peters, D. J. Maskell & I. G. Charles, (2009) Comprehensive identification of essential *Staphylococcus aureus* genes using Transposon-Mediated Differential Hybridisation (TMDH). *BMC genomics* **10**: 291.
- Chen, Y. & H. P. Erickson, (2008) In vitro assembly studies of FtsZ/tubulin-like proteins (TubZ) from *Bacillus* plasmids: evidence for a capping mechanism. *The Journal of biological chemistry* **283**: 8102-8109.
- Chernomordik, L. V. & M. M. Kozlov, (2003) Protein-lipid interplay in fusion and fission of biological membranes. *Annual review of biochemistry* **72**: 175-207.
- Chien, C. T., P. L. Bartel, R. Sternglanz & S. Fields, (1991) The two-hybrid system: a method to identify and clone genes for proteins that interact with a protein of interest. *Proceedings of the National Academy of Sciences of the United States of America* **88**: 9578-9582.
- Cho, H., H. R. McManus, S. L. Dove & T. G. Bernhardt, (2011) Nucleoid occlusion factor SlmA is a DNA-activated FtsZ polymerization antagonist. *Proceedings of the National Academy of Sciences of the United States of America* **108**: 3773-3778.

- Choi-Rhee, E. & J. E. Cronan, (2003) The biotin carboxylase-biotin carboxyl carrier protein complex of *Escherichia coli* acetyl-CoA carboxylase. *The Journal of biological chemistry* **278**: 30806-30812.
- Choi, K. H., R. J. Heath & C. O. Rock, (2000) beta-ketoacyl-acyl carrier protein synthase III (FabH) is a determining factor in branched-chain fatty acid biosynthesis. *Journal of bacteriology* **182**: 365-370.
- Christensen, H., N. J. Garton, R. W. Horobin, D. E. Minnikin & M. R. Barer, (1999) Lipid domains of mycobacteria studied with fluorescent molecular probes. *Molecular microbiology* **31**: 1561-1572.
- Claessen, D., R. Emmins, L. W. Hamoen, R. A. Daniel, J. Errington & D. H. Edwards, (2008) Control of the cell elongation-division cycle by shuttling of PBP1 protein in *Bacillus subtilis*. *Molecular microbiology* **68**: 1029-1046.
- Clements, M. O., S. P. Watson, R. K. Poole & S. J. Foster, (1999) CtaA of *Staphylococcus aureus* is required for starvation survival, recovery, and cytochrome biosynthesis. *Journal of bacteriology* **181**: 501-507.
- Colavin, A., J. Hsin & K. C. Huang, (2014) Effects of polymerization and nucleotide identity on the conformational dynamics of the bacterial actin homolog MreB. *Proceedings of the National Academy of Sciences of the United States of America* **111**: 3585-3590.
- Conti, J., M. G. Viola & J. L. Camberg, (2015) The bacterial cell division regulators MinD and MinC form polymers in the presence of nucleotide. *FEBS letters* **589**: 201-206.
- Cooke, I. R. & M. Deserno, (2006) Coupling between lipid shape and membrane curvature. *Biophysical journal* **91**: 487-495.
- Cooper, E. L., J. Garcia-Lara & S. J. Foster, (2009) YsxC, an essential protein in *Staphylococcus aureus* crucial for ribosome assembly/stability. *BMC microbiology* **9**: 266.
- Coquel, A. S., J. P. Jacob, M. Primet, A. Demarez, M. Dimiccoli, T. Julou, L. Moisan, A. B. Lindner & H. Berry, (2013) Localization of protein aggregation in *Escherichia coli* is governed by diffusion and nucleoid macromolecular crowding effect. *PLoS computational biology* **9**: e1003038.
- Corbin, B. D., Y. Wang, T. K. Beuria & W. Margolin, (2007) Interaction between cell division proteins FtsE and FtsZ. *Journal of bacteriology* **189**: 3026-3035.
- Corrigan, R. M., J. C. Abbott, H. Burhenne, V. Kaefer & A. Grundling, (2011) c-di-AMP is a new second messenger in *Staphylococcus aureus* with a role in controlling cell size and envelope stress. *PLoS pathogens* **7**: e1002217.
- Corrigan, R. M., I. Campeotto, T. Jeganathan, K. G. Roelofs, V. T. Lee & A. Grundling, (2013) Systematic identification of conserved bacterial c-di-AMP receptor proteins. *Proceedings of the National Academy of Sciences of the United States of America* **110**: 9084-9089.
- Cronan, J. E., Jr. & G. L. Waldrop, (2002) Multi-subunit acetyl-CoA carboxylases. *Progress in lipid research* **41**: 407-435.
- D'Elia, M. A., J. A. Henderson, T. J. Beveridge, D. E. Heinrichs & E. D. Brown, (2009) The N-acetylmannosamine transferase catalyzes the first committed step of teichoic acid assembly in *Bacillus subtilis* and *Staphylococcus aureus*. *Journal of bacteriology* **191**: 4030-4034.
- Dai, K. & J. Lutkenhaus, (1991) ftsZ is an essential cell division gene in *Escherichia coli*. *Journal of bacteriology* **173**: 3500-3506.
- Daniel, R. A. & J. Errington, (2003) Control of cell morphogenesis in bacteria: two distinct ways to make a rod-shaped cell. *Cell* **113**: 767-776.

- Daniel, R. A., M. F. Noirot-Gros, P. Noirot & J. Errington, (2006) Multiple interactions between the transmembrane division proteins of *Bacillus subtilis* and the role of FtsL instability in divisome assembly. *Journal of bacteriology* **188**: 7396-7404.
- Datta, P., A. Dasgupta, S. Bhakta & J. Basu, (2002) Interaction between FtsZ and FtsW of *Mycobacterium tuberculosis*. *The Journal of biological chemistry* **277**: 24983-24987.
- Datta, P., A. Dasgupta, A. K. Singh, P. Mukherjee, M. Kundu & J. Basu, (2006) Interaction between FtsW and penicillin-binding protein 3 (PBP3) directs PBP3 to mid-cell, controls cell septation and mediates the formation of a trimeric complex involving FtsZ, FtsW and PBP3 in mycobacteria. *Molecular microbiology* **62**: 1655-1673.
- de Boer, P., R. Crossley & L. Rothfield, (1992) The essential bacterial cell-division protein FtsZ is a GTPase. *Nature* **359**: 254-256.
- de Leeuw, E., B. Graham, G. J. Phillips, C. M. ten Hagen-Jongman, B. Oudega & J. Luirink, (1999) Molecular characterization of *Escherichia coli* FtsE and FtsX. *Molecular microbiology* **31**: 983-993.
- de Lencastre, H., D. Oliveira & A. Tomasz, (2007) Antibiotic resistant *Staphylococcus aureus*: a paradigm of adaptive power. *Current opinion in microbiology* **10**: 428-435.
- Deane, C. M., L. Salwinski, I. Xenarios & D. Eisenberg, (2002) Protein interactions: two methods for assessment of the reliability of high throughput observations. *Molecular & cellular proteomics : MCP* **1**: 349-356.
- DeDent, A. C., M. McAdow & O. Schneewind, (2007) Distribution of protein A on the surface of *Staphylococcus aureus*. *Journal of bacteriology* **189**: 4473-4484.
- Defeu Soufo, H. J. & P. L. Graumann, (2006) Dynamic localization and interaction with other *Bacillus subtilis* actin-like proteins are important for the function of MreB. *Molecular microbiology* **62**: 1340-1356.
- Defeu Soufo, H. J., C. Reimold, H. Breddermann, H. G. Mannherz & P. L. Graumann, (2015) Translation elongation factor EF-Tu modulates filament formation of actin-like MreB protein in vitro. *Journal of molecular biology* **427**: 1715-1727.
- Dempwolff, F., F. K. Schmidt, A. B. Hervas, A. Stroh, T. C. Rosch, C. N. Riese, S. Dersch, T. Heimerl, D. Lucena, N. Hulsbusch, C. A. Stuermer, N. Takeshita, R. Fischer, B. Eckhardt & P. L. Graumann, (2016) Super Resolution Fluorescence Microscopy and Tracking of Bacterial Flotillin (Reggie) Paralogs Provide Evidence for Defined-Sized Protein Microdomains within the Bacterial Membrane but Absence of Clusters Containing Detergent-Resistant Proteins. *PLoS genetics* **12**: e1006116.
- Denapoli, J., A. K. Tehranchi & J. D. Wang, (2013) Dose-dependent reduction of replication elongation rate by (p)ppGpp in *Escherichia coli* and *Bacillus subtilis*. *Molecular microbiology* **88**: 93-104.
- Dengler, V., P. S. Meier, R. Heusser, P. Kupferschmied, J. Fazekas, S. Friebe, S. B. Stauffer, P. A. Majcherczyk, P. Moreillon, B. Berger-Bachi & N. McCallum, (2012) Deletion of hypothetical wall teichoic acid ligases in *Staphylococcus aureus* activates the cell wall stress response. *FEMS microbiology letters* **333**: 109-120.
- Dervyn, E., M. F. Noirot-Gros, P. Mervelet, S. McGovern, S. D. Ehrlich, P. Polard & P. Noirot, (2004) The bacterial condensin/cohesin-like protein complex acts in DNA repair and regulation of gene expression. *Molecular microbiology* **51**: 1629-1640.
- Deva, T., E. N. Baker, C. J. Squire & C. A. Smith, (2006) Structure of *Escherichia coli* UDP-N-acetylmuramoyl-L-alanine ligase (MurC). *Acta crystallographica. Section D, Biological crystallography* **62**: 1466-1474.

- Di Lallo, G., M. Fagioli, D. Barionovi, P. Ghelardini & L. Paolozzi, (2003) Use of a two-hybrid assay to study the assembly of a complex multicomponent protein machinery: bacterial septosome differentiation. *Microbiology* **149**: 3353-3359.
- Di Paolo, G. & P. De Camilli, (2006) Phosphoinositides in cell regulation and membrane dynamics. *Nature* **443**: 651-657.
- Diez-Gonzalez, F. & J. B. Russell, (1997) Effects of carbonylcyanide-m-chlorophenylhydrazone (CCCP) and acetate on Escherichia coli O157:H7 and K-12: uncoupling versus anion accumulation. *FEMS microbiology letters* **151**: 71-76.
- Din, N., E. M. Quardokus, M. J. Sackett & Y. V. Brun, (1998) Dominant C-terminal deletions of FtsZ that affect its ability to localize in Caulobacter and its interaction with FtsA. *Molecular microbiology* **27**: 1051-1063.
- Divakaruni, A. V., C. Baida, C. L. White & J. W. Gober, (2007) The cell shape proteins MreB and MreC control cell morphogenesis by positioning cell wall synthetic complexes. *Molecular microbiology* **66**: 174-188.
- Divakaruni, A. V., R. R. Loo, Y. Xie, J. A. Loo & J. W. Gober, (2005) The cell-shape protein MreC interacts with extracytoplasmic proteins including cell wall assembly complexes in Caulobacter crescentus. *Proceedings of the National Academy of Sciences of the United States of America* **102**: 18602-18607.
- Doerrler, W. T. & C. R. Raetz, (2002) ATPase activity of the MsbA lipid flippase of Escherichia coli. *The Journal of biological chemistry* **277**: 36697-36705.
- Dominguez-Escobar, J., A. Chastanet, A. H. Crevenna, V. Fromion, R. Wedlich-Soldner & R. Carballido-Lopez, (2011) Processive movement of MreB-associated cell wall biosynthetic complexes in bacteria. *Science* **333**: 225-228.
- Donovan, C. & M. Bramkamp, (2009) Characterization and subcellular localization of a bacterial flotillin homologue. *Microbiology* **155**: 1786-1799.
- Dowhan, W., (1997) Molecular basis for membrane phospholipid diversity: why are there so many lipids? *Annual review of biochemistry* **66**: 199-232.
- Drew, D., M. Lerch, E. Kunji, D. J. Slotboom & J. W. de Gier, (2006) Optimization of membrane protein overexpression and purification using GFP fusions. *Nature methods* **3**: 303-313.
- Driessen, A. J., E. H. Manting & C. van der Does, (2001) The structural basis of protein targeting and translocation in bacteria. *Nature structural biology* **8**: 492-498.
- Duggin, I. G., C. H. Aylett, J. C. Walsh, K. A. Michie, Q. Wang, L. Turnbull, E. M. Dawson, E. J. Harry, C. B. Whitchurch, L. A. Amos & J. Lowe, (2015) CetZ tubulin-like proteins control archaeal cell shape. *Nature* **519**: 362-365.
- Duthie, E. S., (1952) Variation in the antigenic composition of staphylococcal coagulase. *Journal of general microbiology* **7**: 320-326.
- Eberhardt, A., C. N. Hoyland, D. Vollmer, S. Bisle, R. M. Cleverley, O. Johnsborg, L. S. Havarstein, R. J. Lewis & W. Vollmer, (2012) Attachment of capsular polysaccharide to the cell wall in Streptococcus pneumoniae. *Microb Drug Resist* **18**: 240-255.
- Ebersbach, G., E. Galli, J. Moller-Jensen, J. Lowe & K. Gerdes, (2008) Novel coiled-coil cell division factor ZapB stimulates Z ring assembly and cell division. *Molecular microbiology* **68**: 720-735.
- Ebersbach, G. & K. Gerdes, (2005) Plasmid segregation mechanisms. *Annual review of genetics* **39**: 453-479.
- Edwards, D. H. & J. Errington, (1997) The Bacillus subtilis DivIVA protein targets to the division septum and controls the site specificity of cell division. *Molecular microbiology* **24**: 905-915.

- Edwards, D. H., H. B. Thomaidis & J. Errington, (2000) Promiscuous targeting of *Bacillus subtilis* cell division protein DivIVA to division sites in *Escherichia coli* and fission yeast. *The EMBO journal* **19**: 2719-2727.
- El Ghachi, M., A. Bouhss, D. Blanot & D. Mengin-Lecreulx, (2004) The *bacA* gene of *Escherichia coli* encodes an undecaprenyl pyrophosphate phosphatase activity. *The Journal of biological chemistry* **279**: 30106-30113.
- Elowitz, M. B., M. G. Surette, P. E. Wolf, J. B. Stock & S. Leibler, (1999) Protein mobility in the cytoplasm of *Escherichia coli*. *Journal of bacteriology* **181**: 197-203.
- Elsen, N. L., J. Lu, G. Parthasarathy, J. C. Reid, S. Sharma, S. M. Soisson & K. J. Lumb, (2012) Mechanism of action of the cell-division inhibitor PC190723: modulation of FtsZ assembly cooperativity. *Journal of the American Chemical Society* **134**: 12342-12345.
- Emoto, K. & M. Umeda, (2001) Membrane lipid control of cytokinesis. *Cell structure and function* **26**: 659-665.
- Engelman, D. M., (2005) Membranes are more mosaic than fluid. *Nature* **438**: 578-580.
- English, B. P., V. Haurlyuk, A. Sanamrad, S. Tankov, N. H. Dekker & J. Elf, (2011) Single-molecule investigations of the stringent response machinery in living bacterial cells. *Proceedings of the National Academy of Sciences of the United States of America* **108**: E365-373.
- Epanand, R. M., C. Walker, R. F. Epanand & N. A. Magarvey, (2016) Molecular mechanisms of membrane targeting antibiotics. *Biochimica et biophysica acta* **1858**: 980-987.
- Erdmann, N., T. Petroff & B. E. Funnell, (1999) Intracellular localization of P1 ParB protein depends on ParA and *parS*. *Proceedings of the National Academy of Sciences of the United States of America* **96**: 14905-14910.
- Erickson, H. P., (1995) FtsZ, a prokaryotic homolog of tubulin? *Cell* **80**: 367-370.
- Erickson, H. P., D. W. Taylor, K. A. Taylor & D. Bramhill, (1996) Bacterial cell division protein FtsZ assembles into protofilament sheets and minirings, structural homologs of tubulin polymers. *Proceedings of the National Academy of Sciences of the United States of America* **93**: 519-523.
- Ernst, C. M., S. Kuhn, C. J. Slavetinsky, B. Krismer, S. Heilbronner, C. Gekeler, D. Kraus, S. Wagner & A. Peschel, (2015) The lipid-modifying multiple peptide resistance factor is an oligomer consisting of distinct interacting synthase and flippase subunits. *mBio* **6**.
- Ernst, C. M. & A. Peschel, (2011) Broad-spectrum antimicrobial peptide resistance by MprF-mediated aminoacylation and flipping of phospholipids. *Molecular microbiology* **80**: 290-299.
- Ernst, C. M., P. Staubitz, N. N. Mishra, S. J. Yang, G. Hornig, H. Kalbacher, A. S. Bayer, D. Kraus & A. Peschel, (2009) The bacterial defensin resistance protein MprF consists of separable domains for lipid lysinylation and antimicrobial peptide repulsion. *PLoS pathogens* **5**: e1000660.
- Errington, J., (2015) Bacterial morphogenesis and the enigmatic MreB helix. *Nature reviews. Microbiology* **13**: 241-248.
- Espeli, O., C. Lee & K. J. Mariani, (2003) A physical and functional interaction between *Escherichia coli* FtsK and topoisomerase IV. *The Journal of biological chemistry* **278**: 44639-44644.
- Eswaramoorthy, P., M. L. Erb, J. A. Gregory, J. Silverman, K. Pogliano, J. Pogliano & K. S. Ramamurthi, (2011) Cellular architecture mediates DivIVA ultrastructure and regulates min activity in *Bacillus subtilis*. *mBio* **2**.
- Ettema, T. J., A. C. Lindas & R. Bernander, (2011) An actin-based cytoskeleton in archaea. *Molecular microbiology* **80**: 1052-1061.

- Fedtke, I., D. Mader, T. Kohler, H. Moll, G. Nicholson, R. Biswas, K. Henseler, F. Gotz, U. Zahringer & A. Peschel, (2007) A *Staphylococcus aureus* ypfP mutant with strongly reduced lipoteichoic acid (LTA) content: LTA governs bacterial surface properties and autolysin activity. *Molecular microbiology* **65**: 1078-1091.
- Fey, P. D., J. L. Endres, V. K. Yajjala, T. J. Widhelm, R. J. Boissy, J. L. Bose & K. W. Bayles, (2013) A genetic resource for rapid and comprehensive phenotype screening of nonessential *Staphylococcus aureus* genes. *mBio* **4**: e00537-00512.
- Fields, S. & O. Song, (1989) A novel genetic system to detect protein-protein interactions. *Nature* **340**: 245-246.
- Figge, R. M., A. V. Divakaruni & J. W. Gober, (2004) MreB, the cell shape-determining bacterial actin homologue, co-ordinates cell wall morphogenesis in *Caulobacter crescentus*. *Molecular microbiology* **51**: 1321-1332.
- Fischer, M., I. Haase, E. Simmeth, G. Gerisch & A. Muller-Taubenberger, (2004) A brilliant monomeric red fluorescent protein to visualize cytoskeleton dynamics in *Dictyostelium*. *FEBS letters* **577**: 227-232.
- Fisher, M., J. T. Kroon, W. Martindale, A. R. Stuitje, A. R. Slabas & J. B. Rafferty, (2000) The X-ray structure of *Brassica napus* beta-keto acyl carrier protein reductase and its implications for substrate binding and catalysis. *Structure* **8**: 339-347.
- Fishov, I. & C. L. Woldringh, (1999) Visualization of membrane domains in *Escherichia coli*. *Molecular microbiology* **32**: 1166-1172.
- Fleming, T. C., J. Y. Shin, S. H. Lee, E. Becker, K. C. Huang, C. Bustamante & K. Pogliano, (2010) Dynamic SpoIIIE assembly mediates septal membrane fission during *Bacillus subtilis* sporulation. *Genes & development* **24**: 1160-1172.
- Fleurie, A., C. Lesterlin, S. Manuse, C. Zhao, C. Cluzel, J. P. Lavergne, M. Franz-Wachtel, B. Macek, C. Combet, E. Kuru, M. S. VanNieuwenhze, Y. V. Brun, D. Sherratt & C. Grangeasse, (2014a) MapZ marks the division sites and positions FtsZ rings in *Streptococcus pneumoniae*. *Nature* **516**: 259-262.
- Fleurie, A., S. Manuse, C. Zhao, N. Campo, C. Cluzel, J. P. Lavergne, C. Freton, C. Combet, S. Guiral, B. Soufi, B. Macek, E. Kuru, M. S. VanNieuwenhze, Y. V. Brun, A. M. Di Guilmi, J. P. Claverys, A. Galinier & C. Grangeasse, (2014b) Interplay of the serine/threonine-kinase StkP and the paralogs DivIVA and GpsB in pneumococcal cell elongation and division. *PLoS genetics* **10**: e1004275.
- Flock, J. I., G. Froman, K. Jonsson, B. Guss, C. Signas, B. Nilsson, G. Raucchi, M. Hook, T. Wadstrom & M. Lindberg, (1987) Cloning and expression of the gene for a fibronectin-binding protein from *Staphylococcus aureus*. *The EMBO journal* **6**: 2351-2357.
- Ford, M. G., I. G. Mills, B. J. Peter, Y. Vallis, G. J. Praefcke, P. R. Evans & H. T. McMahon, (2002) Curvature of clathrin-coated pits driven by epsin. *Nature* **419**: 361-366.
- Forster, T., (2012) Energy migration and fluorescence. 1946. *Journal of biomedical optics* **17**: 011002.
- Foster, T. J., (2005) Immune evasion by staphylococci. *Nature reviews. Microbiology* **3**: 948-958.
- Fraipont, C., S. Alexeeva, B. Wolf, R. van der Ploeg, M. Schloesser, T. den Blaauwen & M. Nguyen-Disteche, (2011) The integral membrane FtsW protein and peptidoglycan synthase PBP3 form a subcomplex in *Escherichia coli*. *Microbiology* **157**: 251-259.
- Fribourg, P. F., M. Chami, C. O. Sorzano, F. Gubellini, R. Marabini, S. Marco, J. M. Jault & D. Levy, (2014) 3D cryo-electron reconstruction of BmrA, a bacterial

- multidrug ABC transporter in an inward-facing conformation and in a lipidic environment. *Journal of molecular biology* **426**: 2059-2069.
- Frost, A., R. Perera, A. Roux, K. Spasov, O. Destaing, E. H. Egelman, P. De Camilli & V. M. Unger, (2008) Structural basis of membrane invagination by F-BAR domains. *Cell* **132**: 807-817.
- Fu, C., L. Keller, A. Bauer, M. Bronstrup, A. Froidbise, P. Hammann, J. Herrmann, G. Mondesert, M. Kurz, M. Schiell, D. Schummer, L. Toti, J. Wink & R. Muller, (2015) Biosynthetic Studies of Telomycin Reveal New Lipopeptides with Enhanced Activity. *Journal of the American Chemical Society* **137**: 7692-7705.
- Fu, G., T. Huang, J. Buss, C. Coltharp, Z. Hensel & J. Xiao, (2010) In vivo structure of the E. coli FtsZ-ring revealed by photoactivated localization microscopy (PALM). *PloS one* **5**: e12682.
- Galli, E. & K. Gerdes, (2010) Spatial resolution of two bacterial cell division proteins: ZapA recruits ZapB to the inner face of the Z-ring. *Molecular microbiology* **76**: 1514-1526.
- Gandhi, A. & N. P. Shah, (2016) Effect of salt stress on morphology and membrane composition of *Lactobacillus acidophilus*, *Lactobacillus casei*, and *Bifidobacterium bifidum*, and their adhesion to human intestinal epithelial-like Caco-2 cells. *Journal of dairy science* **99**: 2594-2605.
- Garcia-Lara, J., F. Weihs, X. Ma, L. Walker, R. R. Chaudhuri, J. Kasturiarachchi, H. Crossley, R. Golestanian & S. J. Foster, (2015) Supramolecular structure in the membrane of *Staphylococcus aureus*. *Proceedings of the National Academy of Sciences of the United States of America* **112**: 15725-15730.
- Garner, E. C., R. Bernard, W. Wang, X. Zhuang, D. Z. Rudner & T. Mitchison, (2011) Coupled, circumferential motions of the cell wall synthesis machinery and MreB filaments in *B. subtilis*. *Science* **333**: 222-225.
- Gayathri, P., T. Fujii, J. Moller-Jensen, F. van den Ent, K. Namba & J. Lowe, (2012) A bipolar spindle of antiparallel ParM filaments drives bacterial plasmid segregation. *Science* **338**: 1334-1337.
- George Abraham, B., K. S. Sarkisyan, A. S. Mishin, V. Santala, N. V. Tkachenko & M. Karp, (2015) Fluorescent Protein Based FRET Pairs with Improved Dynamic Range for Fluorescence Lifetime Measurements. *PloS one* **10**: e0134436.
- Gerdes, K., M. Howard & F. Szardenings, (2010) Pushing and pulling in prokaryotic DNA segregation. *Cell* **141**: 927-942.
- Ghosal, D., D. Trambaiolo, L. A. Amos & J. Lowe, (2014) MinCD cell division proteins form alternating copolymeric cytomotive filaments. *Nature communications* **5**: 5341.
- Gill, R. L., Jr., J. P. Castaing, J. Hsin, I. S. Tan, X. Wang, K. C. Huang, F. Tian & K. S. Ramamurthi, (2015) Structural basis for the geometry-driven localization of a small protein. *Proceedings of the National Academy of Sciences of the United States of America* **112**: E1908-1915.
- Ginsberg, C., Y. H. Zhang, Y. Yuan & S. Walker, (2006) In vitro reconstitution of two essential steps in wall teichoic acid biosynthesis. *ACS chemical biology* **1**: 25-28.
- Goldberg, I., J. R. Walker & K. Bloch, (1973) Inhibition of lipid synthesis in *Escherichia coli* cells by the antibiotic cerulenin. *Antimicrobial agents and chemotherapy* **3**: 549-554.
- Golding, I. & E. C. Cox, (2006) Physical nature of bacterial cytoplasm. *Physical review letters* **96**: 098102.
- Gomez-Baena, G., O. A. Rangel, A. Lopez-Lozano, J. M. Garcia-Fernandez & J. Diez, (2009) Stress responses in *Prochlorococcus* MIT9313 vs. SS120 involve

- differential expression of genes encoding proteases ClpP, FtsH and Lon. *Research in microbiology* **160**: 567-575.
- Gotz, F. & S. Mayer, (2013) Both terminal oxidases contribute to fitness and virulence during organ-specific *Staphylococcus aureus* colonization. *mBio* **4**: e00976-00913.
- Govindarajan, S., Y. Elisha, K. Nevo-Dinur & O. Amster-Choder, (2013) The general phosphotransferase system proteins localize to sites of strong negative curvature in bacterial cells. *mBio* **4**: e00443-00413.
- Grandchamps, J., M. Nguyen-Disteche, C. Damblon, J. M. Frere & J. M. Ghuysen, (1995) Streptomyces K15 active-site serine DD-transpeptidase: specificity profile for peptide, thiol ester and ester carbonyl donors and pathways of the transfer reactions. *The Biochemical journal* **307** (Pt 2): 335-339.
- Gregory, J. A., E. C. Becker & K. Pogliano, (2008) *Bacillus subtilis* MinC destabilizes FtsZ-rings at new cell poles and contributes to the timing of cell division. *Genes & development* **22**: 3475-3488.
- Grundling, A. & O. Schneewind, (2007a) Genes required for glycolipid synthesis and lipoteichoic acid anchoring in *Staphylococcus aureus*. *Journal of bacteriology* **189**: 2521-2530.
- Grundling, A. & O. Schneewind, (2007b) Synthesis of glycerol phosphate lipoteichoic acid in *Staphylococcus aureus*. *Proceedings of the National Academy of Sciences of the United States of America* **104**: 8478-8483.
- Gunning, P. W., U. Ghoshdastider, S. Whitaker, D. Popp & R. C. Robinson, (2015) The evolution of compositionally and functionally distinct actin filaments. *Journal of cell science* **128**: 2009-2019.
- Gustafsson, N., S. Culley, G. Ashdown, D. M. Owen, P. M. Pereira & R. Henriques, (2016) Fast live-cell conventional fluorophore nanoscopy with ImageJ through super-resolution radial fluctuations. *Nature communications* **7**: 12471.
- Halbedel, S., B. Hahn, R. A. Daniel & A. Flieger, (2012) DivIVA affects secretion of virulence-related autolysins in *Listeria monocytogenes*. *Molecular microbiology* **83**: 821-839.
- Halbedel, S., M. Kawai, R. Breitling & L. W. Hamoen, (2014) SecA is required for membrane targeting of the cell division protein DivIVA in vivo. *Frontiers in microbiology* **5**: 58.
- Hamamoto, H., M. Urai, K. Ishii, J. Yasukawa, A. Paudel, M. Murai, T. Kaji, T. Kuranaga, K. Hamase, T. Katsu, J. Su, T. Adachi, R. Uchida, H. Tomoda, M. Yamada, M. Souma, H. Kurihara, M. Inoue & K. Sekimizu, (2015) Lysocin E is a new antibiotic that targets menaquinone in the bacterial membrane. *Nature chemical biology* **11**: 127-133.
- Hammer, N. D., M. L. Reniere, J. E. Cassat, Y. Zhang, A. O. Hirsch, M. Indriati Hood & E. P. Skaar, (2013) Two heme-dependent terminal oxidases power *Staphylococcus aureus* organ-specific colonization of the vertebrate host. *mBio* **4**.
- Haswell, E. S., R. Phillips & D. C. Rees, (2011) Mechanosensitive channels: what can they do and how do they do it? *Structure* **19**: 1356-1369.
- Hayami, M., A. Okabe, R. Kariyama, M. Abe & Y. Kanemasa, (1979) Lipid composition of *Staphylococcus aureus* and its derived L-forms. *Microbiology and immunology* **23**: 435-442.
- Haydon, D. J., N. R. Stokes, R. Ure, G. Galbraith, J. M. Bennett, D. R. Brown, P. J. Baker, V. V. Barynin, D. W. Rice, S. E. Sedelnikova, J. R. Heal, J. M. Sheridan, S. T. Aiwale, P. K. Chauhan, A. Srivastava, A. Taneja, I. Collins, J. Errington & L. G. Czaplewski, (2008) An inhibitor of FtsZ with potent and selective anti-staphylococcal activity. *Science* **321**: 1673-1675.

- He, X. & K. A. Reynolds, (2002) Purification, characterization, and identification of novel inhibitors of the beta-ketoacyl-acyl carrier protein synthase III (FabH) from *Staphylococcus aureus*. *Antimicrobial agents and chemotherapy* **46**: 1310-1318.
- Heath, R. J. & C. O. Rock, (1995) Enoyl-acyl carrier protein reductase (fabI) plays a determinant role in completing cycles of fatty acid elongation in *Escherichia coli*. *The Journal of biological chemistry* **270**: 26538-26542.
- Heath, R. J. & C. O. Rock, (1996a) Inhibition of beta-ketoacyl-acyl carrier protein synthase III (FabH) by acyl-acyl carrier protein in *Escherichia coli*. *The Journal of biological chemistry* **271**: 10996-11000.
- Heath, R. J. & C. O. Rock, (1996b) Roles of the FabA and FabZ beta-hydroxyacyl-acyl carrier protein dehydratases in *Escherichia coli* fatty acid biosynthesis. *The Journal of biological chemistry* **271**: 27795-27801.
- Heath, R. J., N. Su, C. K. Murphy & C. O. Rock, (2000) The enoyl-[acyl-carrier-protein] reductases FabI and FabL from *Bacillus subtilis*. *The Journal of biological chemistry* **275**: 40128-40133.
- Hennekinne, J. A., M. L. De Buyser & S. Dragacci, (2012) *Staphylococcus aureus* and its food poisoning toxins: characterization and outbreak investigation. *FEMS microbiology reviews* **36**: 815-836.
- Henze, U., T. Sidow, J. Wecke, H. Labischinski & B. Berger-Bachi, (1993) Influence of femB on methicillin resistance and peptidoglycan metabolism in *Staphylococcus aureus*. *Journal of bacteriology* **175**: 1612-1620.
- Herbert, S., A. K. Ziebandt, K. Ohlsen, T. Schafer, M. Hecker, D. Albrecht, R. Novick & F. Gotz, (2010) Repair of global regulators in *Staphylococcus aureus* 8325 and comparative analysis with other clinical isolates. *Infection and immunity* **78**: 2877-2889.
- Hill, N. S., P. J. Buske, Y. Shi & P. A. Levin, (2013) A moonlighting enzyme links *Escherichia coli* cell size with central metabolism. *PLoS genetics* **9**: e1003663.
- Hinshaw, J. E., (2000) Dynamin and its role in membrane fission. *Annual review of cell and developmental biology* **16**: 483-519.
- Hirano, M., H. Mori, T. Onogi, M. Yamazoe, H. Niki, T. Ogura & S. Hiraga, (1998) Autoregulation of the partition genes of the mini-F plasmid and the intracellular localization of their products in *Escherichia coli*. *Molecular & general genetics* : *MGG* **257**: 392-403.
- Holeckova, N., L. Doubravova, O. Massidda, V. Molle, K. Buriankova, O. Benada, O. Kofronova, A. Ulrych & P. Branny, (2015) LocZ is a new cell division protein involved in proper septum placement in *Streptococcus pneumoniae*. *mBio* **6**: e01700-01714.
- Horsburgh, M. J., J. L. Aish, I. J. White, L. Shaw, J. K. Lithgow & S. J. Foster, (2002) sigmaB modulates virulence determinant expression and stress resistance: characterization of a functional rsbU strain derived from *Staphylococcus aureus* 8325-4. *Journal of bacteriology* **184**: 5457-5467.
- Horsburgh, M. J., M. D. Wiltshire, H. Crossley, E. Ingham & S. J. Foster, (2004) PheP, a putative amino acid permease of *Staphylococcus aureus*, contributes to survival in vivo and during starvation. *Infection and immunity* **72**: 3073-3076.
- Hoshino, S. & I. Hayashi, (2012) Filament formation of the FtsZ/tubulin-like protein TubZ from the *Bacillus cereus* pXO1 plasmid. *The Journal of biological chemistry* **287**: 32103-32112.
- Hsieh, C. W., T. Y. Lin, H. M. Lai, C. C. Lin, T. S. Hsieh & Y. L. Shih, (2010) Direct MinE-membrane interaction contributes to the proper localization of MinDE in *E. coli*. *Molecular microbiology* **75**: 499-512.

- Hu, Z. & J. Lutkenhaus, (1999) Topological regulation of cell division in *Escherichia coli* involves rapid pole to pole oscillation of the division inhibitor MinC under the control of MinD and MinE. *Molecular microbiology* **34**: 82-90.
- Hu, Z. & J. Lutkenhaus, (2000) Analysis of MinC reveals two independent domains involved in interaction with MinD and FtsZ. *Journal of bacteriology* **182**: 3965-3971.
- Hu, Z. & J. Lutkenhaus, (2001) Topological regulation of cell division in *E. coli*. spatiotemporal oscillation of MinD requires stimulation of its ATPase by MinE and phospholipid. *Molecular cell* **7**: 1337-1343.
- Hu, Z. & J. Lutkenhaus, (2003) A conserved sequence at the C-terminus of MinD is required for binding to the membrane and targeting MinC to the septum. *Molecular microbiology* **47**: 345-355.
- Hu, Z., A. Mukherjee, S. Pichoff & J. Lutkenhaus, (1999) The MinC component of the division site selection system in *Escherichia coli* interacts with FtsZ to prevent polymerization. *Proceedings of the National Academy of Sciences of the United States of America* **96**: 14819-14824.
- Huang, B., W. Wang, M. Bates & X. Zhuang, (2008) Three-dimensional super-resolution imaging by stochastic optical reconstruction microscopy. *Science* **319**: 810-813.
- Huang, K. C., R. Mukhopadhyay & N. S. Wingreen, (2006) A curvature-mediated mechanism for localization of lipids to bacterial poles. *PLoS computational biology* **2**: e151.
- Hubscher, J., N. McCallum, C. D. Sifri, P. A. Majcherzyk, J. M. Entenza, R. Heusser, B. Berger-Bachi & P. Stutzmann Meier, (2009) MsrR contributes to cell surface characteristics and virulence in *Staphylococcus aureus*. *FEMS microbiology letters* **295**: 251-260.
- Huecas, S. & J. M. Andreu, (2004) Polymerization of nucleotide-free, GDP- and GTP-bound cell division protein FtsZ: GDP makes the difference. *FEBS letters* **569**: 43-48.
- Hunt, A., J. P. Rawlins, H. B. Thomaidis & J. Errington, (2006) Functional analysis of 11 putative essential genes in *Bacillus subtilis*. *Microbiology* **152**: 2895-2907.
- Hussain, M., J. G. Hastings & P. J. White, (1991) A chemically defined medium for slime production by coagulase-negative staphylococci. *Journal of medical microbiology* **34**: 143-147.
- Hwang, L. C., A. G. Vecchiarelli, Y. W. Han, M. Mizuuchi, Y. Harada, B. E. Funnell & K. Mizuuchi, (2013) ParA-mediated plasmid partition driven by protein pattern self-organization. *The EMBO journal* **32**: 1238-1249.
- Ishibashi, M., K. Kurokawa, S. Nishida, K. Ueno, M. Matsuo & K. Sekimizu, (2007) Isolation of temperature-sensitive mutations in *murC* of *Staphylococcus aureus*. *FEMS microbiology letters* **274**: 204-209.
- Ishikawa, S., Y. Kawai, K. Hiramatsu, M. Kuwano & N. Ogasawara, (2006) A new FtsZ-interacting protein, YlmF, complements the activity of FtsA during progression of cell division in *Bacillus subtilis*. *Molecular microbiology* **60**: 1364-1380.
- Ishino, F., W. Park, S. Tomioka, S. Tamaki, I. Takase, K. Kunugita, H. Matsuzawa, S. Asoh, T. Ohta, B. G. Spratt & et al., (1986) Peptidoglycan synthetic activities in membranes of *Escherichia coli* caused by overproduction of penicillin-binding protein 2 and *rodA* protein. *The Journal of biological chemistry* **261**: 7024-7031.
- Izore, T., R. Duman, D. Kureisaite-Ciziene & J. Lowe, (2014) Crenactin from *Pyrobaculum calidifontis* is closely related to actin in structure and forms steep helical filaments. *FEBS letters* **588**: 776-782.

- Jackowski, S., C. M. Murphy, J. E. Cronan, Jr. & C. O. Rock, (1989) Acetoacetyl-acyl carrier protein synthase. A target for the antibiotic thiolactomycin. *The Journal of biological chemistry* **264**: 7624-7629.
- Jacques, N. A., (1983) Membrane perturbation by cerulenin modulates glucosyltransferase secretion and acetate uptake by *Streptococcus salivarius*. *Journal of general microbiology* **129**: 3293-3302.
- Jiang, S., A. Narita, D. Popp, U. Ghoshdastider, L. J. Lee, R. Srinivasan, M. K. Balasubramanian, T. Oda, F. Koh, M. Larsson & R. C. Robinson, (2016) Novel actin filaments from *Bacillus thuringiensis* form nanotubules for plasmid DNA segregation. *Proceedings of the National Academy of Sciences of the United States of America* **113**: E1200-1205.
- Jimenez, M., A. Martos, M. Vicente & G. Rivas, (2011) Reconstitution and organization of *Escherichia coli* proto-ring elements (FtsZ and FtsA) inside giant unilamellar vesicles obtained from bacterial inner membranes. *The Journal of biological chemistry* **286**: 11236-11241.
- Johnson, A. S., S. van Horck & P. J. Lewis, (2004) Dynamic localization of membrane proteins in *Bacillus subtilis*. *Microbiology* **150**: 2815-2824.
- Johnson, S., D. Kruger & H. Labischinski, (1995) FemA of *Staphylococcus aureus*: isolation and immunodetection. *FEMS microbiology letters* **132**: 221-228.
- Jones, L. J., R. Carballido-Lopez & J. Errington, (2001) Control of cell shape in bacteria: helical, actin-like filaments in *Bacillus subtilis*. *Cell* **104**: 913-922.
- Jorasch, P., D. C. Warnecke, B. Lindner, U. Zahringer & E. Heinz, (2000) Novel processive and nonprocessive glycosyltransferases from *Staphylococcus aureus* and *Arabidopsis thaliana* synthesize glycosylglycerolipids, glycosylphospholipids, glycosylsphingolipids and glycosylsterols. *European journal of biochemistry / FEBS* **267**: 3770-3783.
- Jorasch, P., F. P. Wolter, U. Zahringer & E. Heinz, (1998) A UDP glucosyltransferase from *Bacillus subtilis* successively transfers up to four glucose residues to 1,2-diacylglycerol: expression of ypfP in *Escherichia coli* and structural analysis of its reaction products. *Molecular microbiology* **29**: 419-430.
- Jouhet, J., (2013) Importance of the hexagonal lipid phase in biological membrane organization. *Frontiers in plant science* **4**: 494.
- Kaito, C., K. Kurokawa, M. S. Hossain, N. Akimitsu & K. Sekimizu, (2002) Isolation and characterization of temperature-sensitive mutants of the *Staphylococcus aureus* dnaC gene. *FEMS microbiology letters* **210**: 157-164.
- Kaltwasser, M., T. Wiegert & W. Schumann, (2002) Construction and application of epitope- and green fluorescent protein-tagging integration vectors for *Bacillus subtilis*. *Applied and environmental microbiology* **68**: 2624-2628.
- Kanemasa, Y., T. Yoshioka & H. Hayashi, (1972) Alteration of the phospholipid composition of *Staphylococcus aureus* cultured in medium containing NaCl. *Biochimica et biophysica acta* **280**: 444-450.
- Kanfer, J. & E. P. Kennedy, (1964) Metabolism and Function of Bacterial Lipids. II. Biosynthesis of Phospholipids in *Escherichia coli*. *The Journal of biological chemistry* **239**: 1720-1726.
- Karimova, G., N. Dautin & D. Ladant, (2005) Interaction network among *Escherichia coli* membrane proteins involved in cell division as revealed by bacterial two-hybrid analysis. *Journal of bacteriology* **187**: 2233-2243.
- Karimova, G., J. Pidoux, A. Ullmann & D. Ladant, (1998) A bacterial two-hybrid system based on a reconstituted signal transduction pathway. *Proceedings of the National Academy of Sciences of the United States of America* **95**: 5752-5756.

- Kawai, F., M. Shoda, R. Harashima, Y. Sadaie, H. Hara & K. Matsumoto, (2004) Cardiolipin domains in *Bacillus subtilis* marburg membranes. *Journal of bacteriology* **186**: 1475-1483.
- Kawai, Y., R. A. Daniel & J. Errington, (2009) Regulation of cell wall morphogenesis in *Bacillus subtilis* by recruitment of PBP1 to the MreB helix. *Molecular microbiology* **71**: 1131-1144.
- Kawai, Y., J. Marles-Wright, R. M. Cleverley, R. Emmins, S. Ishikawa, M. Kuwano, N. Heinz, N. K. Bui, C. N. Hoyland, N. Ogasawara, R. J. Lewis, W. Vollmer, R. A. Daniel & J. Errington, (2011) A widespread family of bacterial cell wall assembly proteins. *The EMBO journal* **30**: 4931-4941.
- Kawai, Y., R. Mercier, L. J. Wu, P. Dominguez-Cuevas, T. Oshima & J. Errington, (2015) Cell growth of wall-free L-form bacteria is limited by oxidative damage. *Current biology : CB* **25**: 1613-1618.
- Keppler, A., M. Kindermann, S. Gendrezig, H. Pick, H. Vogel & K. Johnsson, (2004a) Labeling of fusion proteins of O6-alkylguanine-DNA alkyltransferase with small molecules in vivo and in vitro. *Methods* **32**: 437-444.
- Keppler, A., H. Pick, C. Arrivoli, H. Vogel & K. Johnsson, (2004b) Labeling of fusion proteins with synthetic fluorophores in live cells. *Proceedings of the National Academy of Sciences of the United States of America* **101**: 9955-9959.
- Kern, T., M. Giffard, S. Hediger, A. Amoroso, C. Giustini, N. K. Bui, B. Joris, C. Bougault, W. Vollmer & J. P. Simorre, (2010) Dynamics characterization of fully hydrated bacterial cell walls by solid-state NMR: evidence for cooperative binding of metal ions. *Journal of the American Chemical Society* **132**: 10911-10919.
- Kiekebusch, D., K. A. Michie, L. O. Essen, J. Lowe & M. Thanbichler, (2012) Localized dimerization and nucleoid binding drive gradient formation by the bacterial cell division inhibitor MipZ. *Molecular cell* **46**: 245-259.
- Kim, S. J., M. Singh & J. Schaefer, (2009) Oritavancin binds to isolated protoplast membranes but not intact protoplasts of *Staphylococcus aureus*. *Journal of molecular biology* **391**: 414-425.
- Kinosita, K., Jr., R. Kataoka, Y. Kimura, O. Gotoh & A. Ikegami, (1981) Dynamic structure of biological membranes as probed by 1,6-diphenyl-1,3,5-hexatriene: a nanosecond fluorescence depolarization study. *Biochemistry* **20**: 4270-4277.
- Kiriukhin, M. Y., D. V. Debabov, D. L. Shinabarger & F. C. Neuhaus, (2001) Biosynthesis of the glycolipid anchor in lipoteichoic acid of *Staphylococcus aureus* RN4220: role of YpfP, the diglucosyldiacylglycerol synthase. *Journal of bacteriology* **183**: 3506-3514.
- Kita, K., K. Konishi & Y. Anraku, (1984) Terminal oxidases of *Escherichia coli* aerobic respiratory chain. II. Purification and properties of cytochrome b558-d complex from cells grown with limited oxygen and evidence of branched electron-carrying systems. *The Journal of biological chemistry* **259**: 3375-3381.
- Kluytmans, J., A. van Belkum & H. Verbrugh, (1997) Nasal carriage of *Staphylococcus aureus*: epidemiology, underlying mechanisms, and associated risks. *Clinical microbiology reviews* **10**: 505-520.
- Koch, H. U., R. Haas & W. Fischer, (1984) The role of lipoteichoic acid biosynthesis in membrane lipid metabolism of growing *Staphylococcus aureus*. *European journal of biochemistry / FEBS* **138**: 357-363.
- Kojima, N., Y. Araki & E. Ito, (1985) Structure of the linkage units between ribitol teichoic acids and peptidoglycan. *Journal of bacteriology* **161**: 299-306.
- Kreiswirth, B. N., S. Lofdahl, M. J. Betley, M. O'Reilly, P. M. Schlievert, M. S. Bergdoll & R. P. Novick, (1983) The toxic shock syndrome exotoxin structural gene is not detectably transmitted by a prophage. *Nature* **305**: 709-712.

- Kruse, T., J. Bork-Jensen & K. Gerdes, (2005) The morphogenetic MreBCD proteins of *Escherichia coli* form an essential membrane-bound complex. *Molecular microbiology* **55**: 78-89.
- Kuriyan, J. & D. Eisenberg, (2007) The origin of protein interactions and allostery in colocalization. *Nature* **450**: 983-990.
- Kuru, E., H. V. Hughes, P. J. Brown, E. Hall, S. Tekkam, F. Cava, M. A. de Pedro, Y. V. Brun & M. S. VanNieuwenhze, (2012) In Situ probing of newly synthesized peptidoglycan in live bacteria with fluorescent D-amino acids. *Angew Chem Int Ed Engl* **51**: 12519-12523.
- Kusaka, J., S. Shuto, Y. Imai, K. Ishikawa, T. Saito, K. Natori, S. Matsuoka, H. Hara & K. Matsumoto, (2016) Septal localization by membrane targeting sequences and a conserved sequence essential for activity at the COOH-terminus of *Bacillus subtilis* cardiolipin synthase. *Research in microbiology* **167**: 202-214.
- Kusumi, A., C. Nakada, K. Ritchie, K. Murase, K. Suzuki, H. Murakoshi, R. S. Kasai, J. Kondo & T. Fujiwara, (2005) Paradigm shift of the plasma membrane concept from the two-dimensional continuum fluid to the partitioned fluid: high-speed single-molecule tracking of membrane molecules. *Annual review of biophysics and biomolecular structure* **34**: 351-378.
- Labischinski, H., K. Ehlert & B. Berger-Bachi, (1998) The targeting of factors necessary for expression of methicillin resistance in staphylococci. *The Journal of antimicrobial chemotherapy* **41**: 581-584.
- Lackner, L. L., D. M. Raskin & P. A. de Boer, (2003) ATP-dependent interactions between *Escherichia coli* Min proteins and the phospholipid membrane in vitro. *Journal of bacteriology* **185**: 735-749.
- Lam, H., W. B. Schofield & C. Jacobs-Wagner, (2006) A landmark protein essential for establishing and perpetuating the polarity of a bacterial cell. *Cell* **124**: 1011-1023.
- Land, A. D. & M. E. Winkler, (2011) The requirement for pneumococcal MreC and MreD is relieved by inactivation of the gene encoding PBP1a. *Journal of bacteriology* **193**: 4166-4179.
- LaRocca, T. J., P. Pathak, S. Chiantia, A. Toledo, J. R. Silvius, J. L. Benach & E. London, (2013) Proving lipid rafts exist: membrane domains in the prokaryote *Borrelia burgdorferi* have the same properties as eukaryotic lipid rafts. *PLoS pathogens* **9**: e1003353.
- Larsen, R. A., C. Cusumano, A. Fujioka, G. Lim-Fong, P. Patterson & J. Pogliano, (2007) Treadmilling of a prokaryotic tubulin-like protein, TubZ, required for plasmid stability in *Bacillus thuringiensis*. *Genes & development* **21**: 1340-1352.
- Le, T. B., M. V. Imakaev, L. A. Mirny & M. T. Laub, (2013) High-resolution mapping of the spatial organization of a bacterial chromosome. *Science* **342**: 731-734.
- Leaver, M. & J. Errington, (2005) Roles for MreC and MreD proteins in helical growth of the cylindrical cell wall in *Bacillus subtilis*. *Molecular microbiology* **57**: 1196-1209.
- Ledala, N., B. Zhang, J. Seravalli, R. Powers & G. A. Somerville, (2014) Influence of iron and aeration on *Staphylococcus aureus* growth, metabolism, and transcription. *Journal of bacteriology* **196**: 2178-2189.
- Lee, C. Y., S. L. Buranen & Z. H. Ye, (1991) Construction of single-copy integration vectors for *Staphylococcus aureus*. *Gene* **103**: 101-105.
- Lee, J. C. & G. C. Stewart, (2003) Essential nature of the mreC determinant of *Bacillus subtilis*. *Journal of bacteriology* **185**: 4490-4498.
- Lee, P. C., C. M. Stopford, A. G. Svenson & A. Rietsch, (2010) Control of effector export by the *Pseudomonas aeruginosa* type III secretion proteins PcrG and PcrV. *Molecular microbiology* **75**: 924-941.

- Lefebvre, M., E. Tetaud, M. Thonnus, B. Salin, F. Boissier, C. Blancard, C. Sauvanet, C. Metzler, B. Espiau, A. Sahin & G. Merlin, (2013) LdFlabarin, a new BAR domain membrane protein of *Leishmania* Flagellum. *PLoS one* **8**: e76380.
- Leis, H. J., G. Fauler, G. N. Rechberger & W. Windischhofer, (2004) Electron-capture mass spectrometry: a powerful tool in biomedical trace level analysis. *Current medicinal chemistry* **11**: 1585-1594.
- Lenarcic, R., S. Halbedel, L. Visser, M. Shaw, L. J. Wu, J. Errington, D. Marenduzzo & L. W. Hamoen, (2009) Localisation of DivIVA by targeting to negatively curved membranes. *The EMBO journal* **28**: 2272-2282.
- Lenn, T., M. C. Leake & C. W. Mullineaux, (2008a) Are Escherichia coli OXPHOS complexes concentrated in specialized zones within the plasma membrane? *Biochemical Society transactions* **36**: 1032-1036.
- Lenn, T., M. C. Leake & C. W. Mullineaux, (2008b) Clustering and dynamics of cytochrome bd-I complexes in the Escherichia coli plasma membrane in vivo. *Molecular microbiology* **70**: 1397-1407.
- Lesley, J. A. & L. Shapiro, (2008) SpoT regulates DnaA stability and initiation of DNA replication in carbon-starved *Caulobacter crescentus*. *Journal of bacteriology* **190**: 6867-6880.
- Letek, M., E. Ordonez, J. Vaquera, W. Margolin, K. Flardh, L. M. Mateos & J. A. Gil, (2008) DivIVA is required for polar growth in the MreB-lacking rod-shaped actinomycete *Corynebacterium glutamicum*. *Journal of bacteriology* **190**: 3283-3292.
- Levin, P. A., P. S. Margolis, P. Setlow, R. Losick & D. Sun, (1992) Identification of *Bacillus subtilis* genes for septum placement and shape determination. *Journal of bacteriology* **174**: 6717-6728.
- Lew, M. D., S. F. Lee, J. L. Ptacin, M. K. Lee, R. J. Twieg, L. Shapiro & W. E. Moerner, (2011) Three-dimensional superresolution colocalization of intracellular protein superstructures and the cell surface in live *Caulobacter crescentus*. *Proceedings of the National Academy of Sciences of the United States of America* **108**: E1102-1110.
- Li, Q. X. & W. Dowhan, (1990) Studies on the mechanism of formation of the pyruvate prosthetic group of phosphatidylserine decarboxylase from *Escherichia coli*. *The Journal of biological chemistry* **265**: 4111-4115.
- Li, S. J. & J. E. Cronan, Jr., (1992) The genes encoding the two carboxyltransferase subunits of *Escherichia coli* acetyl-CoA carboxylase. *The Journal of biological chemistry* **267**: 16841-16847.
- Li, Y., K. Kurokawa, L. Reutimann, H. Mizumura, M. Matsuo & K. Sekimizu, (2007) DnaB and DnaI temperature-sensitive mutants of *Staphylococcus aureus*: evidence for involvement of DnaB and DnaI in synchrony regulation of chromosome replication. *Microbiology* **153**: 3370-3379.
- Liedberg, B., C. Nylander & I. Lundstrom, (1995) Biosensing with surface plasmon resonance--how it all started. *Biosensors & bioelectronics* **10**: i-ix.
- Lindas, A. C., M. Chruszcz, R. Bernander & K. Valegard, (2014) Structure of crenactin, an archaeal actin homologue active at 90 degrees C. *Acta crystallographica. Section D, Biological crystallography* **70**: 492-500.
- Litzlbauer, J., M. Schifferer, D. Ng, A. Fabritius, T. Thestrup & O. Griesbeck, (2015) Large Scale Bacterial Colony Screening of Diversified FRET Biosensors. *PLoS one* **10**: e0119860.
- Liu, L. N., S. J. Bryan, F. Huang, J. Yu, P. J. Nixon, P. R. Rich & C. W. Mullineaux, (2012) Control of electron transport routes through redox-regulated redistribution of respiratory complexes. *Proceedings of the National Academy of Sciences of the United States of America* **109**: 11431-11436.

- Liu, Z., A. Mukherjee & J. Lutkenhaus, (1999) Recruitment of ZipA to the division site by interaction with FtsZ. *Molecular microbiology* **31**: 1853-1861.
- Liu, Z., D. Xing, Q. P. Su, Y. Zhu, J. Zhang, X. Kong, B. Xue, S. Wang, H. Sun, Y. Tao & Y. Sun, (2014) Super-resolution imaging and tracking of protein-protein interactions in sub-diffraction cellular space. *Nature communications* **5**: 4443.
- Longenecker, K. L., G. F. Stamper, P. J. Hajduk, E. H. Fry, C. G. Jakob, J. E. Harlan, R. Edalji, D. M. Bartley, K. A. Walter, L. R. Solomon, T. F. Holzman, Y. G. Gu, C. G. Lerner, B. A. Beutel & V. S. Stoll, (2005) Structure of MurF from *Streptococcus pneumoniae* co-crystallized with a small molecule inhibitor exhibits interdomain closure. *Protein science : a publication of the Protein Society* **14**: 3039-3047.
- Loose, M., E. Fischer-Friedrich, J. Ries, K. Kruse & P. Schwille, (2008) Spatial regulators for bacterial cell division self-organize into surface waves in vitro. *Science* **320**: 789-792.
- Loose, M., K. Kruse & P. Schwille, (2011) Protein self-organization: lessons from the min system. *Annual review of biophysics* **40**: 315-336.
- Lopez, D. & R. Kolter, (2010) Functional microdomains in bacterial membranes. *Genes & development* **24**: 1893-1902.
- Lopian, L., Y. Elisha, A. Nussbaum-Shochat & O. Amster-Choder, (2010) Spatial and temporal organization of the E. coli PTS components. *The EMBO journal* **29**: 3630-3645.
- Lovering, A. L. & N. C. Strynadka, (2007) High-resolution structure of the major periplasmic domain from the cell shape-determining filament MreC. *Journal of molecular biology* **372**: 1034-1044.
- Lowe, J. & L. A. Amos, (1998) Crystal structure of the bacterial cell-division protein FtsZ. *Nature* **391**: 203-206.
- Lowy, F. D., (1998) Staphylococcus aureus infections. *The New England journal of medicine* **339**: 520-532.
- Lu, Y. J., Y. M. Zhang, K. D. Grimes, J. Qi, R. E. Lee & C. O. Rock, (2006) Acyl-phosphates initiate membrane phospholipid synthesis in Gram-positive pathogens. *Molecular cell* **23**: 765-772.
- Luong, T. T. & C. Y. Lee, (2007) Improved single-copy integration vectors for *Staphylococcus aureus*. *Journal of microbiological methods* **70**: 186-190.
- Lutkenhaus, J., (2007) Assembly dynamics of the bacterial MinCDE system and spatial regulation of the Z ring. *Annual review of biochemistry* **76**: 539-562.
- Lutkenhaus, J., (2008) Min oscillation in bacteria. *Advances in experimental medicine and biology* **641**: 49-61.
- Lutkenhaus, J. F., H. Wolf-Watz & W. D. Donachie, (1980) Organization of genes in the ftsA-envA region of the *Escherichia coli* genetic map and identification of a new fts locus (ftsZ). *Journal of bacteriology* **142**: 615-620.
- Ma, B., C. M. Reynolds & C. R. Raetz, (2008) Periplasmic orientation of nascent lipid A in the inner membrane of an *Escherichia coli* LptA mutant. *Proceedings of the National Academy of Sciences of the United States of America* **105**: 13823-13828.
- Ma, L., G. F. King & L. Rothfield, (2004) Positioning of the MinE binding site on the MinD surface suggests a plausible mechanism for activation of the *Escherichia coli* MinD ATPase during division site selection. *Molecular microbiology* **54**: 99-108.
- Ma, X. & W. Margolin, (1999) Genetic and functional analyses of the conserved C-terminal core domain of *Escherichia coli* FtsZ. *Journal of bacteriology* **181**: 7531-7544.
- MacKinnon, R., (2003) Potassium channels. *FEBS letters* **555**: 62-65.

- Majerczyk, C. D., P. M. Dunman, T. T. Luong, C. Y. Lee, M. R. Sadykov, G. A. Somerville, K. Bodi & A. L. Sonenshein, (2010) Direct targets of CodY in *Staphylococcus aureus*. *Journal of bacteriology* **192**: 2861-2877.
- Mani, N., P. Tobin & R. K. Jayaswal, (1993) Isolation and characterization of autolysis-defective mutants of *Staphylococcus aureus* created by Tn917-lacZ mutagenesis. *Journal of bacteriology* **175**: 1493-1499.
- Marbouty, M., C. Saguez, C. Cassier-Chauvat & F. Chauvat, (2009) ZipN, an FtsA-like orchestrator of divisome assembly in the model cyanobacterium *Synechocystis* PCC6803. *Molecular microbiology* **74**: 409-420.
- Margolin, W., (2012) The price of tags in protein localization studies. *Journal of bacteriology* **194**: 6369-6371.
- Marguet, D., P. F. Lenne, H. Rigneault & H. T. He, (2006) Dynamics in the plasma membrane: how to combine fluidity and order. *The EMBO journal* **25**: 3446-3457.
- Marston, A. L. & J. Errington, (1999) Selection of the midcell division site in *Bacillus subtilis* through MinD-dependent polar localization and activation of MinC. *Molecular microbiology* **33**: 84-96.
- Marston, A. L., H. B. Thomaidis, D. H. Edwards, M. E. Sharpe & J. Errington, (1998) Polar localization of the MinD protein of *Bacillus subtilis* and its role in selection of the mid-cell division site. *Genes & development* **12**: 3419-3430.
- Martens, S. & H. T. McMahon, (2008) Mechanisms of membrane fusion: disparate players and common principles. *Nature reviews. Molecular cell biology* **9**: 543-556.
- Martin, P. K., T. Li, D. Sun, D. P. Biek & M. B. Schmid, (1999) Role in cell permeability of an essential two-component system in *Staphylococcus aureus*. *Journal of bacteriology* **181**: 3666-3673.
- Martos, A., M. Jimenez, G. Rivas & P. Schwille, (2012a) Towards a bottom-up reconstitution of bacterial cell division. *Trends in cell biology* **22**: 634-643.
- Martos, A., B. Monterroso, S. Zorrilla, B. Reija, C. Alfonso, J. Mingorance, G. Rivas & M. Jimenez, (2012b) Isolation, characterization and lipid-binding properties of the recalcitrant FtsA division protein from *Escherichia coli*. *PloS one* **7**: e39829.
- Martos, A., Z. Petrasek & P. Schwille, (2013) Propagation of MinCDE waves on free-standing membranes. *Environmental microbiology* **15**: 3319-3326.
- Massengo-Tiasse, R. P. & J. E. Cronan, (2008) *Vibrio cholerae* FabV defines a new class of enoyl-acyl carrier protein reductase. *The Journal of biological chemistry* **283**: 1308-1316.
- Matsumoto, K., H. Hara, I. Fishov, E. Mileykovskaya & V. Norris, (2015) The membrane: transertion as an organizing principle in membrane heterogeneity. *Frontiers in microbiology* **6**: 572.
- Matsuo, M., K. Kurokawa, S. Nishida, Y. Li, H. Takimura, C. Kaito, N. Fukuhara, H. Maki, K. Miura, K. Murakami & K. Sekimizu, (2003) Isolation and mutation site determination of the temperature-sensitive murB mutants of *Staphylococcus aureus*. *FEMS microbiology letters* **222**: 107-113.
- Mazmanian, S. K., G. Liu, H. Ton-That & O. Schneewind, (1999) *Staphylococcus aureus* sortase, an enzyme that anchors surface proteins to the cell wall. *Science* **285**: 760-763.
- Mazmanian, S. K., E. P. Skaar, A. H. Gaspar, M. Humayun, P. Gornicki, J. Jelenska, A. Joachmiak, D. M. Missiakas & O. Schneewind, (2003) Passage of heme-iron across the envelope of *Staphylococcus aureus*. *Science* **299**: 906-909.
- Mazouni, K., F. Domain, C. Cassier-Chauvat & F. Chauvat, (2004) Molecular analysis of the key cytokinetic components of cyanobacteria: FtsZ, ZipN and MinCDE. *Molecular microbiology* **52**: 1145-1158.

- McDevitt, D., P. Francois, P. Vaudaux & T. J. Foster, (1994) Molecular characterization of the clumping factor (fibrinogen receptor) of *Staphylococcus aureus*. *Molecular microbiology* **11**: 237-248.
- McMahon, H. T. & J. L. Gallop, (2005) Membrane curvature and mechanisms of dynamic cell membrane remodelling. *Nature* **438**: 590-596.
- McMahon, H. T., M. M. Kozlov & S. Martens, (2010) Membrane curvature in synaptic vesicle fusion and beyond. *Cell* **140**: 601-605.
- Meeske, A. J., L. T. Sham, H. Kimsey, B. M. Koo, C. A. Gross, T. G. Bernhardt & D. Z. Rudner, (2015) MurJ and a novel lipid II flippase are required for cell wall biogenesis in *Bacillus subtilis*. *Proceedings of the National Academy of Sciences of the United States of America* **112**: 6437-6442.
- Meile, J. C., L. J. Wu, S. D. Ehrlich, J. Errington & P. Noirot, (2006) Systematic localisation of proteins fused to the green fluorescent protein in *Bacillus subtilis*: identification of new proteins at the DNA replication factory. *Proteomics* **6**: 2135-2146.
- Mengin-Lecreulx, D., L. Texier, M. Rousseau & J. van Heijenoort, (1991) The murG gene of *Escherichia coli* codes for the UDP-N-acetylglucosamine: N-acetylmuramyl-(pentapeptide) pyrophosphoryl-undecaprenol N-acetylglucosamine transferase involved in the membrane steps of peptidoglycan synthesis. *Journal of bacteriology* **173**: 4625-4636.
- Meniche, X., R. Otten, M. S. Siegrist, C. E. Baer, K. C. Murphy, C. R. Bertozzi & C. M. Sassetti, (2014) Subpolar addition of new cell wall is directed by DivIVA in mycobacteria. *Proceedings of the National Academy of Sciences of the United States of America* **111**: E3243-3251.
- Mercer, K. L. & D. S. Weiss, (2002) The *Escherichia coli* cell division protein FtsW is required to recruit its cognate transpeptidase, FtsI (PBP3), to the division site. *Journal of bacteriology* **184**: 904-912.
- Mercier, R., Y. Kawai & J. Errington, (2013) Excess membrane synthesis drives a primitive mode of cell proliferation. *Cell* **152**: 997-1007.
- Mercier, R., Y. Kawai & J. Errington, (2014) General principles for the formation and proliferation of a wall-free (L-form) state in bacteria. *eLife* **3**.
- Merino, S., N. Jimenez, R. Molero, L. Bouamama, M. Regue & J. M. Tomas, (2011) A UDP-HexNAc:polyprenol-P GalNAc-1-P transferase (WecP) representing a new subgroup of the enzyme family. *Journal of bacteriology* **193**: 1943-1952.
- Mileykovskaya, E., (2007) Subcellular localization of *Escherichia coli* osmosensory transporter ProP: focus on cardiolipin membrane domains. *Molecular microbiology* **64**: 1419-1422.
- Mileykovskaya, E. & W. Dowhan, (2000) Visualization of phospholipid domains in *Escherichia coli* by using the cardiolipin-specific fluorescent dye 10-N-nonyl acridine orange. *Journal of bacteriology* **182**: 1172-1175.
- Miller, D. J., A. Jerga, C. O. Rock & S. W. White, (2008) Analysis of the *Staphylococcus aureus* DgkB structure reveals a common catalytic mechanism for the soluble diacylglycerol kinases. *Structure* **16**: 1036-1046.
- Miller, M. J. & R. B. Gennis, (1983) The purification and characterization of the cytochrome d terminal oxidase complex of the *Escherichia coli* aerobic respiratory chain. *The Journal of biological chemistry* **258**: 9159-9165.
- Mim, C. & V. M. Unger, (2012) Membrane curvature and its generation by BAR proteins. *Trends in biochemical sciences* **37**: 526-533.
- Miroux, B. & J. E. Walker, (1996) Over-production of proteins in *Escherichia coli*: mutant hosts that allow synthesis of some membrane proteins and globular proteins at high levels. *Journal of molecular biology* **260**: 289-298.

- Mirouze, N., C. Ferret, Z. Yao, A. Chastanet & R. Carballido-Lopez, (2015) MreB-Dependent Inhibition of Cell Elongation during the Escape from Competence in *Bacillus subtilis*. *PLoS genetics* **11**: e1005299.
- Mishra, N. N., S. J. Yang, A. Sawa, A. Rubio, C. C. Nast, M. R. Yeaman & A. S. Bayer, (2009) Analysis of cell membrane characteristics of in vitro-selected daptomycin-resistant strains of methicillin-resistant *Staphylococcus aureus*. *Antimicrobial agents and chemotherapy* **53**: 2312-2318.
- Miyagishima, S. Y., H. Nozaki, K. Nishida, M. Matsuzaki & T. Kuroiwa, (2004) Two types of FtsZ proteins in mitochondria and red-lineage chloroplasts: the duplication of FtsZ is implicated in endosymbiosis. *Journal of molecular evolution* **58**: 291-303.
- Miyazaki, C., M. Kuroda, A. Ohta & I. Shibuya, (1985) Genetic manipulation of membrane phospholipid composition in *Escherichia coli*: *pgsA* mutants defective in phosphatidylglycerol synthesis. *Proceedings of the National Academy of Sciences of the United States of America* **82**: 7530-7534.
- Mohammadi, T., A. Karczmarek, M. Crouvoisier, A. Bouhss, D. Mengin-Lecreulx & T. den Blaauwen, (2007) The essential peptidoglycan glycosyltransferase MurG forms a complex with proteins involved in lateral envelope growth as well as with proteins involved in cell division in *Escherichia coli*. *Molecular microbiology* **65**: 1106-1121.
- Mohammadi, T., V. van Dam, R. Sijbrandi, T. Vernet, A. Zapun, A. Bouhss, M. Diepeveen-de Bruin, M. Nguyen-Disteche, B. de Kruijff & E. Breukink, (2011) Identification of FtsW as a transporter of lipid-linked cell wall precursors across the membrane. *The EMBO journal* **30**: 1425-1432.
- Monahan, L. G., A. T. Liew, A. L. Bottomley & E. J. Harry, (2014) Division site positioning in bacteria: one size does not fit all. *Frontiers in microbiology* **5**: 19.
- Montabana, E. A. & D. A. Agard, (2014) Bacterial tubulin TubZ-Bt transitions between a two-stranded intermediate and a four-stranded filament upon GTP hydrolysis. *Proceedings of the National Academy of Sciences of the United States of America* **111**: 3407-3412.
- Monteiro, J. M., P. B. Fernandes, F. Vaz, A. R. Pereira, A. C. Tavares, M. T. Ferreira, P. M. Pereira, H. Veiga, E. Kuru, M. S. VanNieuwenhze, Y. V. Brun, S. R. Filipe & M. G. Pinho, (2015) Cell shape dynamics during the staphylococcal cell cycle. *Nature communications* **6**: 8055.
- Morell, M., A. Espargaro, F. X. Aviles & S. Ventura, (2008) Study and selection of in vivo protein interactions by coupling bimolecular fluorescence complementation and flow cytometry. *Nature protocols* **3**: 22-33.
- Muchova, K., A. J. Wilkinson & I. Barak, (2011) Changes of lipid domains in *Bacillus subtilis* cells with disrupted cell wall peptidoglycan. *FEMS microbiology letters* **325**: 92-98.
- Mukherjee, A. & J. Lutkenhaus, (1994) Guanine nucleotide-dependent assembly of FtsZ into filaments. *Journal of bacteriology* **176**: 2754-2758.
- Mukherjee, A., C. Saez & J. Lutkenhaus, (2001) Assembly of an FtsZ mutant deficient in GTPase activity has implications for FtsZ assembly and the role of the Z ring in cell division. *Journal of bacteriology* **183**: 7190-7197.
- Mukhopadhyay, R., K. C. Huang & N. S. Wingreen, (2008) Lipid localization in bacterial cells through curvature-mediated microphase separation. *Biophysical journal* **95**: 1034-1049.
- Muller, P., C. Ewers, U. Bertsche, M. Anstett, T. Kallis, E. Breukink, C. Fraipont, M. Terrak, M. Nguyen-Disteche & W. Vollmer, (2007) The essential cell division protein FtsN interacts with the murein (peptidoglycan) synthase PBP1B in *Escherichia coli*. *The Journal of biological chemistry* **282**: 36394-36402.

- Neuhaus, F. C. & J. Baddiley, (2003) A continuum of anionic charge: structures and functions of D-alanyl-teichoic acids in gram-positive bacteria. *Microbiology and molecular biology reviews : MMBR* **67**: 686-723.
- Neumann-Giesen, C., B. Falkenbach, P. Beicht, S. Claasen, G. Luers, C. A. Stuermer, V. Herzog & R. Tikkanen, (2004) Membrane and raft association of reggie-1/flotillin-2: role of myristoylation, palmitoylation and oligomerization and induction of filopodia by overexpression. *The Biochemical journal* **378**: 509-518.
- Nguyen, L. T., J. C. Gumbart, M. Beeby & G. J. Jensen, (2015) Coarse-grained simulations of bacterial cell wall growth reveal that local coordination alone can be sufficient to maintain rod shape. *Proceedings of the National Academy of Sciences of the United States of America* **112**: E3689-3698.
- Nishibori, A., J. Kusaka, H. Hara, M. Umeda & K. Matsumoto, (2005) Phosphatidylethanolamine domains and localization of phospholipid synthases in *Bacillus subtilis* membranes. *Journal of bacteriology* **187**: 2163-2174.
- Nishizawa, M., Y. Yabusaki & M. Kanaoka, (2011) Identification of the catalytic residues of carboxylesterase from *Arthrobacter globiformis* by diisopropyl fluorophosphate-labeling and site-directed mutagenesis. *Bioscience, biotechnology, and biochemistry* **75**: 89-94.
- Niu, L. & J. Yu, (2008) Investigating intracellular dynamics of FtsZ cytoskeleton with photoactivation single-molecule tracking. *Biophysical journal* **95**: 2009-2016.
- Nogales, E., S. G. Wolf & K. H. Downing, (1998) Structure of the alpha beta tubulin dimer by electron crystallography. *Nature* **391**: 199-203.
- Noirclerc-Savoie, M., A. Le Gouellec, C. Morlot, O. Dideberg, T. Vernet & A. Zapun, (2005) In vitro reconstitution of a trimeric complex of DivIB, DivIC and FtsL, and their transient co-localization at the division site in *Streptococcus pneumoniae*. *Molecular microbiology* **55**: 413-424.
- Novick, R. P., (1991) Genetic systems in staphylococci. *Methods in enzymology* **204**: 587-636.
- Ogston, A., (1882) Micrococcus Poisoning. *Journal of anatomy and physiology* **17**: 24-58.
- Ohniwa, R. L., K. Kitabayashi & K. Morikawa, (2013) Alternative cardiolipin synthase Cls1 compensates for stalled Cls2 function in *Staphylococcus aureus* under conditions of acute acid stress. *FEMS microbiology letters* **338**: 141-146.
- Ohno, Y., I. Yano & M. Masui, (1979) Effect of NaCl concentration and temperature on the phospholipid and fatty acid compositions of a moderately halophilic bacterium, *Pseudomonas halosaccharolytica*. *Journal of biochemistry* **85**: 413-421.
- Okuda, S., D. J. Sherman, T. J. Silhavy, N. Ruiz & D. Kahne, (2016) Lipopolysaccharide transport and assembly at the outer membrane: the PEZ model. *Nature reviews. Microbiology* **14**: 337-345.
- Okuno, T., M. Ogoh, H. Tanina, N. Funasaki & K. Kogure, (2009) Direct monitoring of interaction between *Escherichia coli* proteins, MinC and monomeric FtsZ, in solution. *Biological & pharmaceutical bulletin* **32**: 1473-1475.
- Oliva, M. A., S. C. Cordell & J. Lowe, (2004) Structural insights into FtsZ protofilament formation. *Nature structural & molecular biology* **11**: 1243-1250.
- Oliva, M. A., S. Halbedel, S. M. Freund, P. Dutow, T. A. Leonard, D. B. Veprintsev, L. W. Hamoen & J. Lowe, (2010) Features critical for membrane binding revealed by DivIVA crystal structure. *The EMBO journal* **29**: 1988-2001.
- Osawa, M., D. E. Anderson & H. P. Erickson, (2008) Reconstitution of contractile FtsZ rings in liposomes. *Science* **320**: 792-794.

- Osawa, M. & H. P. Erickson, (2011) Inside-out Z rings--constriction with and without GTP hydrolysis. *Molecular microbiology* **81**: 571-579.
- Osawa, M. & H. P. Erickson, (2013) Liposome division by a simple bacterial division machinery. *Proceedings of the National Academy of Sciences of the United States of America* **110**: 11000-11004.
- Over, B., R. Heusser, N. McCallum, B. Schulthess, P. Kupferschmied, J. M. Gaiani, C. D. Sifri, B. Berger-Bachi & P. Stutzmann Meier, (2011) LytR-CpsA-Psr proteins in *Staphylococcus aureus* display partial functional redundancy and the deletion of all three severely impairs septum placement and cell separation. *FEMS microbiology letters* **320**: 142-151.
- Paoletti, L., Y. J. Lu, G. E. Schujman, D. de Mendoza & C. O. Rock, (2007) Coupling of fatty acid and phospholipid synthesis in *Bacillus subtilis*. *Journal of bacteriology* **189**: 5816-5824.
- Park, K. T., W. Wu, K. P. Battaile, S. Lovell, T. Holyoak & J. Lutkenhaus, (2011) The Min oscillator uses MinD-dependent conformational changes in MinE to spatially regulate cytokinesis. *Cell* **146**: 396-407.
- Parry, B. R., I. V. Surovtsev, M. T. Cabeen, C. S. O'Hern, E. R. Dufresne & C. Jacobs-Wagner, (2014) The bacterial cytoplasm has glass-like properties and is fluidized by metabolic activity. *Cell* **156**: 183-194.
- Parsons, J. B. & C. O. Rock, (2013) Bacterial lipids: metabolism and membrane homeostasis. *Progress in lipid research* **52**: 249-276.
- Parthasarathy, R., C. H. Yu & J. T. Groves, (2006) Curvature-modulated phase separation in lipid bilayer membranes. *Langmuir : the ACS journal of surfaces and colloids* **22**: 5095-5099.
- Patching, S. G., (2014) Surface plasmon resonance spectroscopy for characterisation of membrane protein-ligand interactions and its potential for drug discovery. *Biochimica et biophysica acta* **1838**: 43-55.
- Patrick, J. E. & D. B. Kearns, (2008) MinJ (YvjD) is a topological determinant of cell division in *Bacillus subtilis*. *Molecular microbiology* **70**: 1166-1179.
- Peacock, S. J., I. de Silva & F. D. Lowy, (2001) What determines nasal carriage of *Staphylococcus aureus*? *Trends in microbiology* **9**: 605-610.
- Perdih, A., M. Kotnik, M. Hodoscek & T. Solmajer, (2007) Targeted molecular dynamics simulation studies of binding and conformational changes in *E. coli* MurD. *Proteins* **68**: 243-254.
- Pereira, S. F., A. O. Henriques, M. G. Pinho, H. de Lencastre & A. Tomasz, (2007) Role of PBP1 in cell division of *Staphylococcus aureus*. *Journal of bacteriology* **189**: 3525-3531.
- Perozo, E. & D. C. Rees, (2003) Structure and mechanism in prokaryotic mechanosensitive channels. *Current opinion in structural biology* **13**: 432-442.
- Perry, S. E. & D. H. Edwards, (2004) Identification of a polar targeting determinant for *Bacillus subtilis* DivIVA. *Molecular microbiology* **54**: 1237-1249.
- Peschel, A., R. W. Jack, M. Otto, L. V. Collins, P. Staubitz, G. Nicholson, H. Kalbacher, W. F. Nieuwenhuizen, G. Jung, A. Tarkowski, K. P. van Kessel & J. A. van Strijp, (2001) *Staphylococcus aureus* resistance to human defensins and evasion of neutrophil killing via the novel virulence factor MprF is based on modification of membrane lipids with l-lysine. *The Journal of experimental medicine* **193**: 1067-1076.
- Peter, B. J., H. M. Kent, I. G. Mills, Y. Vallis, P. J. Butler, P. R. Evans & H. T. McMahon, (2004) BAR domains as sensors of membrane curvature: the amphiphysin BAR structure. *Science* **303**: 495-499.
- Phillips, R., (2013) In retrospect: The Feynman Lectures on Physics. *Nature* **504**: 30-31.

- Pichoff, S. & J. Lutkenhaus, (2005) Tethering the Z ring to the membrane through a conserved membrane targeting sequence in FtsA. *Molecular microbiology* **55**: 1722-1734.
- Pinho, M. G. & J. Errington, (2003) Dispersed mode of Staphylococcus aureus cell wall synthesis in the absence of the division machinery. *Molecular microbiology* **50**: 871-881.
- Pinho, M. G. & J. Errington, (2004) A divIVA null mutant of Staphylococcus aureus undergoes normal cell division. *FEMS microbiology letters* **240**: 145-149.
- Pinho, M. G. & J. Errington, (2005) Recruitment of penicillin-binding protein PBP2 to the division site of Staphylococcus aureus is dependent on its transpeptidation substrates. *Molecular microbiology* **55**: 799-807.
- Pinho, M. G., M. Kjos & J. W. Veening, (2013) How to get (a)round: mechanisms controlling growth and division of coccoid bacteria. *Nature reviews. Microbiology* **11**: 601-614.
- Pogliano, J., N. Pogliano & J. A. Silverman, (2012) Daptomycin-mediated reorganization of membrane architecture causes mislocalization of essential cell division proteins. *Journal of bacteriology* **194**: 4494-4504.
- Pohl, K., P. Francois, L. Stenz, F. Schlink, T. Geiger, S. Herbert, C. Goerke, J. Schrenzel & C. Wolz, (2009) CodY in Staphylococcus aureus: a regulatory link between metabolism and virulence gene expression. *Journal of bacteriology* **191**: 2953-2963.
- Polka, J. K., J. M. Kollman & R. D. Mullins, (2014) Accessory factors promote AlfA-dependent plasmid segregation by regulating filament nucleation, disassembly, and bundling. *Proceedings of the National Academy of Sciences of the United States of America* **111**: 2176-2181.
- Popp, D., W. Xu, A. Narita, A. J. Brzoska, R. A. Skurray, N. Firth, U. Ghoshdastider, Y. Maeda, R. C. Robinson & M. A. Schumacher, (2010) Structure and filament dynamics of the pSK41 actin-like ParM protein: implications for plasmid DNA segregation. *The Journal of biological chemistry* **285**: 10130-10140.
- Potrykus, K. & M. Cashel, (2008) (p)ppGpp: still magical? *Annual review of microbiology* **62**: 35-51.
- Powell, D. A., M. Duckworth & J. Baddiley, (1975) A membrane-associated lipomannan in micrococci. *The Biochemical journal* **151**: 387-397.
- Prescott, D. J. & P. R. Vagelos, (1970) Acyl carrier protein. XIV. Further studies on beta-ketoacyl acyl carrier protein synthetase from Escherichia coli. *The Journal of biological chemistry* **245**: 5484-5490.
- Price, A. C., K. H. Choi, R. J. Heath, Z. Li, S. W. White & C. O. Rock, (2001) Inhibition of beta-ketoacyl-acyl carrier protein synthases by thiolactomycin and cerulenin. Structure and mechanism. *The Journal of biological chemistry* **276**: 6551-6559.
- Qamar, A. & D. Golemi-Kotra, (2012) Dual roles of FmtA in Staphylococcus aureus cell wall biosynthesis and autolysis. *Antimicrobial agents and chemotherapy* **56**: 3797-3805.
- Qiu, X., A. E. Choudhry, C. A. Janson, M. Grooms, R. A. Daines, J. T. Lonsdale & S. S. Khandekar, (2005) Crystal structure and substrate specificity of the beta-ketoacyl-acyl carrier protein synthase III (FabH) from Staphylococcus aureus. *Protein science : a publication of the Protein Society* **14**: 2087-2094.
- Qoronfleh, M. W., J. E. Gustafson & B. J. Wilkinson, (1998) Conditions that induce Staphylococcus aureus heat shock proteins also inhibit autolysis. *FEMS microbiology letters* **166**: 103-107.
- Qoronfleh, M. W., U. N. Streips & B. J. Wilkinson, (1990) Basic features of the staphylococcal heat shock response. *Antonie van Leeuwenhoek* **58**: 79-86.

- Raetz, C. R. & C. Whitfield, (2002) Lipopolysaccharide endotoxins. *Annual review of biochemistry* **71**: 635-700.
- Ramamurthi, K. S., (2010) Protein localization by recognition of membrane curvature. *Current opinion in microbiology* **13**: 753-757.
- Ramamurthi, K. S., S. Lecuyer, H. A. Stone & R. Losick, (2009) Geometric cue for protein localization in a bacterium. *Science* **323**: 1354-1357.
- Ramamurthi, K. S. & R. Losick, (2009) Negative membrane curvature as a cue for subcellular localization of a bacterial protein. *Proceedings of the National Academy of Sciences of the United States of America* **106**: 13541-13545.
- Raskin, D. M. & P. A. de Boer, (1997) The MinE ring: an FtsZ-independent cell structure required for selection of the correct division site in E. coli. *Cell* **91**: 685-694.
- Raskin, D. M. & P. A. de Boer, (1999) MinDE-dependent pole-to-pole oscillation of division inhibitor MinC in Escherichia coli. *Journal of bacteriology* **181**: 6419-6424.
- Ray, P. H., T. T. Lillich & D. C. White, (1972) Consequences of glycerol deprivation on the synthesis of membrane components in a glycerol auxotroph of Staphylococcus aureus. *Journal of bacteriology* **112**: 413-420.
- Ray, P. H. & D. C. White, (1972) Effect of glycerol deprivation on the phospholipid metabolism of a glycerol auxotroph of Staphylococcus aureus. *Journal of bacteriology* **109**: 668-677.
- Reddy, V. M. & B. Kumar, (2000) Interaction of Mycobacterium avium complex with human respiratory epithelial cells. *The Journal of infectious diseases* **181**: 1189-1193.
- Reichmann, N. T. & A. Grundling, (2011) Location, synthesis and function of glycolipids and polyglycerolphosphate lipoteichoic acid in Gram-positive bacteria of the phylum Firmicutes. *FEMS microbiology letters* **319**: 97-105.
- Reichmann, N. T., C. Picarra Cassona, J. M. Monteiro, A. L. Bottomley, R. M. Corrigan, S. J. Foster, M. G. Pinho & A. Grundling, (2014) Differential localization of LTA synthesis proteins and their interaction with the cell division machinery in Staphylococcus aureus. *Molecular microbiology* **92**: 273-286.
- Reimold, C., H. J. Defeu Soufo, F. Dempwolff & P. L. Graumann, (2013) Motion of variable-length MreB filaments at the bacterial cell membrane influences cell morphology. *Molecular biology of the cell* **24**: 2340-2349.
- Renner, L. D., P. Eswaramoorthy, K. S. Ramamurthi & D. B. Weibel, (2013) Studying biomolecule localization by engineering bacterial cell wall curvature. *PloS one* **8**: e84143.
- Renner, L. D. & D. B. Weibel, (2011) Cardiolipin microdomains localize to negatively curved regions of Escherichia coli membranes. *Proceedings of the National Academy of Sciences of the United States of America* **108**: 6264-6269.
- Rietveld, A. & K. Simons, (1998) The differential miscibility of lipids as the basis for the formation of functional membrane rafts. *Biochimica et biophysica acta* **1376**: 467-479.
- Rodionov, O., M. Lobočka & M. Yarmolinsky, (1999) Silencing of genes flanking the P1 plasmid centromere. *Science* **283**: 546-549.
- Rohrer, S. & B. Berger-Bachi, (2003) Application of a bacterial two-hybrid system for the analysis of protein-protein interactions between FemABX family proteins. *Microbiology* **149**: 2733-2738.
- Rohrer, S., K. Ehlert, M. Tschierske, H. Labischinski & B. Berger-Bachi, (1999) The essential Staphylococcus aureus gene fmhB is involved in the first step of peptidoglycan pentaglycine interpeptide formation. *Proceedings of the National Academy of Sciences of the United States of America* **96**: 9351-9356.

- Romantsov, T., A. R. Battle, J. L. Hendel, B. Martinac & J. M. Wood, (2010) Protein localization in Escherichia coli cells: comparison of the cytoplasmic membrane proteins ProP, LacY, ProW, AqpZ, MscS, and MscL. *Journal of bacteriology* **192**: 912-924.
- Romantsov, T., S. Helbig, D. E. Culham, C. Gill, L. Stalker & J. M. Wood, (2007) Cardiolipin promotes polar localization of osmosensory transporter ProP in Escherichia coli. *Molecular microbiology* **64**: 1455-1465.
- Rosander, A., J. Bjerketorp, L. Frykberg & K. Jacobsson, (2002) Phage display as a novel screening method to identify extracellular proteins. *Journal of microbiological methods* **51**: 43-55.
- Roux, C. M., J. P. DeMuth & P. M. Dunman, (2011) Characterization of components of the Staphylococcus aureus mRNA degradosome holoenzyme-like complex. *Journal of bacteriology* **193**: 5520-5526.
- Rowland, S. L., K. D. Wadsworth, S. A. Robson, C. Robichon, J. Beckwith & G. F. King, (2010) Evidence from artificial septal targeting and site-directed mutagenesis that residues in the extracytoplasmic beta domain of DivIB mediate its interaction with the divisomal transpeptidase PBP 2B. *Journal of bacteriology* **192**: 6116-6125.
- Rowlett, V. W. & W. Margolin, (2015) The Min system and other nucleoid-independent regulators of Z ring positioning. *Frontiers in microbiology* **6**: 478.
- Rubinchik, E., T. Schneider, M. Elliott, W. R. Scott, J. Pan, C. Anklin, H. Yang, D. Dugourd, A. Muller, K. Gries, S. K. Straus, H. G. Sahl & R. E. Hancock, (2011) Mechanism of action and limited cross-resistance of new lipopeptide MX-2401. *Antimicrobial agents and chemotherapy* **55**: 2743-2754.
- Ruiz-Avila, L. B., S. Huecas, M. Artola, A. Vergonos, E. Ramirez-Aportela, E. Cercenado, I. Barasoain, H. Vazquez-Villa, M. Martin-Fontecha, P. Chacon, M. L. Lopez-Rodriguez & J. M. Andreu, (2013) Synthetic inhibitors of bacterial cell division targeting the GTP-binding site of FtsZ. *ACS chemical biology* **8**: 2072-2083.
- Saarikangas, J., H. Zhao, A. Pykalainen, P. Laurinmaki, P. K. Mattila, P. K. Kinnunen, S. J. Butcher & P. Lappalainen, (2009) Molecular mechanisms of membrane deformation by I-BAR domain proteins. *Current biology : CB* **19**: 95-107.
- Saenz, J. P., D. Grosser, A. S. Bradley, T. J. Lagny, O. Lavrynenko, M. Broda & K. Simons, (2015) Hopanoids as functional analogues of cholesterol in bacterial membranes. *Proceedings of the National Academy of Sciences of the United States of America* **112**: 11971-11976.
- Saenz, J. P., E. Sezgin, P. Schwillle & K. Simons, (2012) Functional convergence of hopanoids and sterols in membrane ordering. *Proceedings of the National Academy of Sciences of the United States of America* **109**: 14236-14240.
- Salje, J., F. van den Ent, P. de Boer & J. Lowe, (2011) Direct membrane binding by bacterial actin MreB. *Molecular cell* **43**: 478-487.
- Samuel, G. & P. Reeves, (2003) Biosynthesis of O-antigens: genes and pathways involved in nucleotide sugar precursor synthesis and O-antigen assembly. *Carbohydrate research* **338**: 2503-2519.
- Santos, T. M., T. Y. Lin, M. Rajendran, S. M. Anderson & D. B. Weibel, (2014) Polar localization of Escherichia coli chemoreceptors requires an intact Tol-Pal complex. *Molecular microbiology* **92**: 985-1004.
- Sato, Y., M. Kameya, H. Arai, M. Ishii & Y. Igarashi, (2011) Detecting weak protein-protein interactions by modified far-western blotting. *Journal of bioscience and bioengineering* **112**: 304-307.
- Scheffers, D. & A. J. Driessen, (2001) The polymerization mechanism of the bacterial cell division protein FtsZ. *FEBS letters* **506**: 6-10.

- Scheffers, D. J. & M. G. Pinho, (2005) Bacterial cell wall synthesis: new insights from localization studies. *Microbiology and molecular biology reviews* : **MMBR 69**: 585-607.
- Schirner, K., Y. J. Eun, M. Dion, Y. Luo, J. D. Helmann, E. C. Garner & S. Walker, (2015) Lipid-linked cell wall precursors regulate membrane association of bacterial actin MreB. *Nature chemical biology* **11**: 38-45.
- Schirner, K., L. K. Stone & S. Walker, (2011) ABC transporters required for export of wall teichoic acids do not discriminate between different main chain polymers. *ACS chemical biology* **6**: 407-412.
- Schlag, M., R. Biswas, B. Krismer, T. Kohler, S. Zoll, W. Yu, H. Schwarz, A. Peschel & F. Gotz, (2010) Role of staphylococcal wall teichoic acid in targeting the major autolysin Atl. *Molecular microbiology* **75**: 864-873.
- Schmidt, K. L., N. D. Peterson, R. J. Kustusch, M. C. Wissel, B. Graham, G. J. Phillips & D. S. Weiss, (2004) A predicted ABC transporter, FtsEX, is needed for cell division in Escherichia coli. *Journal of bacteriology* **186**: 785-793.
- Schumacher, M. A., (2012) Bacterial plasmid partition machinery: a minimalist approach to survival. *Current opinion in structural biology* **22**: 72-79.
- Seligman, S. J. & M. R. Pincus, (1987) A model for the three-dimensional structure of peptidoglycan in staphylococci. *Journal of theoretical biology* **124**: 275-292.
- Sham, L. T., E. K. Butler, M. D. Lebar, D. Kahne, T. G. Bernhardt & N. Ruiz, (2014) Bacterial cell wall. MurJ is the flippase of lipid-linked precursors for peptidoglycan biogenesis. *Science* **345**: 220-222.
- Sharpe, M. E., P. M. Hauser, R. G. Sharpe & J. Errington, (1998) Bacillus subtilis cell cycle as studied by fluorescence microscopy: constancy of cell length at initiation of DNA replication and evidence for active nucleoid partitioning. *Journal of bacteriology* **180**: 547-555.
- Shen, B. & J. Lutkenhaus, (2010) Examination of the interaction between FtsZ and MinCN in E. coli suggests how MinC disrupts Z rings. *Molecular microbiology* **75**: 1285-1298.
- Shih, Y. L., I. Kawagishi & L. Rothfield, (2005) The MreB and Min cytoskeletal-like systems play independent roles in prokaryotic polar differentiation. *Molecular microbiology* **58**: 917-928.
- Shiomi, D. & W. Margolin, (2007) A sweet sensor for size-conscious bacteria. *Cell* **130**: 216-218.
- Sieger, B. & M. Bramkamp, (2014) Interaction sites of DivIVA and RodA from Corynebacterium glutamicum. *Frontiers in microbiology* **5**: 738.
- Singer, S. J. & G. L. Nicolson, (1972) The fluid mosaic model of the structure of cell membranes. *Science* **175**: 720-731.
- Singh, J. K., R. D. Makde, V. Kumar & D. Panda, (2007) A membrane protein, EzrA, regulates assembly dynamics of FtsZ by interacting with the C-terminal tail of FtsZ. *Biochemistry* **46**: 11013-11022.
- Skarstad, K., E. Boye & H. B. Steen, (1986) Timing of initiation of chromosome replication in individual Escherichia coli cells. *The EMBO journal* **5**: 1711-1717.
- Smith, E. J., L. Visai, S. W. Kerrigan, P. Speziale & T. J. Foster, (2011) The Sbi protein is a multifunctional immune evasion factor of Staphylococcus aureus. *Infection and immunity* **79**: 3801-3809.
- Smith, G. P., (1985) Filamentous fusion phage: novel expression vectors that display cloned antigens on the virion surface. *Science* **228**: 1315-1317.
- Soldo, B., V. Lazarevic & D. Karamata, (2002) tagO is involved in the synthesis of all anionic cell-wall polymers in Bacillus subtilis 168. *Microbiology* **148**: 2079-2087.

- Sourjik, V. & H. C. Berg, (2002) Binding of the Escherichia coli response regulator CheY to its target measured in vivo by fluorescence resonance energy transfer. *Proceedings of the National Academy of Sciences of the United States of America* **99**: 12669-12674.
- Sourjik, V., A. Vaknin, T. S. Shimizu & H. C. Berg, (2007) In vivo measurement by FRET of pathway activity in bacterial chemotaxis. *Methods in enzymology* **423**: 365-391.
- Sparrow, C. P. & C. R. Raetz, (1985) Purification and properties of the membrane-bound CDP-diglyceride synthetase from Escherichia coli. *The Journal of biological chemistry* **260**: 12084-12091.
- Sperandeo, P., F. K. Lau, A. Carpentieri, C. De Castro, A. Molinaro, G. Deho, T. J. Silhavy & A. Polissi, (2008) Functional analysis of the protein machinery required for transport of lipopolysaccharide to the outer membrane of Escherichia coli. *Journal of bacteriology* **190**: 4460-4469.
- Spitzer, J., (2011) From water and ions to crowded biomacromolecules: in vivo structuring of a prokaryotic cell. *Microbiology and molecular biology reviews* : *MMBR* **75**: 491-506, second page of table of contents.
- Spura, J., L. C. Reimer, P. Wieloch, K. Schreiber, S. Buchinger & D. Schomburg, (2009) A method for enzyme quenching in microbial metabolome analysis successfully applied to gram-positive and gram-negative bacteria and yeast. *Analytical biochemistry* **394**: 192-201.
- Steele, V. R., A. L. Bottomley, J. Garcia-Lara, J. Kasturiarachchi & S. J. Foster, (2011) Multiple essential roles for EzrA in cell division of Staphylococcus aureus. *Molecular microbiology* **80**: 542-555.
- Steiner, W., G. Liu, W. D. Donachie & P. Kuempel, (1999) The cytoplasmic domain of FtsK protein is required for resolution of chromosome dimers. *Molecular microbiology* **31**: 579-583.
- Stokes, K. D. & K. W. Osteryoung, (2003) Early divergence of the FtsZ1 and FtsZ2 plastid division gene families in photosynthetic eukaryotes. *Gene* **320**: 97-108.
- Strahl, H., F. Burmann & L. W. Hamoen, (2014) The actin homologue MreB organizes the bacterial cell membrane. *Nature communications* **5**.
- Strahl, H. & L. W. Hamoen, (2010) Membrane potential is important for bacterial cell division. *Proceedings of the National Academy of Sciences of the United States of America* **107**: 12281-12286.
- Strahl, H. & L. W. Hamoen, (2012) Finding the corners in a cell. *Current opinion in microbiology* **15**: 731-736.
- Strahl, H., S. Ronneau, B. S. Gonzalez, D. Klutsch, C. Schaffner-Barbero & L. W. Hamoen, (2015) Transmembrane protein sorting driven by membrane curvature. *Nature communications* **6**: 8728.
- Strauss, M. P., A. T. Liew, L. Turnbull, C. B. Whitchurch, L. G. Monahan & E. J. Harry, (2012) 3D-SIM super resolution microscopy reveals a bead-like arrangement for FtsZ and the division machinery: implications for triggering cytokinesis. *PLoS biology* **10**: e1001389.
- Stryer, L., (1978) Fluorescence energy transfer as a spectroscopic ruler. *Annual review of biochemistry* **47**: 819-846.
- Sukharev, S. I., P. Blount, B. Martinac, F. R. Blattner & C. Kung, (1994) A large-conductance mechanosensitive channel in E. coli encoded by mscL alone. *Nature* **368**: 265-268.
- Sureka, K., T. Hossain, P. Mukherjee, P. Chatterjee, P. Datta, M. Kundu & J. Basu, (2010) Novel role of phosphorylation-dependent interaction between FtsZ and FipA in mycobacterial cell division. *PloS one* **5**: e8590.

- Swulius, M. T., S. Chen, H. Jane Ding, Z. Li, A. Briegel, M. Pilhofer, E. I. Tocheva, S. R. Lybarger, T. L. Johnson, M. Sandkvist & G. J. Jensen, (2011) Long helical filaments are not seen encircling cells in electron cryotomograms of rod-shaped bacteria. *Biochemical and biophysical research communications* **407**: 650-655.
- Swulius, M. T. & G. J. Jensen, (2012) The helical MreB cytoskeleton in *Escherichia coli* MC1000/pLE7 is an artifact of the N-Terminal yellow fluorescent protein tag. *Journal of bacteriology* **194**: 6382-6386.
- Szeto, T. H., S. L. Rowland & G. F. King, (2001) The dimerization function of MinC resides in a structurally autonomous C-terminal domain. *Journal of bacteriology* **183**: 6684-6687.
- Szollosi, J., P. Nagy, Z. Sebestyeny, S. Damjanovitcha, J. W. Park & L. Matyus, (2002) Applications of fluorescence resonance energy transfer for mapping biological membranes. *Journal of biotechnology* **82**: 251-266.
- Takada, H., S. Fukushima-Tanaka, M. Morita, Y. Kasahara, S. Watanabe, T. Chibazakura, H. Hara, K. Matsumoto & H. Yoshikawa, (2014) An essential enzyme for phospholipid synthesis associates with the *Bacillus subtilis* divisome. *Molecular microbiology* **91**: 242-255.
- Taron, D. J., W. C. Childs, 3rd & F. C. Neuhaus, (1983) Biosynthesis of D-alanyl-lipoteichoic acid: role of diglyceride kinase in the synthesis of phosphatidylglycerol for chain elongation. *Journal of bacteriology* **154**: 1110-1116.
- Tavares, A. C., P. B. Fernandes, R. Carballido-Lopez & M. G. Pinho, (2015) MreC and MreD Proteins Are Not Required for Growth of *Staphylococcus aureus*. *PloS one* **10**: e0140523.
- Tefsen, B., J. Geurtsen, F. Beckers, J. Tommassen & H. de Cock, (2005) Lipopolysaccharide transport to the bacterial outer membrane in spheroplasts. *The Journal of biological chemistry* **280**: 4504-4509.
- Thanbichler, M. & L. Shapiro, (2006) MipZ, a spatial regulator coordinating chromosome segregation with cell division in *Caulobacter*. *Cell* **126**: 147-162.
- Thanbichler, M., S. C. Wang & L. Shapiro, (2005) The bacterial nucleoid: a highly organized and dynamic structure. *Journal of cellular biochemistry* **96**: 506-521.
- Tinsley, E. & S. A. Khan, (2006) A novel FtsZ-like protein is involved in replication of the anthrax toxin-encoding pXO1 plasmid in *Bacillus anthracis*. *Journal of bacteriology* **188**: 2829-2835.
- Tjalsma, H., V. P. Kontinen, Z. Pragai, H. Wu, R. Meima, G. Venema, S. Bron, M. Sarvas & J. M. van Dijl, (1999) The role of lipoprotein processing by signal peptidase II in the Gram-positive eubacterium *Bacillus subtilis*. Signal peptidase II is required for the efficient secretion of alpha-amylase, a non-lipoprotein. *The Journal of biological chemistry* **274**: 1698-1707.
- Toledo, A., J. T. Crowley, J. L. Coleman, T. J. LaRocca, S. Chiantia, E. London & J. L. Benach, (2014) Selective association of outer surface lipoproteins with the lipid rafts of *Borrelia burgdorferi*. *mBio* **5**: e00899-00814.
- Traag, B. A. & G. P. van Wezel, (2008) The SsgA-like proteins in actinomycetes: small proteins up to a big task. *Antonie van Leeuwenhoek* **94**: 85-97.
- Tramier, M., M. Zahid, J. C. Mevel, M. J. Masse & M. Coppey-Moisan, (2006) Sensitivity of CFP/YFP and GFP/mCherry pairs to donor photobleaching on FRET determination by fluorescence lifetime imaging microscopy in living cells. *Microscopy research and technique* **69**: 933-939.
- Tran, A. X., M. S. Trent & C. Whitfield, (2008) The LptA protein of *Escherichia coli* is a periplasmic lipid A-binding protein involved in the lipopolysaccharide export pathway. *The Journal of biological chemistry* **283**: 20342-20349.

- Treuner-Lange, A., K. Aguiluz, C. van der Does, N. Gomez-Santos, A. Harms, D. Schumacher, P. Lenz, M. Hoppert, J. Kahnt, J. Munoz-Dorado & L. Sogaard-Andersen, (2013) PomZ, a ParA-like protein, regulates Z-ring formation and cell division in *Myxococcus xanthus*. *Molecular microbiology* **87**: 235-253.
- Treuner-Lange, A., E. Macia, M. Guzzo, E. Hot, L. M. Faure, B. Jakobczak, L. Espinosa, D. Alcor, A. Ducret, D. Keilberg, J. P. Castaing, S. Lacas Gervais, M. Franco, L. Sogaard-Andersen & T. Mignot, (2015) The small G-protein MglA connects to the MreB actin cytoskeleton at bacterial focal adhesions. *The Journal of cell biology* **210**: 243-256.
- Tsay, J. T., W. Oh, T. J. Larson, S. Jackowski & C. O. Rock, (1992) Isolation and characterization of the beta-ketoacyl-acyl carrier protein synthase III gene (fabH) from *Escherichia coli* K-12. *The Journal of biological chemistry* **267**: 6807-6814.
- Turing, A. M., (1990) The chemical basis of morphogenesis. 1953. *Bulletin of mathematical biology* **52**: 153-197; discussion 119-152.
- Turner, R. D., A. F. Hurd, A. Cadby, J. K. Hobbs & S. J. Foster, (2013) Cell wall elongation mode in Gram-negative bacteria is determined by peptidoglycan architecture. *Nature communications* **4**: 1496.
- Turner, R. D., E. C. Ratcliffe, R. Wheeler, R. Golestanian, J. K. Hobbs & S. J. Foster, (2010) Peptidoglycan architecture can specify division planes in *Staphylococcus aureus*. *Nature communications* **1**: 26.
- Turner, R. D., W. Vollmer & S. J. Foster, (2014) Different walls for rods and balls: the diversity of peptidoglycan. *Molecular microbiology* **91**: 862-874.
- Tynecka, Z., Z. Szczesniak, A. Malm & R. Los, (1999) Energy conservation in aerobically grown *Staphylococcus aureus*. *Research in microbiology* **150**: 555-566.
- Typas, A., M. Banzhaf, C. A. Gross & W. Vollmer, (2012) From the regulation of peptidoglycan synthesis to bacterial growth and morphology. *Nature reviews. Microbiology* **10**: 123-136.
- Tzagoloff, H. & R. Novick, (1977) Geometry of cell division in *Staphylococcus aureus*. *Journal of bacteriology* **129**: 343-350.
- Uehara, T. & J. T. Park, (2008) Growth of *Escherichia coli*: significance of peptidoglycan degradation during elongation and septation. *Journal of bacteriology* **190**: 3914-3922.
- Uehara, T., K. R. Parzych, T. Dinh & T. G. Bernhardt, (2010) Daughter cell separation is controlled by cytokinetic ring-activated cell wall hydrolysis. *The EMBO journal* **29**: 1412-1422.
- Ursell, T. S., J. Nguyen, R. D. Monds, A. Colavin, G. Billings, N. Ouzounov, Z. Gitai, J. W. Shaevitz & K. C. Huang, (2014) Rod-like bacterial shape is maintained by feedback between cell curvature and cytoskeletal localization. *Proceedings of the National Academy of Sciences of the United States of America* **111**: E1025-1034.
- Vagner, V., E. Dervyn & S. D. Ehrlich, (1998) A vector for systematic gene inactivation in *Bacillus subtilis*. *Microbiology* **144** (Pt 11): 3097-3104.
- Vaknin, A. & H. C. Berg, (2004) Single-cell FRET imaging of phosphatase activity in the *Escherichia coli* chemotaxis system. *Proceedings of the National Academy of Sciences of the United States of America* **101**: 17072-17077.
- van Baarle, S., I. N. Celik, K. G. Kaval, M. Bramkamp, L. W. Hamoen & S. Halbedel, (2013) Protein-protein interaction domains of *Bacillus subtilis* DivIVA. *Journal of bacteriology* **195**: 1012-1021.
- van den Ent, F., L. A. Amos & J. Lowe, (2001) Prokaryotic origin of the actin cytoskeleton. *Nature* **413**: 39-44.

- van den Ent, F., T. Izore, T. A. Bharat, C. M. Johnson & J. Lowe, (2014) Bacterial actin MreB forms antiparallel double filaments. *eLife* **3**: e02634.
- van der Ploeg, R., S. T. Goudelis & T. den Blaauwen, (2015) Validation of FRET Assay for the Screening of Growth Inhibitors of Escherichia coli Reveals Elongasome Assembly Dynamics. *International journal of molecular sciences* **16**: 17637-17654.
- van der Ploeg, R., J. Verheul, N. O. Vischer, S. Alexeeva, E. Hoogendoorn, M. Postma, M. Banzhaf, W. Vollmer & T. den Blaauwen, (2013) Colocalization and interaction between elongasome and divisome during a preparative cell division phase in Escherichia coli. *Molecular microbiology* **87**: 1074-1087.
- Van Munster, E. B., G. J. Kremers, M. J. Adjobo-Hermans & T. W. Gadella, Jr., (2005) Fluorescence resonance energy transfer (FRET) measurement by gradual acceptor photobleaching. *Journal of microscopy* **218**: 253-262.
- van Ooij, C. & R. Losick, (2003) Subcellular localization of a small sporulation protein in Bacillus subtilis. *Journal of bacteriology* **185**: 1391-1398.
- van Teeffelen, S. & Z. Gitai, (2011) Rotate into shape: MreB and bacterial morphogenesis. *The EMBO journal* **30**: 4856-4857.
- van Thor, J. J. & K. J. Hellingwerf, (2002) Fluorescence resonance energy transfer (FRET) applications using green fluorescent protein. Energy transfer to the endogenous chromophores of phycobilisome light-harvesting complexes. *Methods Mol Biol* **183**: 101-119.
- Vats, P. & L. Rothfield, (2007) Duplication and segregation of the actin (MreB) cytoskeleton during the prokaryotic cell cycle. *Proceedings of the National Academy of Sciences of the United States of America* **104**: 17795-17800.
- Vats, P., Y. L. Shih & L. Rothfield, (2009) Assembly of the MreB-associated cytoskeletal ring of Escherichia coli. *Molecular microbiology* **72**: 170-182.
- Vaughan, S., B. Wickstead, K. Gull & S. G. Addinall, (2004) Molecular evolution of FtsZ protein sequences encoded within the genomes of archaea, bacteria, and eukaryota. *Journal of molecular evolution* **58**: 19-29.
- Vecchiarelli, A. G., M. Li, M. Mizuuchi & K. Mizuuchi, (2014) Differential affinities of MinD and MinE to anionic phospholipid influence Min patterning dynamics in vitro. *Molecular microbiology* **93**: 453-463.
- Veiga, H., A. M. Jorge & M. G. Pinho, (2011) Absence of nucleoid occlusion effector Noc impairs formation of orthogonal FtsZ rings during Staphylococcus aureus cell division. *Molecular microbiology* **80**: 1366-1380.
- Veldkamp, K. E. & J. A. van Strijp, (2009) Innate immune evasion by staphylococci. *Advances in experimental medicine and biology* **666**: 19-31.
- Volkov, A., J. Mascarenhas, C. Andrei-Selmer, H. D. Ulrich & P. L. Graumann, (2003) A prokaryotic condensin/cohesin-like complex can actively compact chromosomes from a single position on the nucleoid and binds to DNA as a ring-like structure. *Molecular and cellular biology* **23**: 5638-5650.
- von Stetten, D., M. Noirclerc-Savoye, J. Goedhart, T. W. Gadella, Jr. & A. Royant, (2012) Structure of a fluorescent protein from Aequorea victoria bearing the obligate-monomer mutation A206K. *Acta crystallographica. Section F, Structural biology and crystallization communications* **68**: 878-882.
- Wachi, M., M. Doi, Y. Okada & M. Matsushashi, (1989) New mre genes mreC and mreD, responsible for formation of the rod shape of Escherichia coli cells. *Journal of bacteriology* **171**: 6511-6516.
- Wagner, S., M. M. Klepsch, S. Schlegel, A. Appel, R. Draheim, M. Tarry, M. Hogbom, K. J. van Wijk, D. J. Slotboom, J. O. Persson & J. W. de Gier, (2008) Tuning Escherichia coli for membrane protein overexpression. *Proceedings of the*

- National Academy of Sciences of the United States of America* **105**: 14371-14376.
- Waldo, G. S., B. M. Standish, J. Berendzen & T. C. Terwilliger, (1999) Rapid protein-folding assay using green fluorescent protein. *Nature biotechnology* **17**: 691-695.
- Wall, T., S. Roos, K. Jacobsson, A. Rosander & H. Jonsson, (2003) Phage display reveals 52 novel extracellular and transmembrane proteins from *Lactobacillus reuteri* DSM 20016(T). *Microbiology* **149**: 3493-3505.
- Wang, J. D., G. M. Sanders & A. D. Grossman, (2007) Nutritional control of elongation of DNA replication by (p)ppGpp. *Cell* **128**: 865-875.
- Wang, S., L. Furchtgott, K. C. Huang & J. W. Shaevitz, (2012) Helical insertion of peptidoglycan produces chiral ordering of the bacterial cell wall. *Proceedings of the National Academy of Sciences of the United States of America* **109**: E595-604.
- Wang, X., J. Huang, A. Mukherjee, C. Cao & J. Lutkenhaus, (1997) Analysis of the interaction of FtsZ with itself, GTP, and FtsA. *Journal of bacteriology* **179**: 5551-5559.
- Wang, X. & P. J. Quinn, (2010) Lipopolysaccharide: Biosynthetic pathway and structure modification. *Progress in lipid research* **49**: 97-107.
- Weart, R. B., A. H. Lee, A. C. Chien, D. P. Haeusser, N. S. Hill & P. A. Levin, (2007) A metabolic sensor governing cell size in bacteria. *Cell* **130**: 335-347.
- Weart, R. B. & P. A. Levin, (2003) Growth rate-dependent regulation of medial FtsZ ring formation. *Journal of bacteriology* **185**: 2826-2834.
- Weidenmaier, C. & A. Peschel, (2008) Teichoic acids and related cell-wall glycopolymers in Gram-positive physiology and host interactions. *Nature reviews. Microbiology* **6**: 276-287.
- Weidenmaier, C., A. Peschel, Y. Q. Xiong, S. A. Kristian, K. Dietz, M. R. Yeaman & A. S. Bayer, (2005) Lack of wall teichoic acids in *Staphylococcus aureus* leads to reduced interactions with endothelial cells and to attenuated virulence in a rabbit model of endocarditis. *The Journal of infectious diseases* **191**: 1771-1777.
- White, C. L., A. Kitich & J. W. Gober, (2010) Positioning cell wall synthetic complexes by the bacterial morphogenetic proteins MreB and MreD. *Molecular microbiology* **76**: 616-633.
- Wickner, W., A. J. Driessen & F. U. Hartl, (1991) The enzymology of protein translocation across the *Escherichia coli* plasma membrane. *Annual review of biochemistry* **60**: 101-124.
- Willemsse, J., J. W. Borst, E. de Waal, T. Bisseling & G. P. van Wezel, (2011) Positive control of cell division: FtsZ is recruited by SsgB during sporulation of *Streptomyces*. *Genes & development* **25**: 89-99.
- Wower, I. K., J. Wower & R. A. Zimmermann, (1998) Ribosomal protein L27 participates in both 50 S subunit assembly and the peptidyl transferase reaction. *The Journal of biological chemistry* **273**: 19847-19852.
- Wu, L. J. & J. Errington, (2004) Coordination of cell division and chromosome segregation by a nucleoid occlusion protein in *Bacillus subtilis*. *Cell* **117**: 915-925.
- Wu, L. J. & J. Errington, (2012) Nucleoid occlusion and bacterial cell division. *Nature reviews. Microbiology* **10**: 8-12.
- Wu, L. J., S. Ishikawa, Y. Kawai, T. Oshima, N. Ogasawara & J. Errington, (2009) Noc protein binds to specific DNA sequences to coordinate cell division with chromosome segregation. *The EMBO journal* **28**: 1940-1952.

- Wu, Q. Y. & Q. Liang, (2014) Interplay between curvature and lateral organization of lipids and peptides/proteins in model membranes. *Langmuir : the ACS journal of surfaces and colloids* **30**: 1116-1122.
- Wu, T., A. C. McCandlish, L. S. Gronenberg, S. S. Chng, T. J. Silhavy & D. Kahne, (2006) Identification of a protein complex that assembles lipopolysaccharide in the outer membrane of Escherichia coli. *Proceedings of the National Academy of Sciences of the United States of America* **103**: 11754-11759.
- Xie, J., M. Bogdanov, P. Heacock & W. Dowhan, (2006) Phosphatidylethanolamine and monoglucosyldiacylglycerol are interchangeable in supporting topogenesis and function of the polytopic membrane protein lactose permease. *The Journal of biological chemistry* **281**: 19172-19178.
- Yan, K., K. H. Pearce & D. J. Payne, (2000) A conserved residue at the extreme C-terminus of FtsZ is critical for the FtsA-FtsZ interaction in Staphylococcus aureus. *Biochemical and biophysical research communications* **270**: 387-392.
- Yang, D. C., N. T. Peters, K. R. Parzych, T. Uehara, M. Markovski & T. G. Bernhardt, (2011) An ATP-binding cassette transporter-like complex governs cell-wall hydrolysis at the bacterial cytokinetic ring. *Proceedings of the National Academy of Sciences of the United States of America* **108**: E1052-1060.
- Yansura, D. G. & D. J. Henner, (1984) Use of the Escherichia coli lac repressor and operator to control gene expression in Bacillus subtilis. *Proceedings of the National Academy of Sciences of the United States of America* **81**: 439-443.
- Young, K. D., (2006) The selective value of bacterial shape. *Microbiology and molecular biology reviews : MMBR* **70**: 660-703.
- Young, R. M., J. K. Arnette, D. A. Roess & B. G. Barisas, (1994) Quantitation of fluorescence energy transfer between cell surface proteins via fluorescence donor photobleaching kinetics. *Biophysical journal* **67**: 881-888.
- Zapun, A., T. Vernet & M. G. Pinho, (2008) The different shapes of cocci. *FEMS microbiology reviews* **32**: 345-360.
- Zhang, H. M., Z. Li, M. Tsudome, S. Ito, H. Takami & K. Horikoshi, (2005a) An alkali-inducible flotillin-like protein from Bacillus halodurans C-125. *The protein journal* **24**: 125-131.
- Zhang, W., H. A. Campbell, S. C. King & W. Dowhan, (2005b) Phospholipids as determinants of membrane protein topology. Phosphatidylethanolamine is required for the proper topological organization of the gamma-aminobutyric acid permease (GabP) of Escherichia coli. *The Journal of biological chemistry* **280**: 26032-26038.
- Zhang, Y. H., C. Ginsberg, Y. Yuan & S. Walker, (2006) Acceptor substrate selectivity and kinetic mechanism of Bacillus subtilis TagA. *Biochemistry* **45**: 10895-10904.
- Zhang, Y. M. & C. O. Rock, (2008) Membrane lipid homeostasis in bacteria. *Nature reviews. Microbiology* **6**: 222-233.
- Zhao, H., A. Pykalainen & P. Lappalainen, (2011) I-BAR domain proteins: linking actin and plasma membrane dynamics. *Current opinion in cell biology* **23**: 14-21.
- Zhao, X. J. & H. C. Wu, (1992) Nucleotide sequence of the Staphylococcus aureus signal peptidase II (Isp) gene. *FEBS letters* **299**: 80-84.
- Zhou, X., D. K. Halladin, E. R. Rojas, E. F. Koslover, T. K. Lee, K. C. Huang & J. A. Theriot, (2015) Bacterial division. Mechanical crack propagation drives millisecond daughter cell separation in Staphylococcus aureus. *Science* **348**: 574-578.
- Zieske, K. & P. Schwille, (2014) Reconstitution of self-organizing protein gradients as spatial cues in cell-free systems. *eLife* **3**.

- Zimmerberg, J. & M. M. Kozlov, (2006) How proteins produce cellular membrane curvature. *Nature reviews. Molecular cell biology* **7**: 9-19.
- Zinchuk, V., O. Zinchuk & T. Okada, (2007) Quantitative colocalization analysis of multicolor confocal immunofluorescence microscopy images: pushing pixels to explore biological phenomena. *Acta histochemica et cytochemica* **40**: 101-111.

Chapter 9: Appendix

9.1 Construction of mCherry and mRFPmars1 fusions with membrane proteins

9.1.1 Construction of a PlsY-mCherry fusion in *S. aureus*

In order to construct pAISH-*plsY*-*mCherry*, *plsY* (5'FW23/3'FW23) was amplified using SH1000 genomic DNA as a template and *mCherry* (5'FW24/3'FW24) was amplified using plasmid pMV158-*mCherry* (Dr. S. Mesnage, unpublished) as templates. DNA fragments were cloned into the *HindIII/SwaI* site of pAISH1 using Gibson Assembly (see Fig. 9.1A) and transformed into *E. coli* NEB5 α . Recombinant plasmids were tested by restriction digest with EcoRV resulting in approximately 4500, 2500 and 1000 bp fragments (Fig. 9.1C) and validated by DNA sequencing (GATC Biotech AG, Konstanz, Germany). The resulting plasmid, pAISH-*plsY*-*mCherry* was electroporated into RN4220 and from there transduced into SH1000. Genomic integration at the *plsY* locus was confirmed by PCR amplification of an approximately 900 bp fragment using one primer that binds at the beginning of *plsY* and one primer within the *mCherry* gene (5'FW23/Outward_mCherry) (Fig. 9.1D). No amplification of an approximately 900 bp fragment was seen using SH1000 genomic DNA as a template. The whole *plsY* gene was amplified with the use of primers 5'FW23/3'FW23 resulting in an approximately 600 bp fragment to confirm the PCR and template.

9.1.2 Construction of a CdsA-mCherry fusion in *S. aureus*

In order to construct pAISH-*cdsA*-*mCherry*, *cdsA* (5'FW45/3'FW45) was amplified using SH1000 genomic DNA as a template and *mCherry* (5'FW45/3'FW24) was amplified using plasmid pMV158-*mCherry* (Dr.S.Mesnage, unpublished) as templates. DNA fragments were cloned into the *HindIII/SwaI* site of pAISH1 using Gibson Assembly (see Fig. 9.2A) and transformed into *E. coli* NEB5 α . Recombinant plasmids were tested by restriction digest with PstI and HindIII resulting in approximately 4000, 3000 and 1000 bp fragments (Fig. 9.2C) and validated by DNA sequencing (GATC

Biotech AG, Konstanz, Germany). The resulting plasmid, pAISH-*cdsA-mCherry* was electroporated into RN4220 and from there transduced into SH1000. Genomic integration at the *cdsA* locus was confirmed by PCR amplification of an approximately 1000 bp fragment using one primer that binds at the beginning of *cdsA* and one primer within the *mCherry* gene (5'FW45/Outward_mCherry) (Fig. 9.2D). No amplification of an approximately 1000 bp fragment was seen using SH1000 genomic DNA as a template. The whole *cdsA* gene was amplified with the use of primers 5'FW45/3'FW45 resulting in an approximately 800 bp fragment to confirm the PCR and template.

9.1.3 Construction of a *CdsA-mRFPmars1* fusion in *S. aureus*

In order to construct pAISH-*cdsA-mRFPmars1*, *cdsA* (5'FW47/3'FW47) was amplified using SH1000 genomic DNA as a template and *mRFPmars1* (5'FW48/3'FW48) was amplified using plasmid pTK-RFP (Prajsnar, 2009) as templates. DNA fragments were cloned into the *HindIII/SwaI* site of pAISH1 using Gibson Assembly (Fig. 9.3A) and transformed into *E. coli* NEB5 α . Recombinant plasmids were tested by restriction digest with PstI and HindIII resulting in approximately 4000, 3000 and 1100 bp fragments (Fig. 9.3C) and validated by DNA sequencing (GATC Biotech AG, Konstanz, Germany). The resulting plasmid, pAISH-*cdsA-mRFPmars1* was electroporated into RN4220 and from there transduced into SH1000. Genomic integration at the *cdsA* locus was confirmed by PCR amplification of an approximately 1000 bp fragment using one primer that binds at the beginning of *cdsA* and one primer within the *mRFPmars1* gene (5'FW45/Outward_mRFP) (Fig. 9.3D). No amplification of an approximately 1000 bp fragment was seen using SH1000 genomic DNA as a template. The whole *cdsA* gene was amplified with the use of primers 5'FW45/3'FW45 resulting in an approximately 800 bp fragment to confirm the PCR and template.

9.1.4 Construction of a *PgsA-mRFPmars1* fusion in *S. aureus*

In order to construct pAISH-*pgsA-mRFPmars1*, *pgsA* (5'FW49/3'FW49) was amplified using SH1000 genomic DNA as a template and *mRFPmars1* (5'FW49/3'FW48) was amplified using plasmid pTK-RFP (Prajsnar, 2009) as templates. DNA fragments were cloned into the *HindIII/SwaI* site of pAISH1 using Gibson Assembly (Fig. 9.4A) and transformed into *E. coli* NEB5 α . Recombinant plasmids were tested by restriction digest with PstI resulting in approximately 7000 and 1000 bp fragments (Fig. 9.4C) and validated by DNA sequencing (GATC Biotech AG, Konstanz, Germany). The resulting plasmid, pAISH-*pgsA-mRFPmars1* was electroporated into RN4220 and from there transduced into SH1000. Genomic integration at the *pgsA* locus was confirmed by PCR amplification of an approximately 1000 bp fragment using one primer that binds at the

beginning of *pgsA* and one primer within the *mRFPmars1* gene (5'FW49/Outward_mRFP) (Fig. 9.4D). Amplification of an approximately 1000 bp fragment was also seen using SH1000 genomic DNA as a negative control template which could be explained by non-specific DNA amplification. The whole *pgsA* gene was amplified with the use of primers 5'FW49/3'FW49 resulting in an approximately 600 bp fragment to confirm the PCR and template.

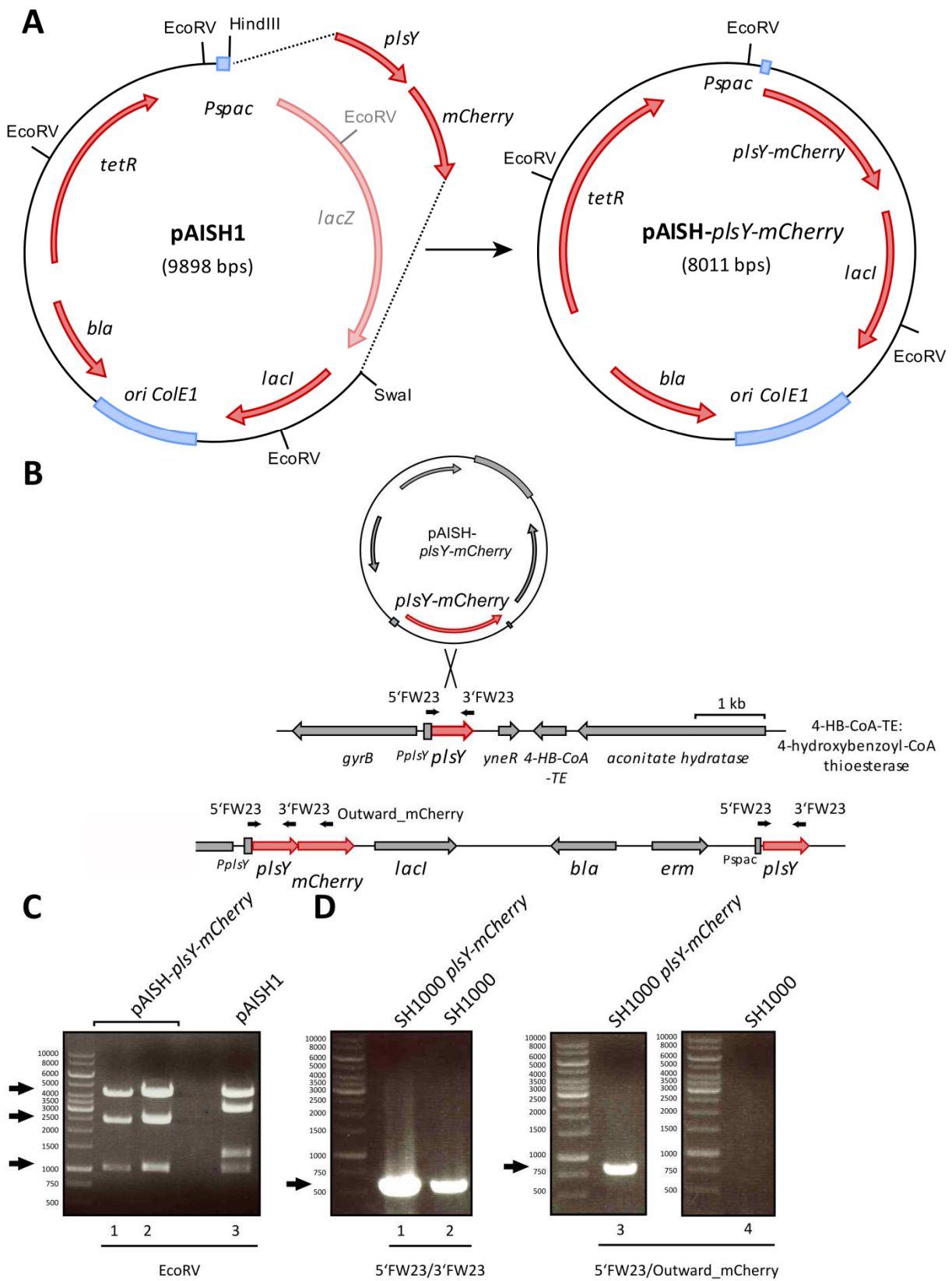


Figure 9.1 Construction of a chromosomal *plsY-mCherry* fusion in *S. aureus*

SH1000

A, Diagram illustrating the construction of pAISH-*plsY*-*mCherry*. **B**, Schematic overview of the native genomic region of *plsY* and post integration of pAISH-*plsY*-*mCherry*. Black arrows indicate primer binding sites. **C**, pAISH-*plsY*-*mCherry* (Lanes 1-2) and pAISH1 (Lane 3) were digested with EcoRV and separated by 1 % (w/v) TAE agarose gel electrophoresis. Bands of approximately 4500, 2500 and 1000 bp fragments, corresponding to pAISH-*plsY*-*mCherry* (Lanes 1-2), respectively, are marked by black arrows. Bands of approximately 4600, 3000, 1500 and 1000 bp fragments correspond to pAISH1 (Lane 3). **D**, Verification of pAISH-*plsY*-*mCherry* integration by PCR using primer pair 5'FW23/Outward_mCherry. PCR products were separated by 1 % (w/v) TAE agarose gel electrophoresis. A band of approximately 900 bp, marked by a black arrow, indicates pAISH-*plsY*-*mCherry* chromosomal integration (Lane 3). No DNA amplification is seen using genomic DNA from SH1000 (Lane 4). PCR amplification of the whole *plsY* gene using primer pair 5'FW23/3'FW23 results in a band of approximately 600 bp, marked by a black arrow (Lanes 1-2).

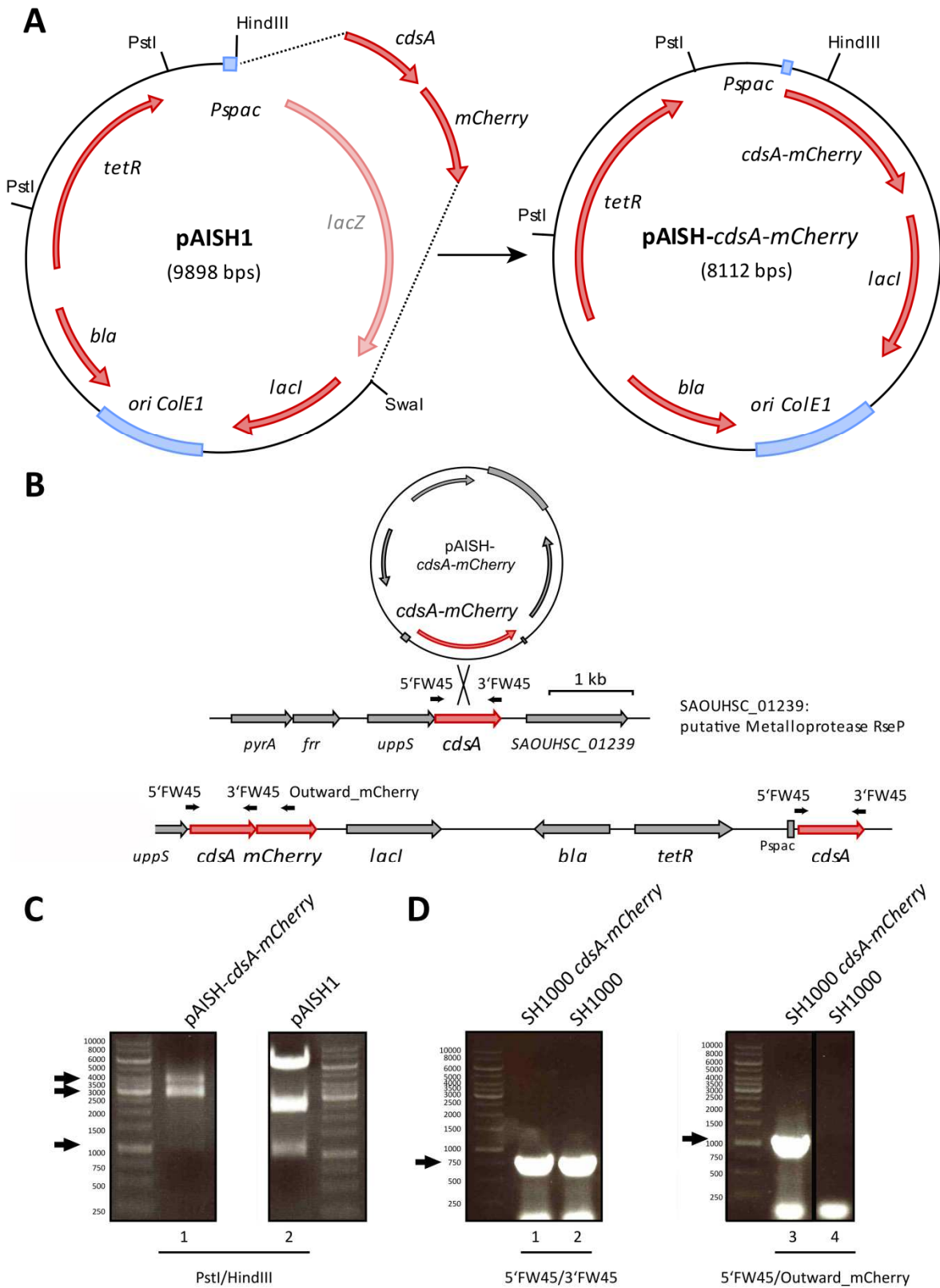


Figure 9.2 Construction of a chromosomal *cdsA-mCherry* fusion in *S. aureus* SH1000

A, Diagram illustrating the construction of pAISH-*cdsA*-*mCherry*. **B**, Schematic overview of the native genomic region of *cdsA* and post integration of pAISH-*cdsA*-*mCherry*. Black arrows indicate primer binding sites. **C**, pAISH-*cdsA*-*mCherry* (Lanes 1-2) and pAISH1 (Lane 3) were digested with PstI and HindIII and separated by 1 % (w/v) TAE agarose gel electrophoresis. Bands of approximately 4000, 3000 and 1000 bp fragments, corresponding to pAISH-*cdsA*-*mCherry* (Lane 1), respectively, are marked by black arrows. Bands of approximately 7500, 2500 and 1000 bp fragments correspond to pAISH1 (Lane 2). **D**, Verification of pAISH-*cdsA*-*mCherry* integration by PCR using primer pair 5'FW45/Outward_mCherry. PCR products were separated by 1 % (w/v) TAE agarose gel electrophoresis. A band of approximately 1000 bp, marked by a black arrow, indicates pAISH-*cdsA*-*mCherry* chromosomal integration (Lane 3). No DNA amplification is seen using genomic DNA from SH1000 (Lane 4). PCR amplification of the whole *cdsA* gene using primer pair 5'FW45/3'FW45 results in a band of approximately 800 bp, marked by a black arrow (Lanes 1-2).

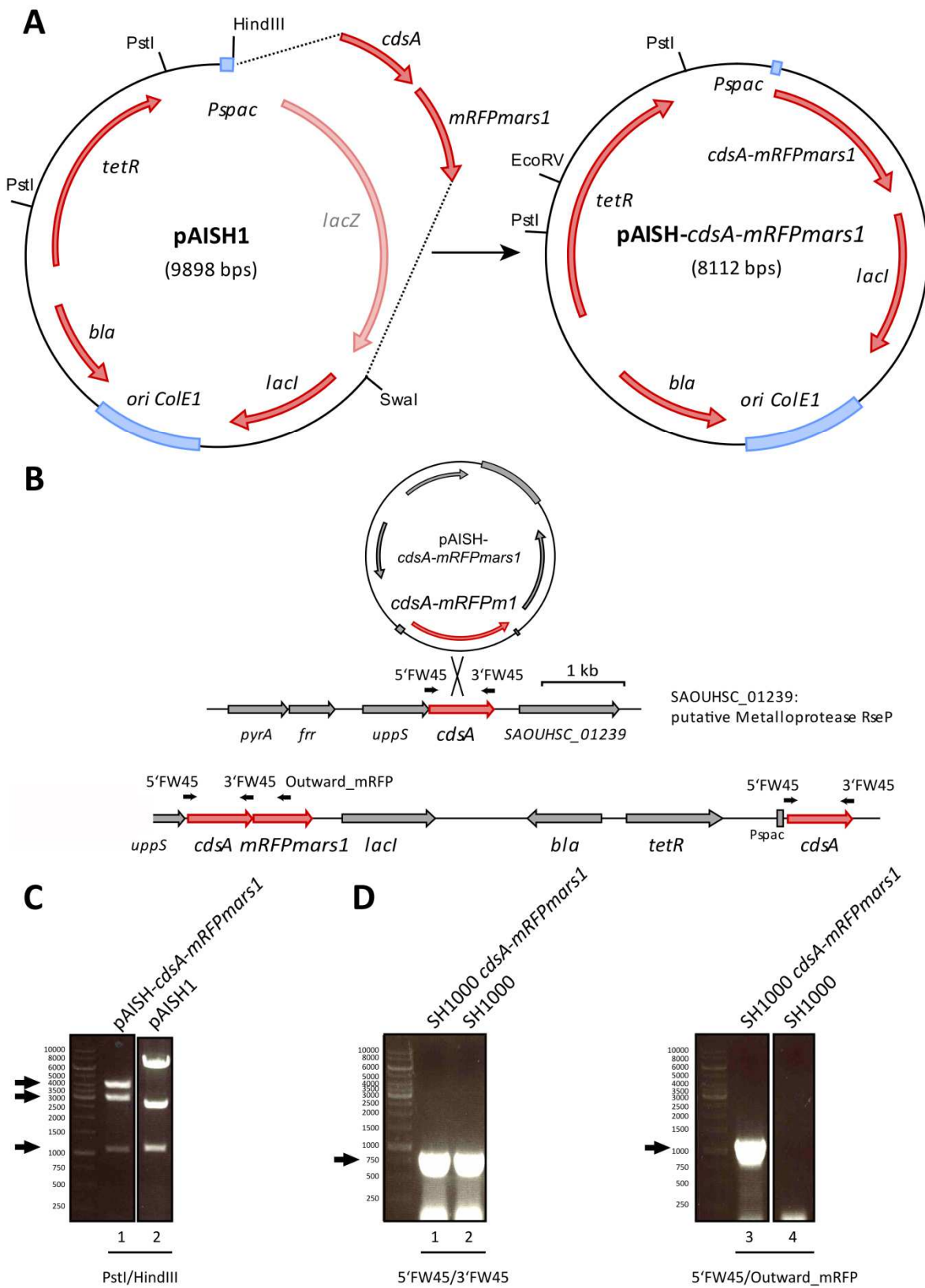


Figure 9.3 Construction of a chromosomal *cdsA-mRFPmars1* fusion in *S. aureus* SH1000

A, Diagram illustrating the construction of pAISH-*cdsA-mRFPmars1*. **B**, Schematic overview of the native genomic region of *cdsA* and post integration of pAISH-*cdsA-mRFPmars1*. Black arrows indicate primer binding sites. **C**, pAISH-*cdsA-mRFPmars1* (Lane 1) and pAISH1 (Lane 2) were digested with PstI and HindIII and separated by 1 % (w/v) TAE agarose gel electrophoresis. Bands of approximately 4000, 3000 and 1100 bp fragments, corresponding to pAISH-*cdsA-mRFPmars1* (Lane 1), respectively, are marked by black arrows. Bands of approximately 7500, 2500 and 1100 bp fragments correspond to pAISH1 (Lane 2). **D**, Verification of pAISH-*cdsA-mRFPmars1* integration by PCR using primer pair 5'FW45/Outward_mRFP. PCR products were separated by 1 % (w/v) TAE agarose gel electrophoresis. A band of approximately 1000 bp, marked by a black arrow, indicates pAISH-*cdsA-mRFPmars1* chromosomal integration (Lane 3). No DNA amplification is seen using genomic DNA from SH1000 (Lane 4). PCR amplification of the whole *cdsA* gene using primer pair 5'FW45/3'FW45 results in a band of approximately 800 bp, marked by a black arrow (Lanes 1-2).

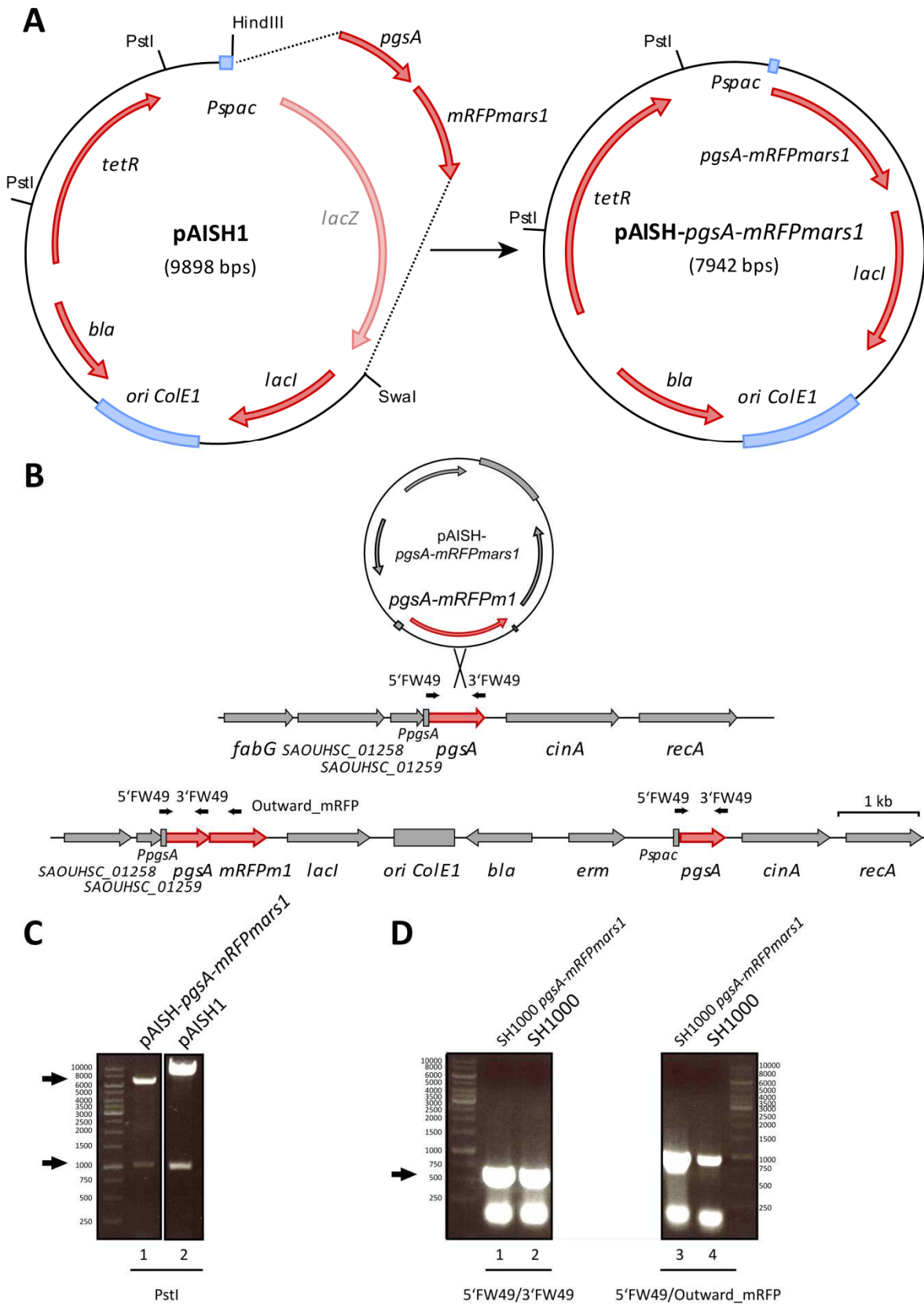


Figure 9.4 Construction of a chromosomal *pgsA-mRFPmars1* fusion in *S. aureus* SH1000

A, Diagram illustrating the construction of pAISH-*pgsA-mRFPmars1*. **B**, Schematic overview of the native genomic region of *pgsA* and post integration of pAISH-*pgsA-mRFPmars1*. Black arrows indicate primer binding sites. **C**, pAISH-*pgsA-mRFPmars1* (Lane 1) and pAISH1 (Lane 2) were digested with PstI and separated by 1 % (w/v) TAE agarose gel electrophoresis. Bands of approximately 7000 and 1000 bp fragments, corresponding to pAISH-*pgsA-mRFPmars1* (Lane 1), respectively, are marked by black arrows. Bands of approximately 9000 and 1000 bp fragments correspond to pAISH1 (Lane 2). **D**, Verification of pAISH-*pgsA-mRFPmars1* integration by PCR using primer pair 5'FW49/Outward_mRFP. PCR products were separated by 1 % (w/v) TAE agarose gel electrophoresis. A band of approximately 1000 bp, marked by a black arrow, indicates pAISH-*pgsA-mRFPmars1* chromosomal integration (Lane 3). Amplification of an approximately 1000 bp fragment was also seen using genomic DNA from SH1000 (Lane 4) which could be due to non-specific DNA amplification. PCR amplification of the whole *pgsA* gene using primer pair 5'FW49/3'FW49 results in a band of approximately 600 bp, marked by a black arrow (Lanes 1-2).

9.1.5 Construction of a PlsY-GFP (tetracycline resistance) fusion in *S.*

aureus

In order to construct pAISH-*plsY-gfp*, *plsY* (5'FW23/3'FW43) was amplified using SH1000 genomic DNA as a template and *gfp* (5'FW44/3'FW44) was amplified using plasmid pMUTIN-*gfp*⁺ as templates. DNA fragments were cloned into the HindIII/SwaI site of pAISH1 using Gibson Assembly (Fig. 9.5A) and transformed into *E. coli* DC10B. Recombinant plasmids were tested by restriction digest with NheI and SacI resulting in approximately 8000 and 750 bp fragments (Fig. 9.5C) and validated by DNA sequencing (GATC Biotech AG, Konstanz, Germany). The resulting plasmid, pAISH-*plsY-gfp* was electroporated into RN4220 and from there transduced into SH1000. Genomic integration at the *plsY* locus was confirmed by PCR amplification of an approximately 1000 bp fragment using one primer that binds in the genome upstream of *plsY* and one primer within the *gfp* gene (Inward_plsY/Outward_gfp) (Fig. 9.5D). No amplification of a 1000 bp fragment was seen using SH1000 genomic DNA as a template.

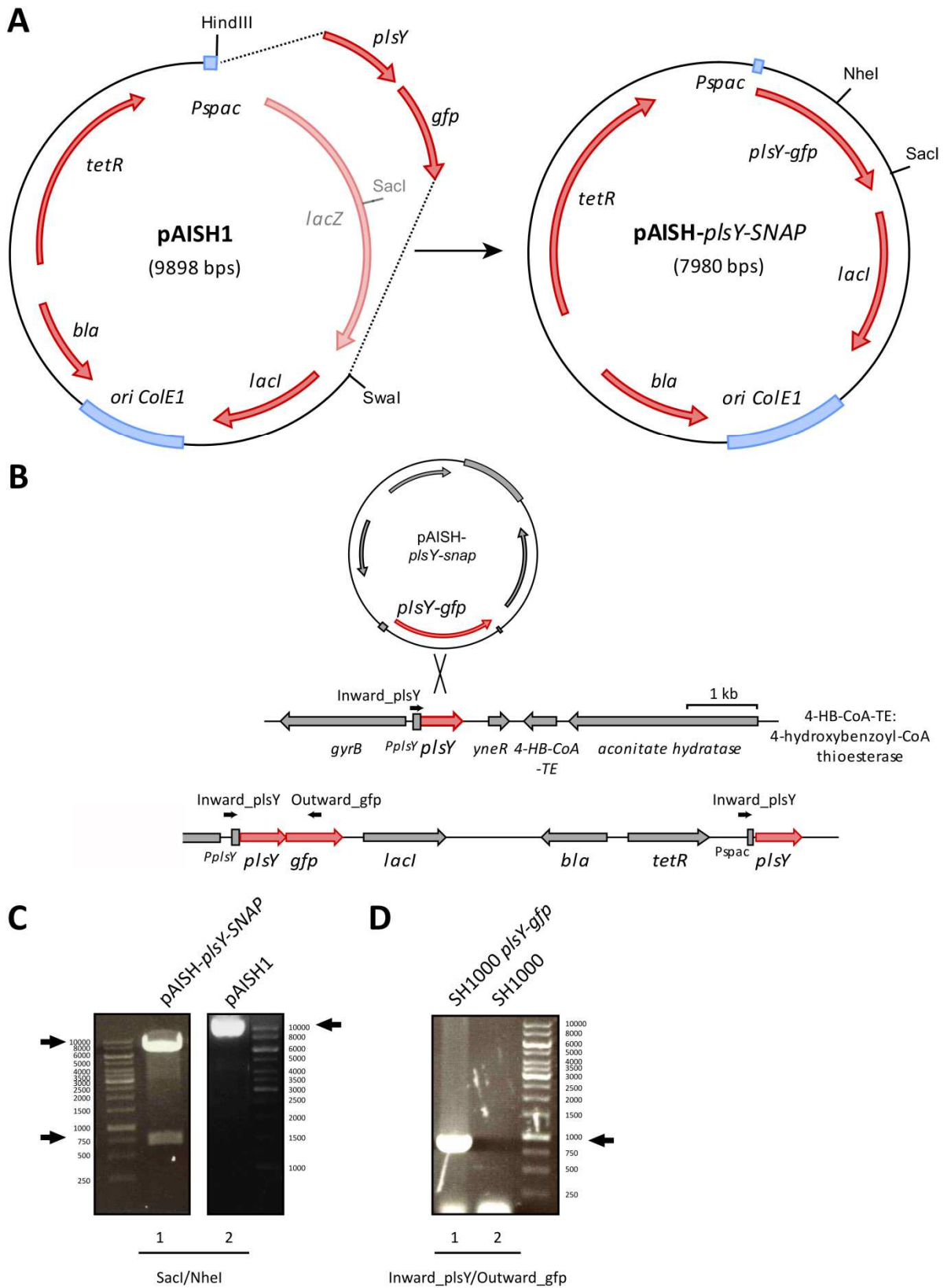


Figure 9.5 Construction of a chromosomal *plsY-gfp* (tetracycline resistance) fusion in *S. aureus* SH1000

A, Diagram illustrating the construction of pAISH-*plsY-gfp*. **B**, Schematic overview of the native genomic region of *plsY* and post integration of pAISH-*plsY-gfp*. Black arrows indicate primer binding sites. **C**, pAISH-*plsY-gfp* (Lane 1) and pAISH1 (Lane 2) were digested with *NheI* and *SacI* and separated by 1 % (w/v) TAE agarose gel electrophoresis. Bands of approximately 8000 and 750 bp fragments, corresponding to pAISH-*plsY-gfp* (Lane 1), respectively, are marked by black arrows. A bands of an approximately 10000 bp fragment corresponds to pAISH1 (Lane 2). **D**, Verification of pAISH-*plsY-gfp* integration by PCR using primer pair Inward_*plsY*/Outward_*gfp*. PCR products were separated by 1 % (w/v) TAE agarose gel electrophoresis. A band of approximately 1000 bp, marked by a black arrow, indicates pAISH-*plsY-gfp* chromosomal integration (Lane 1). No amplification of an approximately 1000 bp fragment was seen using genomic DNA from SH1000 (Lane 2).

9.2 Codon-optimised sequences

9.2.1 Codon-optimised sequence of *mreD*

The sequence of *mreD* from *S. aureus* SH1000 was optimised for the use in *E. coli* using GeneOptimizer® (<https://www.thermofisher.com/uk/en/home/lifescience/cloning/gene-synthesis/genart-gene-synthesis/geneoptimizer.html>). The following figure (Fig. 9.6) shows the original sequence aligned with the optimised sequence.

```
mreD
S.aureus 1 atgcgtacactgtattatTTTTGATAGGTATTTACTATTTATATAGATACTGCAATTGGGCTTCTTA
optimised 1 atgcgtaccctgtattatTTTCTGATTGGTATCCTGCTGTTCTATATTGATACCGCAATTGGTCTGCTGA
          m r t l y y f l i g i l l f y i d t a i g l l
S.aureus 71 TTCGAATGCACATAGGTAAGTTGAACTTGATTGTACCACACCTTACATTTATGTATATTTAATGAT
optimised 71 TTCGGATGCAATTTGGTAAATTTGAACTGGTGTTTGGTCCCGCACTGACCTTATGTATATTTGATGAT
          i p m h i g k f e l v f v p h l t f m y i l m
S.aureus 141 GGTAGTGATCGTGGCTTTGGCGTATCATTATTGCTCAGCATATTTTGGCGTAATGACTGATGTATAC
optimised 141 GGTGGTGATCGGGTTTTGGTGTAGCCTGCTGCTGAGCATTTTTCTGGGTGTTATGACCGATGTTAT
          m v v y r g f g v s l l l s i f l g v m t d v y
S.aureus 211 TTTGGTAGTATTTATGGAGTGACTTATTTGGCTATATATTGTTTTAGCACTTATAGATCGATTCTTTA
optimised 211 TTCGGTAGCATTATGGCGTTTACCTGTTTGGCTATATCTGTCTTCTGGCACTGATCGACCGTTTTTCA
          f g s i y g v y l f g y i l f l a l i d r f f
S.aureus 281 AAATTTTTACAAGATCATTGATGTTATTTCATTATTATATTAGCCAGCACCTTATTATTAGAAGTCTA
optimised 281 AAATCTTCTATAAAGATCATAGCATGCTGTTTCATCATTATCTGGCAAGCACACTGCTGCTGGAAGTTTA
          k i f y k d h s m l f i i i l a s t l l l e v
S.aureus 351 TGTGGCATTAAATATACGGTATGTTAGGATTCATTCAATTTGATATTATTCATTTGTAGTCTTTAGATTA
optimised 351 TGTGGCACTGATTTATGGTATGCTGGGCTTTATCCAGTTTGACATCATTCACTTTGTTGTGTTTCTGCTG
          y v a l i y g m l g f i q f d i i h f v v f r l
S.aureus 421 TTGCCAACATTAATTATGAATTTGTACTGTTGATTATGCTTTATCCGTTGATTATAAAGTTCCTTAAAA
optimised 421 CTGCCGACCTGATTATGAATTTGTGCTGCTGATTATGCTGTACCCGCTGATTATCAAATTTCTGAAAA
          l p t l i m n f v l l i m l y p l i i k f l k
S.aureus 491 AAACAACAATGACATTGACATGAAACGTCGTCGAATGGTAA
optimised 491 AAACAACAAGACATGATGAAACGTCGTCAGTGGTAA
          k t n n d i d m k r r q w -
```

Figure 9.6 Nucleotide alignment of *S. aureus* SH1000 *mreD* with the optimised *mreD* sequence

Sequence alignment of *mreD* from SH1000 (first row) compared to the codon-optimised *mreD* (second row). Green letters indicate translated codon into amino acids in the one letter format. Yellow bars indicate changes in the nucleotide sequence.

9.2.2 Codon-optimised sequence of *eyfp*

The sequence of *eyfp* from plasmid pKASBAR-*ezrA-eyfp* (Wascnik, 2016) was optimised for the use in *E. coli* using GeneOptimizer® (<https://www.thermofisher.com/uk/en/home/life-science/cloning/gene-synthesis/geneart-gene-synthesis/geneoptimizer.html>). The following figure (Fig. 9.7) shows the original sequence aligned with the optimised sequence.

```

eyfp
plasmid 1 atgggtgagcaagggcgaggagctgttcaccgggggtgcccacccctggctcgagctggacggcgacgtaa
optimised 1 atgggtgagcaaaaggtgaagaactgtttaccgggtgttcttccgatctgggtgaaactgggatggatgtta
    m v s k g e e l f t g v v p i l v e l d g d v
plasmid 71 acggccacaagttcagcgtgtccggcgaggggcgatgccacctacggcaagctgaccctgaagtt
optimised 71 atggccacaaaattttcagtttagcgggtgaaggcgaaggtgatgcaacctatggtaaaactgaccctgaaaatt
    n g h k f s v s g e g e g d a t y g k l t l k
plasmid 141 catctgaccaccggcaagctgcccgtgccctggcccaccctcgtgaccaccttcggctacggcctcgacg
optimised 141 tatctgtaccaccggcaaaactgcccgttccgtggccgaccctcgttaccaccttcgggttatggctcgacg
    f i c t t g k l p v p w p t l v t t f g y g l q
plasmid 211 tgcttcgcccgcctaccccgaccacatgaagcagcagcactcttcaagtcgcccatgcccggaaggctacg
optimised 211 tgttttgccagcttatccggatcatatgaaacagcagcattttttcaaaaagcgcgaatgccggaaggttatg
    c f a r y p d h m k q h d f f k s a m p e g y
plasmid 281 tccaggagcgcaccatcttcttcaaggacgcagcgaactacaagaccgcgcgaggtgaagttcgagggg
optimised 281 ttcaagaacgtaccatcttcttcaaaagatgacggcaactataaaaccgcgtgccgaagttaaaattgaaagg
    v q e r t i f f k d d g n y k t r a e v k f e
plasmid 351 cgacaccctgggtgaaccgcatcgagctgaaggcgcacttcaaggaggacggcaacatcctggggcac
optimised 351 tgataccctgggtgaatcgcatgaaactgaaaggcgcacttcaaaaggaggatggtaaatatcctggggcac
    g d t l v n r i e l k g i d f k e d g n i l g h
plasmid 421 aagctggagtagaactacaacagccacaacgtctatatcatggccgacaagcagaagaacggcatcaagg
optimised 421 aaactggaatataattataatagccacaacgtgtacatcatggccgacaaaacagaaaatggcatcaaaag
    k l e y n y n s h n v y i m a d k q k n g i k
plasmid 491 tgaacttcaagatccgcccacaacatcgagggggcagcgtgacgctcgccgaccactaccagcagaacac
optimised 491 tgaacttcaaaatccgccaataatattgaaagctggtagcgttcagctggcagatcattatcagcagaatc
    v n f k i r h n i e g g s v q l a d h y q q n
plasmid 561 ccccatcggcgacggccccgtgctgctgcccgacaaccactacctgagctaccagtcgccctgagcaaaa
optimised 561 cccgatgggtgatgggtccgggtctgctgcccgataatcattatctgagctatcagagcgcaactgagcaaaa
    t p i g d g p v l l p d n h y l s y q s a l s k
plasmid 631 gaccccaacgagaagcgcgatcacatggctcctgctggagttcgtgaccgcccgggatcactctcgcca
optimised 631 gatccggaatgaaaaacgtgatcacatggctcctgctggaaattgttaccgcagcaggtattaccctgggta
    d p n e k r d h m v l l e f v t a a g i t l g
plasmid 701 tggacgagctgtacaagtaa
optimised 701 tggatgaaactgtataaatga
    m d e l y k -

```

Figure 9.7 Nucleotide alignment of *eyfp* with the optimised sequence

Sequence alignment of *eyfp* from pKASBAR-*ezrA-eyfp* (first row) compared to the codon-optimised *eyfp* (second row). Green letters indicate translated codon into amino acids in the one letter format. Yellow bars indicate changes in the nucleotide sequence.